

NASA-CR-172362
19840024340

A Study of Leaside Flow Field Heat Transfer On Shuttle Orbiter Configurations

Leroy C. Baranowski
and H. W. Kipp

MCDONNELL DOUGLAS ASTRONAUTICS COMPANY
-ST. LOUIS DIVISION Saint Louis, Missouri 63166 (314) 232-0232

CONTRACT NAS1-16839

AUGUST 1984



National Aeronautics and
Space Administration

Langley Research Center
Hampton, Virginia 23665

LIBRARY COPY

OCT 2 1984

LANGLEY RESEARCH CENTER
LIBRARY, NASA
HAMPTON, VIRGINIA

NASA Contractor Report 172362

**A Study of Leaside Flow Field
Heat Transfer On Shuttle
Orbiter Configurations**

**Leroy C. Baranowski
and H. W. Kipp**

MCDONNELL DOUGLAS ASTRONAUTICS COMPANY

-ST. LOUIS DIVISION *Saint Louis, Missouri 63166 (314) 232-0232*

CONTRACT NAS1-16839

AUGUST 1984



National Aeronautics and
Space Administration

Langley Research Center
Hampton, Virginia 23665

N84-32410#

TABLE OF CONTENTS

	<u>Page</u>
LIST OF FIGURES.....	iii
NOMENCLATURE.....	vi
SUMMARY.....	1
INTRODUCTION.....	1
TEST DATA.....	4
WING LEESIDE ATTACHED FLOW HEATING CORRELATION.....	5
FUSELAGE UPPER SURFACE HEATING CORRELATION.....	11
FLIGHT PREDICTIONS.....	16
COMPARISON WITH FLIGHT DATA.....	17
WING HEAT TRANSFER.....	18
UPPER FUSELAGE HEAT TRANSFER.....	22
CONCLUSIONS AND RECOMMENDATIONS.....	26
REFERENCES.....	28
FIGURES.....	30
APPENDICES:	
A. THE PHENOMENON OF STRIATION HEATING.....	A1
B. WING AND FUSELAGE LEESIDE TEST DATA.....	B1
C. VARIATIONS OF WING LEESIDE TEST DATA.....	C1
D. BOUNDARIES FOR ATTACHED FLOW ON THE WING LEESIDE SURFACE.....	D1
E. WING HEATING INFLUENCES.....	E1
F. DEFINITION OF WETTED LENGTH FOR UPPER FUSELAGE HEATING CORRELATIONS.....	F1
G. EFFECTS OF FLOW PROCESSING ON HEAT TRANSFER.....	G1
H. WING LEESIDE SURFACE HEATING CORRELATIONS.....	H1
I. UPPER FUSELAGE HEATING CORRELATIONS.....	I1
J. SAMPLE CALCULATIONS.....	J1

LIST OF FIGURES

<u>Figure</u>		<u>Page</u>
1	Shuttle Leeside Flow.....	30
2	Summary of Leeside Heating Tests.....	31
3	Wing Leeside Surface Thermocouple Locations.....	32
4	Fuselage Leeside Surface Thermocouple Locations.....	33
5	Mach 6 Wing Leeside Thermocouple Behavior.....	34
6	Mach 10 Wing Leeside Thermocouple Behavior.....	35
7	Mach 10 Wing Leeside Heating Distribution for Arbitrary Wetted-Length Path.....	36
8	Mach 10 Wing Leeside Heating Distribution for Axial Wetted-Length Path.....	39
9	Wing Leeside Flow Zones.....	42
10	Wing Leeside Flow Zones.....	43
11	Mach 10 Wing Leeside Heating Correlation.....	45
12	Wing Leeside Heating Correlation Parameters.....	50
13	Upper Fuselage Wetted Length Concepts.....	51
14	Upper Fuselage Heat Transfer Profiles, $M_\infty = 10$	52
15	Upper Fuselage Heat Transfer Profiles, $M_\infty = 10$	53
16	Upper Fuselage Heat Transfer Profiles, $M_\infty = 10$	54
17	Upper Fuselage Heat Transfer Profiles, $M_\infty = 6$	55
18	Selected Leeside Oil-Flow Patterns, $M_\infty = 10$	56
19	Selected Leeside Oil-Flow Patterns, $M_\infty = 6$	62
20	Upper Fuselage Heat Transfer Profiles, $M_\infty = 10$	68
21	Upper Fuselage Heat Transfer Profiles, $M_\infty = 10$	69
22	Upper Fuselage Heat Transfer Profiles, $M_\infty = 10$	70
23	Upper Fuselage Heat Transfer Profiles, $M_\infty = 6$	71
24	Upper Fuselage Heat Transfer Profiles, $M_\infty = 6$	72
25	Upper Fuselage Heat Transfer Profiles, $M_\infty = 6$	73
26	Upper Fuselage Heat Transfer Profiles, $M_\infty = 6$	74
27	Upper Fuselage Heat Transfer Profiles, $M_\infty = 6$	75
28	Effective Sweep Angles Measured from Oil-Flow Patterns.....	76
29	Mach 10 Upper Fuselage Centerline Heating Distributions.....	77
30	Mach 6 Upper Fuselage Centerline Heating Distributions.....	78

LIST OF FIGURES (Continued)

<u>Figure</u>		<u>Page</u>
31	Forward Upper Fuselage Heating Correlation Parameters.....	79
32	Aft Upper Fuselage Heating Correlation Parameters.....	80
33	Trajectory History During STS-2 Entry.....	81
34	STS-2 Entry Trajectory and Reference Heating Rates.....	86
35	Reference Heating Rate History During STS-2 Entry.....	87
36	Reynolds Number Variation with Mach Number During STS-2 Entry	88
37	Wing Leaside Correlation Variation with Reynolds Number.....	89
38	Forward Upper Fuselage Correlation Variation with Reynolds Number.....	90
39	Flight Comparison Wing Leaside DFI.....	91
40	Flight Comparison Upper Fuselage DFI.....	92
41	Wing Leaside Heat Flux Histories During STS-2 Entry, $Y/L \approx 0.216$	93
42	Wing Leaside Heat Flux Histories During STS-2 Entry, $Y/L \approx 0.279$	94
43	Wing Leaside Heating Distributions During STS-2 Entry, $\alpha \approx 40^\circ$	95
44	Wing Leaside Heating Distributions During STS-2 Entry, $\alpha \approx 35^\circ$	96
45	Wing Leaside Heating Distributions During STS-2 Entry, $30^\circ \geq \alpha \geq 20^\circ$	97
46	Wing Leaside Flow Definition.....	98
47	Upper Fuselage Heat Flux Histories During STS-2 Entry, $X/L \approx 0.396$	99
48	Upper Fuselage Heat Flux Histories During STS-2 Entry, $X/L \approx 0.496$	100
49	Upper Fuselage Heat Flux Histories During STS-2 Entry, $X/L \approx 0.595$	101
50	Upper Fuselage Heat Flux Histories During STS-2 Entry, $X/L \approx 0.696$	102
51	Upper Fuselage Heat Flux Ratios During STS-2 Entry.....	103
52	Upper Fuselage Heating Distributions During STS-2 Entry, $\alpha \approx 40^\circ$	105
53	Upper Fuselage Heating Distributions During STS-2 Entry, $\alpha \approx 35^\circ$	106
54	Upper Fuselage Heating Distributions During STS-2 Entry, $\alpha \approx 30^\circ$ and 25°	107

LIST OF FIGURES (Continued)

<u>Figure</u>		<u>Page</u>
55	Upper Fuselage Centerline Heating Distributions During STS-2 Entry.....	108
56	Comparison of Upper Fuselage Centerline Heating Distributions	109

NOMENCLATURE

C	multiplier term in correlation expression
DFI	Development Flight Instrumentation
h	heat transfer coefficient
L	orbiter characteristic length, 32.8 m (107.5 ft) full scale
LaRC	Langley Research Center
M	Mach number
n	exponent of normalized wetted length term in correlation expression
\dot{q}	heat transfer rate
Re	Reynolds number
s/L	normalized wetted length
t_E	entry time
T_w	wall temperature
T/C	thermocouple
X/L	normalized longitudinal distance from orbiter nose
Y/L	normalized spanwise distance from orbiter plane of symmetry
α	angle of attack
β	sideslip (yaw) angle
δ	boundary layer thickness
λ	sweep angle
\bar{X}	viscous interaction parameter, M^3/\sqrt{Re}

Subscripts:

axial	wetted length direction parallel to plane of symmetry
c	convective heat transfer

NOMENCLATURE (Continued)

CL	condition at centerline
f	fuselage heat-transfer correlation parameter
L	characteristic length used as distance term in parameter
ref	reference heat transfer, at stagnation point of a scaled 0.305 m (1.0 ft) radius sphere for free stream and wall conditions
s	a sensor or thermocouple related quantity
T/C	condition at location of thermocouple
w	wing heat-transfer correlation parameter
∞	free stream properties used in evaluating parameter

A STUDY OF LEESIDE FLOW FIELD HEAT TRANSFER ON SHUTTLE ORBITER CONFIGURATIONS

Leroy C. Baranowski and H. W. Kipp
McDonnell Douglas Astronautics Company - St. Louis Division

SUMMARY

For lifting re-entry configurations such as the Space Shuttle Orbiter, the aerodynamic heating must be known adequately over the entire vehicle to design the thermal protection system. A coupled inviscid and viscous theoretical solution of the flow about the entire configuration is the desirable and comprehensive approach to defining thermal environments about the spacecraft. While comprehensive numerical flow field solutions for the Shuttle windward surface are becoming available, the leeside is less amenable to such solutions.

The purpose of this study was to develop simplified methods for predicting entry heating on leeside surfaces of the Shuttle orbiter. Wind tunnel heat transfer and oil flow data at Mach 6 and 10 and Reynolds numbers ranging from 0.5×10^6 to 7.3×10^6 were used to develop correlations for the wing upper surface and the top surface of the fuselage. These correlations were extrapolated to flight Reynolds number and compared with heating data obtained during the Shuttle STS-2 reentry. Efforts directed toward the wing leeside surface resulted in an approach which generally agreed with the flight data. Heating predictions for the upper fuselage were less successful due to the extreme complexity of local flow interactions and the associated heating environment.

INTRODUCTION

The purpose of this study was to develop leeside entry heating correlations for the Space Shuttle Orbiter. Wind tunnel thermocouple and oil flow data were used to derive a set of simplified heating methods. These methods were then extrapolated to flight conditions and compared with heating data obtained during entry of the STS-2 orbiter, as this was the first flight for which a full set of entry data was available. The two leeside areas that were examined are the

attached flow region on the wing upper surface and the top surface of the fuselage. These surfaces exhibit many complex flow interactions with attendant effects on pressure and heating distributions. This is especially true on the upper fuselage where formulating a reasonable correlation for off-centerline heating proved very difficult. Efforts directed toward the wing leeward surface resulted in an approach which provided good general agreement with the STS-2 flight data.

Aeroheating analyses of vehicles at large angle of attack usually neglect, or at best, roughly account for heat transfer to the leeward surfaces. Techniques considered conservative are utilized due to lack of knowledge concerning local flow conditions or inadequacies of flow models. Over-expanded pressures are predicted because of failure to account for rapid growth of the boundary layer in the favorable pressure gradient, or flow models simply break down in expanding to the leeward contour.

Prior investigations (refs. 1-10) of leeward heating on delta wings and shuttle configurations have confirmed the deficiencies of using such techniques. Heating rates and pressures measured along the leeward meridian are considerably higher than estimated using two-dimensional streamline methods. The heating at high angle of attack is greater than at zero angle of attack, and can increase off the centerline.

Examination of oil flow patterns for the above-mentioned studies indicates that such phenomena are caused by various interactions of vortices with the leeward surface (refs. 11-12). Heating methods for the shuttle orbiter's leeward centerline which account for these interactions, or at least simulate their influences, have been developed by Zakkay, et.al. (ref. 9) and Helms (ref. 13). However, each technique has its own set of restrictions, and it is not clear if the basic approach employed by either method can be extended to estimate off-centerline heating. Similarly, there is no comprehensive heating method that can be directly applied to the attached flow on the wing leeward surface.

Figure 1a shows an overall view of the three-dimensional flow structures which affect heating on the orbiter's leeward surfaces. The upper fuselage is thought to be dominated by a vortex pair impinging on the top centerline at low to moderate angles of attack (Figures 1b through 1e). Secondary vortices can also occur outboard of the primary pair (Figure 1e). At high angles-of-attack, generally 35° to 40° , vortex impingement moves off of the upper centerline resulting in undulating and roughly axial flow on the top surface, as will be

discussed later. It is suggested that under conditions of off-centerline impingement, a "quasi" boundary layer forms within which embedded vortices may develop (Figure 1e). These vortices are similar to Shuttle sidebody vortices which are discussed in Appendix A. Regardless of angle-of-attack, properties in the upper fuselage vortices are likely to be influenced by flow originating along the strake leading edge and impinging on the side fuselage. This is also illustrated in various parts of Figure 1.

As indicated in Figure 1, flow on the wing upper surface is characterized by an extensive separation which can be accompanied by either a single or double embedded crossflow shock (ref. 2). Properties within the separated region are also influenced by downward flow from the fuselage side. Leading edge conditions can be affected by interactions with the bow and strake shocks. The complicated and unpredictable flow in the separated region was one consideration in choosing to restrict attention in this study to the attached flow region near the wing leading edge. Another consideration was that heating rates associated with the attached flow are generally much higher than those within the separated region. Thus, a correlation for locations preceding separation would be a more significant contribution to the understanding of heating on the wing leeward surface of an entry vehicle.

The goal of this study, as originally envisioned, was to develop simplified methods for computing leeward flow properties and heat transfer, such as might be calculated using the MINIVER computer program (ref. 14) and validate these methods with a NASA/LaRC-furnished data base. It was anticipated that these methods would involve the formulation of "equivalent" two-dimensional flow models, similar to that of reference 13, described by equations relating heat transfer to such major parameters as Mach number, Reynolds number, angle of attack and running length. However, complex heating trends observed in the data base precluded the application of relatively simple flow concepts. This was underscored by an unsuccessful attempt to model flow properties for heating calculations on the wing as illustrated in Appendix G. A further hindrance was the lack of pressure measurements and other local flow properties which could be used as inputs for detailed flow field calculations in the regions of interest. An assessment of trends in heating distributions on the wing revealed that they did not conform to expected variations with wetted length obtained from closed form boundary layer solutions with or without pressure gradient (refs. 15-19). The difficulty encountered with upper fuselage data trends was that the

heating distributions were not axially uniform, nor were the data trends consistent with respect to changes in spanwise location and angle of attack. The origin of complexities in the wing and fuselage heating patterns will be fully addressed in those sections of this report dealing with the development of correlations and comparisons with flight data for the leeward wing attached flow and upper fuselage heating, respectively. The result of these developments was that the approach of this study was altered in order to establish heating correlations adequate for extrapolating test results to flight conditions by employing an equation with a highly generalized format which is capable of duplicating the unusual heating trends observed in the wind tunnel data.

TEST DATA

The previously unpublished test data used in the present study were furnished by the NASA Langley Research Center. These data were obtained in air in their Mach 6 and 10 wind tunnels using a 0.01-scale model of the Space Shuttle orbiter. The data consisted of heat-transfer coefficients (reduced from thin-skin thermocouple measurements normalized by stagnation values on a scaled 1 ft radius sphere) and oil-flow photos. Wind tunnel conditions for the thermocouple tests are summarized in Figure 2. Measurements were made for angles of attack from 20° to 40° at increments of 5° . Free stream Reynolds numbers for the Mach 10 wing and fuselage tests varied from approximately 0.5×10^6 to 2.4×10^6 . Reynolds numbers for the Mach 6 Wing tests spanned the range from 0.8×10^6 to 7.0×10^6 and the Mach 6 fuselage heating data were obtained for Reynolds numbers from 1.1×10^6 to 7.3×10^6 . These Reynolds numbers are based on a model reference length of 0.328 m (12.9 in.). Thermocouple (T/C) locations on the wing and fuselage leeward surfaces are shown in Figures 3 and 4. A value of unity for the recovery factor was used in determining an adiabatic wall temperature for data reduction. A complete set of the test data is included in Appendix B. This tabulation includes data from side fuselage locations, although side fuselage heating was not investigated in the present study (however, Helms utilized these data in his study of side fuselage heating presented in reference 20). Photos of oil-flow patterns on the upper fuselage and wing surfaces were available for the same range of angle of attack over which the heat transfer data were obtained. However oil flow tests at Mach 6 were made at 10° increments instead of every 5° .

The oil flow photographs cover Reynolds numbers from 0.55×10^6 to 2.2×10^6 at Mach 10 and 2.7×10^6 to 7.3×10^6 at Mach 6.

Apparent irregularities in the data from the Mach 6 tests caused the quality of flow at some test conditions to be suspect. This is illustrated by the variations with angle of attack and Reynolds number of Mach 6 data from a few select thermocouples on the wing shown in Figure 5. For comparison, the Mach 10 data from these same thermocouples are shown in Figure 6. These figures show the heating data for thermocouples 28, 29, and 30. The upper set of plots in both figures illustrates the angle of attack dependence of the normalized heating rates for all test Reynolds numbers. The effect of Reynolds number is emphasized in the lower set of graphs. Similar plots for all of the individual wing thermocouples are presented in Appendix C. Thermocouples 28, 29 and 30 were chosen as examples because their location near the wing's leading edge and at about its mid-span (see Figure 3) will minimize, but not entirely eliminate, the influence of flow separation and shock interactions for most test conditions. In comparing the behavior of data in Figures 5 and 6 it is first noted that the Mach 10 data trends are relatively smooth and well-behaved. That is, heat transfer decreases with increased angle of attack and the ratio of heat transfer coefficients remains relatively constant with Reynolds number (i.e., laminar flow). By contrast, there is more scatter for the Mach 6 data (Figure 5) as well as unexplained inconsistencies in the heating variations. At 40° angle of attack the Mach 6 data exhibited a sharp decrease in heating with increasing Reynolds number. This is opposite of the trends at other angles of attack. Also, the Mach 6 heat transfer coefficient ratio initially decreases with increasing Reynolds number which is contrary to the anticipated trends and the Mach 10 data. Model blockage at high angles of attack or growth of the tunnel's boundary layer at low Reynolds numbers are potential sources of these heating variations. The questionable nature of the Mach 6 data at high angles of attack and also at low Reynolds number has been confirmed in private communications with NASA Langley personnel. As a result, the Mach 6 data at 40° angle of attack and the Mach 6 low Reynolds number data were ignored in the correlations. After the fact, some of the omitted data were found to agree with the correlations.

WING LEESIDE ATTACHED FLOW HEATING CORRELATION

Heating distributions in the attached flow region on the wing leeward surface were correlated using the format:

$$h/h_{\text{ref}} = C_w(s/L)^{-n_w} \quad (1)$$

where s is wetted length. The multiplier term C and the exponent n are considered to be dependent on Reynolds number, angle of attack and Mach number. Although equation (1) does not explicitly incorporate these major parameters as independent variables, their effects are contained in the wind tunnel data upon which the correlation is based and they are thereby fully accounted for. A procedure for extrapolating the terms C and n to the shuttle orbiter's entry flight conditions is discussed later.

The format of equation (1) was selected because of its inherent ability to cope with heating induced by a variety of local flow conditions, and because the heat transfer distributions contained in the data base conflicted with trends conventionally associated with either laminar or turbulent flow. Heating tended to decrease more rapidly than the inverse of wetted length ($n \approx 1.0$). This is illustrated for Mach 10 data in Figures 7 and 8 where the dashed line through the data represents a heating rate that is proportional to $(s/L)^{-1.0}$. Attached flow data for Reynolds numbers of approximately 0.55×10^6 , 1.0×10^6 and 2.4×10^6 are shown and both figures contain individual plots for each angle of attack between 20° and 40° .

The difference between Figures 7 and 8 is the way s/L was obtained. For Figure 7, surface patterns in oil flow photographs were used to identify the general direction of flow affecting each thermocouple to establish a wetted length. A different symbol is used for each spanwise location of instrumentation (Figure 3), and marking within a symbol is used for streamline direction, as indicated by the figure legend. The oil flow patterns were sometimes locally indistinct so as to make the flow direction for a given thermocouple uncertain. In this case, the heat rate of that thermocouple was assigned an s/L value which was consistent with flow directions observed for adjacent data points. The s/L values given in Figure 8 were all measured from the wing's leading edge in an axial direction. Axial wetted lengths were obtained from numerical integration of longitudinal wing section drawings assuming a single-shock Newtonian stagnation line location which varied with angle of attack. A comparison of Figures 7 and 8 shows that the latter approach (Figure 8) reduces the data scatter, so these values of s/L were used for the remainder of the wing correlation effort.

The use of axial lengths rather than distance normal to the wing leading edge was based on an examination of oil-flow photos. It was noted that surface

patterns which ordinarily would be categorized as flow normal to the leading edge actually traversed a very complex path in traveling over the leading edge from the stagnation line and onto the wing's upper surface. A flow component parallel to the swept leading edge initially forces the flow outboard. As the flow travels away from the stagnation line and over the leading edge, it changes to an inboard direction and then turns outboard again to approach the flow separation line (Figure 1a). This results in a total path length which is longer than would be calculated by assuming a direction perpendicular to the leading edge, and better approximated by the axial length.

Another trend that was noted in the data is that heating rates for the two most inboard arrays of thermocouples ($Y/L \leq 0.1719$ in Figure 3) seemed anomalously low when plotted using axial path lengths from the leading edge stagnation line. An examination of oil-flow photos suggested that flow in this region of the wing may actually originate on the forward fuselage bottom surface which spreads outboard and over onto the wing's leeside in the transition region between the strake and the swept wing leading edge. Such a large increase in path length over that which would be computed based on distance from the wing's leading edge allows the heating measurements of the inboard thermocouples to fall more nearly in line with the general body of data.

The experimental heating rates in Figures 7 and 8 decrease more rapidly than is indicated by the linear inverse of length ($n = 1.0$). This behavior of heating is in agreement with a rapid growth of the viscous layer ($h \propto 1/\delta$) on the leeside of delta wings noted by Cross and Hankey (ref. 2). Also, boundary layer similar solutions predict that such heating distributions correspond to very favorable pressure gradients (refs. 15-19). A study of references 15-19 indicates that the simultaneous effects of entropy gradients and leading edge bluntness induced pressures may be the primary causes of the sharp decrease in heating as a function of wetted length illustrated in Figures 7 and 8. Entropy gradients cause increased local heat transfer in the region near the wing's leading edge. Higher pressures due to bluntness augment the effect. But heating rates rapidly decrease at points further downstream. (Appendix E contains additional information.) Experimental pressure measurements or detailed flow field computations would be very helpful in further assessing the state of local flow.

Three distinct zones of heating, illustrated in Figure 9, were found to exist in the wing leeside data.

Zone 1 consists of attached flow heating which extends from the wing leading edge stagnation line to the locus of points at which local streamline curvature begins a rapid change of direction (the forward boundary of Zone 2) just upstream of separation. The highest heating is generally associated with the attached flow zone.

Zone 2 encompasses the attached preseparation flow in a region downstream of Zone 1 and ahead of the flow separation line--a region in which the pressure rise associated with the downstream separation propagates upstream in the subsonic portion of the boundary layer. Heating is significantly lower in Zone 2 as compared with Zone 1.

Zone 3 includes the separated flow. Heating rates are usually quite low, and can be erratic, in the separated region.

Oil flow photos show that the boundaries of these three zones change location on the wing's surface in response to variations in angle of attack, Reynolds number and Mach number. Appendix D gives a full account of these movements. In addition, transparencies of thermocouple locations shown in Figure 3 were used to overlay wing upper surface oil flow photographs corresponding to each test condition in order to identify those thermocouples within each of the three zones. This was done to exclude data generated by separation phenomena in the development of a heating correlation for attached flow.

The attached flow data were fit with least squares logarithmic curves. Figure 10a illustrates such a curve fit using selected data from Run 1 ($M_\infty = 9.82$, $Re_{\infty,L} = 0.55 \times 10^6$, $\alpha = 20^\circ$). Some of the data points in this figure are labeled with the corresponding thermocouple number in order to indicate general heating levels on different parts of the wing. Only data from those attached and preseparated flow regions not influenced by shock impingements are shown in order to clearly depict heating trends in the three zones mentioned above. Selected data were also included to indicate the large heating variations occurring in the separated flow. The data trends in this plot display the following characteristics:

- Most of the Zone 1 attached flow data fall within $\pm 20\%$ of the curve fit and all data fall within $\pm 50\%$.
- Most of the Zone 2 preseparation flow data fall below the fit for the Zone 1 heating rates, though a few data points are on the curve. The tendency of the preseparation heat transfer rates to fall below the trend line established by the upstream data is believed to result from a thickening of the boundary layer in the preseparation zone.

- Some of the separated flow data exceeds the attached flow curve fit by more than +50%. The high heat transfer rates in the separated zone appear to be caused by local stagnation points, revealed in the oil flow, and illustrated in Figure 10b, while the extremely low heat transfer data appear to coincide with regions of low surface shear.

The same observations can be applied to Figures 11a through 11e, where selected wing heating plots with corresponding least squares curve fits similar to that of Figure 10a are shown. Plots for all the test conditions are presented in Appendix H. In these figures, all of the attached (Zone 1) and pre-separated (Zone 2) flow data are included, even those thought to be affected by shock interactions. Most of the separated flow data, however, have been omitted. A guide to the state of flow affecting individual thermocouples is given for each test condition. The guide consists of symbols and numbers, defined by an accompanying legend, arranged in a pattern corresponding to the thermocouple locations in Figure 3 for each of the indicated rows of instruments. Also shown is the number of data points used to derive the curve fit and the root-mean-square deviation of the data from the logarithmic correlation.

The data in Figures 11a through 11c show an irregular increase in heating in Zones 1 and 2 with spanwise distance at angles of attack of 20° to 30° . At angles of attack of 35° and 40° , there are insufficient data in Zones 1 and 2 to draw conclusions regarding spanwise heat transfer variation. The observed spanwise increase in heating is consistent with conclusions of a simple analysis of flow processing effects on heat transfer to a reference sphere (Appendix G). However, no way has been found to extend the simple sphere heating analysis model to wing leading edges and thereby to the wing top surface. The leading edge analysis is more complex than that of the sphere because in addition to the parameters required to compute sphere heating, the flow direction relative to the leading edge is required.

The main influence of shock interaction in the data seems to be associated with relatively localized effects due to impingement. Evidence for this can be seen in the higher heating for thermocouple 19 at an angle of attack of 20° (Figure 11a). This thermocouple is near the location thought to be influenced by impingement of the relatively weak strake shock, or intersecting strake and wing shocks. Heating is enhanced only in the region of direct impact and, judging from a lack of a similar response from nearby thermocouples, the effect apparently does not propagate very far downstream. No inboard thermocouples experience elevated heating at higher angles of attack.

The localized heating effects resulting from bow shock interactions outboard on the wing are apparent in the relatively high heating of thermocouple 35 at $\alpha = 25^\circ$ shown in Figure 11b and by the data for $Y/L = 0.2978$ from all angles of attack. At the lower angles of attack, data from thermocouples 41 and 42, which lie outboard of the bow shock interaction and are influenced by flow passing only through the wing shock, are in agreement with measurements made inboard of the bow shock. Further aft, thermocouples 43, 44, and 45 recorded higher heating due to the proximity of the effects from the very strong bow shock impingement which propagates downstream. As angle of attack increases, the bow-shock moves off the wing so that it no longer affects the aft locations. Those data then tend to coalesce with the general body of attached flow heating rates.

The outermost row of thermocouples ($Y/L = 0.3279$) is affected by a combination of flows unlike those that have previously been discussed. Oil flow photographs show that these locations contain a circulation pattern at low angles of attack which generates a wing tip vortex. Increasing the angle of attack causes the bow shock impingement effects to sweep across the area. At very high angles, $\alpha = 35^\circ$ to 40° , a large portion of the wing tip is separated and controlled by reversed flow originating near the wing's trailing edge. Because of the wide variety of local flow conditions at the outer thermocouple locations their heating levels were often incompatible with the main body of attached flow data and were frequently not used in the heating correlation.

Figure 12 summarizes the trends exhibited by the coefficients of equation (1) resulting from the individual curve fits of the wing heating data shown in Figures 11a through 11e and in Appendix H. The variation of the term C_w as a function of angle of attack over the range of Reynolds numbers at Mach 6 and 10 is shown in the lower portions of Figures 12a and 12b, respectively. This coefficient is an indicator of the severity of the heating environment. Its decrease with increasing angle of attack reflects a more pronounced shielding of the leeward regions as well as a greater expansion of flow reaching the upper wing surface at high incidence. Higher Reynolds numbers increase the value of C_w . The Reynolds number plots for Mach 6 and 10 overlap at roughly the same levels for similar Reynolds numbers, which seems to indicate that Mach number exerts only a secondary influence on this coefficient. Figure 12b shows that the exponent n_w becomes larger with increasing angle of attack. This is attributed to the increased effective bluntness of the wing geometry at high angles of attack

causing proportionately stronger gradients in the bluntness-induced leeside pressure distributions. The role of an entropy gradient is difficult to ascertain, but it is thought to make a less significant contribution than bluntness effects to the value of n_w at different model attitudes. Increasing Reynolds number decreases the value of the exponent, demonstrating that the influence of bluntness-induced flow properties on wing leeside heating is reduced at high Reynolds numbers. Plots of n_w for similar Reynolds numbers at both Mach numbers are at approximately the same level, again indicating that Mach number has a secondary effect. The value of n_w at a given angle of attack changes very little as Reynolds number continues to increase.

FUSELAGE UPPER SURFACE HEATING CORRELATION

Heating distributions in the vortex influenced regions on the fuselage upper surface were correlated using the equation:

$$h/h_{CL} = C_F(s/L)^{-n_f} \quad (2)$$

The selection of an appropriate wetted length was the subject of a cursory examination that is discussed in Appendix F. It was not readily apparent how to define the wetted length due to the variety of surface flow directions on top of the fuselage revealed by the oil flow photographs used in this study.

Figure 13 illustrates the three wetted-length concepts that were considered. A wetted-length measured along the fuselage upper surface in a direction normal to the top centerline is shown in Figure 13a. This is a simple definition of s which depends only upon upper fuselage cross sectional geometry. The two remaining concepts made an attempt to incorporate the effects of local flow on nominal heating distributions using measurements of surface flow directions provided in reference 13.

The wetted-length concept of Figure 13b makes use of a line drawn tangent to the inflection point of local vortex-generated surface flow patterns as in reference 13. This line is inclined at a sweep angle of λ . The value of λ is assumed to be constant for all s/L locations on top of the fuselage for a given axial station, so the local flow inflection point can be considered as coincident to any outboard position where a heating calculation is desired. Another line is

constructed which interests the top centerline at the same x/L and is parallel to the inflection-point line. Heating at the outboard point is assumed to be proportional to the local top centerline value in a manner that is related to the distance, $(s/L)\sin \lambda$, between the two respective parallel lines. The quantity s/L is the same as that described in Figure 13a and the modified value of s/L in Figure 13b produces the correct trend in wetted-length expected from an examination of surface flow patterns. The farther outboard a point is, the greater its surface running length from the top centerline in the general direction of λ and also the greater the distance between the parallel lines discussed above. Similarly, the actual running length and the modified s/L for a given outboard position increase with increasing sweep angle. However, this method yields disproportionately small wetted lengths at very high values of λ . For $\lambda \rightarrow 90^\circ$ flow past the location of $h_{T/C}$ would be nearly parallel to the top centerline and is thus associated with a very large physical running length. The largest effective running length that can be predicted from Figure 13b is the distance between the top centerline and the outboard location of interest. Therefore, this approach would be more applicable to moderate values of λ .

Figure 13c depicts the third wetted-length concept that was studied. This approach uses a more straightforward definition of s over the curved upper fuselage in the direction of λ , but it also requires a value of h_{CL} at an axial location ahead of the outboard point where heating calculations are to be made. Appendix F shows how this can be a problem in correlating both wind tunnel and flight data at forward axial stations where the flow originates at top centerline locations for which no measurements have been made. This is particularly true for large sweep angles where the projected top centerline location for the reference value of h_{CL} can fall ahead of the fuselage. This objection may be overcome by applying top centerline heating methods like those of references 9 and 13, assuming that procedures can be developed to extrapolate these techniques to flight conditions.

It was found that the value of s/L defined in Figure 13a correlated the wind-tunnel data as well as the more involved wetted-length definitions in Figures 13b and 13c. Furthermore, its usage avoids the need to extrapolate a flow angle parameter for flight conditions. Wetted-lengths corresponding to the definition of Figure 13a are presented in Figure 4. An attempt was made to refine the correlations resulting from these different values of wetted-length by applying a pressure gradient to allow for the effects of surface curvature.

Approximations using a modified Newtonian pressure gradient (refs. 21-22) showed no significant improvement in the correlations.

The result of applying equation (2), with the above description of s/L , to the Mach 6 and Mach 10 wind tunnel heating data on the fuselage upper surface is shown in Appendix I. Mach 6 data at 40° angle of attack and for $Re_{\infty,L} = 1.1 \times 10^6$ are not included because of flow uncertainties discussed earlier. The curve fits were made using data for $s/L \leq 0.061$. There is generally a large variation between spanwise normalized heating values at different axial locations along the fuselage. This is due to the wide variety of surface flow patterns for the different test conditions which will be discussed below. A single curve fit could not adequately represent all of the data for any test case due to the presence of two distinct heating distributions on the forward and aft regions of the upper fuselage. However, it was determined that two curve fits for each set of wind tunnel data, one for $X/L \leq 0.5$ and the other for $X/L \geq 0.5$, more satisfactorily reproduced the average magnitude and the overall trends in heating in these two areas. This is illustrated in Figures 14 and 15 using data for $M_\infty = 10.16$, $\alpha = 25$ and $Re_{\infty,L} = 0.5 \times 10^6$. The normalized spanwise heating coefficient is plotted versus s/L for each axial location in both figures. Figure 14 shows an attempt at a single curve fit for this test condition. There is a large error in the correlation and it is clear that heating on the forward fuselage is significantly different from the majority of data points over the aft portion. The forward and aft curve fits in Figures 15a and 15b provide improved correlations for those respective areas on the model. Two further examples of the fore and aft dichotomy in upper fuselage heating are shown in Figures 16 and 17. The spanwise heating gradient in the aft region of all of these figures, as well as for the correlations shown in Appendix I, is noticeably less than in the forward region. The fore and aft exponents of wetted length differ by roughly a factor of two for most low angle of attack test cases.

Another common element of the plots contained in Appendix I, as well as in the examples of Figures 14 through 17, is a rise in heating rate at large values of s/L . Surface flow patterns at selected conditions for Mach 10 and 6 in Figures 18 and 19, respectively, illustrate the flow features that are responsible for this trend (also labeled are lines of flow separation on the wings which are discussed in Appendix D). The locally higher rating at $s/L = 0.08$ for all test conditions is associated with attached flow originating from the side fuselage impingement which extends a short distance inboard upon reaching

the upper surface before separating. Indications of increased heating for $s/L = 0.061$ are related to secondary vortex flow at most axial locations for angles of attack less than 30° , as shown in Figure 18a and Figures 19a and 19b at both Mach numbers. The low Reynolds number Mach 10 flow patterns, like those in Figure 18b for $\alpha = 25^\circ$, contain no secondary vortices. However, as shown in the corresponding heating data in Figure 15, heating rates at $s/L = 0.061$ are still somewhat elevated for those test conditions at aft axial locations. The oil patterns in Figure 18b indicate that this is due to the inboard movement of the flow separation line, which is characteristic of the Mach 10 low Reynolds number flow on the rear portion of the fuselage, thus exposing the outer thermocouples to flow originating on the side fuselage.

Figures 18a, 18b, 19a and 19b also demonstrate why the fore and aft fuselage sections exhibit two different heating distributions. The most general explanation of this phenomenon is to be found in the surface flow directions of the primary impingement pattern. The oil flow streaks have a relatively large outboard direction on the forward fuselage and they become nearly parallel to the model's axis over the aft portion. As shown in reference 13, this trend in surface flow-measurements corresponds to decreasing heat rates along the top centerline. The change in flow directions, and in top centerline heating, takes place fairly rapidly with increasing s/L . This results in the aft fuselage values of h/h_{CL} being significantly larger and acquiring a different spanwise distribution than on the forward fuselage.

Another factor which contributes to the character of aft fuselage heating at low to moderate angles of attack that is illustrated in the above figures is the region of flow circulation ahead of the OMS pods and the vertical tail. In general, such features are present for $\alpha \leq 30^\circ$. The spiral patterns just ahead of the OMS pods are a result of the combined flows from the side fuselage impingement and streamwise flow above the fuselage interacting with the blunt forward face of the pods and with the vertical tail. A more extensive flow circulation region is present at high Reynolds numbers, particularly for the Mach 6 test conditions in Figures 19a and 19b. Top centerline heating at these locations is considerably lower than in the primary reattachment zone which dominates the forward fuselage (ref. 13). Coupled with the somewhat higher heating rates throughout the circulation regions, these flow patterns aid in producing large values of h/h_{CL} at aft locations. For example, note the extremely high normalized heating values in Figure 17 at $X/L = 0.731$ for $M_\infty = 6$.

Figures 18c through 18f and 19c show a marked change in high angle of attack ($\alpha \geq 35^\circ$) upper fuselage flow patterns as compared to low α conditions for both Mach 10 and Mach 6. Flow impingement at large Reynolds numbers occurs outboard of the symmetry plane in undulating designs with a central corridor of streamwise flow along the forward section of the top centerline (Figures 18c, 18d and 18e). This central corridor is formed from the combined flow of the outboard vortices. Low Reynolds numbers Mach 10 flow ($\bar{X} > 1$) reduces to a more simple "wavy" pattern with no central corridor (Figure 18f). These flow patterns generally resulted in high heating off of the top centerline so that $h/h_{CL} > 1.0$ at most axial positions for high angles of attack, as demonstrated for several test conditions in Figures 20 through 27. The wind tunnel data of Figures 20 through 22 and Figures 23 through 25 correspond to the flow patterns in Figures 18c through 18e and Figures 19d through 19f, respectively. Figures 20 to 27 indicate that off-centerline heating increased with increasing Reynolds number.

There is usually one axial location for each test condition at high α for which normalized heating is much higher than at any other axial station. In some instances this occurs at $X/L = 0.731$ and for other tests at $X/L = 0.573$, as shown in Figures 20 to 27. In all cases, however, the abnormally high spanwise heating ratio corresponds to the axial location where top centerline heating is at a minimum, which will tend to increase h/h_{CL} . The top centerline minimum heating location can be read directly from a plot of measured surface flow directions as a function of X/L , like the plots in Figure 28 where all available oil flow measurements at both Mach numbers are reproduced from reference 13. The parameter λ represents an "effective" sweep angle, and large values of λ produce low upper centerline heating. The corresponding leeward meridian heating is presented in Figures 29 and 30 for Mach 10 and 6, respectively. Using these plots, the above assertion concerning the relation between the location of very large spanwise heating ratios and minimum top centerline heating rates (large sweep angle flow) can be verified for the test conditions of the data in Figures 20 through 27 and also in Appendix I.

The high angle of attack flow direction measurements in Figure 28 are grouped near $\lambda = 90^\circ$ indicating essentially axial flow patterns similar to some of those shown in Figures 18 and 19. This condition promotes the development of a boundary layer which extends over most of the length along the upper fuselage and over most spanwise locations. In contrast, the many reattachment and separation patterns at low angles of attack allow only truncated boundary layers

aligned with the surface direction in each flow regime. A continuously developing boundary layer will produce an approximately constant level of heating at large distances. This is basically the reason for the low spanwise heating gradients in the data for aft axial locations at high angles of attack.

The values of n_f and C_f resulting from the curve fits presented in Appendix I are summarized in Figure 31 for the forward fuselage data and in Figure 32 for the aft fuselage. It is apparent from a comparison of the two figures that n_f is insensitive to angle of attack at $M = 10$, whereas the $M = 6$ curves show decreasing values of n_f with increasing angle of attack. C_f on the other hand shows a strong dependence on angle of attack for both Mach numbers at the forward locations. At the aft locations the Mach 10 data curve fits result in C_f values which are essentially independent of angle of attack, but the $M = 6$ data show sensitivity to angle of attack consistent with the forward fuselage results.

FLIGHT PREDICTIONS

Utilizing the previously established correlations, heating environments for the leeside surfaces of the wing and upper fuselage were predicted for selected flight conditions during entry of the STS-2 orbiter.

Time histories of various trajectory parameters that were provided by LaRC are presented in Figures 33a through 33e. The abscissa in this figure is the time interval from an altitude of 122 km (400,000 ft). These histories were determined by the method of reference 23 and the parameters are plotted at 50 second intervals.

These parameters are also tabulated in Figure 34 along with associated freestream properties and reference heating rates. Reference heating rates for a constant wall temperature were obtained from the MINIVER (ref. 14) computer program for the stagnation point of a 0.348 m (1.0 ft) radius sphere. Representative time histories of this heat flux are shown in Figure 35.

Flight conditions were selected in or at the end of time intervals during which angle of attack and yaw angles were relatively constant and yaw attitude was minimal. Trajectory points at which predictions of the leeside heating correlations were compared with flight values are denoted by asterisks in Figure 34.

Figure 36 shows the variation of Reynolds number with Mach number in flight compared with the test conditions upon which the correlations are based. The flight Reynolds numbers (based on total length) are nearly an order of magnitude higher than tunnel conditions.

To estimate heating environments, the correlations were extrapolated to flight Reynolds number as shown in Figures 37 and 38. A least-squares logarithmic curve fit of smoothed data from Figures 12 and 31 formed the basis for the extrapolation. In performing the extrapolation, Mach 6 data at Reynolds number of about 10^6 or less were not used since the values of C and n are inconsistent with the body of data and (as discussed under Wing Correlation) are of questionable validity. It may be noted that a convoluted " $-n \log C$ " term is used to determine the exponent for the normalized wetted length. Use of this parameter tends to reduce the scatter previously shown.

COMPARISON WITH FLIGHT DATA

The heating environments extrapolated in the preceding section for the leeside surfaces of the wing and upper fuselage were compared with flight data obtained from Development Flight Instrumentation (DFI) measurements during entry of the STS-2 orbiter. These data were furnished by LaRC.

The flight data consisted of heating rate histories obtained from calorimeter and surface thermocouple measurements. Calorimeters provide a direct measure of the net heat flux to the sensor and require a correction for surface reradiation for the total heating to the surface. Heating rates obtained from surface thermocouple measurements were determined using an inverse, one-dimensional heat transfer method described in reference 24. These are total heating rates to the surface since the inverse solution includes radiation from the surface. These computations were performed at LaRC.

The convective heating rates used in the comparisons were determined by correcting the total heating rates for solar heating and cross-radiation (side fuselage to wing) contributions using the method of reference 25. In this method, all locations on an upper surface are assumed to lie in the same XY plane; that is, local surface contour is not accounted for in the angle of incidence for solar or cross radiation. Also, solar radiation is considered constant and not varied with altitude. These corrections were also provided by LaRC.

The locations of the DFI measurements on the upper wing and fuselage selected for comparison are illustrated in Figures 39 and 40. The locations on the wing are forward and near the midspan. These locations were chosen because they represent the most extensive streamwise distributions of instruments where attached flow on the wings leeward surface is expected. While the outer locations will probably display some influences of shock interactions, the inner locations should be relatively free of such effects. These considerations are in accordance with the guidelines established in Appendix D for determining the region of the wing's upper surface which is affected by attached flow. The locations on the upper fuselage coincide with the area included by test model instrumentation (Figure 3).

In the Development Flight Instrumentation (DFI) coding or number, the letter "R" designates a calorimeter measurement and the "T" a thermocouple. The preceding numbers "07" usually refer to a measurement at the surface.

Wing Heat Transfer. - Histories of normalized heating rates obtained from the wing DFI are compared in Figures 41 and 42 with predictions based on the wind tunnel data correlations of Figure 37. Except for that shown in Figure 41c, the heating rates were obtained from thermocouple measurements. The heating rate history shown in Figure 41c was obtained from a calorimeter measurement corrected for reradiation utilizing the measured surface temperature and an emissivity of 0.90.

Generally, calorimeters are more sensitive (responsive) to changes of heating rate than thermocouples, as illustrated in Figure 41. The lower sensitivity of thermocouples is attributed to thermocouple resolution and the temperature smoothing technique required for solution by the inverse method. However, as shown in Figure 42, the heating rates obtained from thermocouples at the outboard locations tend to exhibit as much sensitivity (or erratic behavior) as from the calorimeter shown in Figure 41c.

The sporadic behavior shown in Figure 42 may possibly be attributed to bow-shock interaction. It is noted that these locations correspond approximately to the vicinity of T/C's 35 and 41 on the test model (Figure 3). Test data at these spanwise locales exhibited the most influence of bow-shock interactions noted in oil-flow photos. The more irregular behavior at the aft location (Figure 42b) is also characteristic of bow-shock interactions observed in test data. Included in these figures for comparison are heating rates extrapolated from the respective correlations. A step-by-step procedure, with three

illustrative examples for utilizing the correlations to predict flight heating, is presented in Appendix J.

The wing heating correlation generally reflects the trend and magnitude of the flight data, and it is perhaps even a bit conservative at early entry times. It appears that the predictions based on the Mach 6 and the Mach 10 wind tunnel data compare equally well with flight data at flight Reynolds numbers below approximately 10^7 . Above Reynolds numbers of 10^7 , predictions based upon the Mach 6 data show better agreement, apparently because of a greater uncertainty in the larger extrapolation of the Mach 10 data.

The credibility of the calorimeter data for entry time before 800 s is uncertain for comparisons relevant to attached flow conditions. The discrepancies during this time period may be caused by separated flow at this relatively aft location and high angle of attack. However, from the definitions of flow regions boundaries in Appendix D, this seems very unlikely.

It does seem more than coincidental that the response of this sensor drops off a "plateau" and agreement commences immediately following the "Push-Over/Pull-Up" (POPU) maneuver during which the angle of attack momentarily decreases to 35° and then returns to the nominal 40° (see Figure 33c). Similar behavior is also observed in the responses of calorimeters on the upper fuselage, and as discussed later, the effect may be partially attributed to solar heating. Whatever the reason, the measurements from this sensor during this time period may be considered suspect.

Figures 43, 44 and 45 compare the flight data sensitivity to s/L with predictions based on the wind tunnel data correlations. Figure 43 compares 40° angle of attack flight data at five times during reentry with predictions based on the Mach 10 tunnel correlations (recall that no correlation was established for the Mach 6 data at $\alpha=40^\circ$). Figure 44 compares 35° angle of attack flight data at two reentry times with predictions based on both the Mach 10 and Mach 6 tunnel tests. Finally, Figure 45 compares flight data at 30° , 25° and 20° angle of attack (each at a single reentry time) with predictions based on both the Mach 10 and Mach 6 tunnel tests. With the exception of some of the calorimeter data, the s/L variations (slopes) of the flight data and tunnel data correlations agree well. Furthermore, the best absolute agreement between flight data and predictions occurs when the flight Mach number and the wind tunnel Mach number are approximately equal. •

The parallel distributions tend to support the extrapolation technique. The flight data would both coalesce (fall on a single line) and agree with the extrapolations if the "effective" wetted lengths were adjusted for possible influence of bow shock interactions. With the higher Mach numbers, the bow shock curves more rapidly and lies closer to the body affecting the three-dimensional flow incident on the wind leading edge. The entropy variation increases and has a steeper gradient. Correspondingly, the velocity vector may also change, possibly moving the stagnation line further toward the lower surface, increasing the wetted length.

The poor agreement between flight data and extrapolated estimates for entry time after 1300 s, when angle of attack is less than 30° , is attributed primarily to turbulent flow. At first, this was thought to be a Mach number effect since the extrapolations from Mach 6 correlations are in better agreement with flight data when the flight Mach number is about the same magnitude (i.e., $M \lesssim 7$). At earlier times and higher flight Mach numbers, the Mach 10 extrapolations appear to agree better with the flight data.

During this time frame, heating increases more rapidly (with time) than predicted by the correlations. The disagreement is more severe for the Mach 10 correlation than for the Mach 6. Reynolds numbers are well above 10^7 , requiring extensive extrapolation of the correlations (Figure 37). Predictions based on extrapolating the Mach 10 correlations are as much as an order-of-magnitude less than the flight data. Even estimates from the Mach 6 correlations for which transitional/turbulent flow was presumed, are somewhat below flight heating rates.

Evidently the variations with Reynolds number are greater than shown in Figure 37 and used for the extrapolations. This is demonstrated by considering the behavior of the convoluted correlation parameter " $\log C_w + n_w$ " illustrated in Figure 46.

The rationale for studying this parameter resulted when, in examining the comparisons, it was observed that the normalized heating rates from the most forward DFI remain relatively constant while angle of attack is 40° . These heating rates compare favorably with the test data in the same vicinity which also appear to remain invariant with Reynolds number (e.g., see data from T/C's 19, 20, 28 and 35 in Appendix C). However, flight Reynolds number during this time frame is also about the same magnitude as for the wind tunnel data and were not varying rapidly (Figure 33e).

The premise for considering this parameter evolves from the basic concept for utilizing the "reference" heating rate or coefficient for normalization. That is, for laminar flow the normalized ratio should be independent of Reynolds number.

Consequently, the right hand side of equation (1) and its logarithm should, for a given wetted length, also remain constant. Normalized wetted-lengths applicable to the correlations (Figure 11) are nominally of the order of 10^{-1} (i.e., $\log(s/L) = -1$). Hence, the term " $\log C_w + n_w$ " should remain invariant with Reynolds number for attached laminar flow.

As shown in Figure 46, use of this parameter coalesces the respective correlations to indicate similar trends and flow conditions. Values of this parameter for similar conditions tend to show agreement within 5%. In Figure 46a it is shown that values for the Mach 6, higher Reynolds numbers and the Mach 10, highest Reynolds number, high angles of attack are insensitive to varying angle of attack. The remaining data, basically for lower Reynolds numbers, indicate a variation with angle of attack, but very little dependence on Mach or Reynolds numbers.

Figure 46b shows the variations of this parameter with Reynolds number, from which the regime of the boundary layer (laminar, transitional, turbulent) may be inferred. First, starting with the higher angles of attack and working down, at the low Reynolds numbers there is a slight increase of " $\log C_w + n_w$ " with Reynolds number, even from the Mach 10 correlations. This slight variation (transitional flow) remains steady to some Reynolds number at which the variation substantially increases (turbulent flow). In the low Reynolds number regime, the variation decreases with decreasing angle of attack until somewhere between 30° and 25° the variation disappears (laminar flow). The Reynolds numbers at which the variations change differ with angle of attack.

In extrapolating the correlation parameters, changes in the boundary layer regime were not taken explicitly into account. Values of the correlation parameters were used without modification. Values for the same or different flow conditions were used in developing the individual extrapolation curves. Either way, the extrapolations almost certainly included more than one boundary layer regime. For example, the lowest Reynolds number, Mach 6 data were initially considered suspect and not used for the extrapolation. As indicated in Figure 46, these data now appear, in retrospect, to be valid and are associated with either laminar or transitional flow, depending on angle of attack.

Furthermore, in developing the Mach 6 extrapolations, the correlations for the next higher Reynolds number (about 2.7×10^6) were used. These data, which also appear to be associated with nonturbulent flow were used with correlations for higher Reynolds numbers for which the flow was turbulent. This resulted in extrapolations which are not strictly applicable to fully developed turbulent flow. Hence, when extrapolating for later entry times when Reynolds numbers are greater than 10^7 , steeper variations with Reynolds number to account for fully developed turbulent flow should have been used. At low angles of attack, the Mach 10 extrapolations were clearly for laminar flow, whereas the low α Mach 6 extrapolations were for quasi-turbulent (but not fully-developed) flow.

It is noteworthy that regardless of the boundary layer regime, attached flow heating on the upper wing varies strongly with wetted length. Furthermore, the variation is insensitive to the regime. These observations are illustrated in Figure 12 where the parameter n , which describes the variation with wetted length is always greater than 1 and takes on values in the range of 1.3 to 1.8 regardless of boundary layer regime. By comparison, in flat plate laminar and fully turbulent flow n should have values of ~ 0.5 and ~ 0.8 respectively.

Upper Fuselage Heat Transfer. - Histories of measurements from the selected calorimeters on the upper fuselage are shown in Figures 47 through 50. Corrections for solar heating and reradiation are not included. The heat flux obtained from the thermocouple measurement V09T9518A is not shown because the data were not available in the form required for automated plotting. Furthermore, since heating rates obtained from thermocouple measurements via inverse solutions include surface reradiation, these rates are inconsistent with calorimeter measurements.

These figures show that heating rates are not available at all the locations for the entire trajectory. In fact, no centerline measurements are available at the comparison time for angle of attack of 20° ($t_E = 1426$ s).

These figures also illustrate the peculiarity mentioned previously (Page 19) regarding the wing calorimeter data. Noting that these heating rates are not normalized, it is observed that all the calorimeter responses remain essentially constant (on a "plateau") during the early portion of the trajectory. The increases for time earlier than 300 s correspond with that of the reference heating rate (Figure 35). This state continues until about 850 s when most of the histories change noticeably. Heating rates decrease rapidly and significantly, although angle of attack and reference heating rate remain relatively constant

until about 1100 s (Figures 33c, 34 and 35). Some of this behavior is attributable to solar heating. It was shown in reference 28 that during the period of 350 to 850 seconds, incident solar radiation varied from approximately 15 to 30 percent of the total heat input to the upper surface. At 850 s, the upper surfaces were rolled abruptly out of the sun, accounting for most of the observed decrease in heat transfer at that time.

It is observed in Figure 49c and 50c that the change in the measured heat flux histories is less noticeable at the outermost locations. These locations are very close to the edge of the upper surface; somewhat analogous to the location of T/C 4 on the test model shown in Figure 4. In this location, the local conditions are most likely dominated by spillage of flow off the strake impinging on the side fuselage, which appears to stabilize the heating.

Ratios of local to centerline heating from the measurements for the same axial location are shown in Figure 51. It is interesting to note in these histories that the ratios are more erratic than the individual heating rates, and the displacement occurring at about 850 s appears enhanced and reversed.

Such events indicate that the centerline and outboard environments during flight are not related, or that heating in the respective areas is controlled by dissimilar mechanisms. If the same flow mechanisms acted on the entire upper surface, the short time excursions in the individual histories would be expected to occur somewhat simultaneously, and with similar amplitudes; therefore the excursions should cancel when the ratio of off centerline to centerline heating is computed. As shown in Figure 51, variations in normalized heating appear to occur more frequently and to have larger displacements than excursions in heating rates for individual instruments. At entry time of about 850 s the heat flux ratios increase rapidly and significantly rather than decreasing, as do the individual heat fluxes, or remaining constant. Another change appears to occur in the time frame around 300 seconds. At this time a "dip" of approximately 100 seconds duration, appears in the heating rate ratios. No specific explanation for this dip has been found, although roll oscillations and the resulting variation of solar radiation appears to be a contributing cause.

Although the wind tunnel data provide no direct evidence of the existence of Gortler vortices on the upper fuselage, it is speculated that the short-time excursions observed in the flight heat flux data may be the result of embedded Gortler vortices within the viscous layer on the upper fuselage. Vortices embedded in boundary layers result in heating undulations normal to the vortex

axes. The undulations can be observed as striations with the aid of thermal mapping techniques (striation heating induced by Gortler vortices on the fuselage sidebody is discussed in Appendix A). Throckmorton noted in reference 25 that short term heating oscillations observed in upper fuselage calorimeter data coincided with Shuttle yaw oscillations. It is suggested that the embedded vortices oscillated laterally as a result of the yaw oscillations. The undulating heat transfer distribution associated with these vortices generated the short interval heat flux excursions measured by the sensors. Since the spacing of the sensors relative to the vortex pattern was not uniform, the effect at the various locations was essentially random.

Comparisons of heating ratios from the flight measurements with extrapolations from the wind tunnel data correlations (Figure 38) for the forward upper fuselage are presented in Figures 52 through 54. Included in each figure is the heating rate obtained from the thermocouple measurement V09T9518A. The flight data were corrected for solar heating and surface reradiation as appropriate.

Since the heating ratios for the outermost locations ($s/L = 0.08$) should be disregarded because of the interactions with flow off the side fuselage discussed earlier, the flight data available for comparisons are rather scarce. In addition, the quantity of available data is further reduced by the intermittent readings of some calorimeters. Finally, evaluation of the comparisons is made more uncertain since the cause of the apparently erratic calorimeter data has not been established.

Agreement between the upper fuselage flight data and the extrapolated correlations is variable. Examination of Figures 52 through 54 shows approximately 12% of the flight data fall within $\pm 10\%$ of the correlations. Another 65% of the flight data are higher than the correlations by more than 10% while the remaining 23% are lower by more than 10%. Furthermore, while the tunnel data correlations predict decreased heating with increasing distance from the centerline many of the flight data show the opposite trend.

A direct comparison between centerline heating measured in flight and the wind tunnel measurements shows some of the same characteristics noted above. Figure 55 shows the normalized centerline heating distribution at the selected time points during entry. In Figure 56 normalized centerline flight heating distributions are superimposed upon the wind tunnel measurements originally shown in Figures 29 and 30. With a few obvious exceptions, the flight heating

rates are higher than comparable wind tunnel measurements (this is consistent with the off-centerline data). Also, the longitudinal variation of the flight data is larger and considerably more erratic than the wind tunnel data. These characteristics are also observed in the off-centerline flight data.

Factors which have the potential for affecting the agreement observed between the test data correlations and the flight data include the following:

1. The set of correlation parameters, $h/h_{CL} = C_f(s/L)^{-nf}$, which was used for the upper fuselage is an obvious candidate. These parameters yield incorrect results at $s/L = 0$ and provide a poor fit to the data for $s/L \lesssim 0.01$. In their relevant range ($0.01 \lesssim s/L \lesssim 0.08$), these parameters fit the wind tunnel data at least moderately well (see Figures 18 through 29). Therefore, it is concluded that the correlation parameters are not the major cause of disagreements between flight data and wind tunnel data correlations.

2. Calorimeter anomalies are candidates because of the "plateau" effect (Page 22) and the short time excursions (Page 23) which characterize these data. It was noted that the ratios of outboard to centerline calorimeter data appear "noisier" than either the centerline or outboard data themselves. These factors cast suspicion on the calorimeter data. On the other hand, as was seen in Figure 56, many carefully selected calorimeter data agree well with corresponding wind tunnel data. In the balance, the suspicion that the calorimeter data contribute to the disagreement seems justified.

3. Dissimilarities between the outboard and centerline flow characteristics were identified above as a possibility. Such dissimilarities can result from several causes. For example, the centerline boundary layer may be laminar while the outboard boundary layer may be turbulent. Presumably, this could result in outboard to centerline heating ratios greater than 1. Another example is the possibility that the centerline and the outboard locations are scrubbed by different vortices. A similar possibility is that the centerline and outboard flows possess different total temperatures and pressures as suggested by the data in reference 9. Such flow dissimilarities are believed to explain some of the heat transfer variations observed above.

4. Differences between the upper body vortex structure in flight and in the wind tunnel are probable. A careful evaluation of the existing data

base might shed light on such differences. Lack of time prevented such an evaluation.

CONCLUSIONS AND RECOMMENDATIONS

Procedures have been developed for predicting aerodynamic heating on the Shuttle upper wing and upper fuselage surfaces. Early attempts to base the prediction procedures on the development of simplified flow models proved unsuccessful, hence the procedures were based on correlating wind tunnel heating data and extrapolating these correlations to flight Reynolds numbers. Predictions using these procedures were then compared with heating data obtained during the Shuttle STS-2 reentry.

The procedure for computing heating for attached flow on the upper wing was shown to provide adequate estimates where the flight vehicle and wind tunnel model experience the same boundary layer flow regime. Fortunately, the lowest Reynolds numbers for significant heating during entry are about equivalent to test Reynolds numbers. Estimates therefore agree quite well with flight data in the laminar and transitional flow regimes. Heating for fully developed turbulent flow is underestimated because of the laminar and/or transitional data used in establishing the extrapolation curves. To establish extrapolations adequate for predicting turbulent flow on the wing leeside surface requires additional test data in this regime.

Evaluation of the technique developed for the forward upper fuselage is difficult because of the scarcity of applicable data. Heating environments and trends observed in the flight and test data are in conflict. Heating on this surface appears to be influenced by many interactions. Identification of the interaction mechanisms and speculation on the significance of each is hampered by lack of data defining the flow field.

In developing the extrapolations and comparing estimates with upper fuselage flight data, assumptions were made regarding flow conditions or influences of interactions based on interpretation of data and trends. This was required due to uncertainty regarding flow field structure. With better knowledge of the flow and refined assumptions, the existing techniques may be improved or extended, or a more accurate method formulated. In order to provide the required knowledge of leeside flow, it is suggested that further analyses and

testing be conducted to quantify the various properties of the three-dimensional flow field which affect leeside heating. For example, an attempt was made to develop a wing heating method by finding a simple heating relationship for the wing leading edge, and then extending the method to include downstream areas. As is documented in Appendix G, the attempt to develop a simple leading edge heating model was unsuccessful because more information is required regarding the flow immediately upstream of the leading edge than can be deduced from the information at hand. It was concluded that in calculating wing heat transfer, an accurate definition of the flow field surrounding the vehicle is needed. Furthermore, the necessity for defining the flow increases significantly with Mach number.

The additional analyses would consist primarily of employing math models to investigate local flow characteristics and trends which were surmised in this study. Among these would be defining the existence and strength of the strake shock, and/or confirming the complex properties of the flow incident on the wing leading edge, and the influence of Mach number on these properties.

Future testing should extend the present heat transfer data by selectively obtaining measurements of surface pressures and of pressure, temperature and velocity profiles in the viscous and inviscid flow layers using survey rakes or probes. These will aid in developing a flow model for local particle paths and provide pressure gradient information for boundary layer computations. The survey data can also probe the rapid growth of the viscous layer on the wing upper surface, local entropy variations, embedded shocks and flow incident on the wing leading edge.

In obtaining the survey data, the investigation of Mach number effects is strongly urged. Together with planform and elevation Schlierens or shadowgraphs, these data would help in evaluating the premises regarding locations and strengths of various shocks and the effect on wing leading-edge flow with movement of the stagnation line.

As last recommendations, two simple tasks are suggested. Using the flight data from the STS-2 entry and the Mach 6 correlations for turbulent flow, redefine the wing extrapolations for the lower angles of attack and turbulent flow; and compare resulting extrapolations with subsequent flight data. On the upper fuselage, reevaluate the extrapolations by comparing with data from subsequent flights where the calorimeters were replaced with surface thermocouples.

REFERENCES

1. Bertram, M. H., Cary, A. M., Jr. and Whitehead, A. H., Jr., "Experiments with Hypersonic Turbulent Boundary Layers on Flat Plates and Delta Wings," AGARD Specialists Meeting on Hypersonic Boundary Layers and Flow Fields, London, England, May 1-3, 1968.
2. Cross, E. J., Jr. and Hankey, W. L., "Investigation of the Leeward Side of a Delta Wing at Hypersonic Speeds," AIAA Paper 68-675, 1968.
3. Whitehead, A. H., Jr. and Keyes, J. W., "Flow Phenomena and Separation over Delta Wings with Trailing-Edge Flaps at Mach 6," AIAA Journal, Vol. 6, No. 12, Dec., 1968, pp 2380-2387.
4. Whitehead, A. H., Jr., "Effect of Vorticies on Delta Wing Lee-Side Heating at Mach 6," AIAA Journal, Vol, 8, No. 3, March, 1970, pp 599-600.
5. Hefner, J. N. and Whitehead, A. H., Jr., "Lee-Side Heating Investigations. Part I - Experimental Lee-Side Heating Studies on a Delta-Wing Orbiter," NASA SPACE Shuttle Technology Conference, Vol I - Aerothermodynamics, Configurations, and Flight Mechanics, NASA TM X-2272, 1971, pp. 267-287.
6. Whitehead, A. H., Jr., Hefner, J. N. and Rao, D. M., "Lee-Surface Vortex Effects over Configurations in Hypersonic Flow," AIAA Paper 72-77, 1972.
7. Hefner, J. N. and Whitehead, A. H., Jr., "Lee-Side Flow Phenomena on Space Shuttle Configurations at Hypersonic Speeds. Part II - Studies of Lee-Side Heating at Hypersonic Mach Numbers," NASA Space Shuttle Aerothermodynamics Technology Conference, Vol II - Heating, NASA TM X-2507, February, 1972, pp. 451-467.
8. Hefner, J. N., "Lee-Surface Heating and Flow Phenomena on Space Shuttle Orbiters at Large Angles of Attack and Hypersonic Speeds," NASA TN D-7088, November, 1972.
9. Zakkay, V., Miyawa, M. and Wang, C. R., "Lee Surface Flow Phenomena over Space Shuttle at Large Angles of Attack at $M_\infty = 6$," New York Univ., NASA CR-132501, 1974, and AIAA Paper 75-148, 1975.
10. Bertin, J. J., Senalug, G., McBride, M. and Willman, R. B., "The Effect of Surface Temperature and Reynolds Number on the Leeward Heat-Transfer for a Shuttle Orbiter," Univ. of Texas at Austin, Aerospace Engineering Report 75002, April, 1975.
11. Bertin, J. J., "A Study of Parameters which Influence Surface Pressure and Heat-Transfer in Separated Regions - A Literature Review," Univ. of Texas at Austin, Aerospace Engineering Report 74004, September, 1974.
12. Dunavant, J. C., Narayan, K. Y. and Walberg, G. D., "A Survey of Leaside Flow and Heat Transfer on Delta Planform Configurations," AIAA Paper 76-118, 1976.
13. Helms, V. T., III, "An Empirical Method for Computing Leaside Centerline Heating on the Space Shuttle Orbiter," AIAA Paper 81-1043, June 1981.

14. Hender, D. R., "A Miniature Version of the JA70 Aerodynamic Heating Computer Program, H800 (MINIVER)," McDonnell Douglas Astronautics Co.-West, MDC G0462, June, 1970, Revised January, 1972.
15. Cohen, C. B. and Reshotko, E., "Similar Solutions for the Compressible Laminar Boundary Layer with Heat Transfer and Pressure Gradient," NACA Report 1293, 1956.
16. Cohen, C. B. and Reshotko, E., "The Compressible Laminar Boundary Layer with Heat Transfer and Arbitrary Pressure Gradient," NACA Report 1294, 1956.
17. Reshotko, E. and Tucker, M., "Approximate Calculation of the Compressible Turbulent Boundary Layer with Heat Transfer and Arbitrary Pressure Gradient," NACA TN 4154, December, 1957.
18. Bertram, M. H. and Feller, W. V., "A Simple Method for Determining Heat Transfer, Skin Friction, and Boundary-Layer Thickness for Hypersonic Laminar Boundary-Layer Flows in a Pressure Gradient," NASA Memo 5-24-9L, June, 1959.
19. Beckwith, I. E. and Cohen, N. B., "Application of Similar Solutions to Calculation of Laminar Heat Transfer on Bodies with Yaw and Large Pressure Gradient in High-Speed Flow," NASA TN D-625, January, 1961.
20. Helms, Vernon T., III, "Leeward Centerline and Side Fuselage Entry Heating Predictions for The Space Shuttle Orbiter" presented at the Langley Conference on Shuttle Performance: Lessons Learned, Langley Research Center, Hampton, VA, NASA CP-2283, March 8-10, 1983.
21. Hankey, W. L., Jr., Neumann, R. D. and Flinn, E. H., "Design Procedures for Computing Aerodynamic Heating at Hypersonic Speeds," WADC TR 59-610, June 1960.
22. Widhopf, G. F., "Laminar, Transitional and Turbulent Measurements on a Yawed Blunt Conical Nose Tip," AF Rpt. SAMS0-TR-72-209, Aerospace Rpt. No. TR-0073 (S3450-60)-1, September, 1972.
23. Compton, H. R., Findlay, J. T., Kelly, G. M. and Heck; M. L., "Shuttle (STS-1) Entry Trajectory Reconstruction", AIAA Paper 81-2459, November 1981
24. Throckmorton, D. A., "Benchmark Aerodynamic Heat Transfer Data From the First Flight of the Space Shuttle Orbiter," AIAA Paper 82-0003, January, 1982.
25. Throckmorton, D. A., "Influence of Radiant Energy Exchange on the Determination of Convective Heat Transfer Rates to Orbiter Leeside Surface During Entry," AIAA Paper 82-0824, June 1982.

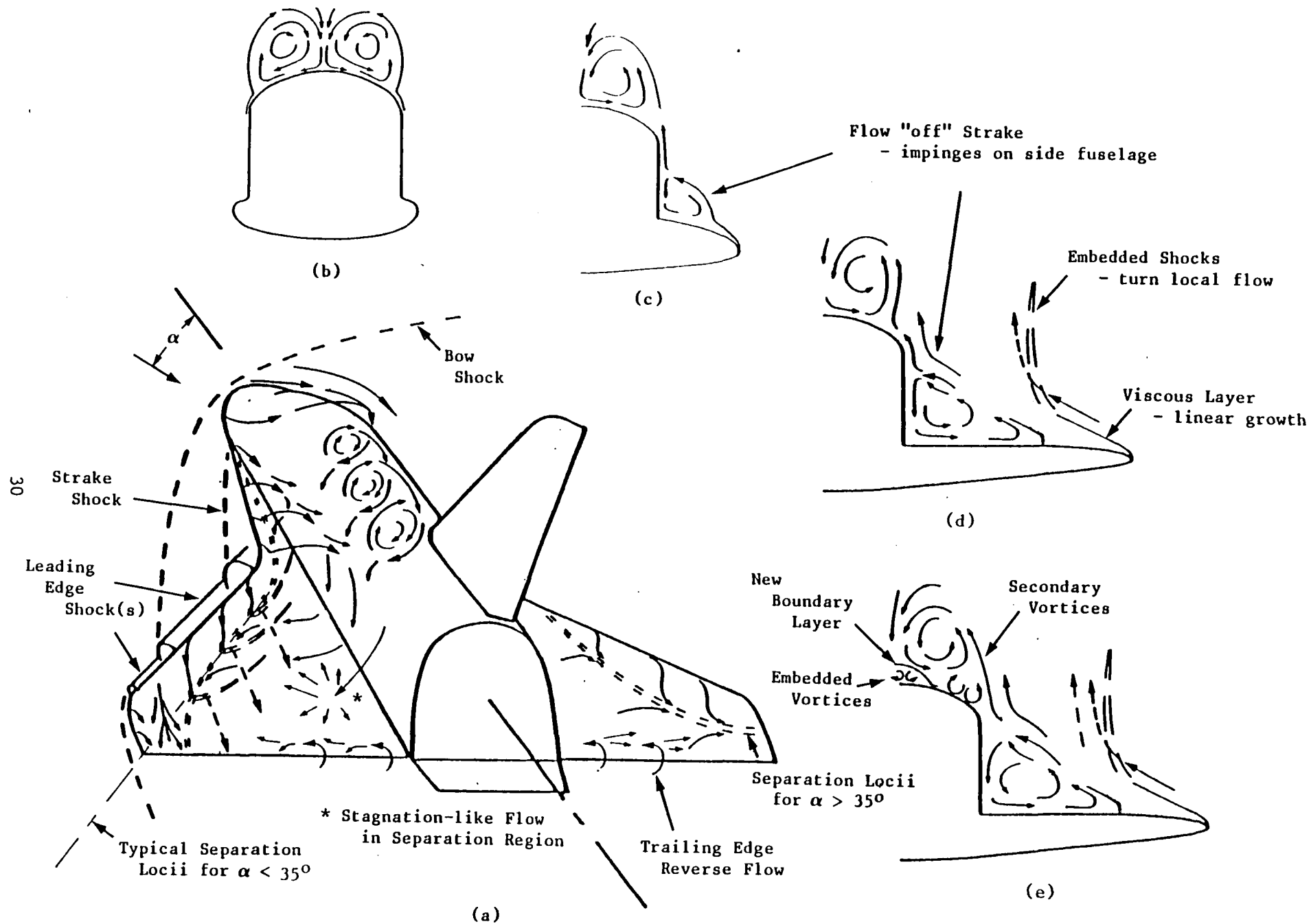


Figure 1 Shuttle Leeside Flow

WING LEESIDE SURFACE

MACH = 10									
RUN NO.	MACH NO.	ALPHA (DEG)	RE (X E6)	T(U) (R)	P(0) (PSI)	T(0) (R)	P(INF) (PSI)	T(INF) (R)	H(REF) (B/F2-S-R)
1	9.82	20.	.55	530.	356.25	1770.42	.00915	90.86	.025530
2	9.82	25.	.55	537.	350.29	1749.94	.00901	89.71	.025307
4	9.82	30.	.55	535.	354.71	1751.00	.00913	89.77	.025468
5	9.82	35.	.55	540.	350.07	1750.15	.00901	89.72	.025299
6	9.82	40.	.55	540.	356.36	1758.20	.00917	90.17	.025530
8	9.98	20.	1.07	533.	732.45	1786.74	.01708	89.13	.035458
10	9.98	25.	1.07	533.	743.49	1785.00	.01735	89.04	.035728
12	9.98	30.	1.03	537.	734.66	1818.73	.01709	90.87	.035520
14	9.98	35.	1.05	540.	729.14	1797.19	.01699	89.69	.035379
20	9.98	40.	1.09	538.	757.84	1796.75	.01767	89.68	.036079
22	10.16	20.	2.50	543.	1763.27	1784.13	.03730	86.37	.053348
3	10.16	25.	2.50	545.	1762.44	1791.31	.03726	86.75	.053338
18	10.16	30.	2.43	535.	1796.95	1794.79	.03801	86.94	.053879
16	10.16	35.	2.43	553.	1777.07	1819.60	.03750	88.25	.053577
7	10.16	40.	2.40	550.	1764.65	1809.81	.03726	87.72	.053380

FUSELAGE LEESIDE SURFACE

MACH = 10									
RUN NO.	MACH NO.	ALPHA (DEG)	RE (X E6)	T(U) (R)	P(0) (PSI)	T(0) (R)	P(INF) (PSI)	T(INF) (R)	H(REF) (B/F2-S-R)
12	10.16	20.	.50	554.	357.5	1666.7	.00738	79.7	.0238235
13	10.16	25.	.50	548.	353.7	1794.8	.00723	86.7	.0238772
14	10.16	30.	.50	543.	350.9	1733.4	.00721	83.3	.0237003
15	10.16	35.	.50	537.	339.6	1778.4	.00694	85.5	.0233508
20	10.16	40.	.50	541.	338.6	1744.2	.00750	84.6	.0242364
3	10.34	20.	1.00	535.	742.6	1819.5	.01360	84.9	.0332186
4	10.34	25.	1.00	542.	743.7	1828.7	.01366	85.4	.0332702
5	10.34	30.	1.00	543.	742.8	1806.5	.01365	84.3	.0332033
6	10.34	35.	1.00	547.	741.9	1807.6	.01364	84.3	.0331859
16	10.34	40.	1.00	533.	743.4	1843.1	.01360	86.1	.0333052
8	10.36	20.	2.40	553.	1784.5	1821.7	.03300	85.1	.0512218
9	10.36	25.	2.40	559.	1788.3	1829.4	.03311	85.4	.0512964
10	10.36	30.	2.40	567.	1807.4	1828.5	.03350	85.4	.0515485
11	10.36	35.	2.40	571.	1787.2	1840.5	.03305	86.0	.0512919
17	10.36	40.	2.40	543.	1801.5	1812.8	.03340	84.6	.0514813

31

MACH = 6									
RUN NO.	MACH NO.	ALPHA (DEG)	RE (X E6)	T(U) (R)	P(0) (PSI)	T(0) (R)	P(INF) (PSI)	T(INF) (R)	H(REF) (B/F2-S-R)
3	6.0	20.	.84	530.	48.11	869.77	.02938	105.32	.026871
7	6.0	25.	.80	530.	47.20	883.65	.02883	107.08	.026651
8	6.0	30.	.85	530.	49.20	875.77	.03055	106.08	.027188
9	6.0	35.	.80	530.	48.32	891.89	.02951	108.12	.026984
5	6.0	20.	2.63	533.	153.80	883.73	.09468	107.14	.048026
10	6.0	25.	2.53	535.	150.12	891.89	.09239	108.10	.047486
13	6.0	30.	2.69	535.	145.65	843.94	.08961	102.10	.046554
17	6.0	35.	2.77	535.	148.50	838.87	.09138	101.46	.046979
22	6.0	40.	3.38	540.	191.52	868.47	.11818	105.22	.053485
6	6.0	20.	5.40	535.	300.0	862.46	.18621	104.51	.066821
11	6.0	25.	5.12	535.	300.0	888.60	.18621	107.82	.067012
15	6.0	30.	4.69	537.	300.0	916.32	.18621	111.35	.067203
18	6.0	35.	5.15	538.	300.0	885.15	.18621	107.39	.066987
21	6.0	40.	5.20	540.	300.0	879.87	.18621	106.72	.066949
2	6.0	20.	6.585	535.	400.0	909.38	.24937	110.51	.077519
12	6.0	25.	7.10	538.	400.0	869.08	.24937	105.39	.077174
16	6.0	30.	7.07	538.	400.0	872.04	.24937	105.77	.077200
19	6.0	35.	7.096	540.	400.0	870.21	.24937	105.54	.077184
20	6.0	40.	6.73	536.	400.0	897.61	.24937	109.01	.077421

MACH = 6									
RUN NO.	MACH NO.	ALPHA (DEG)	RE (X E6)	T(U) (R)	P(0) (PSI)	T(0) (R)	P(INF) (PSI)	T(INF) (R)	H(REF) (B/F2-S-R)
20	6.0	20.	1.10	530.	51.85	799.34	.03167	96.44	.027695
21	6.0	25.	1.10	530.	54.75	808.26	.03345	97.56	.028485
22	6.0	30.	1.10	530.	49.32	797.91	.03012	96.26	.027009
23	6.0	35.	1.10	530.	50.49	801.31	.03084	96.68	.027337
24	6.0	40.	1.10	530.	53.87	801.67	.03292	96.73	.028236
3	6.0	20.	2.70	535.	149.20	882.76	.09182	107.01	.047302
4	6.0	25.	2.70	535.	148.32	891.04	.09127	108.06	.047200
6	6.0	30.	2.70	530.	150.48	877.56	.09261	106.35	.047479
7	6.0	35.	2.70	535.	147.07	878.78	.09049	106.51	.046946
8	6.0	40.	2.70	533.	147.31	877.15	.09064	106.30	.046977
13	6.0	20.	5.40	550.	306.39	886.04	.19023	107.50	.067701
12	6.0	25.	5.40	545.	300.75	875.69	.18668	106.19	.067002
11	6.0	30.	5.40	545.	296.93	903.41	.18427	109.70	.066772
10	6.0	35.	5.40	545.	301.58	913.15	.18720	110.95	.067357
9	6.0	40.	5.40	550.	302.08	904.83	.18751	109.89	.067356
14	6.0	20.	7.30	550.	399.34	893.88	.24895	108.54	.077326
15	6.0	25.	7.30	550.	399.67	888.88	.24916	107.91	.077315
17	6.0	30.	7.30	535.	400.83	895.54	.24990	108.75	.077484
18	6.0	35.	7.30	550.	401.41	887.02	.25027	107.67	.077467
19	6.0	40.	7.30	540.	401.99	898.78	.25063	108.78	.077598

Figure 2 Summary of Leeside Heating Tests

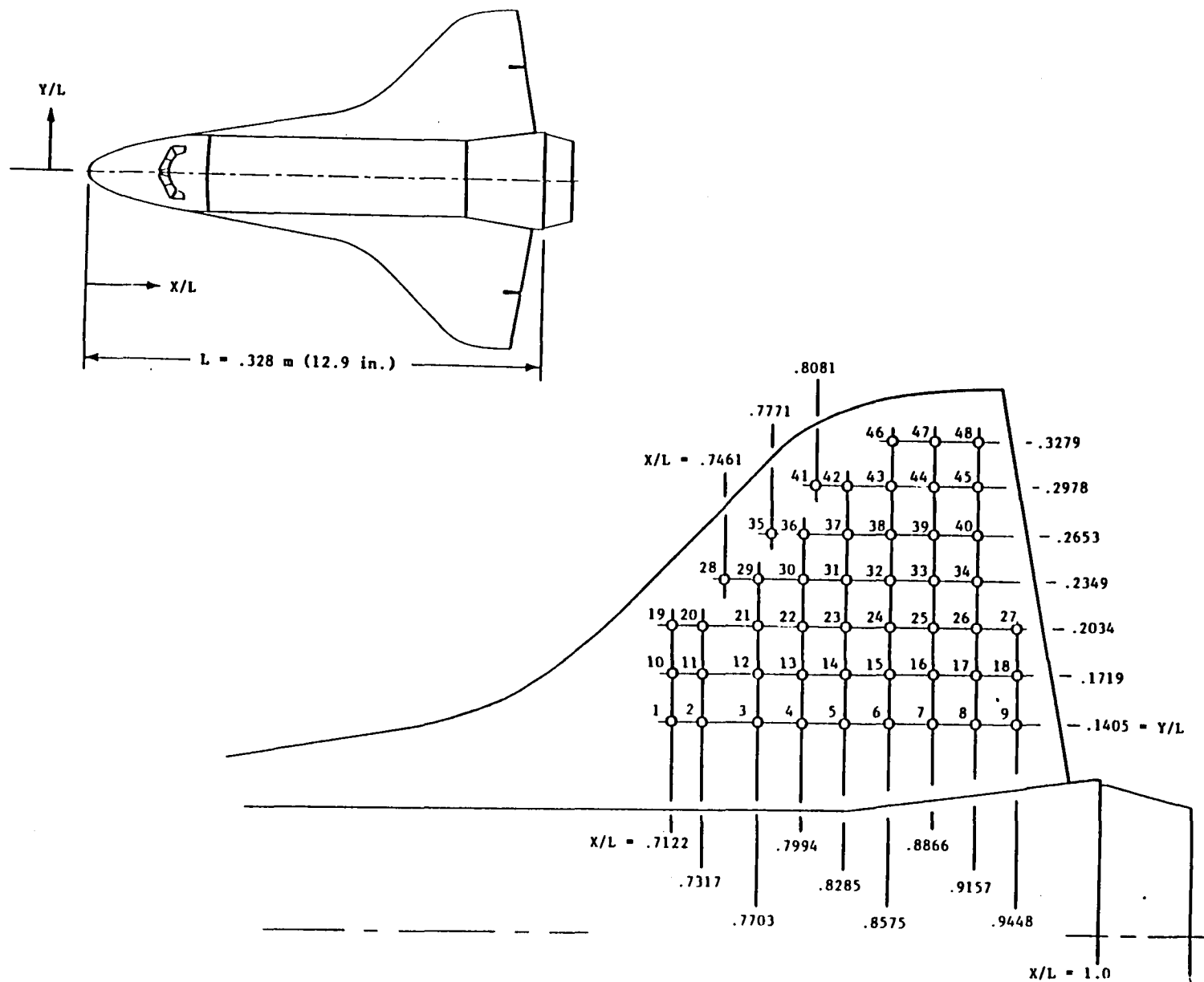
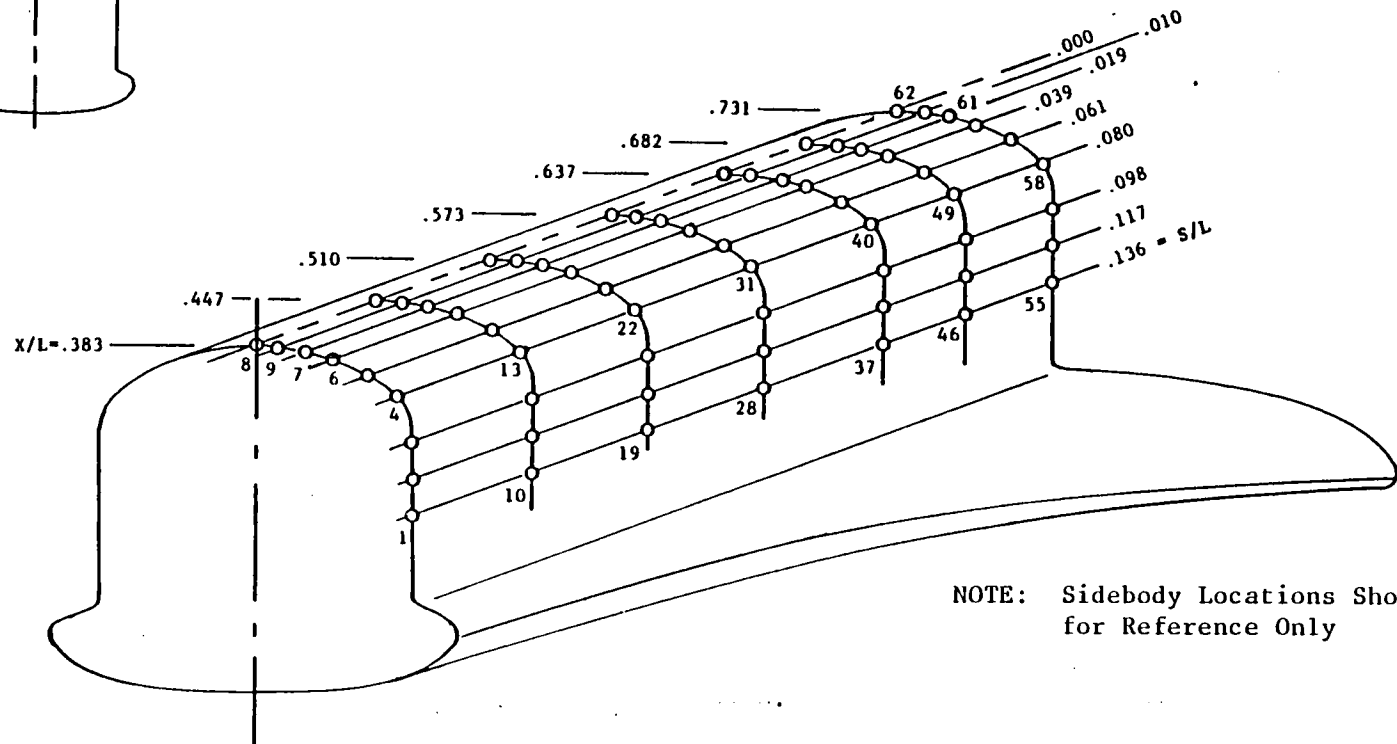
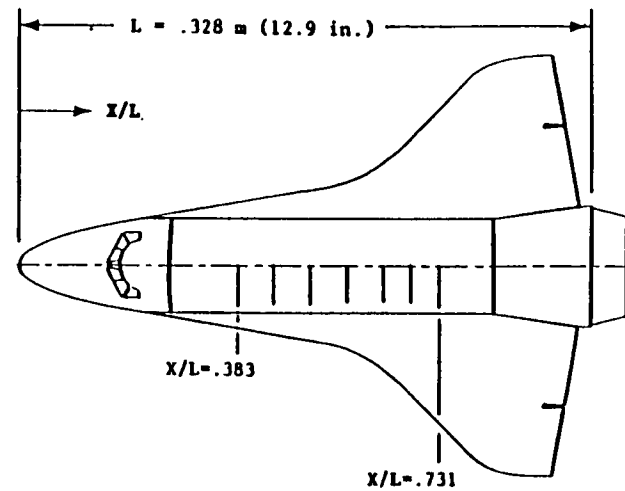
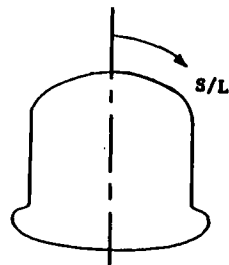


Figure 3 Wing Leeside Surface Thermocouple Locations

X/L =	.383	.447	.510	.573	.637	.682	.731
S/L	THERMOCOUPLE NUMBER						
.000	8	17	26	35	44	53	62
.010	9	18	27	36	45	54	63
.019	7	16	25	34	43	52	61
.039	6	15	24	33	42	51	60
.061	5	14	23	32	41	50	59
.080	4	13	22	31	40	49	58
.098	3	12	21	30	39	48	57
.117	2	11	20	29	38	47	56
.136	1	10	19	28	37	46	55



NOTE: Sidebody Locations Shown
for Reference Only

Figure 4 Fuselage Leeside Surface Thermocouple Locations

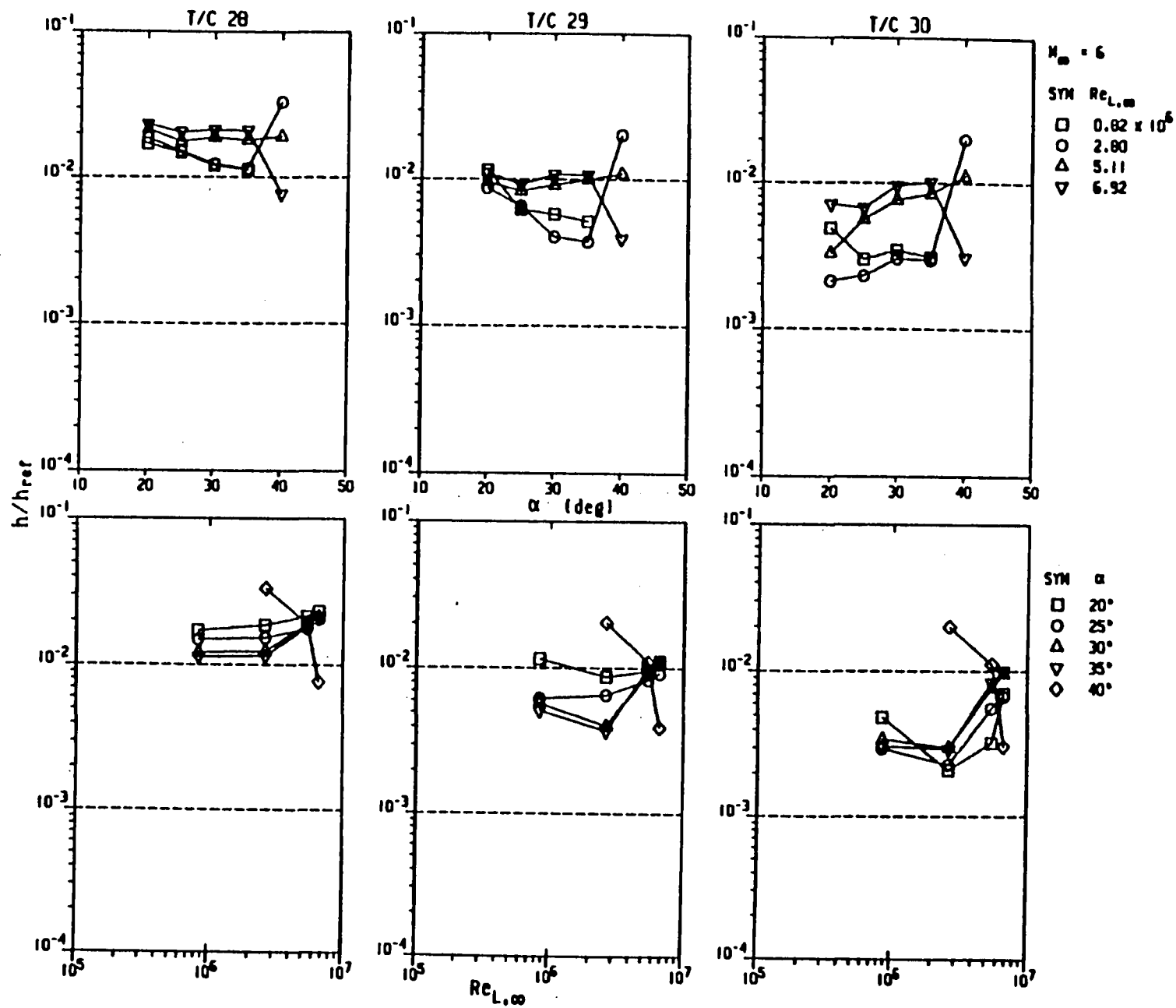


Figure 5 Mach 6 Wing Leeside Thermocouple Behavior

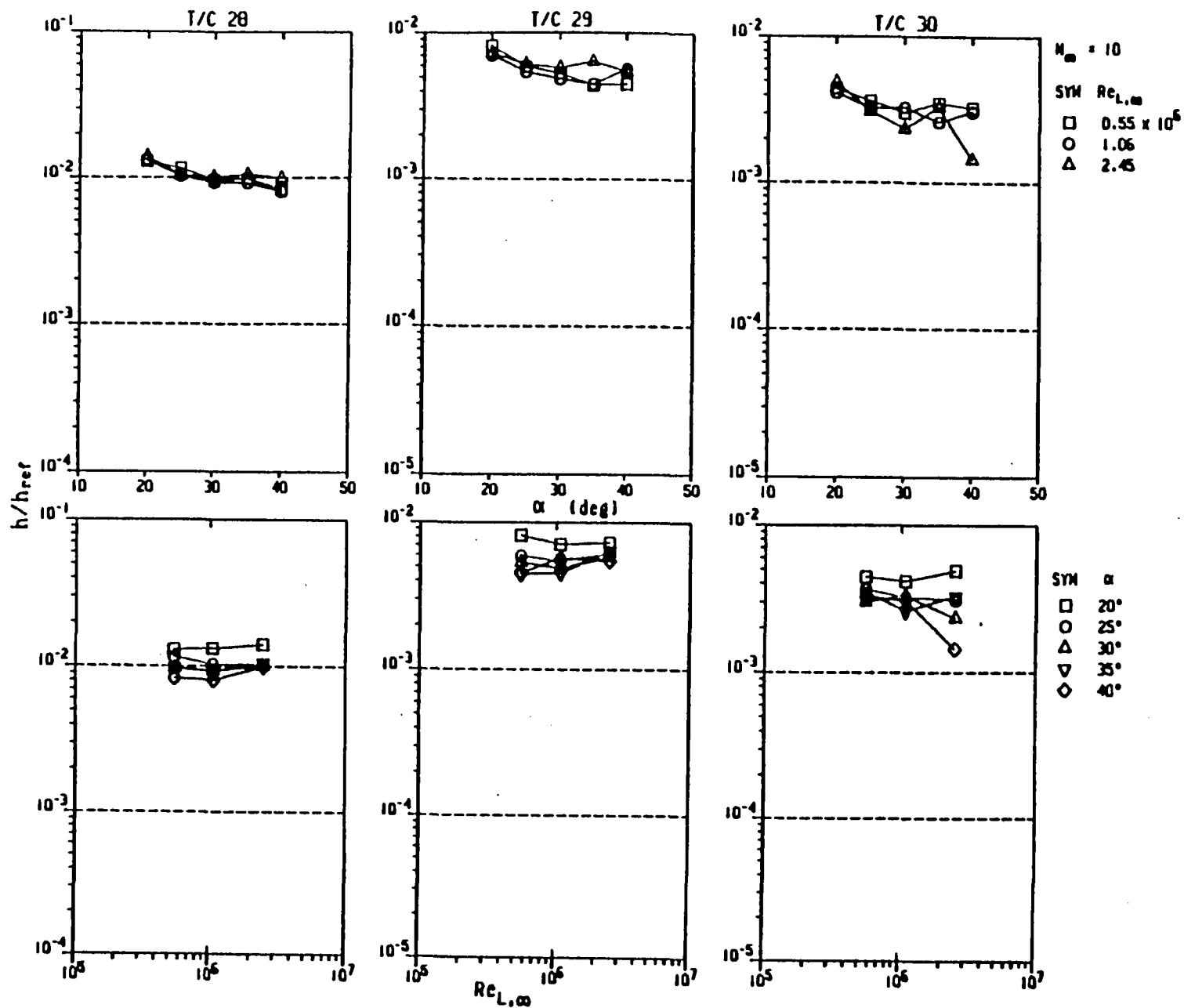


Figure 6 Mach 10 Wing Leaside Thermocouple Behavior

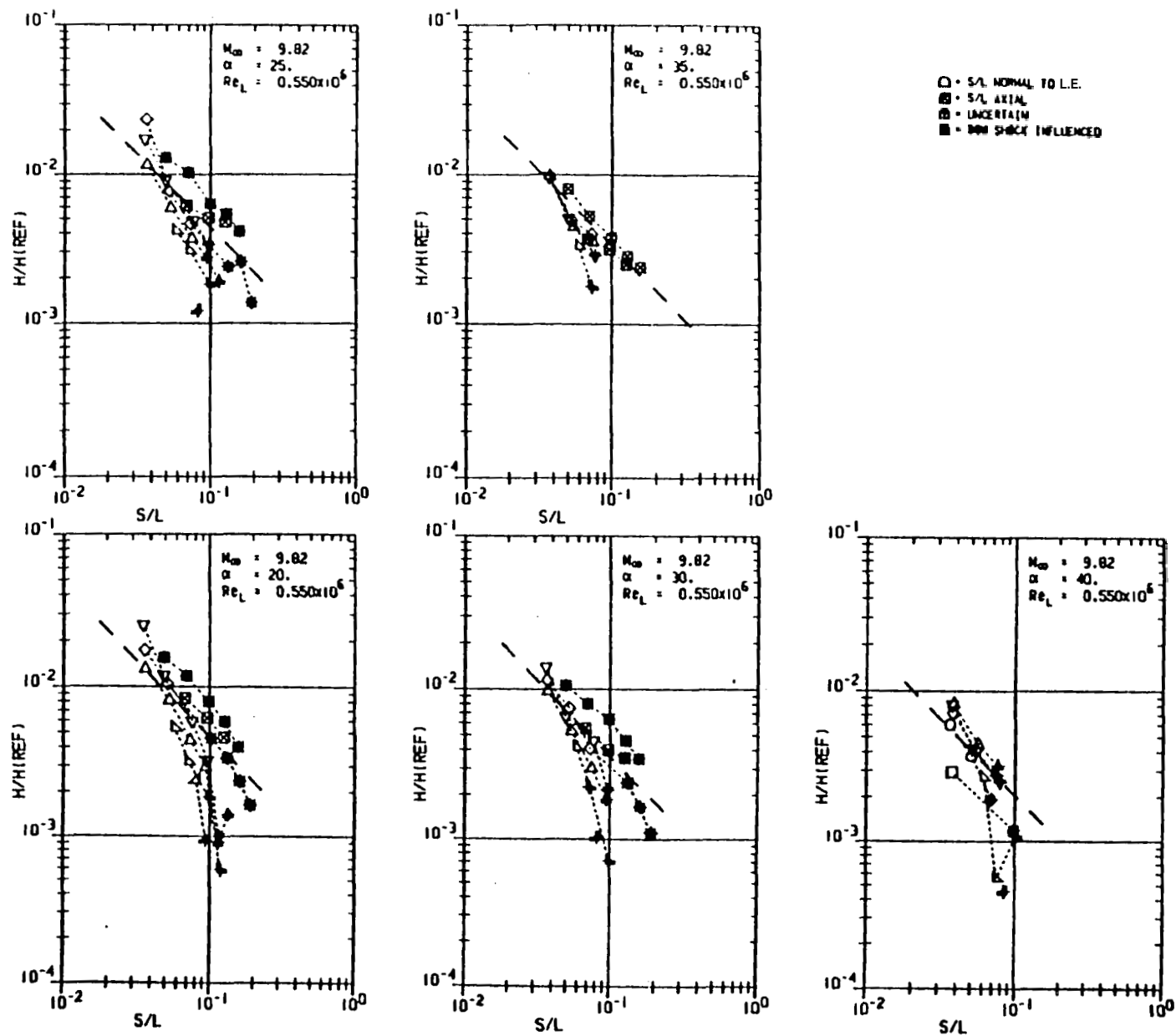


Figure 7a Mach 10 Wing Leeside Heating Distribution for Arbitrary Wetted-Length Path

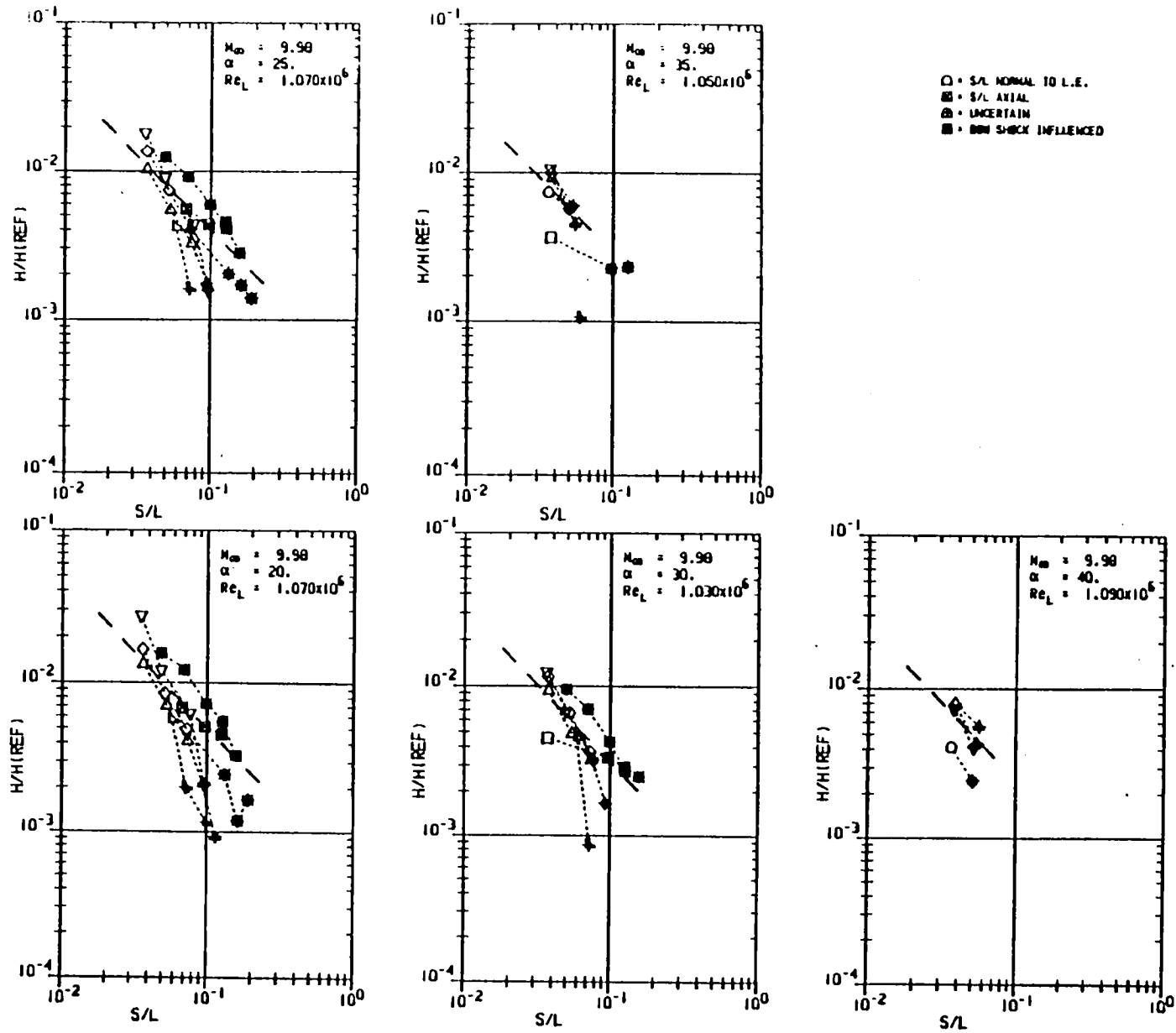


Figure 7b Mach 10 Wing Leeward Heating Distribution for Arbitrary Wetted-Length Path

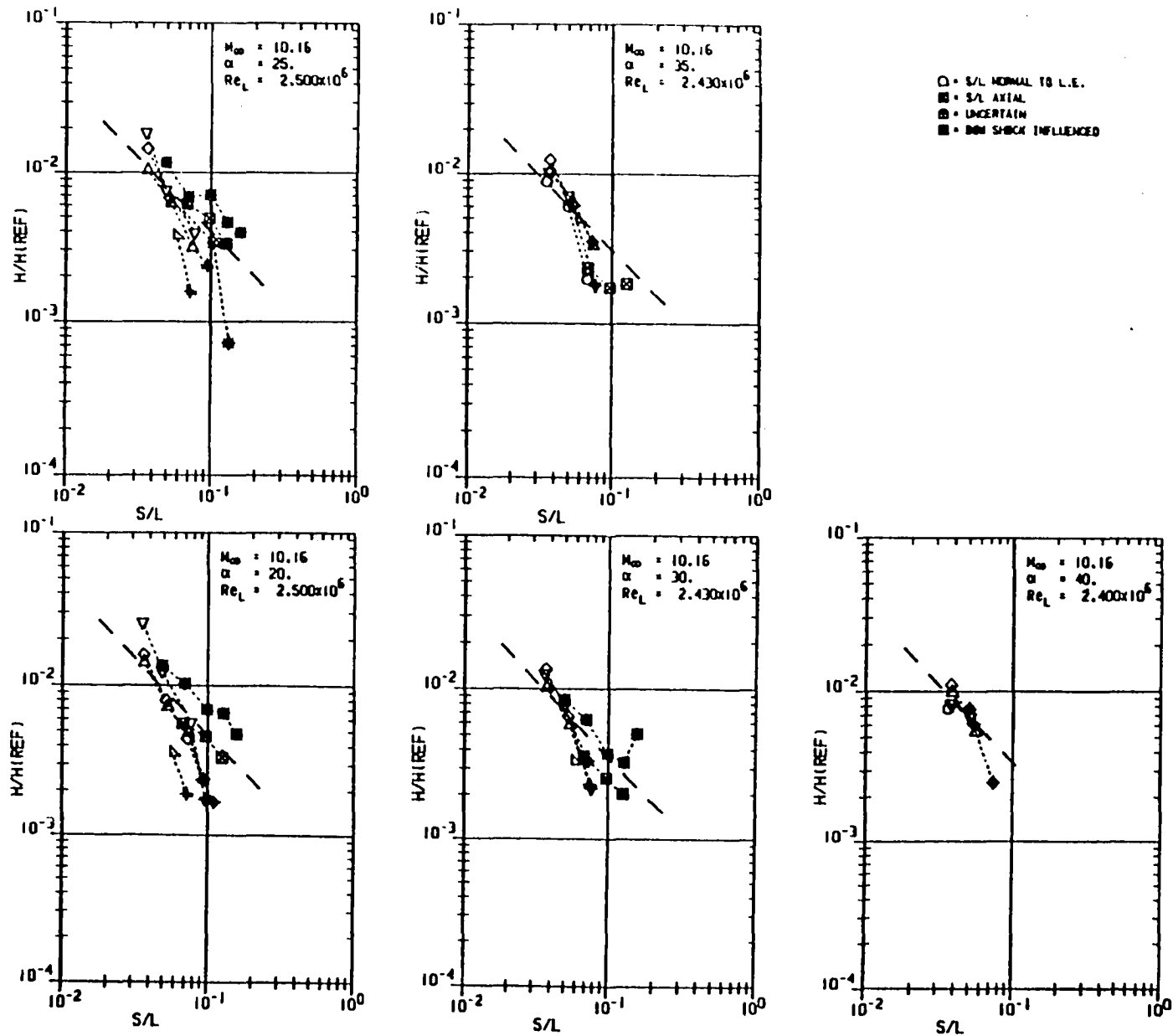


Figure 7c Mach 10 Wing Leaside Heating Distribution for Arbitrary Wetted-Length Path

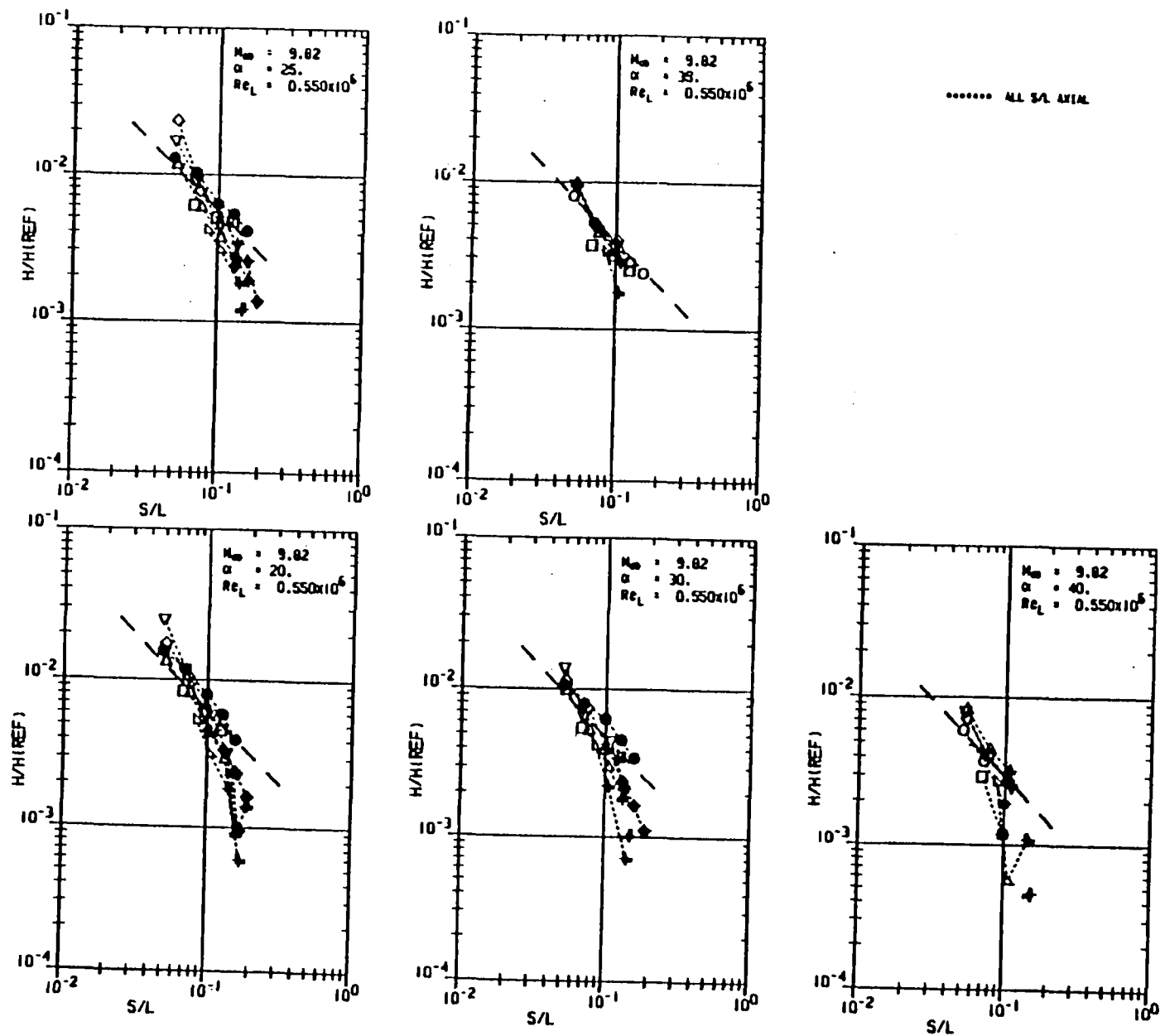


Figure 8a Mach 10 Wing Leeside Heating Distribution for Axial Wetted-Length Path

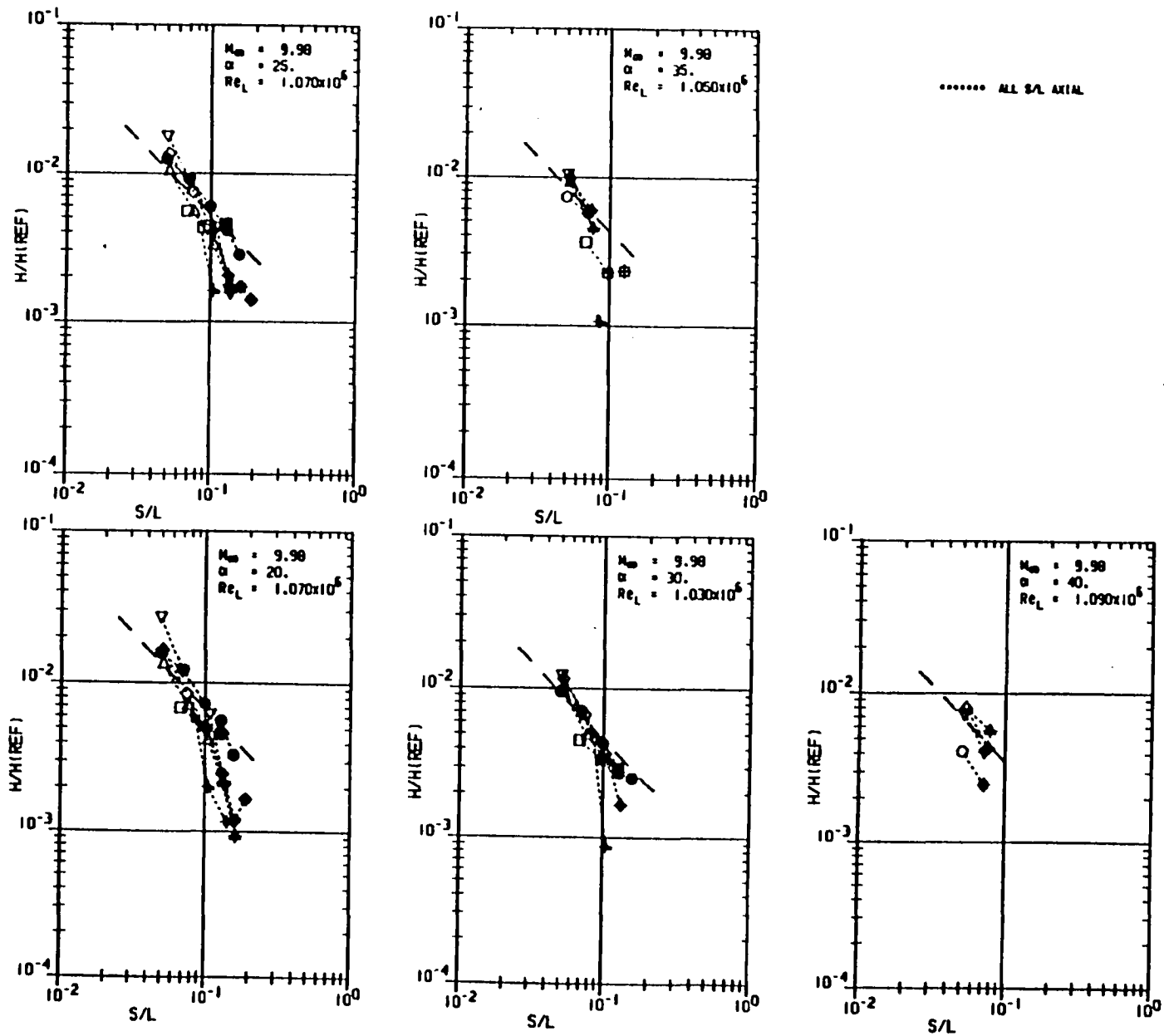


Figure 8b Mach 10 Wing Leeside Heating Distribution for Axial Wetted-Length Path

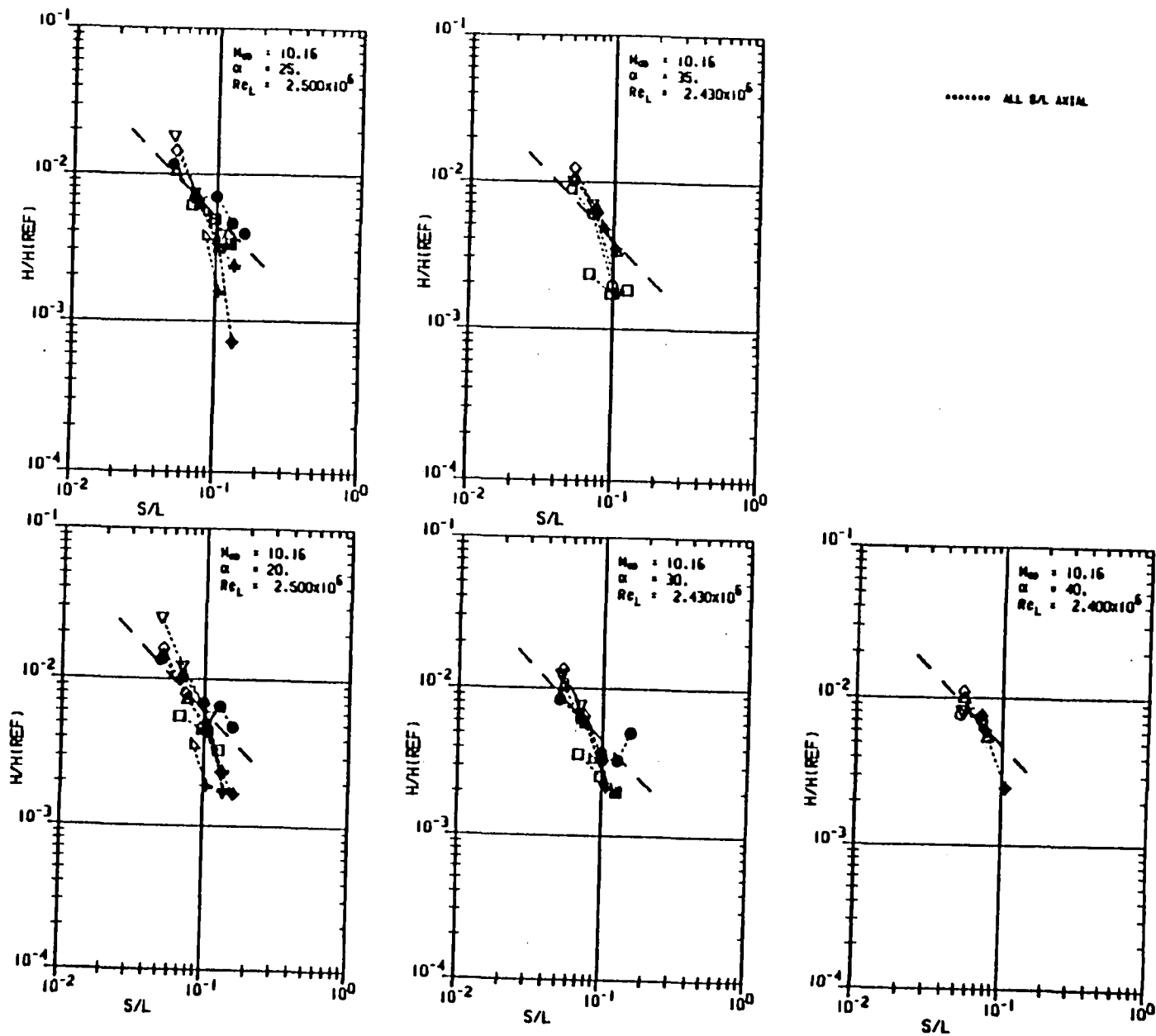


Figure 8c Mach 10 Wing Leeside Heating Distribution for Axial Wetted-Length Path

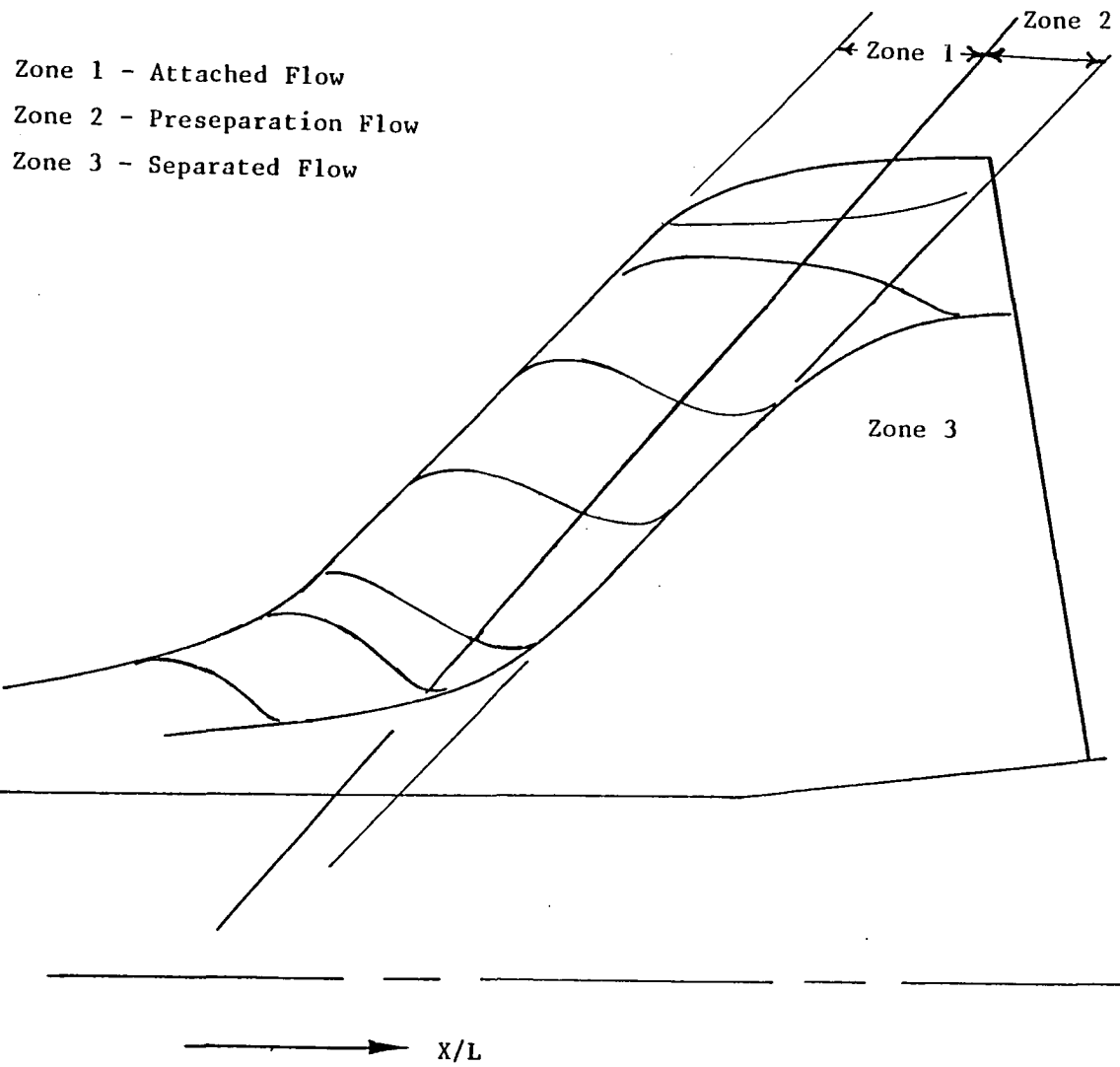


Figure 9 Wing Leaside Flow Zones

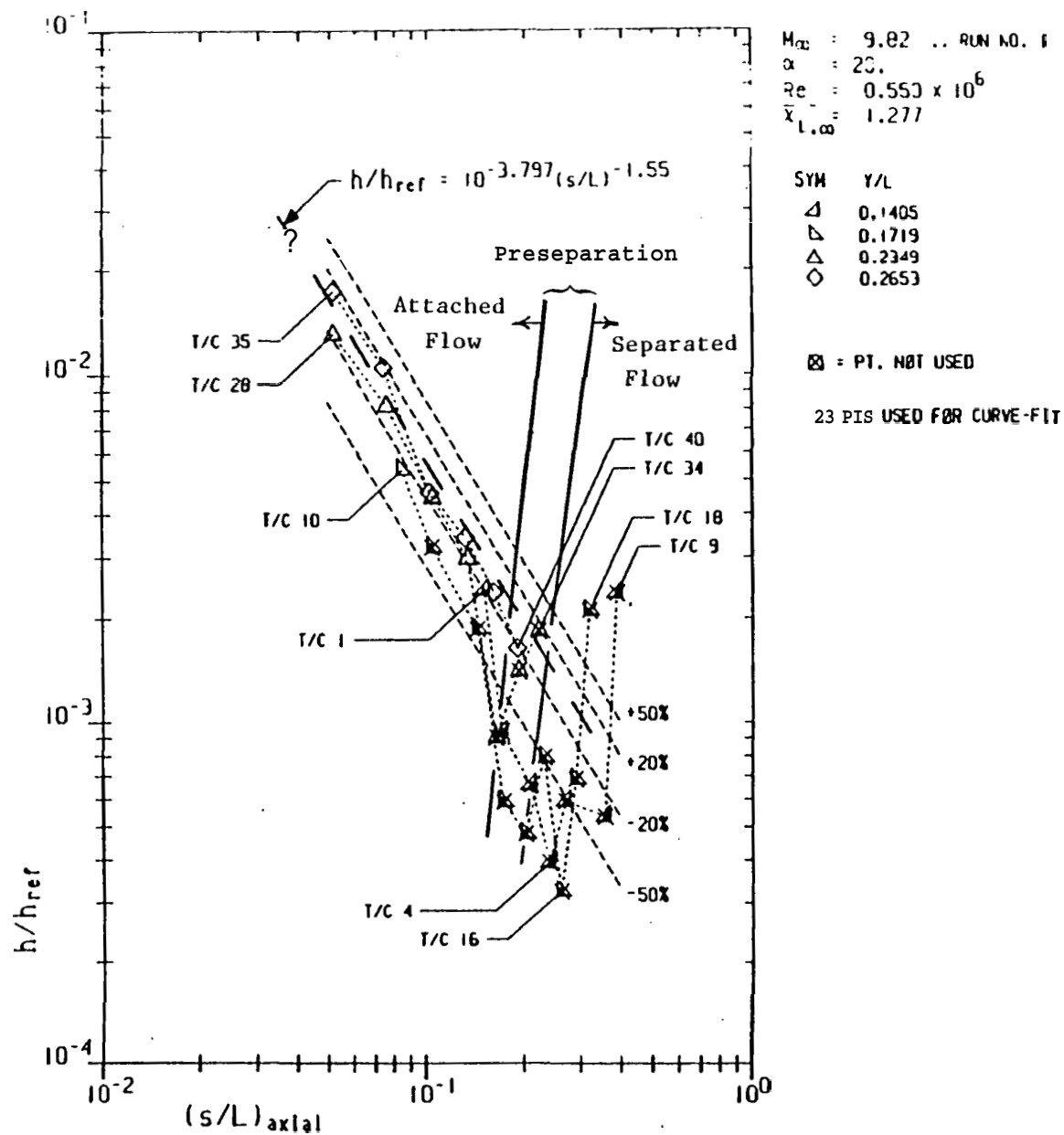
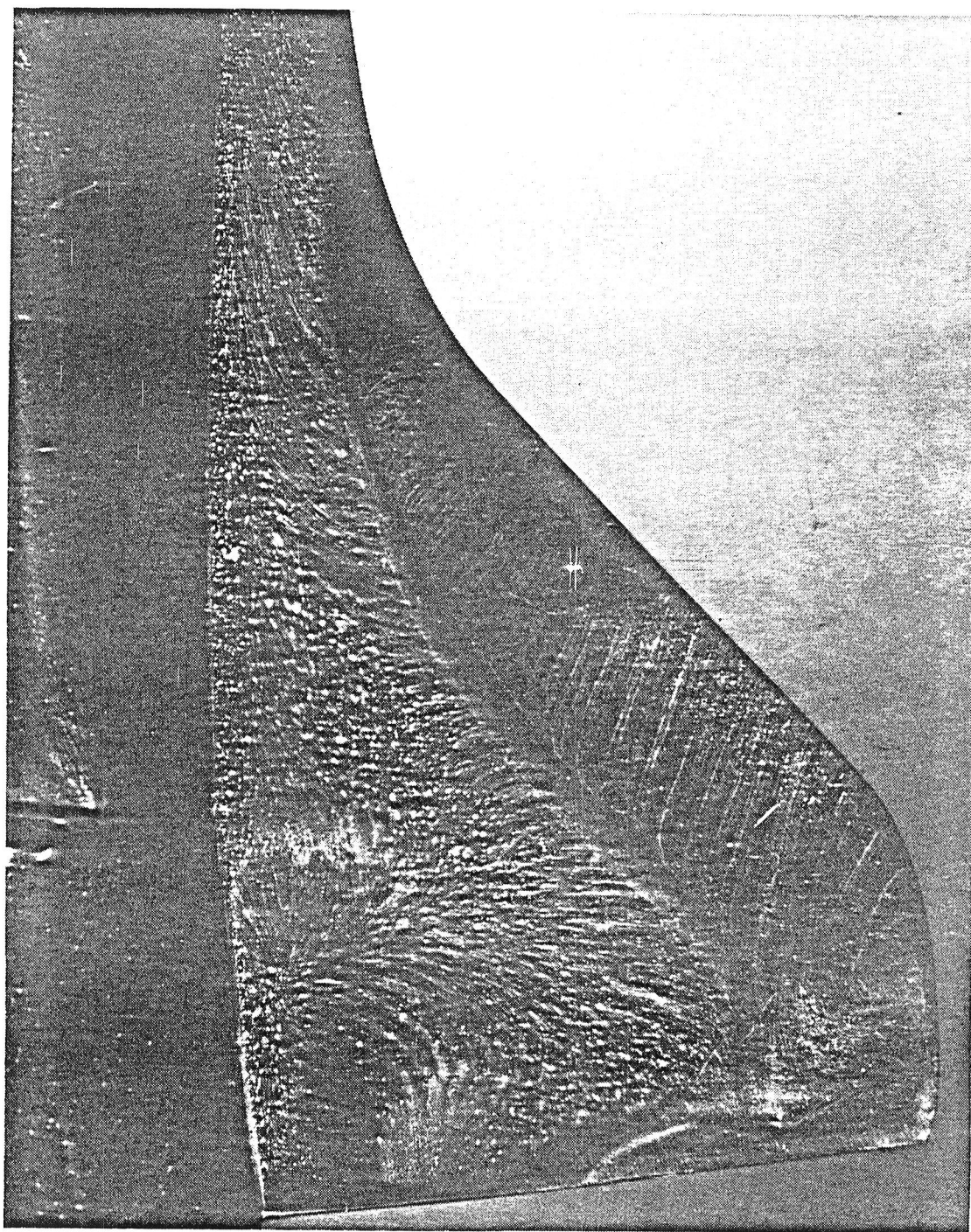


Figure 10a Wing Leaside Flow Zones, Heating Distributions

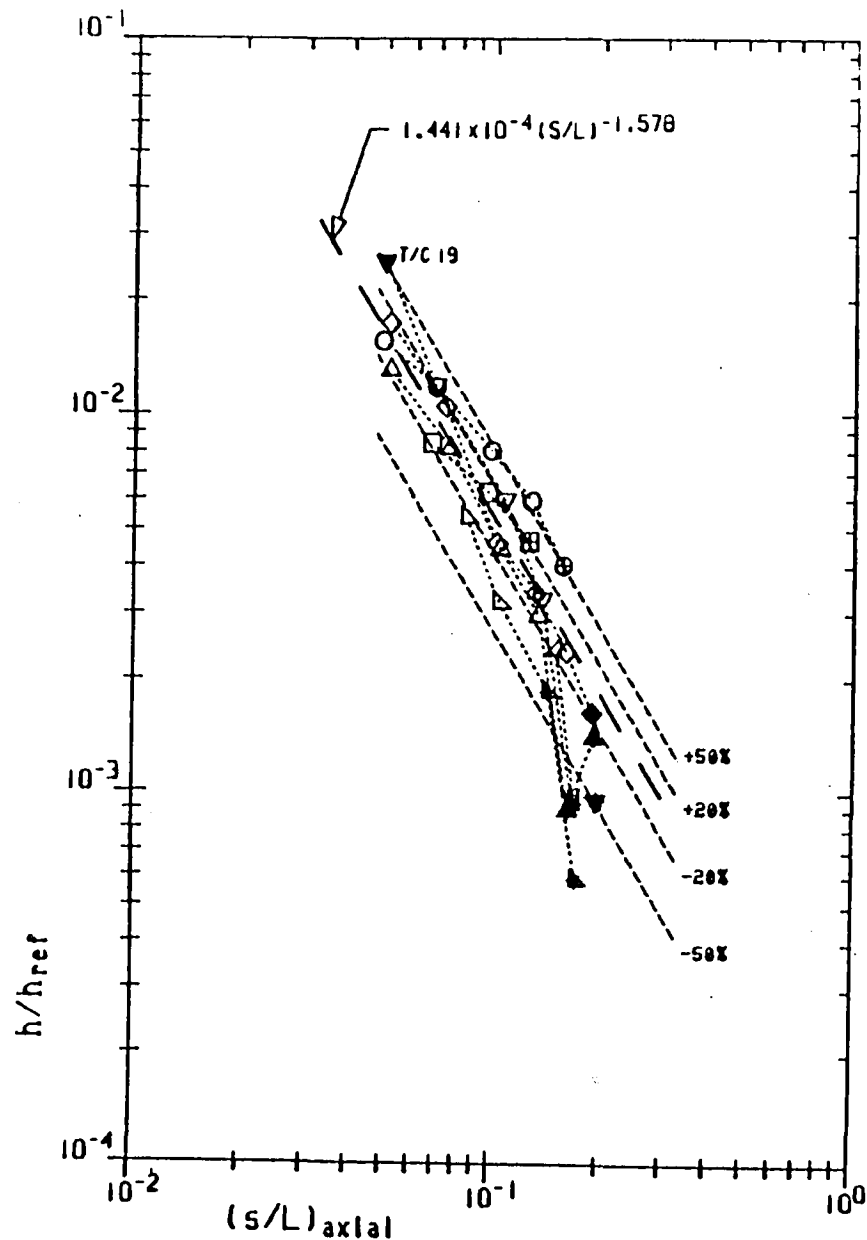


$$\alpha = 40^\circ$$

$$M_\infty = 10$$

$$Re_{\infty,L} = 2.2 \times 10^6$$

Figure 10b Wing Leaside Flow Zones, Separated Flow Stagnation Point



$M_\infty = 9.82$..
 $\alpha = 20^\circ$
 $Re_L = 0.550 \times 10^6$

SYM y/L

\triangle	.1405 .. 1	1-2 0 0 0 0 0 0
∇	.1719 .. 3	1 1 2-2 0 0 0 0
\triangle	.2034 .. 3	-4 1 1 1-2-2 0 0
\diamond	.2349 .. 4	1 1 1 1-2 0
\diamond	.2653 .. 5	1 1 1 1 1-2
\circ	.2978 .. 5	1 1 1 1 2
\square	.3278 .. 3	1 1 2

\emptyset = SEPARATED
 \square = 1 = ATTACHED
 \oplus = 2 = PRESEPARATED
 \bullet = 4 = STRAKE SHOCK?
 \triangle = - - - NOT USED - USUALLY DATA ANOMOLY

24 PTS USED

RMS DEV = 25.85 %

Figure 11a Mach 10 Wing Leeside Heating Correlation, $\alpha = 20^\circ$

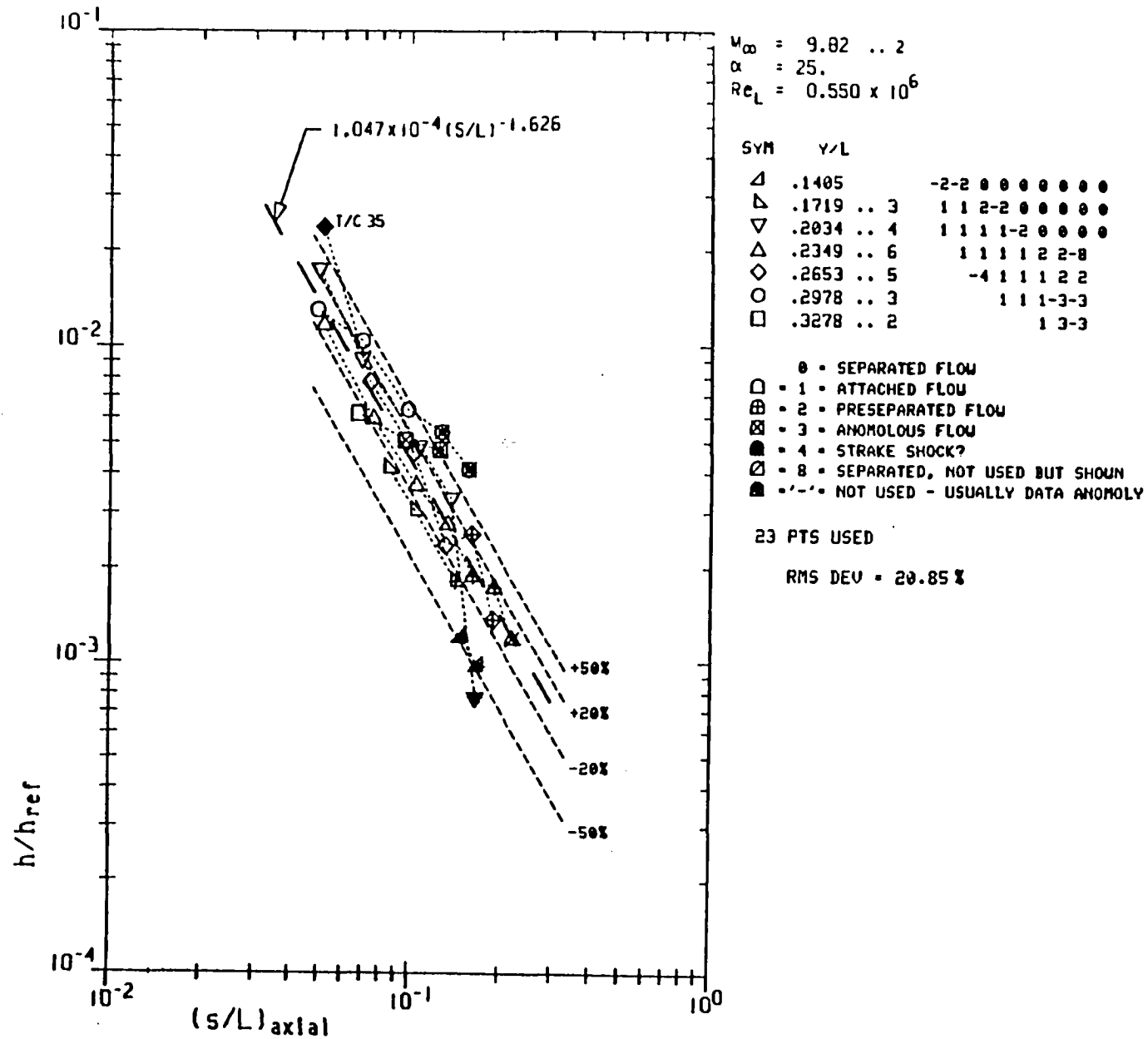


Figure 11b Mach 10 Wing Leeside Heating Correlation, $\alpha = 25^\circ$

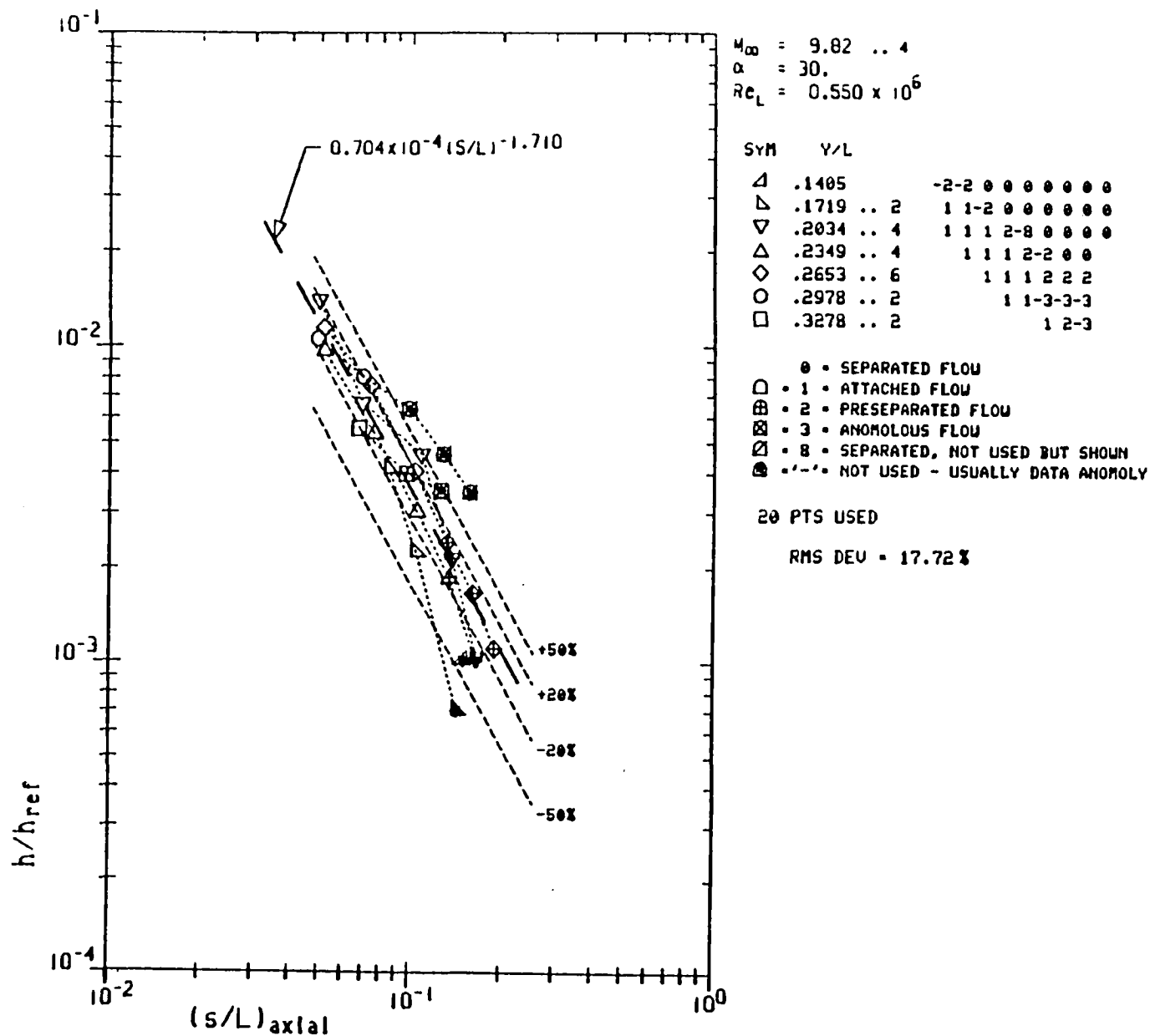


Figure 11c Mach 10 Wing Leeside Heating Correlation, $\alpha = 30^\circ$

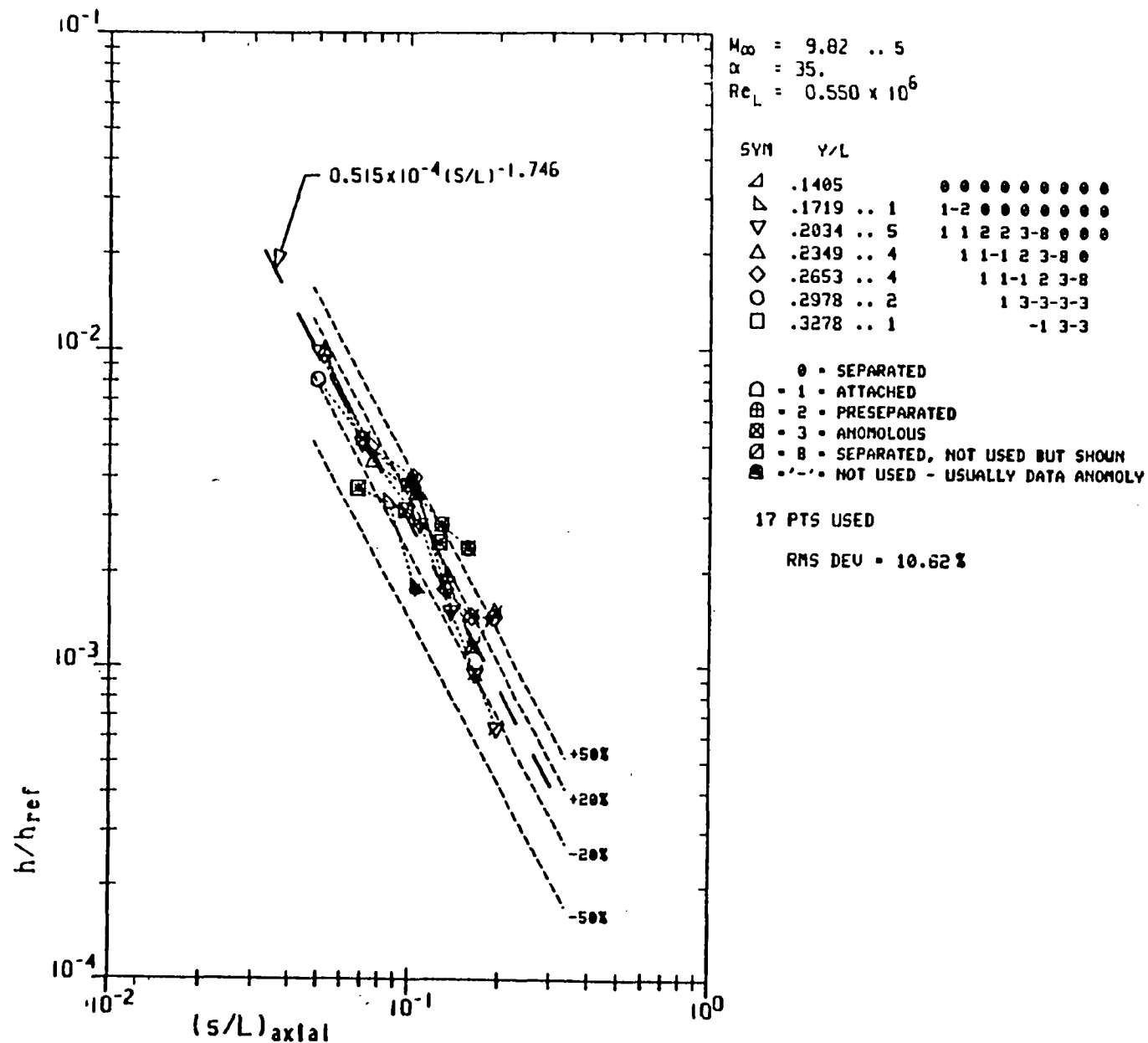


Figure 1ld Mach 10 Wing Leeward Heating Correlation, $\alpha = 35^\circ$

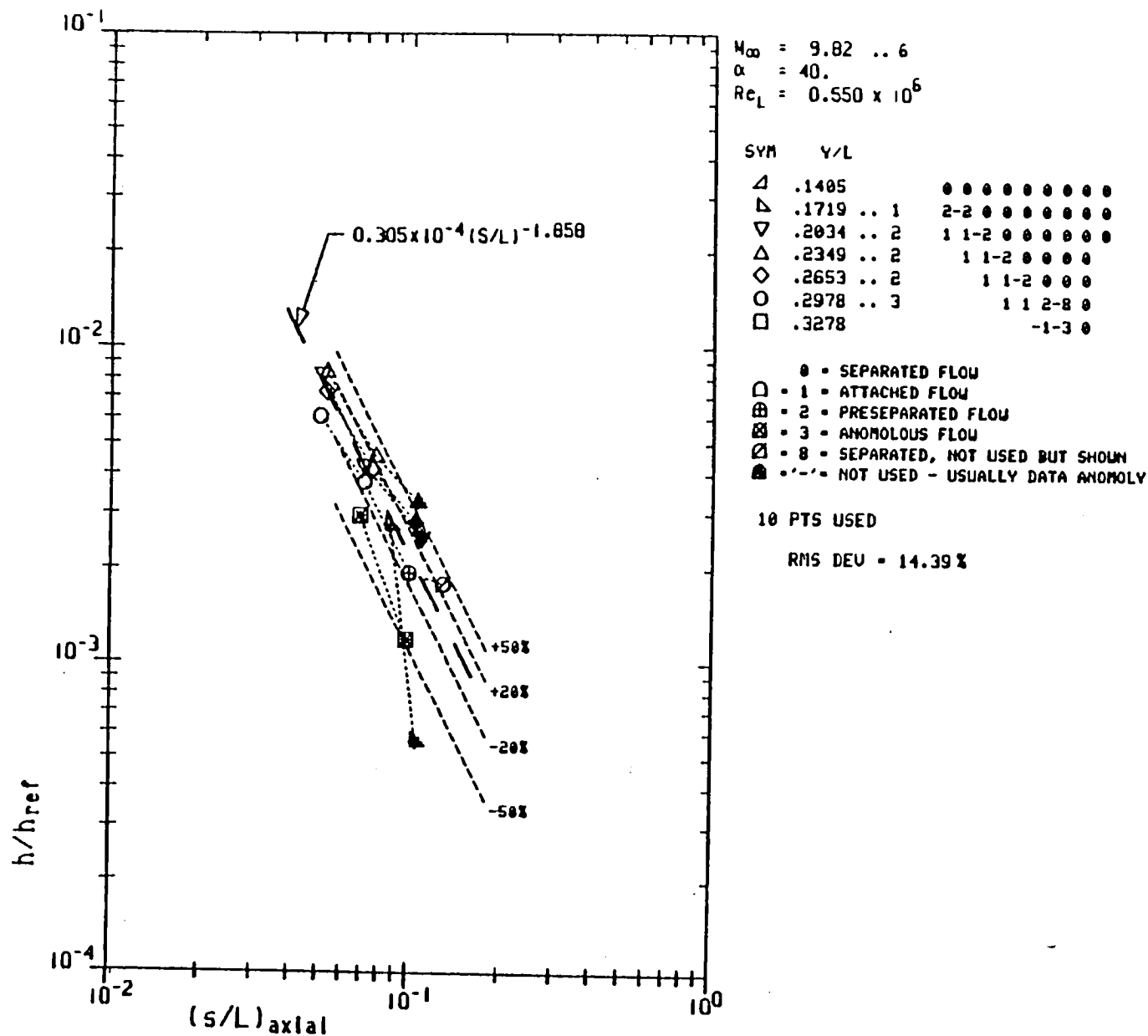


Figure 11e Mach 10 Wing Leeside Heating Correlation, $\alpha = 40^\circ$

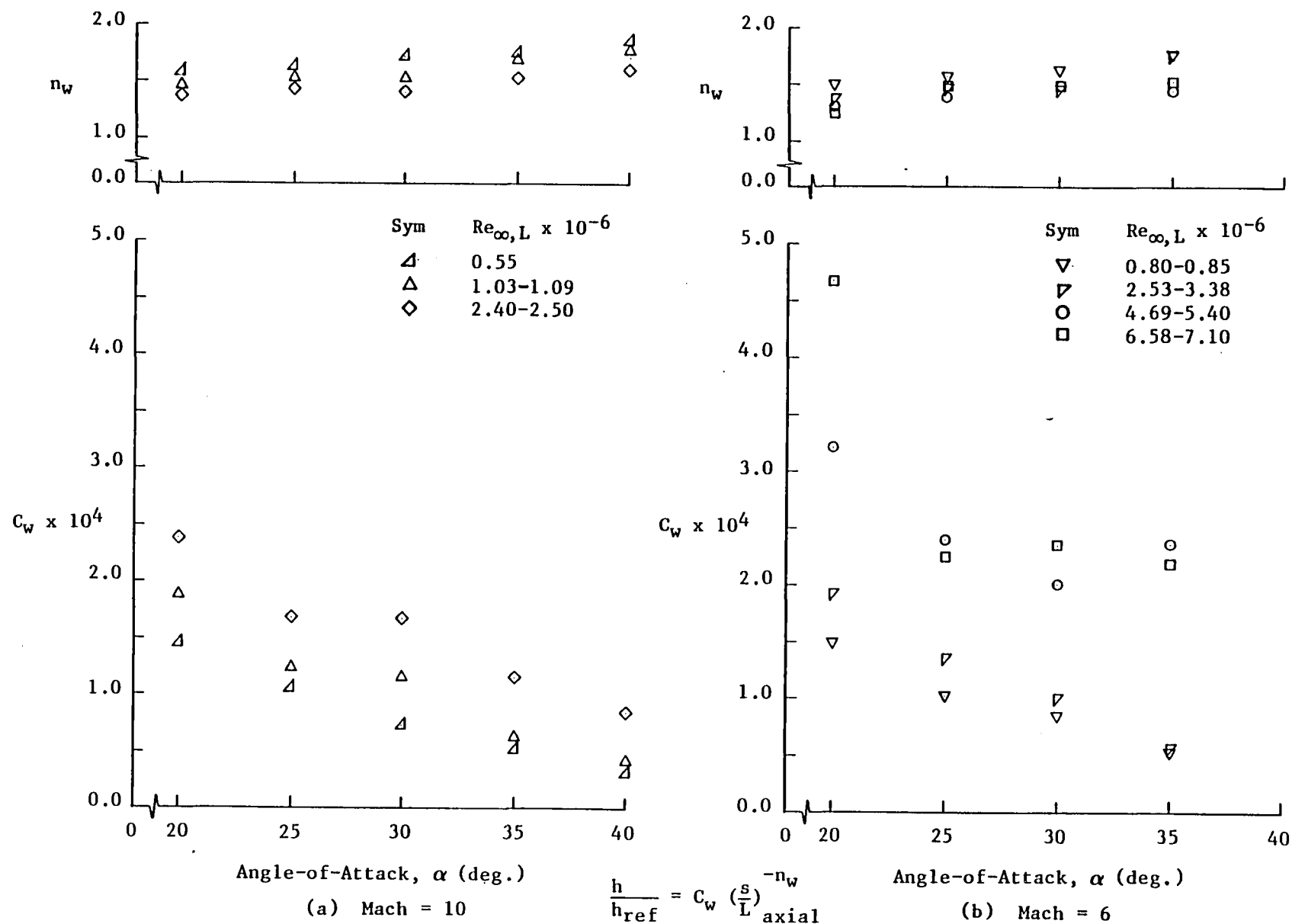
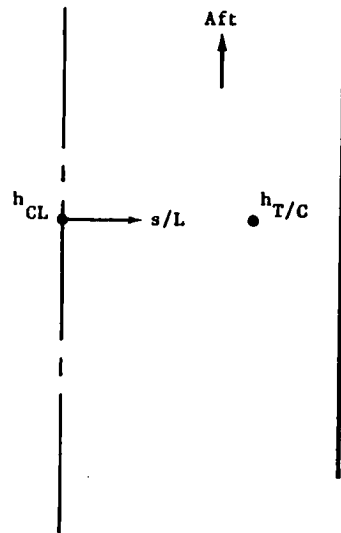
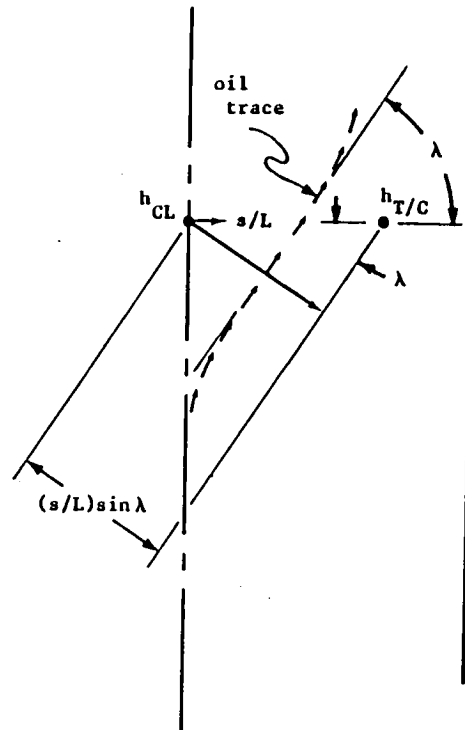
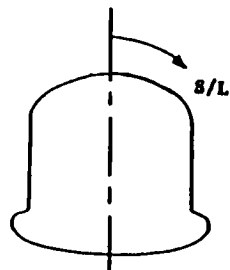


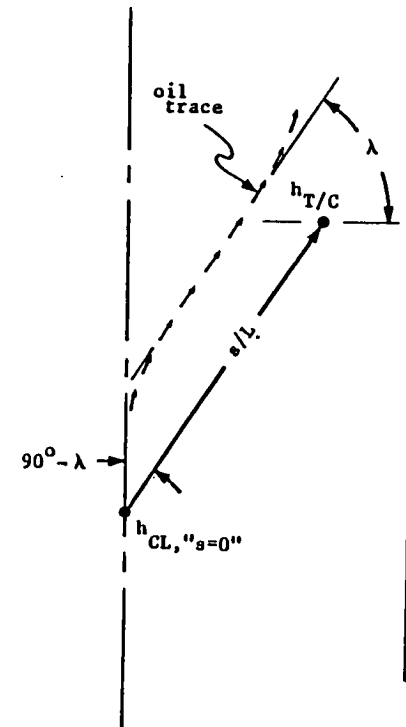
Figure 12 Wing Leeside Heating Correlation Parameters



(a) normal to
centerline



(b) normal to
stagnation line
of effective
swept cylinder



(c) along
"streamline"

Figure 13 Upper Fuselage Wetted-Length Concepts

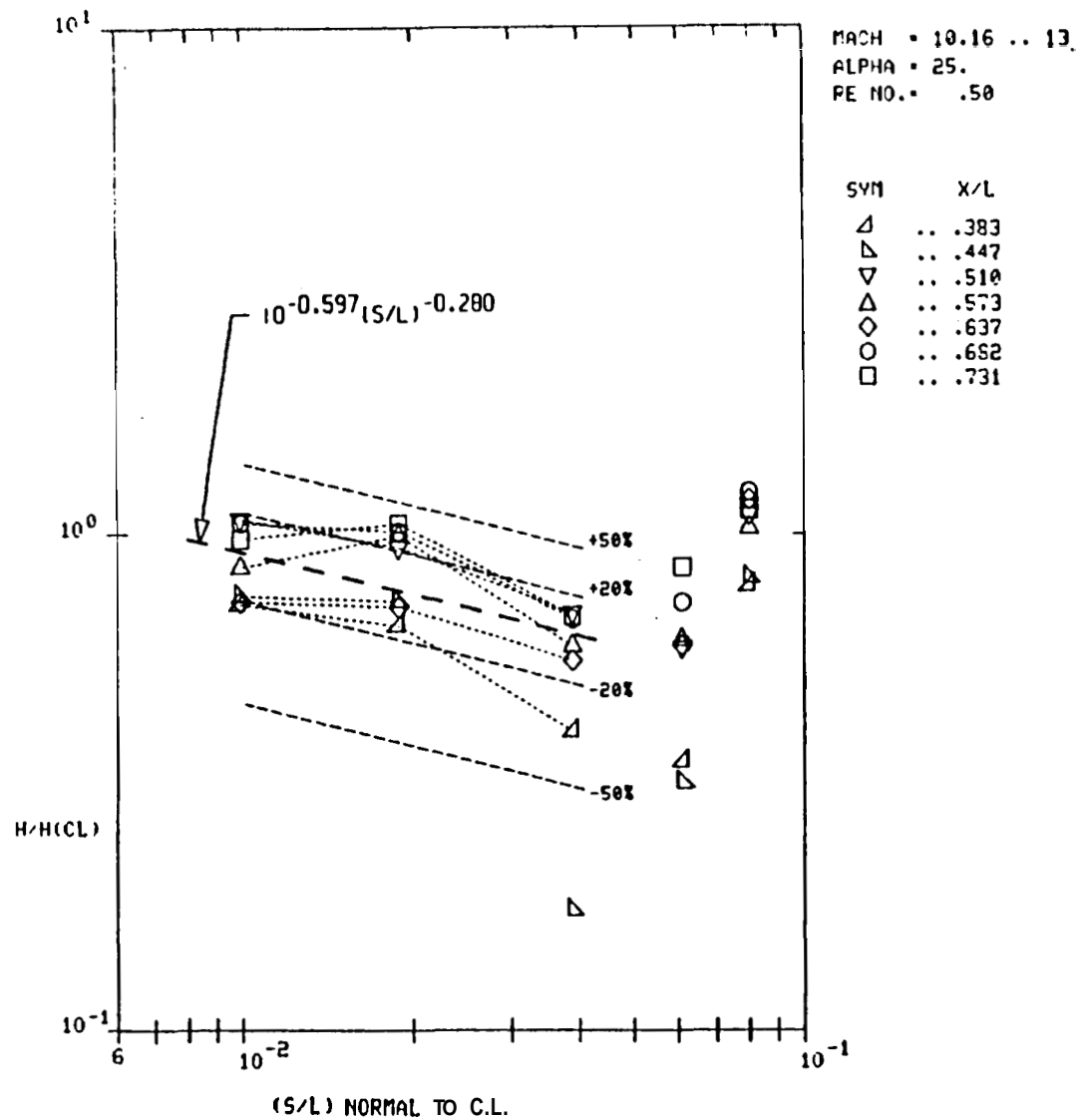


Figure 14 Upper Fuselage Heat Transfer Profiles, $M_\infty = 10$

* Related oil-flow pattern shown in Figure 18b

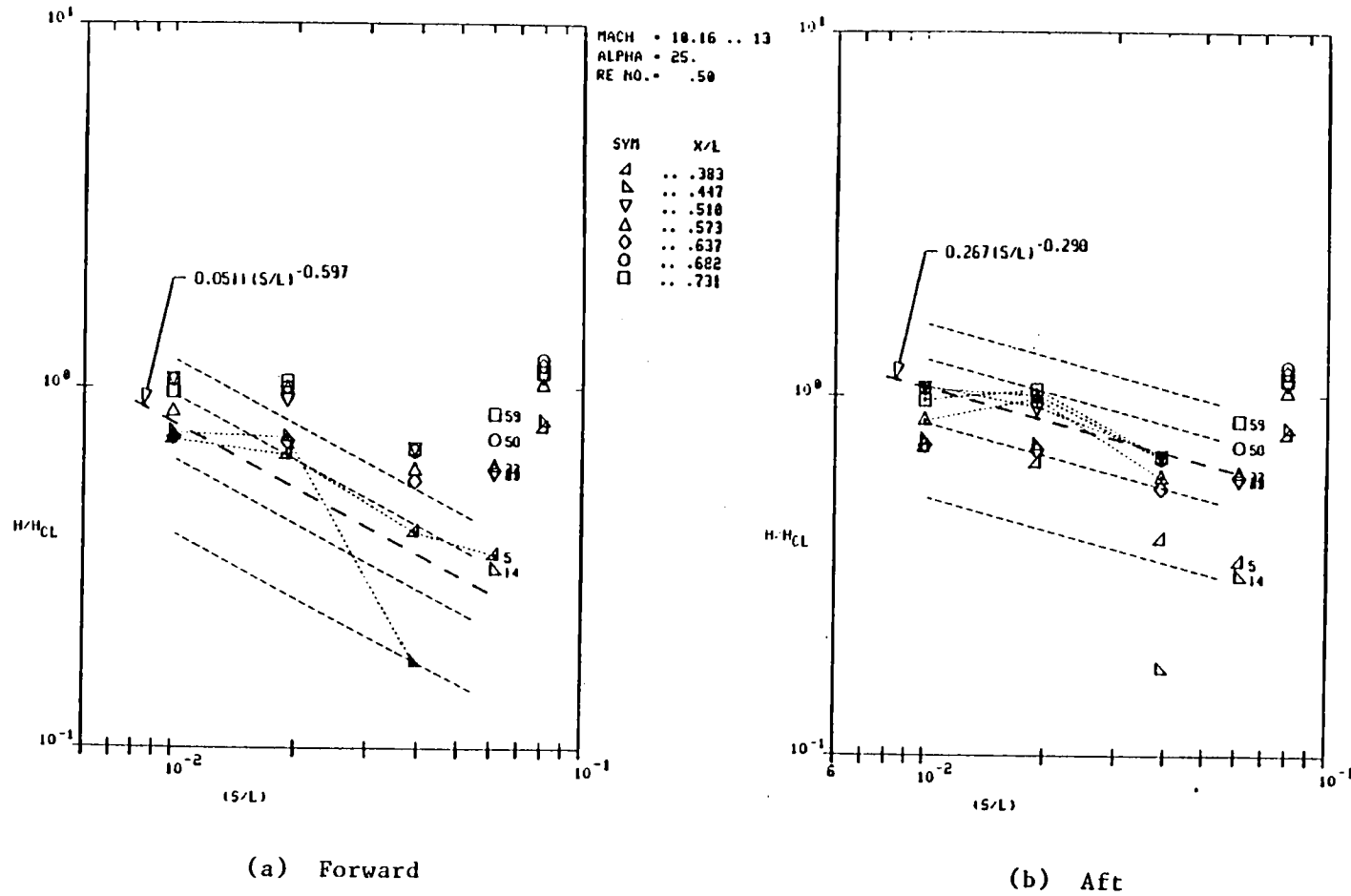


Figure 15 Upper Fuselage Heat Transfer Profiles, $M_\infty = 10$

* Related oil-flow pattern shown in Figure 18a

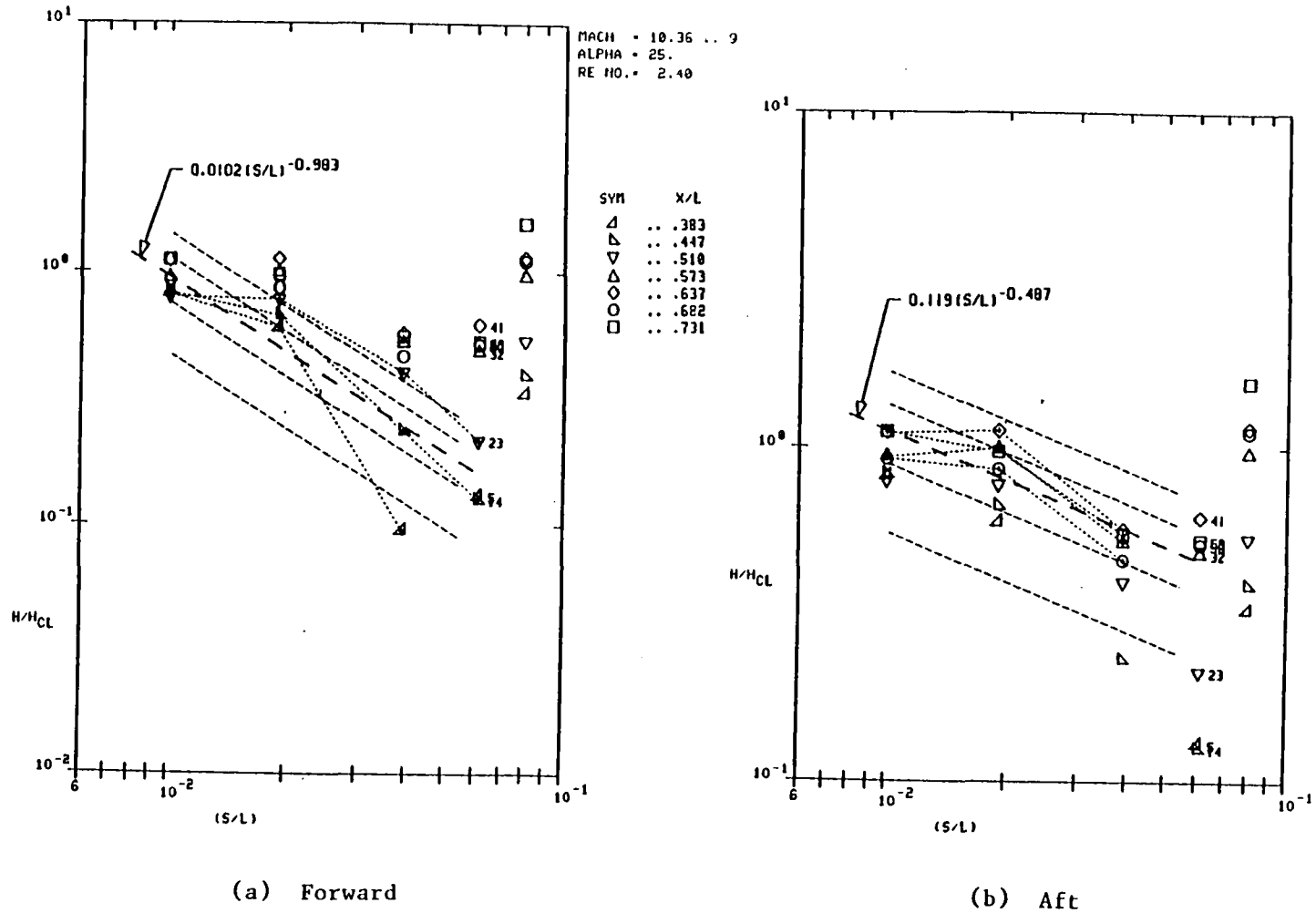


Figure 16 Upper Fuselage Heat Transfer Profiles, $M_\infty = 10$

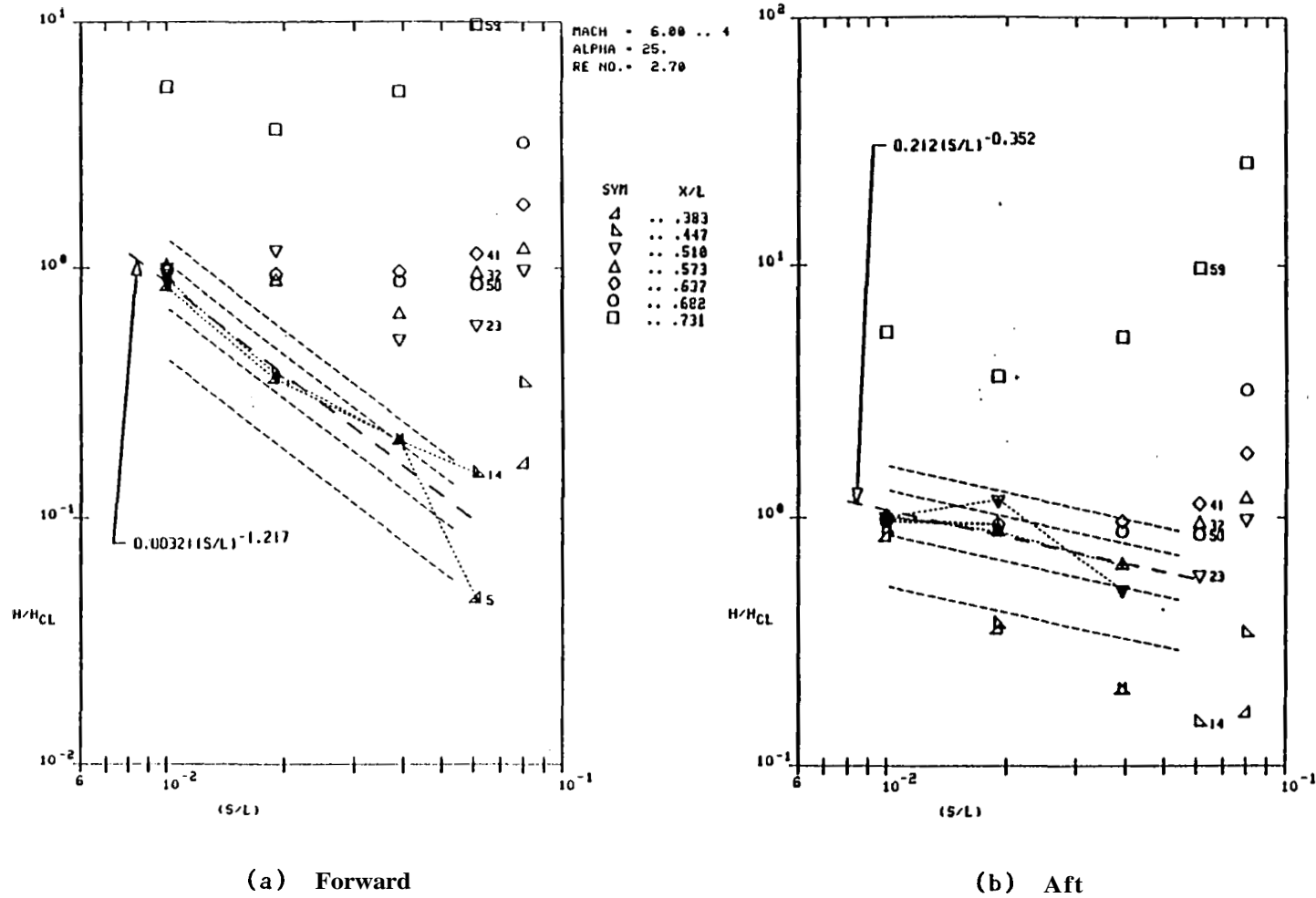
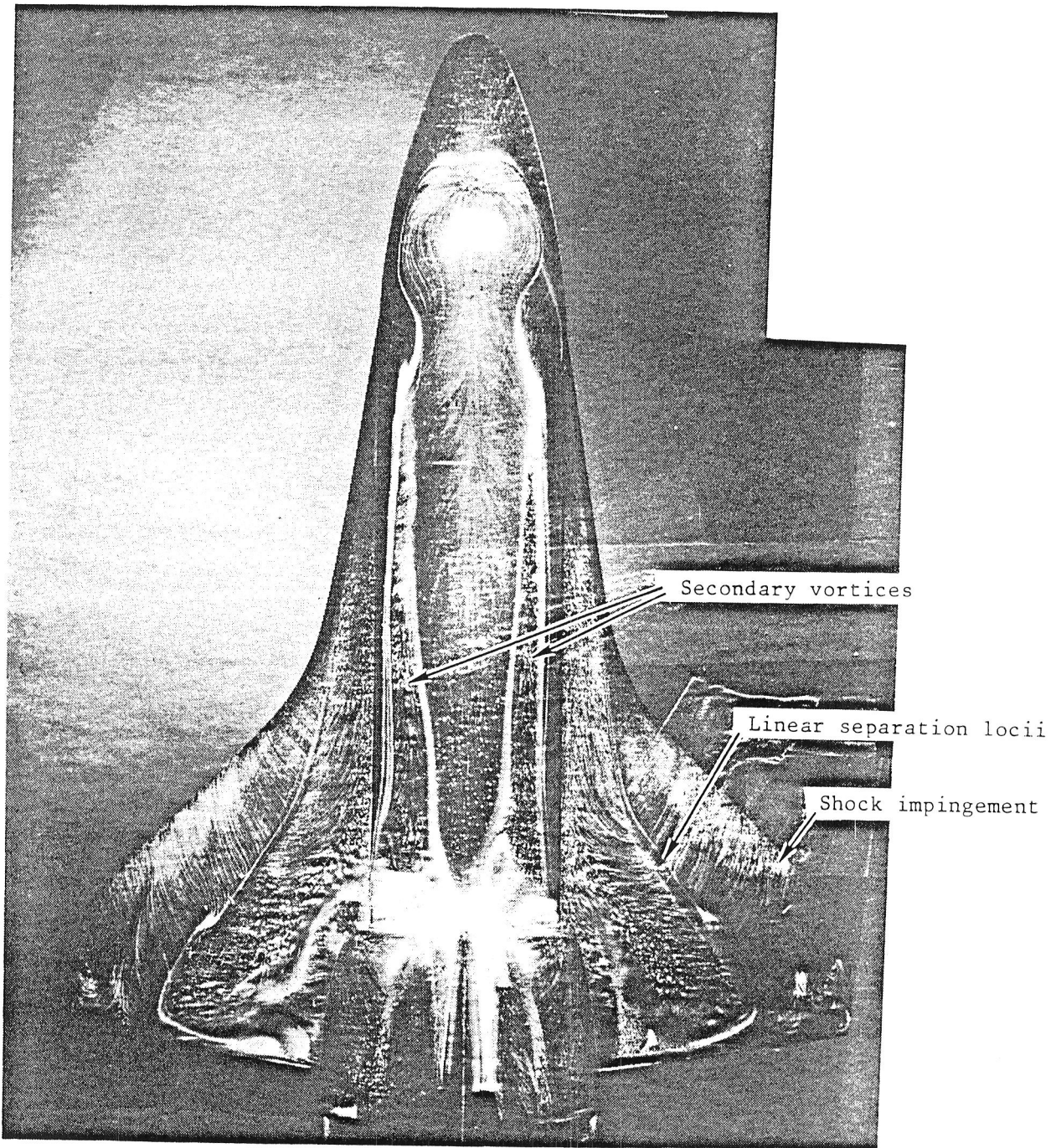


Figure 17 Upper Fuselage Heat Transfer Profiles, $M_\infty = 6$

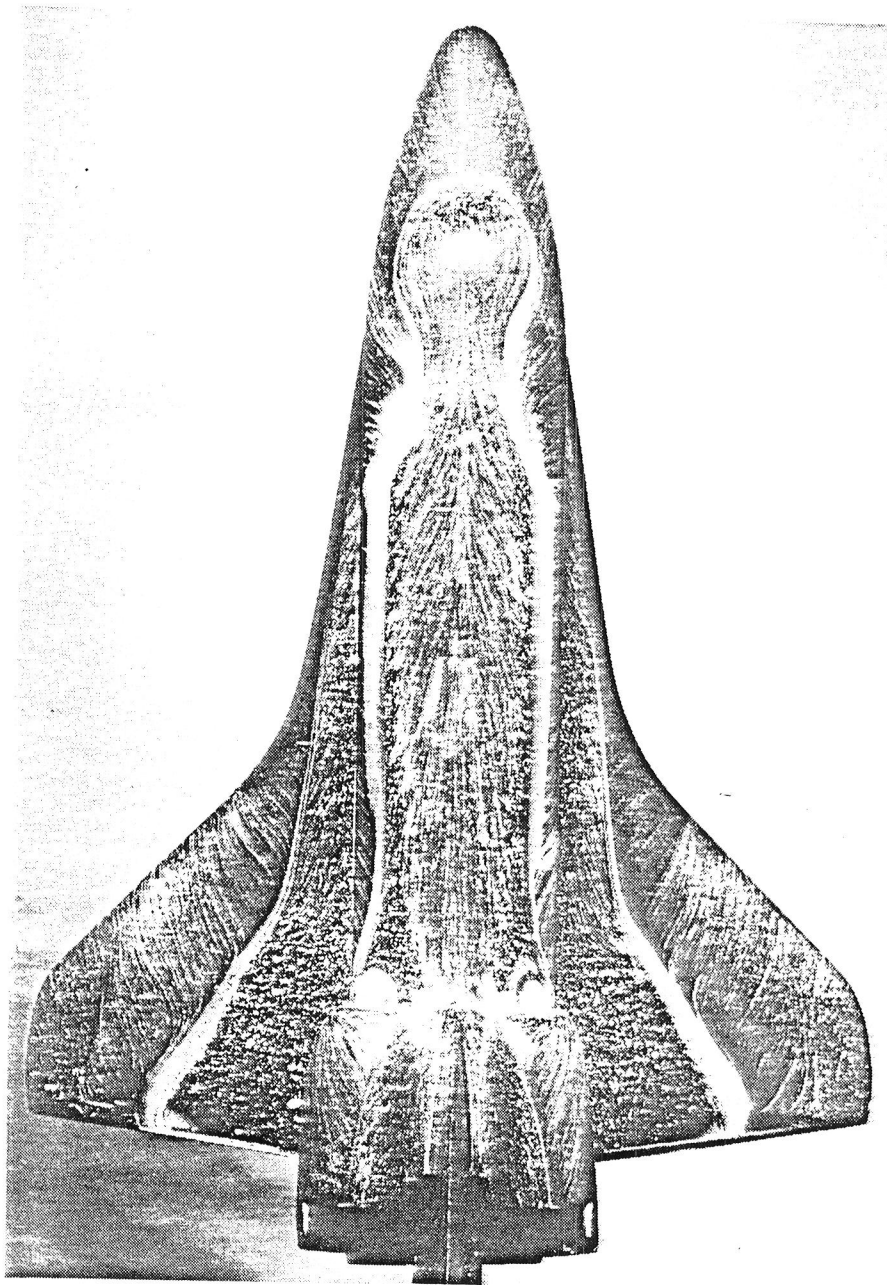


$$\alpha = 25^\circ$$

$$Re_{\infty,L} = 2.2 \times 10^6$$

$$\bar{\chi}_{\infty,L} = 0.67$$

Figure 18a Selected Leaside Oil-Flow Patterns, $M_\infty = 10$

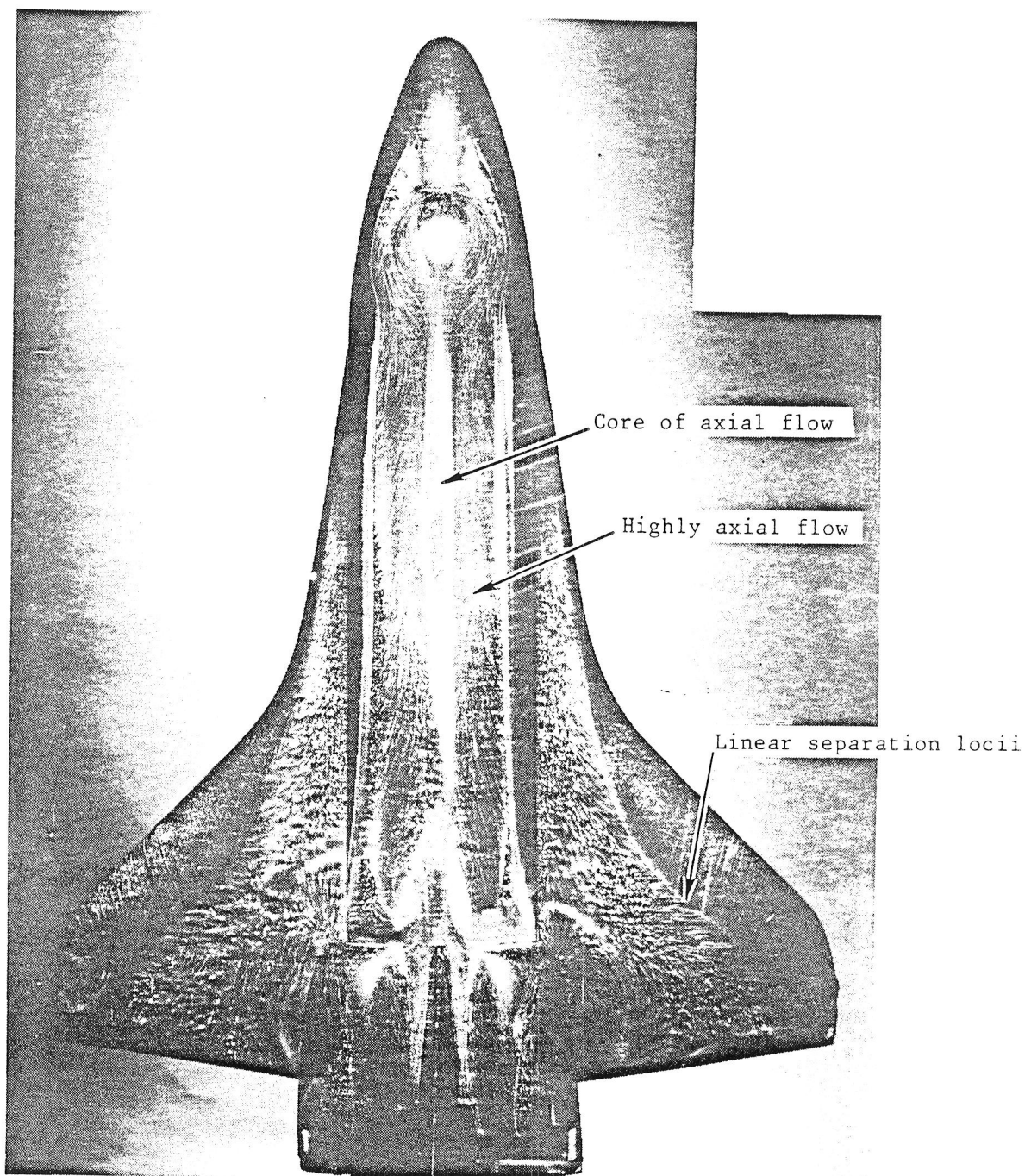


$$\alpha = 25^\circ$$

$$Re_{\infty,L} = .55 \times 10^6$$

$$\bar{\chi}_{\infty,L} = 1.35$$

Figure 18b Selected Leaside Oil-Flow Patterns, $M = 10$ - Continued

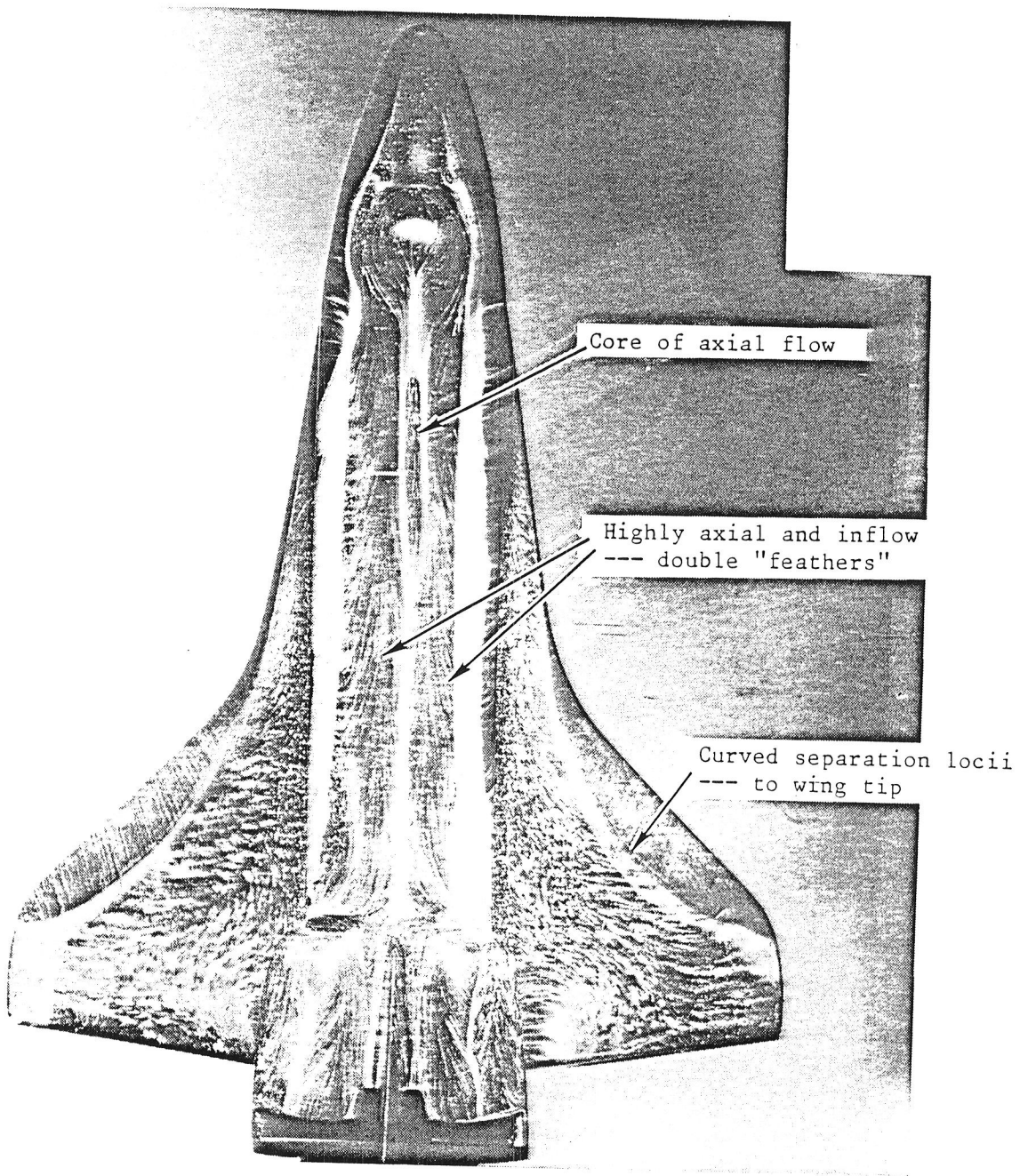


$$\alpha = 35^\circ$$

$$Re_{\infty,L} = 2.2 \times 10^6$$

$$\bar{X}_{\infty,L} = 0.67$$

Figure 18c Selected Leaside Oil-Flow Patterns, $M_\infty = 10$ - Continued

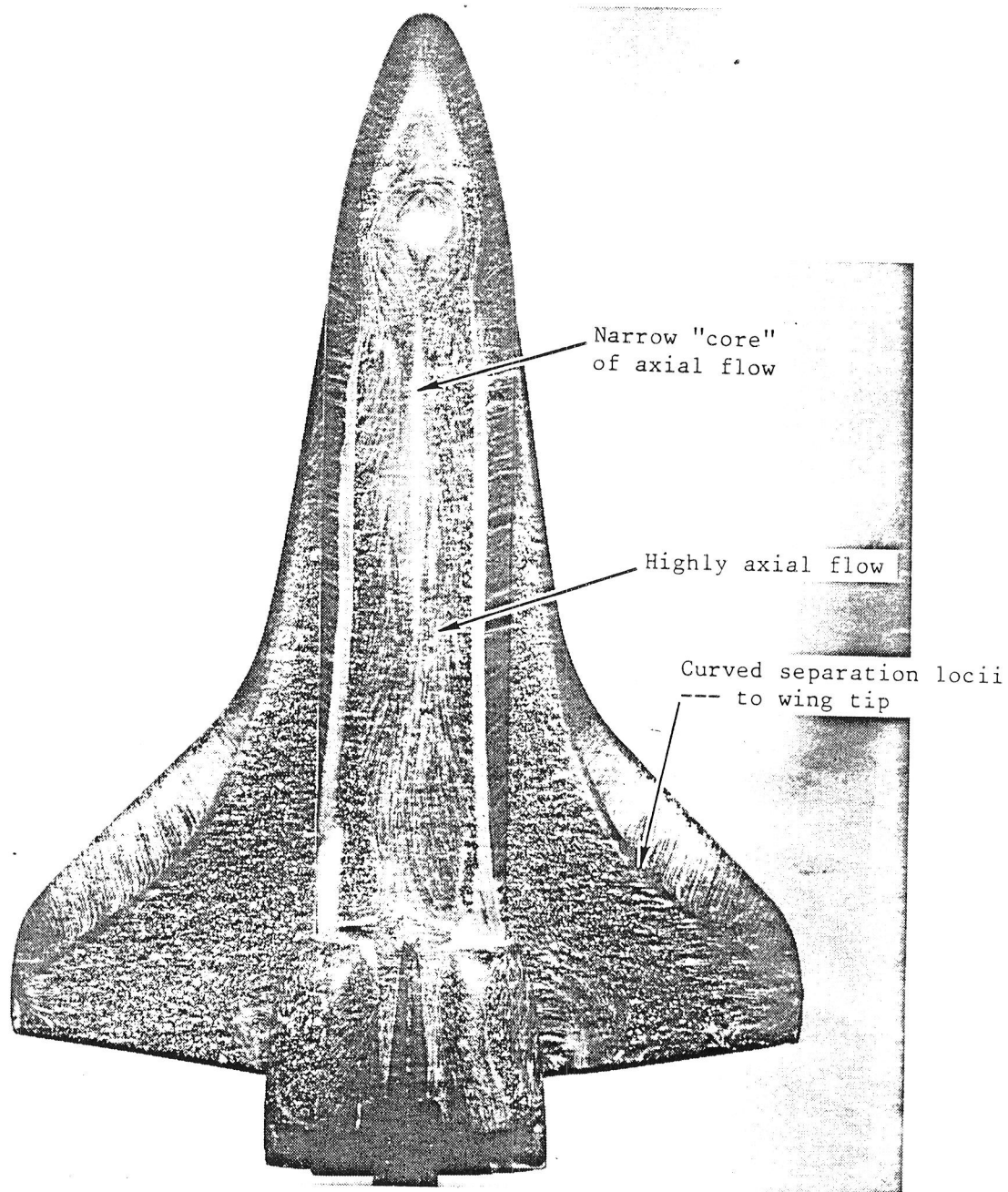


$$\alpha = 40^\circ$$

$$Re_{\infty,L} = 2.2 \times 10^6$$

$$\bar{\chi}_{\infty,L} = 0.67$$

Figure 18d Selected Leaside Oil-Flow Patterns, $M_\infty = 10$ - Continued

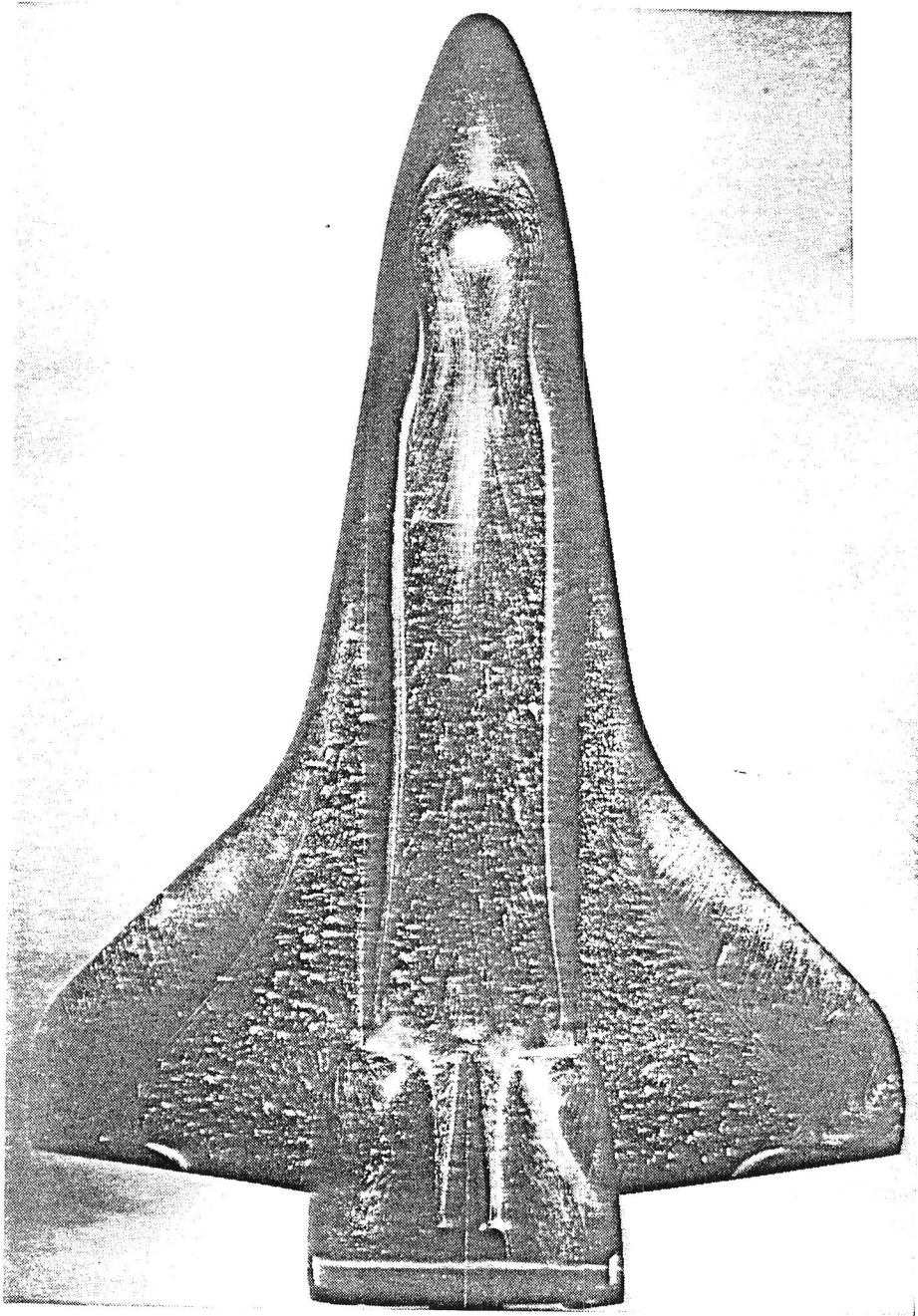


$$\alpha = 40^\circ$$

$$Re_{\infty, L} = 1.1 \times 10^6$$

$$\bar{X}_{\infty, L} = 0.95$$

Figure 18e Selected Leaside Oil-Flow Patterns, $M_\infty = 10$ - Continued

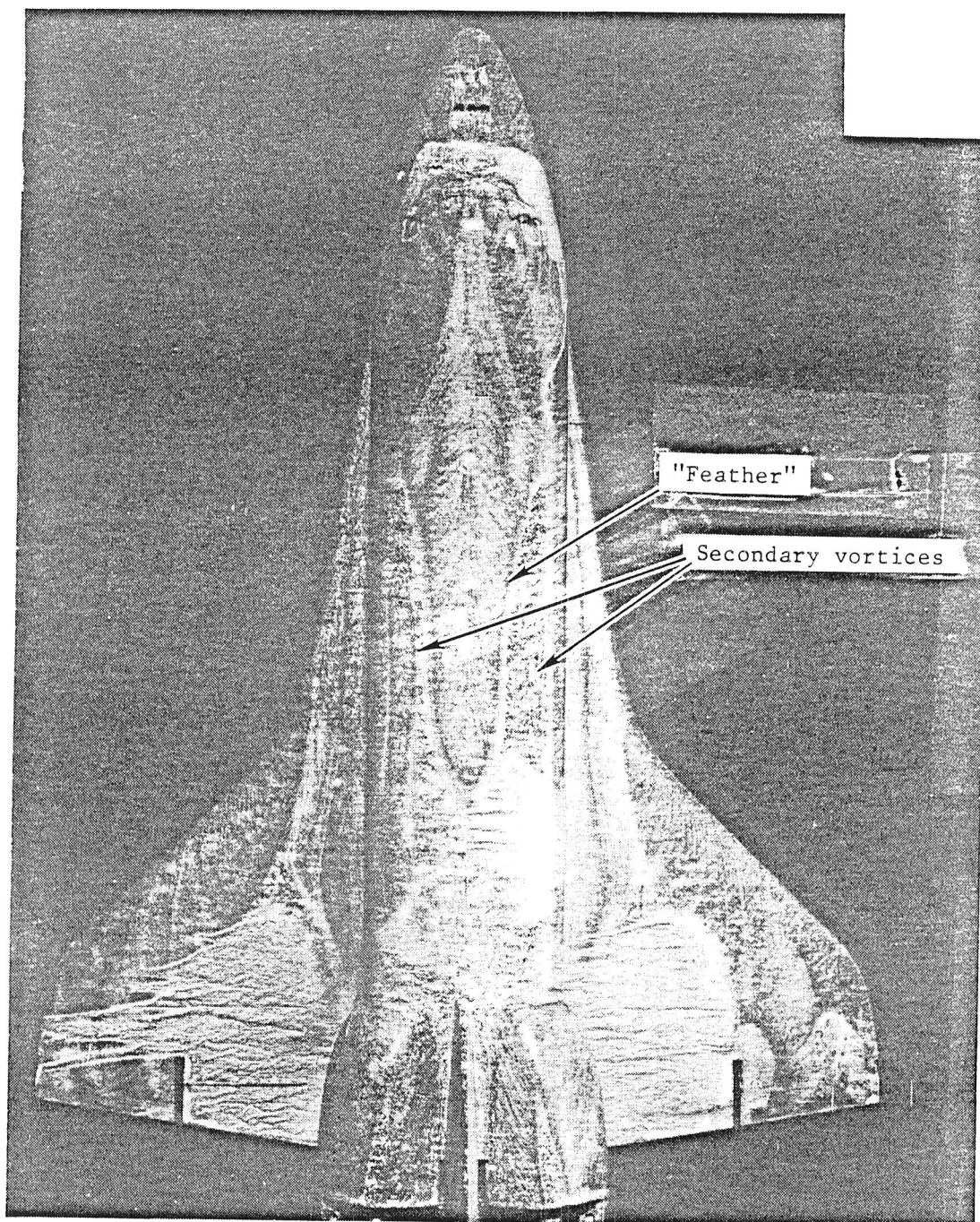


$$\alpha = 35^\circ$$

$$Re_{\infty,L} = .55 \times 10^6$$

$$\bar{\chi}_{\infty,L} = 1.35$$

Figure 18f Selected Leaside Oil-Flow Patterns, $M_\infty = 10$ - Concluded

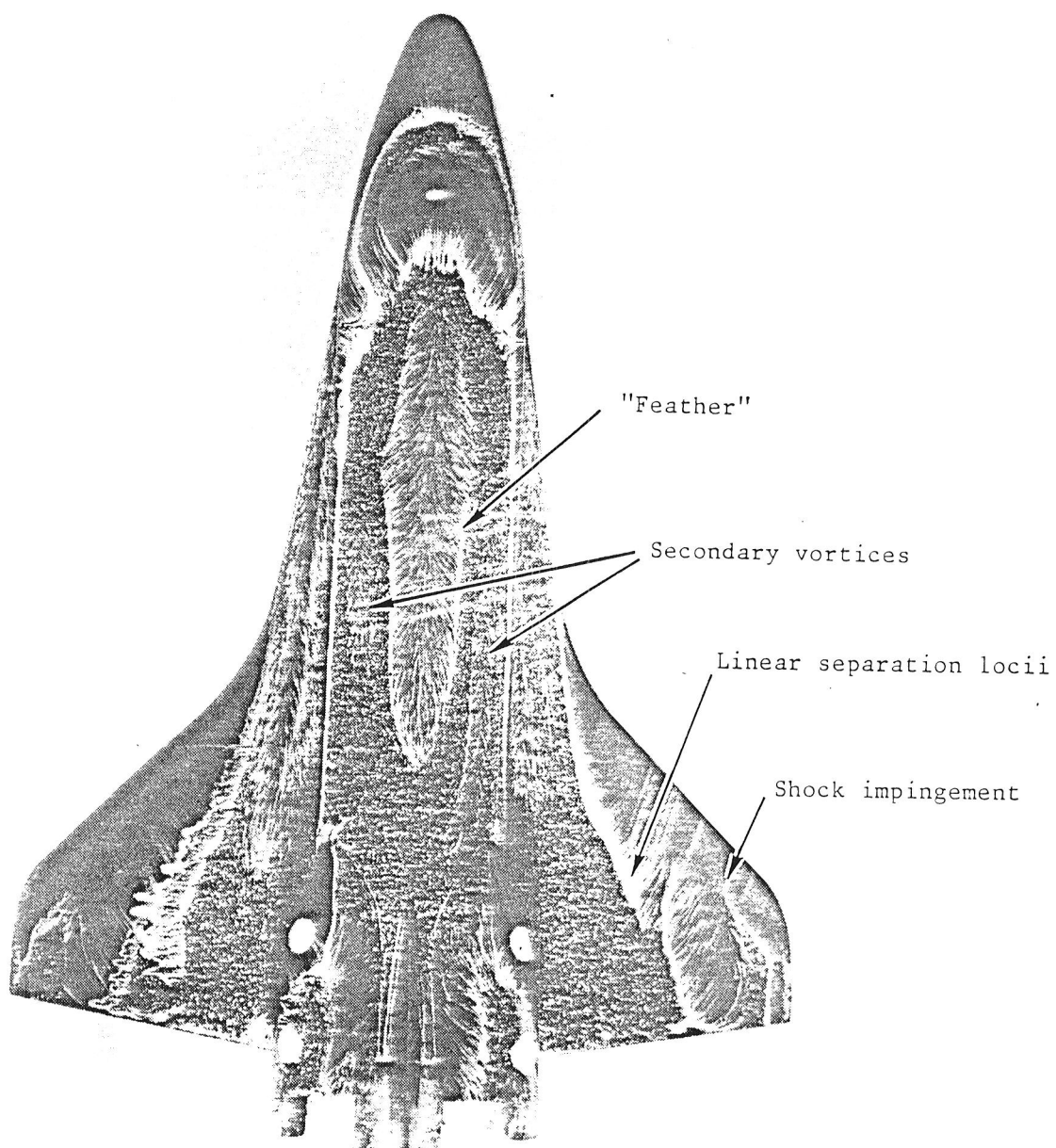


$$\alpha = 20^\circ$$

$$Re_{\infty,L} = 7.3 \times 10^6$$

$$\bar{\chi}_{\infty,L} = 0.080$$

Figure 19a Selected Leeward Oil-Flow Patterns, $M_\infty = 6$

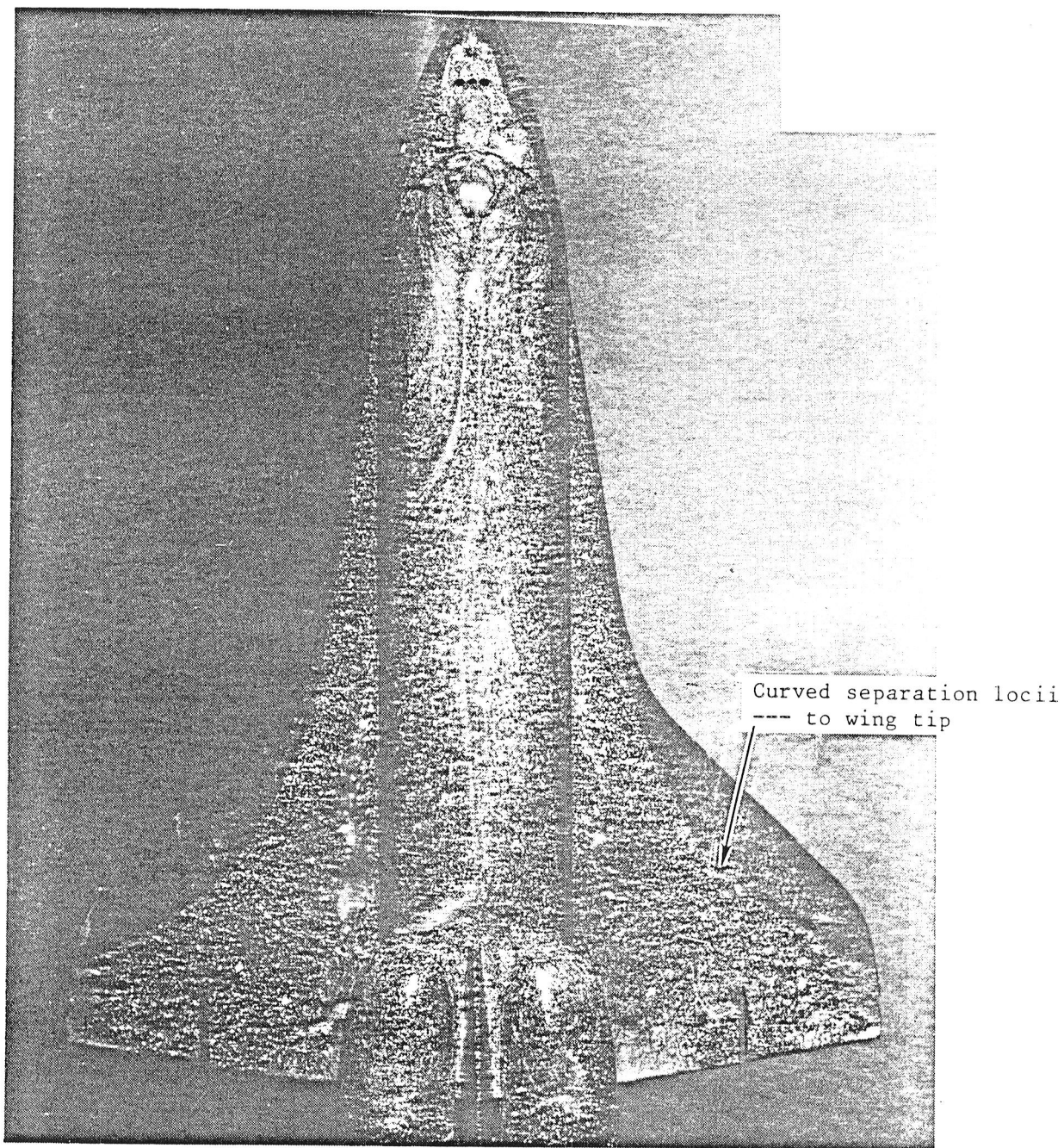


$$\alpha = 20^\circ$$

$$Re_{\infty,L} = 4.8 \times 10^6$$

$$\bar{\chi}_{\infty,L} = 0.098$$

Figure 19b Selected Leaside Oil-Flow Patterns, $M_\infty = 6$ - Continued

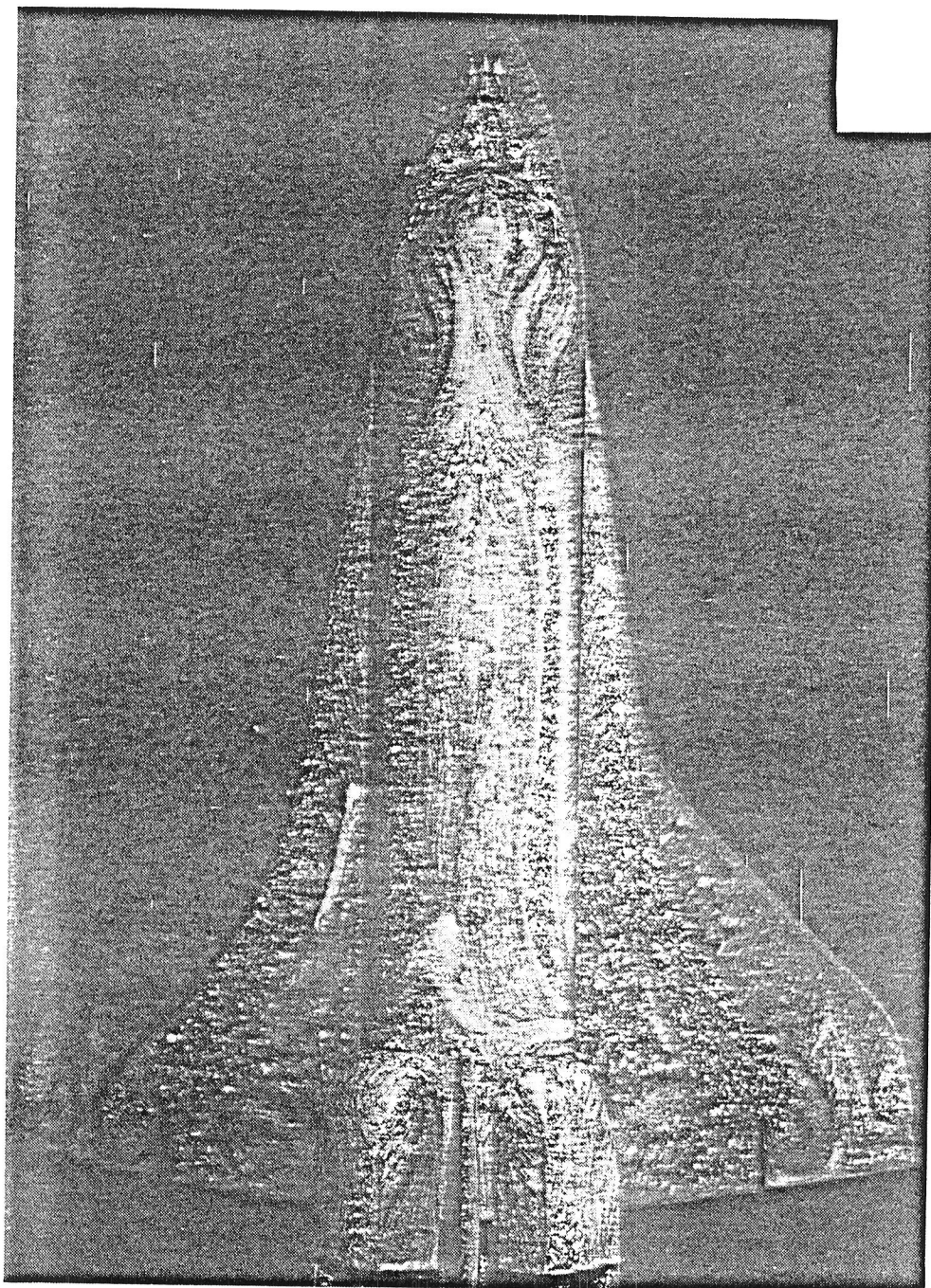


$$\alpha = 40^\circ$$

$$\text{Re}_{\infty, L} = 2.7 \times 10^6$$

$$\bar{\chi}_{\infty, L} = 0.13$$

Figure 19c Selected Leaside Oil-Flow Patterns, $M_\infty = 6$ - Continued

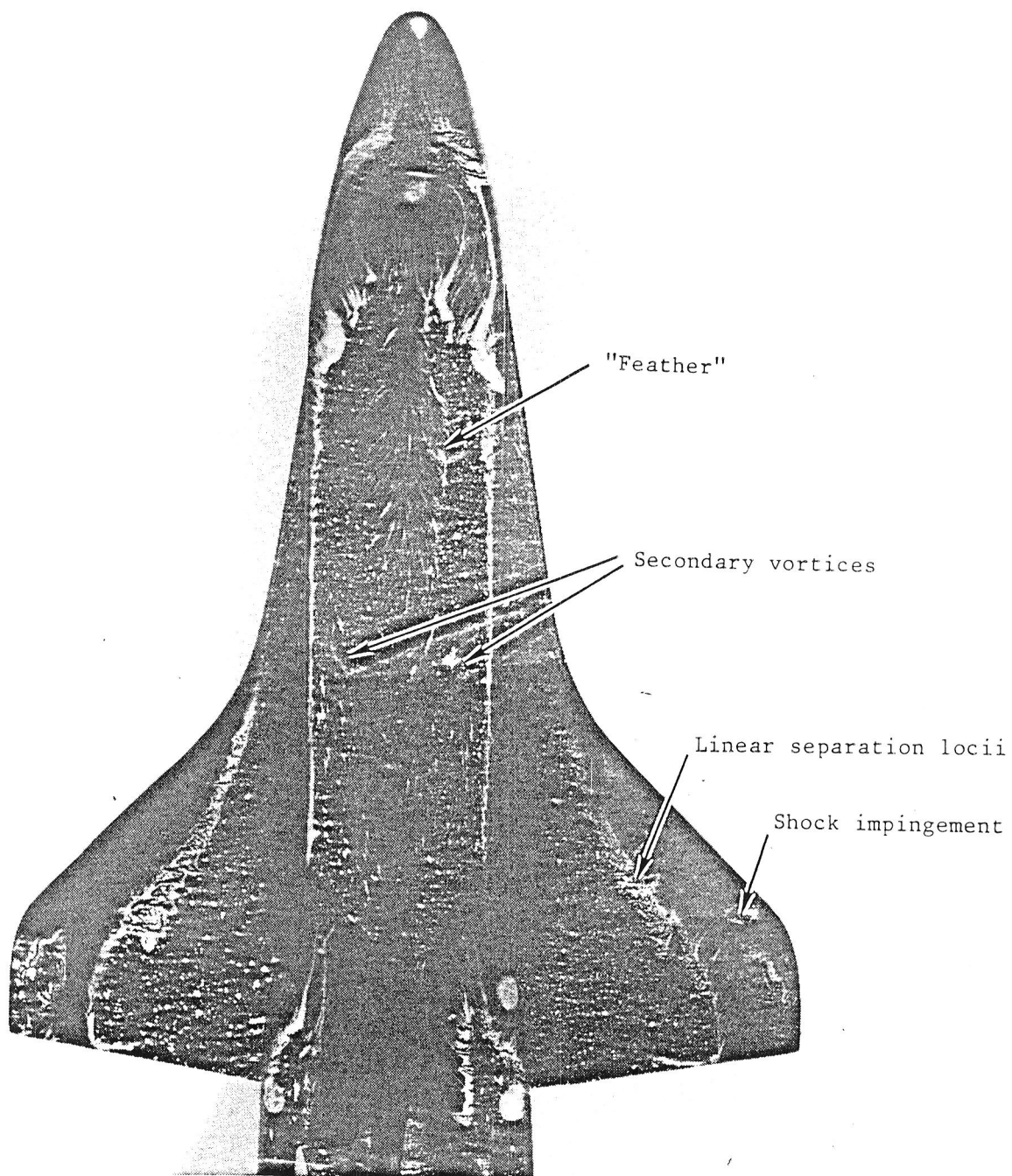


$$\alpha = 30^\circ$$

$$Re_{\infty,L} = 2.7 \times 10^6$$

$$\bar{\chi}_{\infty,L} = 0.13$$

Figure 19d Selected Leeside Oil-Flow Patterns, $M_\infty = 6$ - Continued

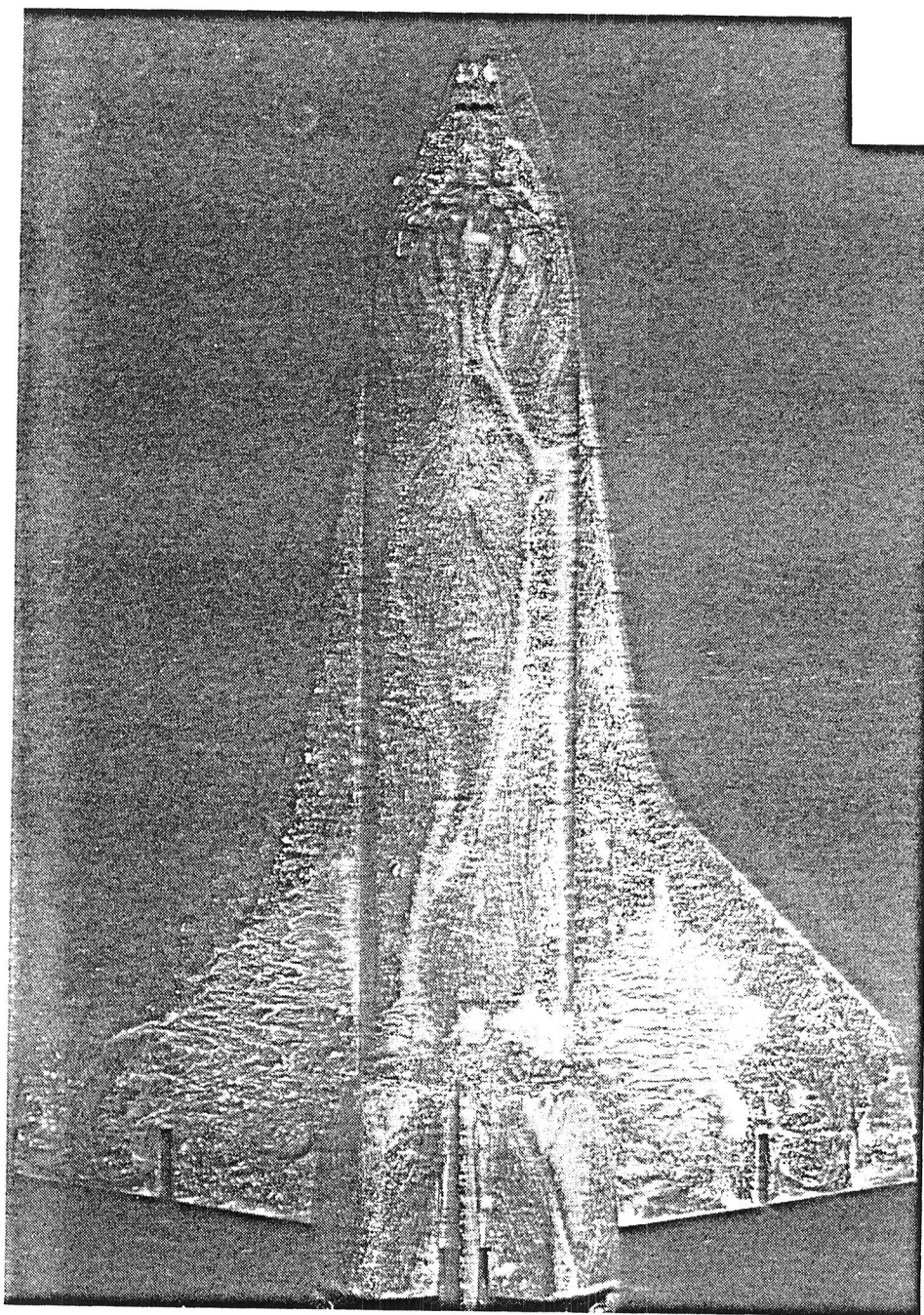


$$\alpha = 30^\circ$$

$$Re_{\infty,L} = 4.8 \times 10^6$$

$$\bar{\chi}_{\infty,L} = 0.098$$

Figure 19e Selected Leaside Oil-Flow Patterns, $M_\infty = 6$ - Continued



$$\alpha = 30^\circ$$

$$\text{Re}_{\infty, L} = 7.3 \times 10^6$$

$$\bar{\chi}_{\infty, L} = 0.08$$

Figure 19f Selected Leaside Oil-Flow Patterns, $M_\infty = 6$ - Concluded

* Related oil-flow pattern shown in Figure 18c

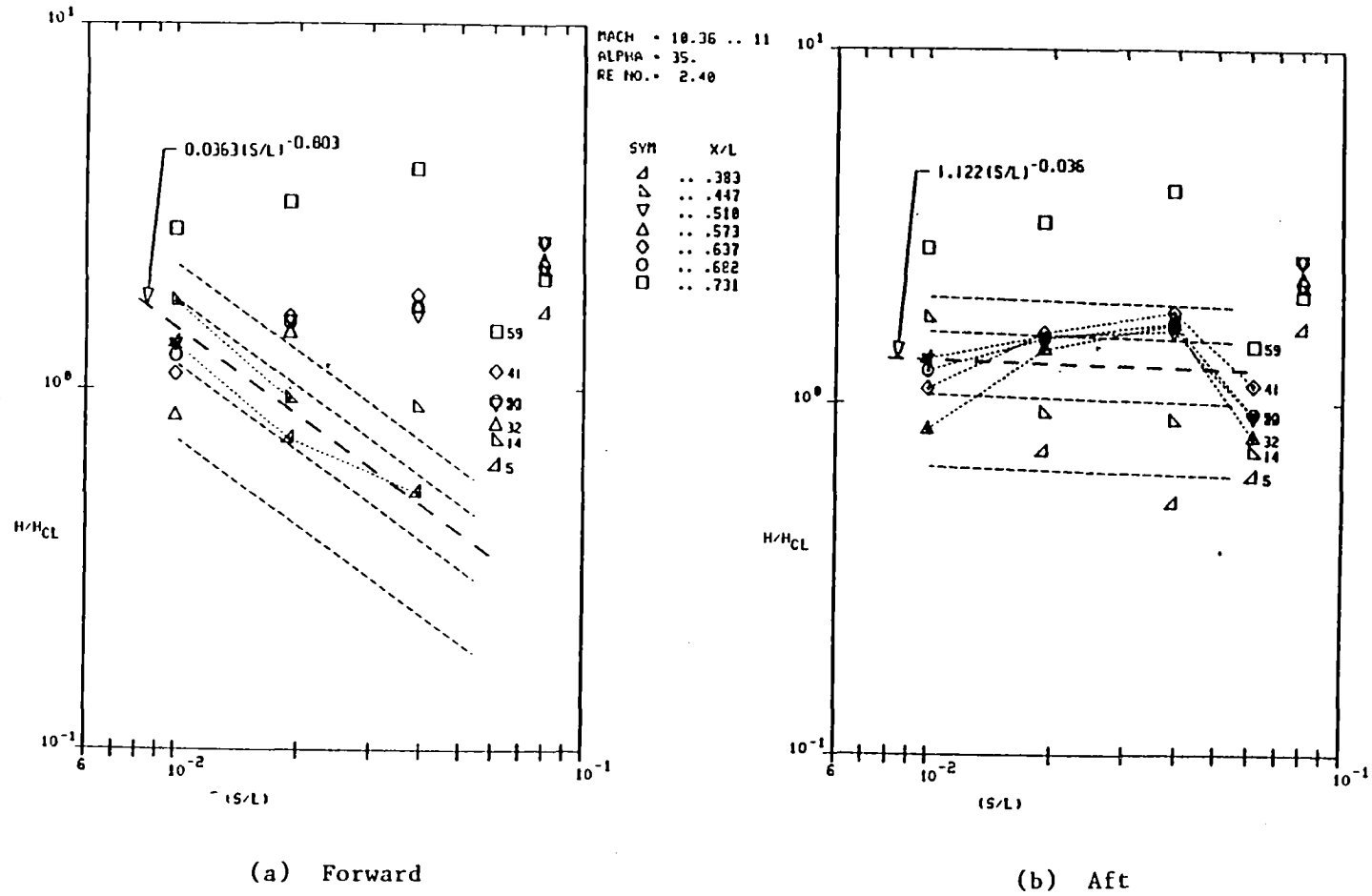


Figure 20 Upper Fuselage Heat Transfer Profiles, $M_\infty = 10$

* Related oil-flow pattern shown in Figure 18d

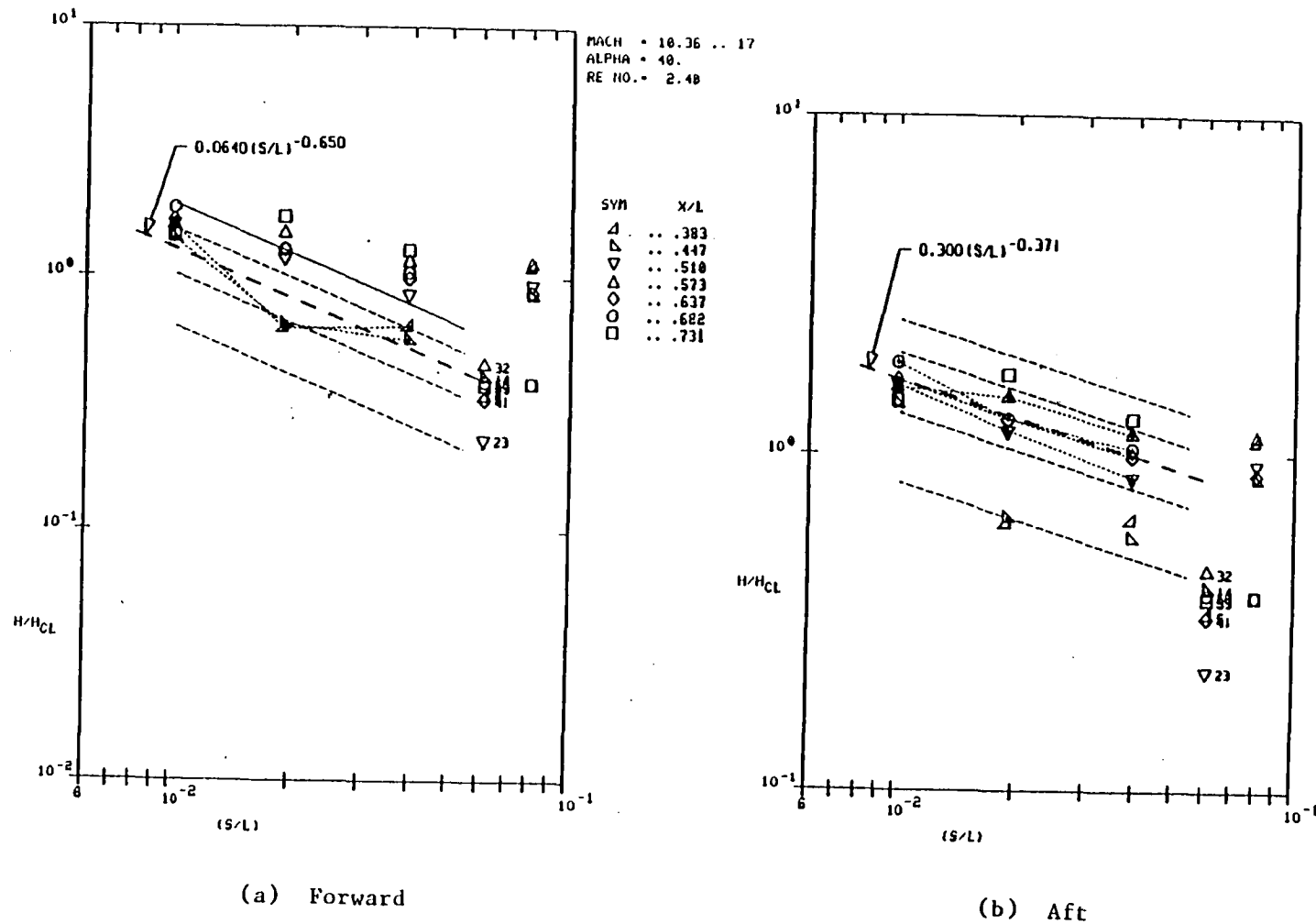


Figure 21 Upper Fuselage Heat Transfer Profiles, $M_\infty = 10$

* Related oil-flow pattern shown in Figure 18e

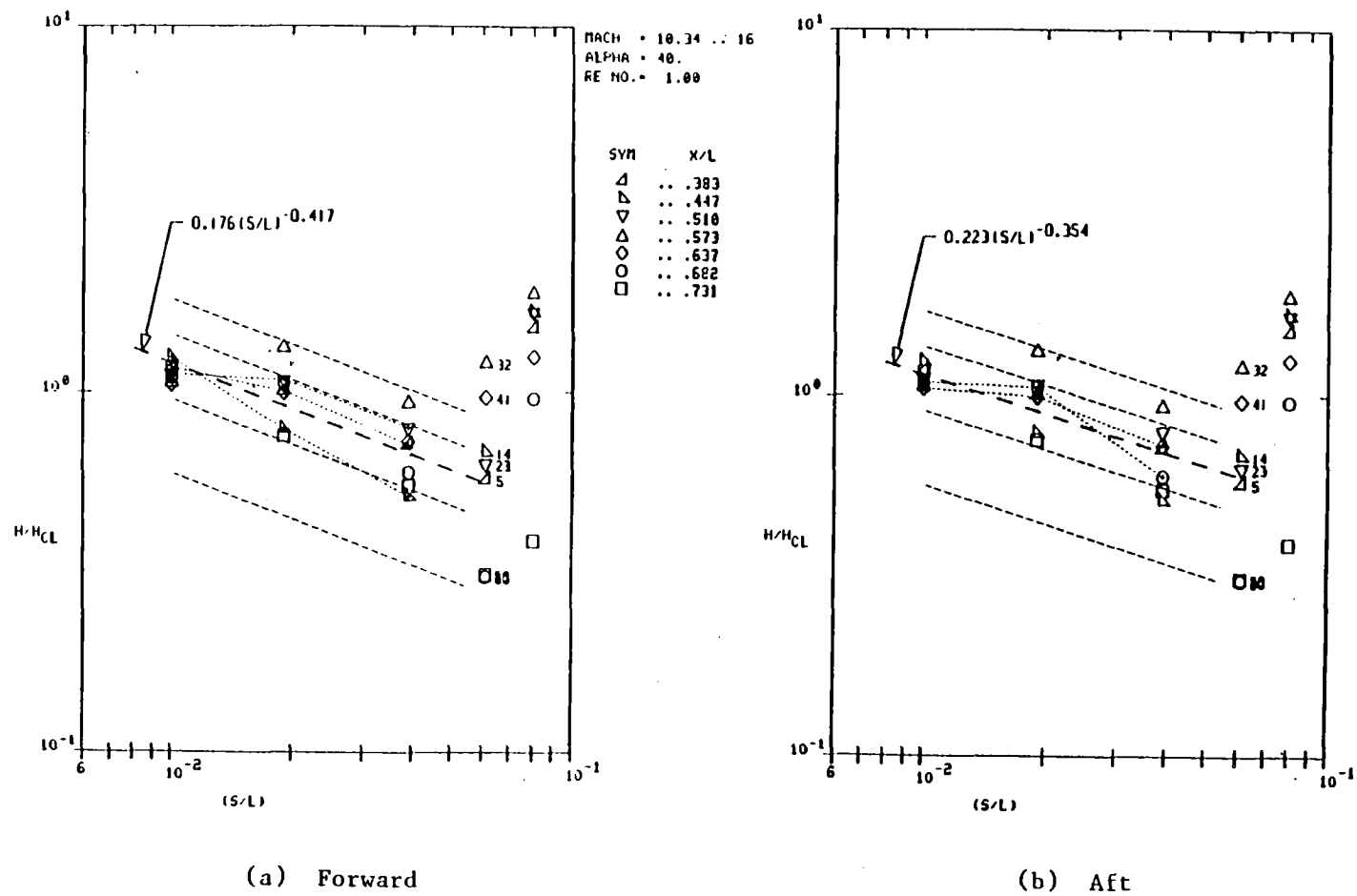


Figure 22 Upper Fuselage Heat Transfer Profiles, $M_\infty = 10$

* Related oil-flow pattern shown in Figure 19d

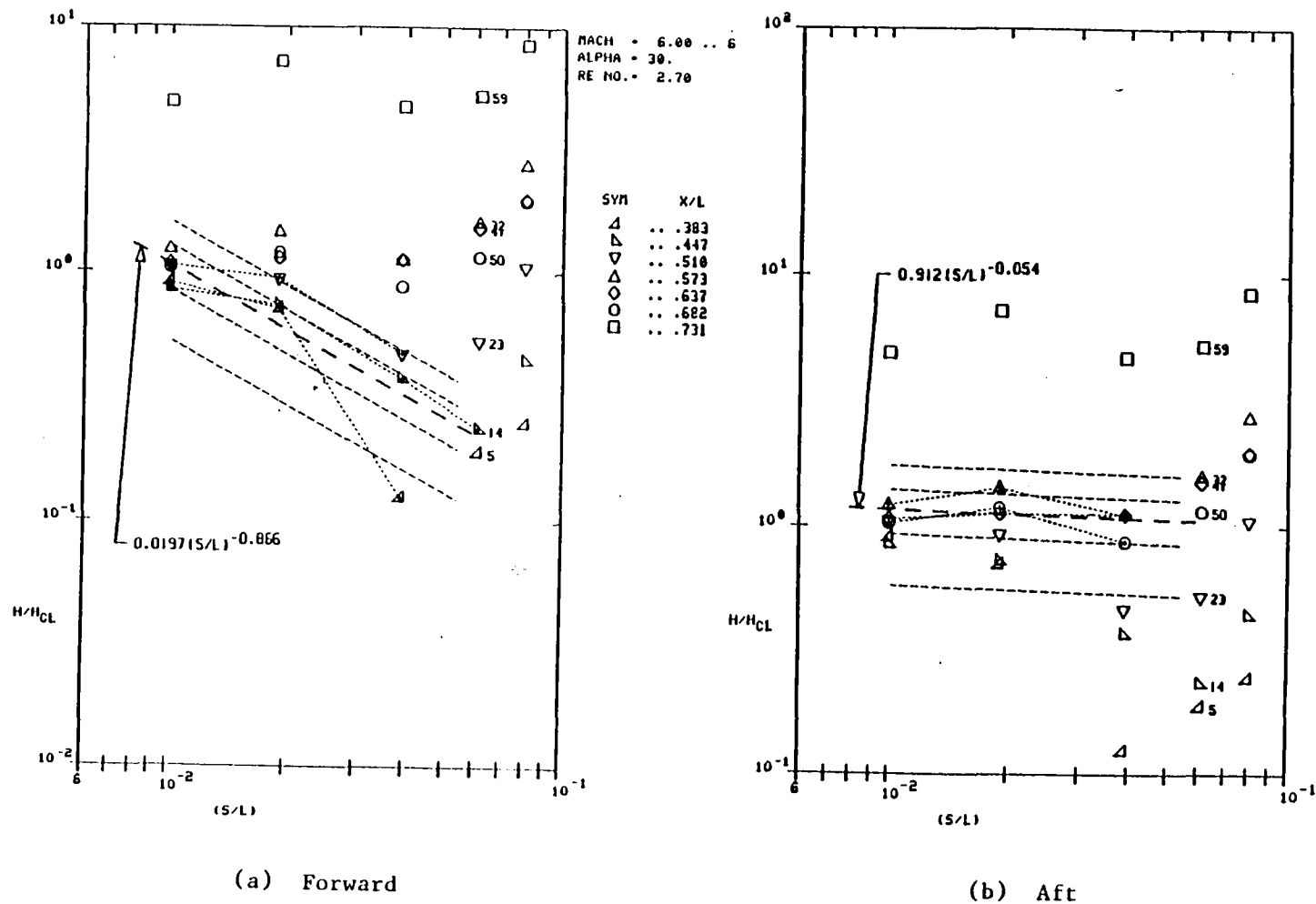


Figure 23 Upper Fuselage Heat Transfer Profiles, $M_\infty = 6$

* Related oil-flow pattern shown in Figure 19e

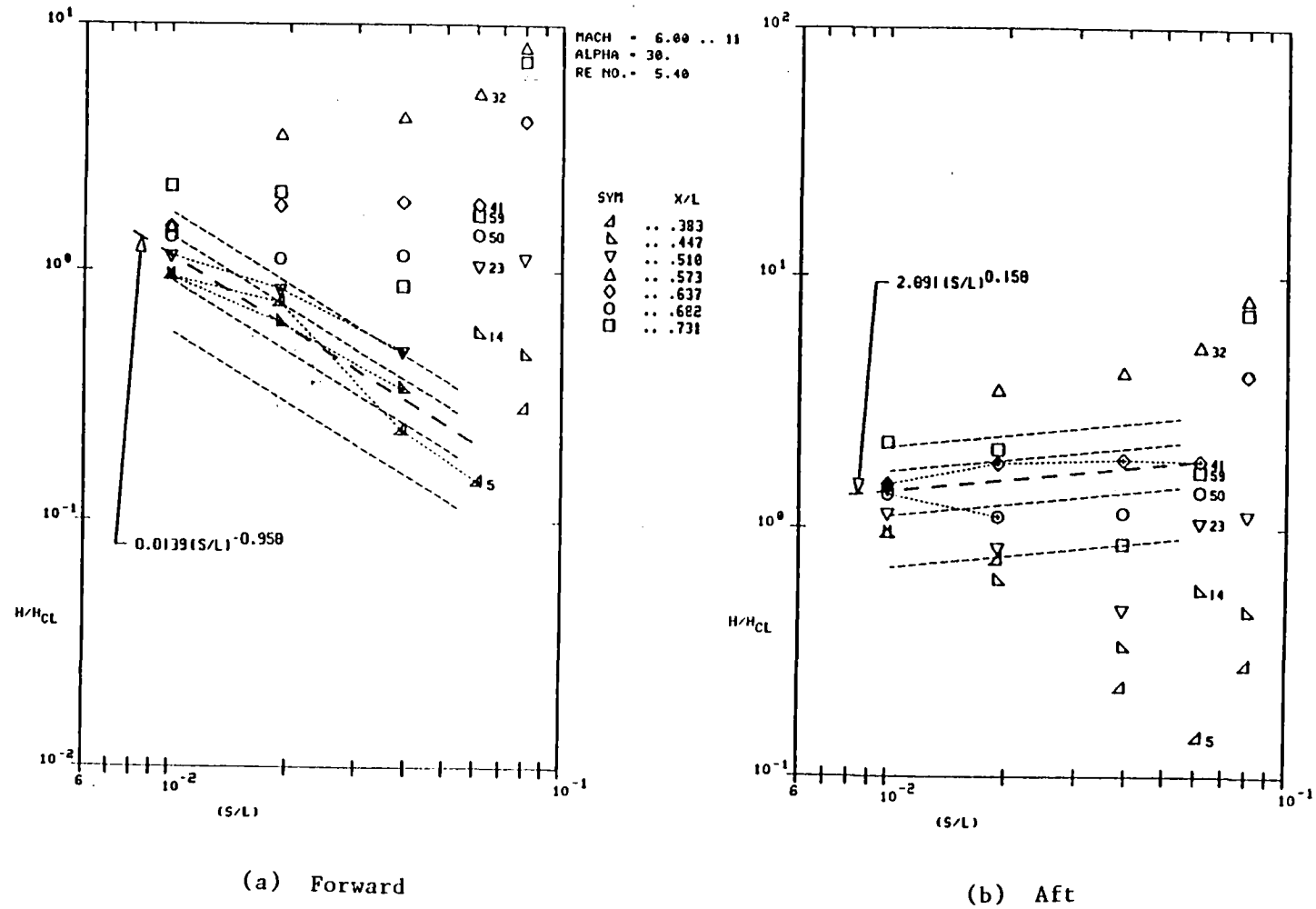


Figure 24 Upper Fuselage Heat Transfer Profiles, $M_{\infty} = 6$

* Related oil-flow pattern shown in Figure 19f

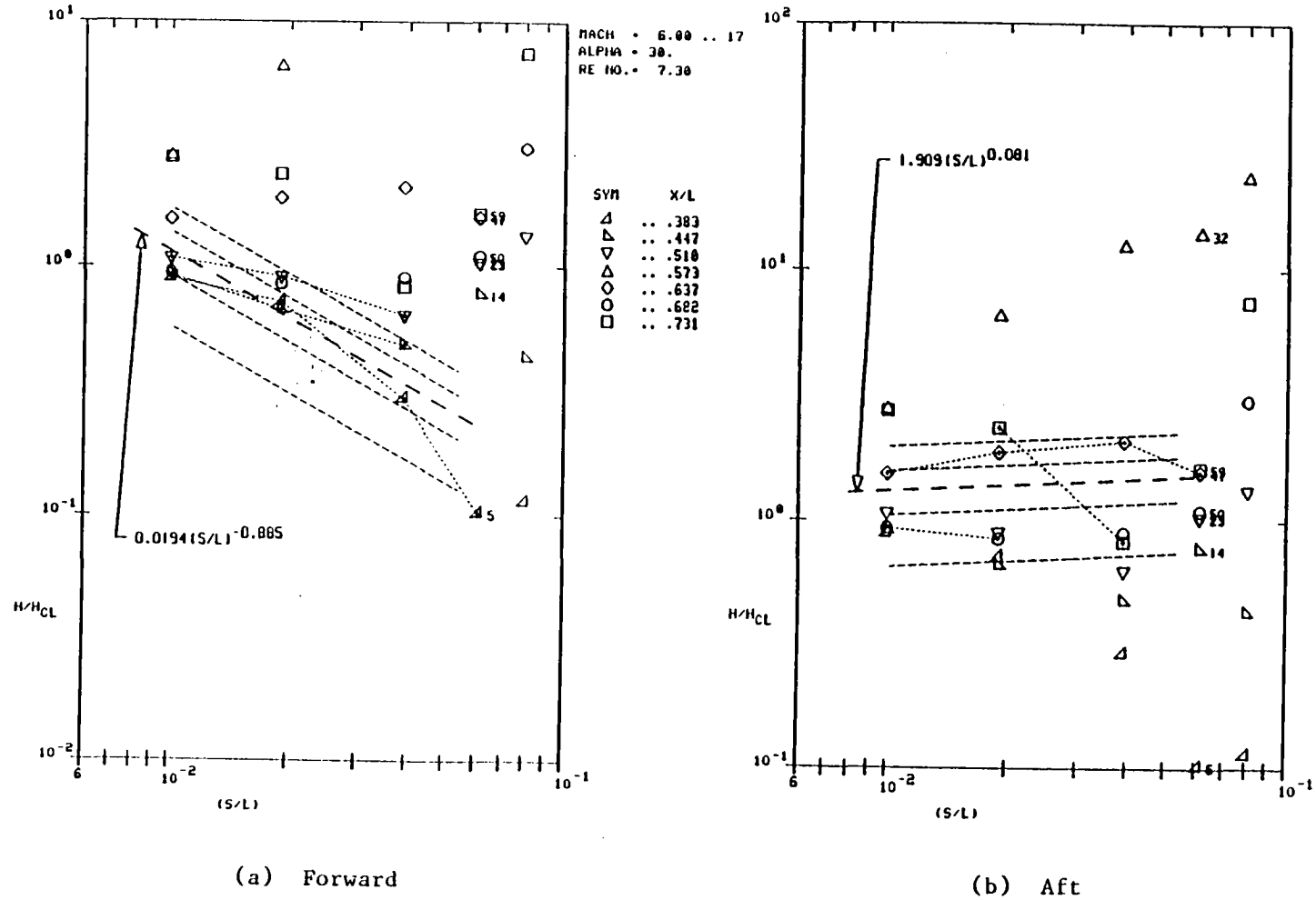


Figure 25 Upper Fuselage Heat Transfer Profiles, $M_\infty = 6$

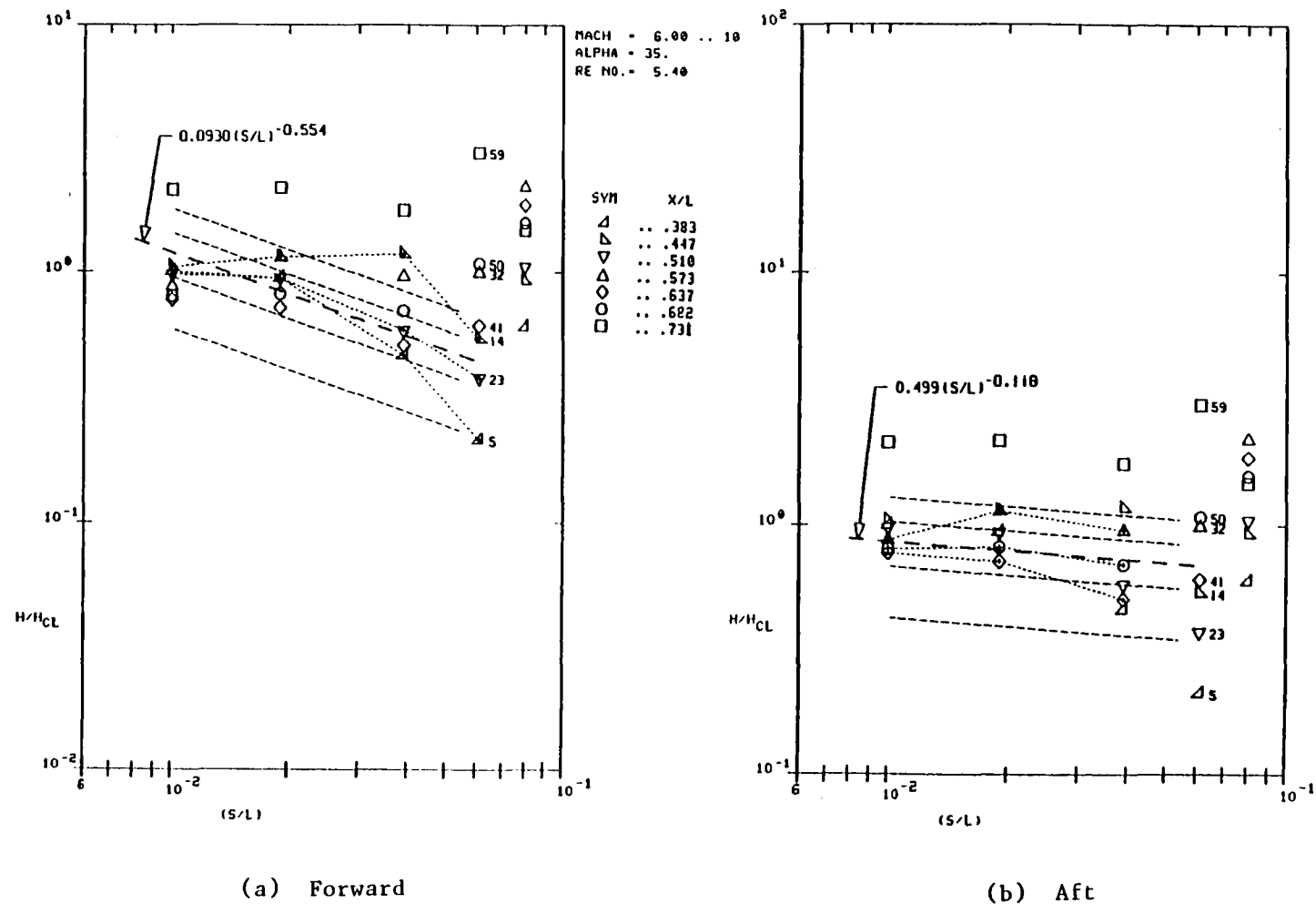


Figure 26 Upper Fuselage Heat Transfer Profiles, $M_\infty = 6$

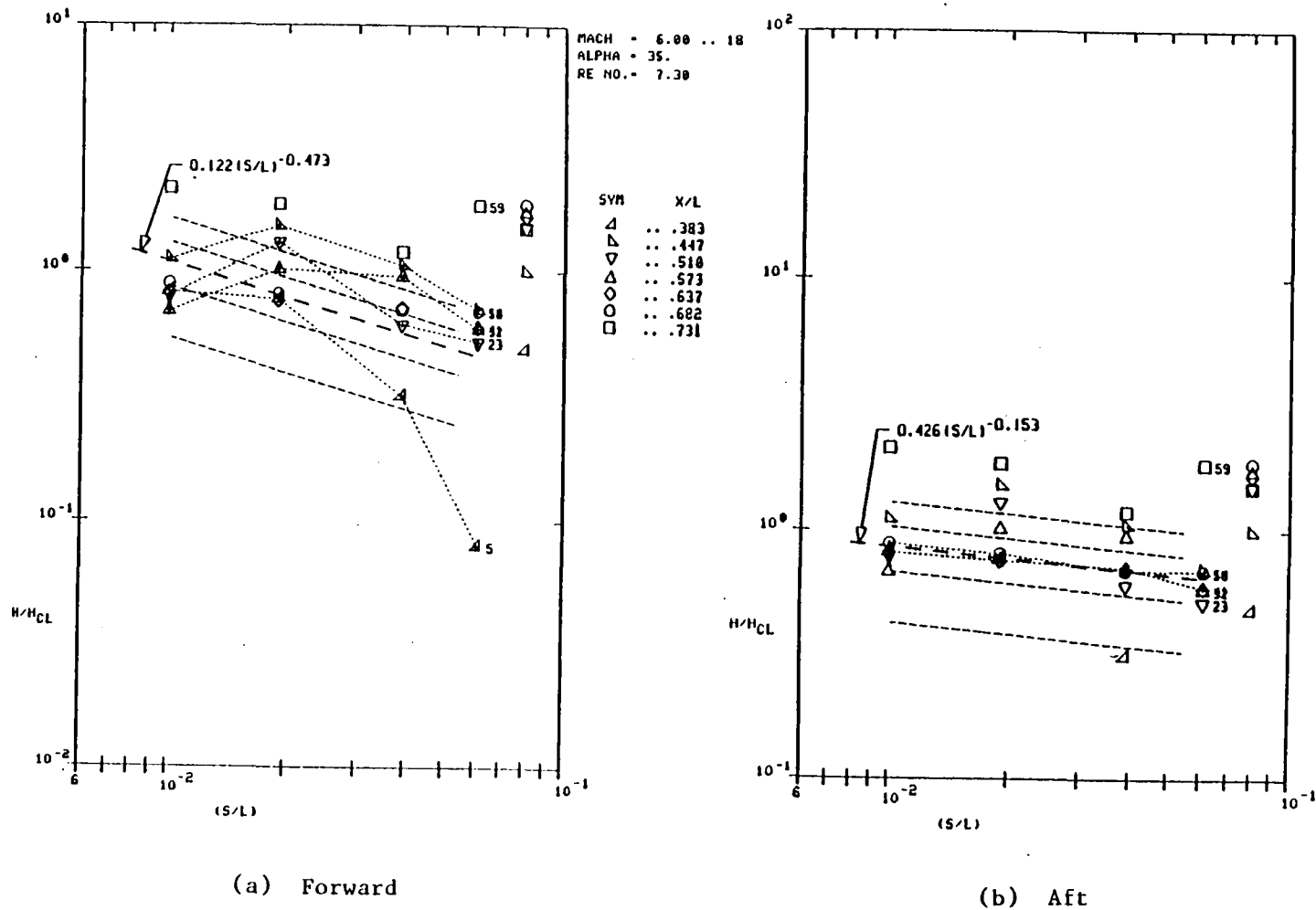
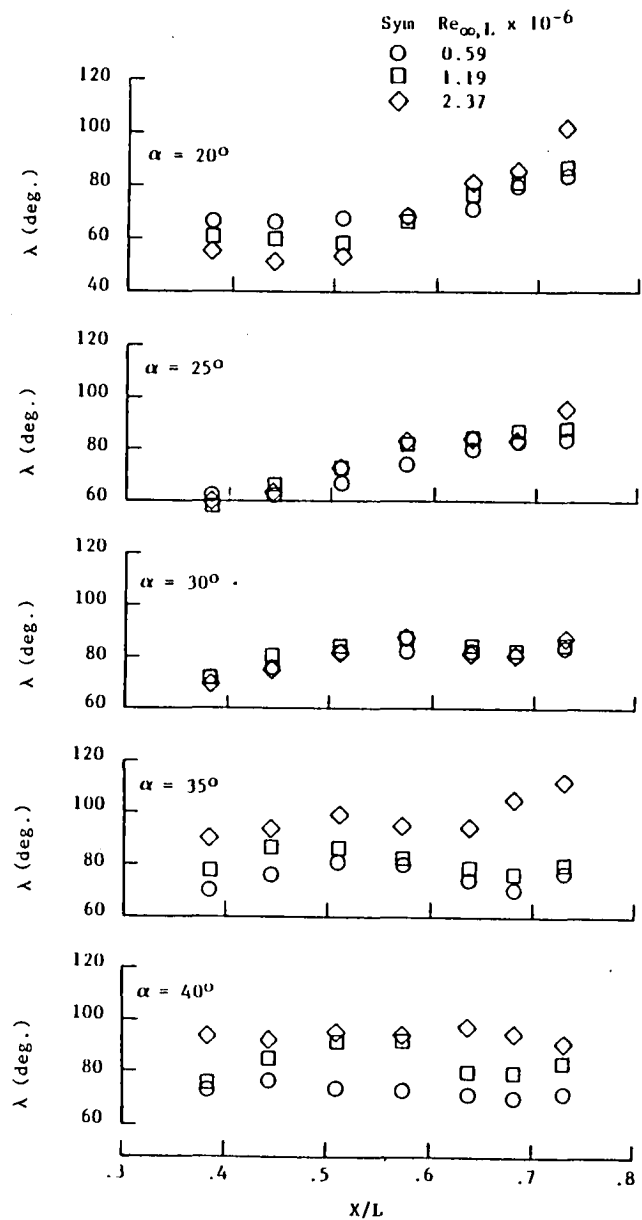
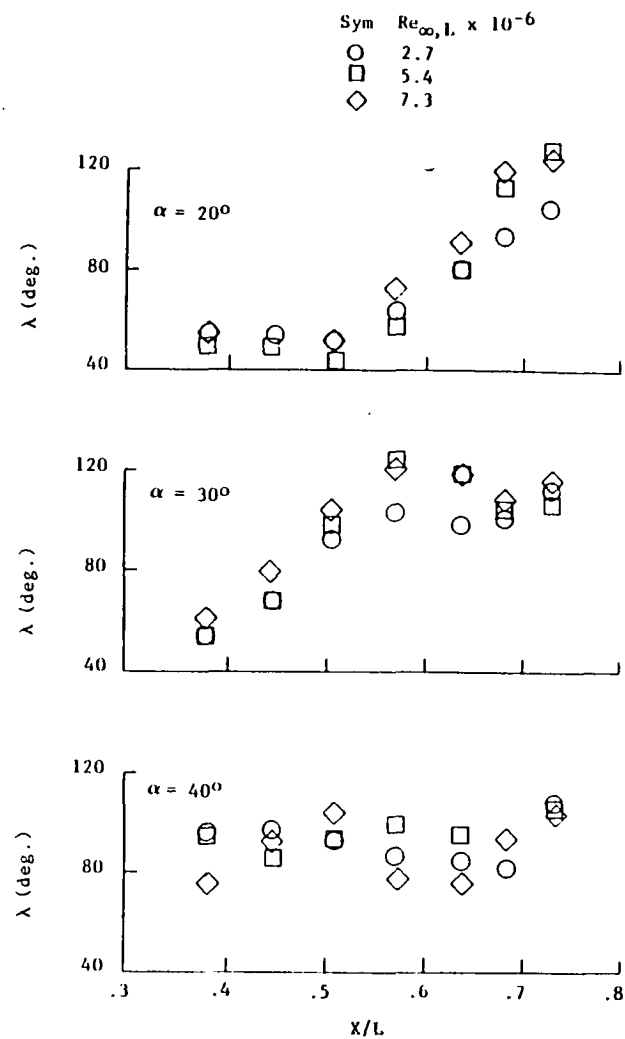


Figure 27 Upper Fuselage Heat Transfer Profiles, $M_\infty = 6$

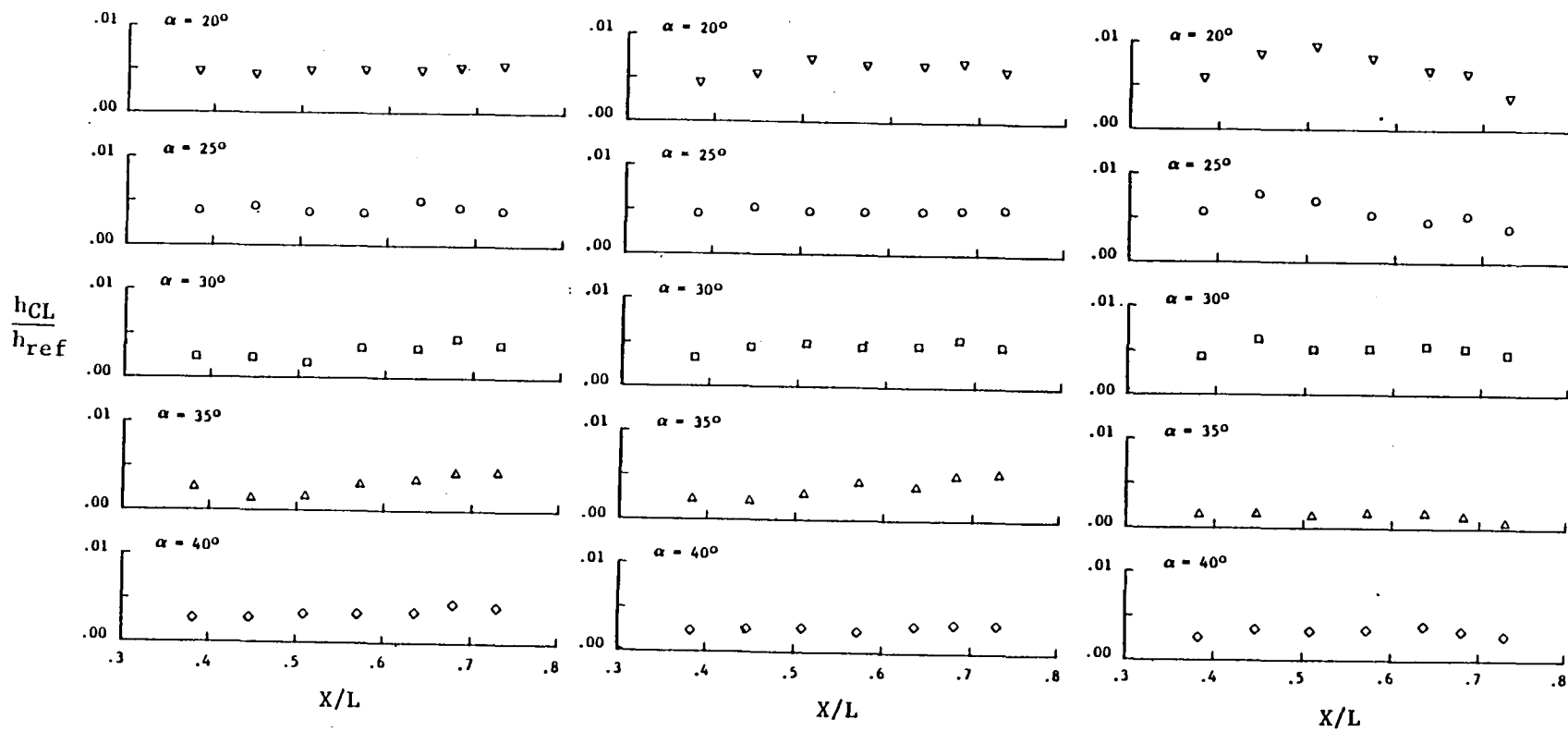


(a) Mach 10



(b) Mach 6

Figure 28 Effective Sweep Angles Measured from Oil-Flow Patterns



(a) $Re_{\infty, L} = 0.5 \times 10^6$

(b) $Re_{\infty, L} = 1.0 \times 10^6$

(c) $Re_{\infty, L} = 2.4 \times 10^6$

Figure 29 Mach 10 Upper Fuselage Centerline Heating Distributions

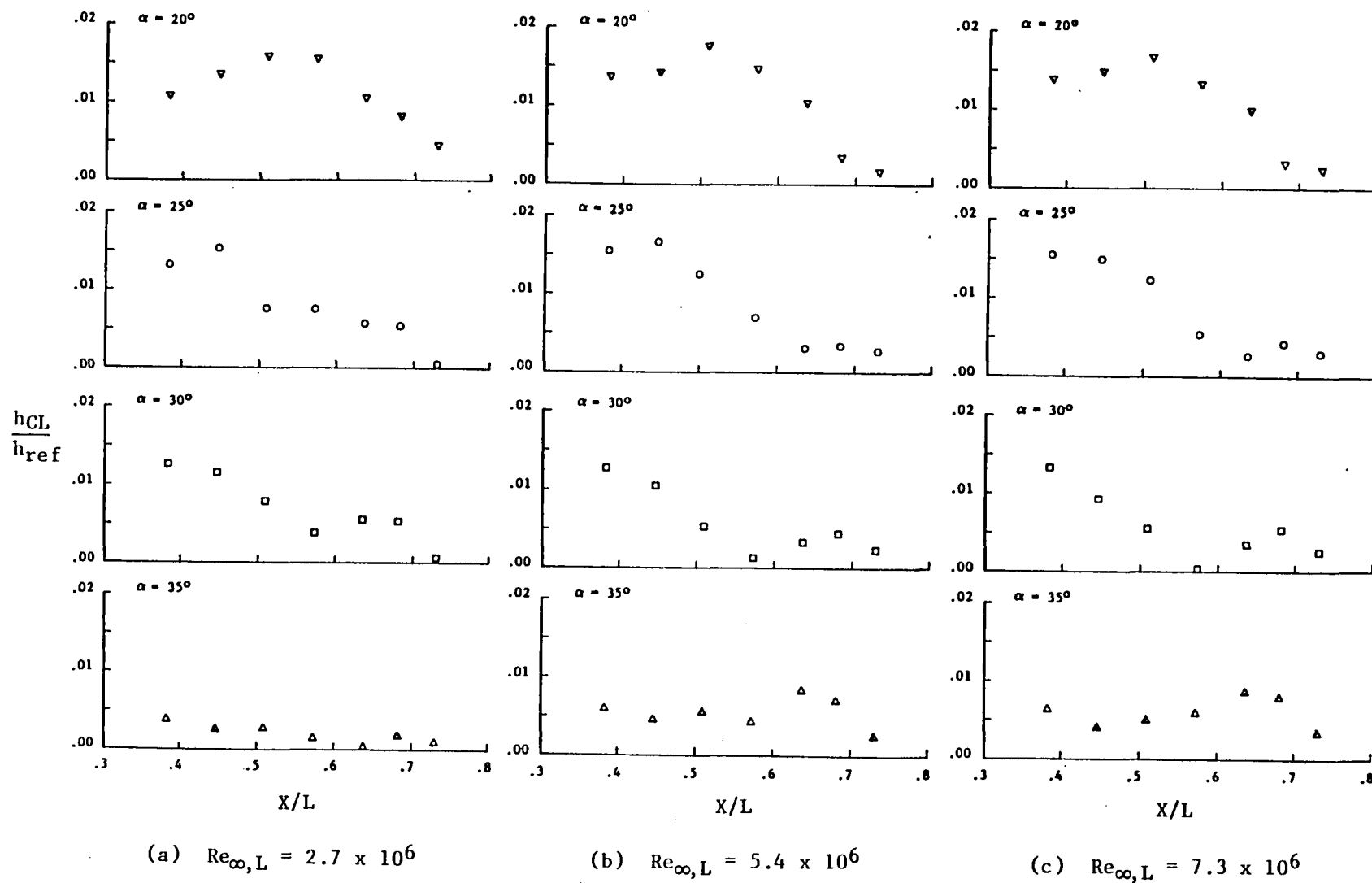
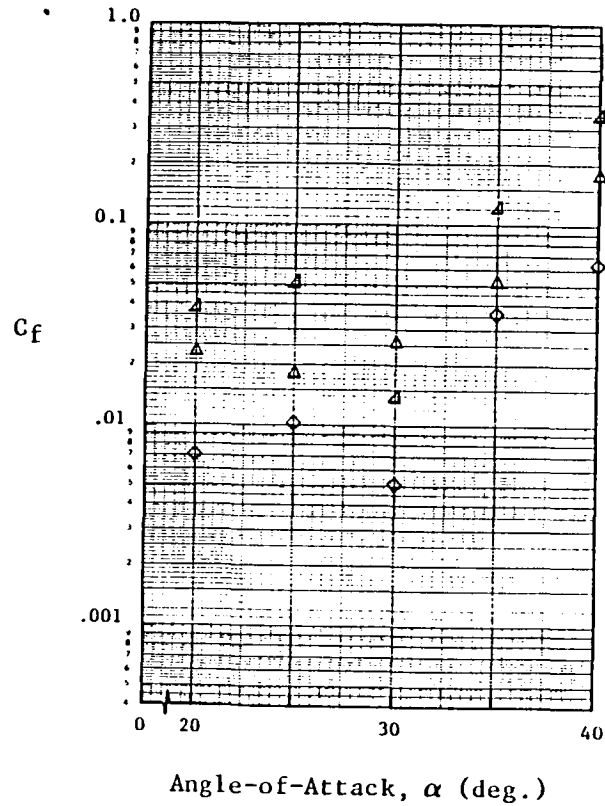
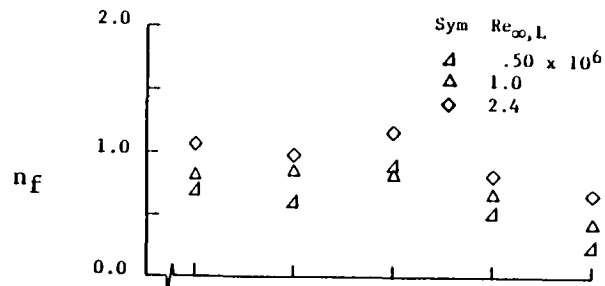
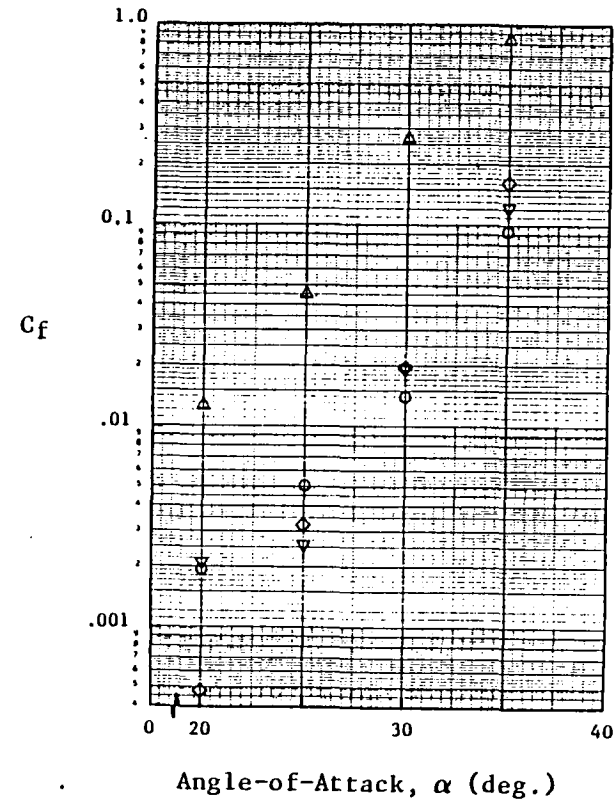
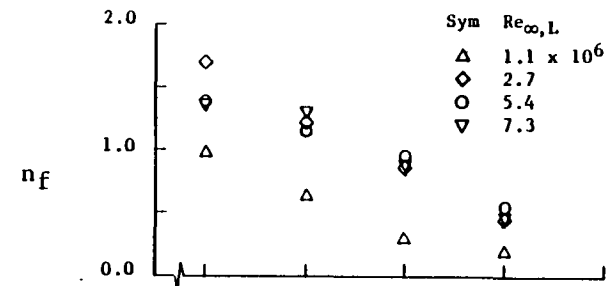


Figure 30 Mach 6 Upper Fuselage Centerline Heating Distributions

$$\frac{h}{h_{CL}} = C_f \left(\frac{s}{L} \right)^{-n_f}$$

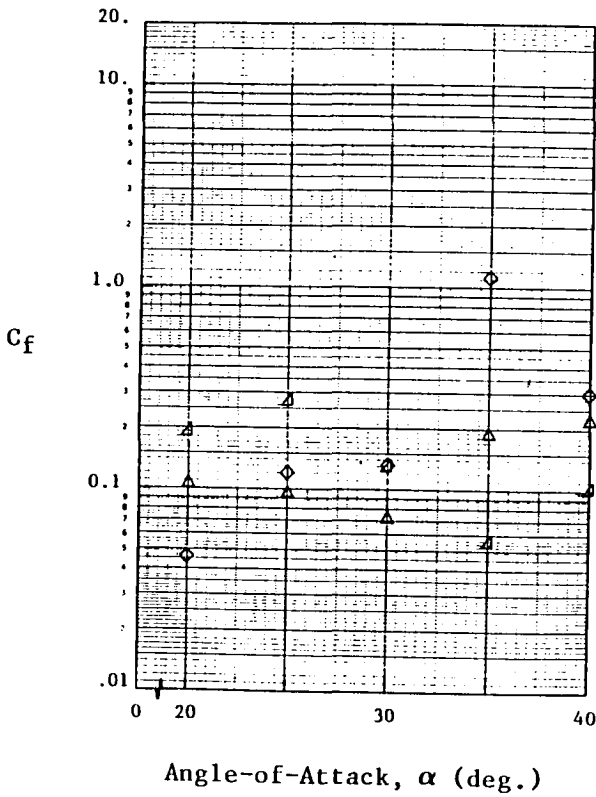
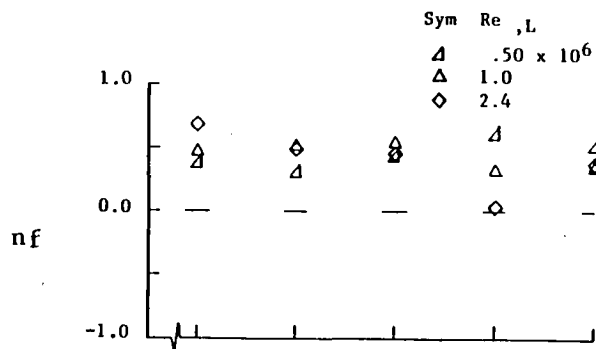


(a) Mach = 10



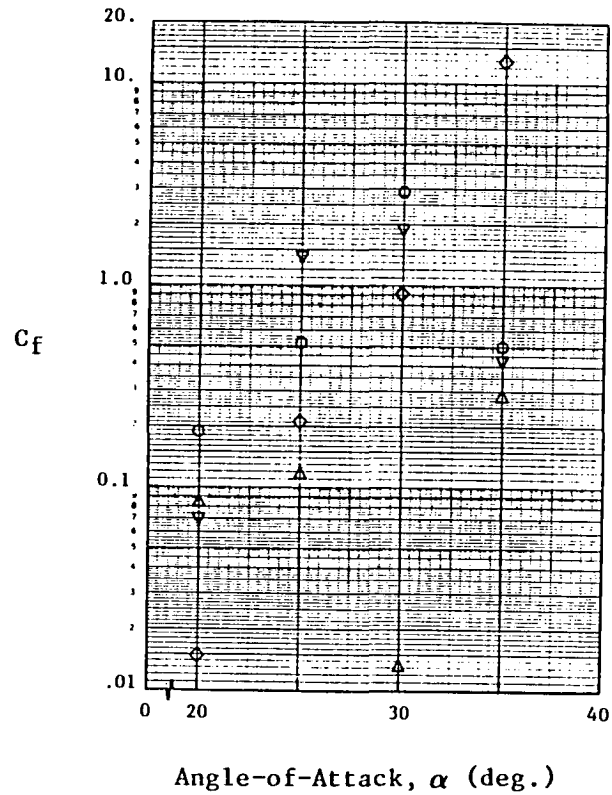
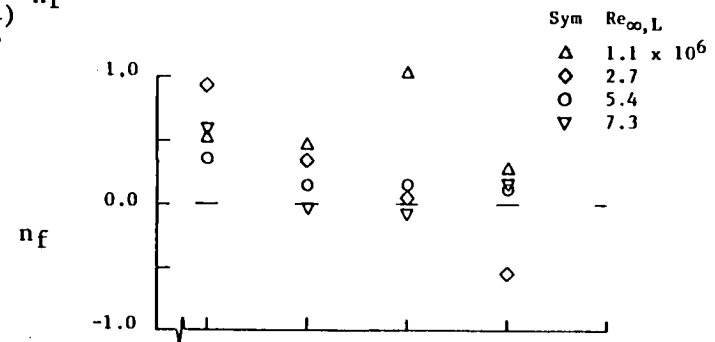
(b) Mach = 6

Figure 31 Forward Upper Fuselage Heating Correlation Parameters



(a) Mach = 10

$$\frac{h}{h_{CL}} = C_f \left(\frac{s}{L} \right)^{-nf}$$



(b) Mach = 6

Figure 32 Aft Upper Fuselage Heating Correlation Parameters

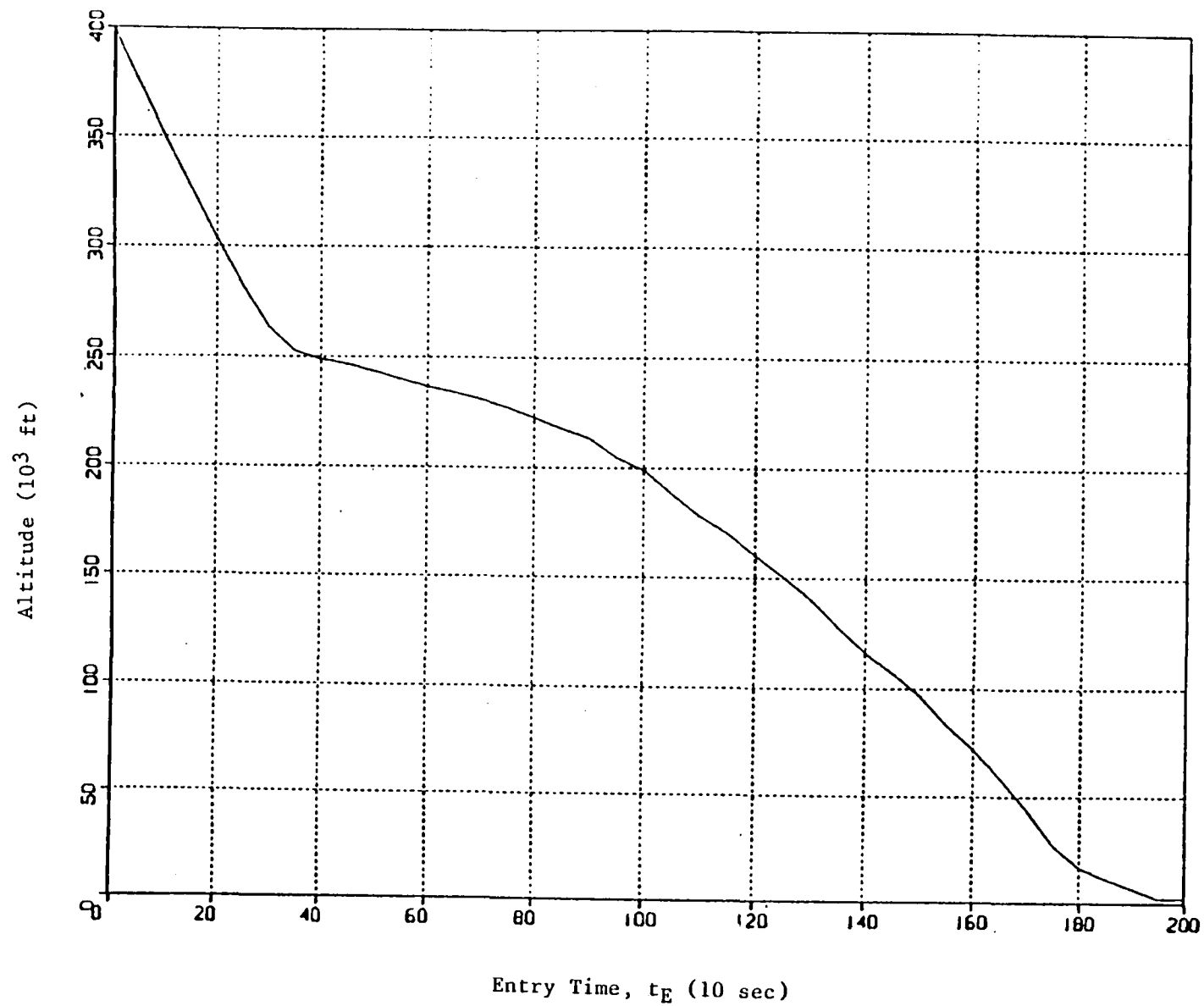


Figure 33a Trajectory History During STS-2 Entry, Altitude

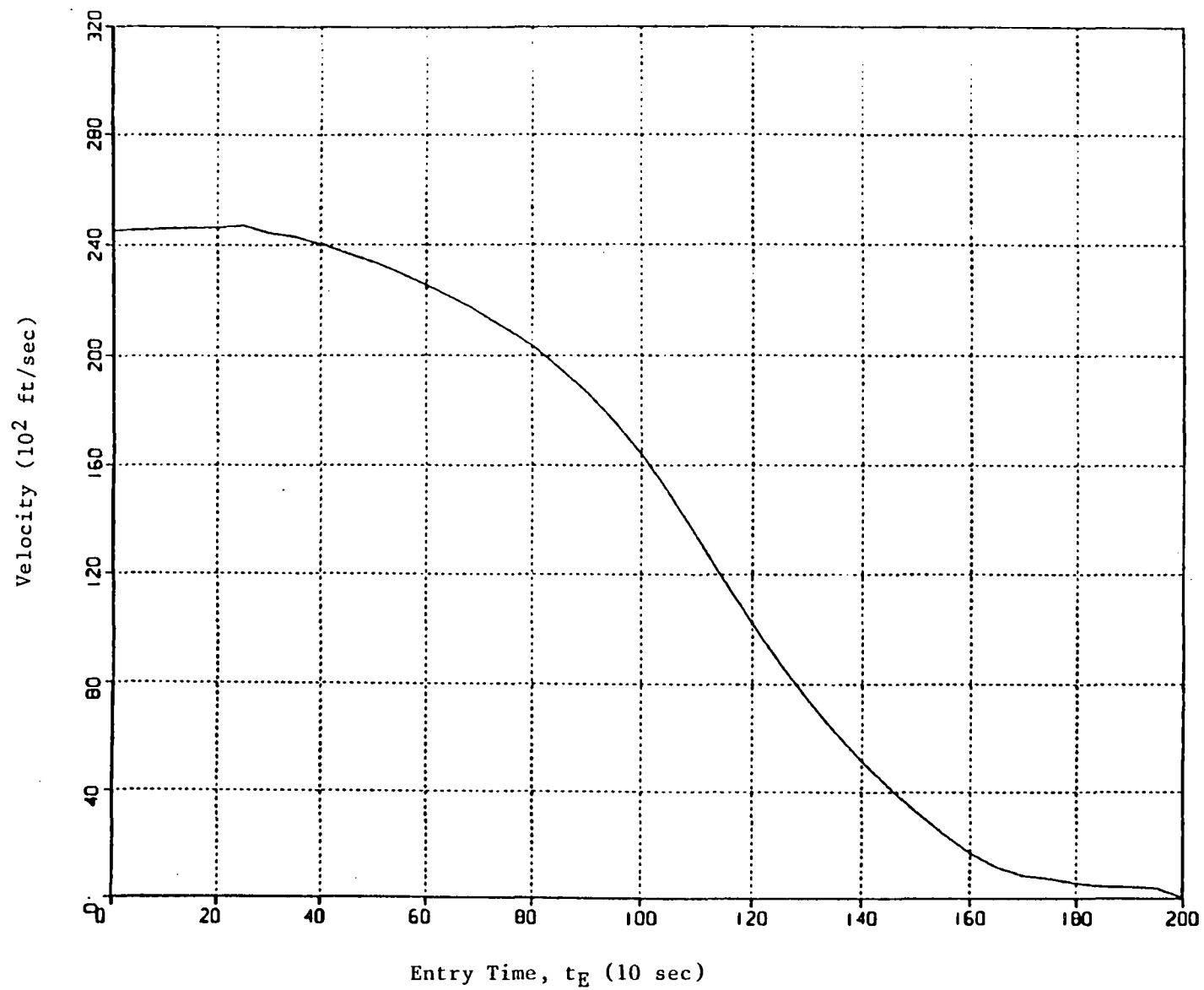


Figure 33b Trajectory History During STS-2 Entry, Velocity

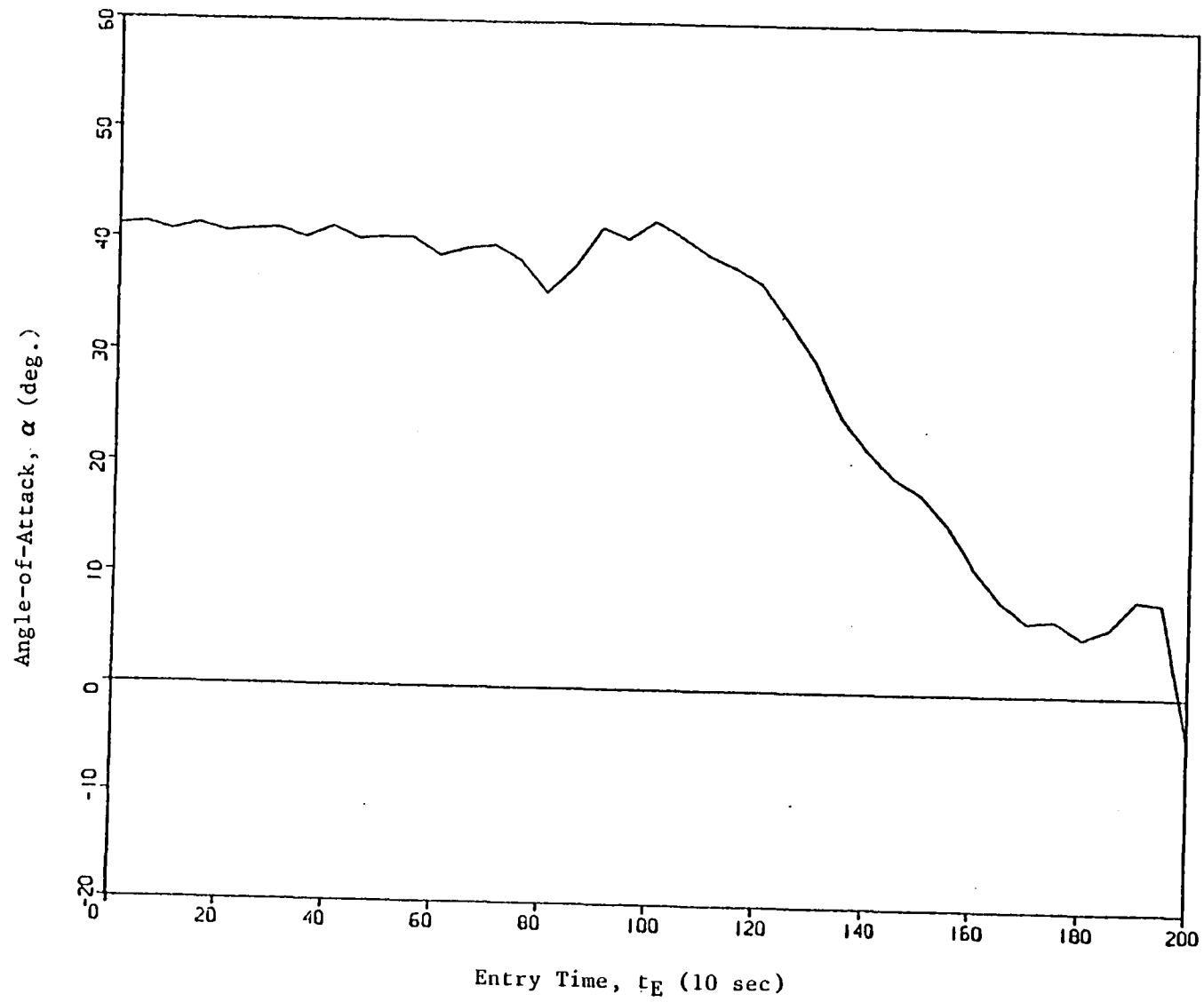


Figure 33c Trajectory History During STS-2 Entry, Angle of Attack

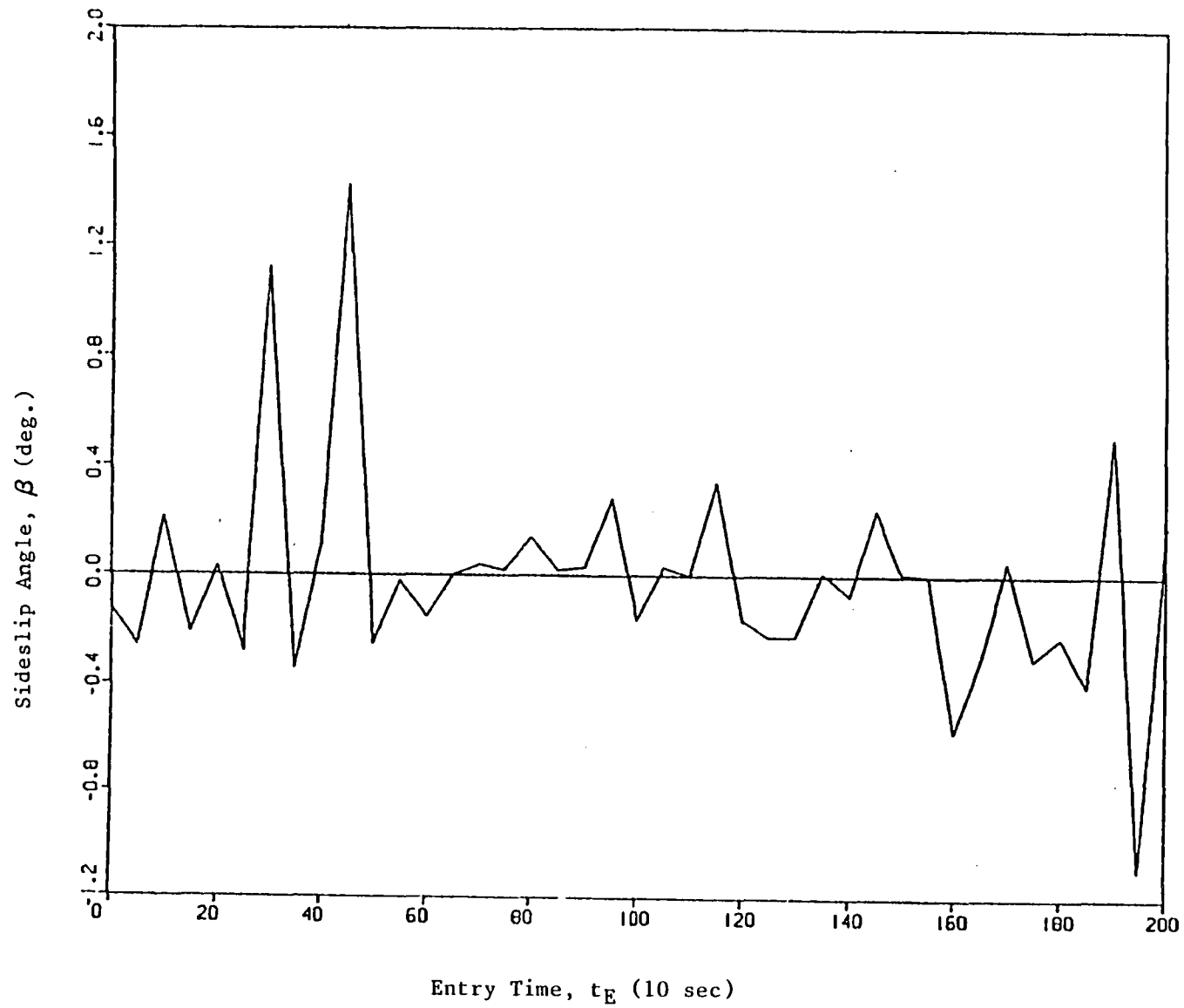


Figure 33d Trajectory History During STS-2 Entry, Sideslip Angle

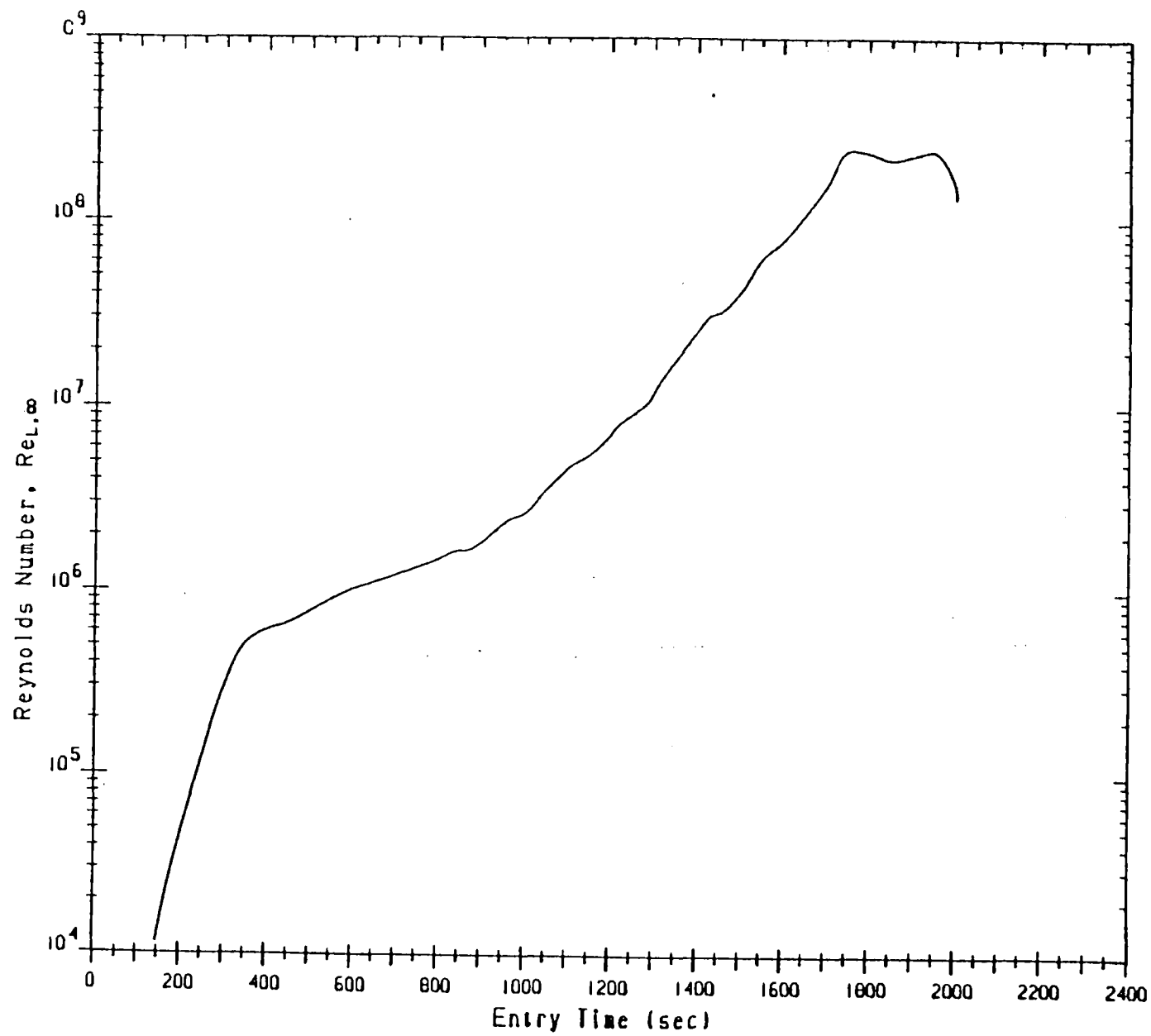


Figure 33e Trajectory History During STS-2 Entry, Reynolds Number

TIME (SEC)	T(U)	Q-REF .. (BTU/FT2/SEC)				ALPHA (DEG)	M-INF	RE-L-INF	BETA (DEG)	U-INF (FPS)	ALTITUDE (KFT)	T-INF (DEG R)	P-INF (PSF)
		0. F	400. F	800. F	1200. F								
0	--	2.2687E+00	2.2145E+00	2.1684E+00	2.1285E+00	41.11	19.62	2.550E+02	-0.13	24516	400.00	650.03	4.7861E-05
50	--	3.6581E+00	3.5707E+00	3.4964E+00	3.4320E+00	41.34	22.26	8.009E+03	-0.26	24547	375.38	506.04	9.6689E-05
100	--	6.4931E+00	6.3380E+00	6.2061E+00	6.0918E+00	40.69	25.04	3.040E+03	0.21	24576	350.92	400.84	2.4061E-04
150	--	9.7964E+00	9.5618E+00	9.3579E+00	9.1800E+00	41.30	27.11	1.161E+04	-0.21	24603	326.83	342.74	6.8695E-04
200	--	1.8780E+01	1.8330E+01	1.7940E+01	1.7599E+01	40.61	27.89	4.375E+04	0.02	24617	303.44	324.11	2.3302E-03
250	--	3.1924E+01	3.1161E+01	3.0499E+01	2.9921E+01	40.82	26.65	1.165E+05	-0.28	24698	281.68	357.50	7.4342E-03
300	--	4.9470E+01	4.8281E+01	4.7246E+01	4.6342E+01	40.93	26.22	2.830E+05	1.11	24438	263.48	361.50	1.8621E-02
350	--	6.4340E+01	6.2786E+01	6.1433E+01	6.0251E+01	40.14	26.21	5.027E+05	-0.34	24279	252.51	357.12	3.2551E-02
400	--	6.8407E+01	6.6742E+01	6.5291E+01	6.4021E+01	41.13	25.94	6.050E+05	0.11	24009	248.74	356.62	3.9502E-02
450	--	6.9455E+01	6.7749E+01	6.6259E+01	6.4954E+01	40.05	25.59	6.626E+05	1.42	23693	246.69	356.80	4.3891E-02
476	--	7.0810E+01	6.9063E+01	6.7535E+01	6.6196E+01	40.34	25.40	7.102E+05	-0.00	23528	245.16	357.19	4.7469E-02
481	*	7.1118E+01	6.9361E+01	6.7825E+01	6.6478E+01	40.32	25.36	7.207E+05	0.05	23496	244.84	357.30	4.8259E-02
500	--	7.2404E+01	7.0609E+01	6.9038E+01	6.7660E+01	40.23	25.20	7.645E+05	-0.25	23369	243.52	357.89	5.1630E-02
550	--	7.4749E+01	7.2873E+01	7.1229E+01	6.9783E+01	40.23	24.69	8.900E+05	-0.02	22985	239.95	360.54	6.1940E-02
600	--	7.6236E+01	7.4295E+01	7.2590E+01	7.1088E+01	38.65	24.08	1.015E+06	-0.15	22541	236.52	364.79	7.3649E-02
650	--	7.5618E+01	7.3663E+01	7.1940E+01	7.0419E+01	39.36	23.44	1.105E+06	-0.00	22076	233.96	369.25	8.3719E-02
700	--	7.5349E+01	7.3365E+01	7.1612E+01	7.0060E+01	39.67	22.67	1.215E+06	0.04	21558	230.83	376.35	9.7633E-02
706	--	7.5378E+01	7.3388E+01	7.1629E+01	7.0071E+01	39.86	22.56	1.230E+06	-0.00	21489	230.41	377.47	9.9683E-02
711	*	7.5373E+01	7.3379E+01	7.1616E+01	7.0054E+01	39.79	22.47	1.242E+06	-0.06	21430	230.05	378.43	1.0140E-01
750	--	7.4927E+01	7.2910E+01	7.1122E+01	6.9534E+01	38.34	21.74	1.336E+06	0.02	20973	227.20	387.17	1.1626E-01
800	--	7.4612E+01	7.2553E+01	7.0720E+01	6.9087E+01	35.50	20.62	1.482E+06	0.14	20340	222.53	404.80	1.4433E-01
803	--	7.4681E+01	7.2617E+01	7.0779E+01	6.9141E+01	35.72	20.56	1.494E+06	0.19	20304	222.23	405.68	1.4631E-01
806	*	7.4774E+01	7.2705E+01	7.0862E+01	6.9219E+01	34.66	20.51	1.506E+06	0.29	20269	221.92	406.58	1.4838E-01
850	--	7.2562E+01	7.0487E+01	6.8630E+01	6.6968E+01	37.86	19.47	1.660E+06	0.02	19513	217.75	418.01	1.7869E-01
863	--	7.0756E+01	6.8715E+01	6.6885E+01	6.5246E+01	39.51	19.25	1.661E+06	-0.34	19316	217.42	418.85	1.8124E-01
866	*	7.0391E+01	6.8355E+01	6.6530E+01	6.4894E+01	40.41	19.20	1.665E+06	-0.20	19266	217.28	419.21	1.8239E-01
900	--	6.8855E+01	6.6805E+01	6.4958E+01	6.3298E+01	41.36	18.37	1.835E+06	0.03	18650	213.33	428.75	2.1640E-01
950	--	6.7827E+01	6.5691E+01	6.3753E+01	6.1999E+01	40.39	16.98	2.325E+06	0.28	17583	204.57	446.15	3.1255E-01
951	--	6.7782E+01	6.5645E+01	6.3705E+01	6.1950E+01	40.34	16.96	2.335E+06	0.23	17561	204.41	446.43	3.1465E-01
956	*	6.7494E+01	6.5353E+01	6.3408E+01	6.1646E+01	40.21	16.82	2.383E+06	0.20	17449	203.63	447.72	3.2483E-01
1000	--	6.0421E+01	5.8378E+01	5.6507E+01	5.4802E+01	42.00	15.68	2.644E+06	-0.16	16394	198.85	454.89	3.9473E-01
1050	--	5.5772E+01	5.3691E+01	5.1762E+01	4.9988E+01	40.62	14.15	3.533E+06	0.03	14975	188.21	466.12	6.0346E-01
1071	--	5.2646E+01	5.0576E+01	4.8646E+01	4.6864E+01	40.07	13.48	3.957E+06	-0.02	14313	183.91	468.96	7.1478E-01
1076	*	5.1753E+01	4.9691E+01	4.7765E+01	4.5985E+01	39.85	13.32	4.061E+06	-0.07	14153	182.91	469.49	7.4343E-01
1100	--	4.7670E+01	4.5638E+01	4.3728E+01	4.1952E+01	38.96	12.58	4.611E+06	0.00	13390	178.06	471.38	8.9892E-01
1150	--	3.7269E+01	3.5388E+01	3.3595E+01	3.1909E+01	37.89	11.05	5.471E+06	0.34	11768	170.29	472.24	1.2174E+00
1200	--	2.8996E+01	2.7204E+01	2.5470E+01	2.3823E+01	36.60	9.60	7.085E+06	-0.16	10205	160.28	469.86	1.8019E+00
1211	--	2.7446E+01	2.5661E+01	2.3927E+01	2.2277E+01	35.67	9.29	7.664E+06	0.14	9861	157.54	468.61	2.0071E+00
1216	*	2.6854E+01	2.5065E+01	2.3325E+01	2.1668E+01	34.78	9.15	7.893E+06	0.10	9707	156.45	468.04	2.0951E+00
1250	--	2.1936E+01	2.0210E+01	1.8515E+01	1.6891E+01	33.28	8.26	9.079E+06	-0.22	8723	150.57	464.40	2.6439E+00
1291	--	1.7300E+01	1.5614E+01	1.3944E+01	1.2331E+01	30.50	7.30	1.107E+07	0.06	7656	142.96	458.33	3.5871E+00
1296	*	1.7065E+01	1.5355E+01	1.3658E+01	1.2019E+01	30.07	7.18	1.159E+07	0.56	7530	141.53	457.04	3.8001E+00
1300	--	1.6797E+01	1.5075E+01	1.3364E+01	1.1711E+01	29.70	7.10	1.206E+07	-0.22	7428	140.33	455.93	3.9893E+00
1341	--	1.3599E+01	1.1820E+01	1.0039E+01	8.3077E+00	25.54	6.25	1.691E+07	0.20	6460	129.75	445.03	6.1595E+00
1346	*	1.3126E+01	1.1351E+01	9.5722E+00	7.8427E+00	25.04	6.14	1.752E+07	0.04	6341	128.59	443.74	6.4643E+00
1350	--	1.2764E+01	1.0992E+01	9.2151E+00	7.4864E+00	24.72	6.06	1.800E+07	0.01	6249	127.68	442.71	6.7138E+00
1400	--	8.9868E+00	7.2177E+00	5.4289E+00	3.6794E+00	21.70	5.09	2.551E+07	-0.07	5171	116.33	429.28	1.0876E+01
1421	--	7.6940E+00	5.9105E+00	4.1020E+00	2.3297E+00	20.23	4.71	2.955E+07	0.35	4748	111.56	423.45	1.3384E+01
1426	*	7.3349E+00	5.5633E+00	3.7656E+00	2.0032E+00	20.08	4.61	3.039E+07	0.01	4648	110.56	422.22	1.3982E+01
1450	--	5.5607E+00	3.9093E+00	2.2287E+00	5.7787E-01	19.37	4.17	3.195E+07	0.24	4180	107.40	418.35	1.6074E+01
1500	--	3.2065E+00	1.6460E+00	4.9987E-02	-1.5229E+00	17.94	3.32	4.157E+07	0.01	3282	97.37	406.31	2.5257E+01
1550	--	1.5208E+00	6.1245E-02	-1.4372E+00	-2.9176E+00	15.26	2.50	6.252E+07	0.01	2423	83.58	391.40	4.8035E+01
1600	--	5.2573E-01	-7.8224E-01	-2.1284E+00	-3.4603E+00	11.35	1.77	7.858E+07	-0.57	1691	72.31	381.73	8.2643E+01
1650	--	7.2897E-02	-1.0449E+00	-2.1968E+00	-3.3375E+00	8.36	1.22	1.090E+08	-0.30	1153	58.62	374.49	1.6232E+02
1700	--	-8.6546E-02	-1.7016E+00	-3.2752E+00	-4.8202E+00	6.62	.94	1.563E+08	0.05	895	43.76	373.51	2.9831E+02

* -- CONDITIONS AT WHICH LEESIDE HEATING ENVIRONMENT ESTIMATED

Figure 34 STS-2 Entry Trajectory and Reference Heating Rates

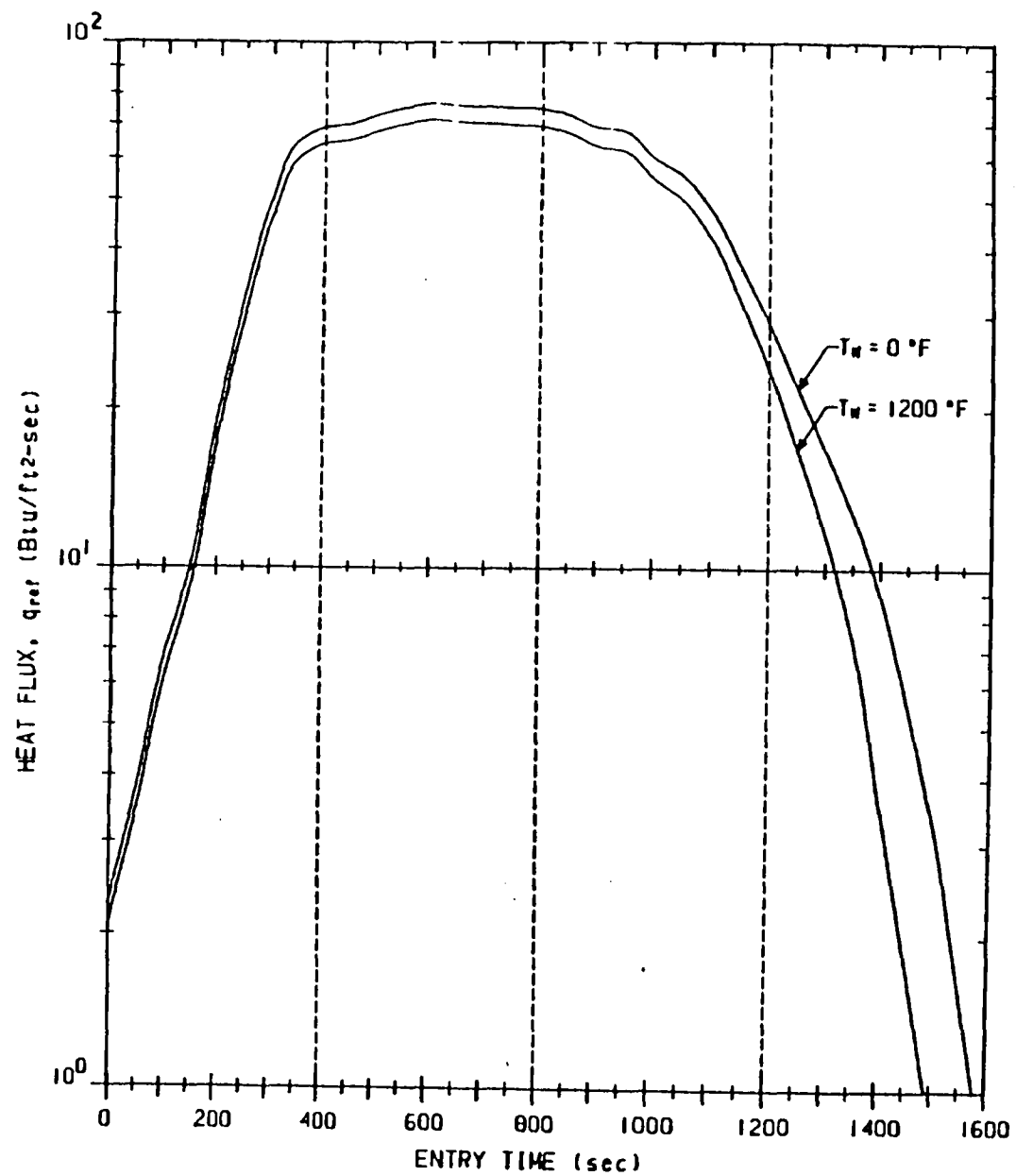


Figure 35 Reference Heating Rate History During STS-2 Entry

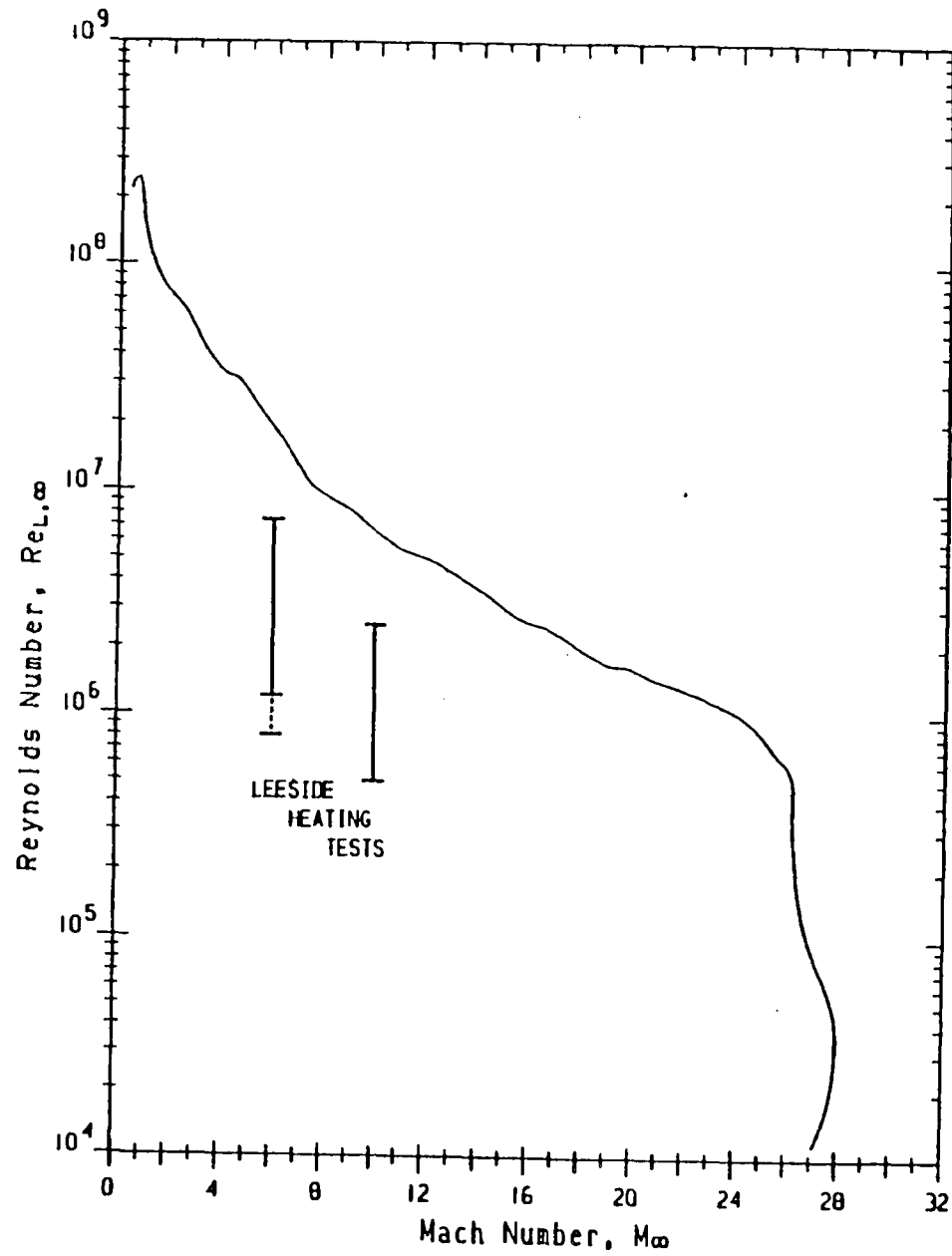
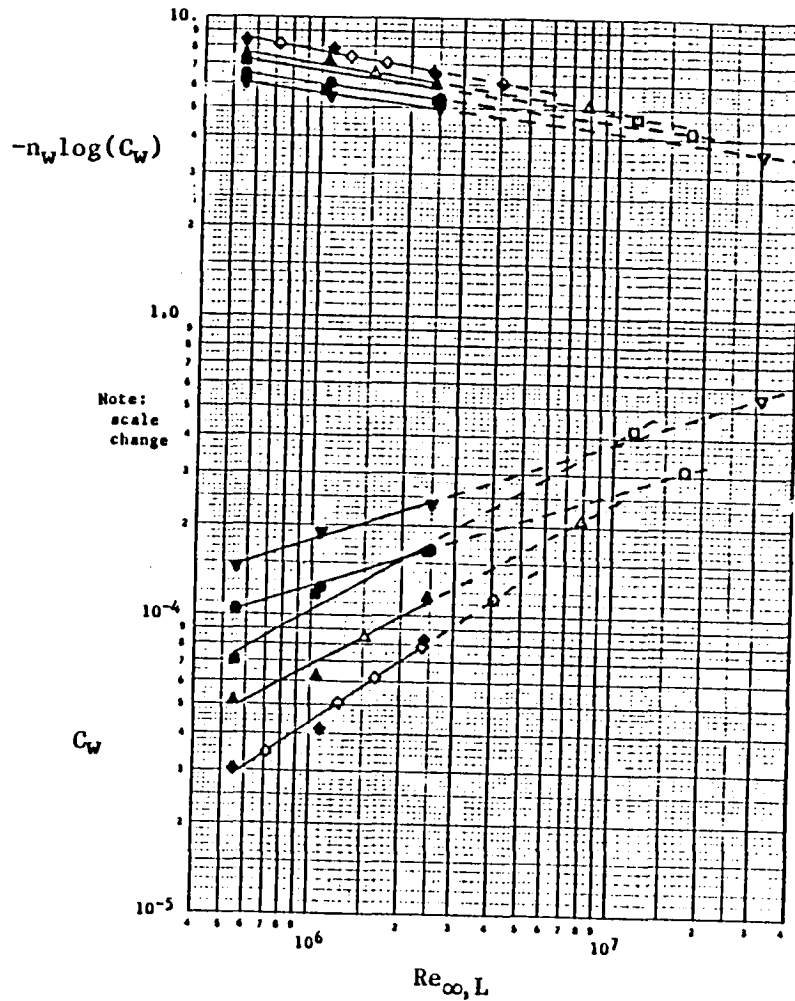


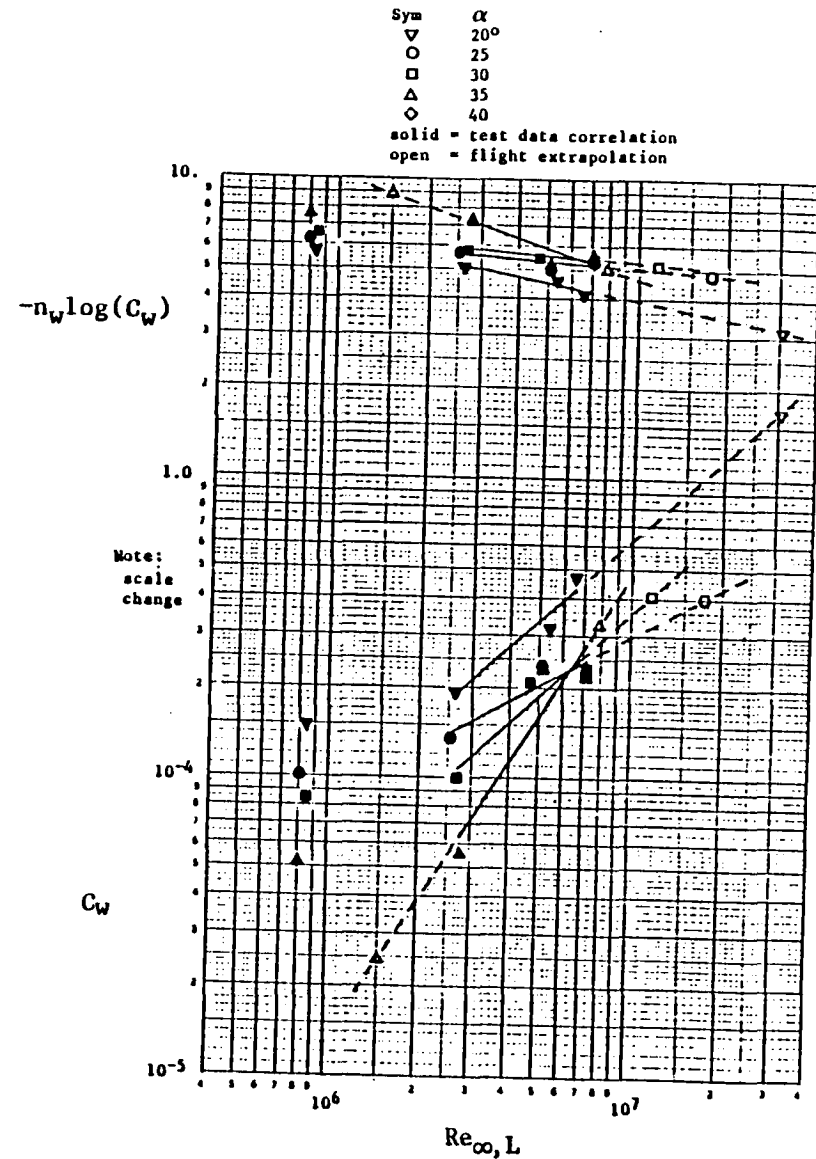
Figure 36 Reynolds Number Variation with Mach Number During STS-2 Entry

$$\frac{h}{h_{ref}} = C_w \left(\frac{s}{L} \right)^{-n_w}$$

68



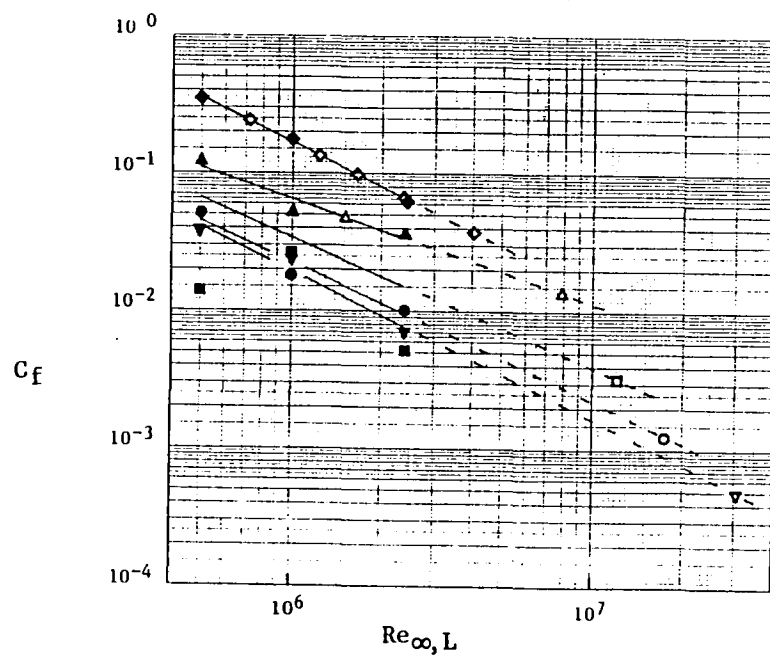
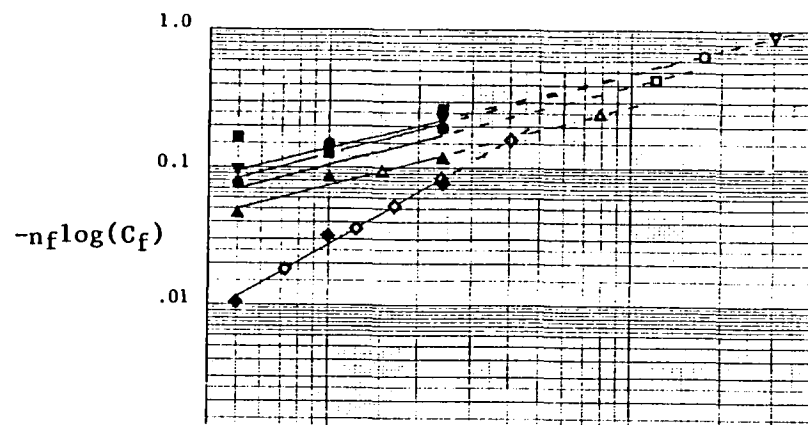
(a) Mach = 10



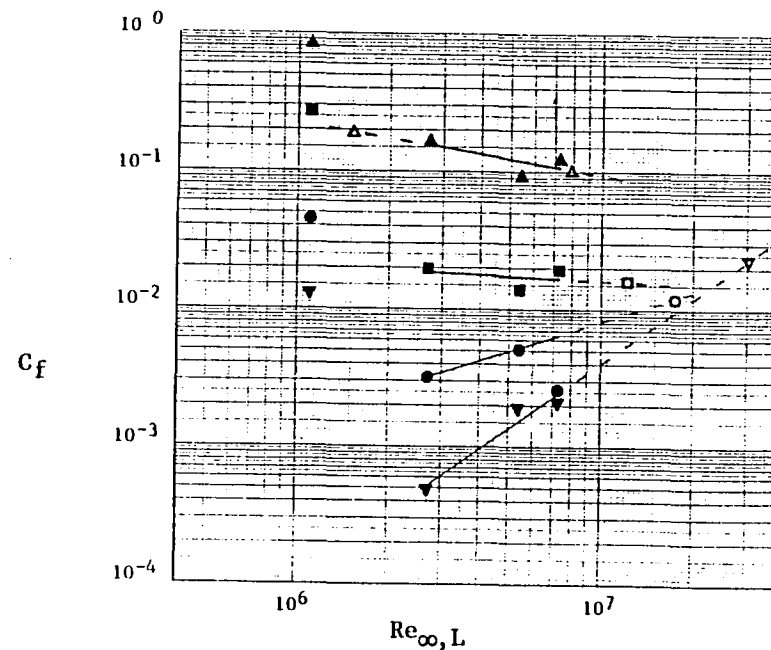
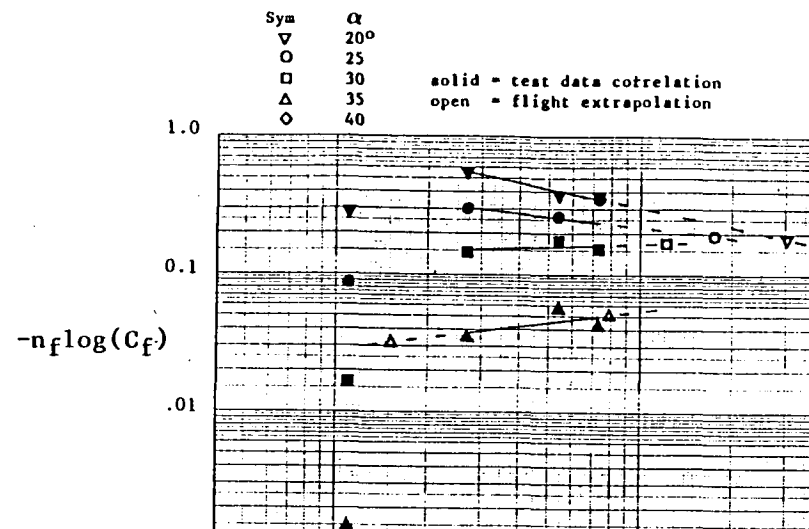
(b) Mach = 6

Figure 37 Wing Leaside Correlation Variations with Reynolds Number

$$\frac{h}{h_{CL}} = C_f \left(\frac{s}{L}\right)^{-n_f}$$



(a) Mach = 10



(b) Mach = 6

Figure 38 Forward Upper Fuselage Correlation Variation with Reynolds Number

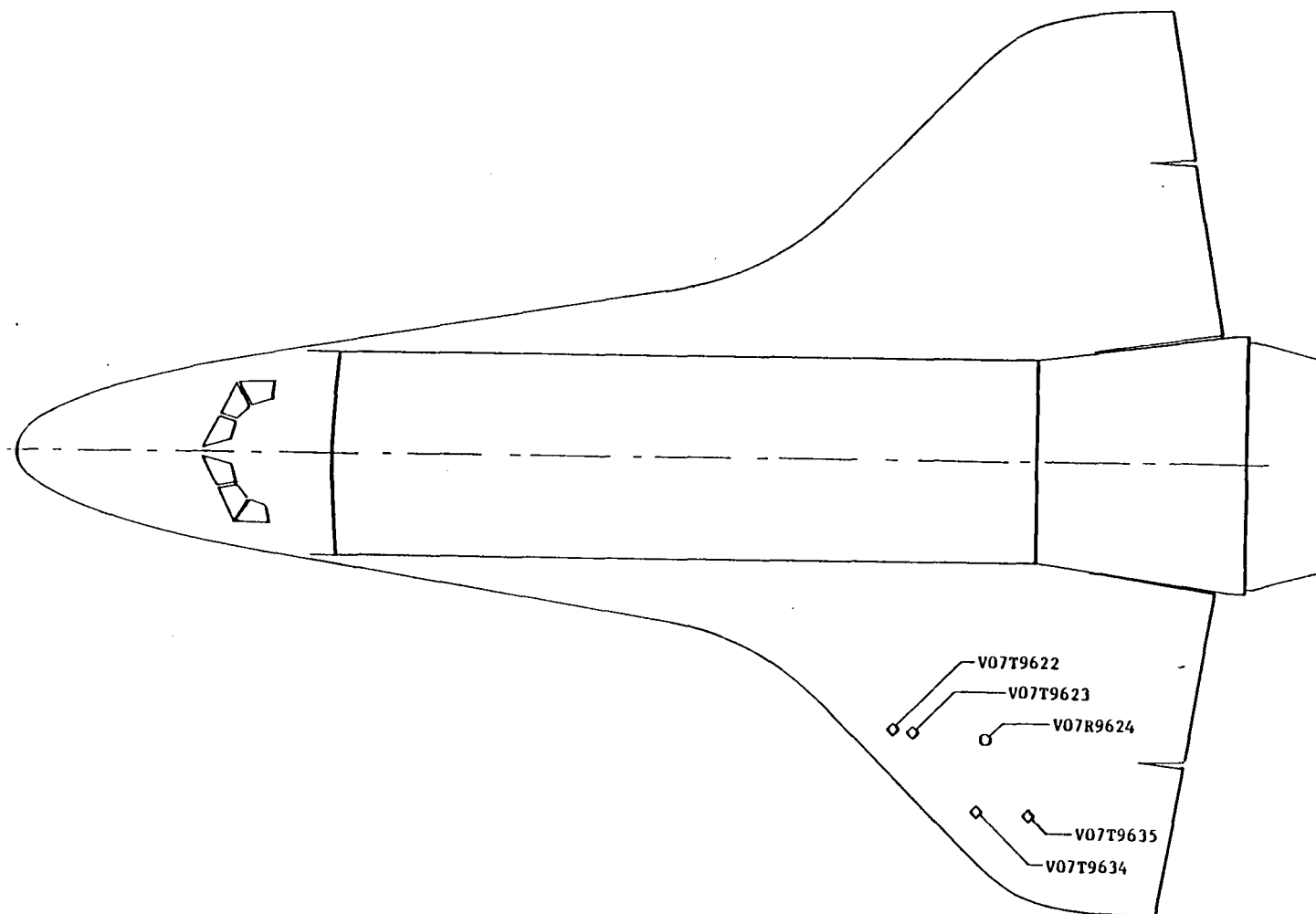


Figure 39 Flight Comparison Wing Leese Side DFI

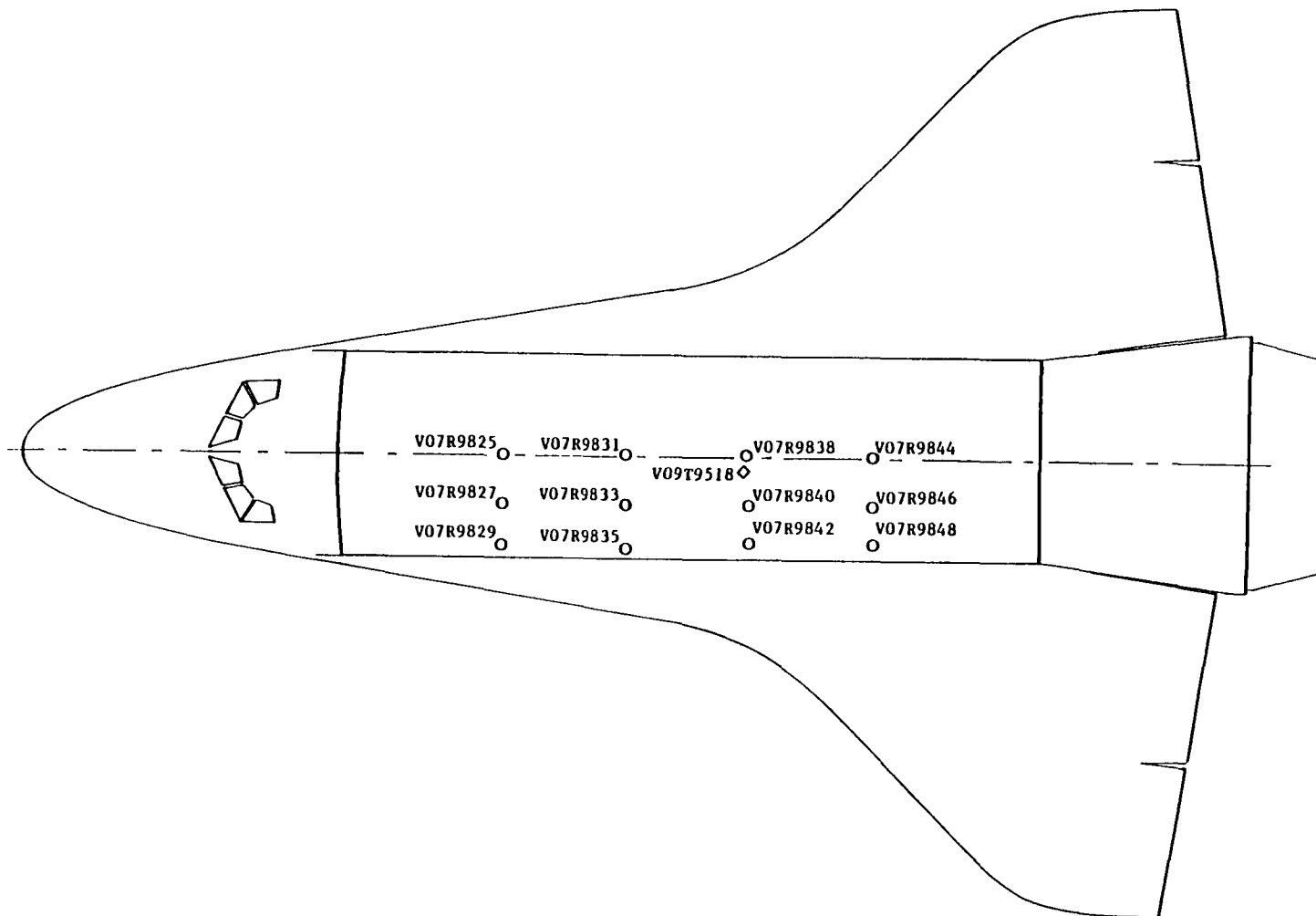
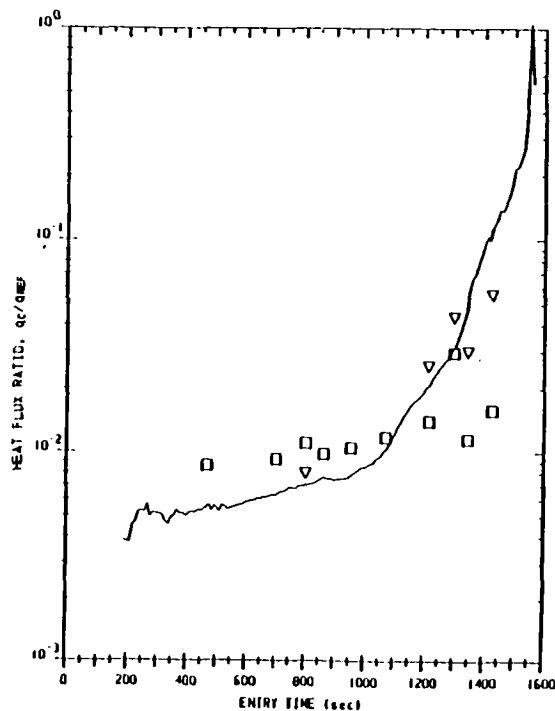


Figure 40 Flight Comparison Upper Fuselage DFI

SYM EXTRAPOLATION

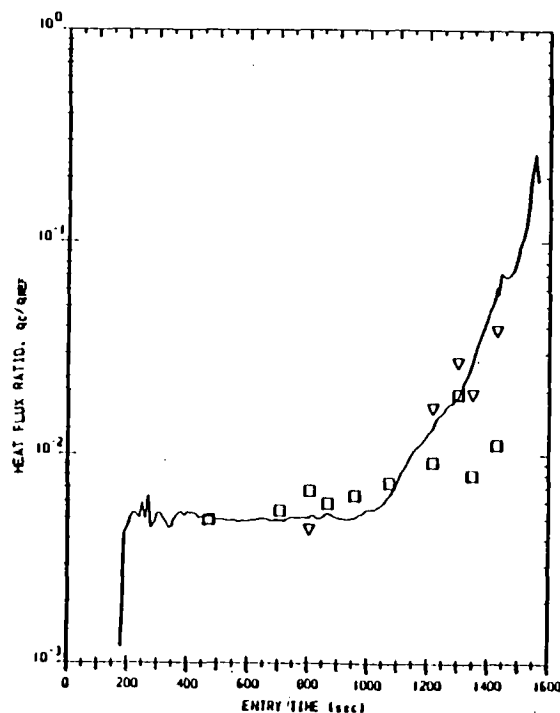
□ M = 10

▽ M = 6



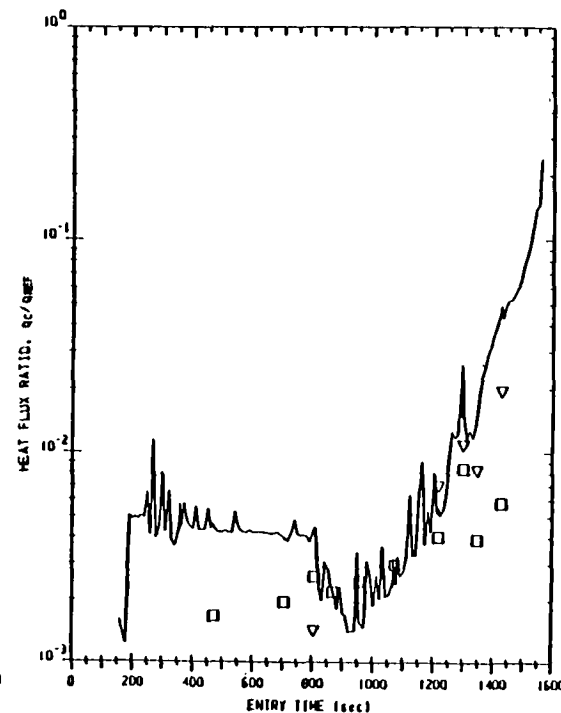
(a) V07T9622A

$X/L = .719$
 $Y/L = .214$
 $.047 \leq s/L \leq .048$



(b) V07T9623A

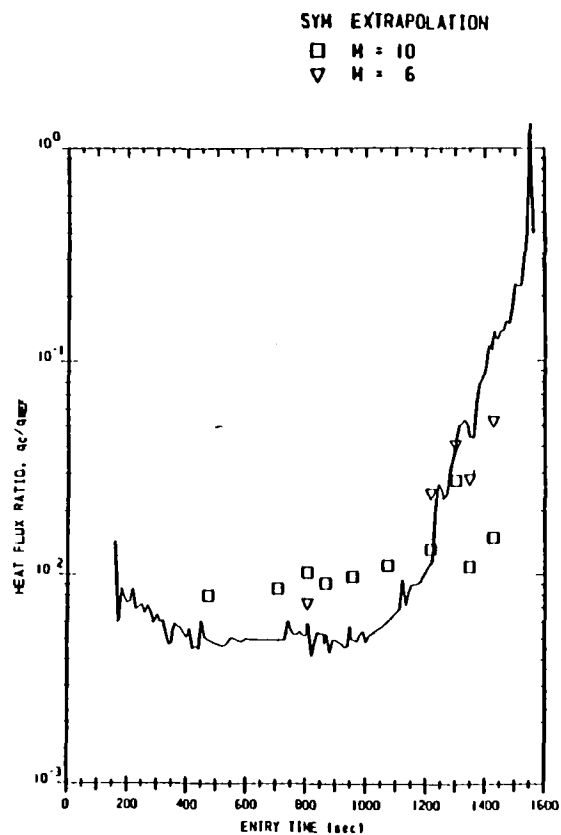
$X/L = .736$
 $Y/L = .214$
 $.064 \leq s/L \leq .066$



(c) V07R9624A

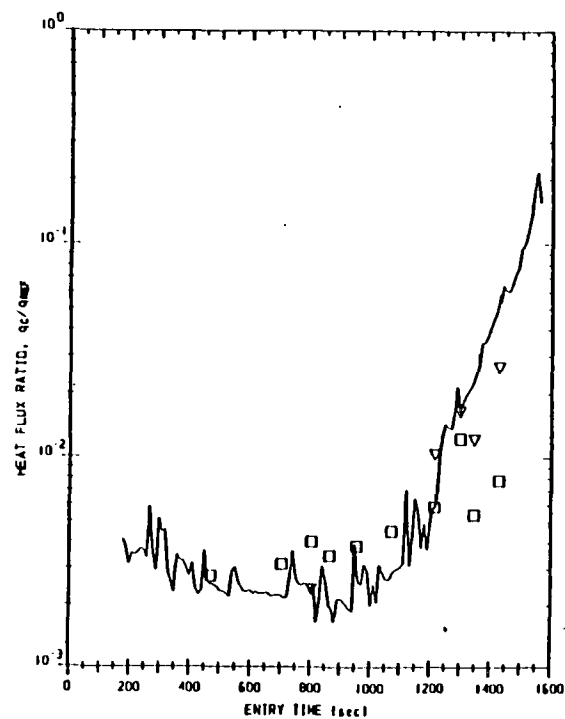
$X/L = .794$
 $Y/L = .218$
 $.117 \leq s/L \leq .119$

Figure 41 Wing Leeside Heat Flux Histories During STS-2 Entry, $Y/L \approx .216$



(a) V07T9634A

$$\begin{aligned} X/L &= .787 \\ Y/L &= .278 \\ .050 \leq s/L &\leq .051 \end{aligned}$$



(b) V07T9635A

$$\begin{aligned} X/L &= .829 \\ Y/L &= .280 \\ .089 \leq s/L &\leq .090 \end{aligned}$$

Figure 42 Wing Leaside Heat Flux Histories During STS-2 Entry, $Y/L \approx .279$

Sym Y/L DFI "V07"
 (+.002) Numbers
 ▽ .216 T9622, T9623, R9624
 △ .279 T9634, T9635

Extrapolation

— Mach 10

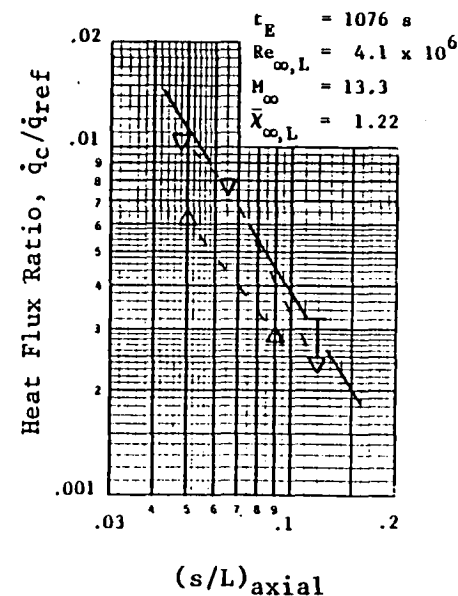
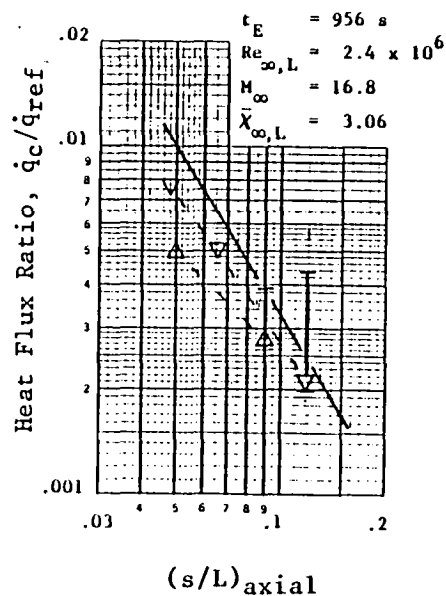
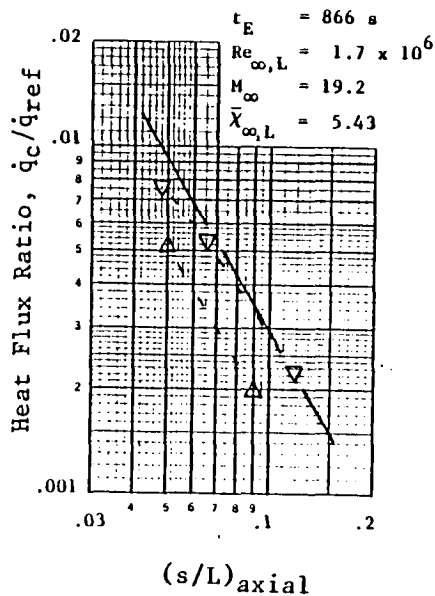
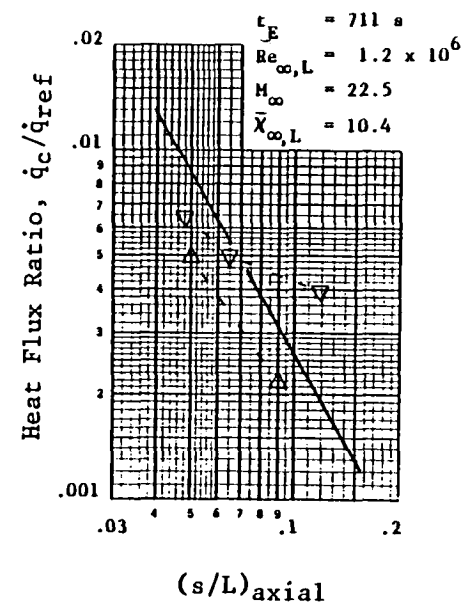
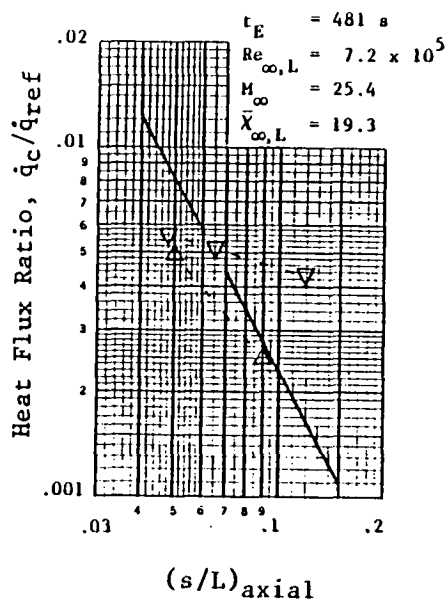


Figure 43 Wing Leeside Heating Distributions During STS-2 Entry, $\alpha \approx 40^\circ$

Sym Y/L DFI "V07"
(+.002) Numbers

▽ .216 T9622, T9623, R9624
△ .279 T9634, T9635

Extrapolation

— Mach 10
— Mach 6

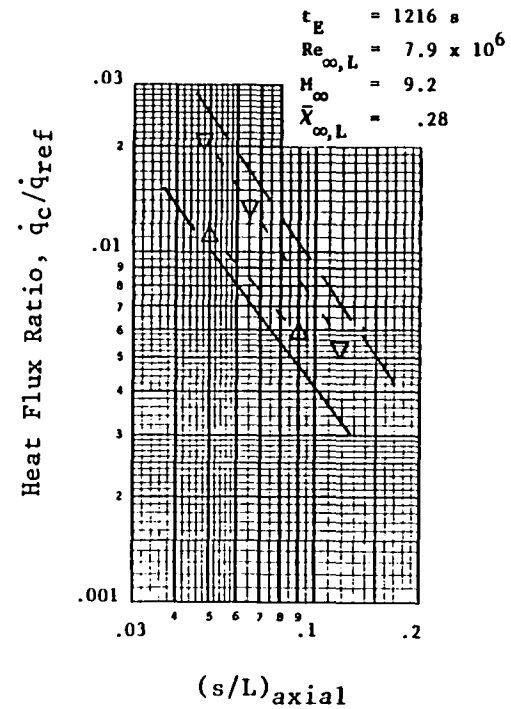
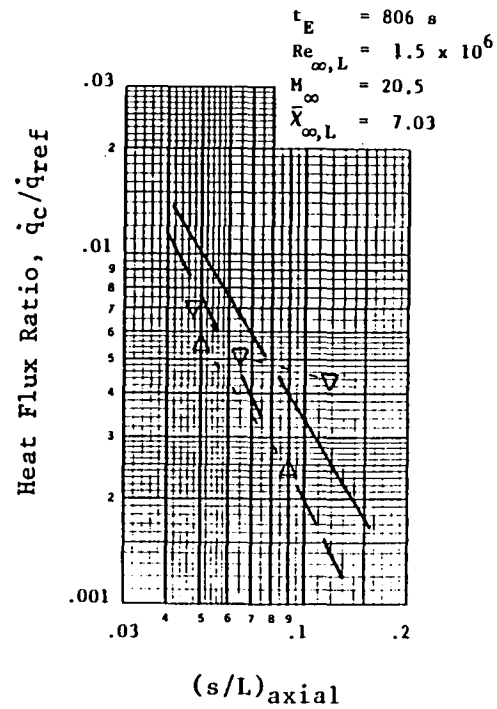
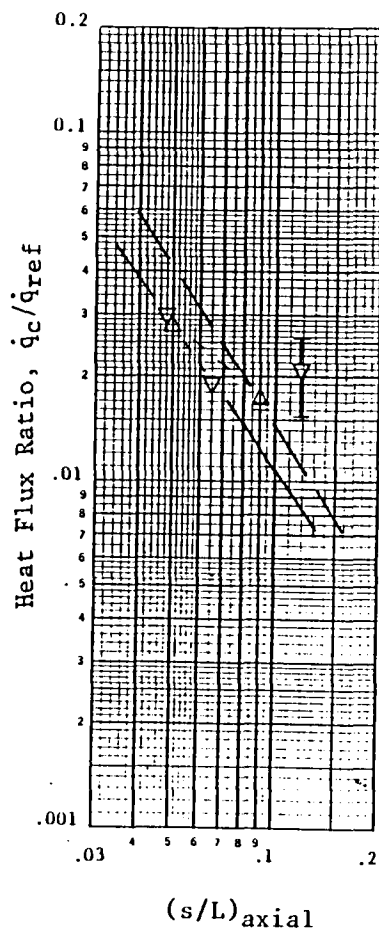
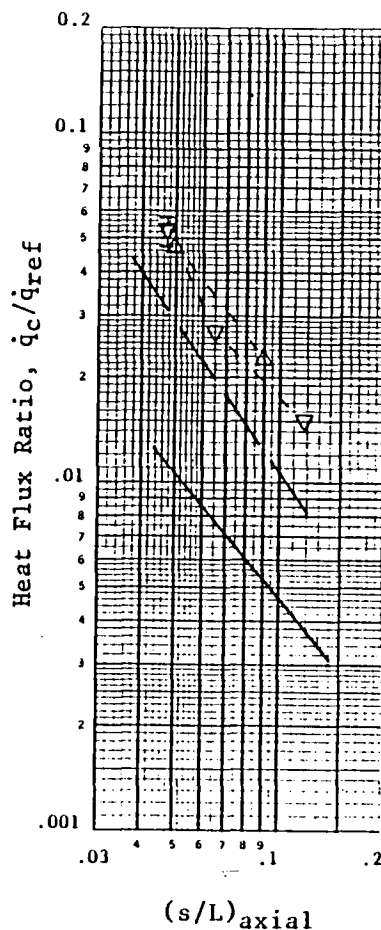


Figure 44 Wing Leaside Heating Distributions During STS-2 Entry, $\alpha \approx 35^\circ$



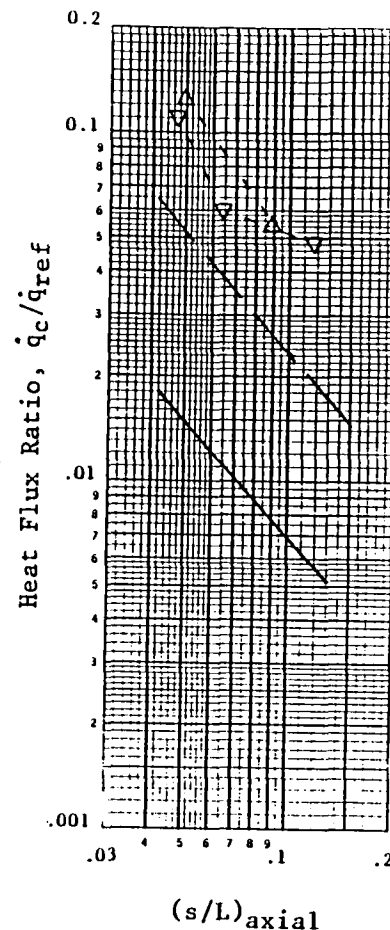
(a) $\alpha \approx 30^\circ$

$t_E = 1296 \text{ s}$
 $Re_{\infty, L} = 1.2 \times 10^7$
 $M_\infty = 7.2$
 $\bar{\chi}_{\infty, L} = .11$



(b) $\alpha \approx 25^\circ$

$t_E = 1346 \text{ s}$
 $Re_{\infty, L} = 1.8 \times 10^7$
 $M_\infty = 6.1$
 $\bar{\chi}_{\infty, L} = .053$



(c) $\alpha \approx 20^\circ$

$t_E = 1426 \text{ s}$
 $Re_{\infty, L} = 3.0 \times 10^7$
 $M_\infty = 4.6$
 $\bar{\chi}_{\infty, L} = .018$

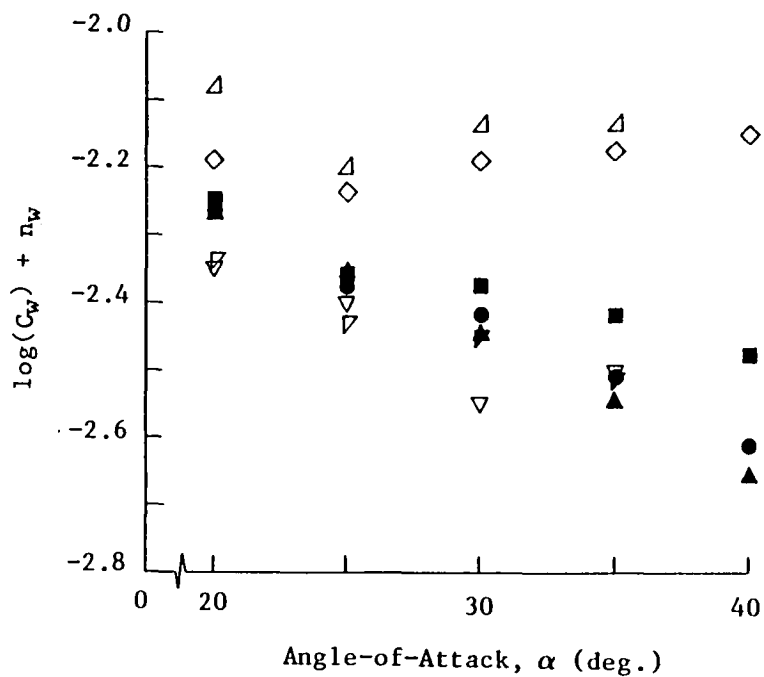
Sym Y/L DFI "V07"
 (+.002) Numbers
 ∇ .216 T9622, T9623, R9624
 Δ .279 T9634, T9635
 — Extrapolation
 — Mach 10
 - - Mach 6

Figure 45 Wing Leeside Heating Distributions During STS-2 Entry, $30^\circ \geq \alpha \geq 20^\circ$

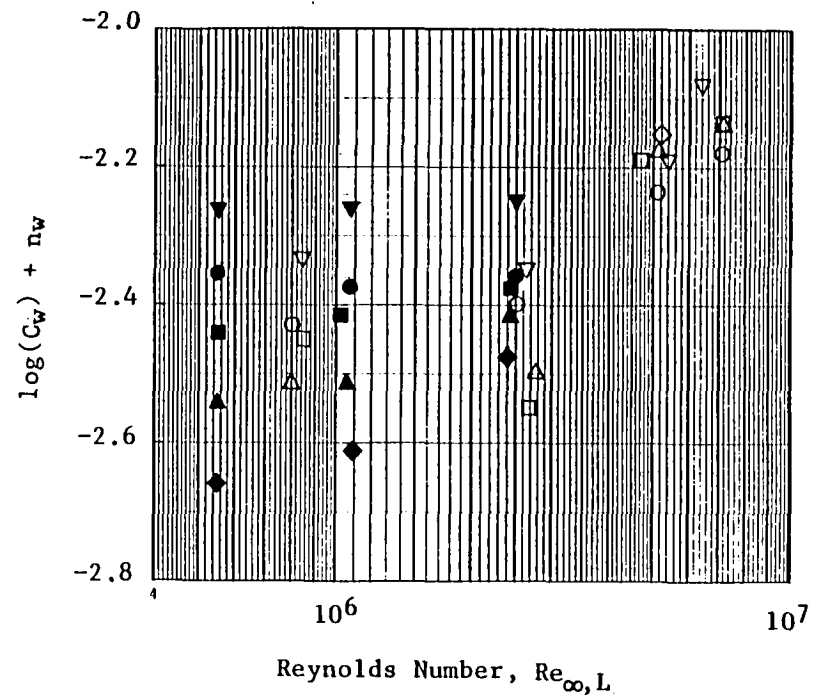
$$\frac{h}{h_{\text{ref}}} = C_w(s/L)^{-n_w}$$

Sym	M_∞	$Re_{\infty,L} \times 10^{-6}$
▲	9.82	0.55
●	9.98	1.03-1.09
■	10.16	2.40-2.50
▽	6.0	0.80-0.85
▽	6.0	2.53-2.77
◇	6.0	4.69-5.15
△	6.0	6.58-7.10

Sym	α
▽	20°
○	25
□	30
△	35
◇	40
filled	$M_\infty = 10$
open	$M_\infty = 6$



(a)

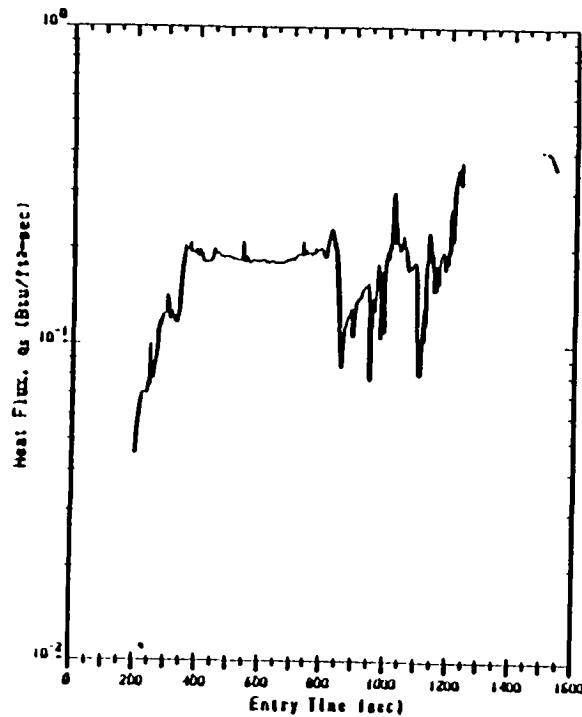


(b)

Figure 46 Wing Leeside Flow Definition

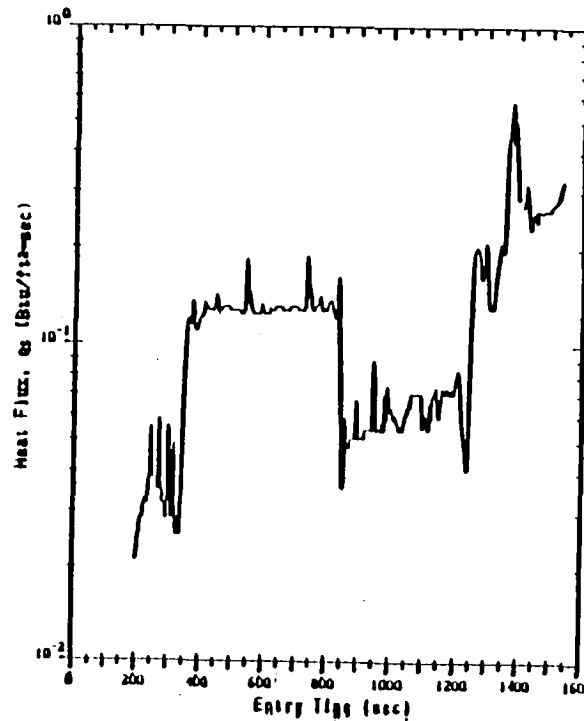
q_s = sensor-measured heat flux (reradiation & solar corrections not included)

66



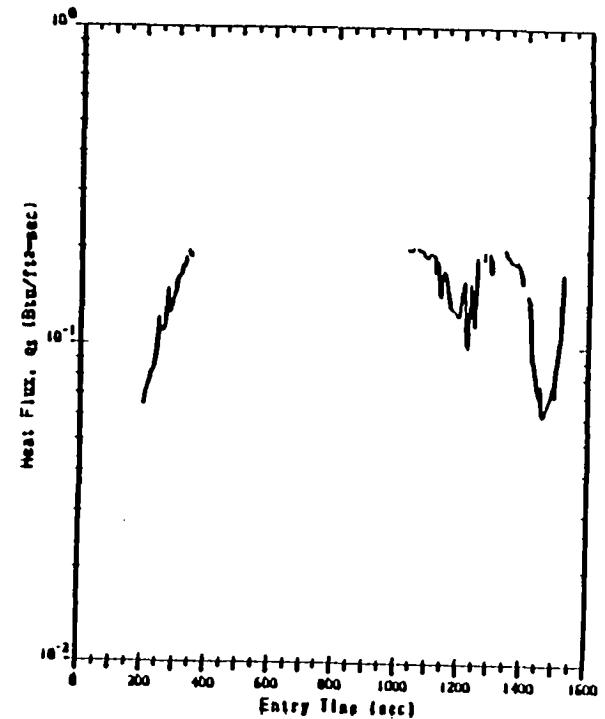
(a) VO7R9825A

Y/L = +.0004
"centerline"



(b) VO7R9827A

Y/L = -.0384
s/L = .0390



(c) VO7R9829A

Y/L = -.0746
s/L = .0825

Figure 47 Upper Fuselage Heat Flux Histories During STS-2 Entry, $X/L \approx .396$

q_s = sensor-measured heat flux (reradiation & solar corrections not included)

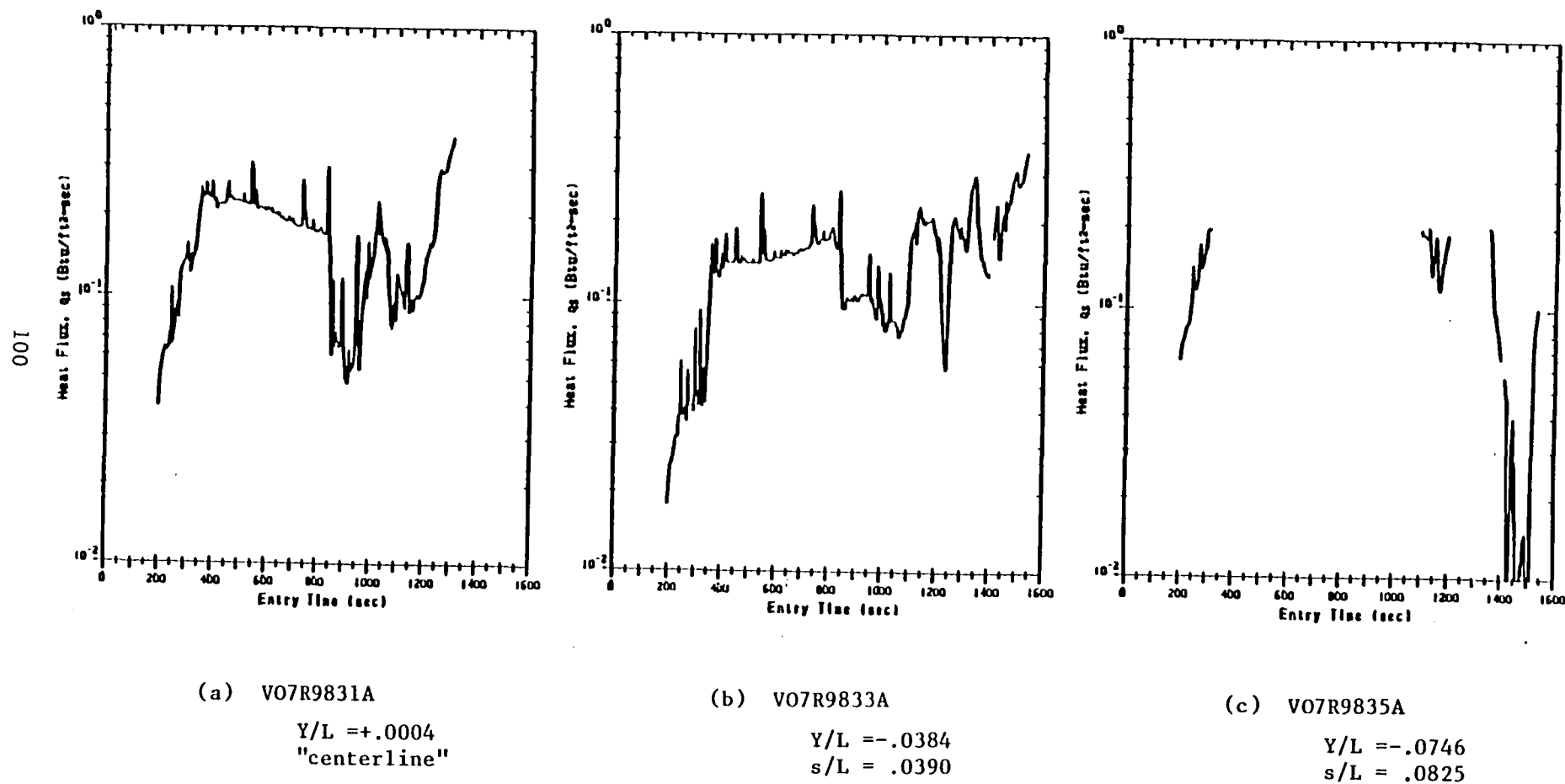


Figure 48 Upper Fuselage Heat Flux Histories During STS-2 Entry, $X/L \cong .496$

q_s = sensor-measured heat flux (reradiation & solar corrections not included)

Note: History from V09T9518A not shown (Surface T/C, X/L = .591, Y/L = -.0116, s/L = .012)

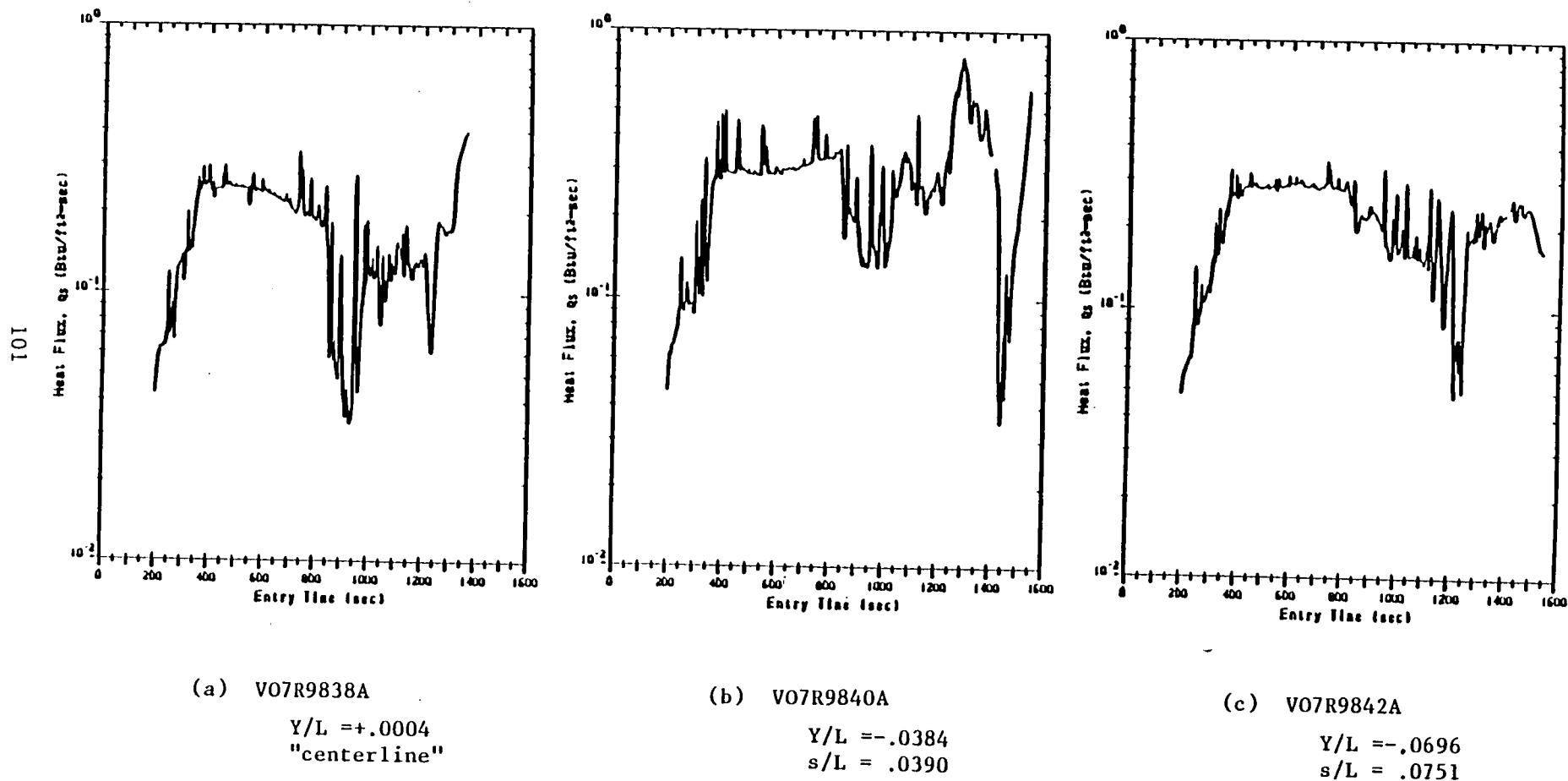


Figure 49 Upper Fuselage Heat Flux Histories During STS-2 Entry, X/L \approx .595

q_s = sensor-measured heat flux (reradiation & solar corrections not included)

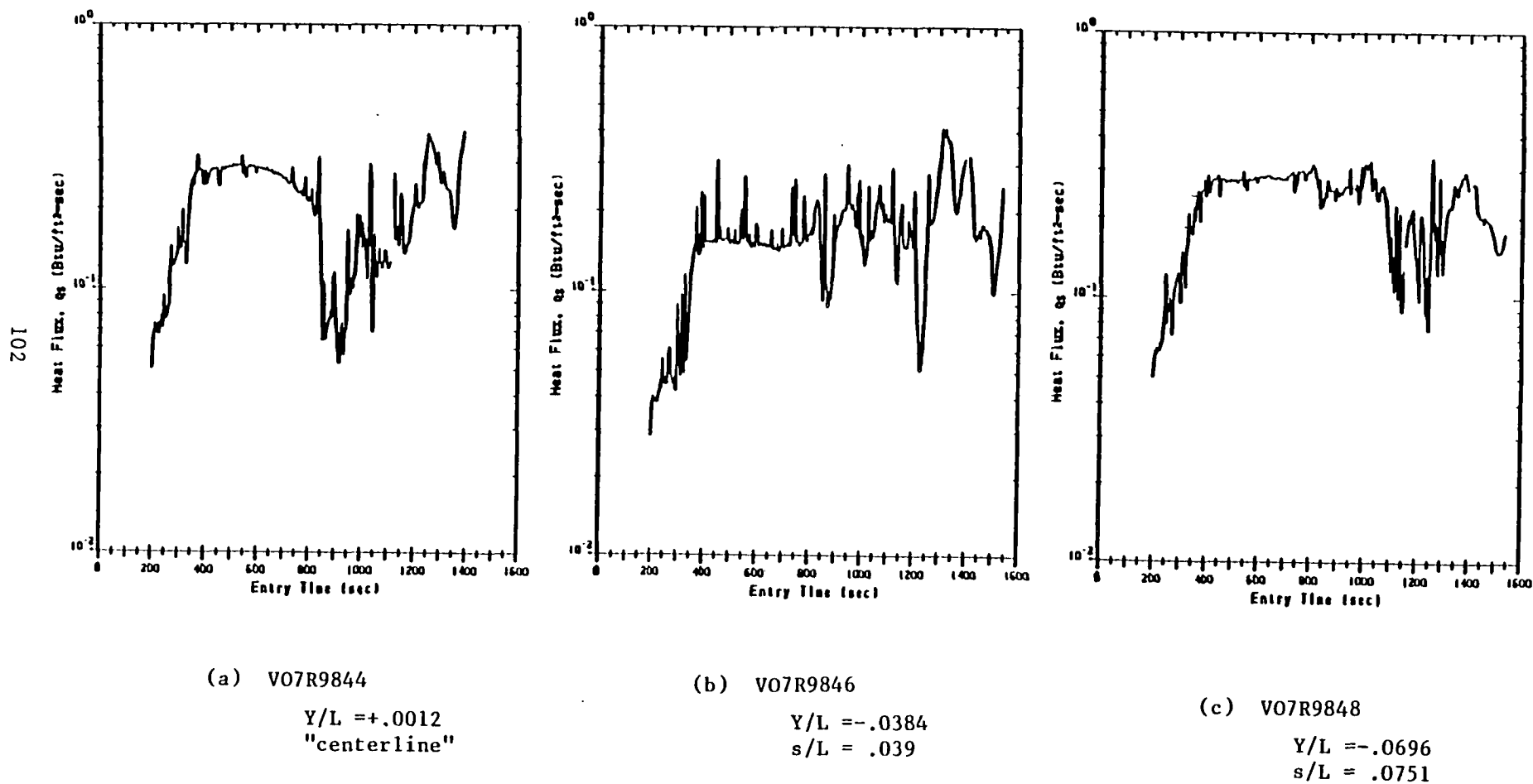
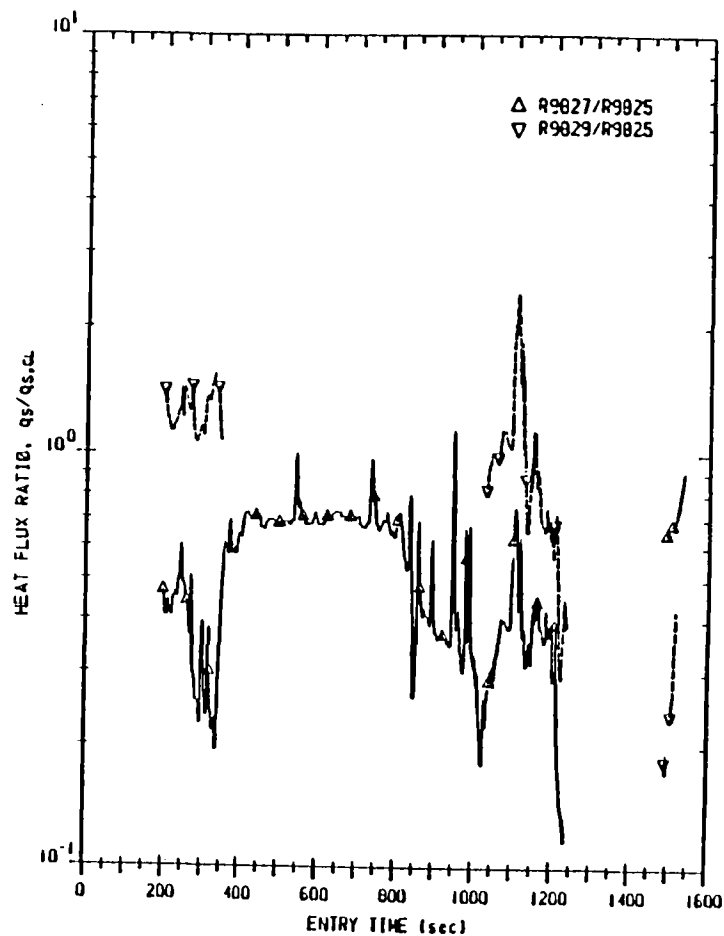
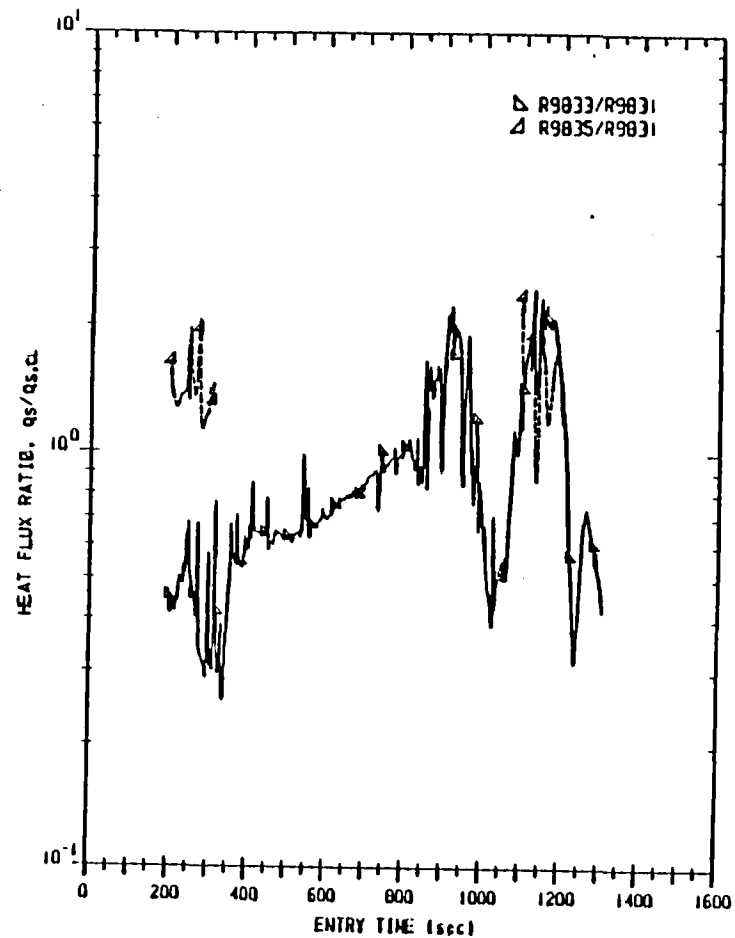


Figure 50 Upper Fuselage Heat Flux Histories During STS-2 Entry, $X/L \approx .696$

q_s = sensor-measured heat flux (reradiation & solar corrections not included)



(i) $X/L \approx .396$

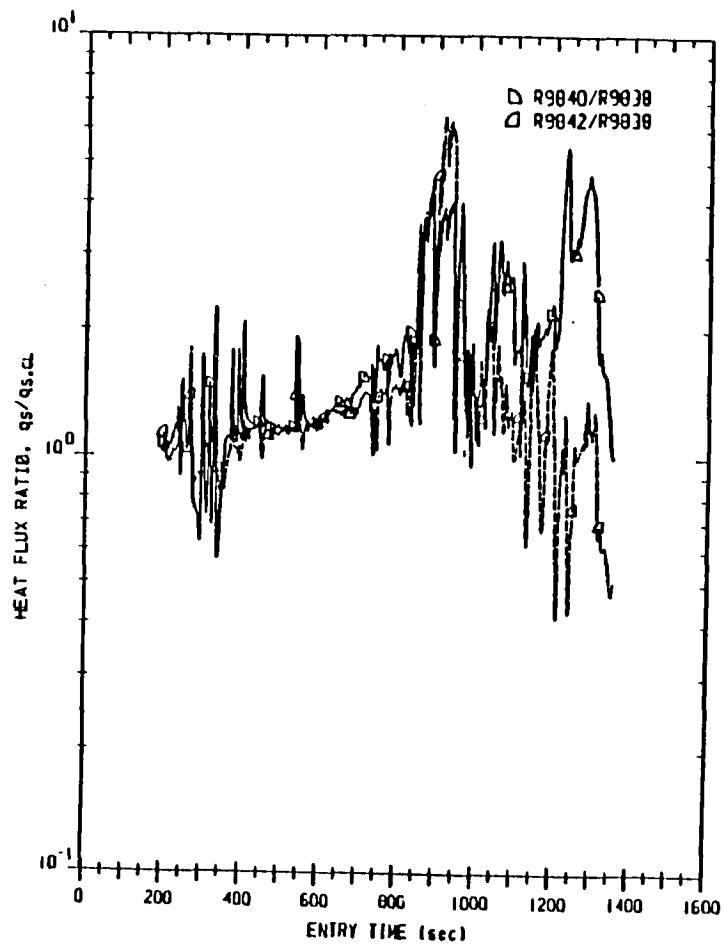


(ii) $X/L \approx .496$

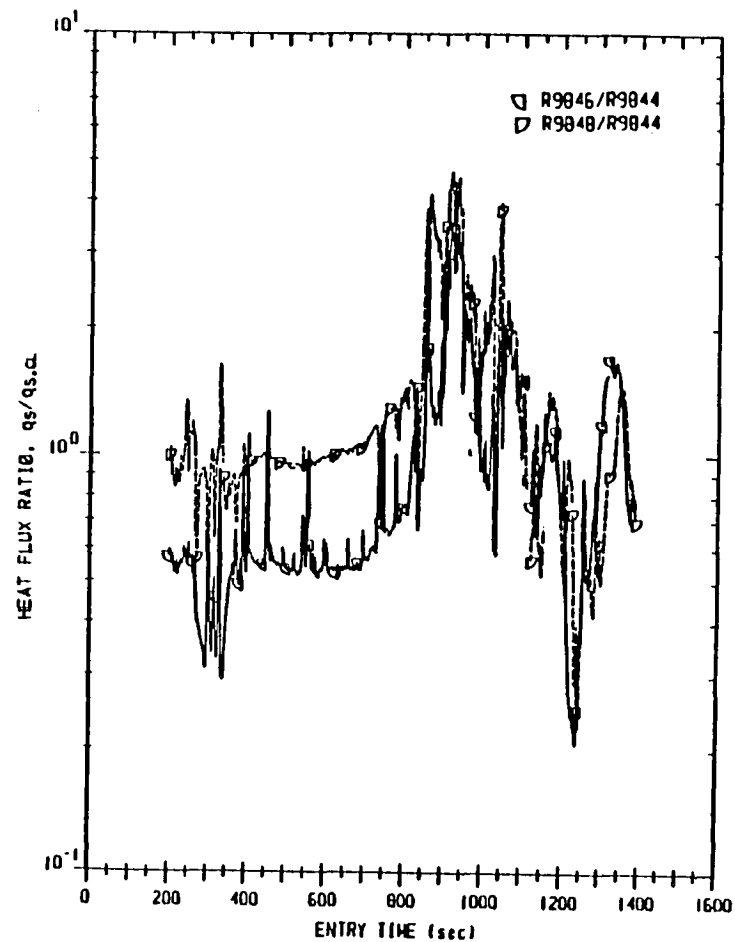
Figure 51a Upper Fuselage Heat Flux Ratios During STS-2 Entry

q_s = sensor-measured heat flux (reradiation & solar corrections not included)

Note: Ratio of T9518/R9838 not included



(i) $X/L \approx .596$



(ii) $X/L \approx .696$

Figure 51b Upper Fuselage Heat Flux Ratios During STS-2 Entry

\dot{q}_c = Convective Heat Flux
(with reradiation and solar corrections)

Sym X/L DFI "V07" & "V09" Numbers
(\approx)

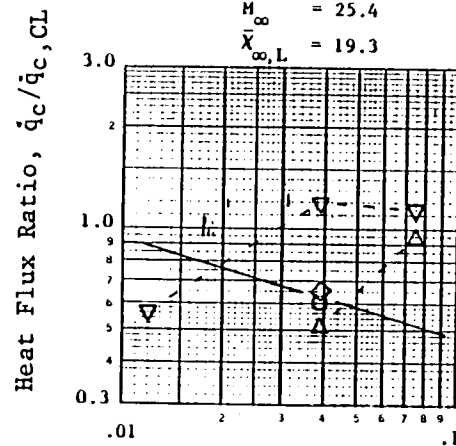
◇ .396 R9825, R9827, R9829
○ .496 R9831, R9833, R9835
▽ .596 R9838, T9518, R9840, R9842
△ .696 R9844, R9846, R9848

s/L = .0 .012 .039 .082/.075

Extrapolation

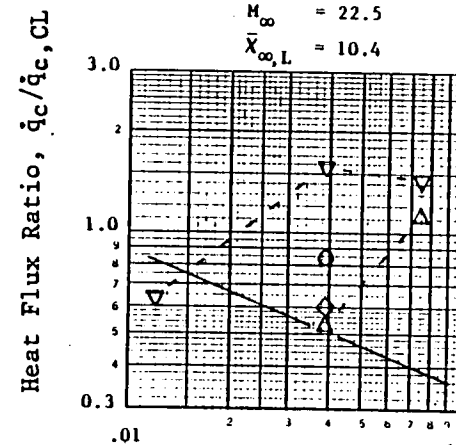
Mach 10

$t_E = 481$ s
 $Re_{\infty,L} = 7.2 \times 10^5$
 $M_{\infty} = 25.4$
 $\bar{X}_{\infty,L} = 19.3$



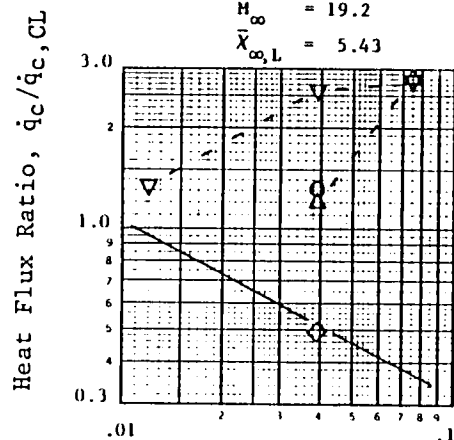
(s/L) normal to CL

$t_E = 711$ s
 $Re_{\infty,L} = 1.2 \times 10^6$
 $M_{\infty} = 22.5$
 $\bar{X}_{\infty,L} = 10.4$



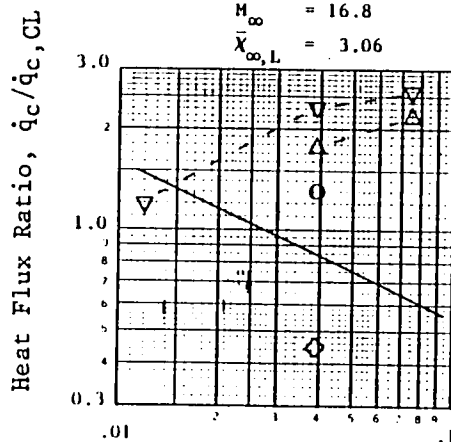
(s/L) normal to CL

$t_E = 866$ s
 $Re_{\infty,L} = 1.7 \times 10^6$
 $M_{\infty} = 19.2$
 $\bar{X}_{\infty,L} = 5.43$



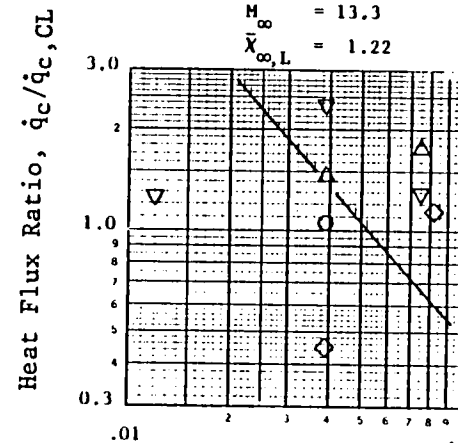
(s/L) normal to CL

$t_E = 956$ s
 $Re_{\infty,L} = 2.4 \times 10^6$
 $M_{\infty} = 16.8$
 $\bar{X}_{\infty,L} = 3.06$



(s/L) normal to CL

$t_E = 1076$ s
 $Re_{\infty,L} = 4.1 \times 10^6$
 $M_{\infty} = 13.3$
 $\bar{X}_{\infty,L} = 1.22$



(s/L) normal to CL

Figure 52 Upper Fuselage Heating Distributions During STS-2 Entry, $\alpha \approx 40^\circ$

\dot{q}_c = Convective Heat Flux
(with reradiation and solar corrections)

Sym X/L DFI "V07" & "V09" Numbers
(\approx)

◇	.396	R9825,	R9827, R9829
○	.496	R9831,	R9833, R9835
▽	.596	R9838, T9518,	R9840, R9842
△	.696	R9844,	R9846, R9848

s/L = .0 .012 .039 .082/.075

Extrapolation

———— Mach 10
———— Mach 6

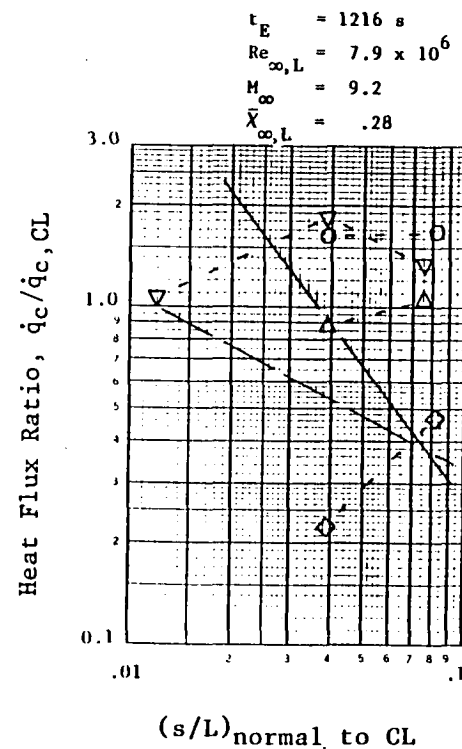
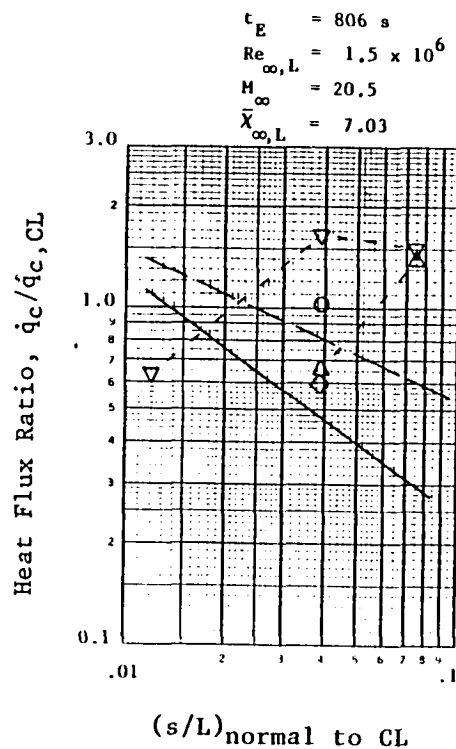
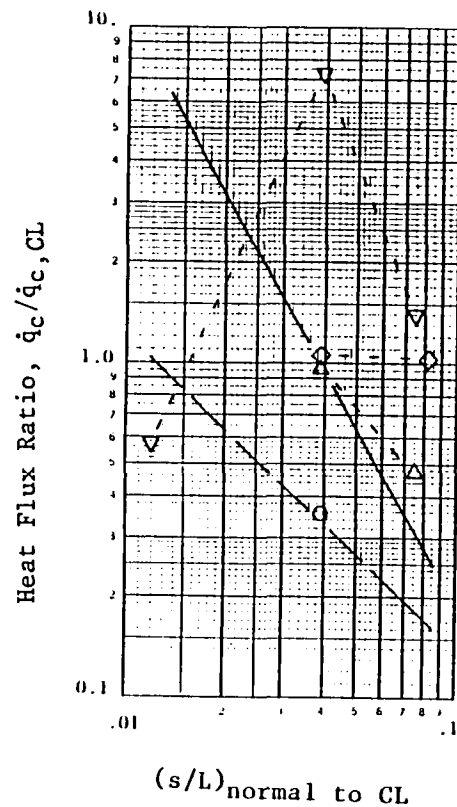
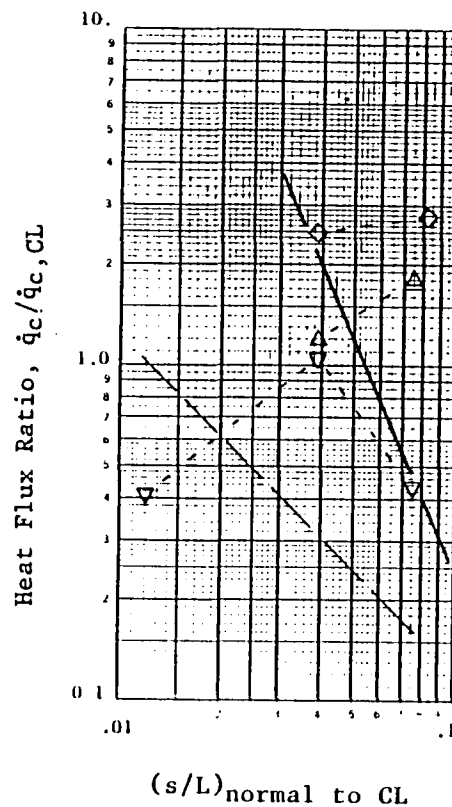


Figure 53 Upper Fuselage Heating Distributions During STS-2 Entry, $\alpha \approx 35^\circ$



(a) $\alpha \approx 30^\circ$

$$\begin{aligned} t_E &= 1296 \text{ s} \\ Re_{\infty,L} &= 1.2 \times 10^7 \\ M_\infty &= 7.2 \\ \bar{\chi}_{\infty,L} &= .11 \end{aligned}$$



(b) $\alpha \approx 25^\circ$

$$\begin{aligned} t_E &= 1346 \text{ s} \\ Re_{\infty,L} &= 1.8 \times 10^7 \\ M_\infty &= 6.1 \\ \bar{\chi}_{\infty,L} &= .053 \end{aligned}$$

\dot{q}_c = Convective Heat Flux
(with reradiation and solar corrections)

Sym	X/L	DFI "V07" & "V09" Numbers (α)
\diamond	.396	R9825, R9827, R9829
\circ	.496	R9831, R9833, R9835
∇	.596	R9838, T9518, R9840, R9842
\triangle	.696	R9844, R9846, R9848

$s/L = .0 \quad .012 \quad .039 \quad .082/.075$

Extrapolation

— — — — — Mach 10
— — — — — Mach 6

Figure 54 Upper Fuselage Heating Distributions During STS-2 Entry, $\alpha \approx 30^\circ$ & 25°

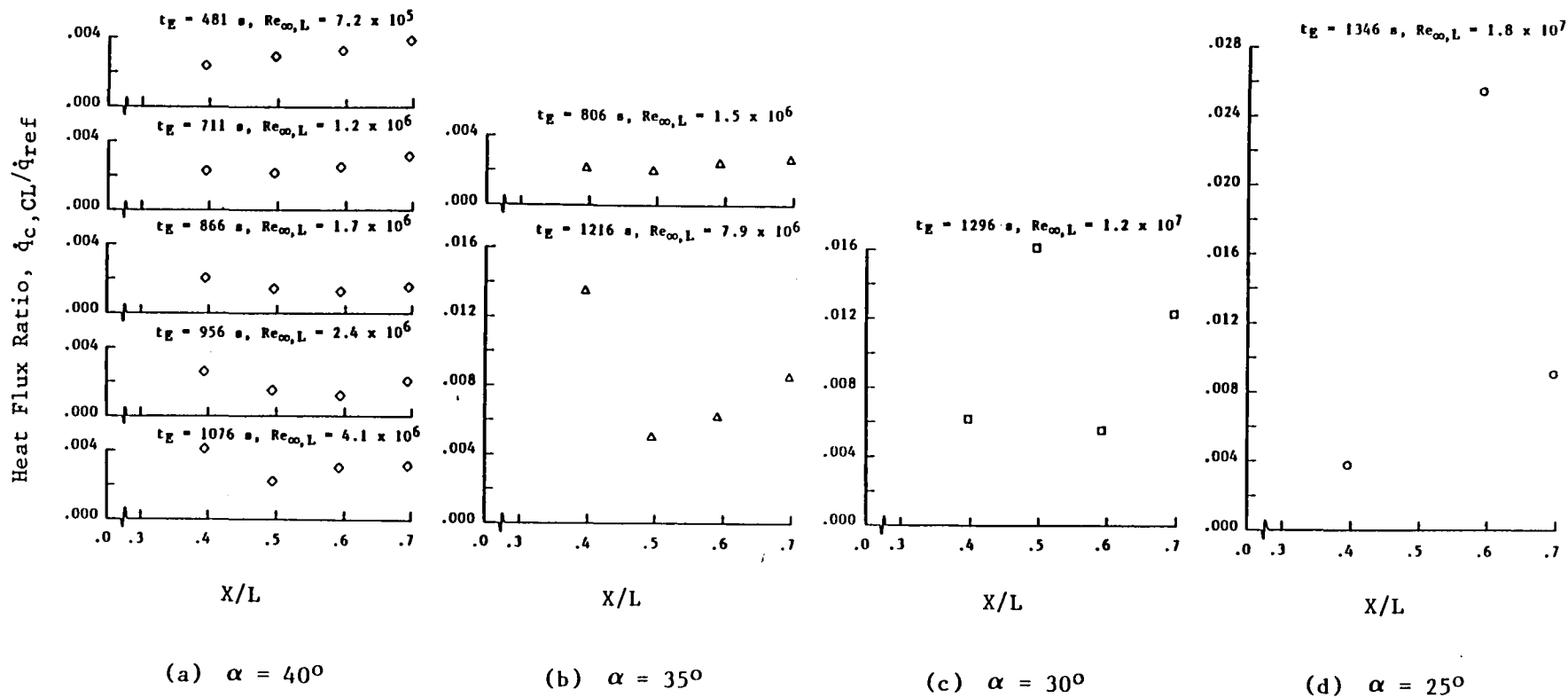
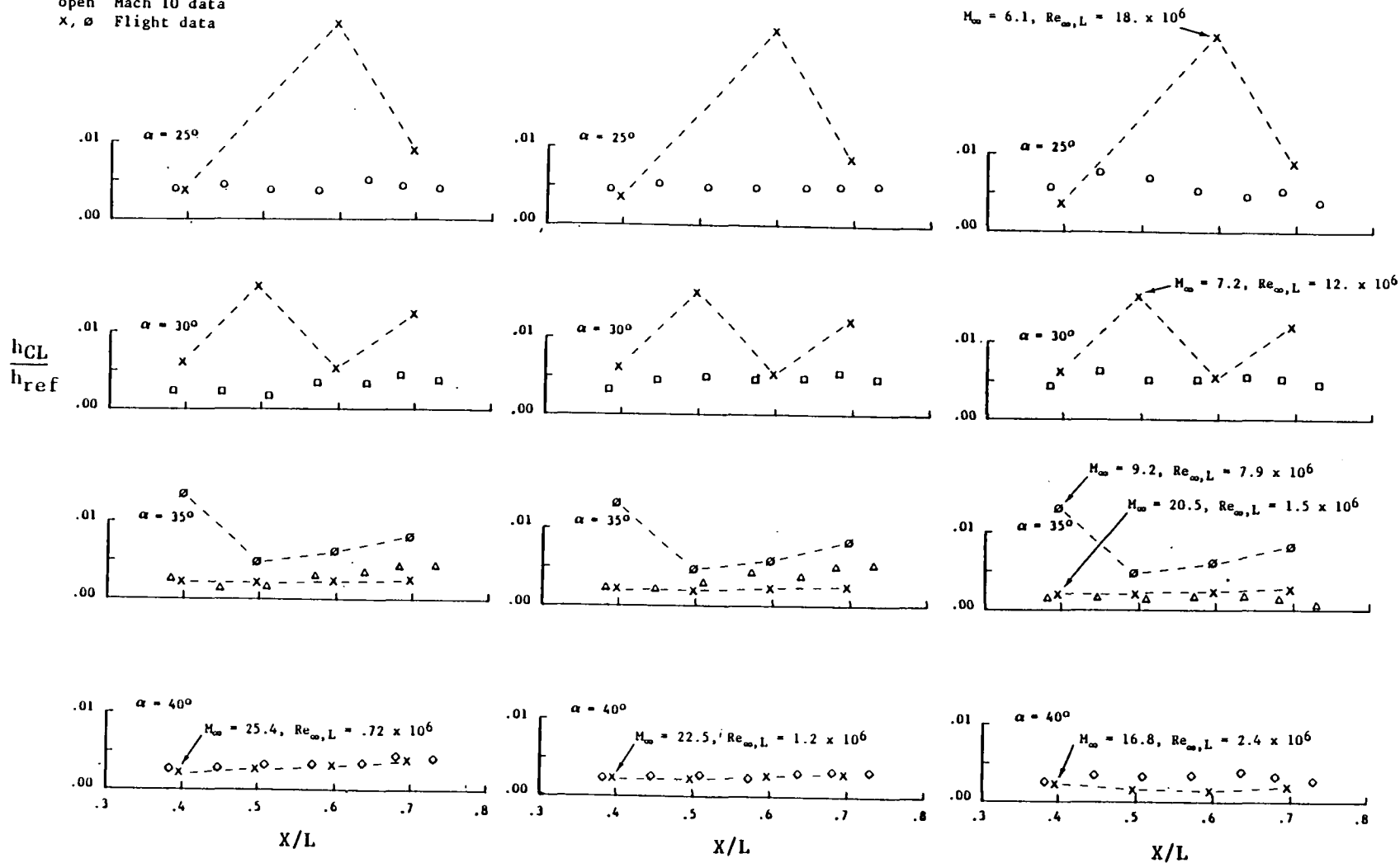


Figure 55 Upper Fuselage Centerline Heating Distributions During STS-2 Entry

Symbol
open Mach 10 data
x, o Flight data



(a) $Re_{\infty,L} = 0.5 \times 10^6$

(b) $Re_{\infty,L} = 1.0 \times 10^6$

(c) $Re_{\infty,L} = 2.4 \times 10^6$

Figure 56a Comparison of Upper Fuselage Centerline Heating Distributions, Mach 10 Data

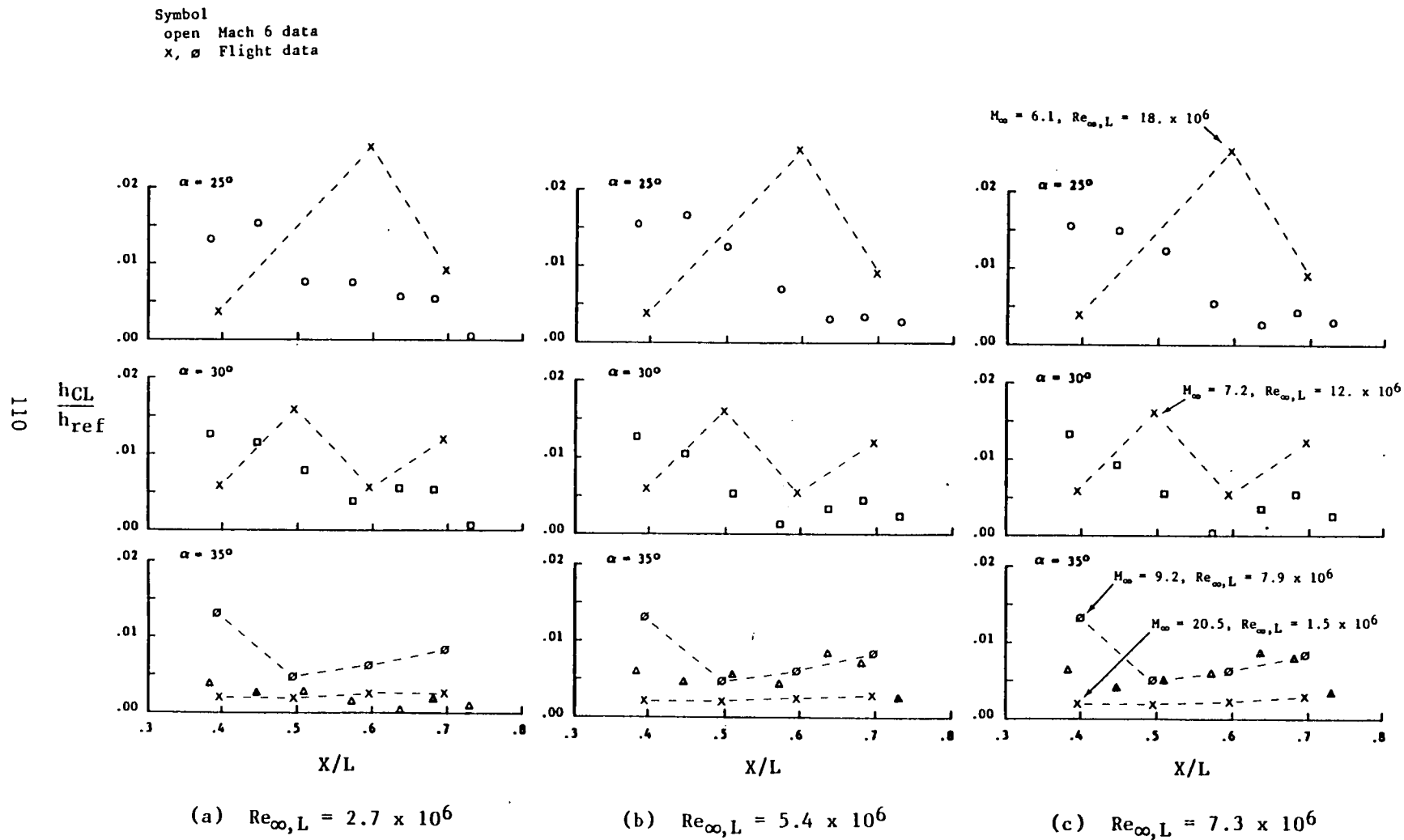


Figure 56b Comparison of Upper Fuselage Centerline Heating Distributions, Mach 6 Data

APPENDIX A

The Phenomenon of Striation Heating*

Prepared by H. W. Kipp

A comprehensive experimental wind tunnel investigation of Shuttle leeside heat transfer was recently conducted by V.T. Helms of NASA Langley Research Center. The tests were conducted with 0.01-scale models at Mach 6 and 10 in the Langley 20 Inch Hypersonic Tunnel and in the Langley Continuous Flow Hypersonic Tunnel. (A2)** Included in the program were tests using thin skin heat transfer models, surface oil flow visualization and phase change thermal mapping. This experimental program provided data for use in Contract NAS1-16839(A1) and for on-going studies of Shuttle leeside heat transfer at NASA LaRC (e.g., reference A3).

Some of the thermal mapping tests revealed a regularly spaced pattern of heat transfer striations or "hot streaks" on the fuselage sidebody. The striations were observed to fall within the region of sidebody vortex impingement above the wing (while the striations were observed only on the Shuttle sidebody, it is speculated that a similar phenomenon may occur on the upper fuselage). Photos of typical striation patterns at 40° angle of attack are shown in Figure A1. These data were taken at Mach 6 at free stream Reynolds numbers based on model length of 2.7×10^6 , 5.4×10^6 and 7.3×10^6 respectively. Examination of the photographs shows the striations become more distinct as well as more closely spaced with increasing Reynolds number. Additional Mach 6 tests at the same three Reynolds numbers revealed similar striation patterns at 20° and 30° angle of attack.

Thermal mapping tests using the same model were also run at Mach 10 at angles of attack of 20°, 30° and 40°. However, the Mach 10 tests were run at Reynolds numbers of 0.5×10^6 , 1×10^6 and 2.4×10^6 , which were significantly lower than in the Mach 6 tests. In contrast with the Mach 6 tests, which revealed varying degrees of striation heating at all angles of attack and Reynolds numbers, striation heating was observed at Mach 10 only at 40° angle of attack (at all three Reynolds numbers).

* This review was prepared using McDonnell Douglas Astronautics Co. Internal Research and Development Funds as a part of IRAD Project No. 122300. This work complements work performed under reference A1.

** Numbers in () are references

Duplicate tests which were run at selected conditions revealed a high degree of repeatability in the striation heating patterns. In an attempt to determine if roughness in the thermal mapping paint might cause the striations, additional tests were run in which the thermal mapping paint was omitted from portions of the model upstream of the striation zone. Omission of the upstream paint had no observable effect on the striation heating patterns. In addition, the model was examined for roughness elements which might have caused the striations; no such roughness was found.

In summary, the 1% wind tunnel model tests conducted by Helms reveal a regular pattern of significant heat transfer variations in the region of flow reattachment on the Shuttle sidebody. These heat transfer striations are demonstrated to depend upon: 1) geometry, 2) angle of attack and 3) Reynolds number. The striations appear not to be caused by model roughness. The effect of wind tunnel Mach number on the striation patterns has not been determined.

A phenomenon similar to Helms' heat transfer striations was observed by Seegmiller during surface oil flow visualization tests on an early Shuttle configuration.^(A4) Seegmiller's surface oil flow tests were conducted at Mach 7.4 in the NASA-Ames 3.5 Foot Hypersonic Wind Tunnel. In these tests, uniformly-spaced streaks were observed on both the elevons and rudders when these control surfaces were deflected and when the test Reynolds number was adequately high.

Figure A2a shows streamline patterns on the lower surface, the elevons and the left rudder. Figure A2b is an enlarged view of the left elevon. The test conditions corresponding to Figures A2a and A2b were:

$$\text{MACH} = 7.4$$

$$R_e = 1.4 \times 10^6 \text{ (vehicle length Reynolds number)}$$

$$\alpha = 15^\circ \text{ (angle of attack)}$$

$$\delta_e = 15^\circ \text{ (elevon deflection)}$$

$$\delta_r = 0^\circ \text{ (rudder deflection)}$$

Figures A2a and A2b show significant boundary layer separation occurred upstream of the elevons. The boundary layer is believed to have been laminar over the entire model. The curved flow separation line and the streamline patterns on the elevon indicate the flow over the elevon was highly three-dimensional. There is no evidence of an organized pattern

of regularly spaced striations anywhere on the model for these test conditions.

Surface flow in the vicinity of the elevons and rudders changes significantly as Reynolds number increases. Figures A3a and A3b show streamline patterns which resulted from increasing the Reynolds number to 2.8×10^6 (and increasing the rudder deflection to 20°). The other test parameters (M_∞ , α and δ_e) are identical to the parameters of Figures A2a and A2b. The increased Reynolds number reduced only slightly the size of the separated zone upstream of the elevon, however a dramatic change occurred in the reattached flow on the elevon (compare Figure A3b with A2b). The reattached flow produces a series of regularly spaced parallel striations in the oil film. These are interpreted as multiple counterrotating vortices within the reattached boundary layer. The striations are also seen on the right rudder (Figure A3a) which was deflected 20° . It is noteworthy that striations did not occur on the undeflected rudder tested at the same Reynolds number (2.8×10^6) nor on the undeflected rudder tested at $Re = 1.4 \times 10^6$. Additional oil flow tests were run at the same elevon deflection and model angle of attack at higher Reynolds numbers (i.e., 3.1×10^6 and 5.7×10^6). As Reynolds numbers increased, striations continued to appear on the elevons and the separated flow zone decreased significantly in size (it became practically non-existent at $Re = 5.7 \times 10^6$). At these higher Reynolds numbers, the striation spacing decreased and striations began to emerge upstream of the elevons. Seegmiller concluded that at $Re = 5.7 \times 10^6$ a turbulent boundary layer had developed on the lower surface of the wing.

Assuming the basic striation-producing mechanism in Helms' thermal mapping tests is the same as in Seegmiller's oil flow tests, the Seegmiller tests corroborate observations based on the thermal mapping data. The following conclusions can be drawn from Seegmiller's data:

- Reynolds number must exceed a critical value before striations can appear.
- Flow turning promotes striations.
- Flow separation (upstream) appears to promote striations but may not be a necessary condition for their formation.

In a review of his comprehensive research on reattaching flows, Ginoux^(A5) describes the development of spatially periodic patterns of counter-rotating streamwise vortices as a fundamental characteristics of flow reattachment. Ginoux performed boundary layer reattachment experiments on six configurations in five wind tunnels. The tests spanned the Mach number rang of 1.5 to 7.0 and included boundary layers which were laminar, transitional and turbulent at reattachment. Figure A4 indicates the scope of the tests.

In his tests of the six configurations listed in Figure A4, Ginoux observed that regularly-spaced streamwise striations formed in subliming surface coatings beginning at the point of boundary layer reattachment. These observations were followed by pitot probe, static pressure probe and hot wire anemometer measurements. The measurements conclusively demonstrated the existance of regularly spaced, counterrotating streamwise vortices within the reattached boundary layer. Tests of up to 3 hours duration demonstrated that the vortices were extremely stable. Vortex spacing was found to be approximately 2.5 times the pre-separation boundary layer thickness. Surface thermocouple measurements showed a sinuosoidal variation of heat transfer with the same period as observed in the pressure measurements and the surface flow visualizations. Peak heat transfer rates produced by the vortices were 50% higher than fully turbulent heating rates measured downstream of the vortices.

Ginoux concluded that the striation phenomenon is a two-stage process associated with laminar and transitional reattaching flows. First, small, irregularly-distributed, model leading edge imperfections trigger disturbances in the boundary layer upstream of separation. As the flow separates and reattaches, a stability mechanism acts to organize the disturbances into a regular pattern of counter-rotating streamwise vortices. These vortices produce significant spanwise variations in boundary layer properties such as velocity, skin friction and heat transfer.

Zakkay and Calarese^(A6) conducted an experimental investigation to determine the possible formation of streamwise vortices in a hypersonic turbulent boundary layer over an axisymmetric configuration with concave curvature. Tests were run in the New York University Mach 6 High

Reynolds Number Tunnel at a free stream Mach number of 5.75 and a Reynolds number of $1.28 \times 10^8 \text{ m}^{-1}$ ($3.9 \times 10^7 \text{ ft}^{-1}$). The model consisted of a 6 inch long axisymmetric flare attached to a .74 m (29 in.) long hollow cylinder (Figure A5). A naturally turbulent boundary layer was established on the cylinder well ahead of the flare. No boundary layer separation was observed on the flare.

Boundary layer profiles of stagnation temperature, static pressure and pitot pressure were measured at a single axial location on the flare where the local surface was inclined 20 degrees to the model axis. The measurements were repeated at other circumferential locations in 5 degree increments. The data showed large regular peripheral variations in static and pitot pressure within the boundary layer but no variations at either the model surface or at the boundary layer edge. Zakkay and Calarese concluded that the admittedly limited results indicated the formation of vortices within the boundary layer.

In another investigation of boundary layer vortices, Olson(A7) studied patterns produced by water flowing axially over sharp smooth metal cones having apex angles of 30° , 60° , 90° and 180° . Striation patterns were observed to form when water flowed over the freshly painted cones. Both laminar and turbulent flow regimes were studied; each resulted in a different vortex pattern. The tests showed that the number of vortex pairs per degree around the periphery of the cone were systematically related to cone angle and flow parameters. These relationships are shown in Figures A6a and A6b from reference A7. Some conclusions which can be drawn from Olsen's study are:

- Striations (boundary layer vortices) can form without flow separation/reattachment.
- Striations are formed by laminar as well as turbulent boundary layers.
- Striation spacing decreases with increasing Reynolds number.
- Turbulent boundary layer striations are more closely spaced than laminar boundary layer striations.

The striation data in references A2 thru A7 were obtained in wind tunnels and in a water-flow facility. Consequently, the possibility exists that striations are artifacts peculiar to ground test facilities and may not occur in free flight. Fortunately a data fragment from the ASSET flight test program provides a tentative answer.

Figure A7 depicts the ASSET lifting reentry flight test vehicle which was designed and tested for the USAF Flight Dynamics Laboratory by McDonnell Aircraft Co.^(A8) Six such vehicles were flown from 1963 to 1965 to explore aerothermodynamic, structural, dynamic and material performance in hypersonic flight. One of the vehicles, the ASV-3, was recovered after a flight of approximately 900 seconds. The ASV-3 was boosted to a speed of approximately 5490 m/s (18,000 ft/sec) at approximately 65 km (213,000 ft.) altitude (Figure A8). At this point, the vehicle was pitched to roughly 40° angle-of-attack. This attitude was maintained nearly constant (in the range of 38-40°) for the next 475 seconds (Figure A9), during which time the airspeed decreased from 5490 to 1980 m/s (18000 to 6500 ft/sec).

Figure A10 shows a post flight view of the left upper fuselage of the ASV-3 ASSET. The photo reveals a regular pattern of "burn marks" resulting from the interaction of volatile contaminants with the hot sidebody. The burn marks demonstrate that the striation phenomenon is not an artifact of wind tunnel testing but can occur in flight. Furthermore, because it is likely that the contaminants evolved over a period of time (measured in seconds or minutes) rather than instantaneously, the vortex flow which produced the striations was relatively steady.

Schlichting^(A9) describes streamwise vortices which can occur in boundary layer flow over concave walls. In such boundary layers, the fluid particles near the concave wall experience a lower centrifugal force than particles nearer the boundary layer edge. Such flows are inherently unstable and provide a mechanism for transition from laminar to turbulent boundary layer flow. When a critical Reynolds number is exceeded, small disturbances will amplify and form a system of streamwise vortices within the boundary layer as shown in Figure A11 (from reference A9). These have been named Gortler vortices after H. Gortler who first solved the equations defining the stability limits for such a system of vortices^(A10).

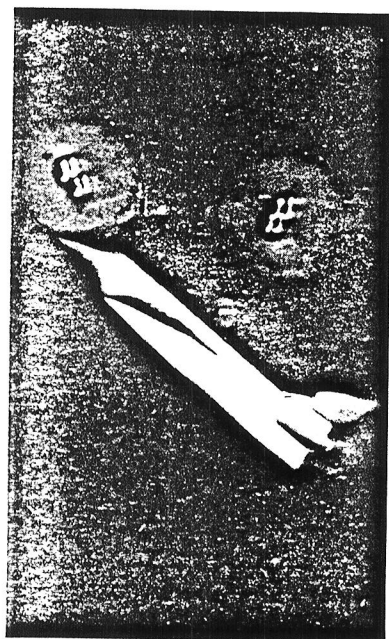
Conclusions:

This review of boundary layer striation phenomena has been limited to data in the author's possession. In spite of the limited scope of the data reviewed, a number of significant conclusions can be drawn.

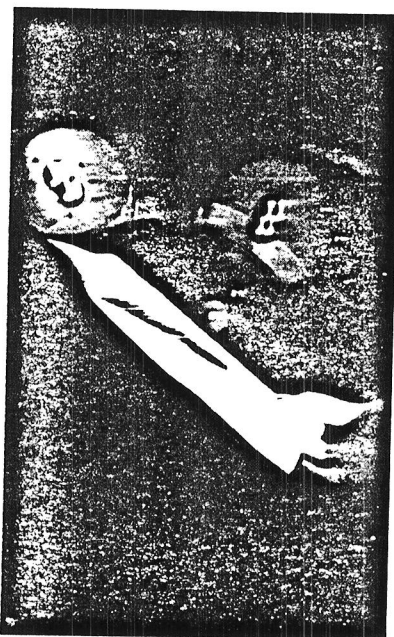
- It appears that the striations identified in references A4, thru A8 are caused by Gortler Vortices. In all instances, the striations occur following turning of the flow in a concave direction.
- Flow reattachment may promote the formation of boundary layer vortices, however, flow reattachment doesn't inevitably result in such vortices. For example, Figure A2 shows an illustration of low Reynolds number flow reattachment without striations.
- Flow reattachment is not necessary to initiate striations. This was demonstrated by Seegmiller^(A4) Zakkay, et al^(A6) and by Olson.^(A7)
- Vortices can occur in laminar or turbulent boundary layers^(A4,A6 & A7)
- Striations can be stable over long periods of time (hours). This was demonstrated by Ginoux.^(A5)
- Boundary layer vortices in transitional flow can induce local heating rates 50% higher than in downstream fully developed turbulent flow and can induce significant excursions in recovery temperature.^(A5)
- Striations occur in flight as well as in wind tunnels.^(A8)

References:

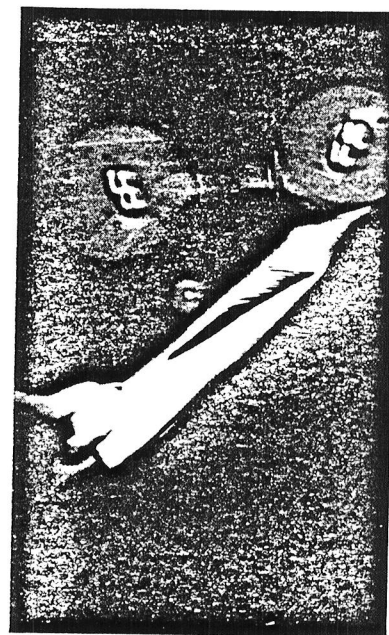
- A1. NASA Contract NAS1-16839, "Study of Leeside Flow and Heat Transfer on Shuttle Orbiter Configuration," 30 September 1981.
- A2. Schaefer, W. T., Jr., "Characteristics of Major Active Wind Tunnels at the Langley Research Center," NASA TM X-1130, 1965.
- A3. Helms, V. T., III, "An Empirical Method for Computing Leeside Heating on the Space Shuttle Orbiter", Paper AIAA-81-1043, AIAA 16th Thermophysics Conference Palo Alto, California, 23-25 June 1981.
- A4. Seegmiller, H. L., "Surface-Flow Visualization Investigation of a Delta Wing Shuttle Configuration at a Mach Number of 7.4 and Several Reynolds Numbers", NASA TM-X-62,036, June 1970.
- A5. Ginoux, J. J., "On Some Properties of Reattaching Laminar and Transitional High Speed Flows", Von Karman Institute, Belgium, Technical Note 53, September 1969.
- A6. Zakkay, V. and Calarese, W., "An Experimental Investigation of Vortex Generation in a Turbulent Boundary Layer Undergoing Adverse Pressure Gradient", NASA CR-2037, June 1972.
- A7. Olson, R. M., "Streamwise Vortex Patterns on Cones", pp 95-102, Studies in Heat Transfer - A Festschrift for E.R.G. Eckert, edited by J. P. Hartnett, T. F. Irvine, Jr., E. Pfender and E. M. Sparrow, McGraw Hill book Co., New York, 1979.
- A8. Pagel, L. L., Beardsley, P. P. and Gaumer, G. R., "ASSET Volume IV Correlative Analysis of Heat Transfer Data", AFFDL-TR-65-31, Volume IX, April 1966.
- A9. Schlichting, Hermann, "Boundary Layer Theory", 4th Ed., McGraw Hill, New York 1960.
- A10. Gortler, H., "Über eine dreidimensionale Instabilität laminarer Grenzschichten an konkaven Wänden", Nachr. Wiss. Ges. Göttingen, Math. Phys. Klasse, New Series 2, No. 1 (1940); see also ZAMM 21, 250-252 (1941).



$Re_\infty =$
 2.7×10^6



$Re_\infty =$
 5.4×10^6



$Re_\infty =$
 7.3×10^6

Figure A1 Hot Streaks on Shuttle Sidebody

Mach = 6 $\alpha = 40^\circ$

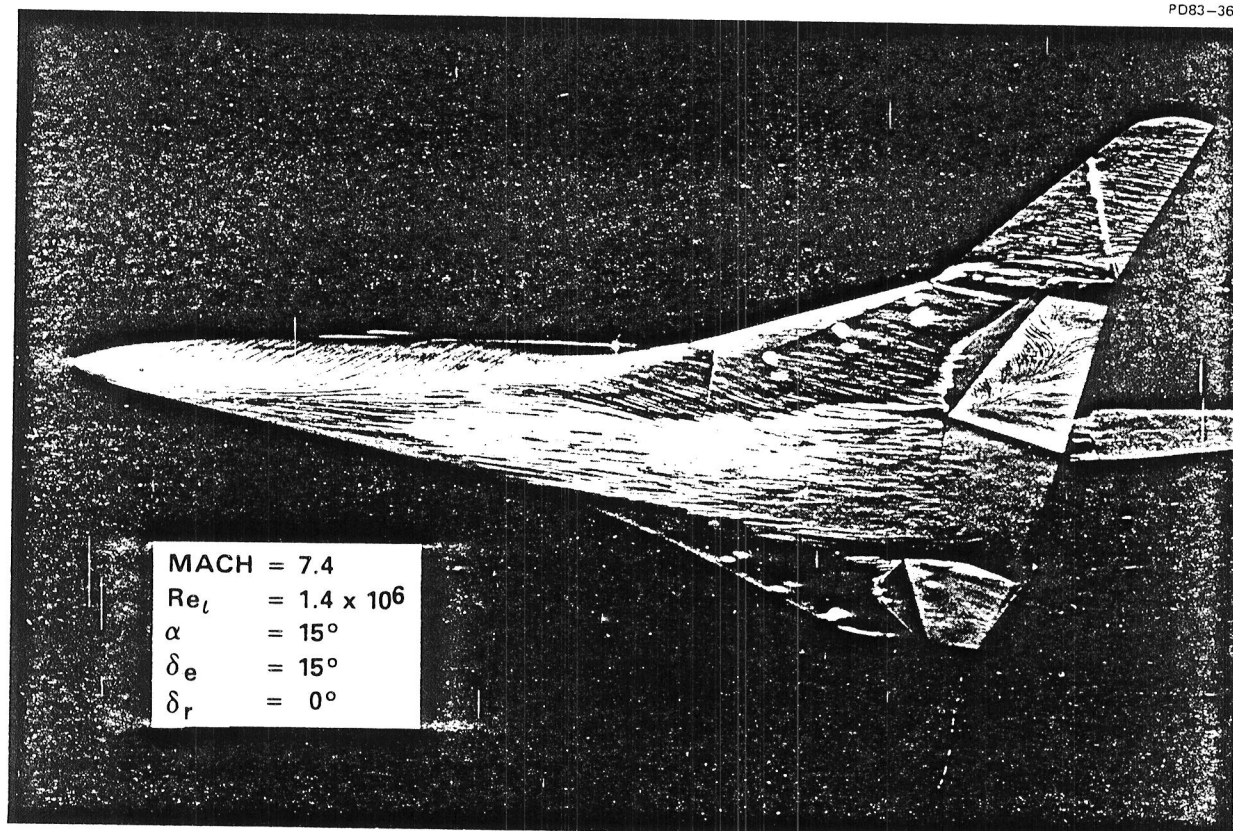


Figure A2a Lower Surface Oil Flow Visualization
 $Re_l = 1.4 \times 10^6$

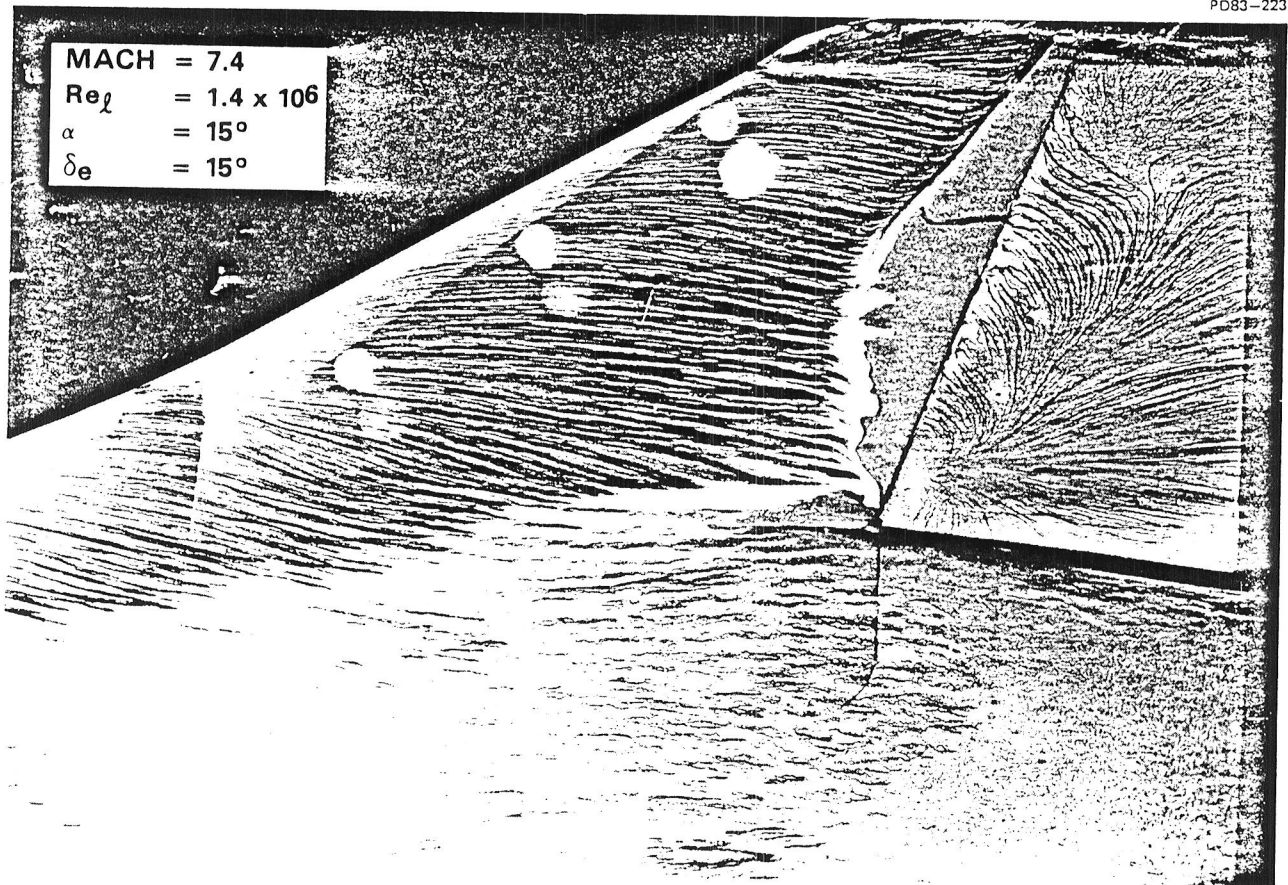


Figure A2b Left Wing and Elevon

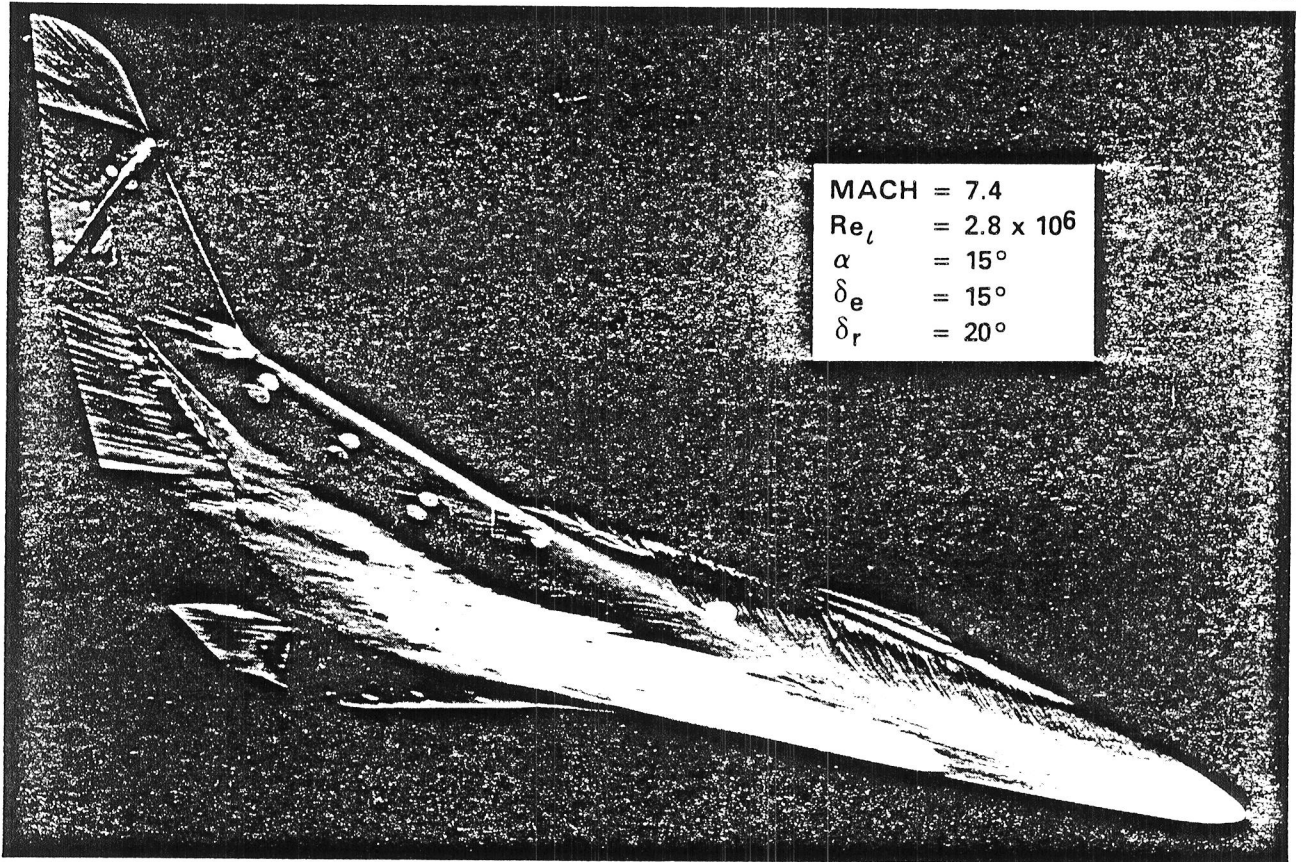


Figure A3a Lower Surface and Right Side
 $Re_l = 2.8 \times 10^6$

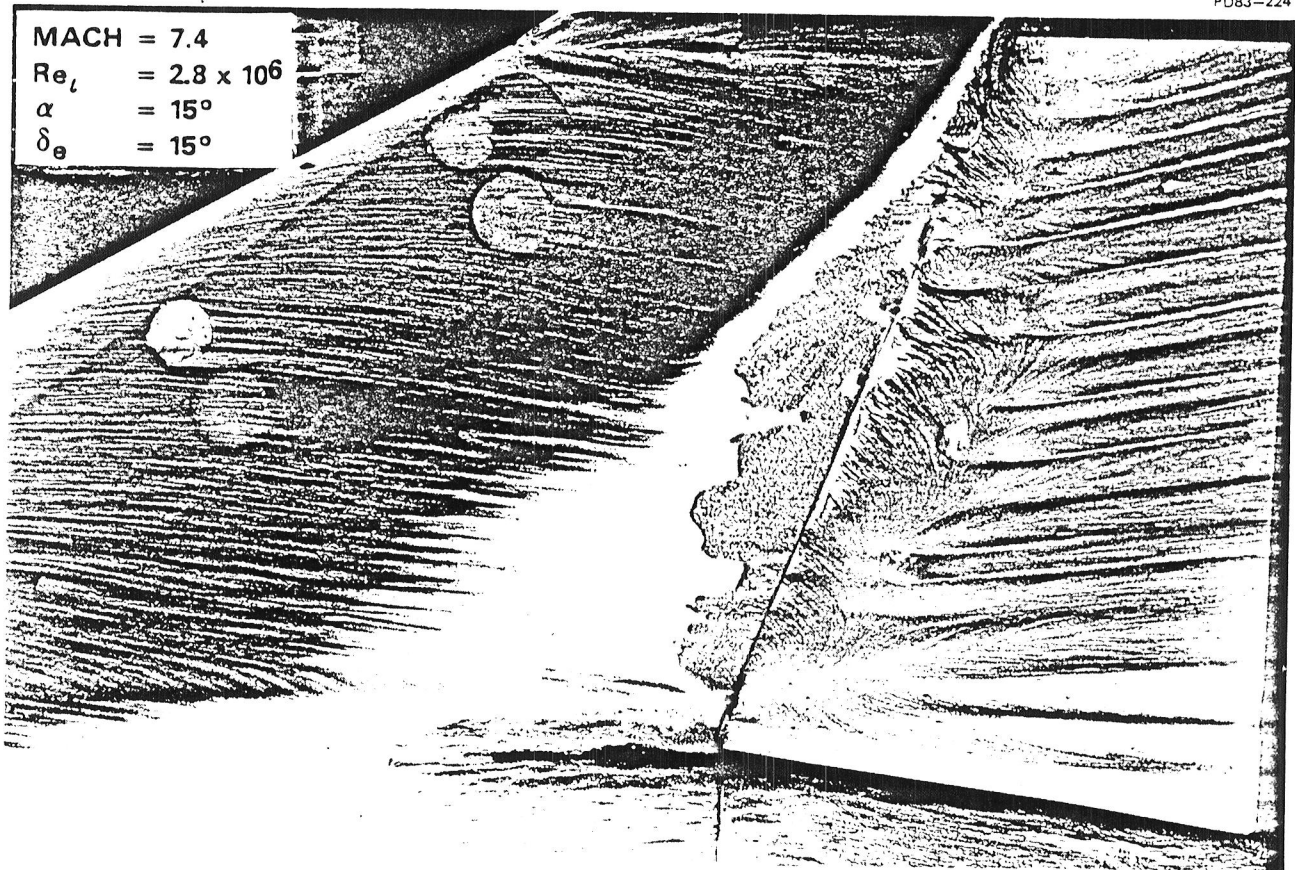


Figure A3b Left Wing and Elevon

<u>CONFIGURATIONS</u>	<u>MACH</u>
BACKWARD FACING STEPS	1.5, 2.25, 2.67, 5.3, 7.0
FORWARD FACING STEP	2.02
BLUNT FLAT PLATE	2.25
FLAT PLATE WITH FLAP	2.25
DELTA WING WITH BACKWARD FACING STEP	2.25
HOLLOW CYLINDER-FLARE	2.25, 5.3
<u>MEASUREMENTS</u>	<u>REYNOLDS NUMBER AT SEPARATION</u>
SUBLIMING COATINGS	$10^5 - 10^6$
SURFACE OIL FLOW	
STATIC PRESSURE	
SURFACE THERMOCOUPLES	<u>REATTACHMENT FLOW STATES</u>
HOT WIRE ANEMOMETER	LAMINAR
SCHLIERENS/SHADOWGRAPHS	TRANSITIONAL
	TURBULENT

Figure A4 Scope of Ginoux Flow Reattachment Test

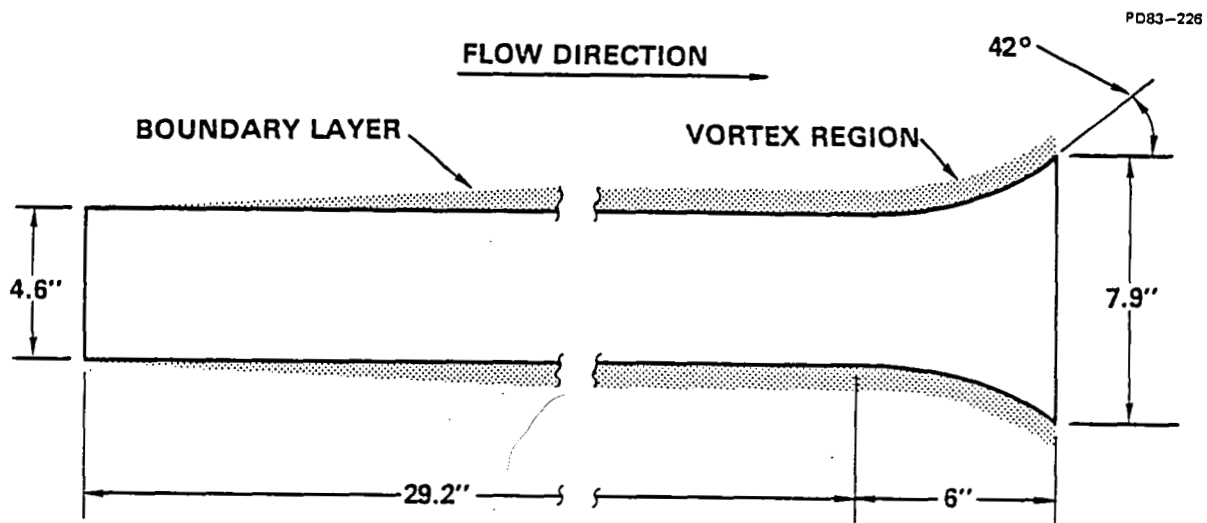


Figure A5 NYU Turbulent Vortex Model

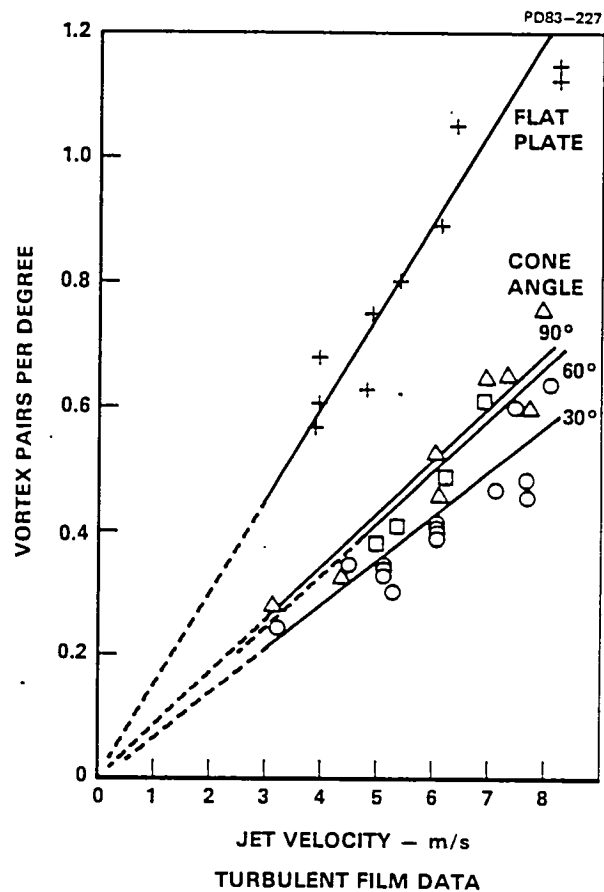
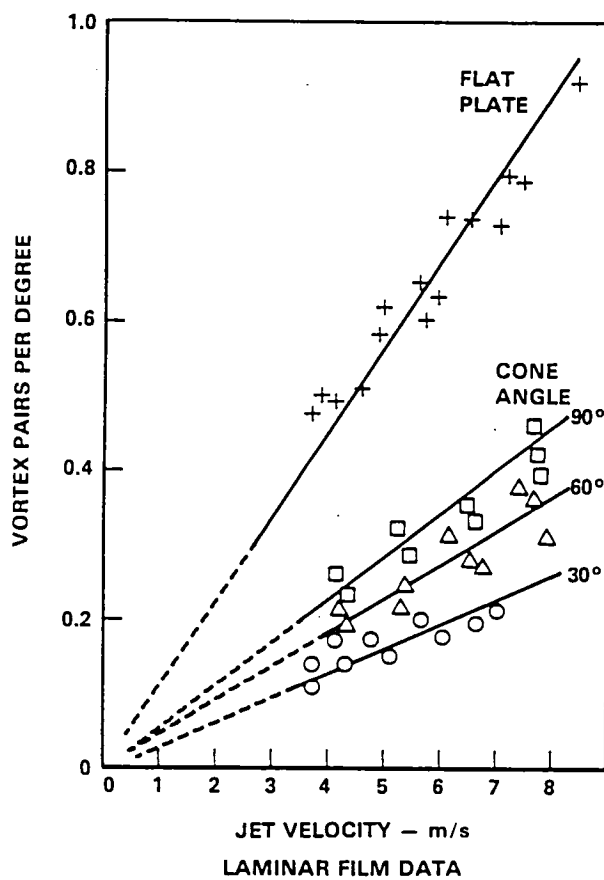
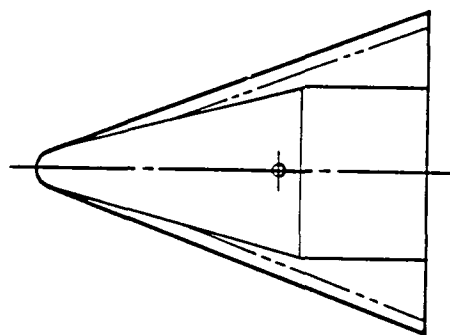


Figure A6 Vortex Spacing on Cones

PD83-228



LENGTH	68.82 INCHES
SPAN	54.88 INCHES
HEIGHT	32.79 INCHES
WING SWEEP	70 DEGREES (TRUE)
WING AREA	14 SQUARE FEET
NOSE TIP RADIUS	3 INCHES
LEADING EDGE RADIUS	2 INCHES
AVERAGE WEIGHT	
AEROTHERMODYNAMIC	
STRUCTURAL VEHICLE	1130 POUNDS
AEROTHERMODYNAMIC	
ELASTIC VEHICLE	1225 POUNDS

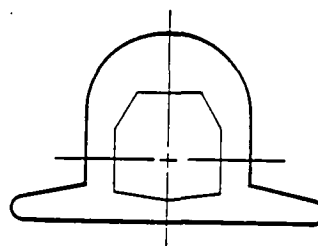
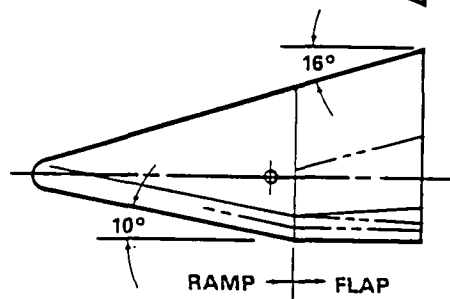


Figure A7 ASSET Vehicle Configuration

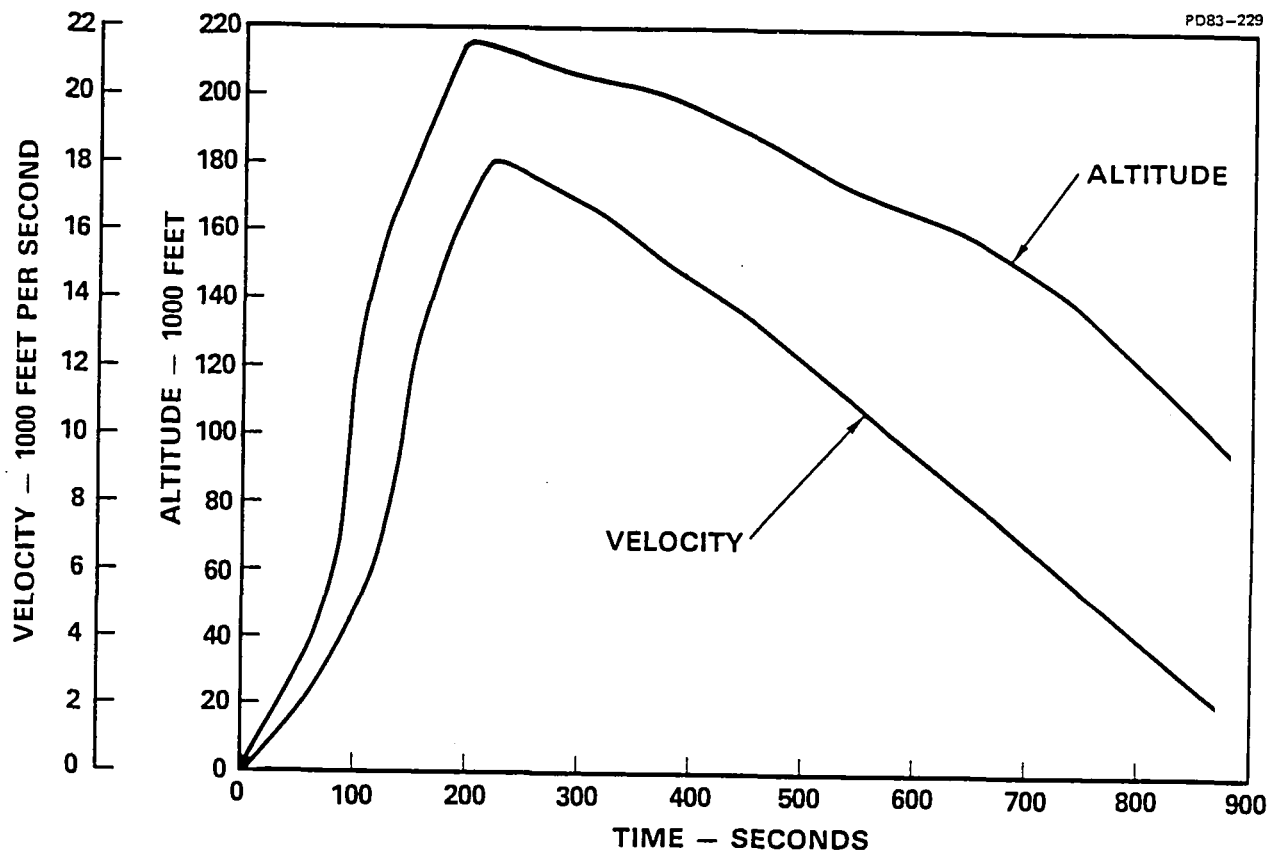


Figure A8 ASV-3 Flight Test Trajectory Parameters

TIME (SECONDS)	ANGLE-OF- ATTACK α_v (DEGREES)	ANGLE-OF- SIDESLIP β_v (DEGREES)	MACH NO.	TIME (SECONDS)	ANGLE-OF- ATTACK α_v (DEGREES)	ANGLE-OF- SIDESLIP β_v (DEGREES)	MACH NO.
10	3.836	6.533	---	210	1.582	-0.276	---
20	-0.623	1.532	---	218	1.400	-0.240	---
30	1.967	0.633	---	225	39.900	-1.940	17.7
40	3.351	0.309	---	239	39.200	-1.200	17
50	2.951	-0.086	---	283	38.800	-1.160	16
60	3.190	-0.075	---	330	38.500	-1.000	15
70	1.982	-1.227	---	380	38.400	-0.440	14
80	2.156	0.862	---	424	38.300	-0.620	13
90	-1.557	-0.657	---	467	38.300	-1.000	12
100	-6.335	-0.459	---	509	38.400	-0.950	11
110	-8.031	0.404	---	547	38.500	-0.640	10
120	-9.188	0.119	---	584	38.500	-0.500	9
130	-10.158	-0.092	---	622	38.600	-0.600	8
140	-6.963	-0.077	---	660	38.700	-0.860	7
150	-0.901	-0.060	---	700	38.100	-0.420	6
160	3.167	-0.657	---	740	36.600	-0.320	5
170	3.225	-0.602	---	779	34.500	-0.200	4
180	2.841	-0.515	---	825	31.200	-0.400	3
190	2.438	-0.432	---	880	28.500	-0.050	2
200	2.018	-0.352	---	913	24.500	0.360	1.5

Figure A9 ASV-3 Flight Parameters

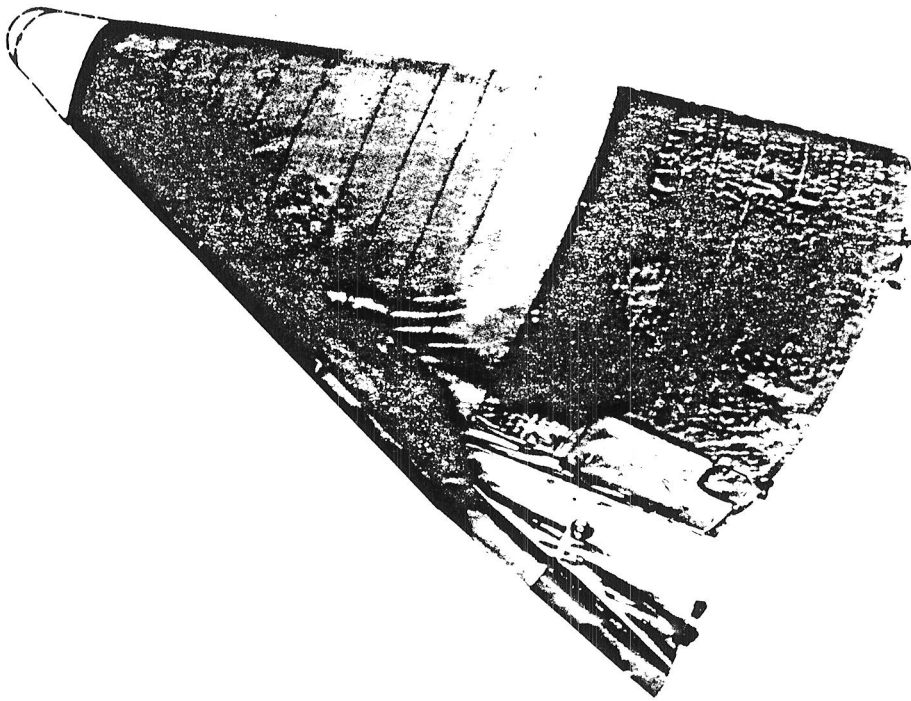


Figure A10 Post-Flight Asset

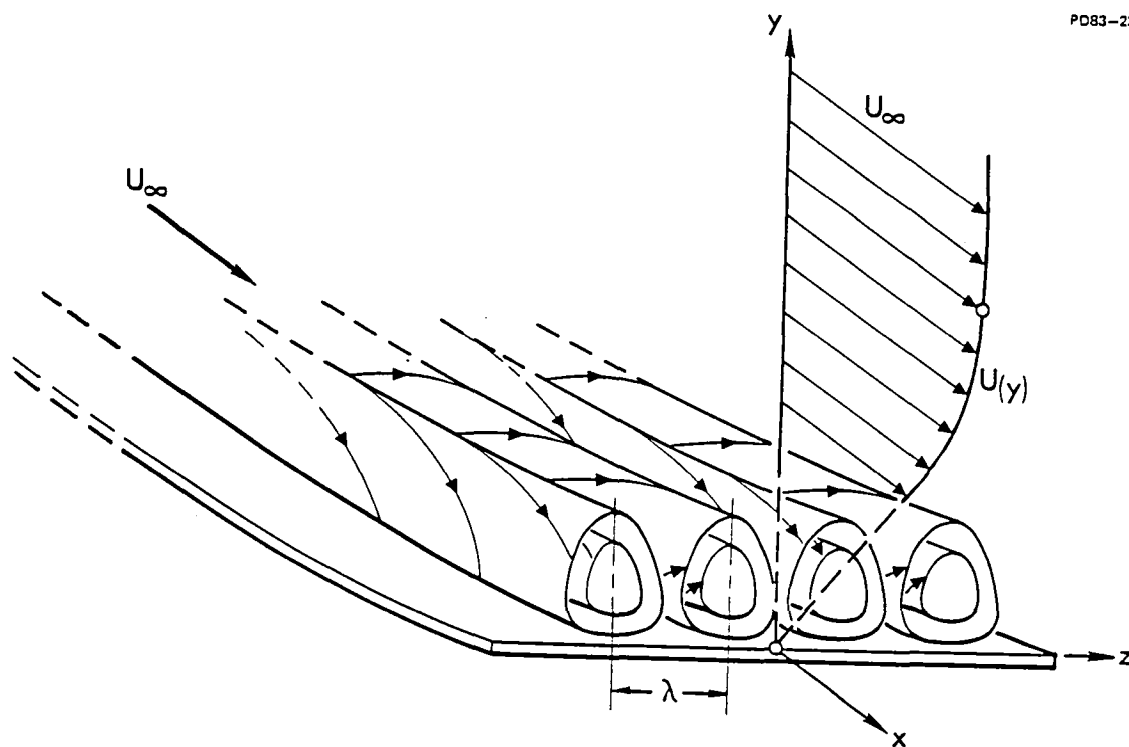


Figure A11 Gortler Vortices

APPENDIX B

Wing and Fuselage Leaside Test Data

This Appendix tabulates the reduced test data from the wing and fuselage leaside heating tests.

For completeness the summary and drawings of thermocouple locations from the main text are also included in Figures B1 thru B3.

WING LEESIDE SURFACE

MACH = 10									
RUN NO.	MACH NO.	ALPHA (DEG)	RE (X EG)	T(U) (R)	P(0) (PSI)	T(0) (R)	P(INF) (PSI)	T(INF) (R)	H(REF) (B/F2-S-R)
1	9.82	20.	.55	530.	356.25	1770.42	.00915	90.86	.025530
2	9.82	25.	.55	537.	350.29	1749.94	.00901	89.71	.025307
4	9.82	30.	.55	535.	354.71	1751.00	.00913	89.77	.025468
5	9.82	35.	.55	540.	350.07	1750.15	.00901	89.72	.025299
6	9.82	40.	.55	540.	356.36	1758.20	.00917	90.17	.025530
8	9.98	20.	1.07	533.	732.45	1786.74	.01708	89.13	.035458
10	9.98	25.	1.07	533.	743.49	1785.00	.01735	89.04	.035728
12	9.98	30.	1.03	537.	734.66	1818.73	.01709	90.87	.035520
14	9.98	35.	1.05	540.	729.14	1797.19	.01699	89.69	.035379
20	9.98	40.	1.09	538.	757.84	1796.75	.01767	89.68	.036079
22	10.16	20.	2.50	543.	1763.27	1784.13	.03730	86.37	.053348
3	10.16	25.	2.50	545.	1762.44	1791.31	.03726	86.75	.053338
18	10.16	30.	2.43	535.	1796.95	1794.79	.03801	86.94	.053879
16	10.16	35.	2.43	553.	1777.07	1819.60	.03750	88.25	.053577
7	10.16	40.	2.40	550.	1764.65	1809.81	.03726	87.72	.053380

MACH = 6									
RUN NO.	MACH NO.	ALPHA (DEG)	RE (X EG)	T(U) (R)	P(0) (PSI)	T(0) (R)	P(INF) (PSI)	T(INF) (R)	H(REF) (B/F2-S-R)
3	6.0	20.	.84	530.	48.11	869.77	.02938	105.32	.026871
7	6.0	25.	.80	530.	47.20	883.65	.02883	107.08	.026651
8	6.0	30.	.85	530.	49.20	875.77	.03055	106.08	.027188
9	6.0	35.	.80	530.	48.32	891.89	.02951	108.12	.026984
5	6.0	20.	2.63	533.	153.80	883.73	.09468	107.14	.048026
10	6.0	25.	2.53	535.	150.12	891.89	.09239	108.10	.047486
13	6.0	30.	2.69	535.	145.65	843.94	.08961	102.10	.046554
17	6.0	35.	2.77	535.	148.50	838.87	.09138	101.46	.046979
22	6.0	40.	3.38	540.	191.52	868.47	.11818	105.22	.053485
6	6.0	20.	5.40	535.	300.0	862.46	.18621	104.51	.066821
11	6.0	25.	5.12	535.	300.0	888.60	.18621	107.82	.067012
15	6.0	30.	4.69	537.	300.0	916.32	.18621	111.35	.067203
18	6.0	35.	5.15	538.	300.0	885.15	.18621	107.39	.066987
21	6.0	40.	5.20	540.	300.0	879.87	.18621	106.72	.066949
2	6.0	20.	6.585	535.	400.0	909.38	.24937	110.51	.077519
12	6.0	25.	7.10	538.	400.0	869.08	.24937	105.39	.077174
16	6.0	30.	7.07	538.	400.0	872.04	.24937	105.77	.077200
19	6.0	35.	7.096	540.	400.0	870.21	.24937	105.54	.077184
20	6.0	40.	6.73	536.	400.0	897.61	.24937	109.01	.077421

FUSELAGE LEESIDE SURFACE

MACH = 10									
RUN NO.	MACH NO.	ALPHA (DEG)	RE (X EG)	T(U) (R)	P(0) (PSI)	T(0) (R)	P(INF) (PSI)	T(INF) (R)	H(REF) (B/F2-S-R)
12	10.16	20.	.50	554.	357.5	1666.7	.00738	79.7	.0238235
13	10.16	25.	.50	548.	353.7	1794.8	.00723	86.7	.0238772
14	10.16	30.	.50	543.	350.9	1733.4	.00721	83.3	.0237003
15	10.16	35.	.50	537.	339.6	1778.4	.00694	85.5	.0233508
20	10.16	40.	.50	541.	338.6	1744.2	.00750	84.6	.0242364
3	10.34	20.	1.00	535.	742.6	1819.5	.01360	84.9	.0332186
4	10.34	25.	1.00	542.	743.7	1828.7	.01366	85.4	.0332702
5	10.34	30.	1.00	543.	742.8	1806.5	.01365	84.3	.0332033
6	10.34	35.	1.00	547.	741.9	1807.6	.01364	84.3	.0331859
16	10.34	40.	1.00	533.	743.4	1843.1	.01360	86.1	.0333052
8	10.36	20.	2.40	553.	1784.5	1821.7	.03300	85.1	.0512218
9	10.36	25.	2.40	559.	1788.3	1829.4	.03311	85.4	.0512964
10	10.36	30.	2.40	567.	1807.4	1828.5	.03350	85.4	.0515485
11	10.36	35.	2.40	571.	1787.2	1840.5	.03305	86.0	.0512919
17	10.36	40.	2.40	543.	1801.5	1812.8	.03340	84.6	.0514813

MACH = 6									
RUN NO.	MACH NO.	ALPHA (DEG)	RE (X EG)	T(U) (R)	P(0) (PSI)	T(0) (R)	P(INF) (PSI)	T(INF) (R)	H(REF) (B/F2-S-R)
20	6.0	20.	1.10	530.	51.85	799.34	.03167	96.44	.027695
21	6.0	25.	1.10	530.	54.75	808.26	.03345	97.56	.028485
22	6.0	30.	1.10	530.	49.32	797.91	.03012	96.26	.027009
23	6.0	35.	1.10	530.	50.49	801.31	.03084	96.68	.027337
24	6.0	40.	1.10	530.	53.87	801.67	.03292	96.73	.028236
3	6.0	20.	2.70	535.	149.20	882.76	.09182	107.01	.047302
4	6.0	25.	2.70	535.	148.32	891.04	.09127	108.06	.047200
6	6.0	30.	2.70	530.	150.48	877.56	.09261	106.35	.047479
7	6.0	35.	2.70	535.	147.07	878.78	.09049	106.51	.046946
8	6.0	40.	2.70	533.	147.31	877.15	.09064	106.30	.046977
13	6.0	20.	5.40	550.	306.39	886.04	.19023	107.50	.067701
12	6.0	25.	5.40	545.	300.75	875.69	.18668	106.19	.067002
11	6.0	30.	5.40	545.	296.93	903.41	.18427	109.70	.066772
10	6.0	35.	5.40	545.	301.58	913.15	.18720	110.95	.067357
9	6.0	40.	5.40	550.	302.08	904.83	.18751	109.89	.067356
14	6.0	20.	7.30	550.	399.34	893.88	.24895	108.54	.077326
15	6.0	25.	7.30	550.	399.67	888.88	.24916	107.91	.077315
17	6.0	30.	7.30	535.	400.83	895.54	.24990	108.75	.077484
18	6.0	35.	7.30	550.	401.41	887.02	.25027	107.67	.077467
19	6.0	40.	7.30	540.	401.99	898.78	.25063	108.78	.077598

Figure B1 Summary of Test Conditions for Leeside Heating Tests

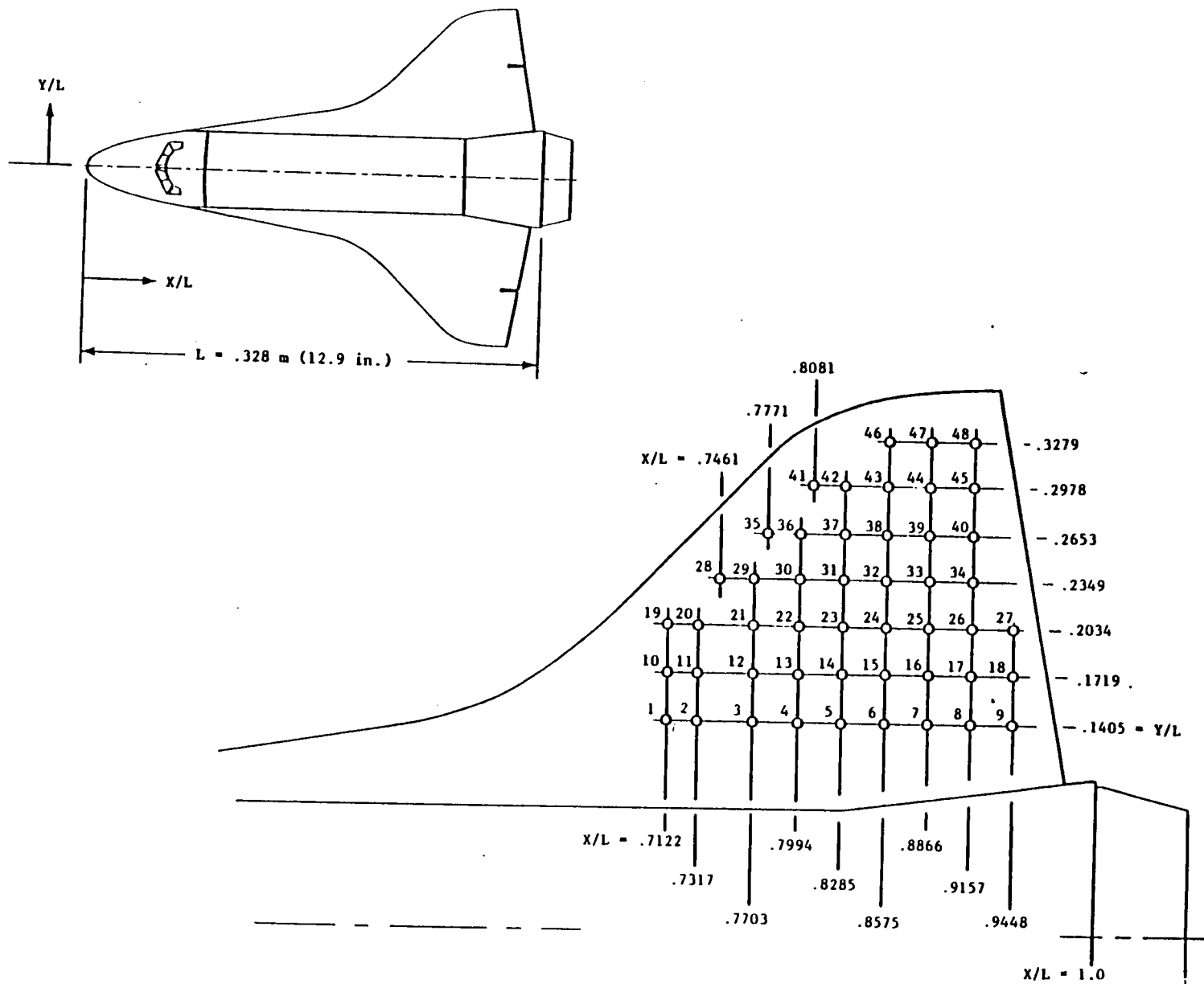


Figure B2 Wing Leeside Surface Thermocouple Locations

X/L =	.383	.447	.510	.573	.637	.682	.731
S/L	THERMOCOUPLE NUMBER						
.000	8	17	26	35	44	53	62
.010	9	18	27	36	45	54	63
.019	7	16	25	34	43	52	61
.039	6	15	24	33	42	51	60
.061	5	14	23	32	41	50	59
.080	4	13	22	31	40	49	58
.098	3	12	21	30	39	48	57
.117	2	11	20	29	38	47	56
.136	1	10	19	28	37	46	55

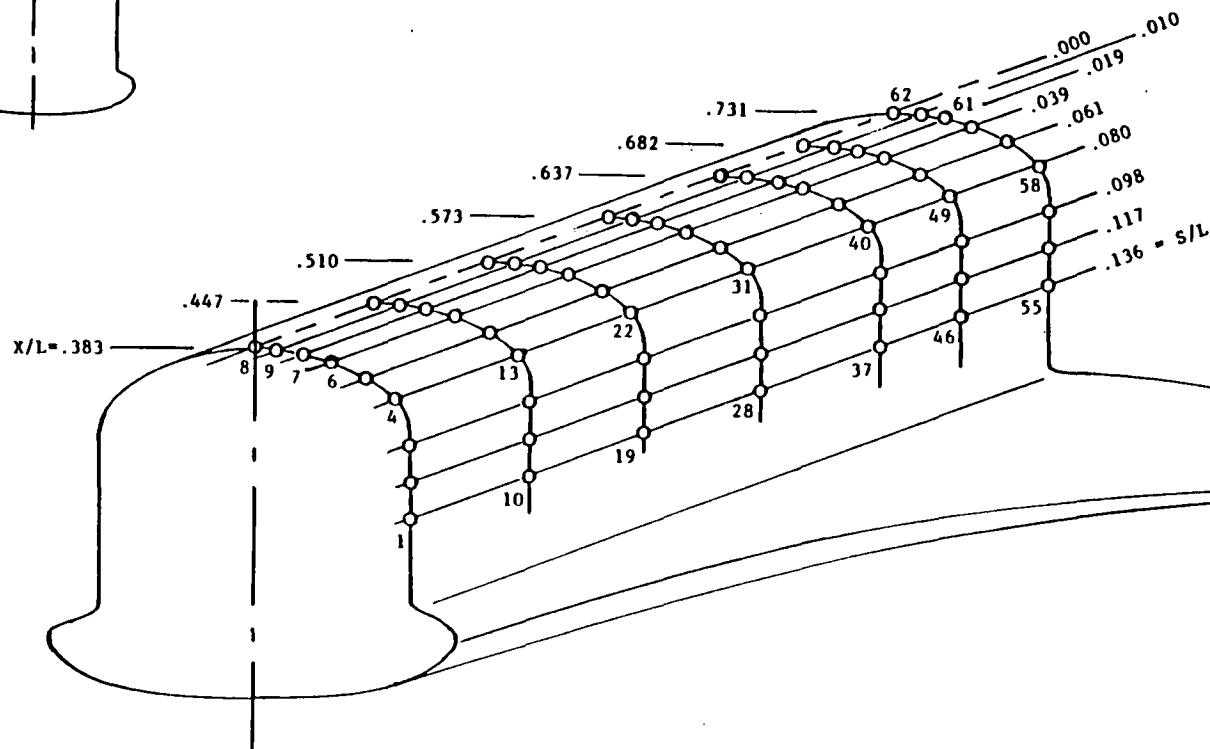
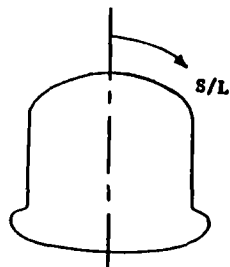
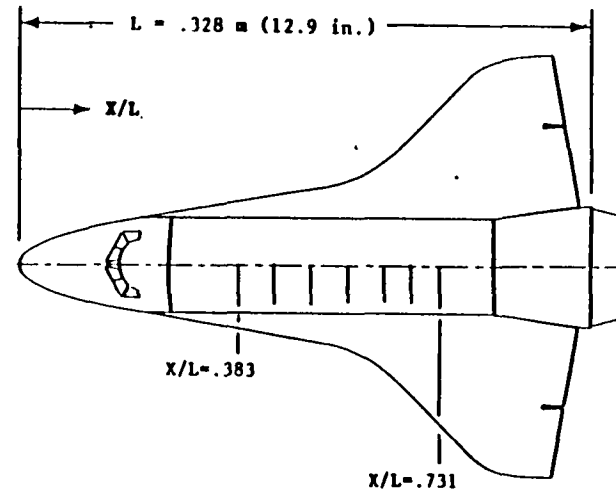


Figure B3 Fuselage Leeside Surface Thermocouple Locations

WING LEESIDE SURFACE ... MACH = 10

RUN NO.	MACH NO.	ALPHA (DEG)	RE (X E6)	T(U) (R)	P(0) (PSI)	T(0) (R)	P(INF) (PSI)	T(INF) (R)	H(REF) (B/F2-S-R)
---------	----------	-------------	-----------	----------	------------	----------	--------------	------------	-------------------

T/C	H/H(REF)	T/C	H/H(REF)	T/C	H/H(REF)	T/C	H/H(REF)
-----	----------	-----	----------	-----	----------	-----	----------

1	9.82	20.	.55	530.	356.25	1770.42	.00915	90.86	.025530
---	------	-----	-----	------	--------	---------	--------	-------	---------

(1)	.0024086	(2)	.00094109	(3)	.00066255	(4)	.00039577
(5)	.00059448	(6)	.000064715	(7)	.000015913	(8)	.00053619
(9)	.0023671	(10)	.0053484	(11)	.0032011	(12)	.0018591
(13)	.00059104	(14)	.00047809	(15)	.00079541	(16)	.00032524
(17)	.00068745	(18)	.0021054	(19)	.025329	(20)	.011876
(21)	.0059685	(22)	.0032877	(23)	.00099522	(24)	.00096135
(25)	.00094205	(26)	.00080951	(27)	.0019403	(28)	.013040
(29)	.0081473	(30)	.0044391	(31)	.0029651	(32)	.00090589
(33)	.0014083	(34)	.0018398	(35)	.017340	(36)	.010459
(37)	.0046071	(38)	.0034051	(39)	.0023718	(40)	.0016383
(41)	.015533	(42)	.011761	(43)	.0080312	(44)	.0059301
(45)	.0040240	(46)	.0083998	(47)	.0062463	(48)	.0046485

2	9.82	25.	.55	537.	350.29	1749.94	.00901	89.71	.025307
---	------	-----	-----	------	--------	---------	--------	-------	---------

(1)	.0012084	(2)	.00097690	(3)	.00051361	(4)	.00038578
(5)	.00021543	(6)	.00067289	(7)	.00022711	(8)	.00095075
(9)	.0020297	(10)	.0041223	(11)	.0030330	(12)	.0018137
(13)	.000002142	(14)	.00074386	(15)	.00027369	(16)	.00081541
(17)	.0010599	(18)	.0016408	(19)	.017359	(20)	.0091019
(21)	.0048677	(22)	.0033327	(23)	.00077944	(24)	.00124615
(25)	.00069126	(26)	.00204311	(27)	.0024376	(28)	.011595
(29)	.0059008	(30)	.0036481	(31)	.0027458	(32)	.0018871
(33)	.0017309	(34)	.0011883	(35)	.023680	(36)	.0076990
(37)	.0046275	(38)	.0023640	(39)	.0025612	(40)	.0013714
(41)	.012991	(42)	.010327	(43)	.0063083	(44)	.0053765
(45)	.0041113	(46)	.0061547	(47)	.0050699	(48)	.0047334

3	10.16	25.	2.50	545.	1762.44	1791.31	.03726	86.75	.053338
---	-------	-----	------	------	---------	---------	--------	-------	---------

(1)	.0017558	(2)	.0011619	(3)	.00024403	(4)	.00052966
(5)	.0017457	(6)	.00046074	(7)	.00093561	(8)	.0017491
(9)	.0025823	(10)	.0037104	(11)	.0015774	(12)	.0011400
(13)	.0010460	(14)	.0029290	(15)	.00047217	(16)	.00082683
(17)	.0019600	(18)	.0023233	(19)	.018588	(20)	.0076046
(21)	.0039100	(22)	.0015221	(23)	.0021857	(24)	.00071293
(25)	.00087508	(26)	.0014745	(27)	.0016539	(28)	.010342
(29)	.0061578	(30)	.0030945	(31)	.0023599	(32)	.00052214
(33)	.00073813	(34)	.0013659	(35)	.014470	(36)	.0067193
(37)	.0033496	(38)	.00072817	(39)	.0010854	(40)	.0014962
(41)	.011696	(42)	.0068529	(43)	.0070596	(44)	.0045947
(45)	.0039187	(46)	.0061396	(47)	.0048914	(48)	.0033125

WING LEESIDE SURFACE ... MACH = 10 --- CONTINUED

RUN NO.	MACH NO.	ALPHA (DEG)	RE (X E6)	T(U) (R)	P(0) (PSI)	T(0) (R)	P(INF) (PSI)	T(INF) (R)	H(REF) (B/F2-S-R)
---------	----------	-------------	-----------	----------	------------	----------	--------------	------------	-------------------

T/C	H/H(REF)	T/C	H/H(REF)	T/C	H/H(REF)	T/C	H/H(REF)
-----	----------	-----	----------	-----	----------	-----	----------

4	9.82	30.	.55	535.	354.71	1751.00	.00913	89.77	.025468
---	------	-----	-----	------	--------	---------	--------	-------	---------

(1)	.0010246	(2)	.00014215	(3)	.00022746	(4)	.00011206
(5)	.00034558	(6)	.00047408	(7)	.00082361	(8)	.00098272
(9)	.00076642	(10)	.0041347	(11)	.0022564	(12)	.00070820
(13)	.000016923	(14)	.000016156	(15)	.00074581	(16)	.00041172
(17)	.0013286	(18)	.00093111	(19)	.013902	(20)	.0066394
(21)	.0045866	(22)	.0021521	(23)	.0010365	(24)	.00033655
(25)	.00052649	(26)	.00090023	(27)	.0015686	(28)	.0096450
(29)	.0053175	(30)	.0030192	(31)	.0018628	(32)	.0010486
(33)	.0012399	(34)	.0015684	(35)	.011403	(36)	.0075309
(37)	.0040675	(38)	.0024181	(39)	.0016629	(40)	.0011096
(41)	.010559	(42)	.0080202	(43)	.0063730	(44)	.0046064
(45)	.0034914	(46)	.0055379	(47)	.0039919	(48)	.0035328

5	9.82	35.	.55	540.	350.07	1750.15	.00901	89.72	.025299
---	------	-----	-----	------	--------	---------	--------	-------	---------

(1)	.00086108	(2)	.0010768	(3)	.00013256	(4)	.00013353
(5)	.00052184	(6)	.00067749	(7)	.00074048	(8)	.0014971
(9)	.00066656	(10)	.0032999	(11)	.0017736	(12)	.00052815
(13)	.000084829	(14)	.00070465	(15)	.00068622	(16)	.0012335
(17)	.00085826	(18)	.0020575	(19)	.0098199	(20)	.0051089
(21)	.0028426	(22)	.0015111	(23)	.00096014	(24)	.00064597
(25)	.0010548	(26)	.0014178	(27)	.0013294	(28)	.0098321
(29)	.0044491	(30)	.0035128	(31)	.0019337	(32)	.0011537
(33)	.0014877	(34)	.0012933	(35)	.0095526	(36)	.0049534
(37)	.0039741	(38)	.0017665	(39)	.0014469	(40)	.0014373
(41)	.0080388	(42)	.0052609	(43)	.0037776	(44)	.0028292
(45)	.0023886	(46)	.0036861	(47)	.0031382	(48)	.0024832

6	9.82	40.	.55	540.	356.36	1758.20	.00917	90.17	.025530
---	------	-----	-----	------	--------	---------	--------	-------	---------

(1)	.00046389	(2)	.00015122	(3)	.00037749	(4)	.00063043
(5)	.00075629	(6)	.00069081	(7)	.00033496	(8)	.00041570
(9)	.00091132	(10)	.0027476	(11)	.00056894	(12)	.0011031
(13)	.00089982	(14)	.0012646	(15)	.0016600	(16)	.00075652
(17)	.00094126	(18)	.0013513	(19)	.0082184	(20)	.0042679
(21)	.0025315	(22)	.00070079	(23)	.0010689	(24)	.00088275
(25)	.00080412	(26)	.00041858	(27)	.00091303	(28)	.0082834
(29)	.0045098	(30)	.0032508	(31)	.0015520	(32)	.0010524
(33)	.00083198	(34)	.0011921	(35)	.0072308	(36)	.0041277
(37)	.0028090	(38)	.0012023	(39)	.00041157	(40)	.00059072
(41)	.0060619	(42)	.0037656	(43)	.0019395	(44)	.0017893
(45)	.0014147	(46)	.0029519	(47)	.0011910	(48)	.0013651

WING LEESIDE SURFACE ... MACH = 10 --- CONTINUED

RUN NO.	MACH NO.	ALPHA (DEG)	RE (X E6)	T(U) (R)	P(0) (PSI)	T(0) (R)	P(INF) (PSI)	T(INF) (R)	H(REF) (B/F2-S-R)
		T/C	H/H(REF)	T/C	H/H(REF)	T/C	H/H(REF)	T/C	H/H(REF)

7	10.16	40.	2.40	550.	1764.65	1809.81	.03726	87.72	.053380
---	-------	-----	------	------	---------	---------	--------	-------	---------

(1)	.00273479	(2)	.00135572	(3)	.00087486	(4)	.00074928
(5)	.0011944	(6)	.0012712	(7)	.0021169	(8)	.0013920
(9)	.0020015	(10)	.0013211	(11)	.0017222	(12)	.00054251
(13)	.0026530	(14)	.0028549	(15)	.0017602	(16)	.0034065
(17)	.0021169	(18)	.0018040	(19)	.0084147	(20)	.0068191
(21)	.0011395	(22)	.0033153	(23)	.0041758	(24)	.0029947
(25)	.0024195	(26)	.0026311	(27)	.0040684	(28)	.0099206
(29)	.0054765	(30)	.0014435	(31)	.0064219	(32)	.0014662
(33)	.0020639	(34)	.0028228	(35)	.011055	(36)	.0061691
(37)	.0025135	(38)	.0011118	(39)	.0029673	(40)	.0033160
(41)	.0077794	(42)	.0076947	(43)	.0020428	(44)	.0016675
(45)	.0060042	(46)	.00012279	(47)	.0015811	(48)	.0021081

8	9.98	20.	1.07	533.	732.45	1786.74	.01708	89.13	.035458
---	------	-----	------	------	--------	---------	--------	-------	---------

(1)	.0013201	(2)	.00018701	(3)	.000088307	(4)	.00070293
(5)	.00028645	(6)	.00041433	(7)	.00051412	(8)	.00099471
(9)	.0020951	(10)	.0057471	(11)	.0020248	(12)	.0011603
(13)	.00065922	(14)	.00057064	(15)	.00072189	(16)	.00069835
(17)	.0014161	(18)	.0018631	(19)	.027542	(20)	.012120
(21)	.0063379	(22)	.0020983	(23)	.00094717	(24)	.00085865
(25)	.00087579	(26)	.0011157	(27)	.0023511	(28)	.013233
(29)	.0070695	(30)	.0041458	(31)	.0021466	(32)	.00092889
(33)	.0016015	(34)	.0018303	(35)	.016511	(36)	.0085131
(37)	.0049504	(38)	.0024816	(39)	.0011985	(40)	.0016673
(41)	.015689	(42)	.012188	(43)	.0073239	(44)	.0056279
(45)	.0033239	(46)	.00688019	(47)	.0051804	(48)	.0045802

10	9.98	25.	1.07	533.	743.49	1785.00	.01735	89.04	.035728
----	------	-----	------	------	--------	---------	--------	-------	---------

(1)	.0017727	(2)	.00030742	(3)	.000099278	(4)	.000022500
(5)	.00031454	(6)	.00027562	(7)	.00066529	(8)	.0012811
(9)	.0014648	(10)	.0041541	(11)	.0016059	(12)	.00069912
(13)	.00021868	(14)	.00040428	(15)	.00012835	(16)	.0011944
(17)	.0018277	(18)	.0025541	(19)	.018280	(20)	.0091183
(21)	.0044004	(22)	.0015545	(23)	.00080851	(24)	.00031134
(25)	.0012112	(26)	.0018067	(27)	.0019545	(28)	.010315
(29)	.0054404	(30)	.0032214	(31)	.0017562	(32)	.00059777
(33)	.0017760	(34)	.0016561	(35)	.013689	(36)	.0074478
(37)	.0040344	(38)	.0020270	(39)	.0017064	(40)	.0013959
(41)	.012589	(42)	.0092385	(43)	.0059815	(44)	.0040999
(45)	.0027994	(46)	.00554739	(47)	.0043881	(48)	.0045421

WING LEESIDE SURFACE ... MACH = 10 --- CONTINUED

RUN NO.	MACH NO.	ALPHA (DEG)	RE (X E6)	T(U) (R)	P(0) (PSI)	T(0) (R)	P(INF) (PSI)	T(INF) (R)	H(REF) (B/F2-S-R)
		T/C	H/H(REF)	T/C	H/H(REF)	T/C	H/H(REF)	T/C	H/H(REF)

12	9.98	30.	1.03	537.	734.66	1818.73	.01709	90.87	.035520
----	------	-----	------	------	--------	---------	--------	-------	---------

(1)	.0012534	(2)	.00050064	(3)	.000086823	(4)	.00026833
(5)	.00032267	(6)	.00063709	(7)	.00057785	(8)	.0015751
(9)	.0011486	(10)	.0046350	(11)	.00086388	(12)	.00015987
(13)	.000010955	(14)	.00014777	(15)	.00064911	(16)	.00093129
(17)	.0011212	(18)	.0019979	(19)	.012372	(20)	.0068662
(21)	.0032591	(22)	.00099566	(23)	.00094399	(24)	.0000028345
(25)	.00047424	(26)	.0011083	(27)	.0017570	(28)	.0092812
(29)	.0048737	(30)	.0032772	(31)	.0024246	(32)	.00058866
(33)	.0010857	(34)	.0014830	(35)	.011474	(36)	.0067182
(37)	.0037020	(38)	.0016716	(39)	.0021342	(40)	.0015973
(41)	.0095545	(42)	.0071162	(43)	.0043301	(44)	.0027353
(45)	.0025346	(46)	.00455579	(47)	.0033856	(48)	.0029378

14	9.98	35.	1.05	540.	729.14	1797.19	.01699	89.69	.035379
----	------	-----	------	------	--------	---------	--------	-------	---------

(1)	.00053099	(2)	.00094557	(3)	.00078966	(4)	.00073017
(5)	.00053812	(6)	.00041627	(7)	.0019522	(8)	.0012434
(9)	.0024944	(10)	.0010696	(11)	.0020606	(12)	.0011364
(13)	.0011439	(14)	.00038907	(15)	.0015350	(16)	.0012721
(17)	.0017937	(18)	.0032804	(19)	.010714	(20)	.0057522
(21)	.0021022	(22)	.0020734	(23)	.0014891	(24)	.0012627
(25)	.0023046	(26)	.0021038	(27)	.0031825	(28)	.0091883
(29)	.0045103	(30)	.0026036	(31)	.0015285	(32)	.0010476
(33)	.0012747	(34)	.0015899	(35)	.0099362	(36)	.0059879
(37)	.0032580	(38)	.0010860	(39)	.00045620	(40)	.0018705
(41)	.0073874	(42)	.0056942	(43)	.0030999	(44)	.0022035
(45)	.0026741	(46)	.0036247	(47)	.0022577	(48)	.0023202

16	10.16	35.	2.43	553.	1777.07	1819.60	.03750	88.25	.053577
----	-------	-----	------	------	---------	---------	--------	-------	---------

(1)	.0019457	(2)	.00088419	(3)	.00044770	(4)	.00089874
(5)	.0037551	(6)	.00046027	(7)	.0016024	(8)	.00021833
(9)	.00082187	(10)	.0049173	(11)	.0016926	(12)	.00093021
(13)	.0019996	(14)	.0061175	(15)	.00073741	(16)	.0010547
(17)	.0013014	(18)	.0017501	(19)	.010328	(20)	.0071913
(21)	.0017793	(22)	.0019847	(23)	.0089881	(24)	.0014300
(25)	.0011402	(26)	.0012408	(27)	.0026021	(28)	.010579
(29)	.0064059	(30)	.0032911	(31)	.0043909	(32)	.00036989
(33)	.0011895	(34)	.0016431	(35)	.012471	(36)	.0061845
(37)	.0035059	(38)	.00072999	(39)	.0019405	(40)	.0015914
(41)	.0089009	(42)	.0060268	(43)	.0019684	(44)	.0027422
(45)	.0055646	(46)	.0023340	(47)	.0017267	(48)	.0018294

WING LEESIDE SURFACE ... MACH = 10 --- CONCLUDED

RUN NO.	MACH NO.	ALPHA (DEG)	RE (X EG)	T(U) (R)	P(0) (PSI)	T(0) (R)	P(INF) (PSI)	T(INF) (R)	H(REF) (B/F2-S-R)
---------	----------	-------------	-----------	----------	------------	----------	--------------	------------	-------------------

T/C	H/H(REF)	T/C	H/H(REF)	T/C	H/H(REF)	T/C	H/H(REF)
-----	----------	-----	----------	-----	----------	-----	----------

18	10.16	30.	2.43	535.	1796.95	1794.79	.03801	86.94	.053879
----	-------	-----	------	------	---------	---------	--------	-------	---------

(1)	.0020768	(2)	.00099714	(3)	.00034104	(4)	.00056356
(5)	.0022600	(6)	.00038040	(7)	.00097876	(8)	.0015732
(9)	.0016634	(10)	.0033320	(11)	.00092446	(12)	.00083344
(13)	.0010316	(14)	.0069111	(15)	.00030912	(16)	.00091856
(17)	.0016701	(18)	.0019966	(19)	.012522	(20)	.0078464
(21)	.0022026	(22)	.0015407	(23)	.0045893	(24)	.00096732
(25)	.00071928	(26)	.0011704	(27)	.0020624	(28)	.010117
(29)	.0057992	(30)	.0023446	(31)	.0022912	(32)	.00036141
(33)	.0010362	(34)	.0016278	(35)	.013336	(36)	.0065864
(37)	.0033681	(38)	.00074546	(39)	.0017051	(40)	.0015799
(41)	.0084607	(42)	.0062947	(43)	.0037457	(44)	.0032920
(45)	.0050921	(46)	.0036224	(47)	.0025826	(48)	.0020209

20	9.98	40.	1.09	538.	757.84	1796.75	.01767	89.68	.036079
----	------	-----	------	------	--------	---------	--------	-------	---------

(1)	.0011830	(2)	.00038183	(3)	.000065503	(4)	.00088392
(5)	.0012736	(6)	.0014243	(7)	.0013197	(8)	.0012946
(9)	.0018934	(10)	.0035147	(11)	.00012428	(12)	.00029253
(13)	.00067431	(14)	.0021745	(15)	.0016257	(16)	.0015464
(17)	.0018703	(18)	.0014181	(19)	.0074734	(20)	.0041305
(21)	.0013114	(22)	.0011361	(23)	.0032432	(24)	.0019937
(25)	.0012384	(26)	.0016605	(27)	.0020730	(28)	.0080228
(29)	.0057097	(30)	.0030678	(31)	.0032648	(32)	.0011858
(33)	.0012295	(34)	.0021952	(35)	.0080083	(36)	.0043931
(37)	.0020838	(38)	.0016586	(39)	.0019872	(40)	.0016517
(41)	.0041556	(42)	.0024826	(43)	.0016960	(44)	.0025743
(45)	.0031891	(46)	.0016179	(47)	.0016725	(48)	.0017143

22	10.16	20.	2.50	543.	1763.27	1784.13	.03730	86.37	.053348
----	-------	-----	------	------	---------	---------	--------	-------	---------

(1)	.0018843	(2)	.00087815	(3)	.00038319	(4)	.00032228
(5)	.00095817	(6)	.0024784	(7)	.00097098	(8)	.00083520
(9)	.0017313	(10)	.0035832	(11)	.0019041	(12)	.00053248
(13)	.00054005	(14)	.0023490	(15)	.00068946	(16)	.00052395
(17)	.00043918	(18)	.0013704	(19)	.025725	(20)	.012318
(21)	.0057259	(22)	.0017380	(23)	.0010134	(24)	.0010006
(25)	.00041759	(26)	.00046956	(27)	.0014993	(28)	.014084
(29)	.0072641	(30)	.0048867	(31)	.0024105	(32)	.00080078
(33)	.00045556	(34)	.00086257	(35)	.015834	(36)	.0079670
(37)	.0044735	(38)	.0023632	(39)	.0016783	(40)	.00099421
(41)	.013448	(42)	.010282	(43)	.0069722	(44)	.0065967
(45)	.0048062	(46)	.0056353	(47)	.0046319	(48)	.0033483

WING LEESIDE SURFACE ... MACH = 6

RUN NO.	MACH NO.	ALPHA (DEG)	RE (X E6)	T(U) (R)	P(0) (PSI)	T(0) (R)	P(INF) (PSI)	T(INF) (R)	H(REF) (B/F2-S-R)
		T/C	H/H(REF)	T/C	H/H(REF)	T/C	H/H(REF)	T/C	H/H(REF)

2	6.0	20.	6.585	535.	400.0	909.38	.24937	110.51	.077519
---	-----	-----	-------	------	-------	--------	--------	--------	---------

(1)	.0067941	(2)	.0052101	(3)	.0041850	(4)	.0048410
(5)	.0072619	(6)	.010427	(7)	.010884	(8)	.010616
(9)	.0095170	(10)	.0050312	(11)	.0012227	(12)	.0014967
(13)	.0035018	(14)	.0048618	(15)	.0059438	(16)	.0061699
(17)	.0073805	(18)	.0085319	(19)	.021047	(20)	.010217
(21)	.0041708	(22)	.0033269	(23)	.0086604	(24)	.0012781
(25)	.0045513	(26)	.0070531	(27)	.010578	(28)	.023249
(29)	.011065	(30)	.0070622	(31)	.0083256	(32)	.0036962
(33)	.0067014	(34)	.0081011	(35)	.023335	(36)	.011614
(37)	.0087781	(38)	.0020419	(39)	.0066524	(40)	.0083729
(41)	.018812	(42)	.013831	(43)	.0085841	(44)	.0087947
(45)	.0079488	(46)	.0074245	(47)	.0065471	(48)	.0079711

3	6.0	20.	.84	530.	48.11	869.77	.02938	105.32	.026871
---	-----	-----	-----	------	-------	--------	--------	--------	---------

(1)	.0027951	(2)	.0015280	(3)	.0012221	(4)	.0017518
(5)	.00095819	(6)	.0020600	(7)	.0010116	(8)	.00012328
(9)	.0016907	(10)	.0054426	(11)	.0013283	(12)	.0010659
(13)	.00079334	(14)	.0012958	(15)	.0011077	(16)	.0016786
(17)	.0009638	(18)	.0027965	(19)	.012176	(20)	.0078417
(21)	.0038546	(22)	.0024030	(23)	.0012122	(24)	.0012121
(25)	.00065445	(26)	.0012226	(27)	.0039825	(28)	.017099
(29)	.011475	(30)	.0048328	(31)	.0029701	(32)	.00080959
(33)	.0010722	(34)	.0021855	(35)	.015711	(36)	.011167
(37)	.0046062	(38)	.0021000	(39)	.0026478	(40)	.0020745
(41)	.015333	(42)	.013413	(43)	.0074221	(44)	.0062090
(45)	.0053016	(46)	.0095107	(47)	.0078321	(48)	.0071728

5	6.0	20.	2.63	533.	153.80	883.73	.09468	107.14	.048026
---	-----	-----	------	------	--------	--------	--------	--------	---------

(1)	.0011551	(2)	.0016482	(3)	.0020233	(4)	.0025014
(5)	.0020464	(6)	.0033042	(7)	.0065590	(8)	.0024041
(9)	.0050545	(10)	.0011140	(11)	.0015152	(12)	.00095126
(13)	.0011211	(14)	.0022239	(15)	.0016987	(16)	.0024073
(17)	.0019303	(18)	.0033895	(19)	.013932	(20)	.0068052
(21)	.0028210	(22)	.0021704	(23)	.0016090	(24)	.0023725
(25)	.0015149	(26)	.00085177	(27)	.0058385	(28)	.018661
(29)	.0086779	(30)	.0021042	(31)	.0020701	(32)	.0018826
(33)	.0022572	(34)	.0016199	(35)	.017505	(36)	.0085155
(37)	.0033224	(38)	.0028186	(39)	.0025330	(40)	.0013704
(41)	.013375	(42)	.0089166	(43)	.0043879	(44)	.0030578
(45)	.0029131	(46)	.0061519	(47)	.0044501	(48)	.0051844

WING LEESIDE SURFACE ... MACH = 6 --- CONTINUED

RUN NO.	MACH NO.	ALPHA (DEG)	RE (X E6)	T(U) (R)	P(0) (PSI)	T(0) (R)	P(INF) (PSI)	T(INF) (R)	H(REF) (B/F2-S-R)
		T/C	H/H(REF)	T/C	H/H(REF)	T/C	H/H(REF)	T/C	H/H(REF)

6	6.0	20.	5.40	535.	300.0	862.46	.18621	104.51	.066821
---	-----	-----	------	------	-------	--------	--------	--------	---------

(1)	.0038095	(2)	.0045038	(3)	.0049909	(4)	.0031383
(5)	.0052890	(6)	.0077100	(7)	.010681	(8)	.0069778
(9)	.0066714	(10)	.0046751	(11)	.0020434	(12)	.0012314
(13)	.0023098	(14)	.0046826	(15)	.0034700	(16)	.0043331
(17)	.0058637	(18)	.0064889	(19)	.017716	(20)	.0085856
(21)	.0030890	(22)	.0030079	(23)	.0066553	(24)	.0032171
(25)	.0043883	(26)	.0030536	(27)	.0078271	(28)	.021444
(29)	.0095038	(30)	.0032499	(31)	.0043752	(32)	.0042360
(33)	.0051040	(34)	.0040741	(35)	.021861	(36)	.010314
(37)	.0052431	(38)	.0025014	(39)	.0042923	(40)	.0045454
(41)	.017376	(42)	.013056	(43)	.0064079	(44)	.0048555
(45)	.0033232	(46)	.0050971	(47)	.0044157	(48)	.0029235

7	6.0	25.	.80	530.	47.20	883.65	.02883	107.08	.026651
---	-----	-----	-----	------	-------	--------	--------	--------	---------

(1)	.00085146	(2)	.0024060	(3)	.00014626	(4)	.00083357
(5)	.0025029	(6)	.0016068	(7)	.00082587	(8)	.00018076
(9)	.00010266	(10)	.0032812	(11)	.00042908	(12)	.0012253
(13)	.00066430	(14)	.0010027	(15)	.0021496	(16)	.0022633
(17)	.0016432	(18)	.00013435	(19)	.012099	(20)	.0064373
(21)	.0028712	(22)	.0031853	(23)	.0021546	(24)	.00084730
(25)	.0016509	(26)	.00047471	(27)	.0023146	(28)	.014848
(29)	.0061832	(30)	.0029661	(31)	.0030191	(32)	.00078792
(33)	.0015671	(34)	.0020054	(35)	.015494	(36)	.0067853
(37)	.0028736	(38)	.00026142	(39)	.0025552	(40)	.0022707
(41)	.011174	(42)	.0072288	(43)	.0051725	(44)	.0027536
(45)	.0034741	(46)	.0057856	(47)	.0071635	(48)	.0057305

8	6.0	30.	.85	530.	49.20	875.77	.03055	106.08	.027188
---	-----	-----	-----	------	-------	--------	--------	--------	---------

(1)	.0024068	(2)	.00080646	(3)	.00113786	(4)	.00043844
(5)	.00082200	(6)	.000077443	(7)	.00010954	(8)	.00050235
(9)	.00037480	(10)	.0023864	(11)	.00176078	(12)	.00076229
(13)	.00114900	(14)	.0010056	(15)	.00075806	(16)	.00044309
(17)	.0010861	(18)	.00069500	(19)	.012202	(20)	.0051606
(21)	.0028492	(22)	.0024308	(23)	.0020260	(24)	.00071140
(25)	.00089918	(26)	.00110841	(27)	.0023346	(28)	.012081
(29)	.0057376	(30)	.0034312	(31)	.0033631	(32)	.00073066
(33)	.0015185	(34)	.0017599	(35)	.011228	(36)	.0054527
(37)	.0031446	(38)	.00209222	(39)	.0010550	(40)	.00065122
(41)	.0099849	(42)	.0070140	(43)	.0038560	(44)	.0022350
(45)	.0022779	(46)	.0055120	(47)	.0053609	(48)	.0044594

WING LEESIDE SURFACE ... MACH = 6 --- CONTINUED

RUN NO.	MACH NO.	ALPHA (DEG)	RE (X E6)	T(U) (R)	P(0) (PSI)	T(0) (R)	P(INF) (PSI)	T(INF) (R)	H(REF) (B/F2-S-R)
---------	----------	-------------	-----------	----------	------------	----------	--------------	------------	-------------------

T/C	H/H(REF)	T/C	H/H(REF)	T/C	H/H(REF)	T/C	H/H(REF)
-----	----------	-----	----------	-----	----------	-----	----------

9	6.0	35.	.80	530.	48.32	891.89	.02951	108.12	.026984
---	-----	-----	-----	------	-------	--------	--------	--------	---------

(1)	.0009865	(2)	.0117646	(3)	.00121316	(4)	.00047006
(5)	.00069435	(6)	.00065868	(7)	.00041756	(8)	.00049389
(9)	.0015664	(10)	.0016901	(11)	.00141868	(12)	.00106429
(13)	.00031233	(14)	.00017407	(15)	.00094309	(16)	.00110599
(17)	.00092347	(18)	.00061738	(19)	.010965	(20)	.0046545
(21)	.0025533	(22)	.0020977	(23)	.0031900	(24)	.00057125
(25)	.00134278	(26)	.00163861	(27)	.0029233	(28)	.011282
(29)	.0051255	(30)	.0030743	(31)	.0034195	(32)	.00098795
(33)	.00098032	(34)	.00090661	(35)	.010878	(36)	.0048783
(37)	.0024666	(38)	.00147422	(39)	.00034621	(40)	.0012088
(41)	.0072764	(42)	.0030834	(43)	.0020580	(44)	.0025200
(45)	.0013587	(46)	.0048609	(47)	.0048885	(48)	.0034981

10	6.0	25.	2.53	535.	150.12	891.89	.09239	108.10	.047486
----	-----	-----	------	------	--------	--------	--------	--------	---------

(1)	.0030729	(2)	.0017197	(3)	.0020991	(4)	.00272866
(5)	.0015894	(6)	.0013556	(7)	.00095487	(8)	.000078982
(9)	.0016326	(10)	.0017181	(11)	.0017500	(12)	.0021051
(13)	.0032329	(14)	.0033108	(15)	.0021952	(16)	.0016912
(17)	.0012706	(18)	.0028529	(19)	.012567	(20)	.0063972
(21)	.0024130	(22)	.0032695	(23)	.0086818	(24)	.0039802
(25)	.0020051	(26)	.00209861	(27)	.0037030	(28)	.015207
(29)	.0065241	(30)	.0022899	(31)	.0034730	(32)	.0032556
(33)	.0030828	(34)	.0027436	(35)	.014338	(36)	.0072650
(37)	.0043178	(38)	.0014662	(39)	.0029006	(40)	.0036301
(41)	.010782	(42)	.0064931	(43)	.0031964	(44)	.0039972
(45)	.0046999	(46)	.0040662	(47)	.0030651	(48)	.0032239

11	6.0	25.	5.12	535.	300.0	888.60	.18621	107.82	.067012
----	-----	-----	------	------	-------	--------	--------	--------	---------

(1)	.0029906	(2)	.0018676	(3)	.0028788	(4)	.00224786
(5)	.0016779	(6)	.0034494	(7)	.0055500	(8)	.0063813
(9)	.0053641	(10)	.0023750	(11)	.0022860	(12)	.0011202
(13)	.0033702	(14)	.0056373	(15)	.00095075	(16)	.0030030
(17)	.0039658	(18)	.0048539	(19)	.015011	(20)	.0089761
(21)	.0027009	(22)	.0026043	(23)	.010616	(24)	.0036844
(25)	.0023689	(26)	.0037501	(27)	.0066300	(28)	.017729
(29)	.0082716	(30)	.0055858	(31)	.0078887	(32)	.0028790
(33)	.0037137	(34)	.0031753	(35)	.016478	(36)	.0082693
(37)	.0076239	(38)	.0022627	(39)	.0050650	(40)	.0048456
(41)	.015999	(42)	.010458	(43)	.0041319	(44)	.0061893
(45)	.010274	(46)	.0038449	(47)	.0048375	(48)	.0057992

WING LEESIDE SURFACE ... MACH = 6 --- CONTINUED

RUN NO.	MACH NO.	ALPHA (DEG)	RE (X E6)	T(U) (R)	P(0) (PSI)	T(0) (R)	P(INF) (PSI)	T(INF) (R)	H(REF) (B/F2-S-R)
---------	----------	-------------	-----------	----------	------------	----------	--------------	------------	-------------------

T/C	H/H(REF)	T/C	H/H(REF)	T/C	H/H(REF)	T/C	H/H(REF)
-----	----------	-----	----------	-----	----------	-----	----------

12	6.0	25.	7.10	538.	400.0	869.08	.24937	105.39	.077174
----	-----	-----	------	------	-------	--------	--------	--------	---------

(1)	.0050599	(2)	.0038745	(3)	.0020612	(4)	.0043431
(5)	.0041511	(6)	.0056473	(7)	.0073644	(8)	.0065114
(9)	.0067297	(10)	.0057109	(11)	.00060345	(12)	.0011979
(13)	.0016488	(14)	.0064478	(15)	.0033554	(16)	.0041749
(17)	.0051881	(18)	.0053172	(19)	.018997	(20)	.010509
(21)	.0034071	(22)	.0032819	(23)	.014145	(24)	.00078654
(25)	.0034400	(26)	.0049611	(27)	.0069144	(28)	.020571
(29)	.0091432	(30)	.0066986	(31)	.011432	(32)	.0032513
(33)	.0065738	(34)	.0051447	(35)	.018371	(36)	.0076955
(37)	.0095045	(38)	.0029128	(39)	.0064289	(40)	.0068133
(41)	.018464	(42)	.010509	(43)	.0049078	(44)	.0084914
(45)	.014151	(46)	.0058950	(47)	.0073333	(48)	.0061661

13	6.0	30.	2.69	535.	145.65	843.94	.08961	102.10	.046554
----	-----	-----	------	------	--------	--------	--------	--------	---------

(1)	.0039962	(2)	.0031304	(3)	.0020854	(4)	.0019440
(5)	.00076619	(6)	.00079342	(7)	.0012807	(8)	.00094089
(9)	.0016385	(10)	.0033795	(11)	.0018881	(12)	.0017458
(13)	.0035176	(14)	.0044297	(15)	.0016749	(16)	.0015535
(17)	.0025827	(18)	.0021930	(19)	.0084756	(20)	.0037885
(21)	.0030308	(22)	.0032954	(23)	.012439	(24)	.0043457
(25)	.0019116	(26)	.0027175	(27)	.0036022	(28)	.012335
(29)	.0040249	(30)	.0029981	(31)	.0063259	(32)	.0032742
(33)	.0016154	(34)	.0022444	(35)	.011851	(36)	.0044922
(37)	.0047234	(38)	.00095617	(39)	.0035677	(40)	.0033314
(41)	.0071434	(42)	.0050488	(43)	.0019119	(44)	.0035808
(45)	.0049063	(46)	.0046910	(47)	.0042547	(48)	.0037582

15	6.0	30.	4.69	537.	300.0	916.32	.18621	111.35	.067203
----	-----	-----	------	------	-------	--------	--------	--------	---------

(1)	.0054589	(2)	.0039351	(3)	.0034761	(4)	.0041353
(5)	.0032560	(6)	.0053489	(7)	.0056447	(8)	.0044261
(9)	.0037218	(10)	.0051634	(11)	.0023015	(12)	.0017949
(13)	.0049293	(14)	.0087376	(15)	.0032823	(16)	.0034620
(17)	.0052752	(18)	.0052861	(19)	.015720	(20)	.010112
(21)	.0044485	(22)	.0057092	(23)	.016760	(24)	.0043515
(25)	.0034204	(26)	.0045514	(27)	.0079993	(28)	.018805
(29)	.0091113	(30)	.0076368	(31)	.012073	(32)	.0048316
(33)	.0066116	(34)	.0059515	(35)	.019179	(36)	.010053
(37)	.010904	(38)	.00093959	(39)	.0055210	(40)	.0052192
(41)	.016631	(42)	.012697	(43)	.0037100	(44)	.0057795
(45)	.013691	(46)	.0075638	(47)	.0084939	(48)	.0071807

WING LEESIDE SURFACE ... MACH = 6 --- CONTINUED

RUN NO.	MACH NO.	ALPHA (DEG)	RE (X E6)	T(U) (R)	P(0) (PSI)	T(0) (R)	P(INF) (PSI)	T(INF) (R)	H(REF) (B/F2-S-R)
		T/C	H/H(REF)	T/C	H/H(REF)	T/C	H/H(REF)	T/C	H/H(REF)

16	6.0	30.	7.07	538.	400.0	872.04	.24937	105.77	.077200
----	-----	-----	------	------	-------	--------	--------	--------	---------

(1)	.0072163	(2)	.0058324	(3)	.0047598	(4)	.0056241
(5)	.0056073	(6)	.0055890	(7)	.0055448	(8)	.0047290
(9)	.0056875	(10)	.0067332	(11)	.0026805	(12)	.0011148
(13)	.0059570	(14)	.010886	(15)	.0049414	(16)	.0066412
(17)	.0065287	(18)	.0059893	(19)	.019245	(20)	.011761
(21)	.0053170	(22)	.0078839	(23)	.020308	(24)	.0052383
(25)	.0046940	(26)	.0069027	(27)	.0091770	(28)	.021306
(29)	.010799	(30)	.0095716	(31)	.016761	(32)	.0060802
(33)	.0093259	(34)	.0086709	(35)	.020622	(36)	.011321
(37)	.012244	(38)	.0043650	(39)	.0066412	(40)	.0077635
(41)	.019431	(42)	.016111	(43)	.0051670	(44)	.011281
(45)	.019677	(46)	.0082992	(47)	.010073	(48)	.010070

17	6.0	35.	2.77	535.	148.50	838.87	.09138	101.46	.046979
----	-----	-----	------	------	--------	--------	--------	--------	---------

(1)	.0037746	(2)	.0027292	(3)	.0021010	(4)	.0012537
(5)	.0014715	(6)	.0013767	(7)	.0035132	(8)	.0011633
(9)	.0021940	(10)	.0035544	(11)	.0015511	(12)	.00089069
(13)	.0029890	(14)	.0037917	(15)	.0024593	(16)	.0012116
(17)	.0014852	(18)	.00065983	(19)	.0089739	(20)	.0047493
(21)	.0020428	(22)	.0020540	(23)	.014926	(24)	.0031181
(25)	.0021874	(26)	.0020371	(27)	.0035020	(28)	.011430
(29)	.0037147	(30)	.0029340	(31)	.0095517	(32)	.0018327
(33)	.0019298	(34)	.0010110	(35)	.010848	(36)	.0050392
(37)	.0057051	(38)	.0015734	(39)	.0022749	(40)	.0022074
(41)	.010708	(42)	.0080479	(43)	.0018251	(44)	.0026704
(45)	.0056680	(46)	.0038382	(47)	.0035678	(48)	.0033321

18	6.0	35.	5.15	538.	300.0	885.15	.18621	107.39	.066987
----	-----	-----	------	------	-------	--------	--------	--------	---------

(1)	.0057641	(2)	.0054809	(3)	.0042137	(4)	.0041066
(5)	.0023027	(6)	.0050999	(7)	.0068992	(8)	.0037853
(9)	.0032991	(10)	.0063036	(11)	.0026809	(12)	.00159729
(13)	.0054167	(14)	.010937	(15)	.0030243	(16)	.0057745
(17)	.0060605	(18)	.0041546	(19)	.015110	(20)	.010644
(21)	.0039664	(22)	.0066376	(23)	.021086	(24)	.0048146
(25)	.0034980	(26)	.0053384	(27)	.0076953	(28)	.018062
(29)	.0099947	(30)	.0084015	(31)	.016030	(32)	.0059566
(33)	.0065651	(34)	.0066536	(35)	.017124	(36)	.010449
(37)	.013017	(38)	.0037458	(39)	.0055256	(40)	.0060175
(41)	.017770	(42)	.015912	(43)	.0038122	(44)	.0084922
(45)	.015134	(46)	.0067271	(47)	.0068393	(48)	.0075487

WING LEESIDE SURFACE ... MACH = 6 --- CONTINUED

RUN NO.	MACH NO.	ALPHA (DEG)	RE (X E6)	T(U) (R)	P(0) (PSI)	T(0) (R)	P(INF) (PSI)	T(INF) (R)	H(REF) (B/F2-S-R)
		T/C	H/H(REF)	T/C	H/H(REF)	T/C	H/H(REF)	T/C	H/H(REF)

19	6.0	35.	7.096	540.	400.0	870.21	.24937	105.54	.077184
----	-----	-----	-------	------	-------	--------	--------	--------	---------

(1)	.0084024	(2)	.0072456	(3)	.0060035	(4)	.0056978
(5)	.0055394	(6)	.0089560	(7)	.0087606	(8)	.0056471
(9)	.0068391	(10)	.0074960	(11)	.0032773	(12)	.0014310
(13)	.0076104	(14)	.014707	(15)	.0059737	(16)	.0055750
(17)	.010190	(18)	.0059914	(19)	.018273	(20)	.012243
(21)	.0058906	(22)	.0081661	(23)	.024702	(24)	.0063402
(25)	.0052844	(26)	.0079251	(27)	.0088448	(28)	.021053
(29)	.010756	(30)	.010109	(31)	.020009	(32)	.0075914
(33)	.010485	(34)	.0079553	(35)	.020023	(36)	.011778
(37)	.015676	(38)	.0048423	(39)	.0079112	(40)	.0074374
(41)	.021867	(42)	.019800	(43)	.0058024	(44)	.011223
(45)	.020097	(46)	.0081125	(47)	.0090008	(48)	.0099351

20	6.0	40.	6.73	536.	400.0	897.61	.24937	109.01	.077421
----	-----	-----	------	------	-------	--------	--------	--------	---------

(1)	.0024499	(2)	.0013541	(3)	.00078960	(4)	.0012927
(5)	.0012430	(6)	.00058565	(7)	.0028326	(8)	.00085862
(9)	.0020670	(10)	.0033231	(11)	.0015678	(12)	.0012107
(13)	.0019106	(14)	.0039507	(15)	.0017695	(16)	.0014012
(17)	.0013492	(18)	.0011359	(19)	.0066359	(20)	.0044366
(21)	.0011070	(22)	.0015502	(23)	.011450	(24)	.0024283
(25)	.0016302	(26)	.00092972	(27)	.0030904	(28)	.0076808
(29)	.0039245	(30)	.0030684	(31)	.0079057	(32)	.0015504
(33)	.0015845	(34)	.00087134	(35)	.0072366	(36)	.0040622
(37)	.0055326	(38)	.0013475	(39)	.0017563	(40)	.0017594
(41)	.0084678	(42)	.0075832	(43)	.0010691	(44)	.0011431
(45)	.0041935	(46)	.0026279	(47)	.0029002	(48)	.0024627

21	6.0	40.	5.20	540.	300.0	879.87	.18621	106.72	.066949
----	-----	-----	------	------	-------	--------	--------	--------	---------

(1)	.0072750	(2)	.0042333	(3)	.0046724	(4)	.0044318
(5)	.0036258	(6)	.0085797	(7)	.0080381	(8)	.0036572
(9)	.0056934	(10)	.0076360	(11)	.0039391	(12)	.0017369
(13)	.0076786	(14)	.012176	(15)	.0053921	(16)	.0044100
(17)	.0067168	(18)	.0050480	(19)	.015187	(20)	.013162
(21)	.0061129	(22)	.0090790	(23)	.027750	(24)	.0077509
(25)	.0056839	(26)	.0061862	(27)	.0091793	(28)	.019112
(29)	.010933	(30)	.011099	(31)	.019277	(32)	.0084363
(33)	.0083261	(34)	.0045405	(35)	.018029	(36)	.010570
(37)	.016558	(38)	.0047677	(39)	.0056594	(40)	.0069322
(41)	.022392	(42)	.019322	(43)	.0049022	(44)	.0099724
(45)	.016479	(46)	.0059713	(47)	.0067798	(48)	.0075038

WING LEESIDE SURFACE ... MACH = 6 --- CONCLUDED

RUN NO.	MACH NO.	ALPHA (DEG)	RE (X E6)	T(0) (R)	P(0) (PSI)	T(0) (R)	P(INF) (PSI)	T(INF) (R)	H(REF) (B/F2-S-R)
---------	----------	-------------	-----------	----------	------------	----------	--------------	------------	-------------------

T/C	H/H(REF)	T/C	H/H(REF)	T/C	H/H(REF)	T/C	H/H(REF)
-----	----------	-----	----------	-----	----------	-----	----------

22	6.0	40.	3.38	540.	191.52	868.47	.11818	105.22	.053485
----	-----	-----	------	------	--------	--------	--------	--------	---------

(1) .013843	(2) .010212	(3) .0084906	(4) .0084882
(5) .0061903	(6) .011839	(7) .013130	(8) .0074702
(9) .011280	(10) .015210	(11) .0075295	(12) .0043626
(13) .013031	(14) .017750	(15) .011478	(16) .0126020
(17) .016589	(18) .0092619	(19) .028721	(20) .022647
(21) .011319	(22) .016783	(23) .041000	(24) .012176
(25) .010340	(26) .013176	(27) .016646	(28) .033016
(29) .020239	(30) .019955	(31) .031779	(32) .015749
(33) .016721	(34) .011342	(35) .032085	(36) .020764
(37) .028696	(38) .010474	(39) .011710	(40) .011762
(41) .039731	(42) .031029	(43) .010267	(44) .020796
(45) .032543	(46) .012340	(47) .016720	(48) .017383

FUSELAGE LEESIDE SURFACE ... MACH = 10

RUN NO.	MACH NO.	ALPHA (DEG)	RE (X E6)	T(U) (R)	P(0) (PSI)	T(0) (R)	P(INF) (PSI)	T(INF) (R)	H(REF) (B/F2-S-R)
		T/C	H/H(REF)	T/C	H/H(REF)	T/C	H/H(REF)	T/C	H/H(REF)

3	10.34	20.	1.00	535.	742.6	1819.5	.01360	84.9	.0332186
---	-------	-----	------	------	-------	--------	--------	------	----------

(1)	.022834	(2)	.012888	(3)	.010317	(4)	.0032192
(5)	.0015757	(6)	.00092934	(7)	.0024298	(8)	.0043651
(9)	.0036549	(10)	.024044	(11)	.021413	(12)	.013217
(13)	.0031676	(14)	.0017797	(15)	.0014277	(16)	.0045055
(17)	.0054332	(18)	.0050623	(19)	.018487	(20)	.025238
(21)	.018134	(22)	.0041921	(23)	.0014503	(24)	.0022224
(25)	.0045520	(26)	.0072519	(27)	.0062054	(28)	.0093209
(29)	.021416	(30)	.023336	(31)	.0046715	(32)	.0017997
(33)	.0025947	(34)	.0056335	(35)	.0065524	(36)	.0060351
(37)	.0065304	(38)	.013888	(39)	.021453	(40)	.0058029
(41)	.0033034	(42)	.0027354	(43)	.0047639	(44)	.0065028
(45)	.0054245	(46)	.0051257	(47)	.0098072	(48)	.017231
(49)	.0081143	(50)	.0028658	(51)	.0029191	(52)	.0053459
(53)	.0068751	(54)	.0056576	(55)	.0034427	(56)	.0082669
(57)	.013631	(58)	.0093761	(59)	.0024615	(60)	.0031253
(61)	.0049221	(62)	.0058162	(63)	.0054923		

4	10.34	25.	1.00	542.	743.7	1828.7	.01366	85.4	.0332702
---	-------	-----	------	------	-------	--------	--------	------	----------

(1)	.023772	(2)	.018993	(3)	.011617	(4)	.0026685
(5)	.0015334	(6)	.00082577	(7)	.0029622	(8)	.0046196
(9)	.0031020	(10)	.015113	(11)	.024883	(12)	.019101
(13)	.0042633	(14)	.0016259	(15)	.0016750	(16)	.0042287
(17)	.0052064	(18)	.0042779	(19)	.0093367	(20)	.019426
(21)	.023415	(22)	.0053222	(23)	.0019541	(24)	.0020079
(25)	.0040937	(26)	.0047926	(27)	.0047494	(28)	.0049215
(29)	.011852	(30)	.018567	(31)	.0054621	(32)	.0022015
(33)	.0022628	(34)	.0041107	(35)	.0048496	(36)	.0045957
(37)	.0039595	(38)	.0079529	(39)	.012208	(40)	.0058238
(41)	.0026077	(42)	.0026260	(43)	.0041670	(44)	.0048842
(45)	.0043816	(46)	.0027245	(47)	.0061248	(48)	.010031
(49)	.0058331	(50)	.0025498	(51)	.0026640	(52)	.0031890
(53)	.0049544	(54)	.0041972	(55)	.0021274	(56)	.0047508
(57)	.007684	(58)	.0056237	(59)	.0028416	(60)	.0027944
(61)	.0033624	(62)	.0051200	(63)	.0040027		

FUSELAGE LEESIDE SURFACE ... MACH = 10 --- CONTINUED

RUN NO.	MACH NO.	ALPHA (DEG)	RE (X E6)	T(U) (R)	P(0) (PSI)	T(0) (R)	P(INF) (PSI)	T(INF) (R)	H(REF) (B/F2-S-R)
		T/C	H/H(REF)	T/C	H/H(REF)	T/C	H/H(REF)	T/C	H/H(REF)

5	10.34	30.	1.00	543.	742.8	1806.5	.01365	84.3	.0332033
---	-------	-----	------	------	-------	--------	--------	------	----------

(1)	.017438	(2)	.022364	(3)	.015077	(4)	.0034947
(5)	.00076156	(6)	.00065768	(7)	.0021155	(8)	.0032288
(9)	.0034033	(10)	.011405	(11)	.018885	(12)	.020544
(13)	.0033199	(14)	.0014340	(15)	.0013970	(16)	.0031950
(17)	.0043639	(18)	.0040982	(19)	.0065065	(20)	.013221
(21)	.017965	(22)	.0042707	(23)	.0026325	(24)	.0016497
(25)	.0039330	(26)	.0048782	(27)	.0039872	(28)	.0051855
(29)	.010428	(30)	.014490	(31)	.0038312	(32)	.0021070
(33)	.0030293	(34)	.0035447	(35)	.0045705	(36)	.0040053
(37)	.0034465	(38)	.0069157	(39)	.011552	(40)	.0050358
(41)	.0024704	(42)	.0020841	(43)	.0034818	(44)	.0047410
(45)	.0040510	(46)	.0020072	(47)	.0061216	(48)	.00928455
(49)	.0048913	(50)	.0018899	(51)	.0020891	(52)	.0040720
(53)	.0054231	(54)	.0042593	(55)	.0012890	(56)	.0028110
(57)	.0063068	(58)	.0048253	(59)	.0025139	(60)	.0025974
(61)	.0041455	(62)	.0046318	(63)	.0041701		

6	10.34	35.	1.00	547.	741.9	1807.6	.01364	84.3	.0331859
---	-------	-----	------	------	-------	--------	--------	------	----------

(1)	.015447	(2)	.020303	(3)	.016267	(4)	.0035601
(5)	.0015795	(6)	.00080837	(7)	.0022033	(8)	.0022124
(9)	.0018231	(10)	.0095381	(11)	.016166	(12)	.018632
(13)	.0047103	(14)	.0025577	(15)	.00076295	(16)	.0023501
(17)	.0020725	(18)	.0019526	(19)	.0067838	(20)	.013483
(21)	.016236	(22)	.0050968	(23)	.0018943	(24)	.0016852
(25)	.00236	(26)	.0028125	(27)	.0031511	(28)	.0048614
(29)	.010341	(30)	.015442	(31)	.0040284	(32)	.0020154
(33)	.00095058	(34)	.0022132	(35)	.0041669	(36)	.0031456
(37)	.0030788	(38)	.0057020	(39)	.011259	(40)	.0047126
(41)	.0025681	(42)	.0023136	(43)	.0040744	(44)	.0038323
(45)	.0031265	(46)	.00062195	(47)	.0032568	(48)	.0079723
(49)	.0043351	(50)	.0024778	(51)	.0023222	(52)	.0037899
(53)	.0050141	(54)	.0040421	(55)	.00046064	(56)	.0014245
(57)	.0033391	(58)	.0043263	(59)	.0021727	(60)	.0025104
(61)	.0033470	(62)	.0052552	(63)	.0034084		

FUSELAGE LEESIDE SURFACE ... MACH = 10 --- CONTINUED

RUN NO.	MACH NO.	ALPHA (DEG)	RE (X E6)	T(U) (R)	P(0) (PSI)	T(0) (R)	P(INF) (PSI)	T(INF) (R)	H(REF) (B/F2-S-R)
				T/C	H/H(REF)	T/C	H/H(REF)	T/C	H/H(REF)

8	10.36	20.	2.40	553.	1784.5	1821.7	.03300	85.1	.0512218
---	-------	-----	------	------	--------	--------	--------	------	----------

(1)	.024532	(2)	.011555	(3)	.0088172	(4)	.0024035
(5)	.00094089	(6)	.00085846	(7)	.0032915	(8)	.0058722
(9)	.0049963	(10)	.033730	(11)	.021444	(12)	.013095
(13)	.0022308	(14)	.0011643	(15)	.0020051	(16)	.0058029
(17)	.0085160	(18)	.0072820	(19)	.022366	(20)	.032603
(21)	.017386	(22)	.0031773	(23)	.0011565	(24)	.0022027
(25)	.0067851	(26)	.0093591	(27)	.0078792	(28)	.0097865
(29)	.032086	(30)	.026134	(31)	.0036867	(32)	.0015585
(33)	.0026472	(34)	.0067002	(35)	.008116	(36)	.0069568
(37)	.0068970	(38)	.016059	(39)	.031945	(40)	.0041904
(41)	.0027251	(42)	.0029011	(43)	.0059039	(44)	.0067333
(45)	.0063430	(46)	.0051299	(47)	.010054	(48)	.026236
(49)	.0066408	(50)	.0028665	(51)	.0023342	(52)	.0050882
(53)	.0063201	(54)	.0062045	(55)	.0037932	(56)	.0081761
(57)	.015834	(58)	.0094683	(59)	.002376	(60)	.0018707
(61)	.0044049	(62)	.0036162	(63)	.0050815		

9	10.36	25.	2.40	559.	1788.3	1829.4	.03311	85.4	.0512964
---	-------	-----	------	------	--------	--------	--------	------	----------

(1)	.028817	(2)	.018954	(3)	.011696	(4)	.0019078
(5)	.00074908	(6)	.00054484	(7)	.0034373	(8)	.0057085
(9)	.0046803	(10)	.017445	(11)	.029182	(12)	.018361
(13)	.0030493	(14)	.00098029	(15)	.0018274	(16)	.0052027
(17)	.0077243	(18)	.0064025	(19)	.0099971	(20)	.023854
(21)	.025886	(22)	.0037662	(23)	.0015097	(24)	.0027983
(25)	.0053975	(26)	.0069334	(27)	.0055243	(28)	.0055690
(29)	.013123	(30)	.024161	(31)	.0051097	(32)	.0025803
(33)	.0027868	(34)	.0052506	(35)	.0052834	(36)	.0049643
(37)	.0036914	(38)	.0086077	(39)	.014410	(40)	.0052855
(41)	.0028673	(42)	.0026415	(43)	.0051645	(44)	.0045921
(45)	.0050722	(46)	.0020209	(47)	.0058138	(48)	.012168
(49)	.0058477	(50)	.0027262	(51)	.0024457	(52)	.0045397
(53)	.0052455	(54)	.0048453	(55)	.00069319	(56)	.0042384
(57)	.0078771	(58)	.0059919	(59)	.0020386	(60)	.002125
(61)	.0037296	(62)	.0038211	(63)	.0042558		

FUSELAGE LEESIDE SURFACE ... MACH = 10 --- CONTINUED

RUN NO.	MACH NO.	ALPHA (DEG)	RE (X E6)	T(U) (R)	P(0) (PSI)	T(0) (R)	P(INF) (PSI)	T(INF) (R)	H(REF) (B/F2-S-R)
				T/C	H/H(REF)	T/C	H/H(REF)	T/C	H/H(REF)

10	10.36	30.	2.40	567.	1807.4	1828.5	.03350	85.4	.0515485
----	-------	-----	------	------	--------	--------	--------	------	----------

(1)	.018902	(2)	.022005	(3)	.015237	(4)	.0029438
(5)	.0012667	(6)	.00060671	(7)	.0027472	(8)	.0042203
(9)	.0038900	(10)	.011395	(11)	.020547	(12)	.020186
(13)	.0033853	(14)	.00095443	(15)	.0013856	(16)	.0042701
(17)	.0062904	(18)	.0062390	(19)	.0081874	(20)	.015073
(21)	.020118	(22)	.0039046	(23)	.0010627	(24)	.0022878
(25)	.0053934	(26)	.0051111	(27)	.0052205	(28)	.0048440
(29)	.011886	(30)	.015908	(31)	.0047632	(32)	.0021514
(33)	.0029526	(34)	.005281	(35)	.0051508	(36)	.0048399
(37)	.0025161	(38)	.0072643	(39)	.014033	(40)	.0038318
(41)	.0018578	(42)	.0030189	(43)	.0054297	(44)	.0054291
(45)	.0050531	(46)	.00050826	(47)	.0038914	(48)	.0097781
(49)	.0050616	(50)	.0022430	(51)	.0029411	(52)	.0045795
(53)	.0052441	(54)	.0051129	(55)	.00026055	(56)	.0011332
(57)	.0048878	(58)	.0044287	(59)	.0013548	(60)	.0022262
(61)	.0047916	(62)	.0045688	(63)	.0043582		

11	10.36	35.	2.40	571.	1787.2	1840.5	.03305	86.0	.0512919
----	-------	-----	------	------	--------	--------	--------	------	----------

(1)	.014794	(2)	.019765	(3)	.016564	(4)	.0026344
(5)	.0010106	(6)	.00084836	(7)	.0011866	(8)	.0016296
(9)	.0021634	(10)	.0098508	(11)	.016933	(12)	.017979
(13)	.0034473	(14)	.0011825	(15)	.0014523	(16)	.0015241
(17)	.0016299	(18)	.0028183	(19)	.0070263	(20)	.014505
(21)	.016983	(22)	.0035385	(23)	.0012783	(24)	.0022100
(25)	.0021364	(26)	.0013819	(27)	.0018402	(28)	.0030005
(29)	.0087794	(30)	.016424	(31)	.0038438	(32)	.0013688
(33)	.0028533	(34)	.0024197	(35)	.0017096	(36)	.0014374
(37)	.00076684	(38)	.0039025	(39)	.0077108	(40)	.0041903
(41)	.0018696	(42)	.0030016	(43)	.0026200	(44)	.0016604
(45)	.0018240	(46)	.00079700	(47)	.00099558	(48)	.0035000
(49)	.0029310	(50)	.0012500	(51)	.0022504	(52)	.0020307
(53)	.0013368	(54)	.0016513	(55)	.0014190	(56)	.0016066
(57)	.0018517	(58)	.0011288	(59)	.00081247	(60)	.0022239
(61)	.0018047	(62)	.00055996	(63)	.0015272		

FUSELAGE LEESIDE SURFACE ... MACH = 10 --- CONTINUED

RUN NO.	MACH NO.	ALPHA (DEG)	RE (X E6)	T(U) (R)	P(0) (PSI)	T(0) (R)	P(INF) (PSI)	T(INF) (R)	H(REF) (B/F2-S-R)
		T/C	H/H(REF)	T/C	H/H(REF)	T/C	H/H(REF)	T/C	H/H(REF)

12	10.16	20.	.50	554.	357.5	1666.7	.00738	79.7	.0238235
----	-------	-----	-----	------	-------	--------	--------	------	----------

(1)	.01947	(2)	.012711	(3)	.0083408	(4)	.0033065
(5)	.0025641	(6)	.0016037	(7)	.0027139	(8)	.0047576
(9)	.0032223	(10)	.017406	(11)	.019902	(12)	.012096
(13)	.0041598	(14)	.0018299	(15)	.001452	(16)	.0034293
(17)	.0043841	(18)	.0032532	(19)	.012682	(20)	.019489
(21)	.01756	(22)	.0045506	(23)	.0017582	(24)	.0013977
(25)	.0041707	(26)	.0048489	(27)	.0049506	(28)	.0072934
(29)	.01476	(30)	.018975	(31)	.0046036	(32)	.0013815
(33)	.0027529	(34)	.0035841	(35)	.0049157	(36)	.0047739
(37)	.0048373	(38)	.0089729	(39)	.014816	(40)	.0053949
(41)	.0021377	(42)	.0032941	(43)	.0046693	(44)	.004874
(45)	.004802	(46)	.0039453	(47)	.0076004	(48)	.01255
(49)	.006108	(50)	.0038041	(51)	.0027923	(52)	.0040793
(53)	.0052414	(54)	.0046585	(55)	.0037398	(56)	.0061372
(57)	.0094058	(58)	.0069125	(59)	.0038718	(60)	.002802
(61)	.0034125	(62)	.0053765	(63)	.0050997		

13	10.16	25.	.50	548.	353.7	1794.8	.00723	86.7	.0238772
----	-------	-----	-----	------	-------	--------	--------	------	----------

(1)	.018531	(2)	.017462	(3)	.012033	(4)	.0030417
(5)	.0013643	(6)	.0015700	(7)	.0025382	(8)	.0038859
(9)	.0028000	(10)	.013011	(11)	.017328	(12)	.017016
(13)	.0035632	(14)	.0014022	(15)	.00077542	(16)	.00321
(17)	.0043955	(18)	.0032961	(19)	.0085416	(20)	.014334
(21)	.01567	(22)	.0040939	(23)	.0022296	(24)	.0026119
(25)	.003527	(26)	.0037733	(27)	.0040244	(28)	.0057784
(29)	.009498	(30)	.012791	(31)	.0038172	(32)	.0022887
(33)	.0022246	(34)	.0036901	(35)	.0037436	(36)	.0031968
(37)	.0042556	(38)	.0070357	(39)	.0098476	(40)	.0057816
(41)	.0029656	(42)	.002773	(43)	.0035444	(44)	.0049816
(45)	.0036339	(46)	.0034680	(47)	.0051857	(48)	.0085593
(49)	.0051537	(50)	.0031092	(51)	.0028848	(52)	.0043026
(53)	.0042827	(54)	.0044836	(55)	.0019380	(56)	.0053533
(57)	.0064421	(58)	.0043669	(59)	.0033641	(60)	.002689
(61)	.0041067	(62)	.0039429	(63)	.0038389		

FUSELAGE LEESIDE SURFACE ... MACH = 10 --- CONTINUED

RUN NO.	MACH NO.	ALPHA (DEG)	RE (X E6)	T(U) (R)	P(0) (PSI)	T(0) (R)	P(INF) (PSI)	T(INF) (R)	H(REF) (B/F2-S-R)
		T/C	H/H(REF)	T/C	H/H(REF)	T/C	H/H(REF)	T/C	H/H(REF)

14	10.16	30.	.50	543.	350.9	1733.4	.00721	83.3	.0237003
----	-------	-----	-----	------	-------	--------	--------	------	----------

(1)	.015929	(2)	.018492	(3)	.01347	(4)	.0041177
(5)	.0010448	(6)	.0015135	(7)	.0013752	(8)	.0024303
(9)	.0022422	(10)	.0086716	(11)	.014418	(12)	.016113
(13)	.0039161	(14)	.0013474	(15)	.0015652	(16)	.00093383
(17)	.0023312	(18)	.0018013	(19)	.0085529	(20)	.010071
(21)	.01217	(22)	.0040417	(23)	.0026734	(24)	.00085243
(25)	.002901	(26)	.0017261	(27)	.0036839	(28)	.004302
(29)	.010247	(30)	.011616	(31)	.0041127	(32)	.0026371
(33)	.0026676	(34)	.0023719	(35)	.0034375	(36)	.0034852
(37)	.0038449	(38)	.0070386	(39)	.0096904	(40)	.0050868
(41)	.00284	(42)	.0015178	(43)	.0029824	(44)	.0033422
(45)	.0036354	(46)	.0032048	(47)	.0052159	(48)	.0085767
(49)	.0042955	(50)	.0027214	(51)	.0025556	(52)	.003259
(53)	.0043053	(54)	.0034786	(55)	.002008	(56)	.003955
(57)	.0070432	(58)	.0040086	(59)	.0024295	(60)	.0023615
(61)	.0024453	(62)	.0037779	(63)	.0034505		

15	10.16	35.	.50	537.	339.6	1778.4	.00694	85.5	.0233508
----	-------	-----	-----	------	-------	--------	--------	------	----------

(1)	.013683	(2)	.017851	(3)	.015496	(4)	.0031256
(5)	.0014897	(6)	.0013968	(7)	.0027824	(8)	.0026298
(9)	.0013533	(10)	.0093436	(11)	.014211	(12)	.016536
(13)	.0039981	(14)	.0021794	(15)	.0016498	(16)	.00080254
(17)	.0012832	(18)	.0014861	(19)	.0067567	(20)	.012051
(21)	.014124	(22)	.0043383	(23)	.0015164	(24)	.0015222
(25)	.0022275	(26)	.0015843	(27)	.0024944	(28)	.0044551
(29)	.0092677	(30)	.012413	(31)	.0040615	(32)	.0022377
(33)	.0018831	(34)	.0032545	(35)	.0030042	(36)	.0033469
(37)	.0037344	(38)	.0061782	(39)	.0091981	(40)	.0034971
(41)	.0010680	(42)	.0015506	(43)	.0019517	(44)	.0035128
(45)	.0031782	(46)	.0022913	(47)	.0045002	(48)	.0080193
(49)	.0042595	(50)	.0021501	(51)	.0031032	(52)	.0029388
(53)	.0042805	(54)	.0037035	(55)	.0014876	(56)	.0015058
(57)	.0045077	(58)	.0052656	(59)	.0028244	(60)	.001455
(61)	.0028257	(62)	.0043295	(63)	.0039359		

FUSELAGE LEESIDE SURFACE ... MACH = 10 --- CONTINUED

RUN NO.	MACH NO.	ALPHA (DEG)	RE (X E6)	T(U) (R)	P(0) (PSI)	T(0) (R)	P(INF) (PSI)	T(INF) (R)	H(REF) (B/F2-S-R)
		T/C	H/H(REF)	T/C	H/H(REF)	T/C	H/H(REF)	T/C	H/H(REF)

16	10.34	40.	1.00	533.	743.4	1843.1	.01360	86.1	.0333052
----	-------	-----	------	------	-------	--------	--------	------	----------

(1)	.014031	(2)	.018131	(3)	.017658	(4)	.0036109
(5)	.0013898	(6)	.0017285	(7)	.0024228	(8)	.0024104
(9)	.0028092	(10)	.0090174	(11)	.01591	(12)	.018471
(13)	.0043263	(14)	.0017897	(15)	.0013491	(16)	.0020612
(17)	.0026087	(18)	.0032319	(19)	.0061604	(20)	.012833
(21)	.017309	(22)	.0044751	(23)	.0017126	(24)	.0021545
(25)	.0029059	(26)	.0026964	(27)	.0030131	(28)	.0034323
(29)	.0077803	(30)	.014116	(31)	.0042496	(32)	.0027409
(33)	.0021264	(34)	.0030062	(35)	.0022808	(36)	.0024114
(37)	.0016802	(38)	.0038871	(39)	.0081944	(40)	.0037161
(41)	.0028779	(42)	.0021755	(43)	.002957	(44)	.002975
(45)	.0031128	(46)	.000703	(47)	.0015968	(48)	.0039876
(49)	.0031152	(50)	.0010127	(51)	.0019528	(52)	.0034185
(53)	.0032413	(54)	.0035311	(55)	.0013448	(56)	.0014837
(57)	.001818	(58)	.0012652	(59)	.0010234	(60)	.00178044
(61)	.0024424	(62)	.0032228	(63)	.003747		

17	10.36	40.	2.40	543.	1801.5	1812.8	.03340	84.6	.0514813
----	-------	-----	------	------	--------	--------	--------	------	----------

(1)	.015054	(2)	.016818	(3)	.015104	(4)	.0028840
(5)	.00089577	(6)	.0016821	(7)	.0016396	(8)	.0026335
(9)	.0041375	(10)	.0093441	(11)	.017371	(12)	.017630
(13)	.0029495	(14)	.0014049	(15)	.0019649	(16)	.0022503
(17)	.003466	(18)	.004841	(19)	.0050661	(20)	.013722
(21)	.018787	(22)	.0030916	(23)	.00076094	(24)	.0028226
(25)	.0038573	(26)	.0032848	(27)	.0052505	(28)	.0020869
(29)	.0060983	(30)	.01448	(31)	.0037933	(32)	.0015271
(33)	.0038501	(34)	.004926	(35)	.003357	(36)	.0052687
(37)	.00075342	(38)	.001863	(39)	.0052194	(40)	.0033852
(41)	.0012859	(42)	.0038214	(43)	.004909	(44)	.0038626
(45)	.0063621	(46)	.00032373	(47)	.0010134	(48)	.0012085
(49)	.0012537	(50)	.0012697	(51)	.0033901	(52)	.0041394
(53)	.0032576	(54)	.0060362	(55)	.0009176	(56)	.0010454
(57)	.0018324	(58)	.0010576	(59)	.0010385	(60)	.0035113
(61)	.0047026	(62)	.0027516	(63)	.0039581		

FUSELAGE LEESIDE SURFACE ... MACH = 10 --- CONCLUDED

RUN NO.	MACH NO.	ALPHA (DEG)	RE (X E6)	T(U) (R)	P(0) (PSI)	T(0) (R)	P(INF) (PSI)	T(INF) (R)	H(REF) (B/F2-S-R)
		T/C	H/H(REF)	T/C	H/H(REF)	T/C	H/H(REF)	T/C	H/H(REF)

20	10.16	40.	.50	541.	338.6	1744.2	.00750	84.6	.0242364
----	-------	-----	-----	------	-------	--------	--------	------	----------

(1)	.013396	(2)	.015918	(3)	.016261	(4)	.0033936
(5)	.0016389	(6)	.000004999	(7)	.0022519	(8)	.0027189
(9)	.0026261	(10)	.0088728	(11)	.015792	(12)	.016062
(13)	.0046174	(14)	.001604	(15)	.0020712	(16)	.0020021
(17)	.0018566	(18)	.0024626	(19)	.0069827	(20)	.011371
(21)	.015954	(22)	.0048875	(23)	.0015805	(24)	.0027274
(25)	.0027961	(26)	.0032116	(27)	.0027061	(28)	.0037308
(29)	.0084915	(30)	.013028	(31)	.0043705	(32)	.0020597
(33)	.0022775	(34)	.0027135	(35)	.0032132	(36)	.0030442
(37)	.0020671	(38)	.0042419	(39)	.0077074	(40)	.0037652
(41)	.0031121	(42)	.0013957	(43)	.0030971	(44)	.0035253
(45)	.0033467	(46)	.00031328	(47)	.0025942	(48)	.004783
(49)	.0039378	(50)	.0022363	(51)	.0025357	(52)	.0035311
(53)	.0043025	(54)	.0037043	(55)	.0010233	(56)	.0006841
(57)	.001327	(58)	.0016771	(59)	.0017584	(60)	.0021089
(61)	.0043437	(62)	.0040574	(63)	.0047781		

FUSELAGE LEESIDE SURFACE ... MACH = 6

RUN NO.	MACH NO.	ALPHA (DEG)	RE (X E6)	T(U) (R)	P(0) (PSI)	T(0) (R)	P(INF) (PSI)	T(INF) (R)	H(REF) (B/F2-S-R)
				T/C	H/H(REF)	T/C	H/H(REF)	T/C	H/H(REF)

3	6.0	20.	2.70	535.	149.20	882.76	.09182	107.01	.047302
---	-----	-----	------	------	--------	--------	--------	--------	---------

(1)	.031852	(2)	.014667	(3)	.0098209	(4)	.0023480
(5)	.000082514	(6)	.00071732	(7)	.0067475	(8)	.010862
(9)	.0091293	(10)	.045676	(11)	.025239	(12)	.016234
(13)	.0038661	(14)	.0005786	(15)	.0029217	(16)	.0092478
(17)	.013507	(18)	.013429	(19)	.050261	(20)	.033964
(21)	.018414	(22)	.0059226	(23)	.0019690	(24)	.0017968
(25)	.0096711	(26)	.015844	(27)	.015303	(28)	.033146
(29)	.046426	(30)	.024496	(31)	.0049194	(32)	.0029221
(33)	.0011689	(34)	.010415	(35)	.015478	(36)	.014146
(37)	.019200	(38)	.047409	(39)	.035481	(40)	.0065036
(41)	.0024776	(42)	.0023086	(43)	.0077440	(44)	.010485
(45)	.011428	(46)	.012752	(47)	.037908	(48)	.036588
(49)	.0084082	(50)	.0033364	(51)	.0025864	(52)	.0087652
(53)	.0081972	(54)	.0064871	(55)	.010309	(56)	.026896
(57)	.038047	(58)	.0099682	(59)	.0032641	(60)	.0088566
(61)	.016078	(62)	.0053700	(63)	.0065742		

4	6.0	25.	2.70	535.	148.32	891.04	.09127	108.06	.047200
---	-----	-----	------	------	--------	--------	--------	--------	---------

(1)	.039211	(2)	.022373	(3)	.012825	(4)	.0021501
(5)	.00062584	(6)	.0026816	(7)	.0047178	(8)	.013108
(9)	.010993	(10)	.036918	(11)	.038430	(12)	.019057
(13)	.0052933	(14)	.0022917	(15)	.0031116	(16)	.0057628
(17)	.015216	(18)	.013729	(19)	.023856	(20)	.046788
(21)	.029103	(22)	.0075966	(23)	.0045569	(24)	.0039949
(25)	.0090514	(26)	.0076516	(27)	.0077323	(28)	.011569
(29)	.035186	(30)	.043491	(31)	.0090096	(32)	.0071862
(33)	.0049555	(34)	.0067163	(35)	.0075880	(36)	.0077336
(37)	.0061345	(38)	.017452	(39)	.035562	(40)	.0098565
(41)	.0062210	(42)	.0052943	(43)	.0051822	(44)	.0054640
(45)	.0054445	(46)	.0029928	(47)	.010423	(48)	.028652
(49)	.016575	(50)	.0044286	(51)	.0045647	(52)	.0048507
(53)	.0051506	(54)	.0049927	(55)	.00057243	(56)	.0078394
(57)	.018778	(58)	.015791	(59)	.0059700	(60)	.0031801
(61)	.0022222	(62)	.00061073	(63)	.0033201		

FUSELAGE LEESIDE SURFACE ... MACH = 6 --- CONTINUED

RUN NO.	MACH NO.	ALPHA (DEG)	RE (X E6)	T(U) (R)	P(0) (PSI)	T(0) (R)	P(INF) (PSI)	T(INF) (R)	H(REF) (B/F2-S-R)
				T/C	H/H(REF)	T/C	H/H(REF)	T/C	H/H(REF)

6	6.0	30.	2.70	530.	150.48	877.56	.09261	106.35	.047479
---	-----	-----	------	------	--------	--------	--------	--------	---------

(1)	.030152	(2)	.0026176	(3)	.015693	(4)	.0031564
(5)	.0024165	(6)	.0015858	(7)	.0090346	(8)	.012699
(9)	.011458	(10)	.019349	(11)	.034348	(12)	.023509
(13)	.0051524	(14)	.0027207	(15)	.0043139	(16)	.0084440
(17)	.011487	(18)	.0097843	(19)	.0087433	(20)	.027992
(21)	.033768	(22)	.0084276	(23)	.0042348	(24)	.0037590
(25)	.0074641	(26)	.0079182	(27)	.0083760	(28)	.0054301
(29)	.024246	(30)	.026377	(31)	.010590	(32)	.0061594
(33)	.0043414	(34)	.0055695	(35)	.0038783	(36)	.0047357
(37)	.0035682	(38)	.0092800	(39)	.018015	(40)	.011090
(41)	.0084294	(42)	.0062901	(43)	.0063403	(44)	.0055783
(45)	.0059879	(46)	.00072839	(47)	.0041664	(48)	.0085013
(49)	.010313	(50)	.0061085	(51)	.0046285	(52)	.0063000
(53)	.0052690	(54)	.0054560	(55)	.0019323	(56)	.0015573
(57)	.0046985	(58)	.0058547	(59)	.0036020	(60)	.0032232
(61)	.0049211	(62)	.00068139	(63)	.0033447		

7	6.0	35.	2.70	535.	147.07	878.78	.09049	106.51	.046946
---	-----	-----	------	------	--------	--------	--------	--------	---------

(1)	.019446	(2)	.023644	(3)	.018030	(4)	.0036287
(5)	.0013749	(6)	.0026720	(7)	.0044403	(8)	.0038835
(9)	.0034032	(10)	.013192	(11)	.021479	(12)	.021111
(13)	.0056931	(14)	.0010218	(15)	.0025608	(16)	.0039650
(17)	.0027007	(18)	.0030545	(19)	.0072352	(20)	.018083
(21)	.021321	(22)	.0043030	(23)	.0021887	(24)	.0032876
(25)	.0035708	(26)	.0028327	(27)	.0029364	(28)	.0022163
(29)	.011268	(30)	.019930	(31)	.0058338	(32)	.0034405
(33)	.0049146	(34)	.0026070	(35)	.0016408	(36)	.0014664
(37)	.0018639	(38)	.0043475	(39)	.0089356	(40)	.0063887
(41)	.0034952	(42)	.0063238	(43)	.0053455	(44)	.00032383
(45)	.0028136	(46)	.00183829	(47)	.0014815	(48)	.0019647
(49)	.0031655	(50)	.0059113	(51)	.0037141	(52)	.0034667
(53)	.0019441	(54)	.00036804	(55)	.0023047	(56)	.0022486
(57)	.0018465	(58)	.00060541	(59)	.0069401	(60)	.0049624
(61)	.0017610	(62)	.0010294	(63)	.0034973		

FUSELAGE LEESIDE SURFACE ... MACH = 6 --- CONTINUED

RUN NO.	MACH NO.	ALPHA (DEG)	RE (X E6)	T(U) (R)	P(0) (PSI)	T(0) (R)	P(INF) (PSI)	T(INF) (R)	H(REF) (B/F2-S-R)
				T/C	H/H(REF)	T/C	H/H(REF)	T/C	H/H(REF)

8	6.0	40.	2.70	533.	147.31	877.15	.09064	106.30	.046977
---	-----	-----	------	------	--------	--------	--------	--------	---------

(1)	.018533	(2)	.022619	(3)	.016259	(4)	.0042957
(5)	.0014172	(6)	.0028998	(7)	.0047061	(8)	.0028565
(9)	.0031246	(10)	.0096493	(11)	.022607	(12)	.019325
(13)	.0049202	(14)	.0013477	(15)	.0031903	(16)	.0052127
(17)	.0041498	(18)	.0044304	(19)	.0032644	(20)	.015976
(21)	.021447	(22)	.0060215	(23)	.0017750	(24)	.0045615
(25)	.0079974	(26)	.0059774	(27)	.0075998	(28)	.00053936
(29)	.0053390	(30)	.015221	(31)	.0068565	(32)	.0021264
(33)	.0069072	(34)	.0098074	(35)	.0068467	(36)	.0084701
(37)	.0024028	(38)	.0013457	(39)	.0036296	(40)	.0028971
(41)	.0039880	(42)	.0062035	(43)	.0068097	(44)	.0070848
(45)	.0091154	(46)	.0044740	(47)	.0035710	(48)	.0024172
(49)	.0019458	(50)	.0043495	(51)	.0055601	(52)	.0049261
(53)	.0079511	(54)	.0081056	(55)	.0048939	(56)	.0063639
(57)	.0062134	(58)	.0017075	(59)	.0037372	(60)	.0047983
(61)	.010050	(62)	.00059336	(63)	.0071427		

9	6.0	40.	5.40	550.	302.08	904.83	.18751	109.89	.067356
---	-----	-----	------	------	--------	--------	--------	--------	---------

(1)	.018347	(2)	.018060	(3)	.013978	(4)	.0027373
(5)	.000035660	(6)	.0025786	(7)	.0049692	(8)	.0043892
(9)	.0057738	(10)	.014882	(11)	.021312	(12)	.016094
(13)	.0032394	(14)	.00072936	(15)	.0027651	(16)	.0056674
(17)	.0064498	(18)	.0070113	(19)	.0080242	(20)	.027108
(21)	.024021	(22)	.0044406	(23)	.00069178	(24)	.0025171
(25)	.0054771	(26)	.0053036	(27)	.0055910	(28)	.0021582
(29)	.014926	(30)	.040806	(31)	.010724	(32)	.0030376
(33)	.0042622	(34)	.0040449	(35)	.0041883	(36)	.0039071
(37)	.0012378	(38)	.0045498	(39)	.010705	(40)	.0086440
(41)	.0051524	(42)	.0044575	(43)	.0060488	(44)	.0055941
(45)	.0053899	(46)	.00083943	(47)	.00059041	(48)	.000036778
(49)	.0031579	(50)	.0080387	(51)	.0060694	(52)	.0051944
(53)	.0044854	(54)	.0054181	(55)	.0056016	(56)	.0045689
(57)	.0026608	(58)	.00041759	(59)	.0033530	(60)	.0064231
(61)	.0067838	(62)	.0017487	(63)	.0080120		

FUSELAGE LEESIDE SURFACE ... MACH = 6 --- CONTINUED

RUN NO.	MACH NO.	ALPHA (DEG)	RE (X E6)	T(U) (R)	P(0) (PSI)	T(0) (R)	P(INF) (PSI)	T(INF) (R)	H(REF) (B/F2-S-R)
				T/C	H/H(REF)	T/C	H/H(REF)	T/C	H/H(REF)

10	6.0	35.	5.40	545.	301.58	913.15	.18720	110.95	.067357
----	-----	-----	------	------	--------	--------	--------	--------	---------

(1)	.021683	(2)	.021610	(3)	.015452	(4)	.0035624
(5)	.0012618	(6)	.0027440	(7)	.0055561	(8)	.0058873
(9)	.0058861	(10)	.015354	(11)	.023970	(12)	.017066
(13)	.0042321	(14)	.0024734	(15)	.0053692	(16)	.0052244
(17)	.0045684	(18)	.0047735	(19)	.010792	(20)	.023899
(21)	.023802	(22)	.0057269	(23)	.0020624	(24)	.0031962
(25)	.0051316	(26)	.0054443	(27)	.0053274	(28)	.0042799
(29)	.026895	(30)	.042845	(31)	.0091810	(32)	.0041527
(33)	.0040059	(34)	.0047789	(35)	.0041888	(36)	.0036690
(37)	.0026239	(38)	.0099611	(39)	.028224	(40)	.015287
(41)	.0050439	(42)	.0042109	(43)	.0059338	(44)	.0082272
(45)	.0063816	(46)	.0010987	(47)	.0038035	(48)	.0095602
(49)	.011036	(50)	.0075964	(51)	.0049243	(52)	.0057589
(53)	.0070230	(54)	.0056521	(55)	.0041700	(56)	.0029530
(57)	.0041905	(58)	.0037374	(59)	.0076521	(60)	.0044760
(61)	.0055050	(62)	.0025406	(63)	.0054072		

11	6.0	30.	5.40	545.	296.93	903.41	.18427	109.70	.066772
----	-----	-----	------	------	--------	--------	--------	--------	---------

(1)	.029038	(2)	.023066	(3)	.014556	(4)	.0036236
(5)	.0018407	(6)	.0029396	(7)	.0095062	(8)	.012767
(9)	.012113	(10)	.023170	(11)	.030364	(12)	.017384
(13)	.0049079	(14)	.0059479	(15)	.0035538	(16)	.0065218
(17)	.010527	(18)	.0099651	(19)	.016066	(20)	.035958
(21)	.029181	(22)	.0060926	(23)	.0056850	(24)	.0025720
(25)	.0045312	(26)	.0053605	(27)	.0061595	(28)	.0068336
(29)	.032480	(30)	.037997	(31)	.0093509	(32)	.0060370
(33)	.0047664	(34)	.0040433	(35)	.0011604	(36)	.0016948
(37)	.0046266	(38)	.019394	(39)	.045842	(40)	.013404
(41)	.0061230	(42)	.0062065	(43)	.0059847	(44)	.0033040
(45)	.0049294	(46)	.0023659	(47)	.0086750	(48)	.032148
(49)	.017456	(50)	.0059710	(51)	.0049209	(52)	.0047559
(53)	.0042697	(54)	.0058134	(55)	.0053237	(56)	.0017013
(57)	.017013	(58)	.016573	(59)	.0038800	(60)	.0020148
(61)	.0047663	(62)	.0023162	(63)	.0050510		

FUSELAGE LEESIDE SURFACE ... MACH = 6 --- CONTINUED

RUN NO.	MACH NO.	ALPHA (DEG)	RE (X E6)	T(U) (R)	P(0) (PSI)	T(0) (R)	P(INF) (PSI)	T(INF) (R)	H(REF) (B/F2-S-R)
		T/C	H/H(REF)	T/C	H/H(REF)	T/C	H/H(REF)	T/C	H/H(REF)

12	6.0	25.	5.40	545.	300.75	875.69	.18668	106.19	.067002
----	-----	-----	------	------	--------	--------	--------	--------	---------

(1)	.037257	(2)	.020101	(3)	.011938	(4)	.0032134
(5)	.0012522	(6)	.0035095	(7)	.0088461	(8)	.015516
(9)	.013688	(10)	.038337	(11)	.028653	(12)	.014762
(13)	.0050379	(14)	.0047210	(15)	.0039964	(16)	.0091821
(17)	.016634	(18)	.015922	(19)	.034118	(20)	.046790
(21)	.021527	(22)	.0068374	(23)	.0055960	(24)	.0035671
(25)	.0091616	(26)	.012527	(27)	.011555	(28)	.015989
(29)	.047327	(30)	.033340	(31)	.0082612	(32)	.0096256
(33)	.0056086	(34)	.0056900	(35)	.0070331	(36)	.0056810
(37)	.010395	(38)	.036945	(39)	.045511	(40)	.0084174
(41)	.0092875	(42)	.0056085	(43)	.0039411	(44)	.0031030
(45)	.0034730	(46)	.0056029	(47)	.0249070	(48)	.044946
(49)	.010436	(50)	.0079389	(51)	.0054812	(52)	.0030918
(53)	.0033529	(54)	.0039071	(55)	.0065777	(56)	.017887
(57)	.038395	(58)	.011896	(59)	.0057301	(60)	.0022453
(61)	.0040523	(62)	.0027966	(63)	.0068495		

13	6.0	20.	5.40	550.	306.39	886.04	.19023	107.50	.067701
----	-----	-----	------	------	--------	--------	--------	--------	---------

(1)	.020153	(2)	.012446	(3)	.0073463	(4)	.0013425
(5)	.00075792	(6)	.0023937	(7)	.0078798	(8)	.013698
(9)	.0011586	(10)	.039636	(11)	.022669	(12)	.013721
(13)	.0033267	(14)	.0015836	(15)	.0037557	(16)	.0093671
(17)	.014180	(18)	.013495	(19)	.050812	(20)	.026520
(21)	.020265	(22)	.0064408	(23)	.0040574	(24)	.0026643
(25)	.010512	(26)	.017648	(27)	.016472	(28)	.036381
(29)	.033853	(30)	.020862	(31)	.0063348	(32)	.0025779
(33)	.0019318	(34)	.0091280	(35)	.014728	(36)	.013287
(37)	.027400	(38)	.039470	(39)	.024557	(40)	.0070898
(41)	.0058914	(42)	.0036128	(43)	.0066310	(44)	.010396
(45)	.0093395	(46)	.017107	(47)	.034176	(48)	.024224
(49)	.0072898	(50)	.0047573	(51)	.0035333	(52)	.0038084
(53)	.0035145	(54)	.0036305	(55)	.011682	(56)	.025255
(57)	.024701	(58)	.0063763	(59)	.0043177	(60)	.0089503
(61)	.0072495	(62)	.0016513	(63)	.0071980		

FUSELAGE LEESIDE SURFACE ... MACH = 6 --- CONTINUED

RUN NO.	MACH NO.	ALPHA (DEG)	RE (X E6)	T(U) (R)	P(0) (PSI)	T(0) (R)	P(INF) (PSI)	T(INF) (R)	H(REF) (B/F2-S-R)
		T/C	H/H(REF)	T/C	H/H(REF)	T/C	H/H(REF)	T/C	H/H(REF)

14	6.0	20.	7.30	550.	399.34	893.88	.24895	108.54	.077326
----	-----	-----	------	------	--------	--------	--------	--------	---------

(1)	.018732	(2)	.012349	(3)	.0085351	(4)	.0023998
(5)	.00074418	(6)	.0011028	(7)	.0086023	(8)	.013924
(9)	.013148	(10)	.040283	(11)	.026009	(12)	.013481
(13)	.0030365	(14)	.0019051	(15)	.0034758	(16)	.0096207
(17)	.014763	(18)	.013543	(19)	.047409	(20)	.026009
(21)	.026472	(22)	.0073070	(23)	.0044914	(24)	.0036334
(25)	.011217	(26)	.016706	(27)	.016407	(28)	.035157
(29)	.031235	(30)	.020967	(31)	.0064193	(32)	.0025293
(33)	.0026038	(34)	.0097186	(35)	.012288	(36)	.011947
(37)	.026115	(38)	.036613	(39)	.027087	(40)	.0069211
(41)	.0055578	(42)	.0043917	(43)	.0071464	(44)	.0097952
(45)	.0090850	(46)	.016831	(47)	.032864	(48)	.025780
(49)	.0084324	(50)	.0044271	(51)	.0039648	(52)	.0037812
(53)	.0031838	(54)	.0033816	(55)	.012315	(56)	.024289
(57)	.024484	(58)	.0073122	(59)	.0036955	(60)	.0055404
(61)	.0063444	(62)	.0024834	(63)	.0080903		

15	6.0	25.	7.30	550.	399.67	888.88	.24916	107.91	.077315
----	-----	-----	------	------	--------	--------	--------	--------	---------

(1)	.035864	(2)	.019085	(3)	.011934	(4)	.0032250
(5)	.0010070	(6)	.0017308	(7)	.0087963	(8)	.015637
(9)	.012654	(10)	.044587	(11)	.027978	(12)	.015047
(13)	.0045520	(14)	.0050386	(15)	.0034151	(16)	.0086710
(17)	.014891	(18)	.013624	(19)	.038909	(20)	.049688
(21)	.023880	(22)	.0067260	(23)	.0071768	(24)	.0034127
(25)	.0080833	(26)	.012181	(27)	.011251	(28)	.020315
(29)	.055572	(30)	.035836	(31)	.0090466	(32)	.0083689
(33)	.0011006	(34)	.0043889	(35)	.0053601	(36)	.0041720
(37)	.011531	(38)	.040001	(39)	.043152	(40)	.0089628
(41)	.0079345	(42)	.0058175	(43)	.0038189	(44)	.0026996
(45)	.0028435	(46)	.0055956	(47)	.026869	(48)	.039626
(49)	.0097676	(50)	.0079188	(51)	.0056117	(52)	.0039431
(53)	.0042401	(54)	.0043909	(55)	.0076268	(56)	.020391
(57)	.039161	(58)	.0099812	(59)	.0057846	(60)	.0030991
(61)	.0047339	(62)	.0029760	(63)	.0079450		

FUSELAGE LEESIDE SURFACE ... MACH = 6 --- CONTINUED

RUN NO.	MACH NO.	ALPHA (DEG)	RE (X E6)	T(U) (R)	P(0) (PSI)	T(0) (R)	P(INF) (PSI)	T(INF) (R)	H(REF) (B/F2-S-R)
				T/C	H/H(REF)	T/C	H/H(REF)	T/C	H/H(REF)

17	6.0	30.	7.30	535.	400.83	895.54	.24990	108.75	.077484
----	-----	-----	------	------	--------	--------	--------	--------	---------

(1)	.031982	(2)	.023844	(3)	.015707	(4)	.0015153
(5)	.0013585	(6)	.0039214	(7)	.0094946	(8)	.013186
(9)	.011757	(10)	.032389	(11)	.038104	(12)	.020278
(13)	.0040631	(14)	.0072557	(15)	.0045248	(16)	.0062475
(17)	.0093214	(18)	.0085730	(19)	.025007	(20)	.050100
(21)	.034943	(22)	.0073012	(23)	.0057006	(24)	.0035093
(25)	.0049642	(26)	.0054650	(27)	.0058892	(28)	.012457
(29)	.052100	(30)	.047395	(31)	.0093337	(32)	.0055327
(33)	.0049254	(34)	.0025843	(35)	.00039665	(36)	.0011031
(37)	.0080090	(38)	.029554	(39)	.053644	(40)	.010666
(41)	.0055358	(42)	.0073427	(43)	.0066061	(44)	.0035166
(45)	.0054215	(46)	.0070563	(47)	.013447	(48)	.041305
(49)	.016648	(50)	.0060482	(51)	.0049480	(52)	.0046789
(53)	.0054862	(54)	.0051433	(55)	.0081944	(56)	.010272
(57)	.021028	(58)	.019556	(59)	.0042429	(60)	.0021700
(61)	.0061444	(62)	.0026067	(63)	.0071821		

18	6.0	35.	7.30	550.	401.41	887.02	.25027	107.67	.077467
----	-----	-----	------	------	--------	--------	--------	--------	---------

(1)	.023052	(2)	.020815	(3)	.014281	(4)	.0030924
(5)	.00050600	(6)	.0020137	(7)	.0048840	(8)	.0063225
(9)	.0051956	(10)	.019464	(11)	.029843	(12)	.019382
(13)	.0040375	(14)	.0028387	(15)	.0042447	(16)	.0060970
(17)	.0040436	(18)	.0044767	(19)	.016644	(20)	.040579
(21)	.034264	(22)	.0074413	(23)	.0025922	(24)	.0030348
(25)	.0064168	(26)	.0049473	(27)	.0039198	(28)	.0062872
(29)	.038552	(30)	.047951	(31)	.010141	(32)	.0034596
(33)	.0055767	(34)	.0059588	(35)	.0058709	(36)	.0040327
(37)	.0054410	(38)	.012089	(39)	.036045	(40)	.014281
(41)	.0050932	(42)	.0061231	(43)	.0065130	(44)	.0085293
(45)	.0069900	(46)	.0025132	(47)	.0048515	(48)	.012066
(49)	.014673	(50)	.0054818	(51)	.0055177	(52)	.0063878
(53)	.0078743	(54)	.0070014	(55)	.0046149	(56)	.0063219
(57)	.0064240	(58)	.0051116	(59)	.0063060	(60)	.0040833
(61)	.0063439	(62)	.0034269	(63)	.0073223		

FUSELAGE LEESIDE SURFACE ... MACH = 6 --- CONTINUED

RUN NO.	MACH NO.	ALPHA (DEG)	RE (X E6)	T(U) (R)	P(0) (PSI)	T(0) (R)	P(INF) (PSI)	T(INF) (R)	H(REF) (B/F2-S-R)
				T/C	H/H(REF)	T/C	H/H(REF)	T/C	H/H(REF)

19	6.0	40.	7.30	540.	401.99	898.78	.25063	108.78	.077598
----	-----	-----	------	------	--------	--------	--------	--------	---------

(1)	.022532	(2)	.020627	(3)	.016271	(4)	.0039368
(5)	.00050845	(6)	.0025426	(7)	.0053570	(8)	.0062084
(9)	.0068330	(10)	.020425	(11)	.029237	(12)	.021338
(13)	.0054512	(14)	.00093893	(15)	.0030574	(16)	.0044134
(17)	.0048931	(18)	.0046946	(19)	.015294	(20)	.047060
(21)	.037716	(22)	.0083806	(23)	.0021451	(24)	.0045583
(25)	.0065482	(26)	.0042640	(27)	.0042588	(28)	.0044684
(29)	.023470	(30)	.053359	(31)	.011882	(32)	.0040035
(33)	.0054281	(34)	.0060765	(35)	.0063695	(36)	.0063396
(37)	.0040521	(38)	.0080003	(39)	.018657	(40)	.015324
(41)	.0052624	(42)	.0056165	(43)	.0078908	(44)	.0070280
(45)	.0071624	(46)	.0022556	(47)	.0035742	(48)	.0039510
(49)	.0062663	(50)	.011007	(51)	.0080421	(52)	.0062681
(53)	.0057588	(54)	.0063779	(55)	.0063021	(56)	.0062554
(57)	.0054908	(58)	.0023378	(59)	.0046812	(60)	.0083583
(61)	.0079799	(62)	.0027007	(63)	.0067920		

20	6.0	20.	1.10	530.	51.85	799.34	.03167	96.44	.027695
----	-----	-----	------	------	-------	--------	--------	-------	---------

(1)	.028767	(2)	.012945	(3)	.0075422	(4)	.0034989
(5)	.00038535	(6)	.0066337	(7)	.0055888	(8)	.0091780
(9)	.0058194	(10)	.037996	(11)	.026470	(12)	.017358
(13)	.0029962	(14)	.0012229	(15)	.0055789	(16)	.0058949
(17)	.010556	(18)	.011272	(19)	.035827	(20)	.035701
(21)	.021199	(22)	.0063823	(23)	.0022689	(24)	.0054460
(25)	.0087712	(26)	.010092	(27)	.0096378	(28)	.012889
(29)	.043442	(30)	.020475	(31)	.0046905	(32)	.0010983
(33)	.0035971	(34)	.0075862	(35)	.010273	(36)	.0094696
(37)	.014052	(38)	.030343	(39)	.037391	(40)	.0078267
(41)	.0041603	(42)	.0050516	(43)	.0090610	(44)	.010090
(45)	.010054	(46)	.010434	(47)	.018134	(48)	.036027
(49)	.011275	(50)	.0034024	(51)	.0044635	(52)	.0061496
(53)	.010123	(54)	.0092839	(55)	.0067284	(56)	.014163
(57)	.028796	(58)	.0073337	(59)	.0019877	(60)	.0034276
(61)	.0076541	(62)	.0024592	(63)	.0065789		

FUSELAGE LEESIDE SURFACE ... MACH = 6 --- CONTINUED

RUN NO.	MACH NO.	ALPHA (DEG)	RE (X E6)	T(U) (R)	P(0) (PSI)	T(0) (R)	P(INF) (PSI)	T(INF) (R)	H(REF) (B/F2-S-R)
		T/C	H/H(REF)	T/C	H/H(REF)	T/C	H/H(REF)	T/C	H/H(REF)

21	6.0	25.	1.10	530.	54.75	808.26	.03345	97.56	.028485
----	-----	-----	------	------	-------	--------	--------	-------	---------

(1)	.033438	(2)	.022897	(3)	.012251	(4)	.0039276
(5)	.0016275	(6)	.0059901	(7)	.0054567	(8)	.0095419
(9)	.0078978	(10)	.024206	(11)	.035512	(12)	.016127
(13)	.0086934	(14)	.0020417	(15)	.0018540	(16)	.0060275
(17)	.012045	(18)	.0092815	(19)	.014324	(20)	.034843
(21)	.032563	(22)	.0073769	(23)	.0042221	(24)	.0049963
(25)	.0081478	(26)	.010557	(27)	.0092179	(28)	.0091973
(29)	.019913	(30)	.036972	(31)	.010809	(32)	.0046468
(33)	.0038532	(34)	.0074061	(35)	.0084482	(36)	.0068353
(37)	.0082338	(38)	.010402	(39)	.021689	(40)	.013175
(41)	.0051051	(42)	.0034171	(43)	.0075840	(44)	.0084364
(45)	.0065378	(46)	.0060646	(47)	.0052119	(48)	.017400
(49)	.0055693	(50)	.0049090	(51)	.0038583	(52)	.0056753
(53)	.0063251	(54)	.0074247	(55)	.0040438	(56)	.0027402
(57)	.0092514	(58)	.0029169	(59)	.0057442	(60)	.0036123
(61)	.0047391	(62)	.0018821	(63)	.0086747		

22	6.0	30.	1.10	530.	49.32	797.91	.03012	96.26	.027009
----	-----	-----	------	------	-------	--------	--------	-------	---------

(1)	.022211	(2)	.019699	(3)	.017806	(4)	.0051958
(5)	.0051094	(6)	.0059528	(7)	.0071151	(8)	.0087100
(9)	.0066695	(10)	.013259	(11)	.021456	(12)	.028963
(13)	.0081948	(14)	.0022252	(15)	.0056896	(16)	.011081
(17)	.010356	(18)	.010512	(19)	.0099015	(20)	.022521
(21)	.027413	(22)	.0096049	(23)	.0045886	(24)	.0065141
(25)	.0097412	(26)	.0084667	(27)	.0080306	(28)	.0061813
(29)	.013653	(30)	.019417	(31)	.011296	(32)	.0043066
(33)	.0019533	(34)	.0093791	(35)	.0065794	(36)	.0096055
(37)	.0034613	(38)	.0064113	(39)	.014888	(40)	.0060160
(41)	.0039090	(42)	.0069546	(43)	.0062931	(44)	.0071523
(45)	.0094887	(46)	.0041844	(47)	.0055110	(48)	.0078555
(49)	.0084346	(50)	.0040247	(51)	.0070445	(52)	.0061231
(53)	.0065603	(54)	.0054167	(55)	.0028601	(56)	.0015471
(57)	.0038091	(58)	.0024520	(59)	.0031305	(60)	.0055382
(61)	.0075919	(62)	.0036963	(63)	.0067484		

FUSELAGE LEESIDE SURFACE ... MACH = 6 --- CONCLUDED

RUN NO.	MACH NO.	ALPHA (DEG)	RE (X E6)	T(U) (R)	P(0) (PSI)	T(0) (R)	P(INF) (PSI)	T(INF) (R)	H(REF) (B/F2-S-R)
		T/C	H/H(REF)	T/C	H/H(REF)	T/C	H/H(REF)	T/C	H/H(REF)

23	6.0	35.	1.10	530.	50.49	801.31	.03084	96.68	.027337
----	-----	-----	------	------	-------	--------	--------	-------	---------

(1)	.015535	(2)	.019414	(3)	.020808	(4)	.0061473
(5)	.0045261	(6)	.0028717	(7)	.0045864	(8)	.0021812
(9)	.0037929	(10)	.012811	(11)	.012305	(12)	.025895
(13)	.0081712	(14)	.0022020	(15)	.0051434	(16)	.0048690
(17)	.0019200	(18)	.0044066	(19)	.0047853	(20)	.017000
(21)	.019294	(22)	.0094270	(23)	.0036598	(24)	.0056450
(25)	.0077252	(26)	.0036539	(27)	.0041092	(28)	.0039075
(29)	.0094597	(30)	.015479	(31)	.0065783	(32)	.0026445
(33)	.0049605	(34)	.0044749	(35)	.0046570	(36)	.0030901
(37)	.0024282	(38)	.0055386	(39)	.0064446	(40)	.0051613
(41)	.0023756	(42)	.0030029	(43)	.0050403	(44)	.0053717
(45)	.0066917	(46)	.0033505	(47)	.0021184	(48)	.00025994
(49)	.0011973	(50)	.0030908	(51)	.0038776	(52)	.0057547
(53)	.0051068	(54)	.0042081	(55)	.0046063	(56)	.0049443
(57)	.0014445	(58)	.00030343	(59)	.00063867	(60)	.0050790
(61)	.0037373	(62)	.0023151	(63)	.0043844		

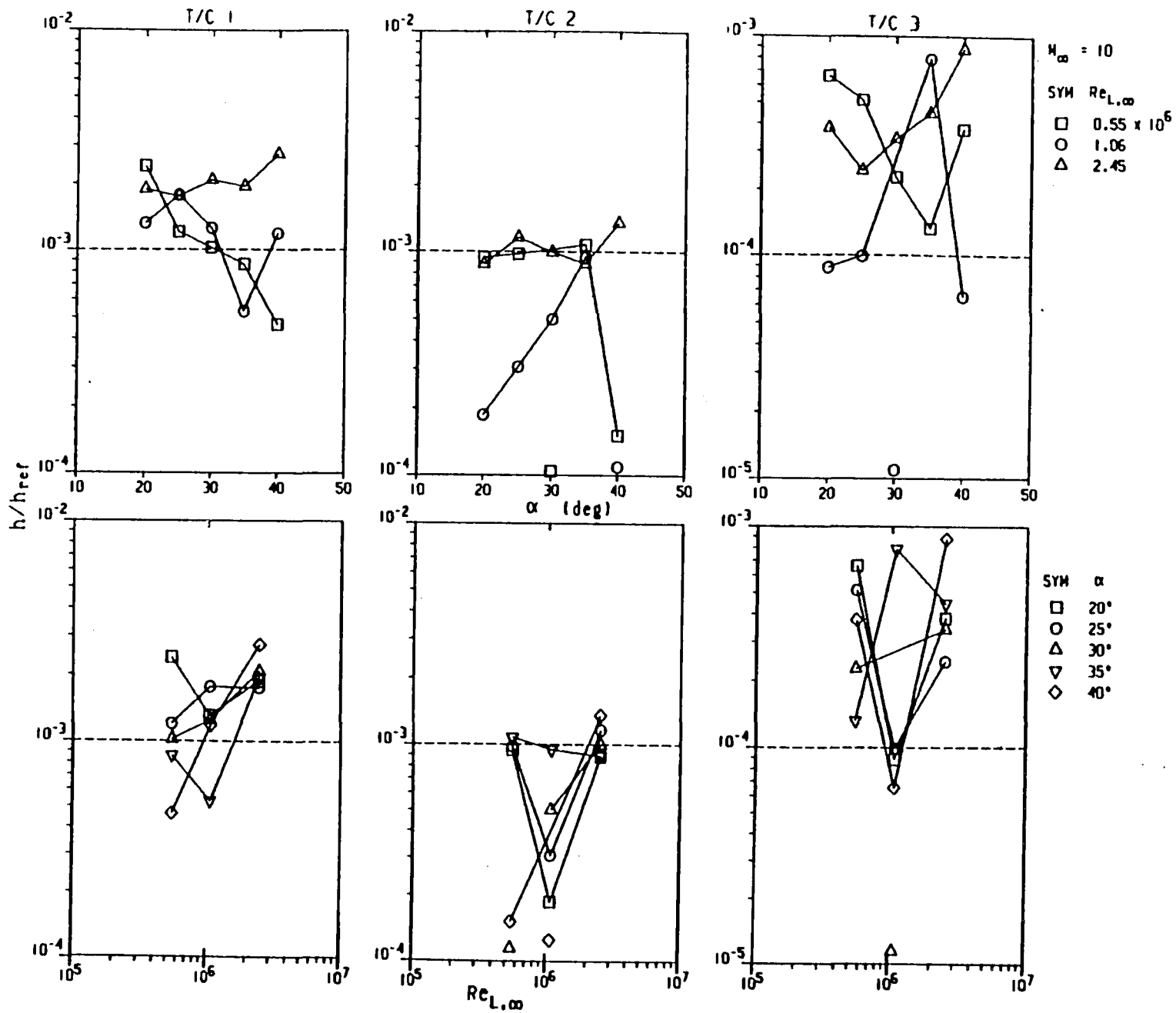
24	6.0	40.	1.10	530.	53.87	801.67	.03292	96.73	.028236
----	-----	-----	------	------	-------	--------	--------	-------	---------

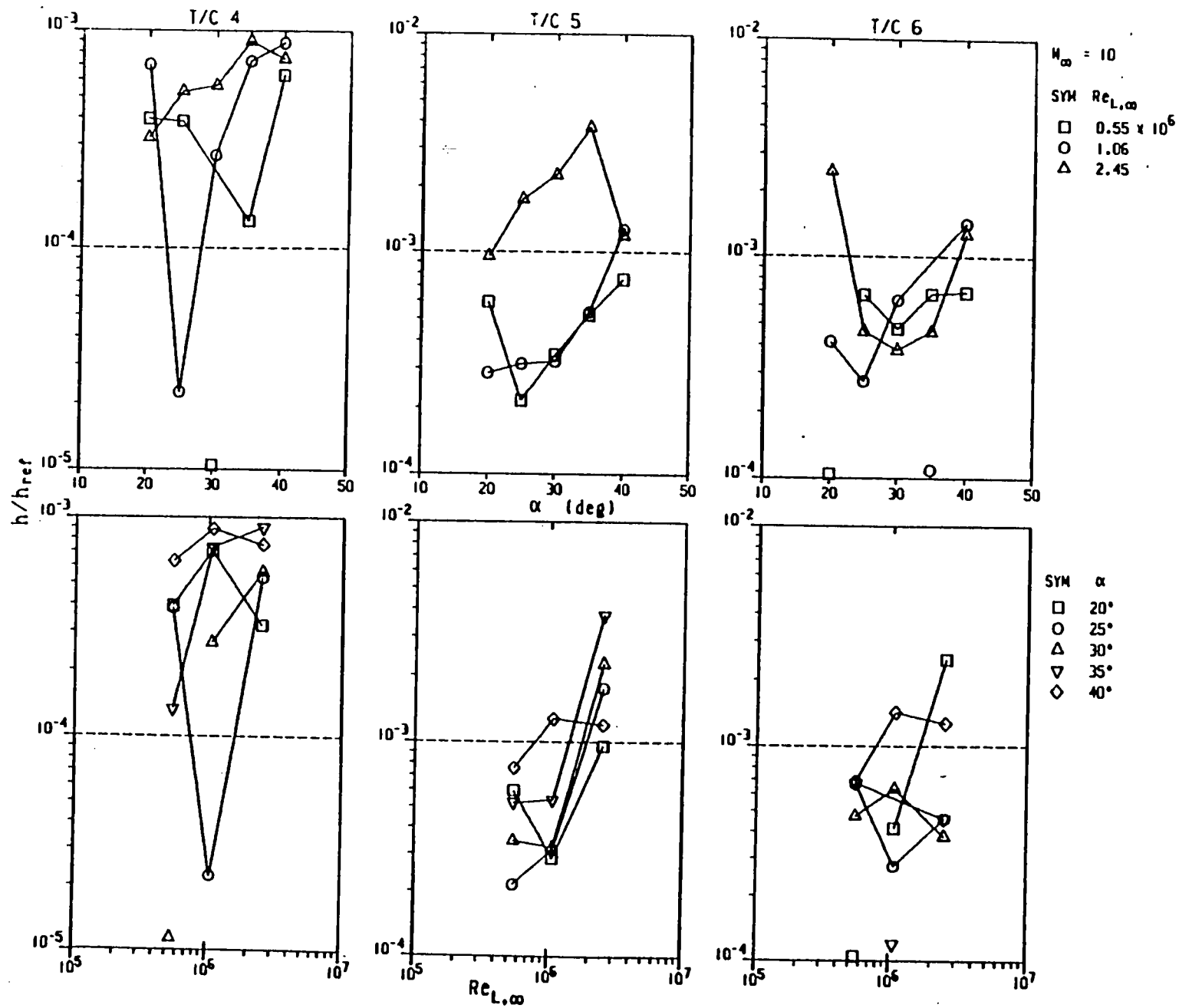
(1)	.015460	(2)	.017635	(3)	.018080	(4)	.0058836
(5)	.0020696	(6)	.0093702	(7)	.0033342	(8)	.0039051
(9)	.0025684	(10)	.0067824	(11)	.015509	(12)	.022860
(13)	.0040829	(14)	.0043179	(15)	.0051246	(16)	.0033633
(17)	.0072095	(18)	.0048821	(19)	.0071815	(20)	.027768
(21)	.028504	(22)	.0059903	(23)	.0031286	(24)	.0053758
(25)	.0083028	(26)	.0092445	(27)	.011755	(28)	.0042695
(29)	.011897	(30)	.017259	(31)	.012481	(32)	.0053964
(33)	.0044507	(34)	.0044722	(35)	.0075481	(36)	.0068555
(37)	.0063778	(38)	.0077490	(39)	.030283	(40)	.011188
(41)	.0048695	(42)	.0050973	(43)	.0063820	(44)	.0046594
(45)	.0072553	(46)	.0058810	(47)	.010474	(48)	.018619
(49)	.0023182	(50)	.0042697	(51)	.0067109	(52)	.0076566
(53)	.0077554	(54)	.0066754	(55)	.0043501	(56)	.015603
(57)	.019474	(58)	.0036473	(59)	.0015462	(60)	.0095635
(61)	.015265	(62)	.0075511	(63)	.012903		

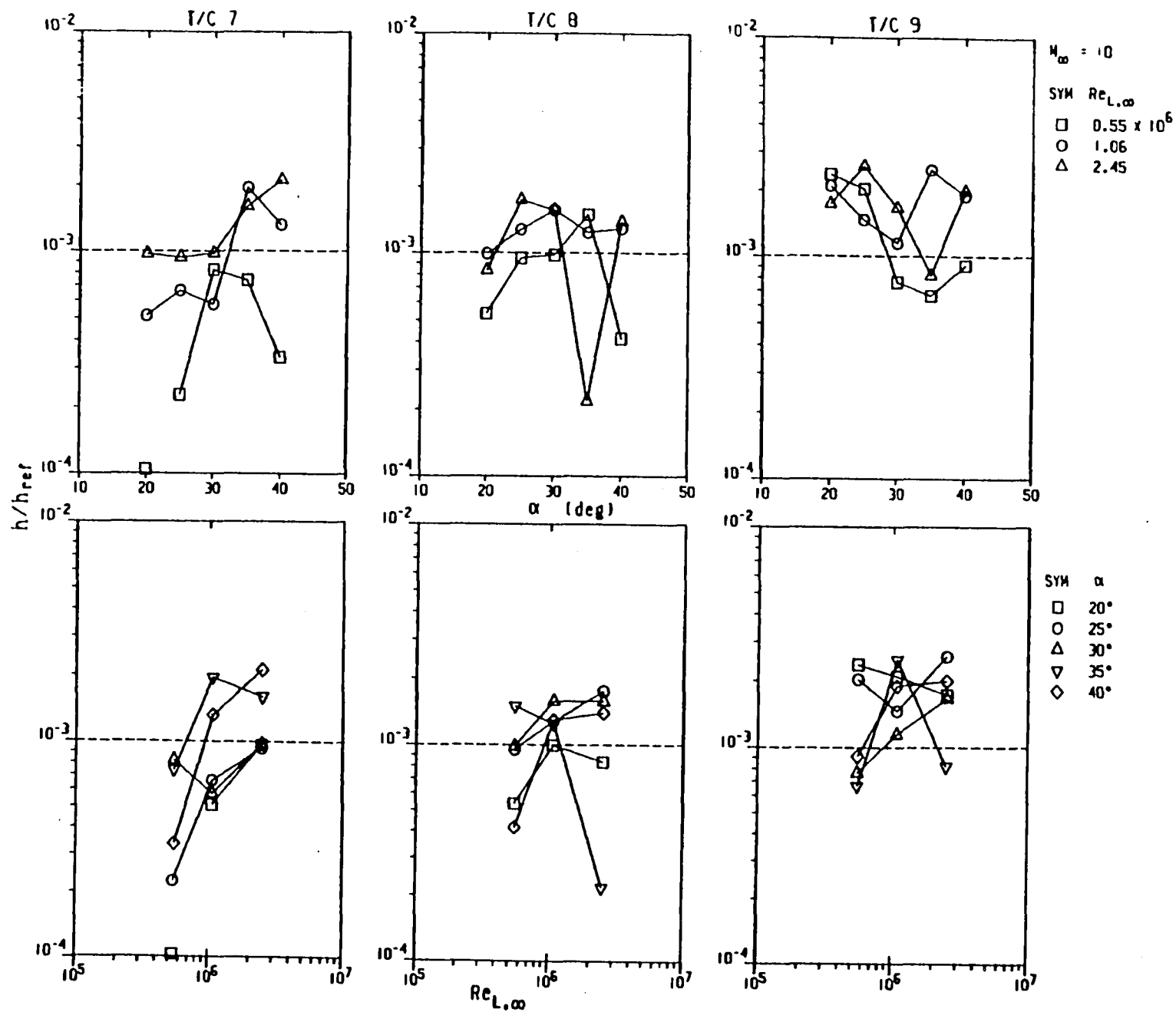
APPENDIX C

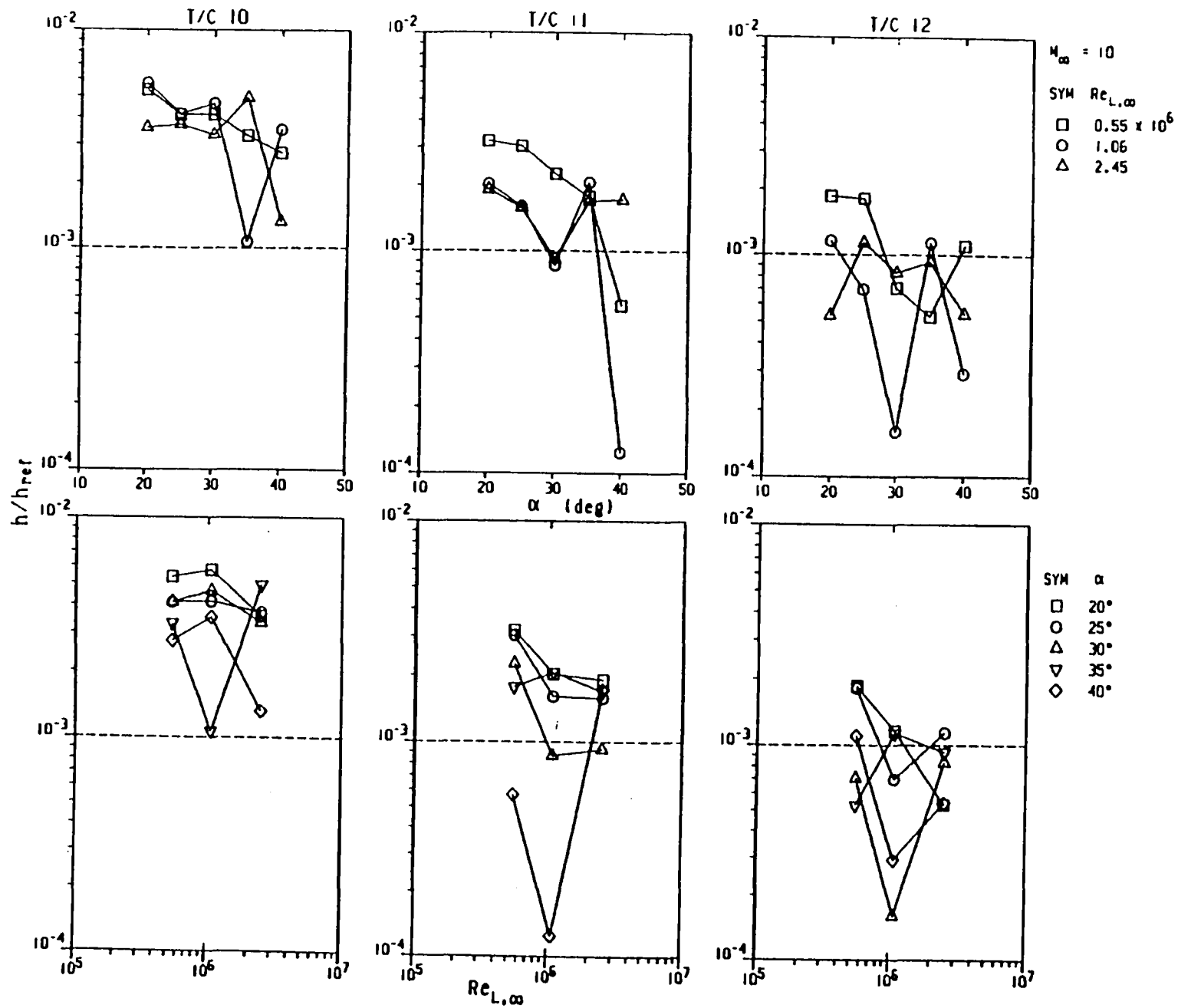
Variations of Wing Leaside Test Data

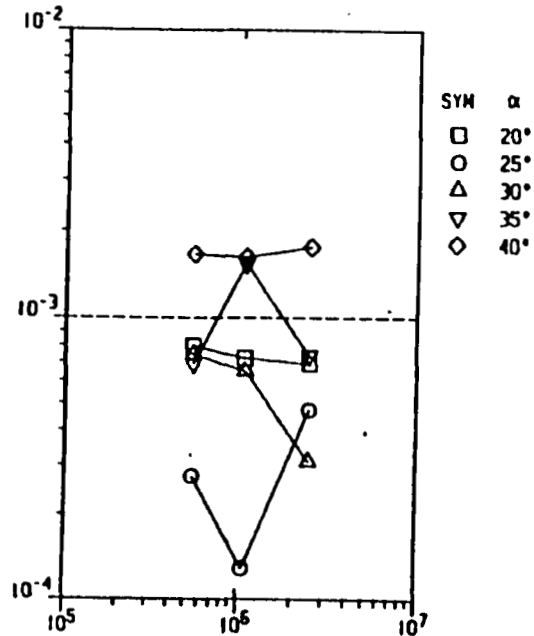
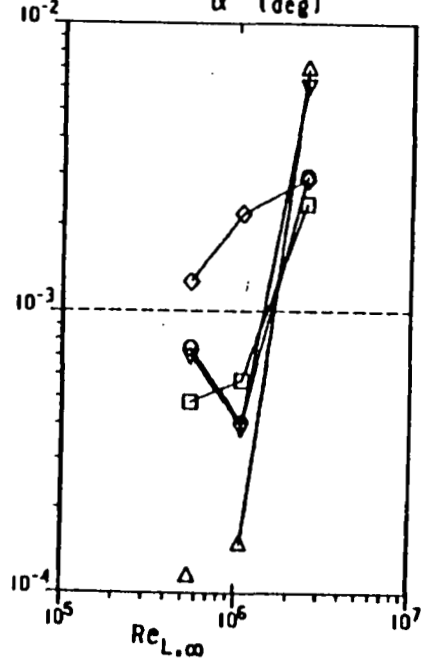
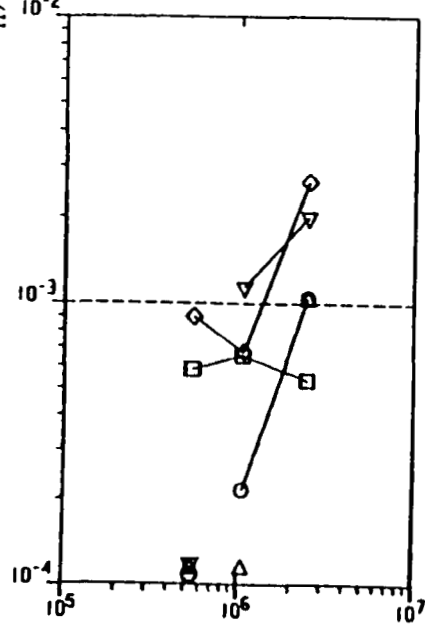
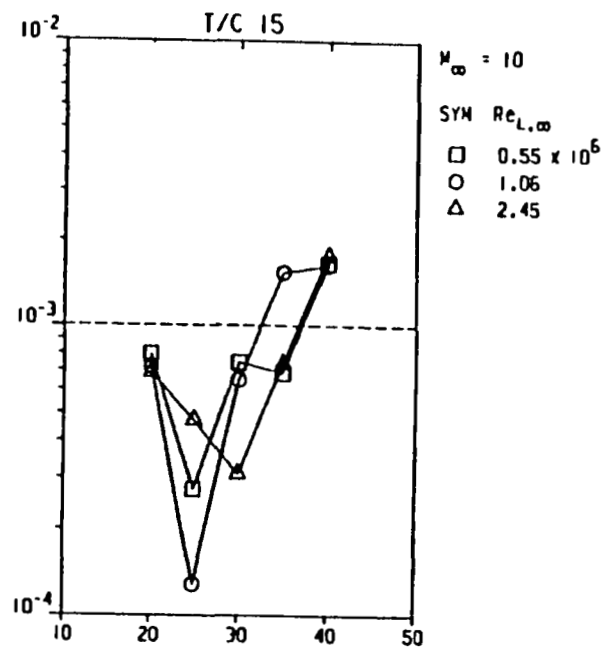
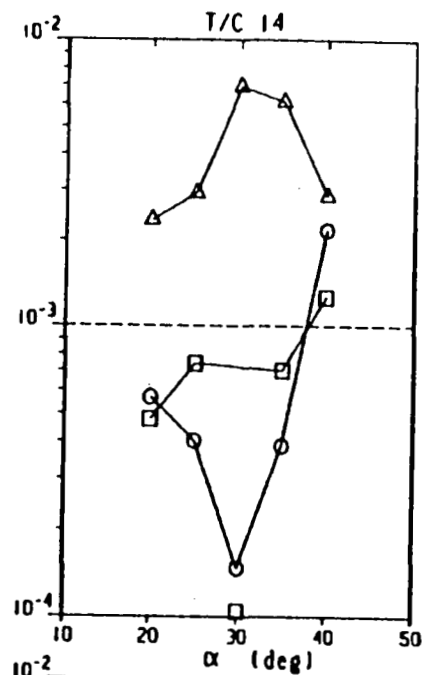
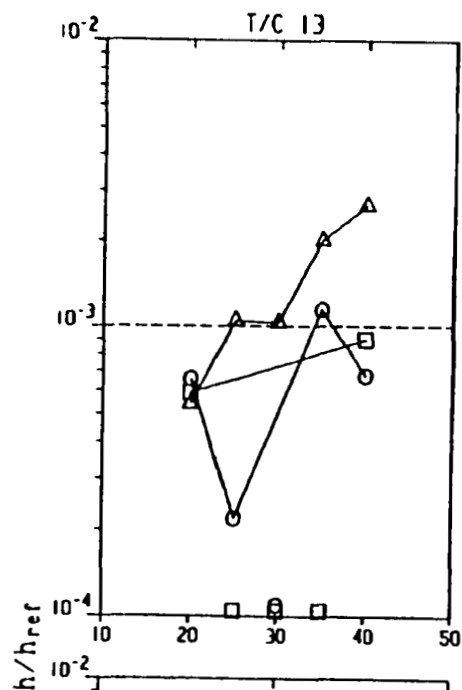
Variations of individual wing leaside thermocouple data with angle-of-attack and free-stream Reynolds number are presented herein.

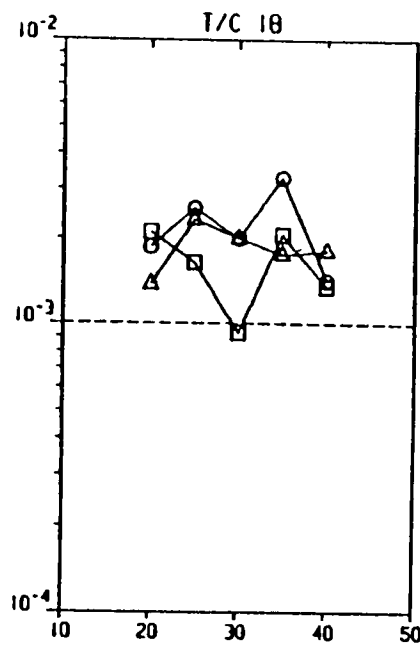
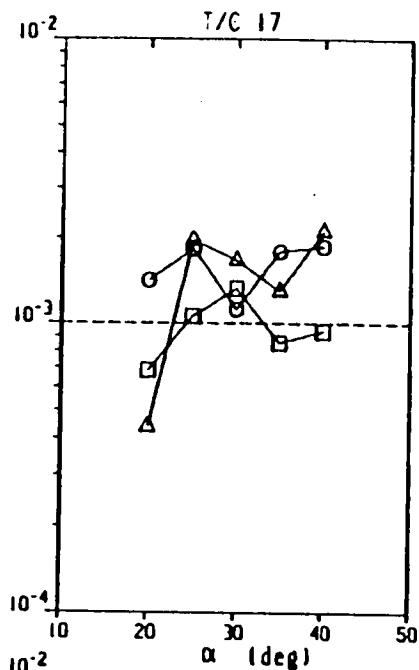
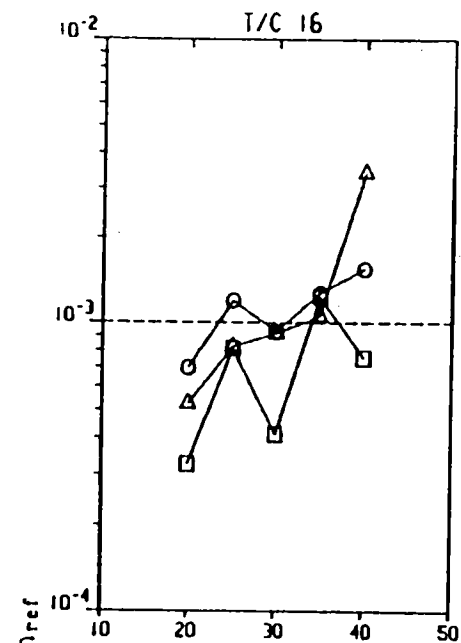












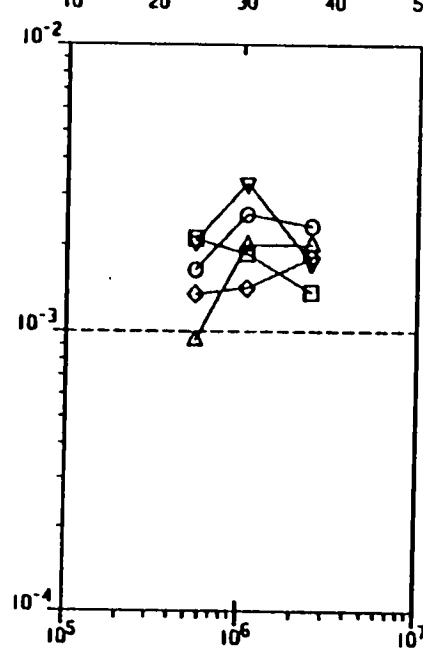
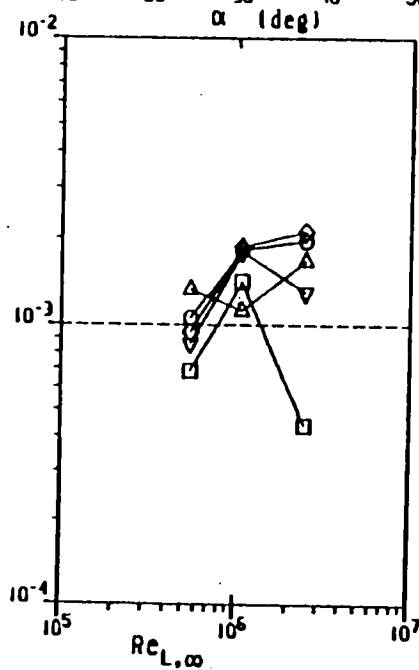
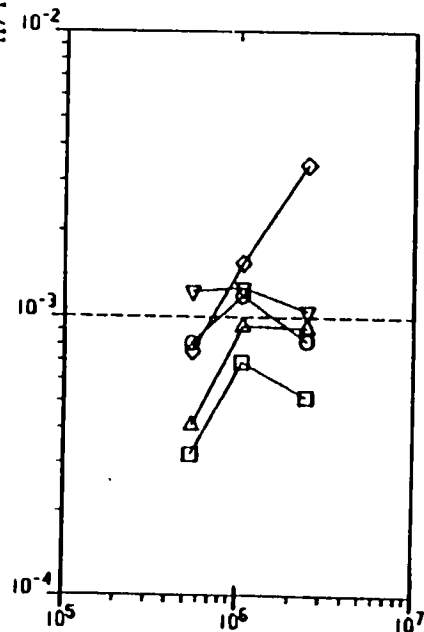
$M_\infty = 10$

SYM $Re_{L,\infty}$

□ 0.55×10^6

○ 1.06

△ 2.45



SYM α

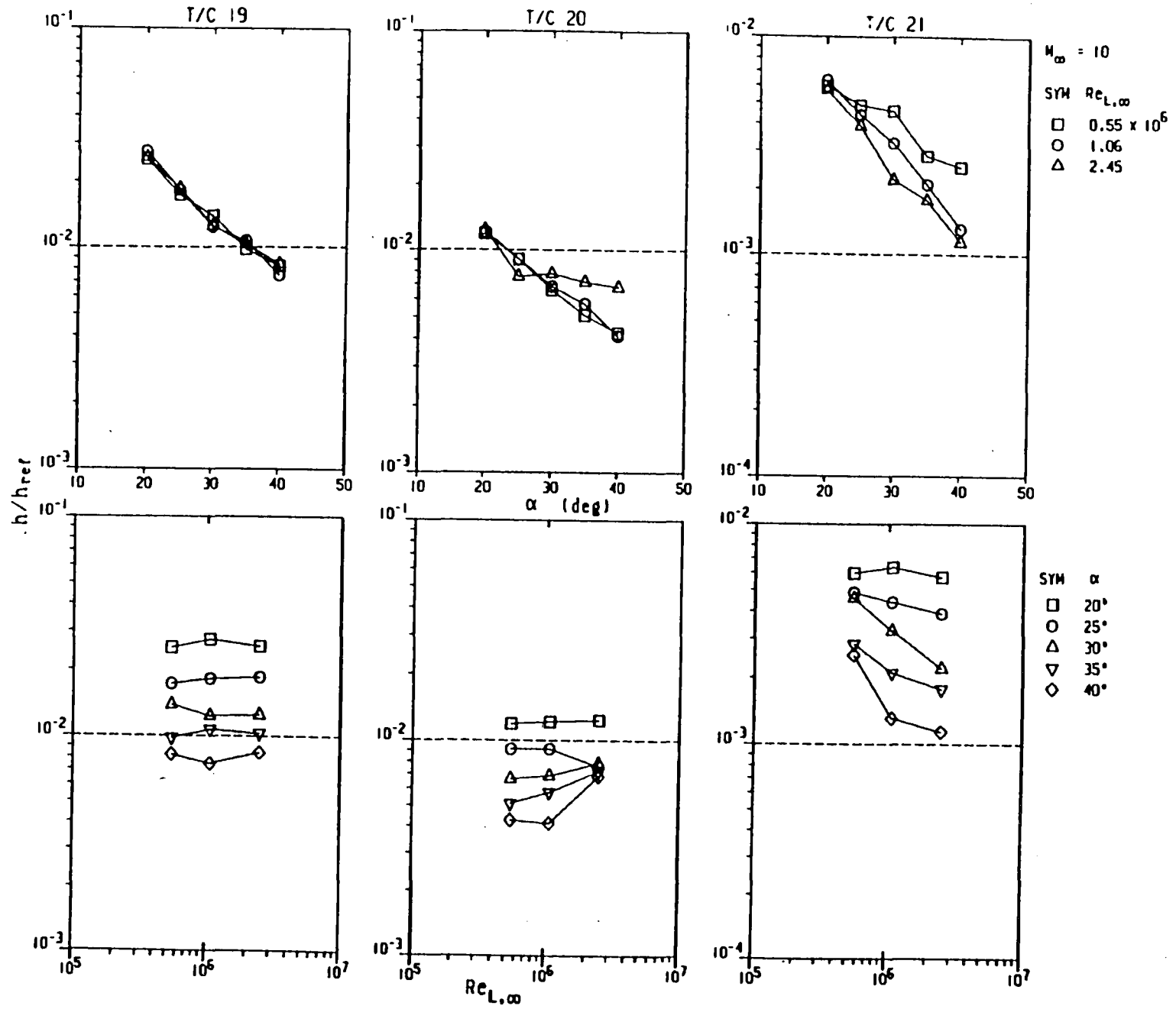
□ 20°

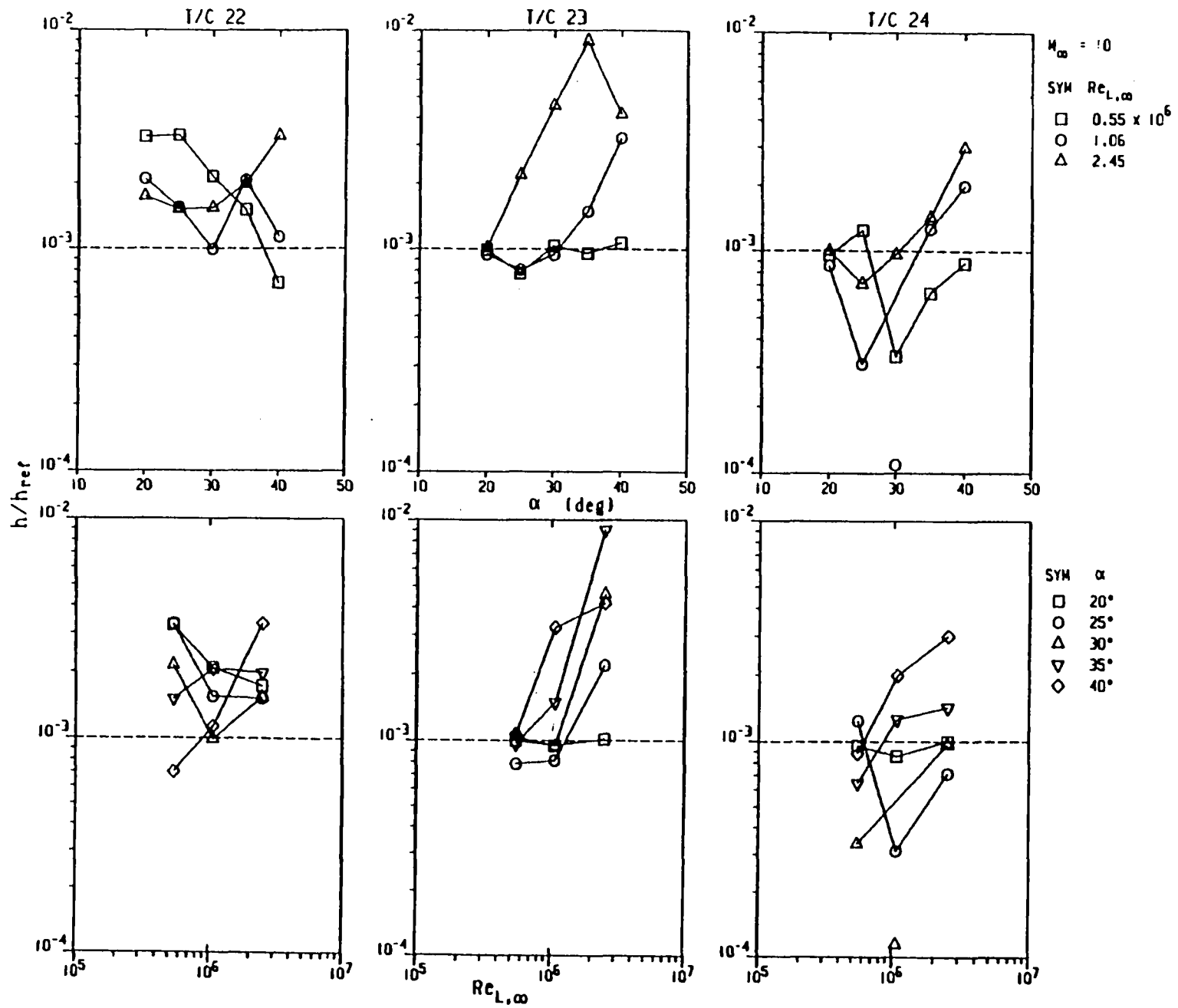
○ 25°

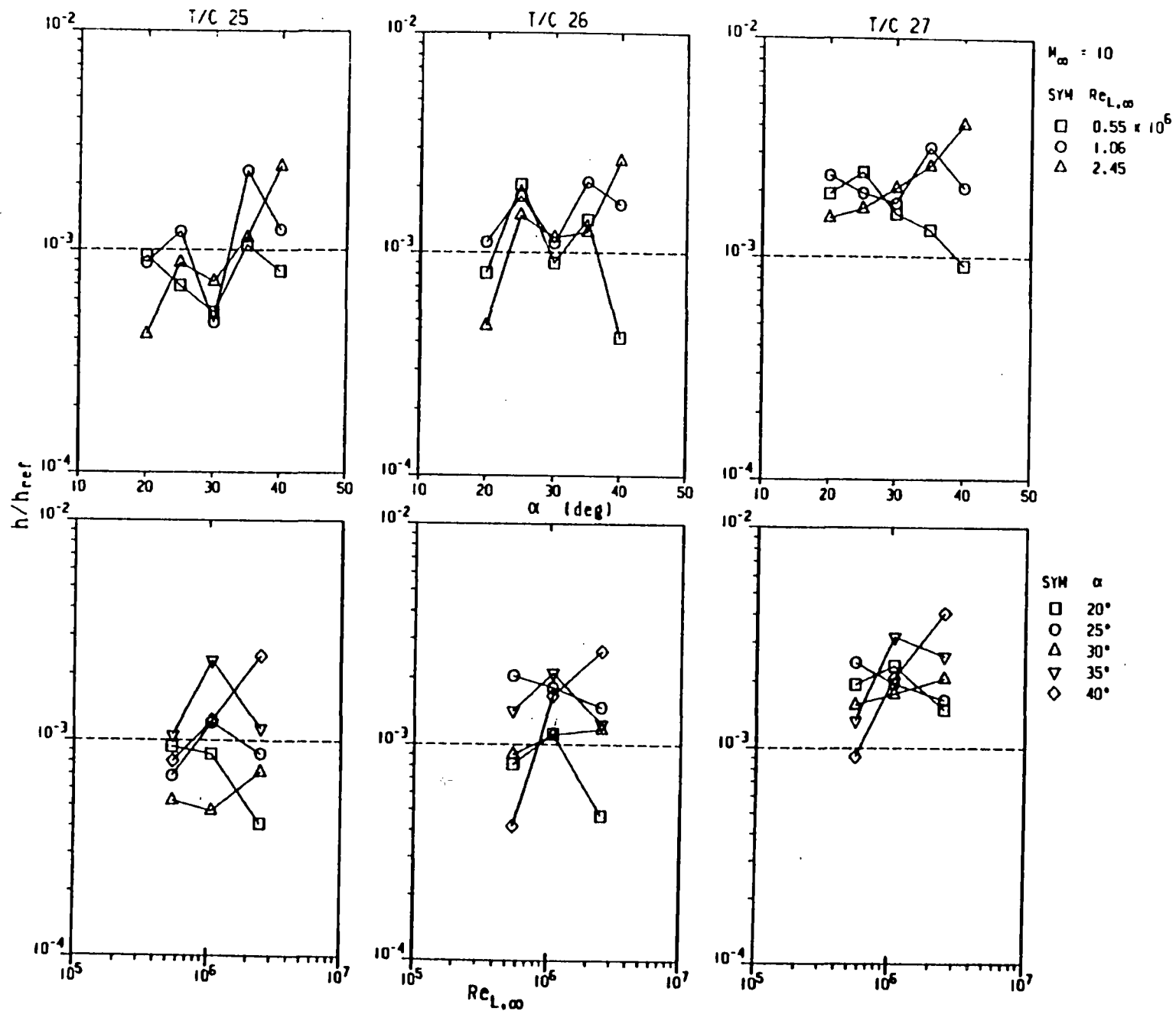
△ 30°

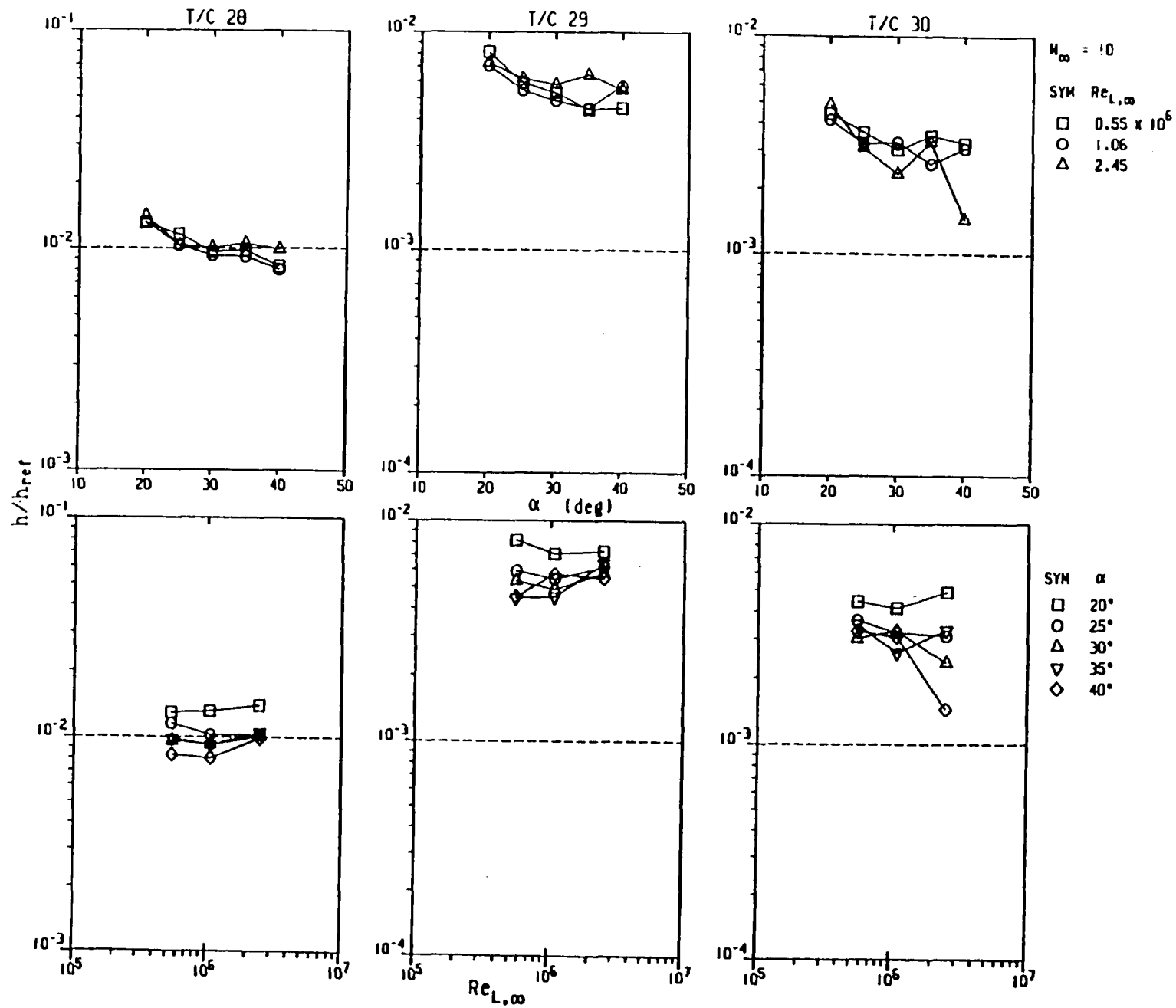
▽ 35°

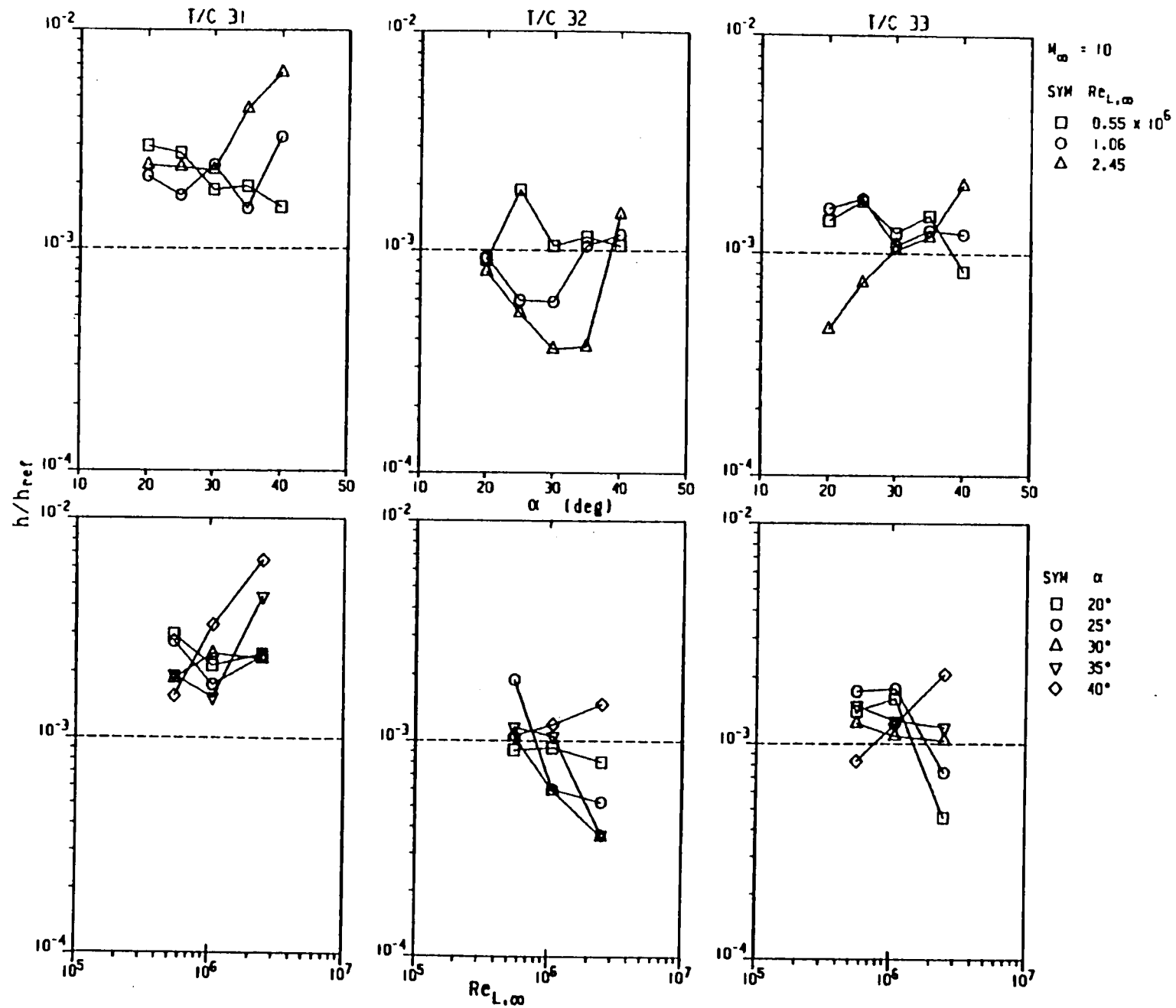
◇ 40°

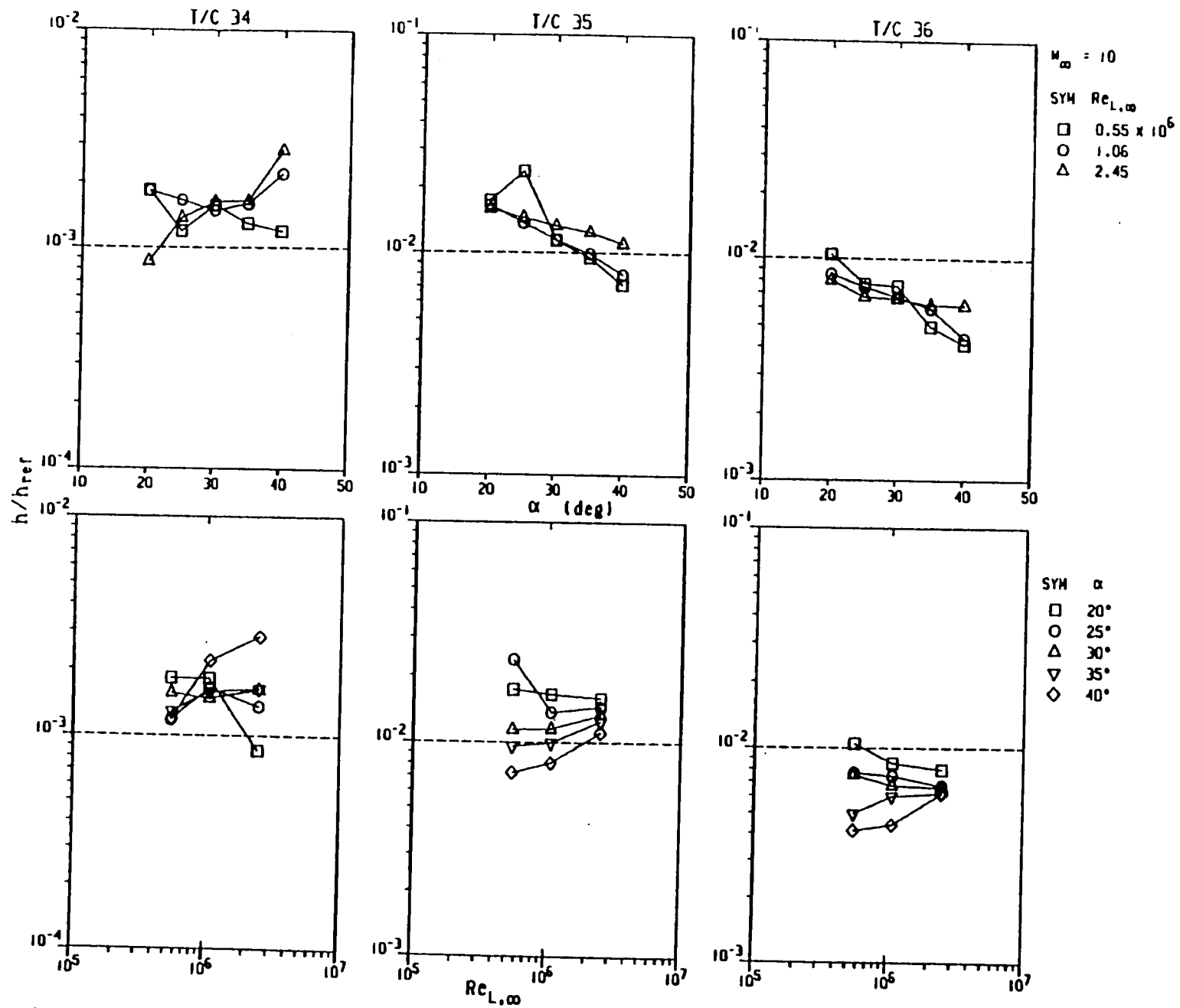


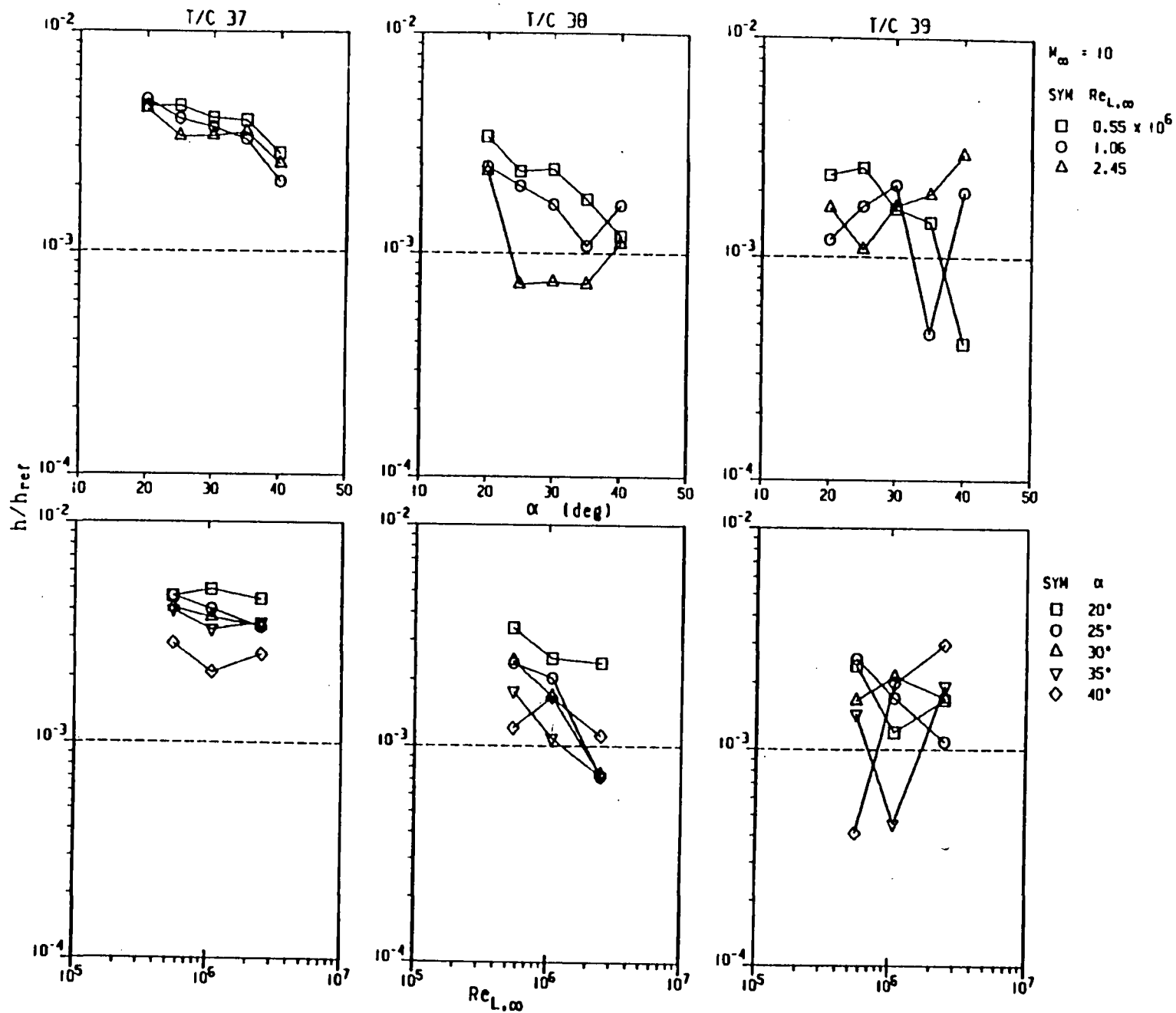


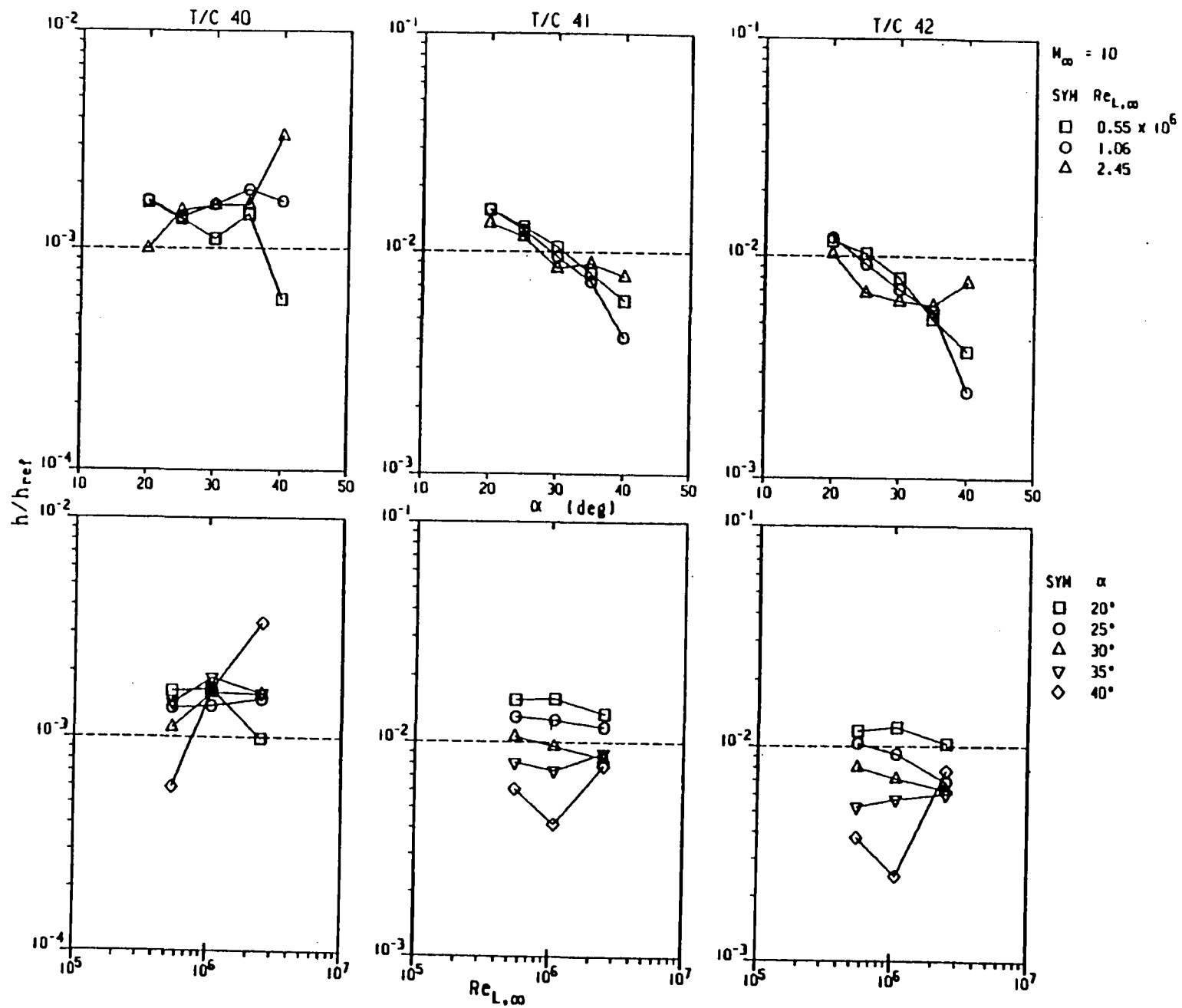


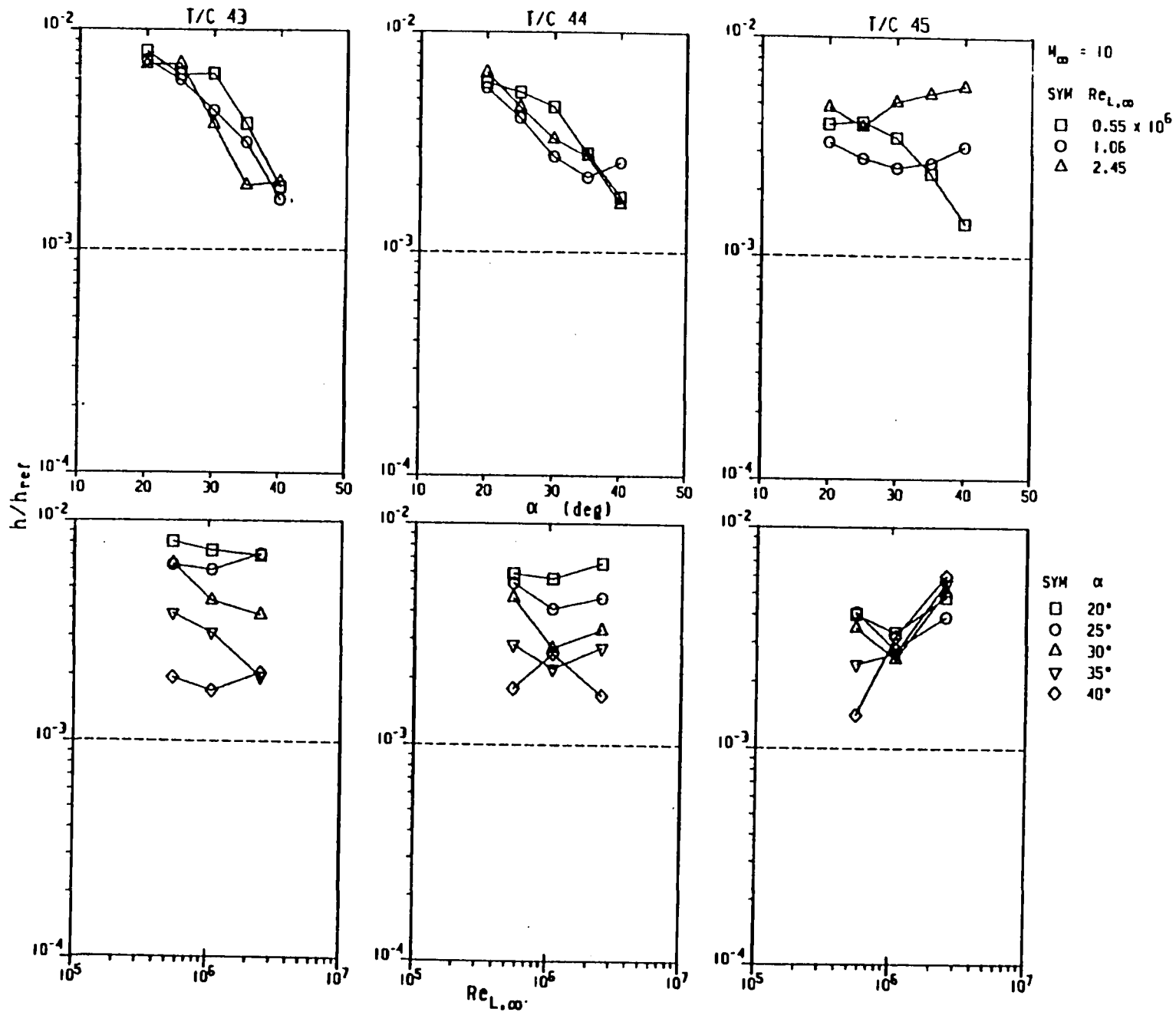


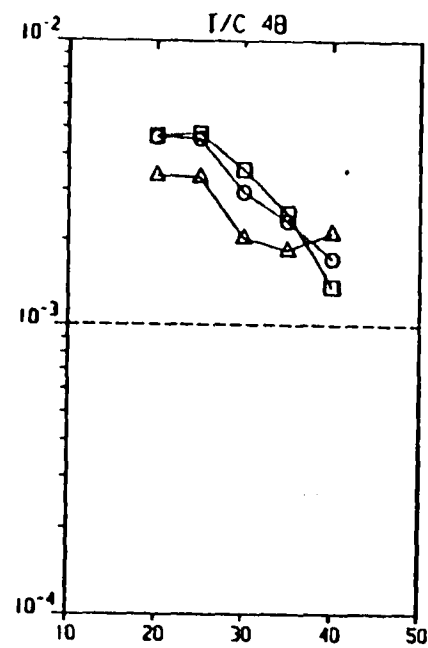
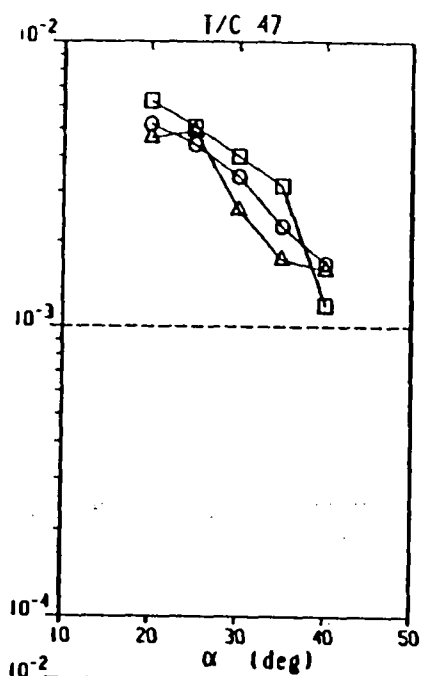
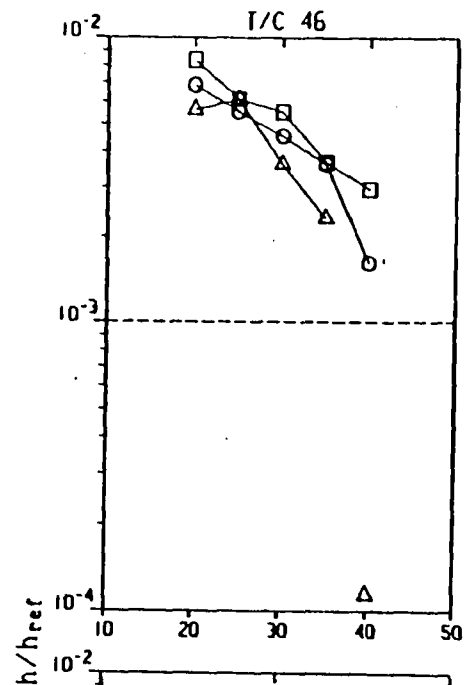








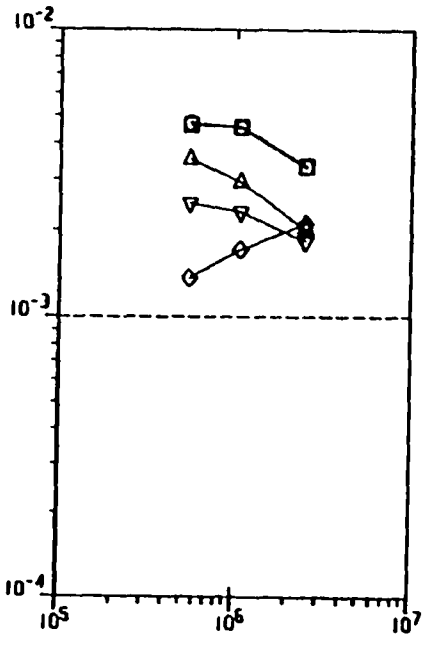
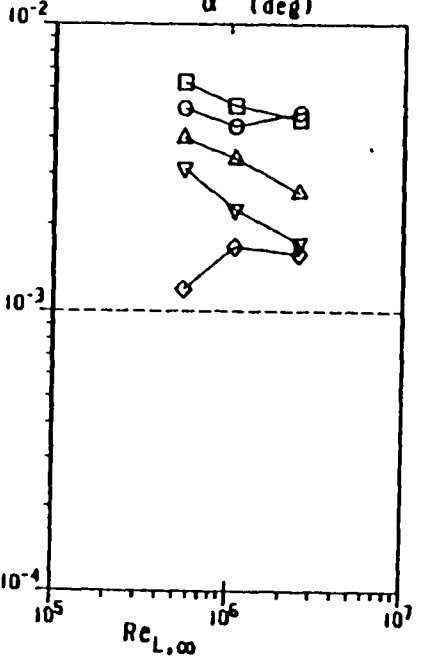
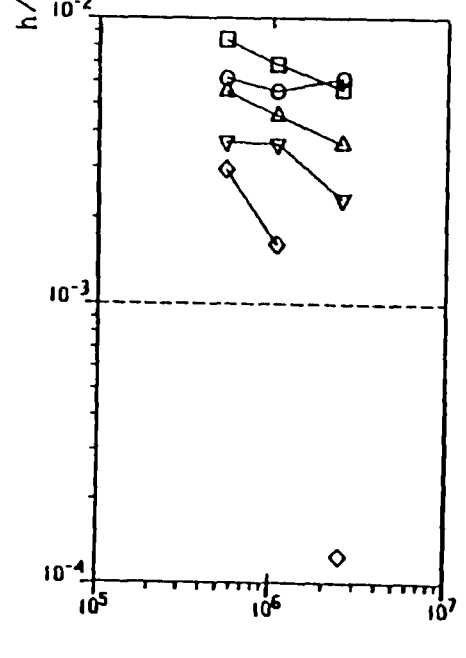




$M_\infty = 10$

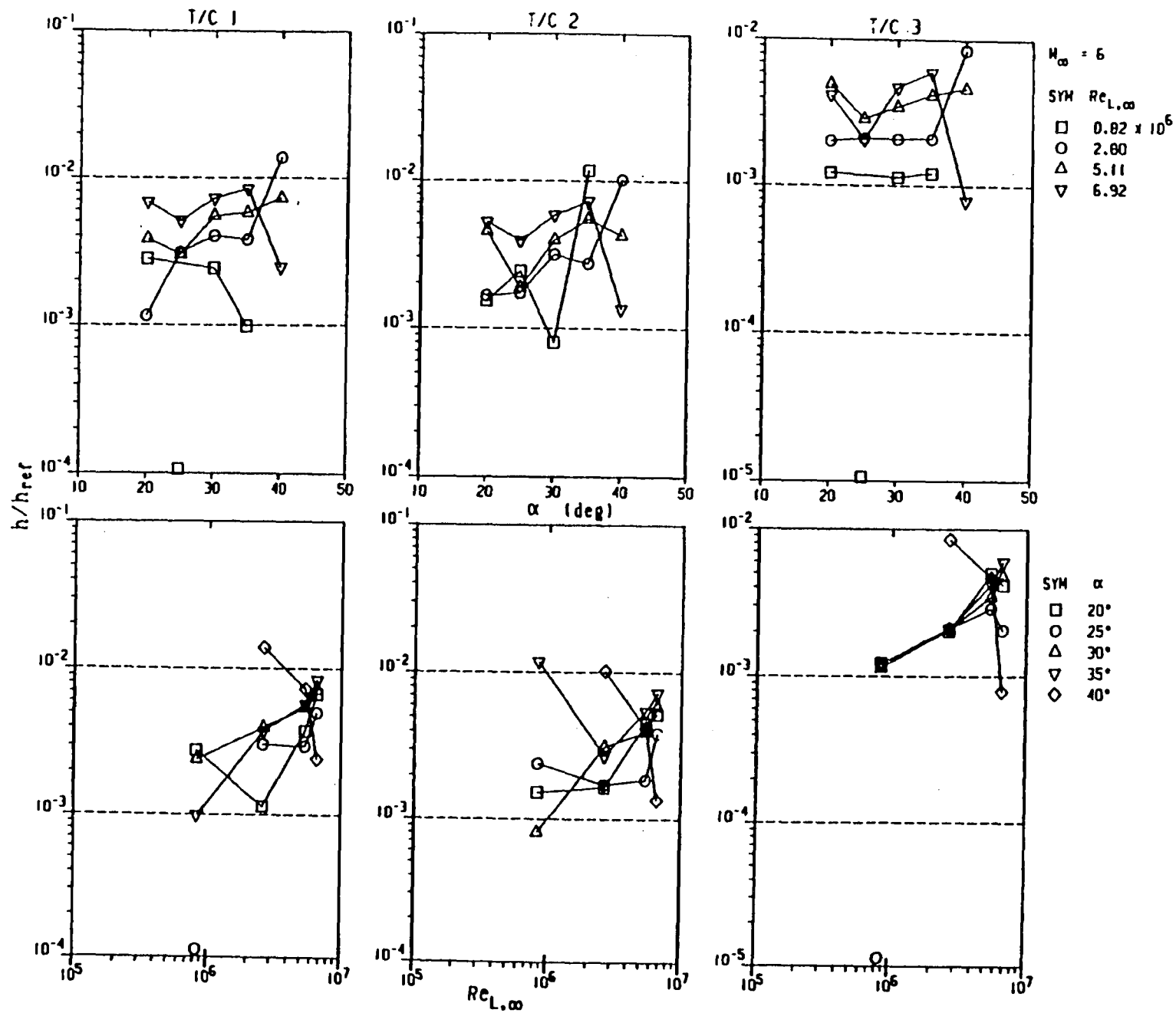
SYM $Re_{L,\infty}$

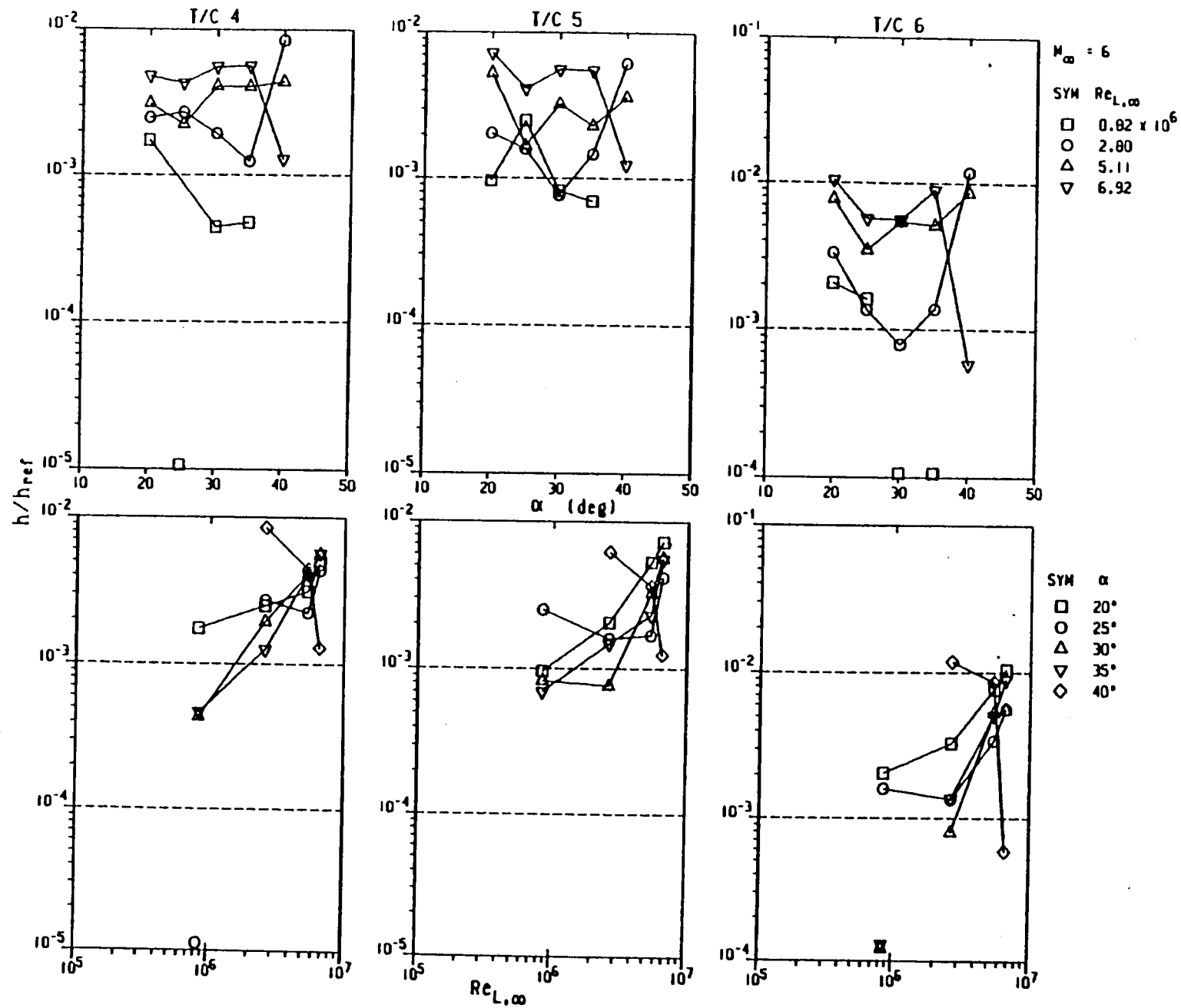
□ 0.55×10^6
 ○ 1.06
 △ 2.45

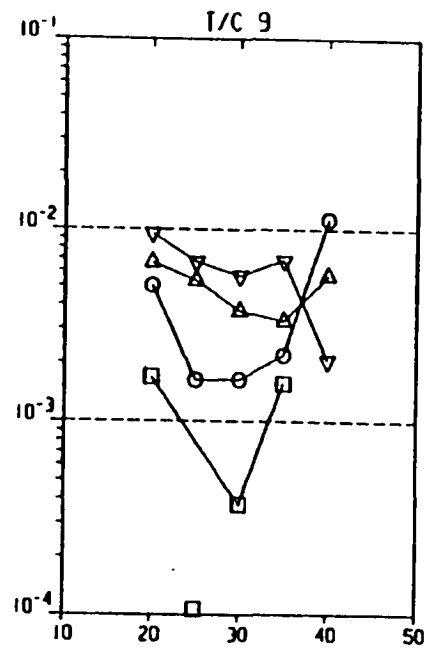
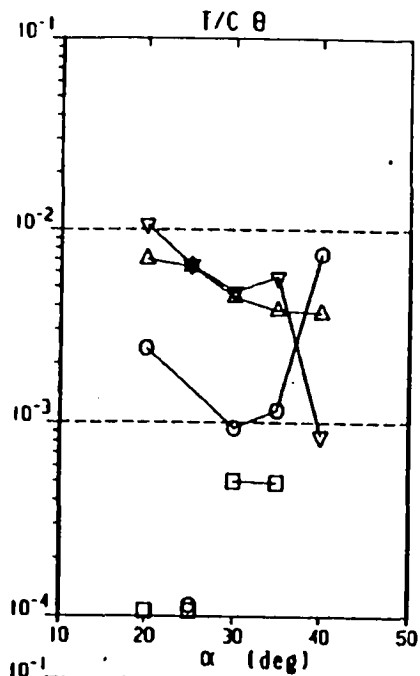
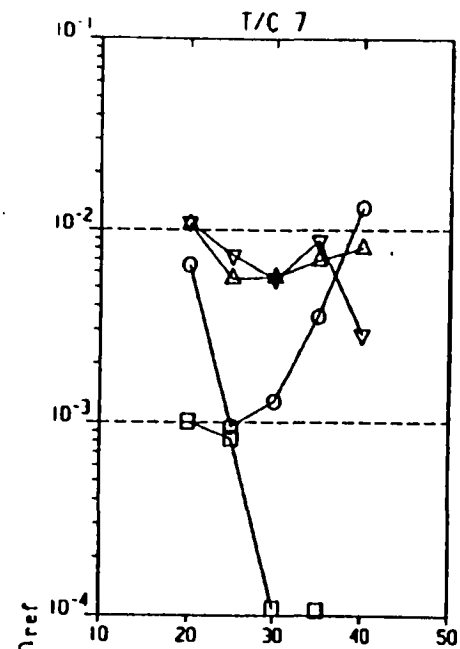


SYM α

□ 20°
 ○ 25°
 △ 30°
 ▽ 35°
 ◇ 40°







$M_\infty = 6$

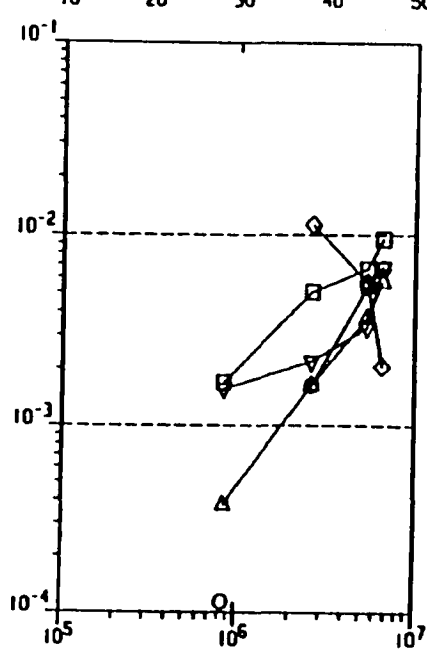
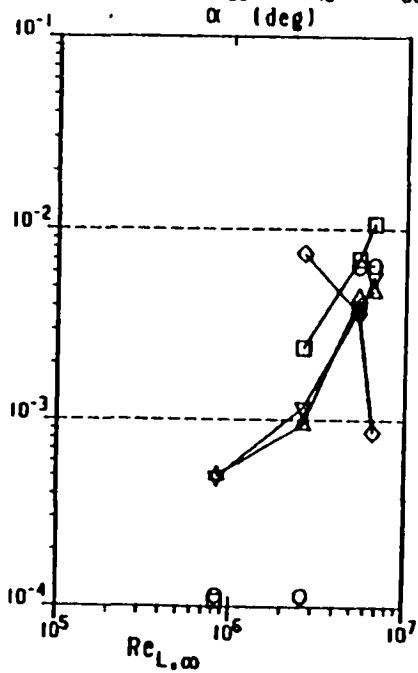
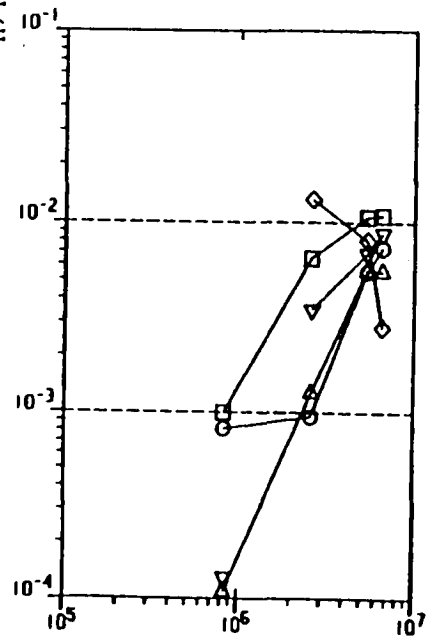
SYM $Re_{L,\infty}$

□ 0.82×10^6

○ 2.80

△ 5.11

▽ 6.92



SYM α

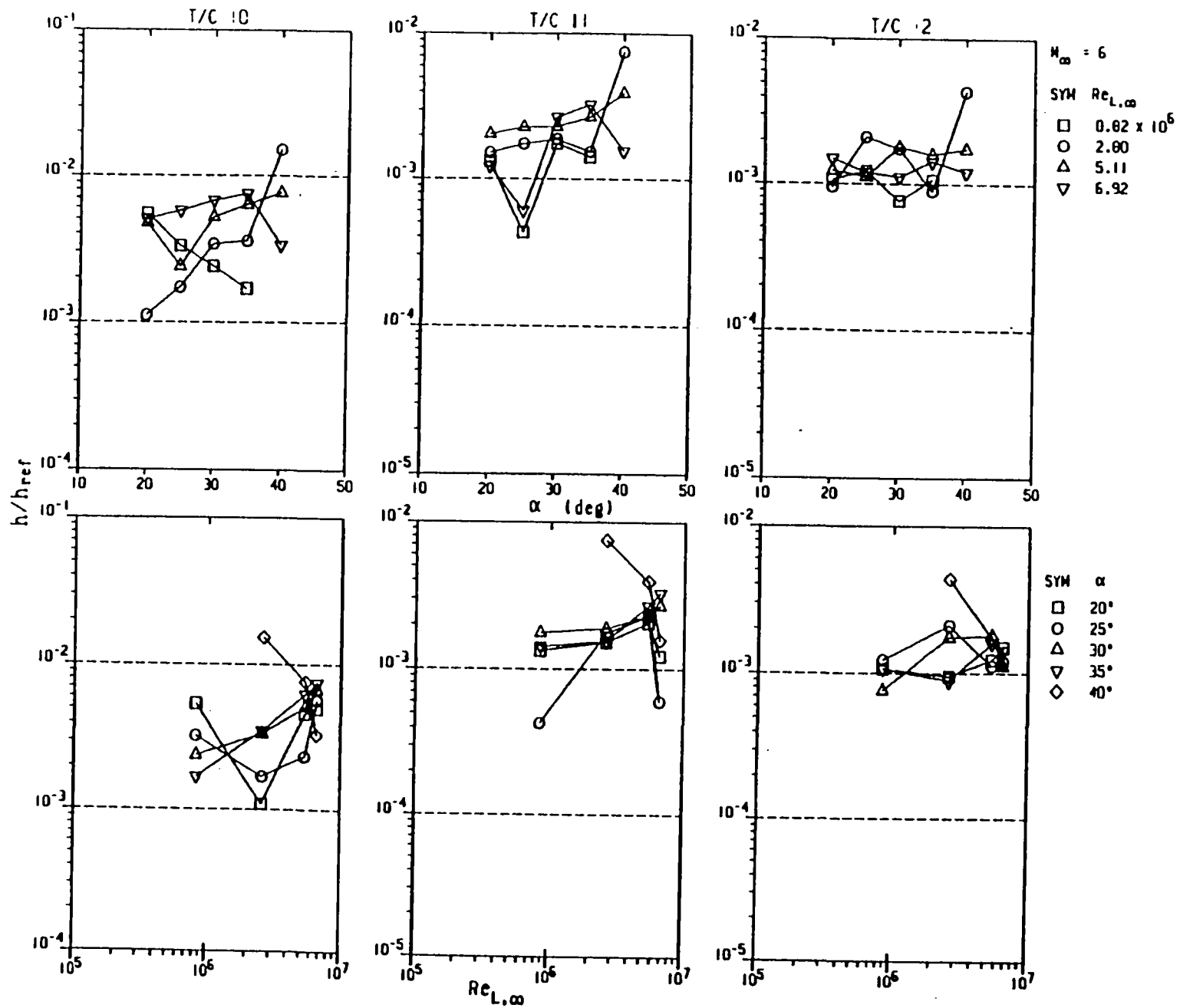
□ 20°

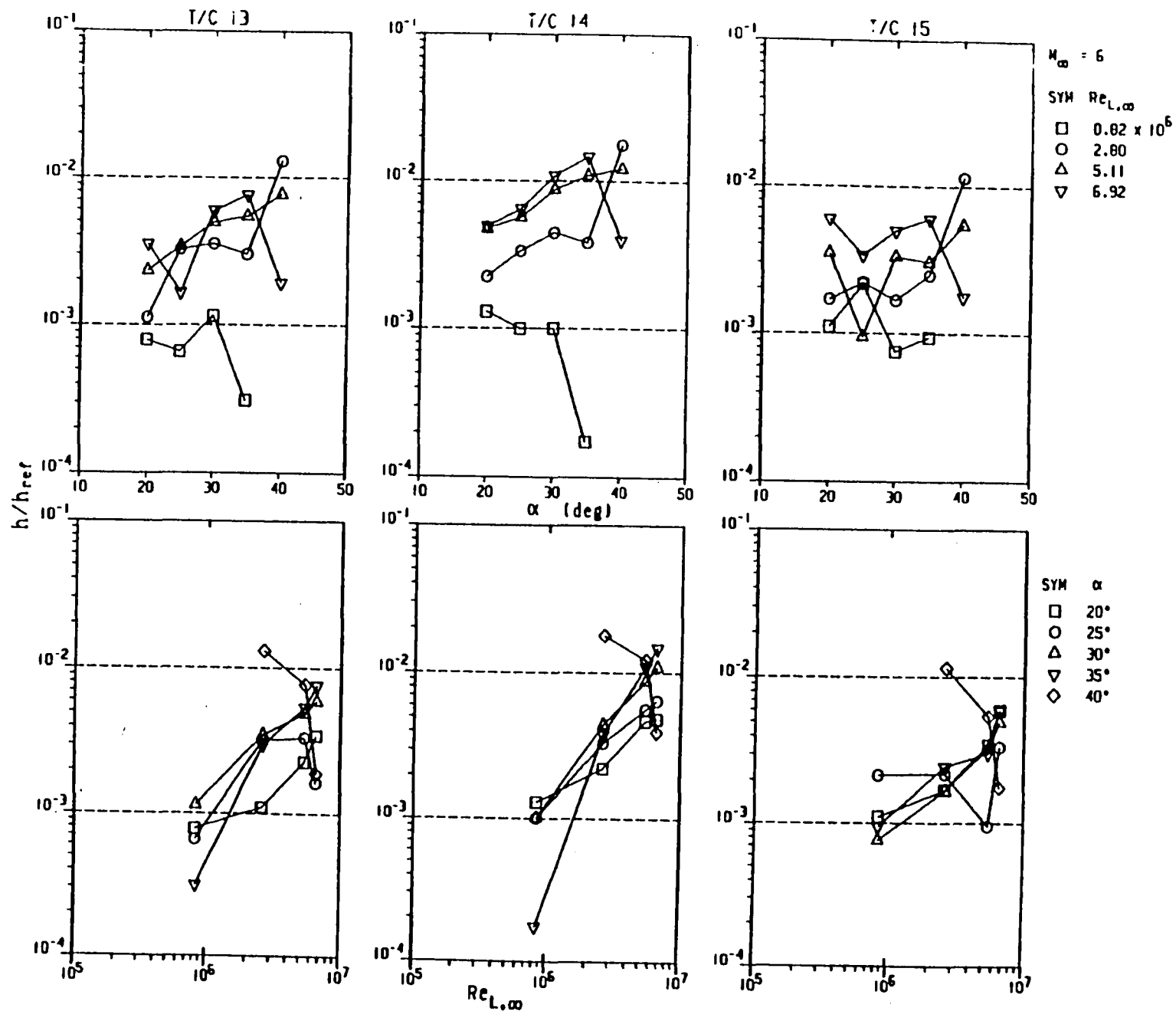
○ 25°

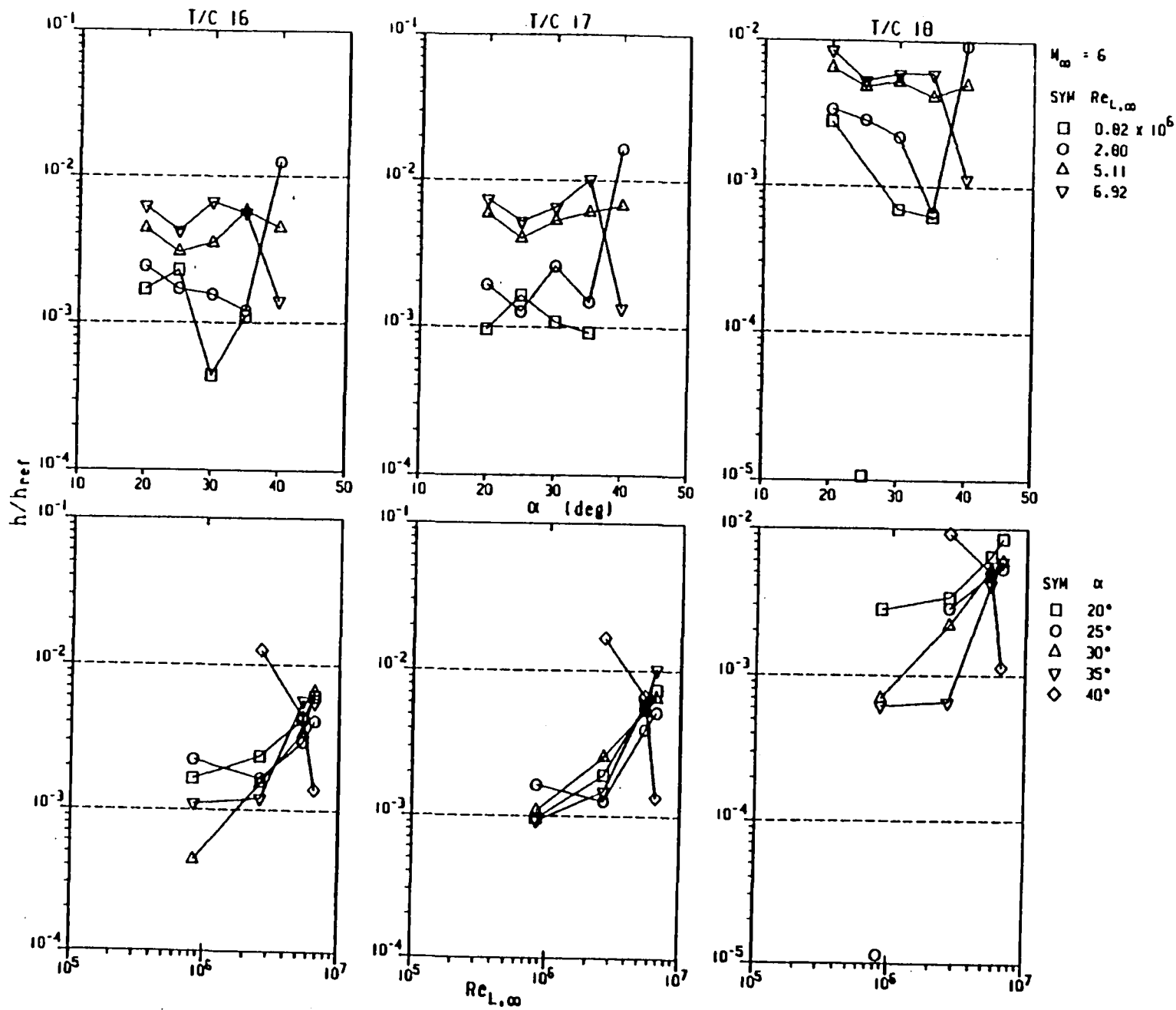
△ 30°

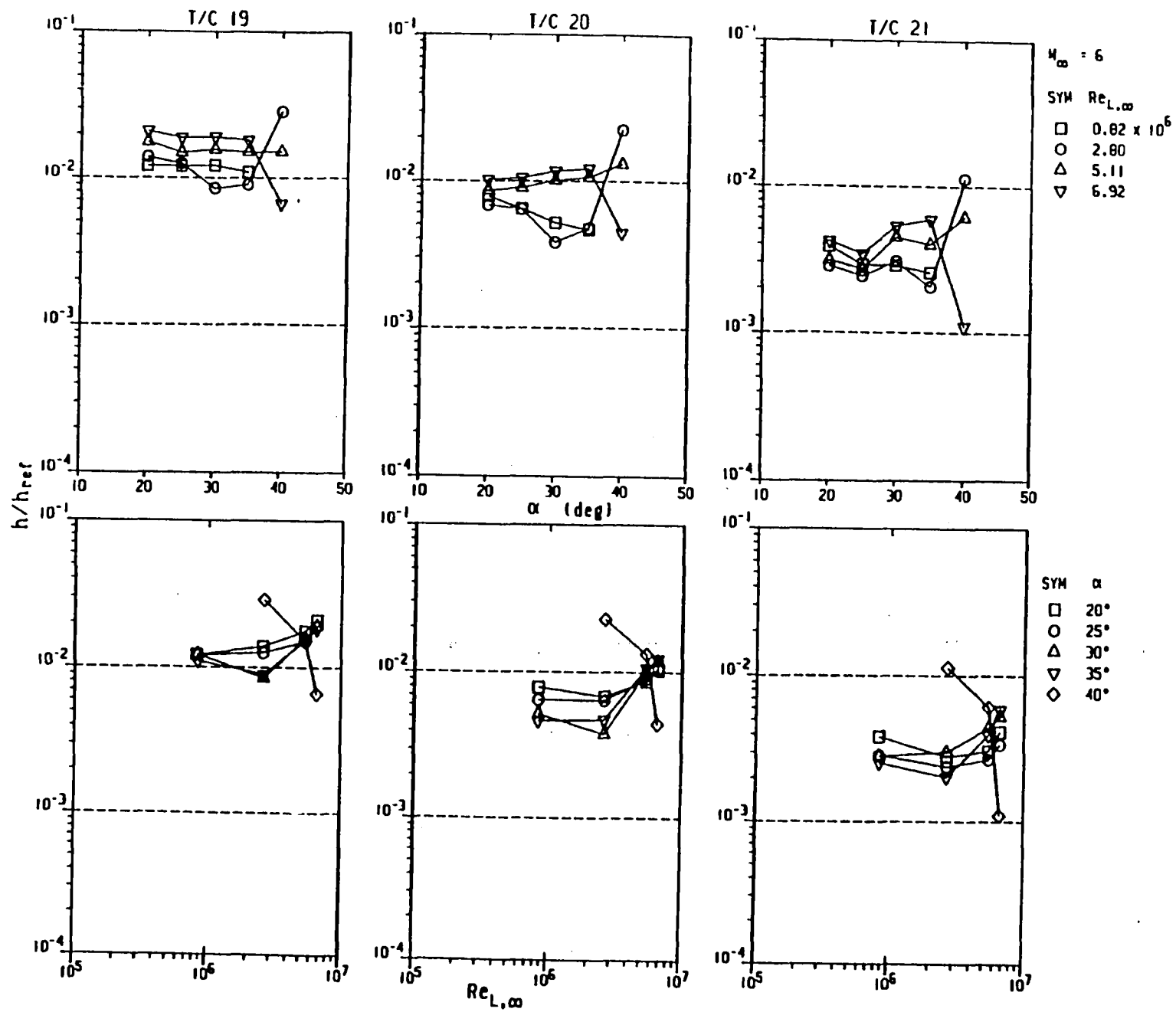
▽ 35°

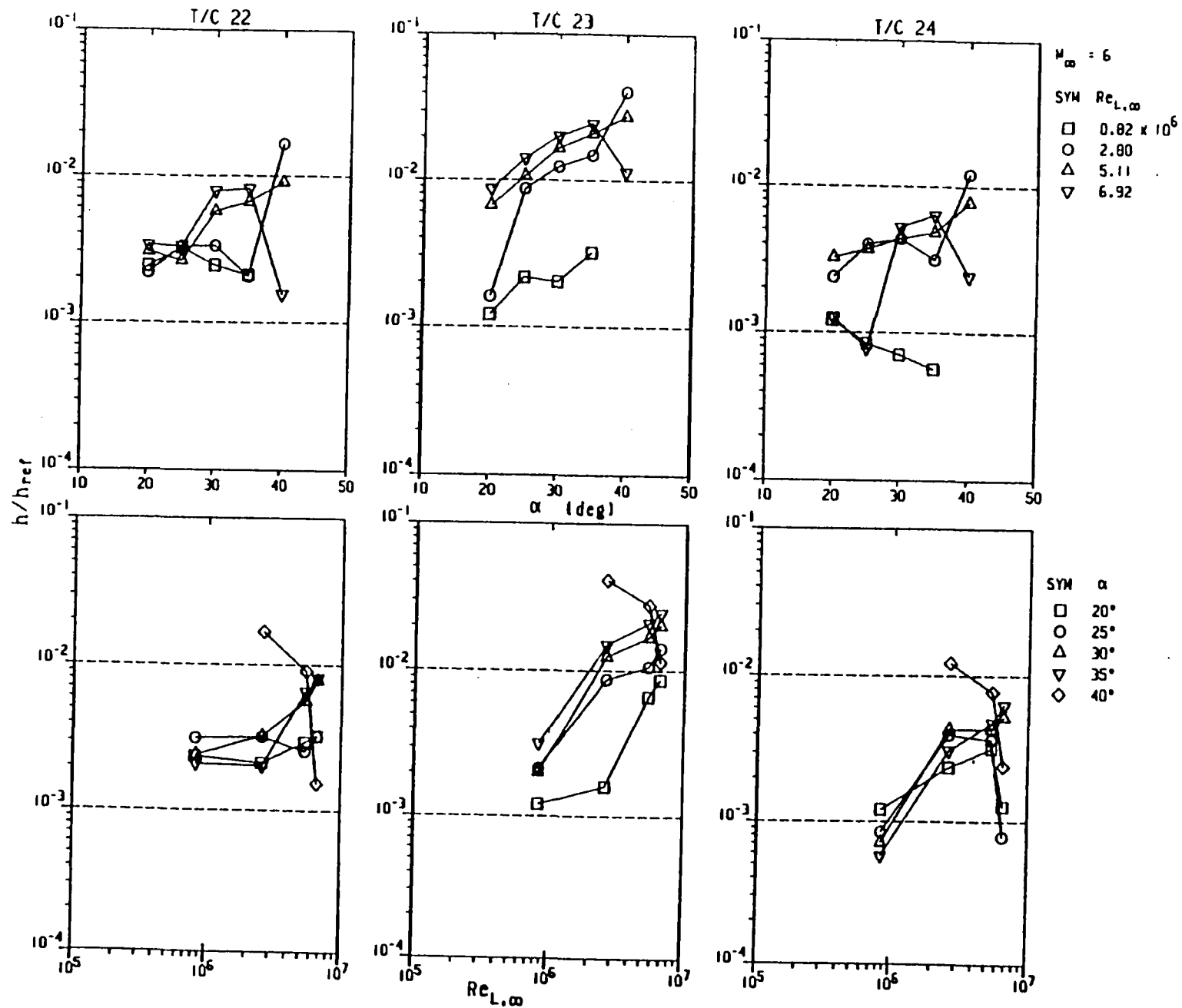
◇ 40°

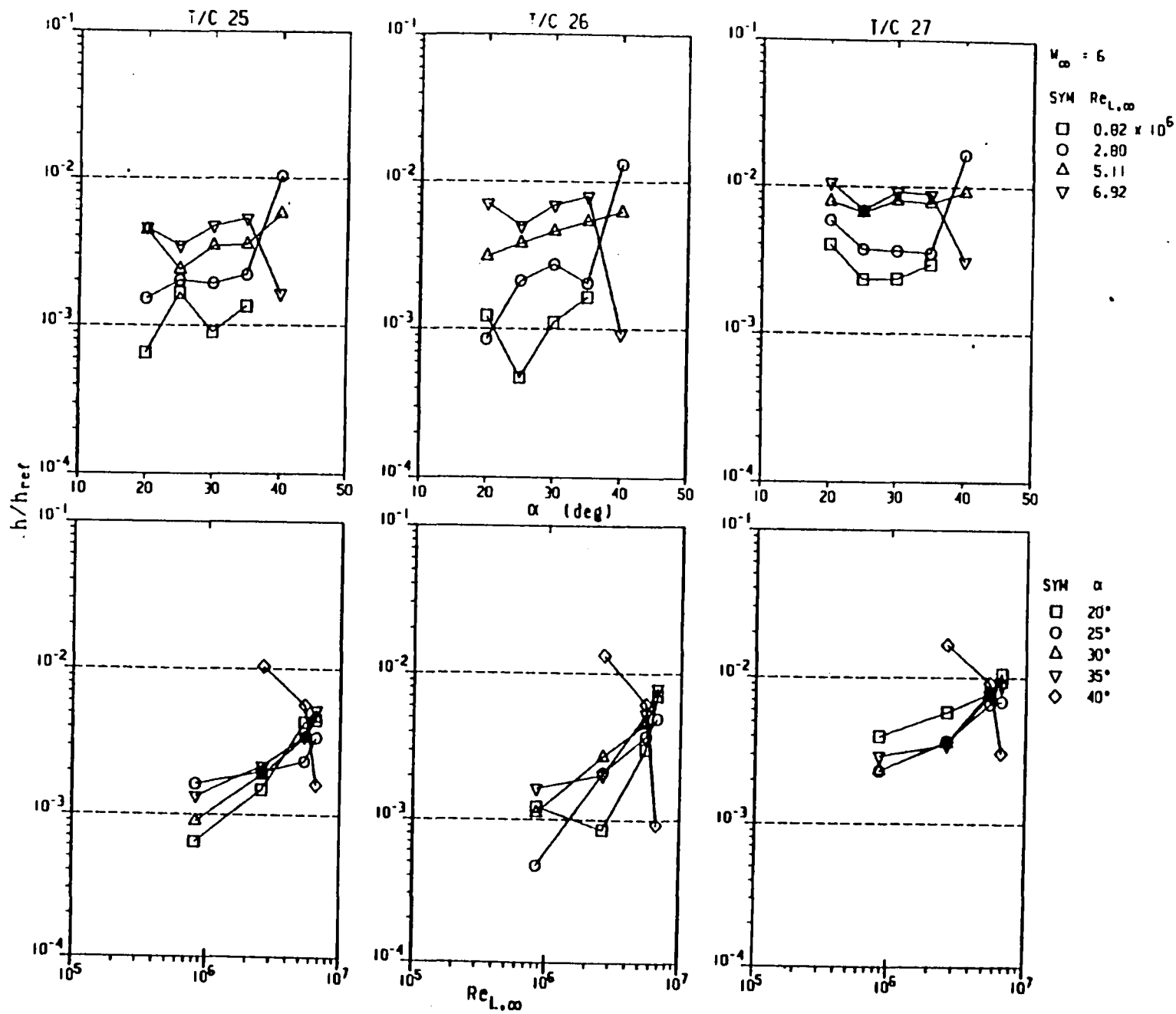


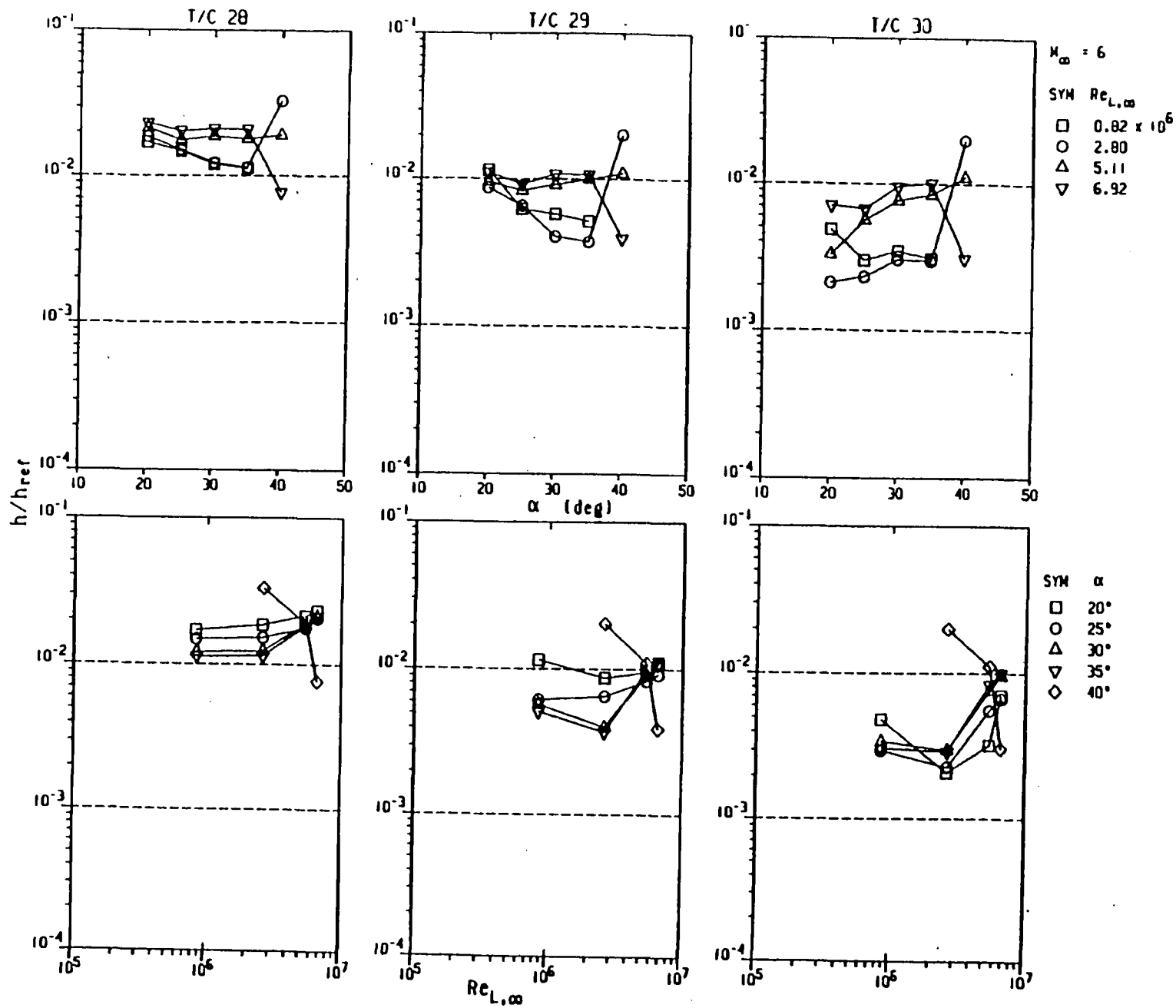


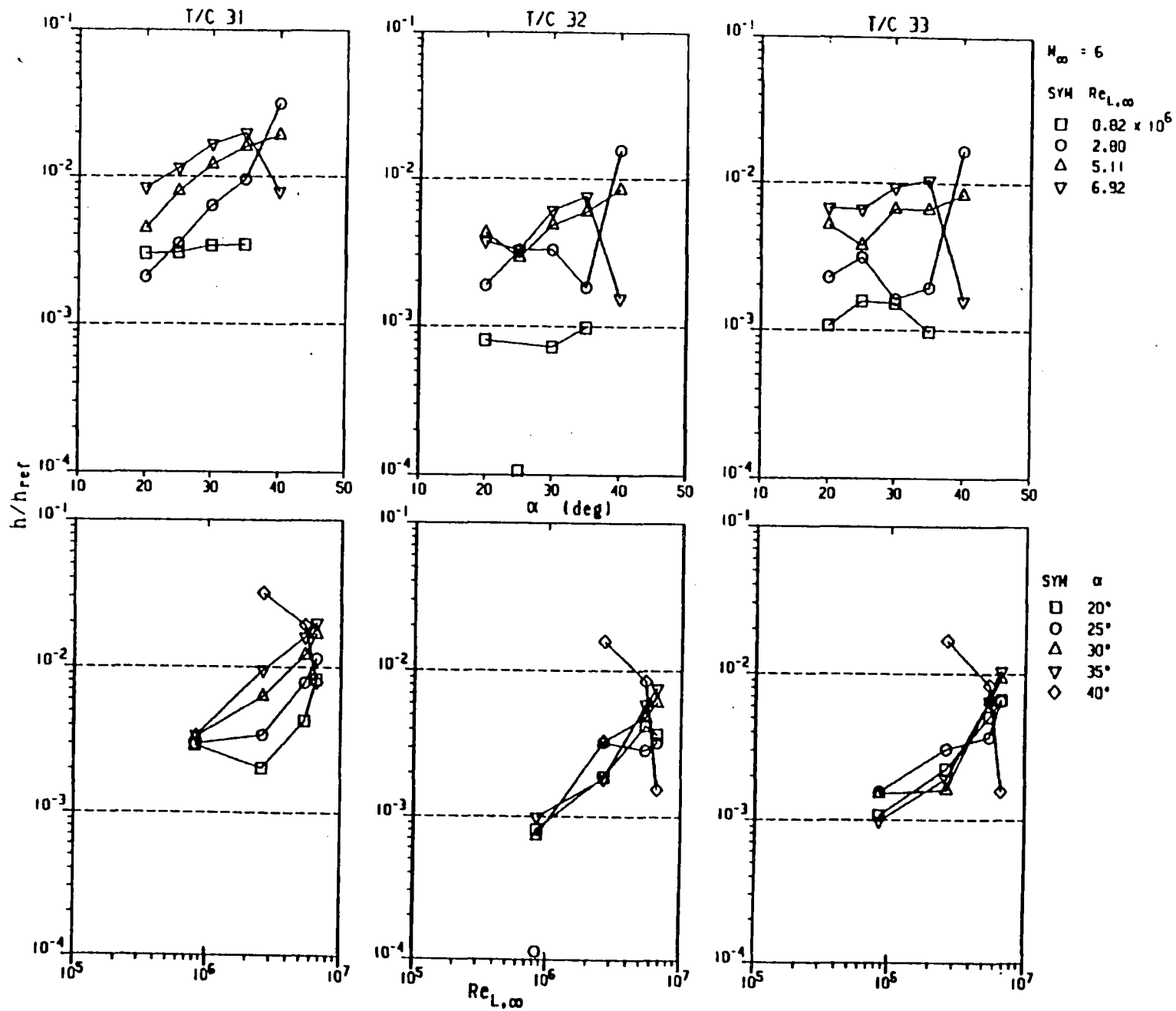


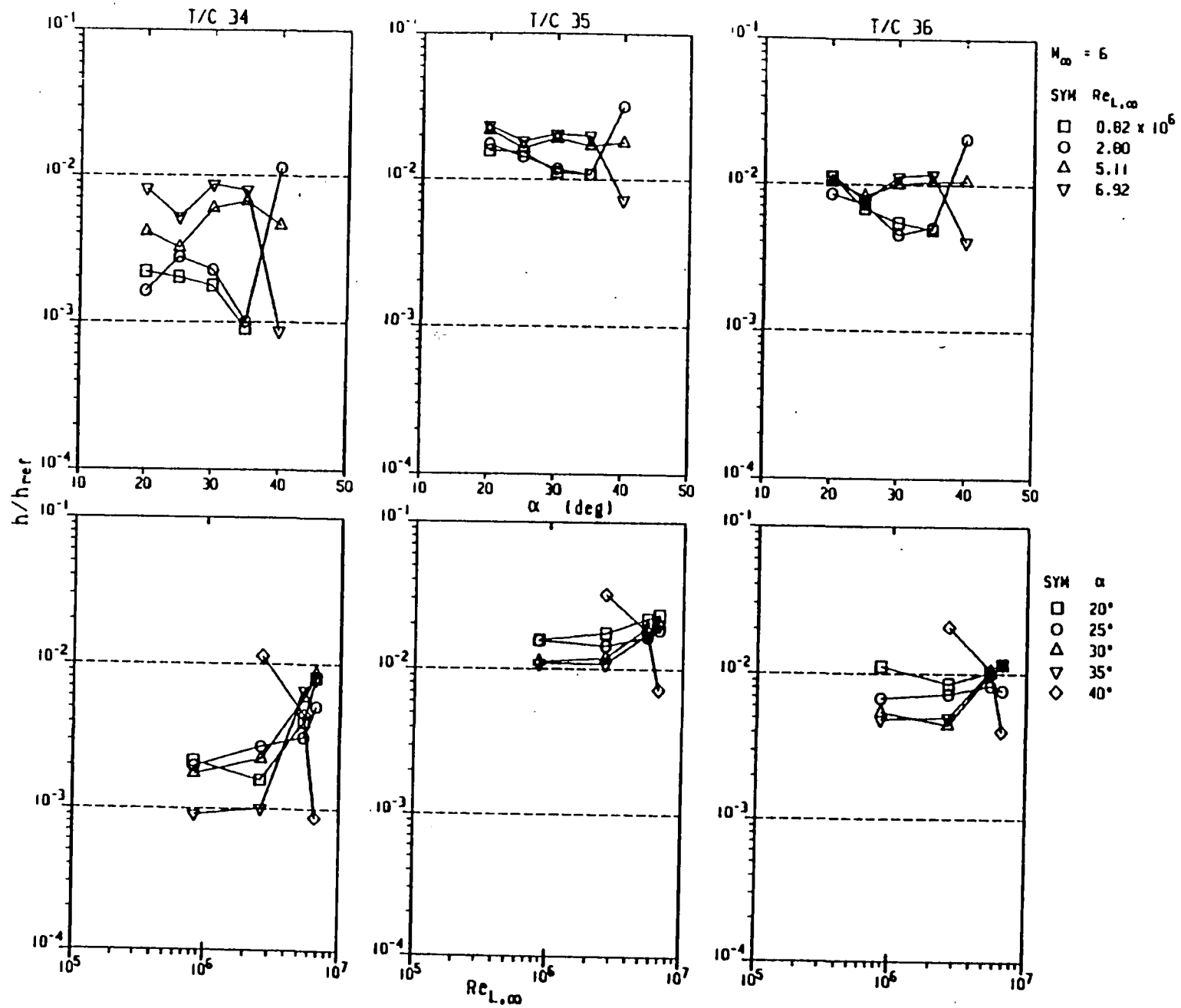


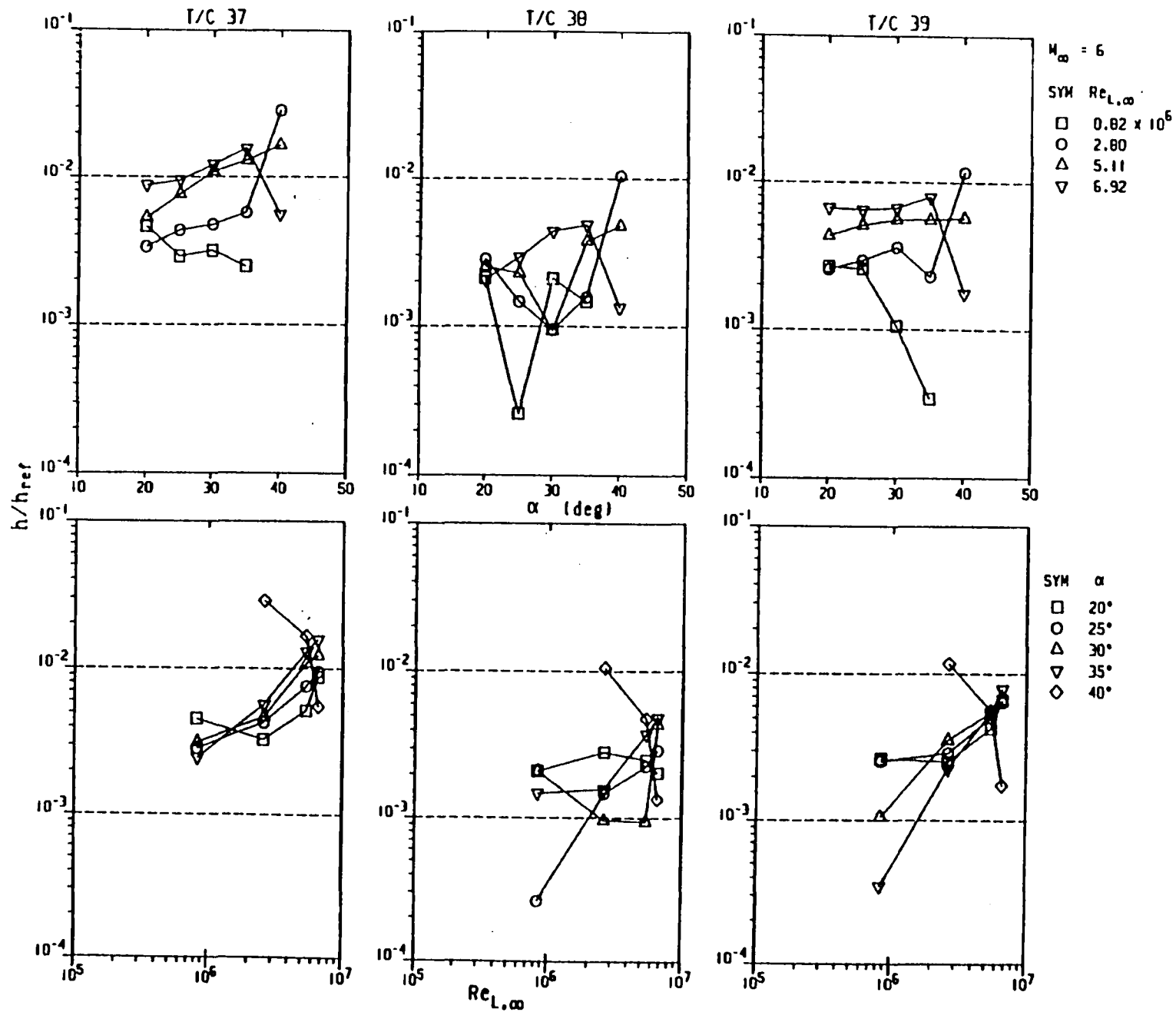


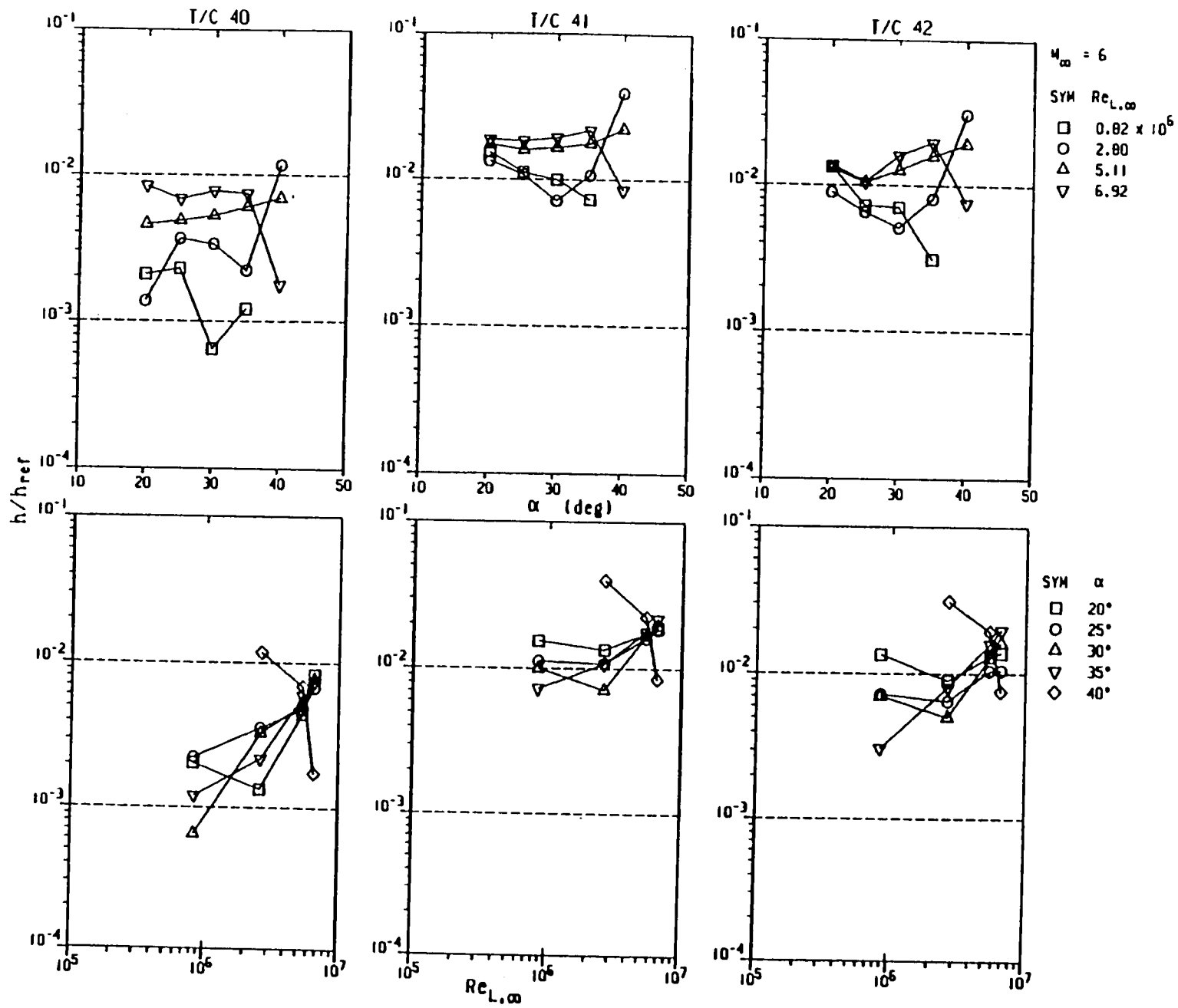


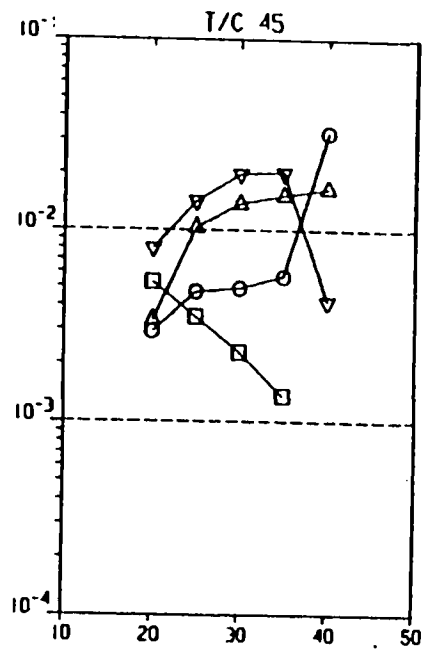
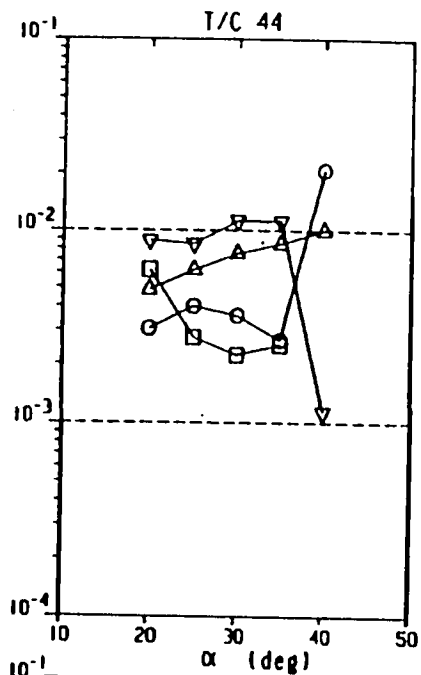
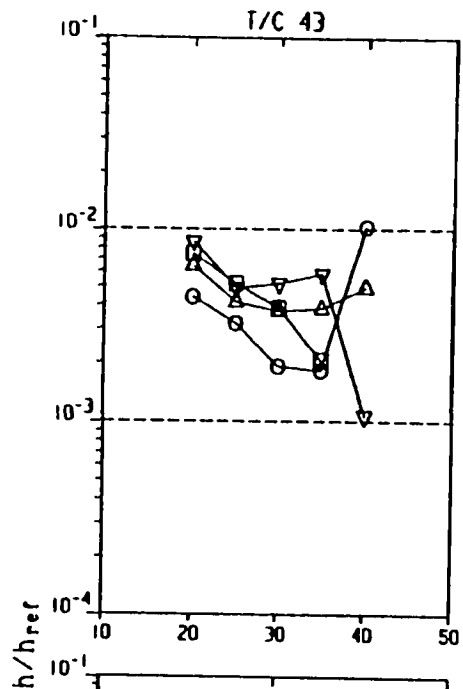












$M_\infty = 6$

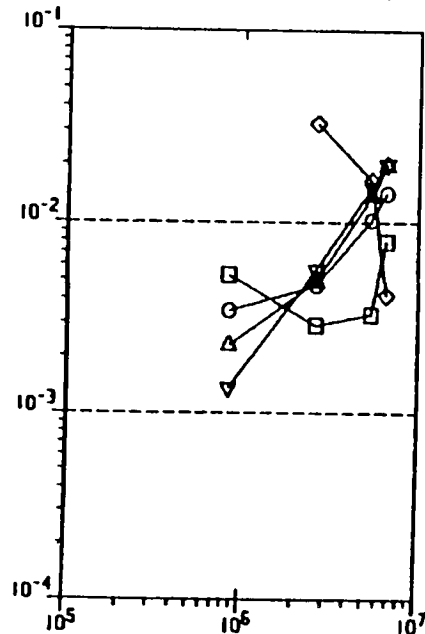
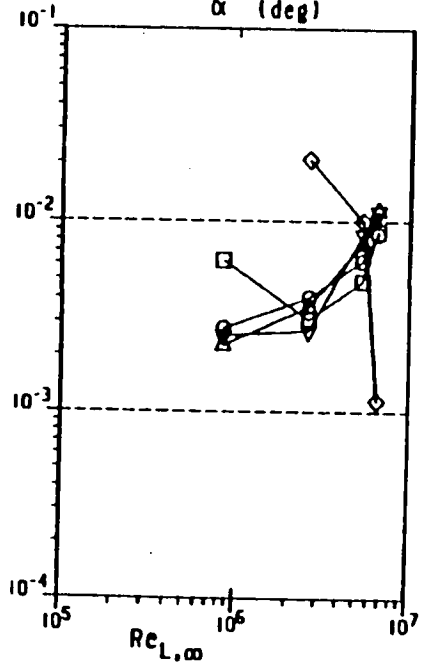
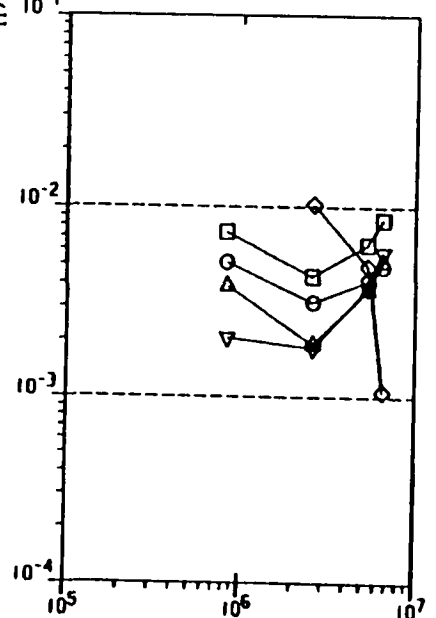
SYM $Re_{L,\infty}$

□ 0.82×10^6

○ 2.80

△ 5.11

▽ 6.92



SYM α

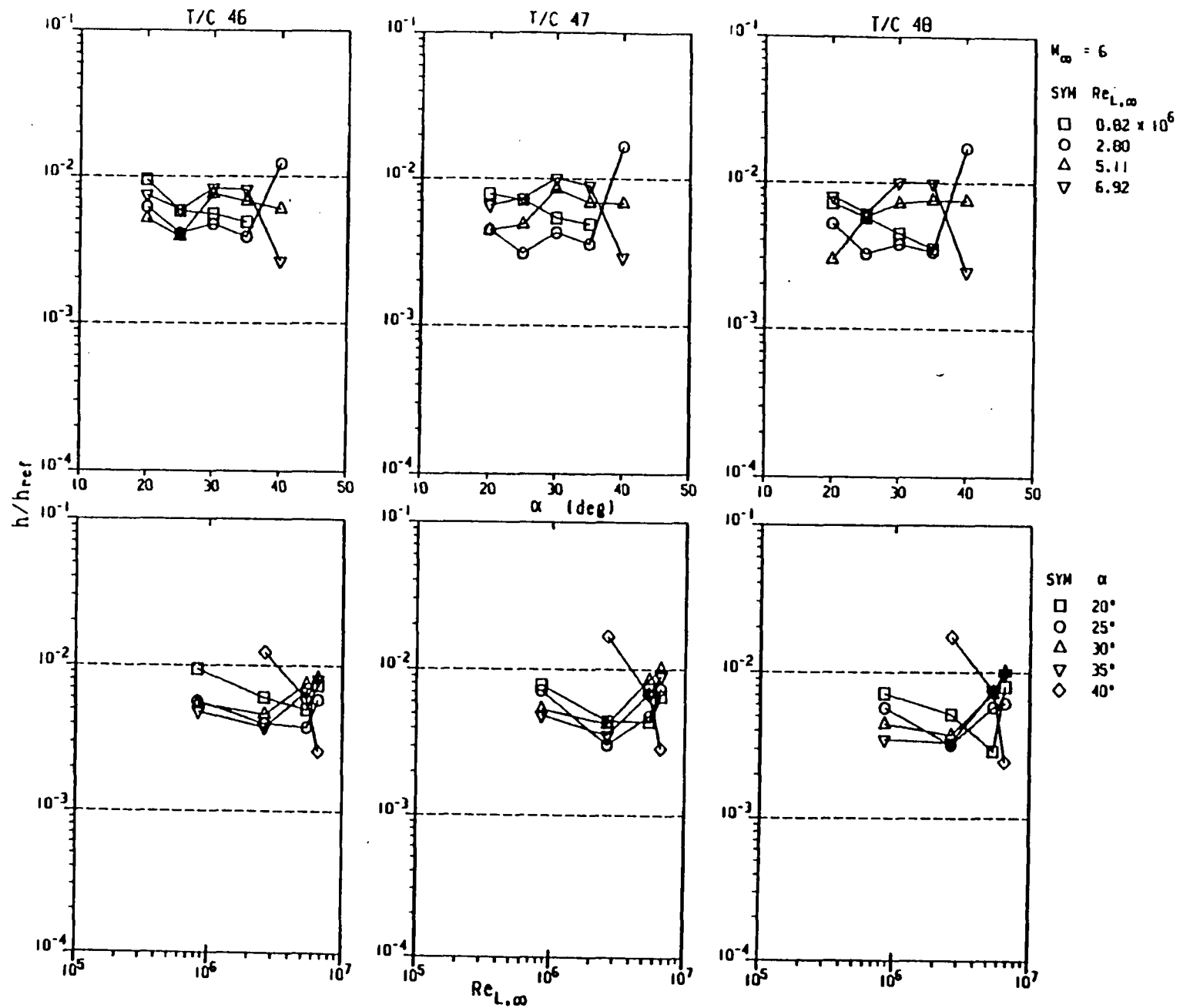
□ 20°

○ 25°

△ 30°

▽ 35°

◇ 40°



APPENDIX D

Boundaries for Attached Flow on the Wing Leaside Surface

This appendix defines and discusses the behavior of simplified boundaries for the zone of attached flow on the wing leaside surface. For completeness, the definition of flow zones from the main text is repeated here in Figure D1.

For the purpose of studying the behavior of the attached-flow zone (in terms of changing size and location), simple straight-line segments shown in Figure D2 were used to approximate the boundaries of the attached flow regions observed on oil flow photos.

Heat transfer within the region of preseparation flow or the "envelope of limiting streamlines" (that region where the curvature of streamlines changes rapidly to converge into the locus of separation) is of the same order as that in the separated flow region. For all practical purposes, and as shown for $\alpha < 40^\circ$ in Figures 18 and 19 of the main text, the boundary for this region is roughly a straight line (at an angle, γ_{eff} , in the horizontal plane with respect to the model's axis) through the locus of these streamline inflection points as illustrated in Figure D2.

This effective boundary is considered to have an inboard limit defined by X_e/L , Y_e/L and an outboard limit defined by Y_f/L . The inner limit is the most inboard or aft location before the boundary would traverse the curved envelope of limiting streamlines in transitioning from strake to wing. The boundary may be thought of as originating from or "pivoting" about that point (by the angle γ_{eff}). The outer limit is the intersection with a line ($Y/L = Y_f/L = \text{constant}$) parallel to the vehicle axis, through the locus of streamline inflection points as the locus of actual separation is curved by the influence of the bow shock interaction. Hence, flow is considered "attached" if,

$$Y/L \geq Y_f/L; \quad \text{for } X/L > 0$$

$$\text{or, } Y/L > Y_e/L + (X/L - X_e/L)\tan(\gamma_{eff}); \quad \text{for } X/L > X_e/L$$

$$\text{or, } Y/L \geq Y_e/L; \quad \text{for } X/L \leq X_e/L.$$

As shown in Figure D2, any location above and/or to the left of the dashed line is in the attached flow region.

Also shown in this figure is the angle γ_{sep} for the line running approximately through the locus of actual separation. This latter angle is not used in defining the region of attached flow heating, but is useful in corroborating the behavior of the boundaries. For example, the oil-flow photos (Figures 18 and 19 of main text) tend to indicate a base-pressure induced separation at $\alpha = 40^\circ$, and conical separation at the lower angles of attack. This is also evidenced by the variation of γ_{sep} shown in Figure D3a. For $\alpha \leq 30^\circ$, it appears to vary linearly with α , and then increases more rapidly indicative of deviation from conical flow. Actually, the values of $\alpha = 40^\circ$ might be somewhat misleading since the locus of separation is very much curved. This linear relationship concurs with the findings of other investigations and is considered a verification of conical flow. For example, Cross and Hankey^{(D1)*} showed a similar correlation for this parameter in the form $(\gamma_{sep} - \mu)$, using the Mach angle $\mu = \sin^{-1}(1/M_\infty)$ to account for Mach number variations (for a sharp delta wing with no fuselage). For comparison, the variation of this parameter is included in Figure D3b. The use of μ only tends to increase the deviation between Mach 6 and 10 measurements. This is taken as support of the double-shock (bow and wing leading edge) hypothesis for the leeward flow. That is, having passed through the bow shock, the Mach number for flow upstream of the wing is approximately the same for both freestream Mach numbers.

The variation of the "effective" angle γ_{eff} is shown in Figure D4a. Similarly, γ_{eff} appears to vary linearly with angle of attack for $\alpha \leq 30^\circ$, and then increases more rapidly. Comparing the two separation angles as in Figure D4b indicates a definite linear relationship, although it does appear that the Mach 6 and Mach 10 measurements do not lie on the same correlation. On the other hand, there is more uncertainty associated with the Mach 6 measurements due to saw-cuts in the trailing edge of the model's wing made to simulate clearance gaps between the ailerons. Scale-wise these gaps appear too large and there is evidence their presence influences the flow separation phenomenon, especially at the lower angles of attack.

Movement of the boundary limits is shown in Figures D5a through D5c. A number of characteristics of the boundary movement are revealed in these plots. The lateral coordinate of the inboard limit (Y_e/L) appears to remain relatively constant for $\alpha \leq 30^\circ$. The outboard limit (Y_f/L) continues to increase over the same range of angles of attack, indicative of the outboard movement of bow-shock impingement.

* Number in () is reference

No values of Y_f/L are shown for $\alpha = 40^\circ$ since the locus of separation extends out to the wing tip. Also, the values of both limits are further outboard for Mach = 6, as expected, but the variations still tend to parallel those for Mach = 10.

These parameters tend to vary smoothly and behave consistently for angles of attack up to 30 degrees. However, their values are not as well behaved at higher angles of attack. This is also reflected by the longitudinal coordinate (X_e/L) of the "pivot" point, or inner limit. It tends to move forward for $\alpha \leq 30^\circ$, and then suddenly increase

The movement of the "pivot" point is better illustrated in Figure D6. That is, as α increases, X_e decreases while Y_e remains essentially constant (and somewhat independent of Reynolds number), resulting in an almost straight forward movement of the point. With continued increase of attitude, the point moves outboard almost parallel to the wing leading edge ($\tan 45^\circ = 1 = dY_e/dX_e$) to some spanwise location dependent on Reynolds number. With further increases in α , the point resumes a straight/forward movement to the leading edge. Note that the parallel movement (between straight/forward movements) generally occurs at $\alpha > 30^\circ$, indicative of a transition in the flow and coinciding with the inconsistencies mentioned earlier. The dashed lines joining two measurements signify repeat measurements at the same angle of attack. Again the disparity in the Mach 6 measurements is quite evident. Whether this can be attributed to the out-of-scale aileron gaps is unknown at this time.

The typical movement of the "effective" boundary for attached flow, as predicted using these parameters is demonstrated in Figure D7. It is noted that with the first straight/forward movement of the pivot point ($Y_e/L = \text{const.}$), the inclination (Y_{eff}) of the spanwise boundary remains relatively constant. From the correlation of Y_{eff} and Y_e/L shown in Figure D8, it does appear that the two parameters are linearly related, but possibly dependent on Mach number. The longitudinal coordinate (X_f) of the outboard limit also appears to remain relatively constant; at least, for the example cited. This trend might be worthy of further study. However, it is suspected that the resulting longitudinal track is Reynolds number dependent.

References:

- D1. Cross, E. J., Jr. and Hankey, W. L., "Investigation of the Leeward Side of a Delta Wing at Hypersonic Speeds," AIAA Paper 68-675, 1968.

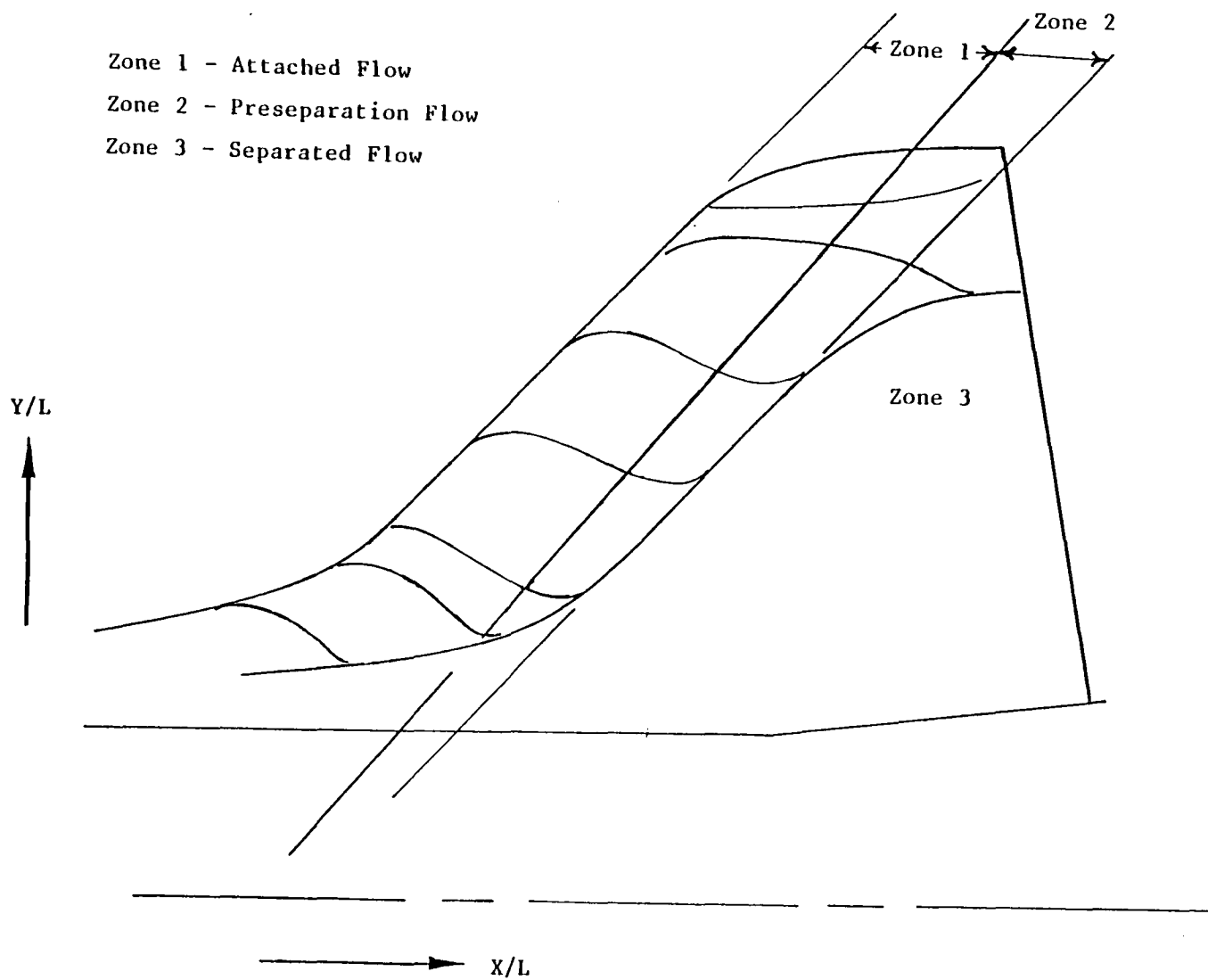


Figure D1 Wing Leeward Flow Zones

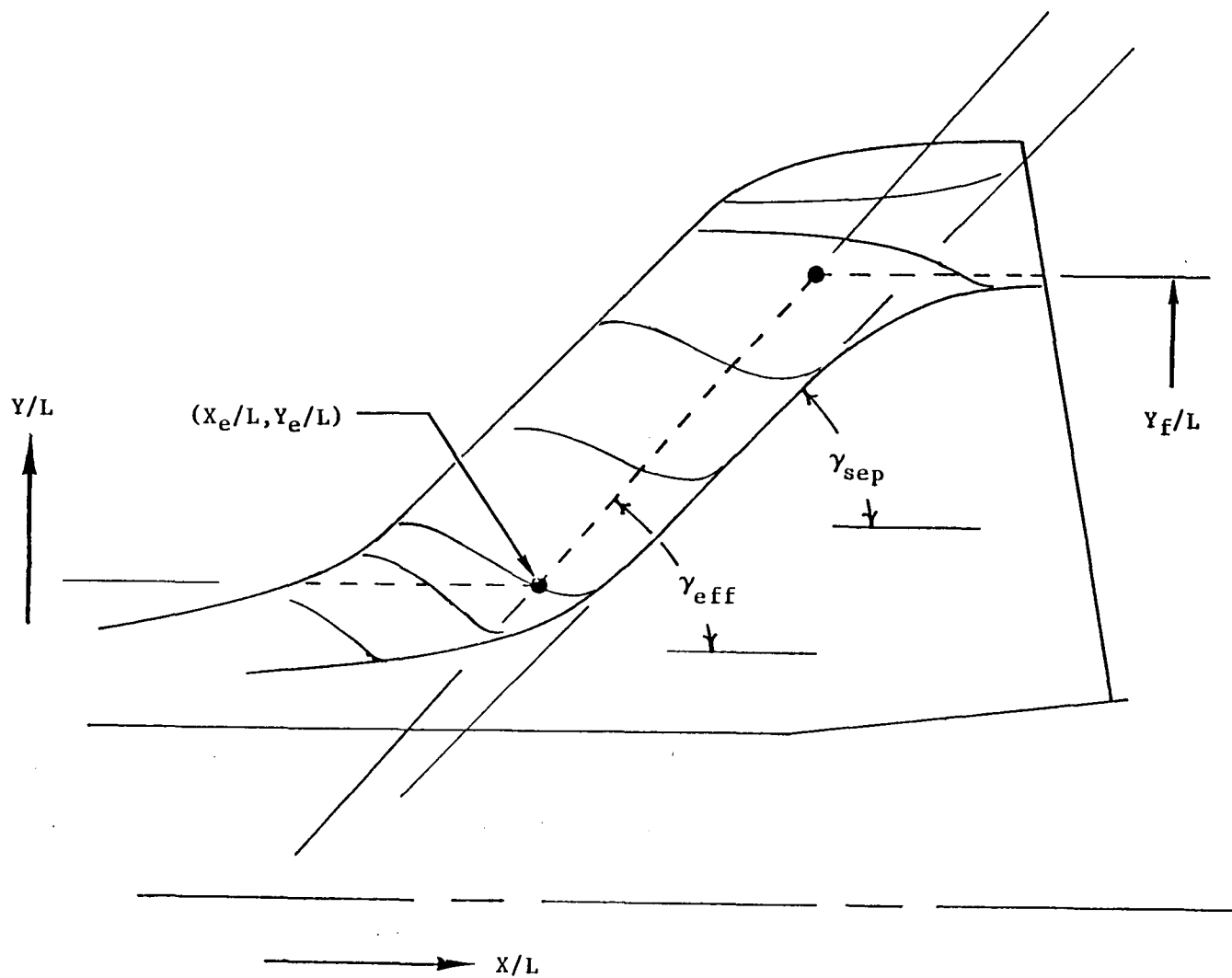
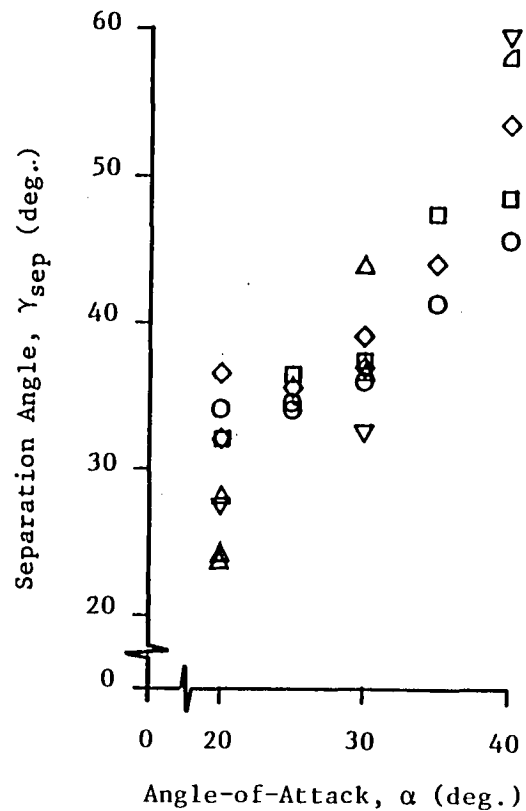
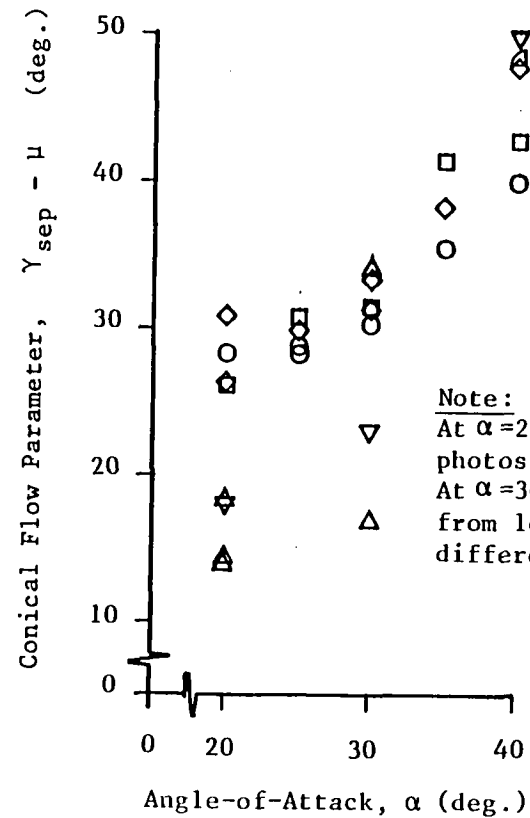


Figure D2 Definition of "Effective" Boundary Parameters



(a)



(b)

Sym	Mach	$Re_L \times 10^{-6}$
○	10	.55
□	10	1.1
◇	10	2.2
▽	6	2.7
△	6	5.4
△	6	7.3

Note:
 At $\alpha = 20^\circ$, three
 photos were measured.
 At $\alpha = 30^\circ$, measurements
 from left and right wings
 differed significantly.

Figure D3 Variation of Separation Angle

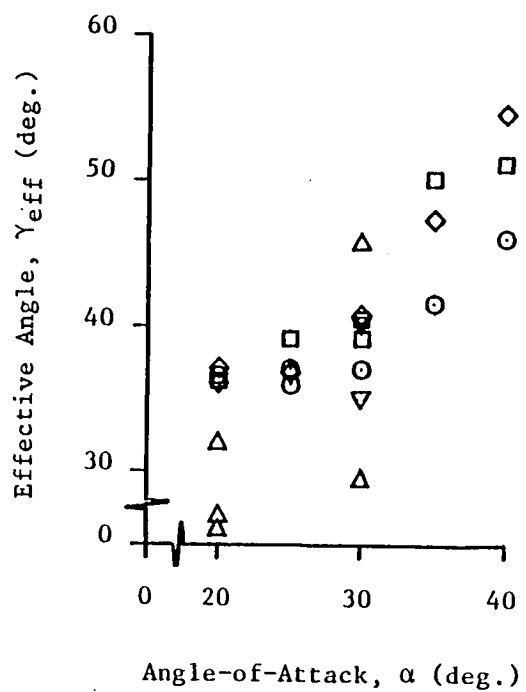


Figure D4a Effective Angle Variation

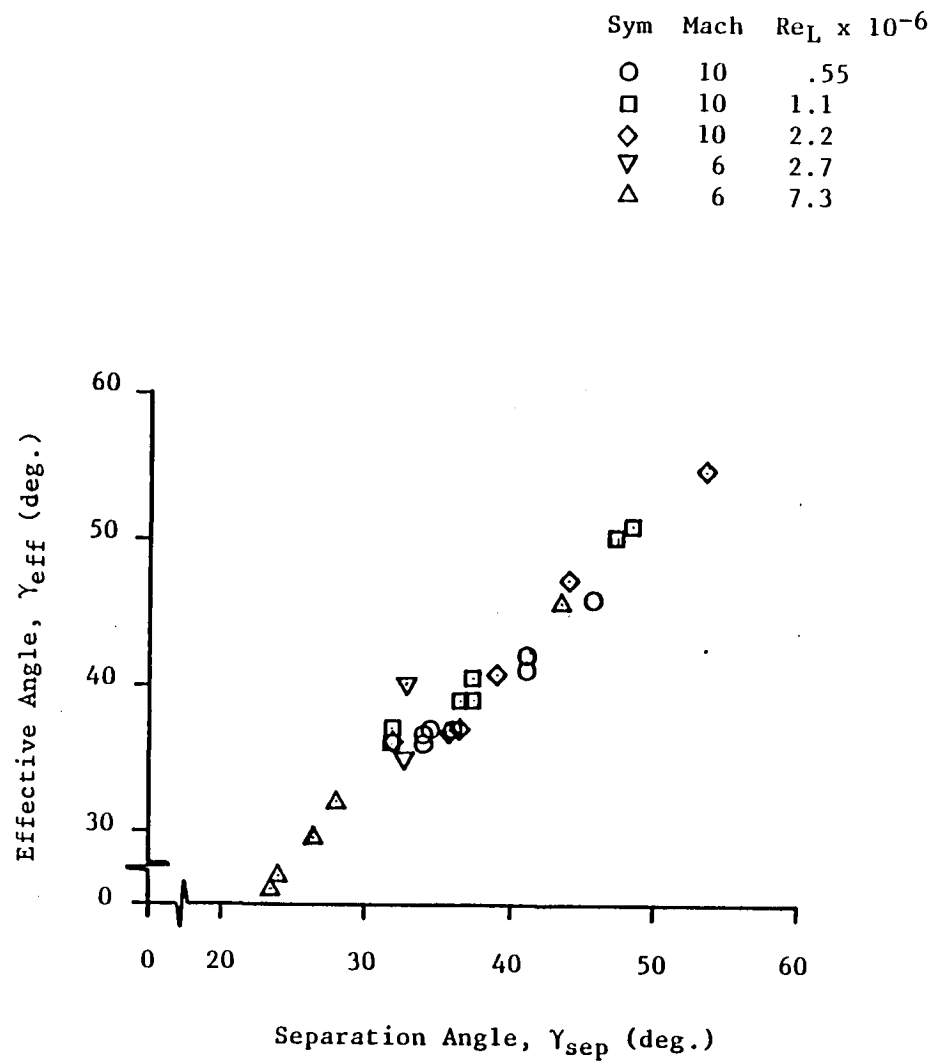


Figure D4b Correlation of Angles

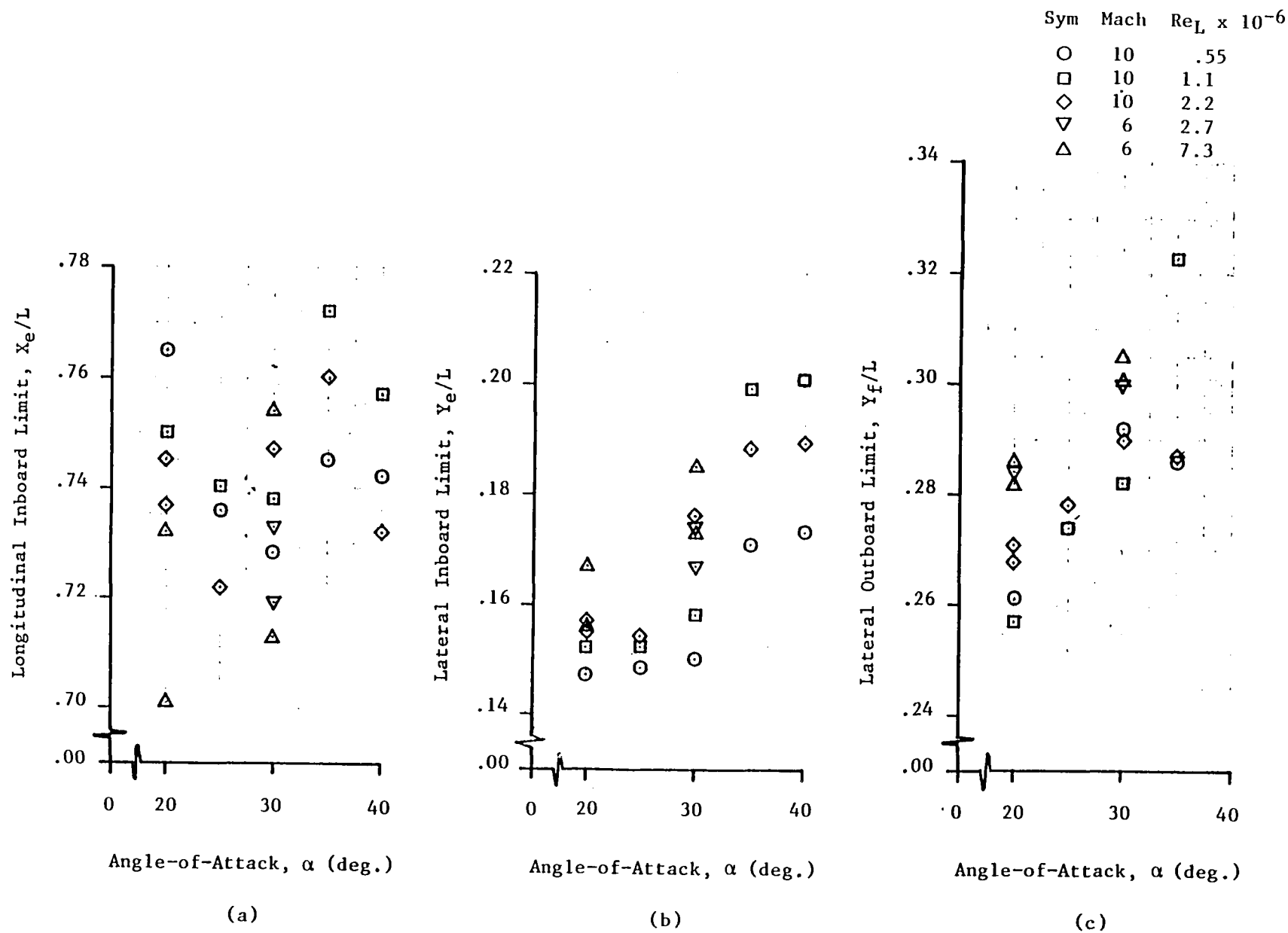


Figure D5 Variation of Limits for Attached-Flow Effective Boundaries

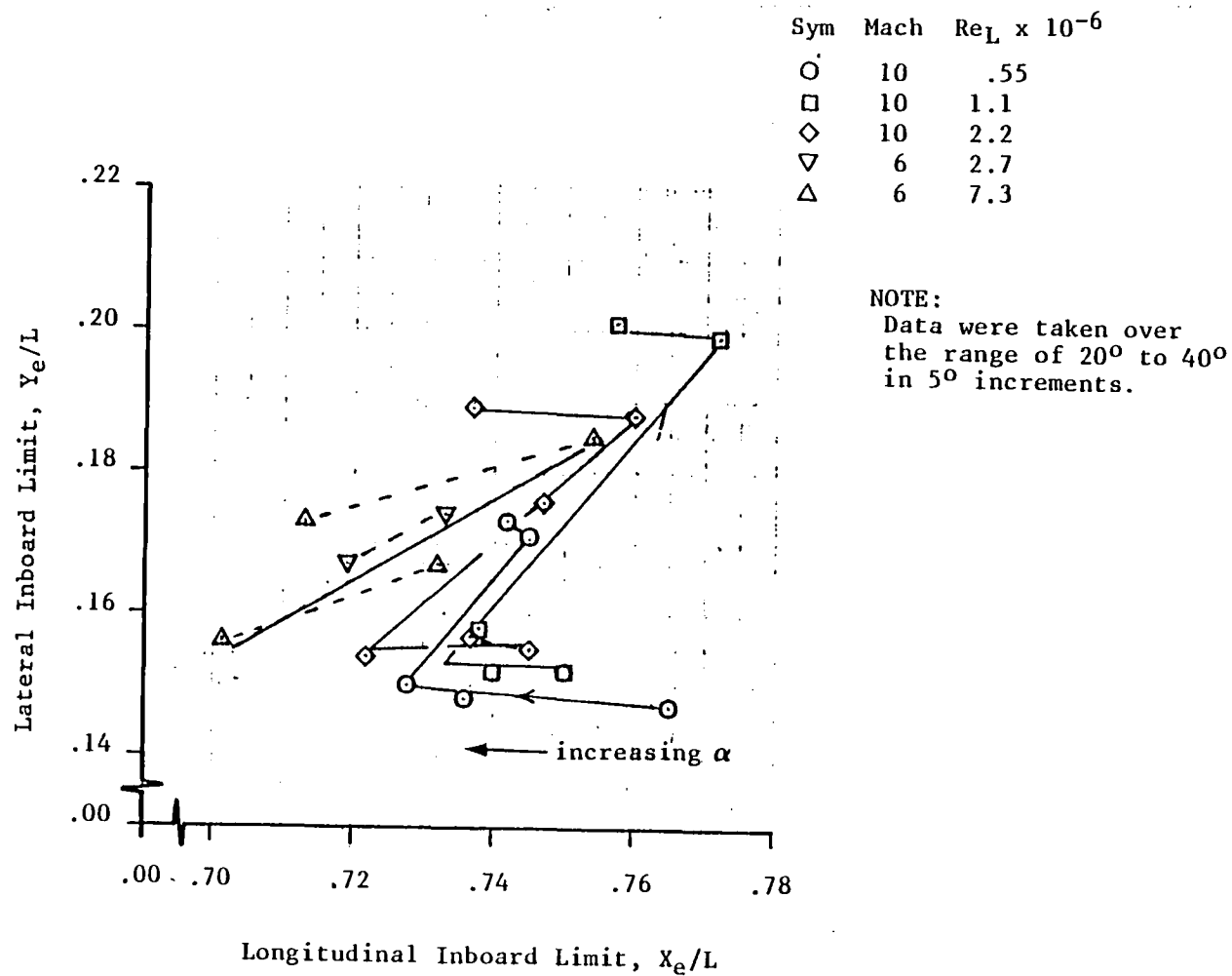


Figure D6 Movement of Attached-Flow Pivot Point

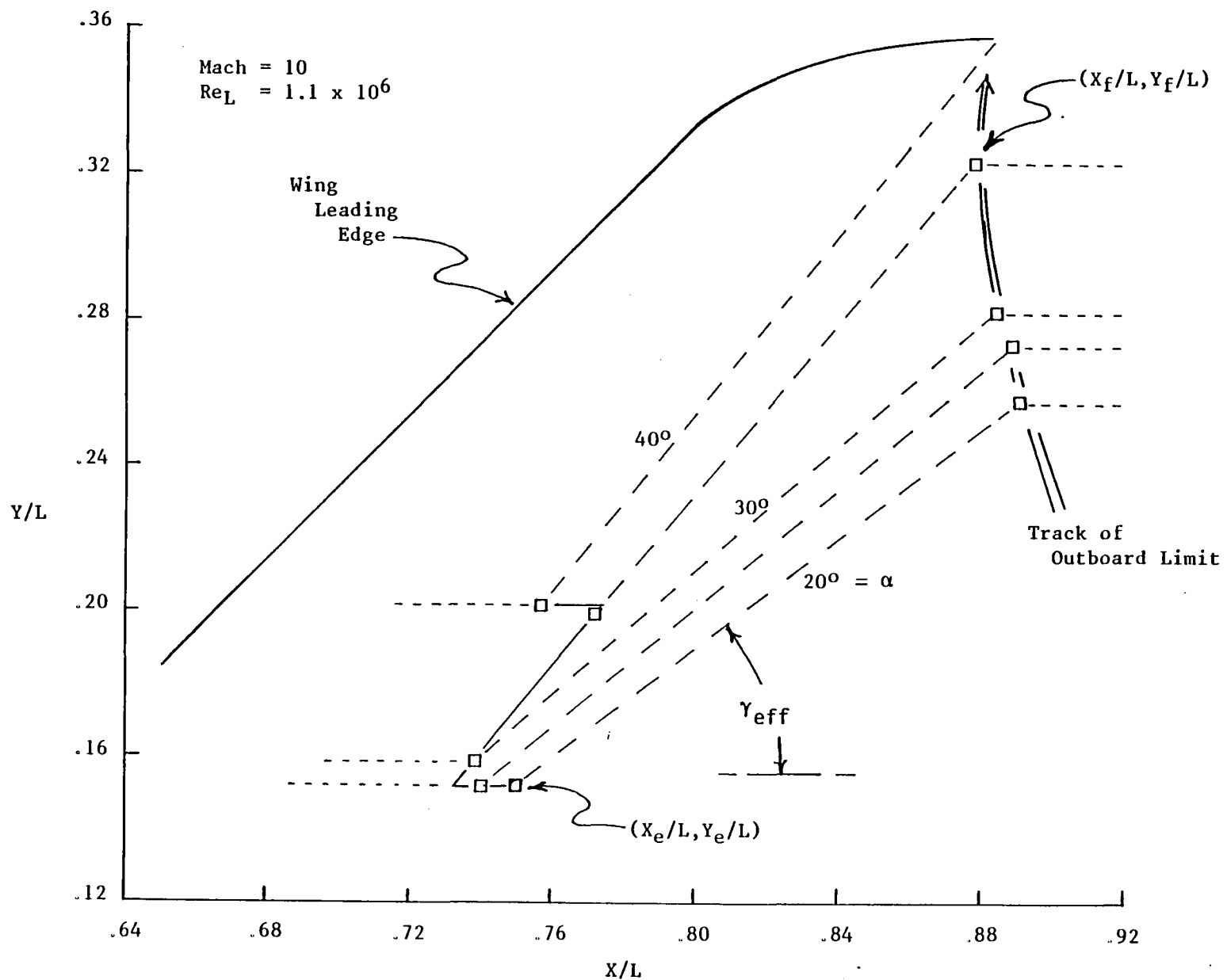


Figure D7 Movement of Attached-Flow Boundary

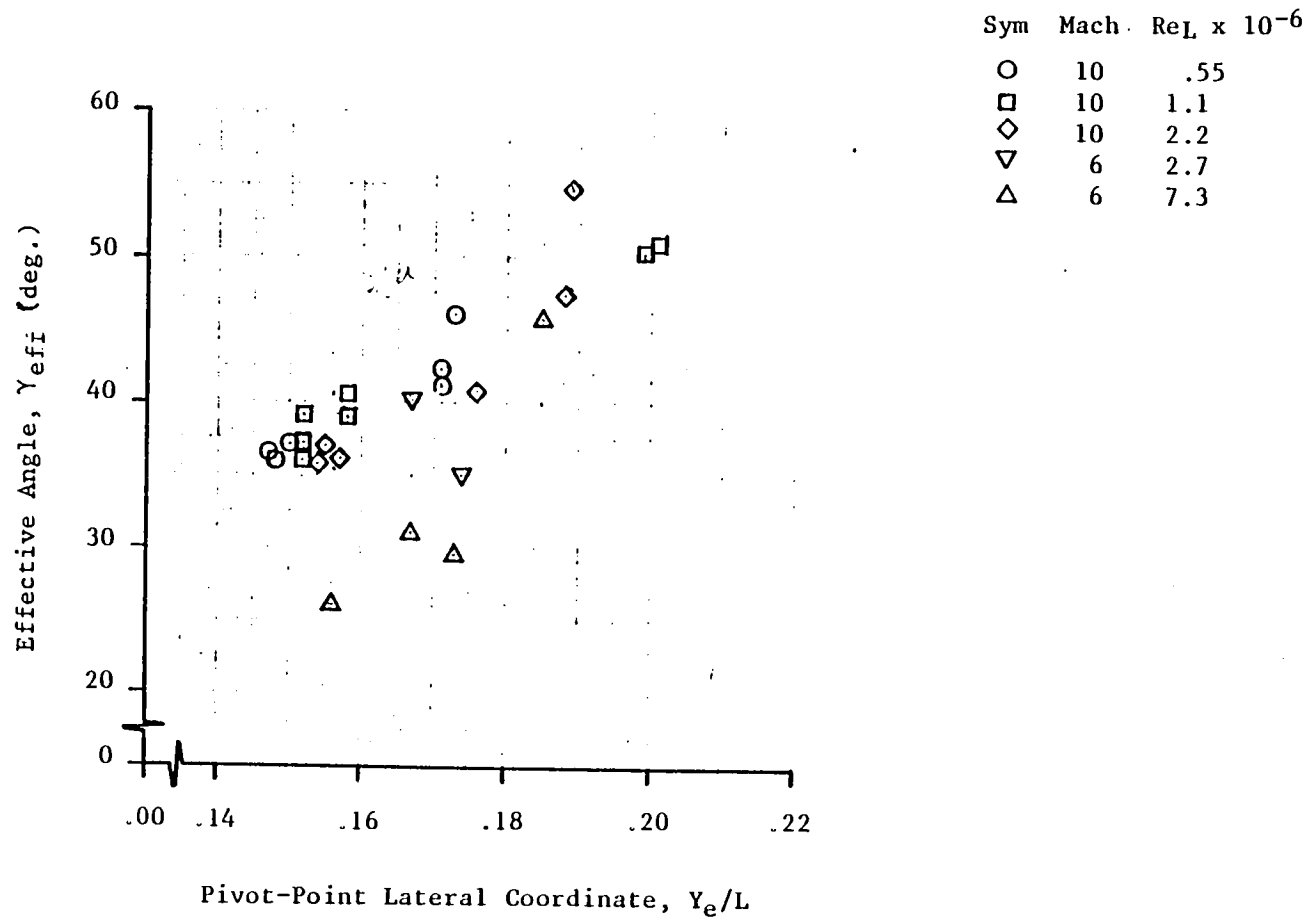


Figure D8 Correlation of Effective Angle and Pivot-Point Movement

APPENDIX E

Wing Heating Influences

This appendix discusses a cursory investigation conducted in an effort to explain the large gradients observed in heating distributions on the wing leeward surface. Heating rates are analyzed in the form $h \propto s^{-n}$ where $n \geq 1.0$. Values for n of 0.5 in laminar flow or 0.2 under turbulent conditions would normally be expected for flow in a zero pressure gradient.

References E1 through E9 (listed alphabetically) were utilized with possible causes attributed to:

- (1) A Newtonian-like pressure distribution (due to surface curvature)
- (2) viscous interaction (boundary-layer displacement) induced pressures
- (3) local flow entropy gradient (boundary-layer entrainment) effects, and/or
- (4) leading-edge bluntness induced pressure effects.

The first cause was readily dismissed because the wing surface is essentially flat where the thermocouples were located.

The possible effect of viscous interaction was examined in more detail, primarily because of significance attributed to the viscous interaction parameter $\bar{X} = M_\infty^3 / Re_\infty^{1/2}$ in References E7, E8 and E9, plus others. A strong interaction theory ($\bar{X} \gg 1$) is formulated in reference E8 which yields an induced pressure of $p \propto \bar{X}$ (i.e. $p \propto s^{-1/2}$) and an associated heat transfer of $h \propto s^{-3/4}$. A pressure variation of this order is also corroborated by data. (E3 & E9) For a power-law variation of pressure, a similar result for heat transfer can be obtained from other developments. (E3 - E6)

Samples of correlations of Mach 10 data for $h \propto s^{-n}$ for the influence of viscous interaction are presented in Figures E1 and E2 for $n = 3/4$ and 1.0, respectively, where $\bar{X}_{s,\infty} \rightarrow \infty$ as $s \rightarrow 0$. For these Mach 10 data $\bar{X} > 1$, but the scatter of data is enhanced (the parameter hs^n should have a constant value). The correlations for $n = 1$ exhibit less scatter than those for $n = 3/4$ (from theory), again indicating n should have a value greater than unity. Typical correlations of Mach 6 data represented in Figure E3 show an increase in scatter compared with the Mach 10 data. The increased scatter may be partially attributed to smaller difference between adiabatic wall temperatures and model surface temperatures and a lower magnitude of heat transfer, and possibility of turbulent flow for the Mach 6 tests.

* Numbers in () are references

For boundary-layer similar solutions, a value of $n = .9375$ corresponds to an infinite favorable pressure gradient, and solutions are imaginary for $n > 1.0$. (E3 & E4) That is, for more severe pressure variations ($p < s^{-1}$), nonsimilar solutions or "locally" similar concepts using equations of References E5 and E6 would be required. In Reference E6, it is shown that flows with arbitrary larger values of n may exist; however, Falkner-Skan type solutions are similarly limited. Extrapolation of the existing solutions is suggested, but the adequacy of such extrapolation is unknown.

The viscous interaction parameter, \bar{X} , shown in these figures was computed for free-stream conditions. When using this parameter for evaluating the interaction on the wing it should be computed for flow conditions upstream of the wing--i.e., for flow within the fuselage bow shock--which would probably yield a $\bar{X} < 1.0$ for the Mach 10 data. For the Mach 6 data, typically represented in Figure E3, \bar{X} would be even lower. Actually, in the correlation of the wing data for both Mach numbers $n \geq 1.20$. Hence, it is felt that the observed heat transfer variation is not induced by primarily viscous interaction. If any viscous interaction is present, it is most likely acting simultaneously with or overpowered by the effects of the last two causes--entropy gradients and bluntness effects.

The effect of entropy gradient is difficult to ascertain because of the requirement for nonsimilar boundary layer solutions and simultaneous flow field computation. Basically, an entropy gradient caused by flow passing through a leading-edge shock of varying strength (due to curvature) produces vorticity in the flow and a finite value of the normal velocity gradient at the edge of the boundary layer. Generally, this results in increased local heat transfer where the boundary layer is affected. Once the flow containing entropy gradients (i.e. entropy layer) is "swallowed" by the boundary layer, heating rates rapidly approach values corresponding to flow downstream of sharp leading edges.

The increase in pressures on surfaces following a blunt leading edge has long been known, and "blast-wave" theory has been shown to adequately correlate this behavior. (E4) As shown in this same reference, pressure gradients on a leeward surface in hypersonic flow can be very significant (an example cited therein shows the pressure can decrease an order of magnitude on a leeward surface). Corresponding heat transfer distributions should similarly deviate from the flat plate values, but are difficult to correlate because of the limitations of similar solutions, as mentioned earlier, and the complex calculation procedures required. Heating variations similar to those for attached flow on the Shuttle model's wing leeside

surface (Figure 6 in main text) (i.e., $h \propto s^{-n}$; $n \approx 1$) have been observed previously for a blunted slab in the region of the leading edge/slab junction, and in unpublished data for the Shuttle delta-wing booster^(E3). As stated in references E4 and E8, bluntness-induced effects are important and are usually limited to region close to the leading edge ($s/t \leq 4$, where t is the leading edge thickness or diameter). It seems likely that the effects of bluntness-induced pressures are reflected in the present data to some degree.

Conclusions:

From this investigation it appears that both bluntness-induced pressures and entropy gradients may be possible causes for the approximately s^{-n} (where $n > 1.0$) variation in wing leeside heating. This hypothesis can be examined by calculating heat transfer on the upper wing surface using an available non-similar boundary layer code.^(E10) Experimental surface pressure distributions (if available) or computed values could be used as input for the boundary layer calculations. Boundary layer edge entropy variation could be computed with the aid of an assumed leading edge shock shape by matching inviscid mass flow with mass flow within the boundary layer. While the suggested investigation is conceptually simple, it would have required more time than was available in the current study.

References:

- E1. Beckwith, I. E. and Cohen, N. B., "Application of Similar Solutions to Calculation of Laminar Heat Transfer on Bodies with Yaw and Large Pressure Gradient in High-Speed Flow", NASA TN D-625, January 1961.
- E2. Bertram, M. H., "Boundary-Layer Displacement Effects in Air at Mach Numbers of 6.8 and 9.6", NACA TN 4133, February 1958.
- E3. Bertram, M. H. and Feller, W. V., "A Simple Method for Determining Heat Transfer, Skin Friction, and Boundary-Layer Thickness for Hypersonic Laminar Boundary-Layer Flows in a Pressure Gradient", NASA Memo 5-24-59L, June 1959.
- E4. Bertram, M. H. and Henderson, A. Jr., "Effects of Boundary-Layer Displacement and Leading-Edge Bluntness on Pressure Distribution, Skin Friction, and Heat Transfer of Bodies at Hypersonic Speeds", NACA TN 4301, July 1958.
- E5. Cohen, C. B. and Reshotko, E., "Similar Solutions for the Compressible Laminar Boundary Layer with Heat Transfer and Pressure Gradient", NACA Report 1293, 1956.
- E6. Cohen, C. B. and Reshotko, E., "The Compressible Laminar Boundary Layer with Heat Transfer and Arbitrary pressure Gradient", NACA Report 1294, 1956.
- E7. Cross, E. J. Jr. and Hankey, W. L., "Investigation of the Leeward Side of a Delta Wing at Hypersonic Speeds", AIAA Paper 68-675, 1968.
- E8. Dorrance, W. H., "Viscous Hypersonic Flow", McGraw-Hill book Co., New York, N. Y., 1962.
- E9. Hurley, F. X., "Leeward Surface in Hypersonic Viscous Interaction", Trans of the ASME, Journal of Applied Mech. June 1968, Pg 412-414.
- E10. Cebeci, T., Smith, A.M.O., & Wang, L. D., "A Finite-Difference Method for Calculating Compressible Laminar and Turbulent Boundary Layers", McDonnell Douglas Report DAC-67131, Part I, March 1969.

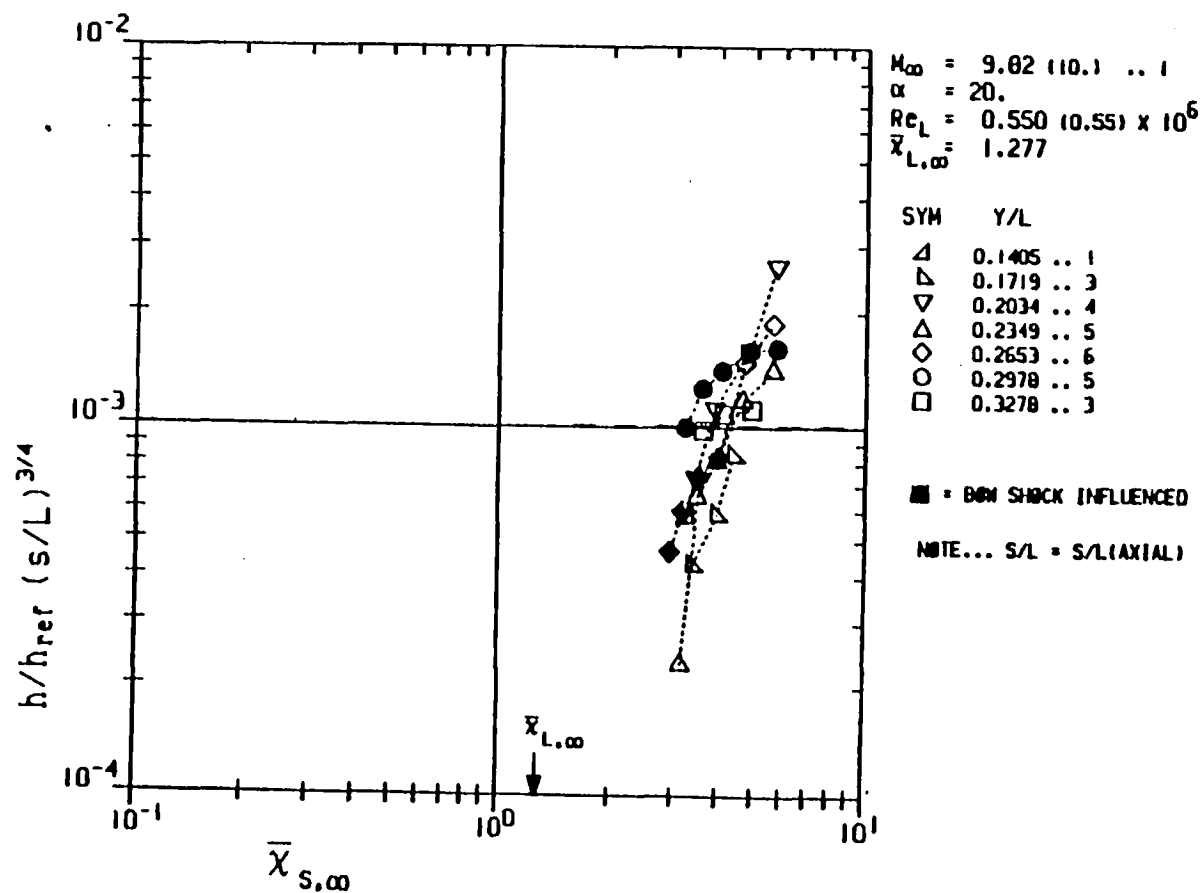


Figure E1a Mach 10 Influence of Viscous Interaction on Wing Leaside Heating Correlation - $n = 3/4$

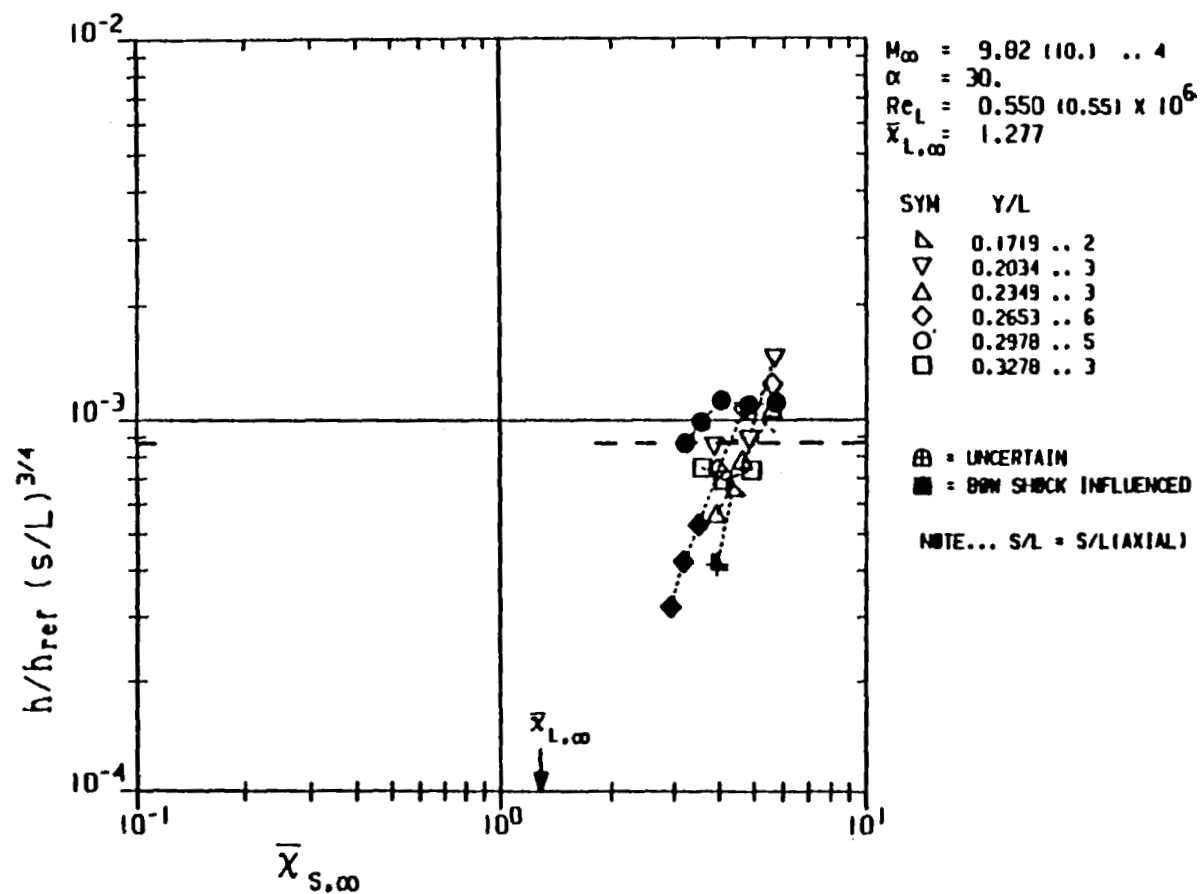


Figure E1b Mach 10 Influence of Viscous Interaction on Wing Leeside Heating Correlation - $n = 3/4$

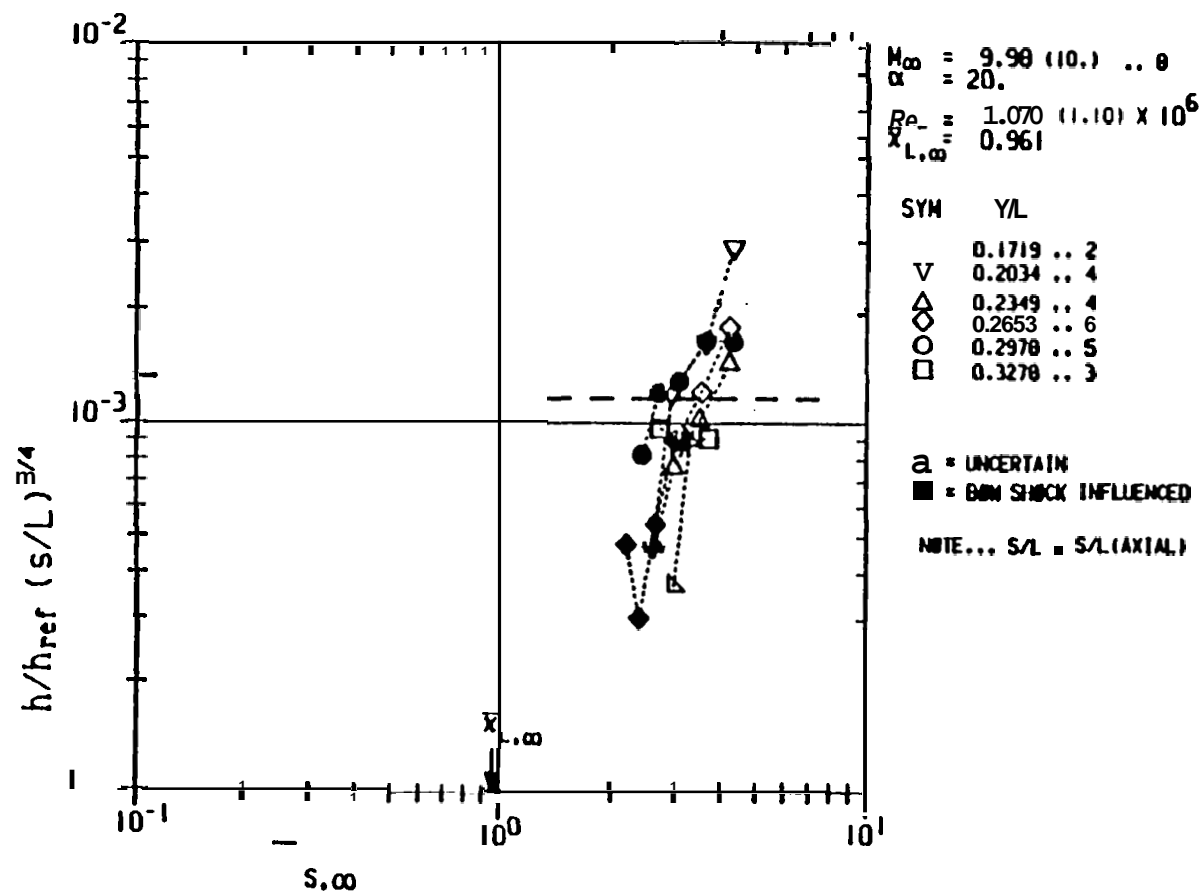


Figure Elc Mach 10 Influence of Viscous Interaction on Wing Leeside
heating Correlation - $n = 3/4$

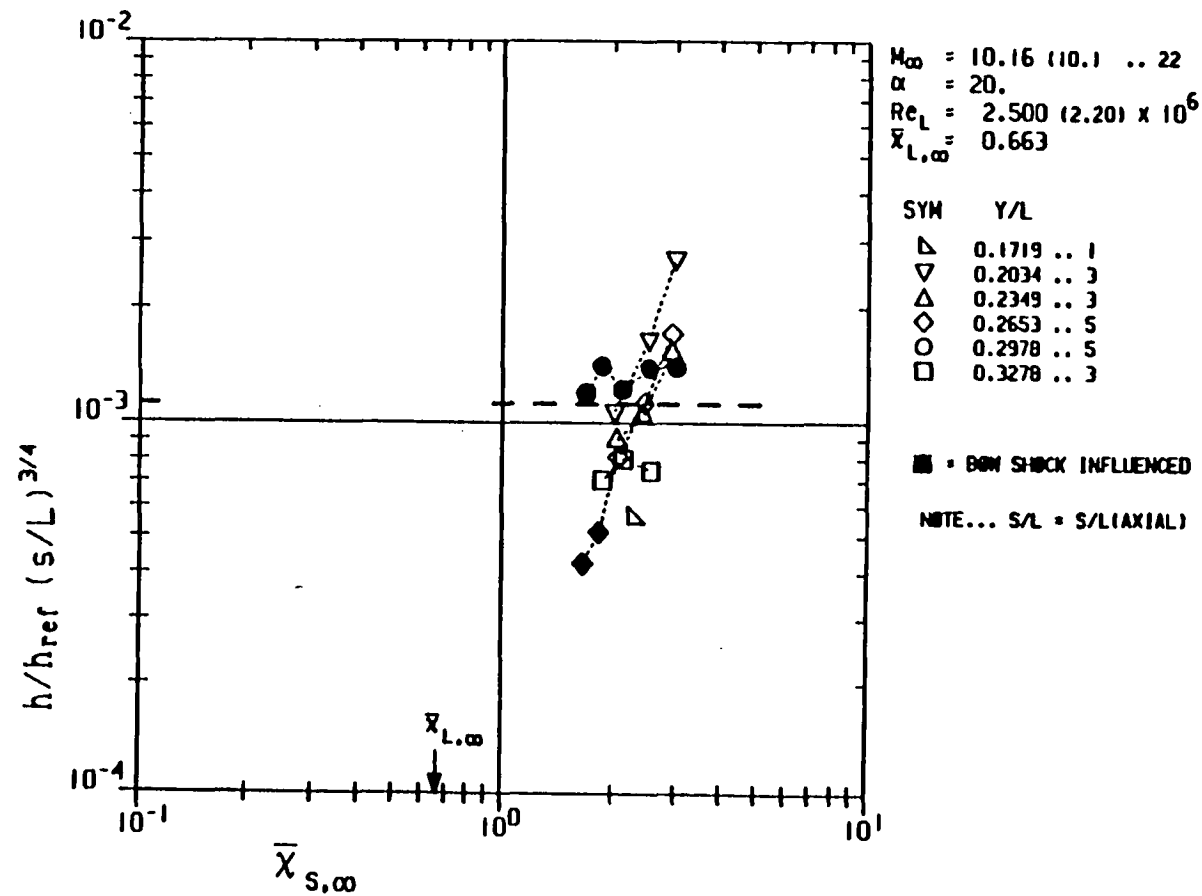


Figure Eld Mach 10 Influence of Viscous Interaction on Wing Leeside Heating Correlation - $n = 3/4$

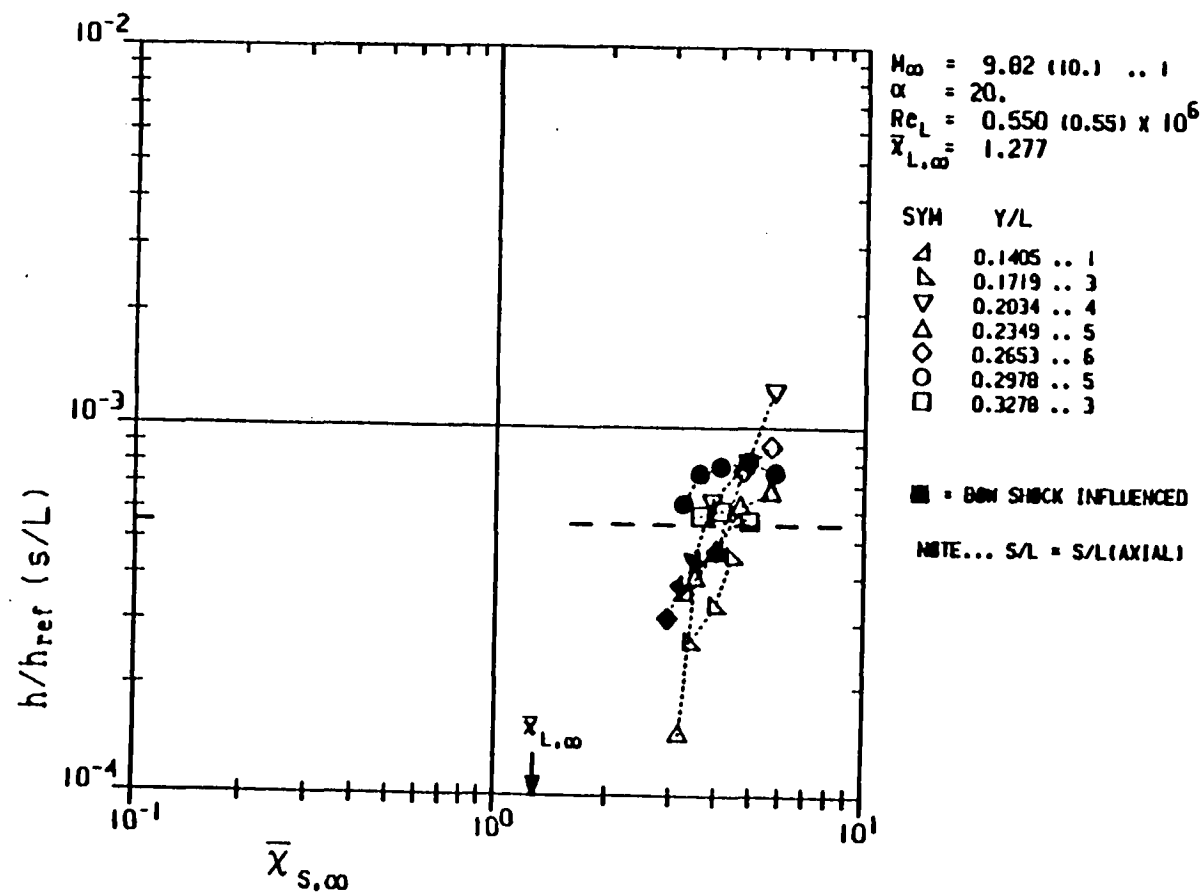


Figure E2a Mach 10 Influence of Viscous Interaction on Wing Leeside Heating Correlation - $n = 1.0$

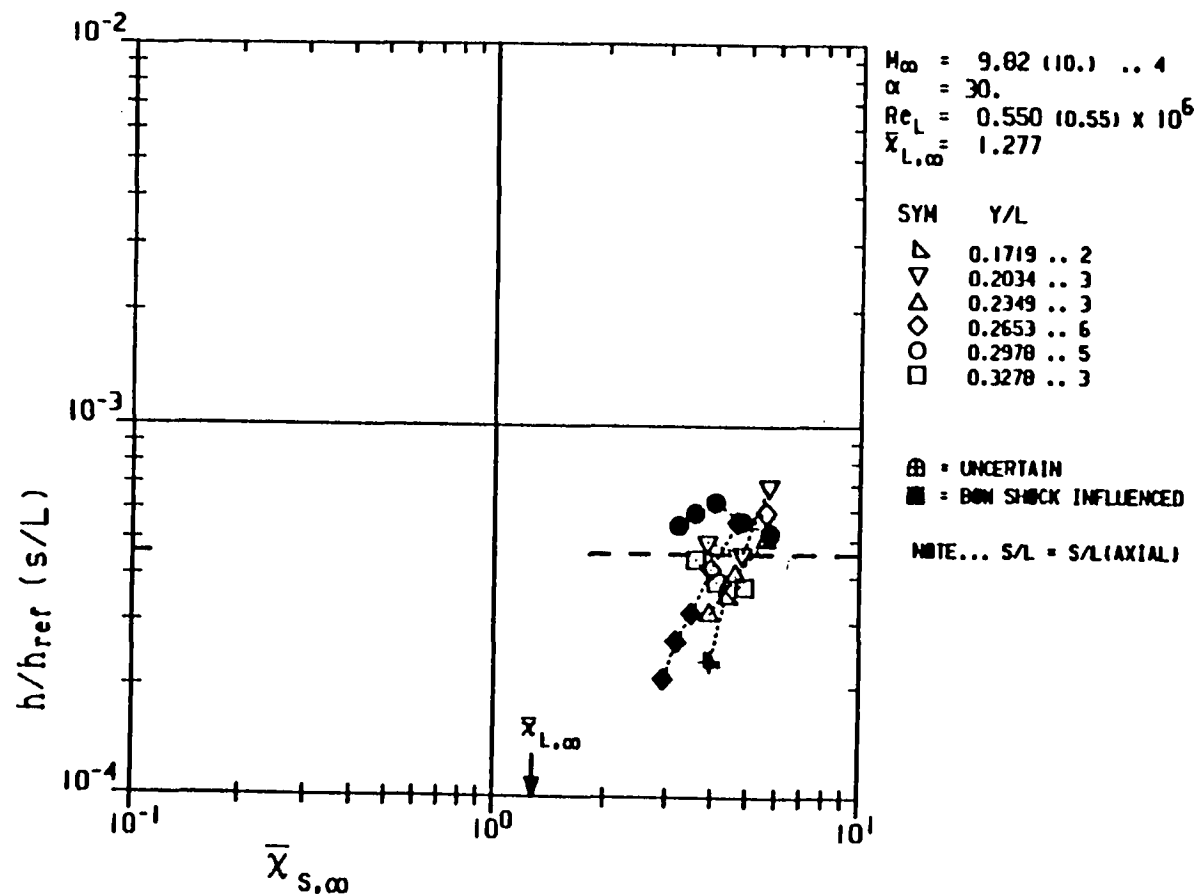


Figure E2b Mach 10 Influence of Viscous Interaction on Wing Leeside Heating Correlation - $n = 1.0$

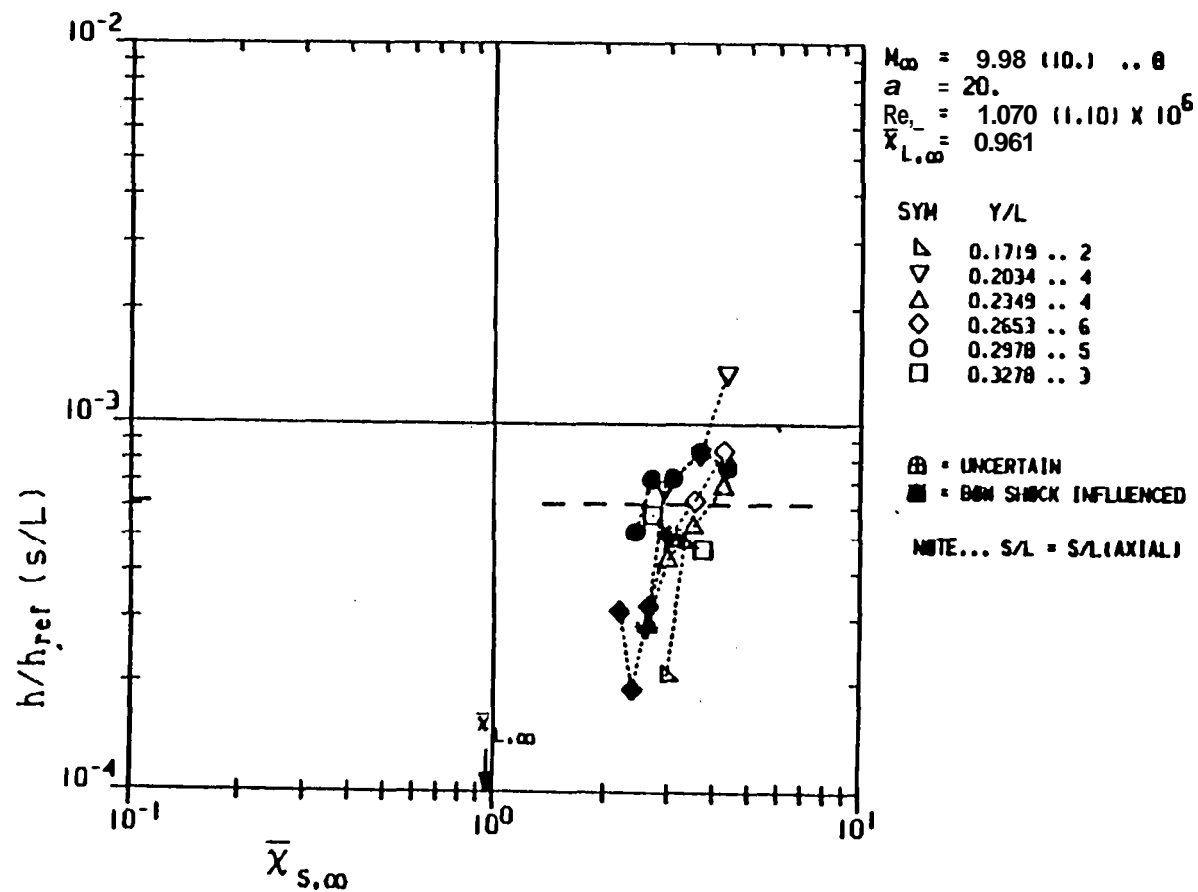


Figure E2c Mach 10 Influence of Viscous Interaction on Wing Leaside Heating Correlation - $n = 1.0$

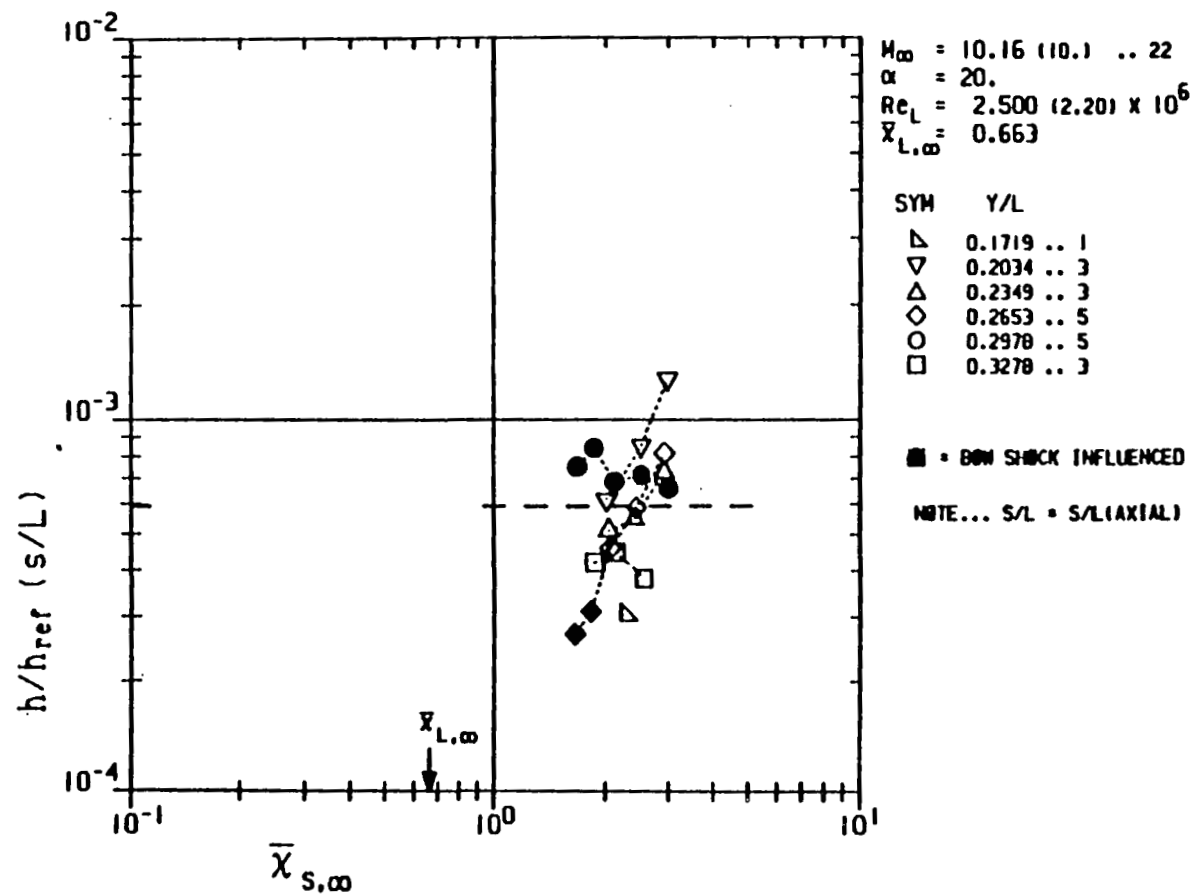


Figure E2d Mach 10 Influence of Viscous Interaction on Wing Leaside Heating Correlation - $n = 1.0$

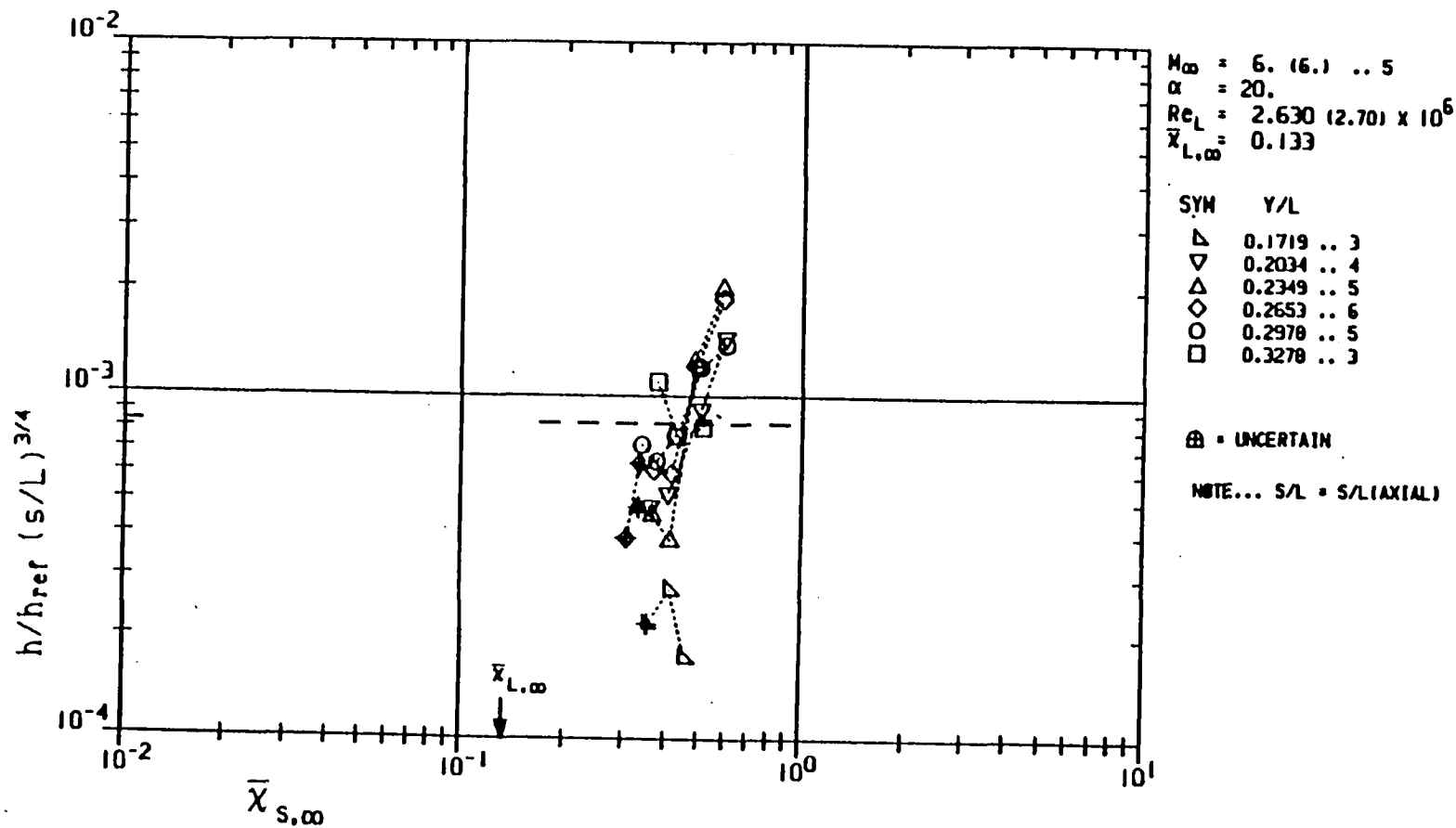


Figure E3a Mach 6 Influence of Viscous Interaction on Wing Leaside Heating Correlation - $n = 3/4$

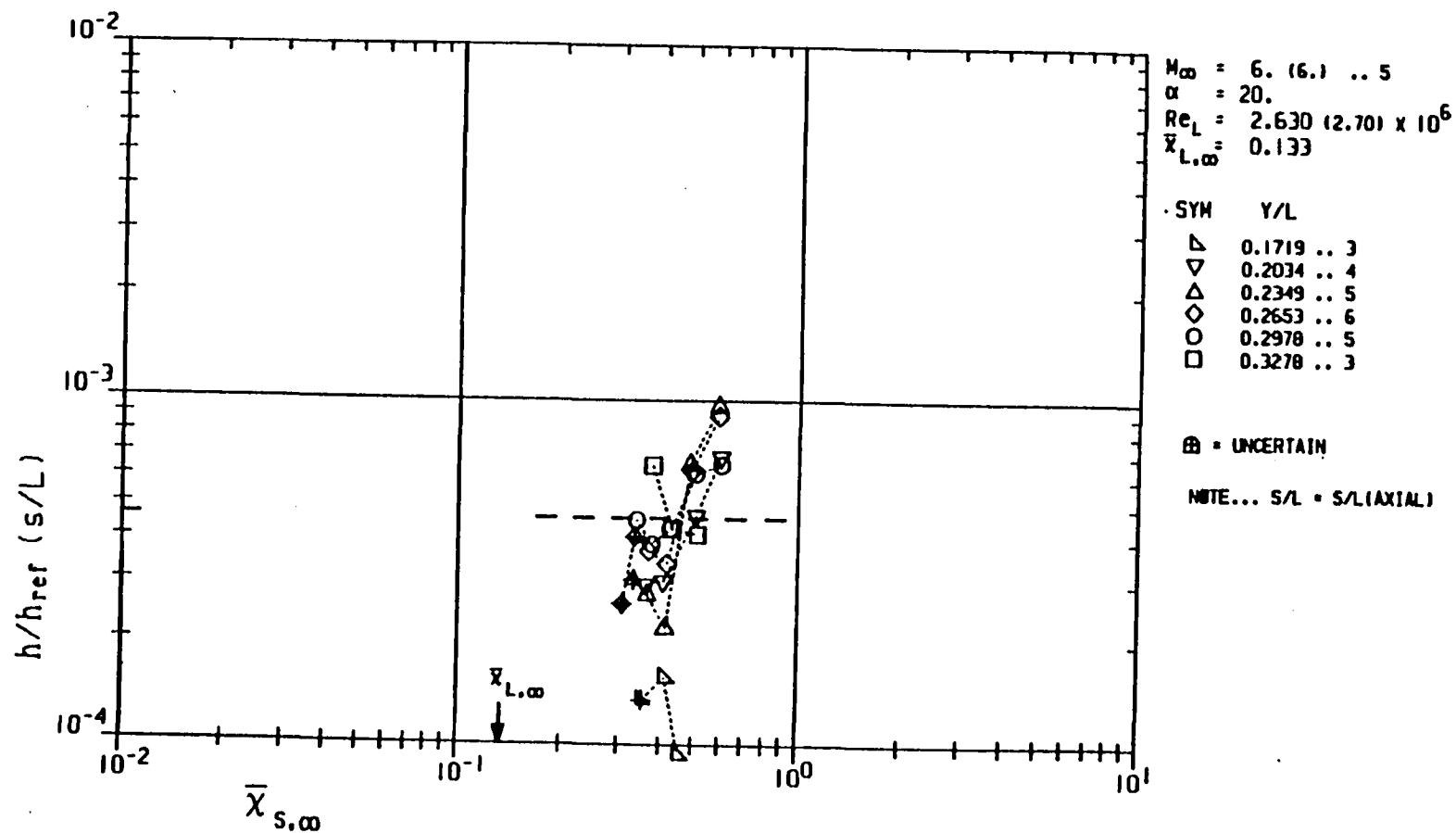


Figure E3b Mach 6 Influence of Viscous Interaction on Wing Leaside Heating Correlation - $n = 1.0$

APPENDIX F

Definition of Wetted Length for Upper Fuselage Heating Correlations

In this appendix the useage of various formulations of wetted length are evaluated for correlating the vortex-induced heat transfer on the upper fuselage.

In an effort to complement the work of reference F1, the heat transfer data were ratioed to the corresponding distribution along the upper centerline. In keeping with the concept of a swept-cylinder, correlations were evaluated for wetted length and sweep angles. The wetted paths considered are illustrated in Figure F1 and included directions

- 1) normal to the upper centerline,
- 2) along a "streamline", determined from oil-flow photos, and
- 3) normal to the stagnation line of the "effective" swept cylinder for centerline heat transfer.

Streamlines of constant flow angle were assumed in the above, using flow angles furnished by V. T. Helms of LaRC.

Some examples of these correlations are shown in Figures F2 through F4, for the low Reynolds number, Mach 10 data and angles of attack from 20° to 40°. In these figures all data on the upper surface are included, but only the data points joined with dashed lines are used in the correlations. These data are considered to be in the attached flow (feather-pattern) region. Although not used in the correlations, the data outside the feather pattern are included to illustrate the entire upper surface distribution, and as will be seen from the figures, the correlations provide a good estimate for an "average" value of heating in this region.

Figure F2 shows the heating distributions and correlations using wetted-distance normal to the upper centerline (Figure F1a). For angles of attack up to 35°, these data may be correlated by a relation of the form

$$\frac{h}{h_{CL}} = 0.23(\pm 10\%) \cdot \left(\frac{s}{L}\right)^{0.30(\pm 8\%)} \quad (F1)$$

It is interesting to note the exponent value of 0.3 on the wetted distance term, indicative of turbulent heating (in agreement with reference F1).

Another correlation is shown in Figure F3 where the wetted length along the streamline is used and the centerline heat transfer at the origin of the streamline is utilized for normalization (Figure F1b). When streamlines were projected forward of $X/L = .383$ for which heat transfer data were not available, centerline heat

transfer was obtained from equation (7) of reference F1 using sweep angles, λ , provided. An "X" in the symbol indicates data not used in the correlation because the streamlines were projected forward of the range of available sweep angles ($X/L = 0.3$), and $h_{s=0}$ was obtained by linear extrapolation. Wetted distances along streamlines were obtained by integrating along a constant-angle streamline (in the XY plane) over the curved upper fuselage surface. The origin of a streamline was determined from the relation

$$\left(\frac{X}{L}\right)_{s=0} = \left(\frac{X}{L}\right)_{T/C} - \frac{\left(\frac{Y}{L}\right)_{T/C}}{\tan \epsilon} \quad (F2)$$

where $\epsilon = 90 - \lambda$ is the flow angle between the centerline and streamline. Surface curvature was obtained from the approximate definition of the upper surface mold-line

$$\frac{(Y/L)^2}{.006832} + \frac{(Z/L - .33614)^2}{.002574} = 1.0 \quad (F3)$$

As shown in Figure F3 the exponent on the wetted length term is very small. In fact, for angles-of-attack greater than 20° , this negative exponent has a value less than 0.05 indicative of relatively constant heat transfer along these "streamlines". If feasible, confirmation of this trend from thermal mapping test data might be worthwhile. The other interesting feature of this correlation is the increase of the multiplier or constant (10^{-m}) with angle-of-attack, approaching unity at about 30° , then dropping to a constant value at the higher angles-of-attack. However, the large scatter of the data in this format tends to lessen the creditability of the above observations.

The last correlation is shown in Figure F4 where the parameter $(s/L)\sin$ is used (Figure Flc). The uniqueness of this parameter goes back to the treatment of upper centerline heating in reference F1 and the preceding (although somewhat dubious) findings. In essence, in reference F1, the heating along the upper centerline is treated as stagnation-line heat transfer along a cylinder of varying sweep angle. That is, the upper centerline can be thought of as a line tangent to an infinite swept cylinder at the stagnation line of the cylinder. The cylinder can move along this line; and as it does, cants or rotates itself (and its stagnation line) at vary angles of sweep relative to flow parallel to the centerline. Hence, a point on the centerline is also a point on a swept cylinder stagnation line

along which the heat transfer is relatively constant as indicated above for heating angle a "streamline" of constant sweep/flow angle. In other words, the "streamline" is equivalent to the stagnation line of a swept cylinder tangent to the centerline. Heat transfer is relatively constant along the stagnation line; and the component $(s/L) \sin \lambda$ is the wetted distance on this cylinder normal to the stagnation line. Note that this parameter is only approximated by use of the $(\sin \lambda)$ term; actual wetted distance probably should be integrated, or using equation (3), the use of the associated deflection angle might be evaluated.

As shown in comparing Figures F2 and F4, no significant alterations of the correlations result in using this parameter.

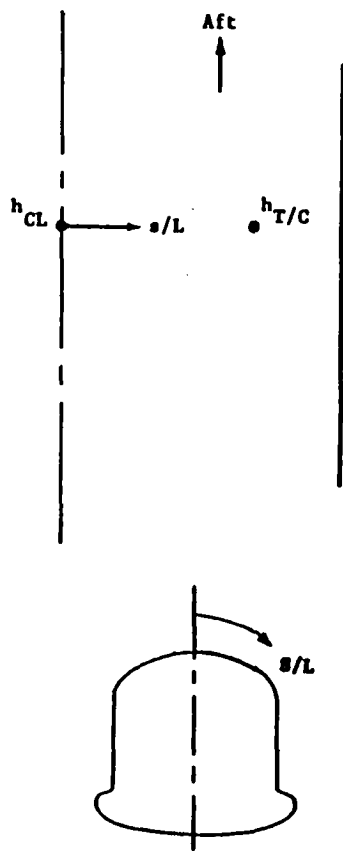
Conclusions:

From the preceding examination it is concluded that use of the wetted distance normal to the upper centerline provides an appropriate parameter for correlating the heating distribution on the upper fuselage surface. Correlations obtained using this parameter are consistent and compare with expected trends. Its usage is very simple and straightforward, and the need for attendant flow or sweep angle is not required. Results using a streamline approach reveal some interesting findings, but require further study to establish their creditability. Accounting for the influence of local sweep angle did not improve the correlations.

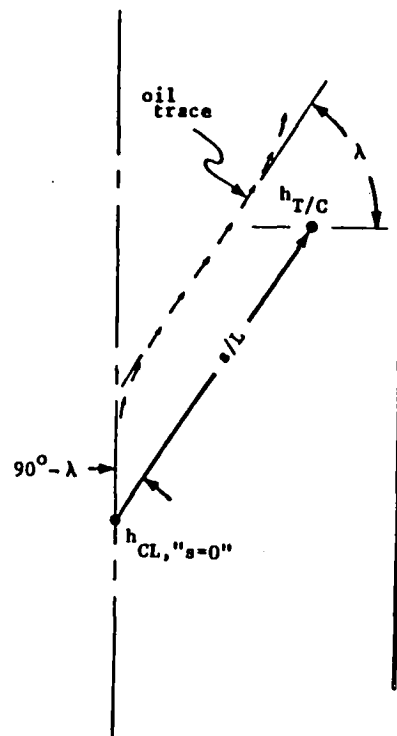
Keep in mind though, this is only a very cursory examination using data for a very low Reynolds number. Results of a more extensive examination may conflict with the above.

References:

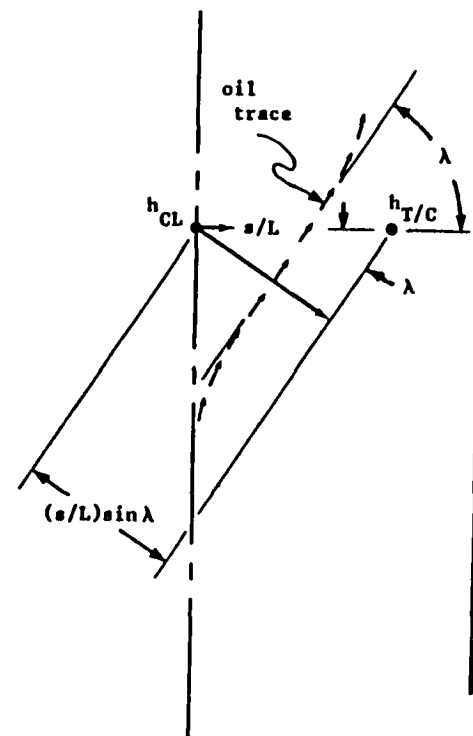
- F1. Helms, V. T., III, "An Empirical Method for Computing Leeward Centerline Heating on the Space Shuttle Orbiter," AIAA Paper 81-1043, June 1981.



(a) normal to centerline



(b) along a "streamline" of constant flow angle



(c) normal to the stagnation line of the effective swept cylinder

Figure F1 Upper Fuselage Wetted-Length Parameters

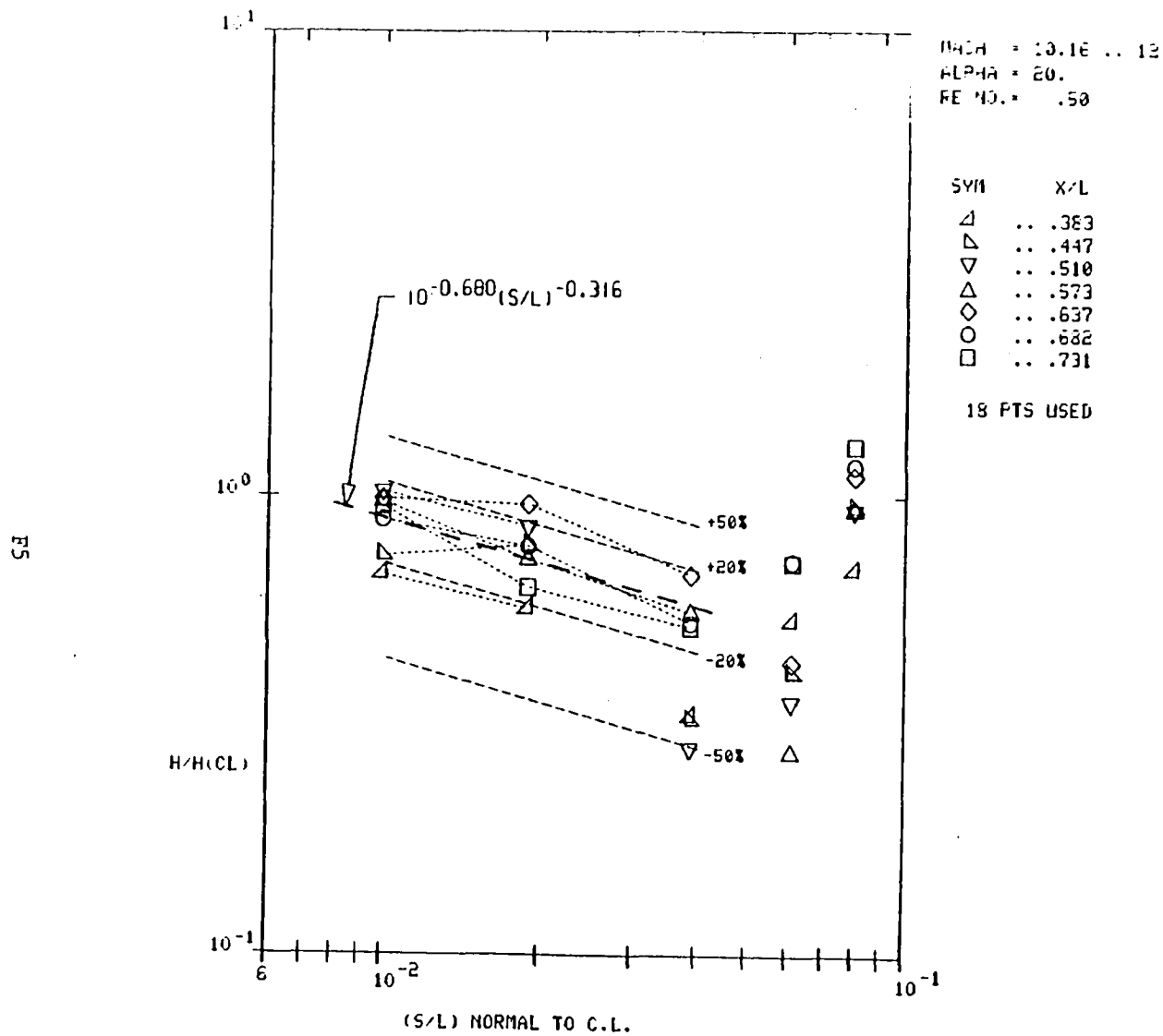


Figure F2a Upper Fuselage Heat Transfer Profiles

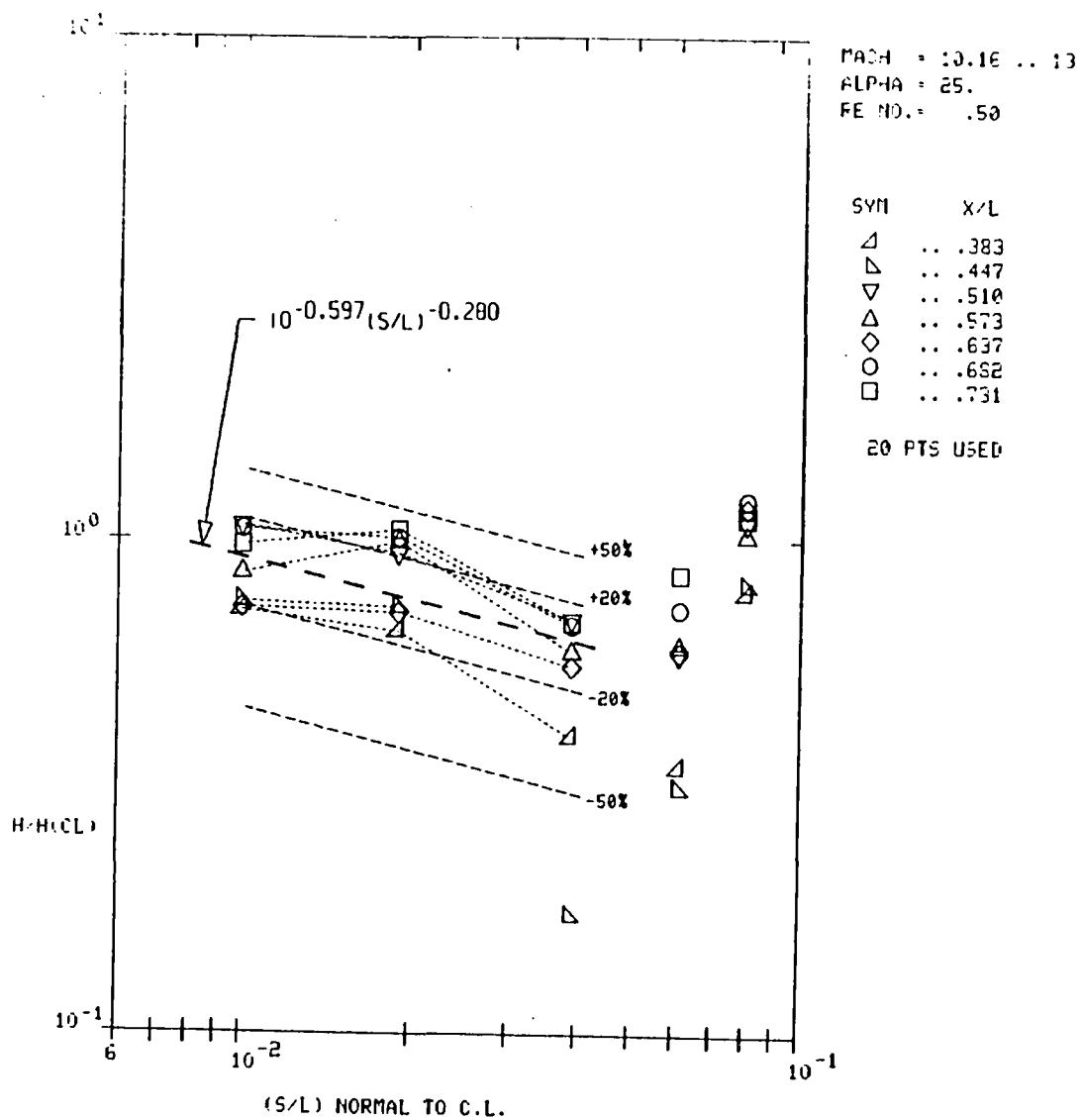


Figure F2b Upper Fuselage Heat Transfer Profiles - Continued

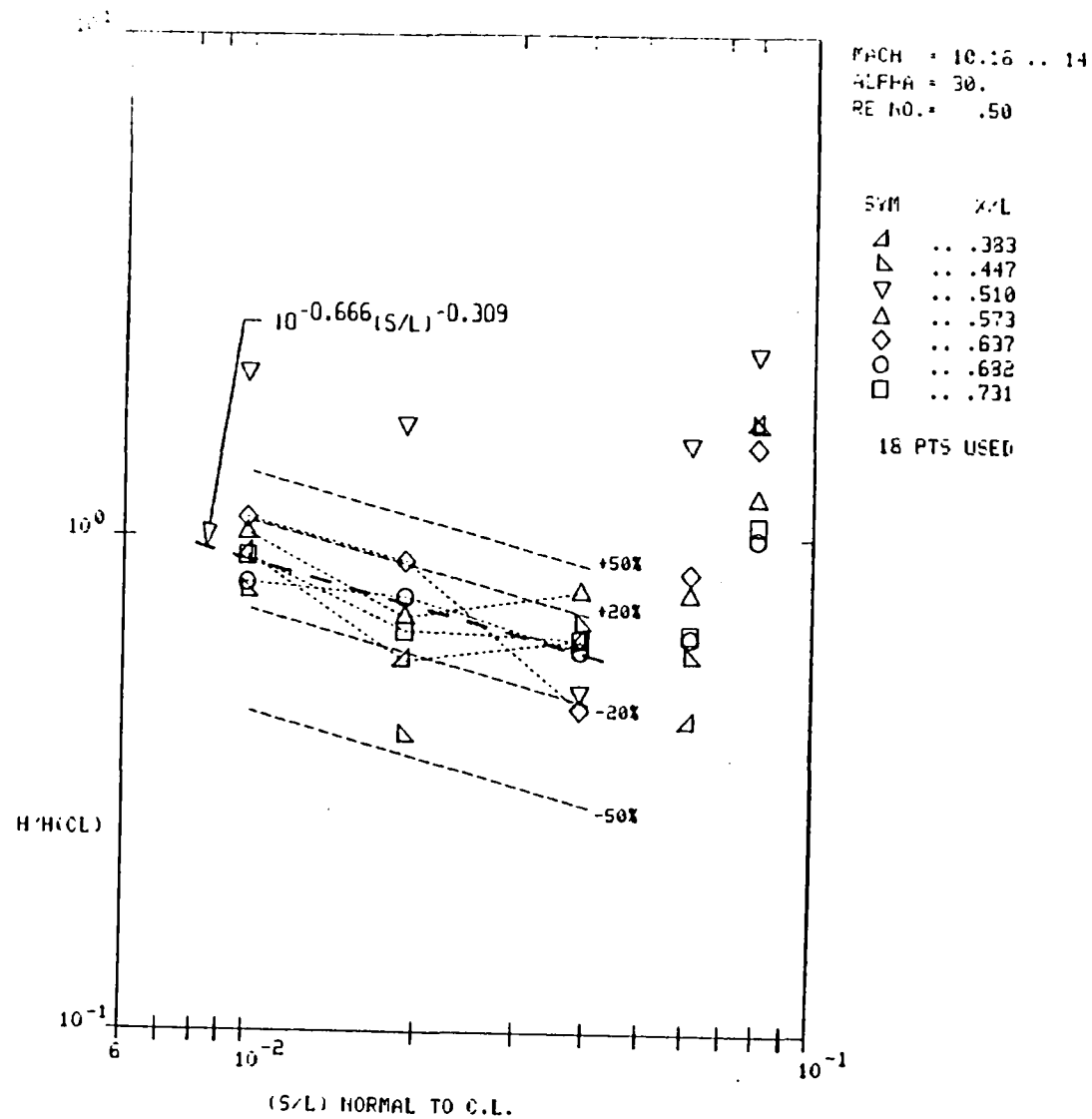


Figure F2c Upper Fuselage Heat Transfer Profiles - Continued

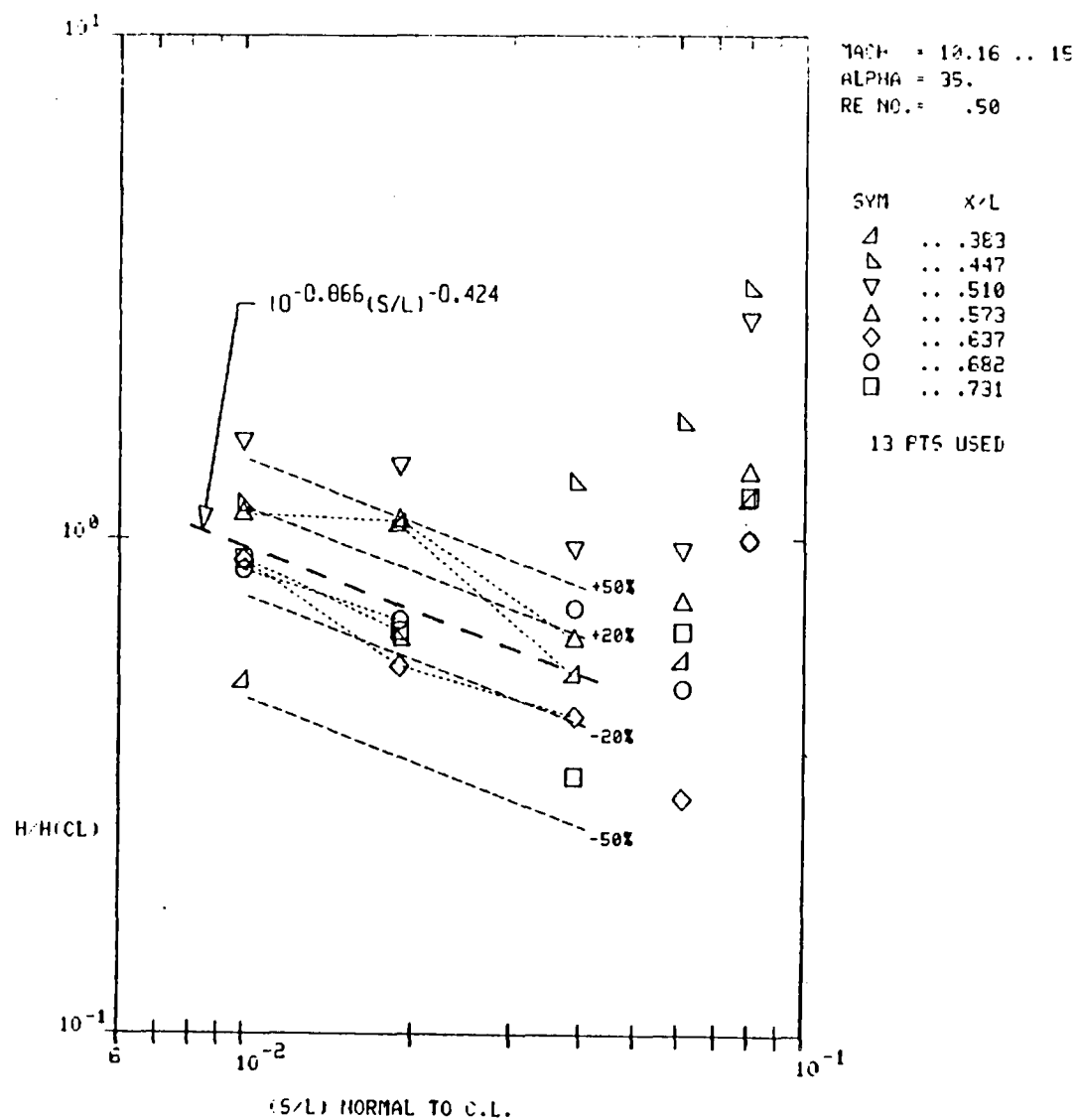


Figure F2d Upper Fuselage Heat Transfer Profiles - Continued

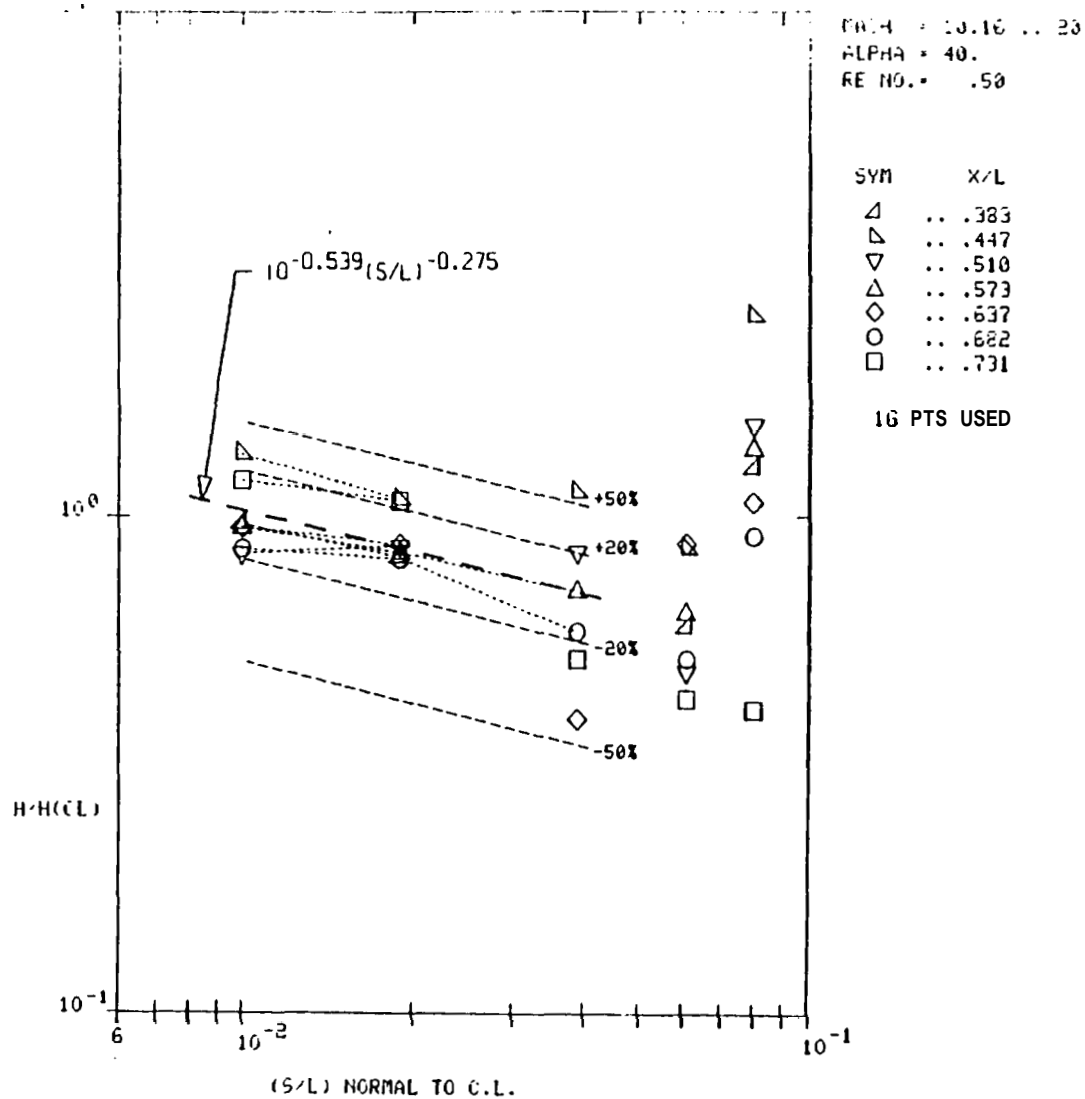


Figure F2e Upper Fuselage Heat Transfer Profiles - concluded

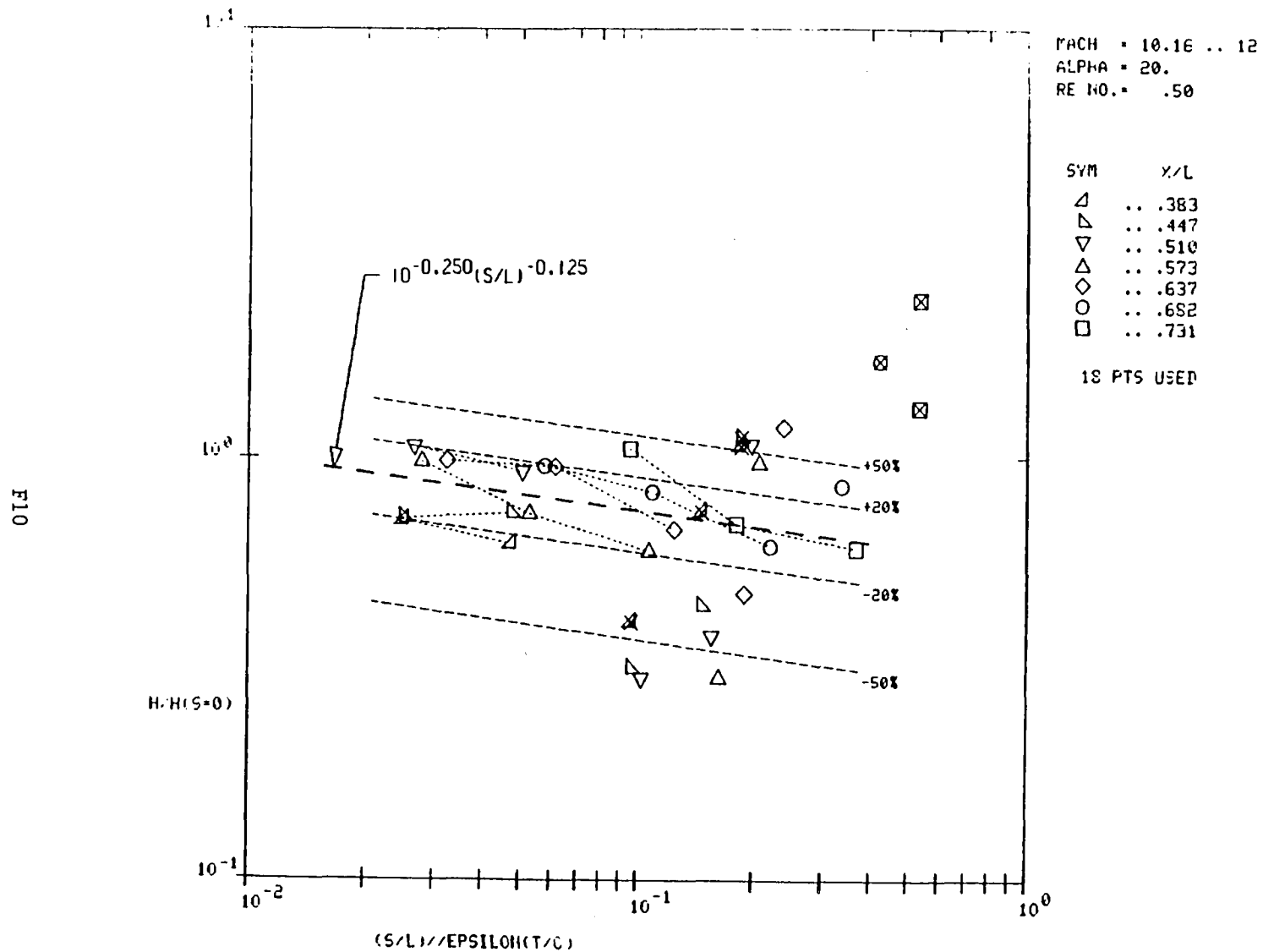


Figure F3a Upper Fuselage Heat Transfer Along Streamlines

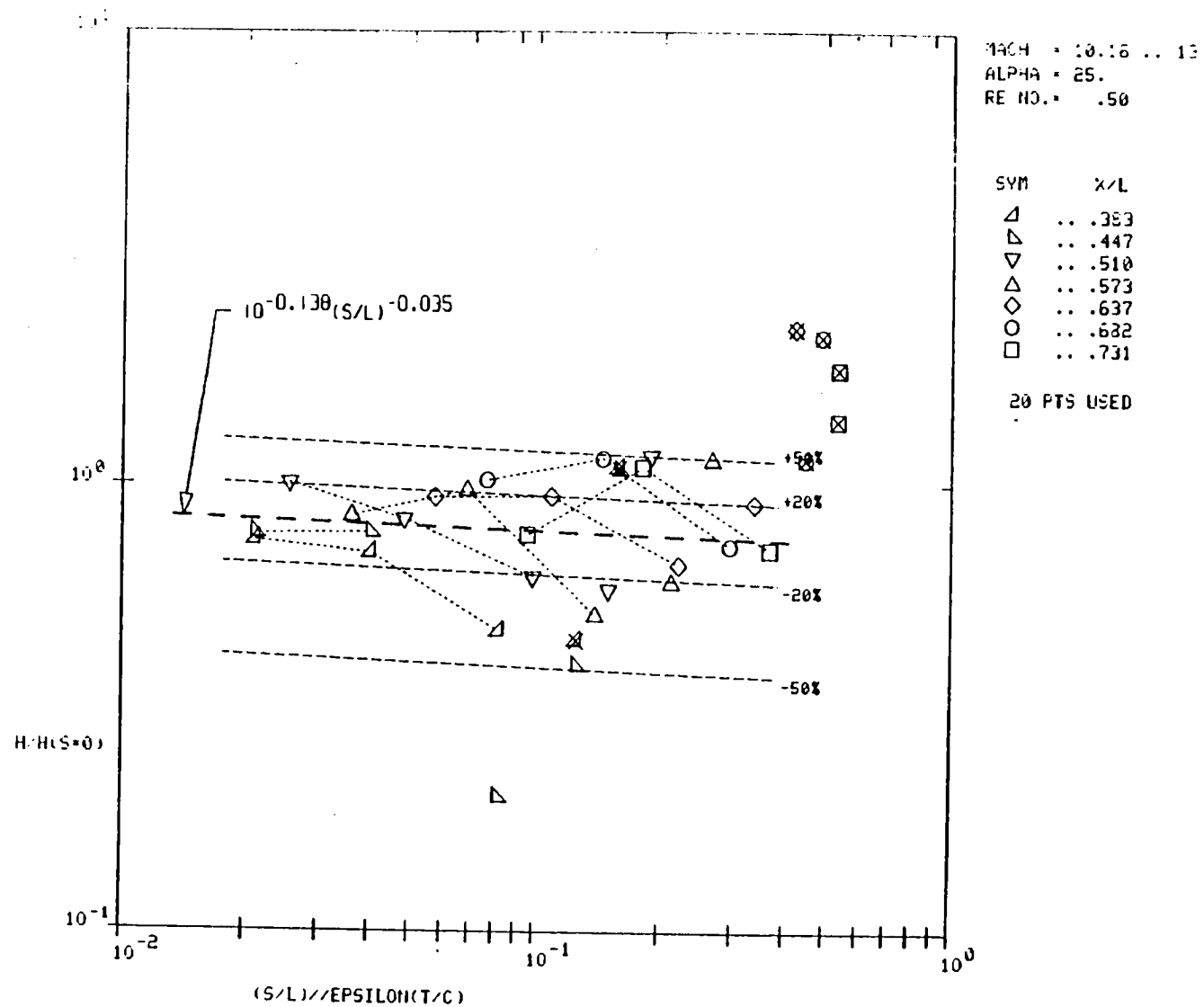


Figure F3b Upper Fuselage Heat Transfer Along Streamlines - Continued

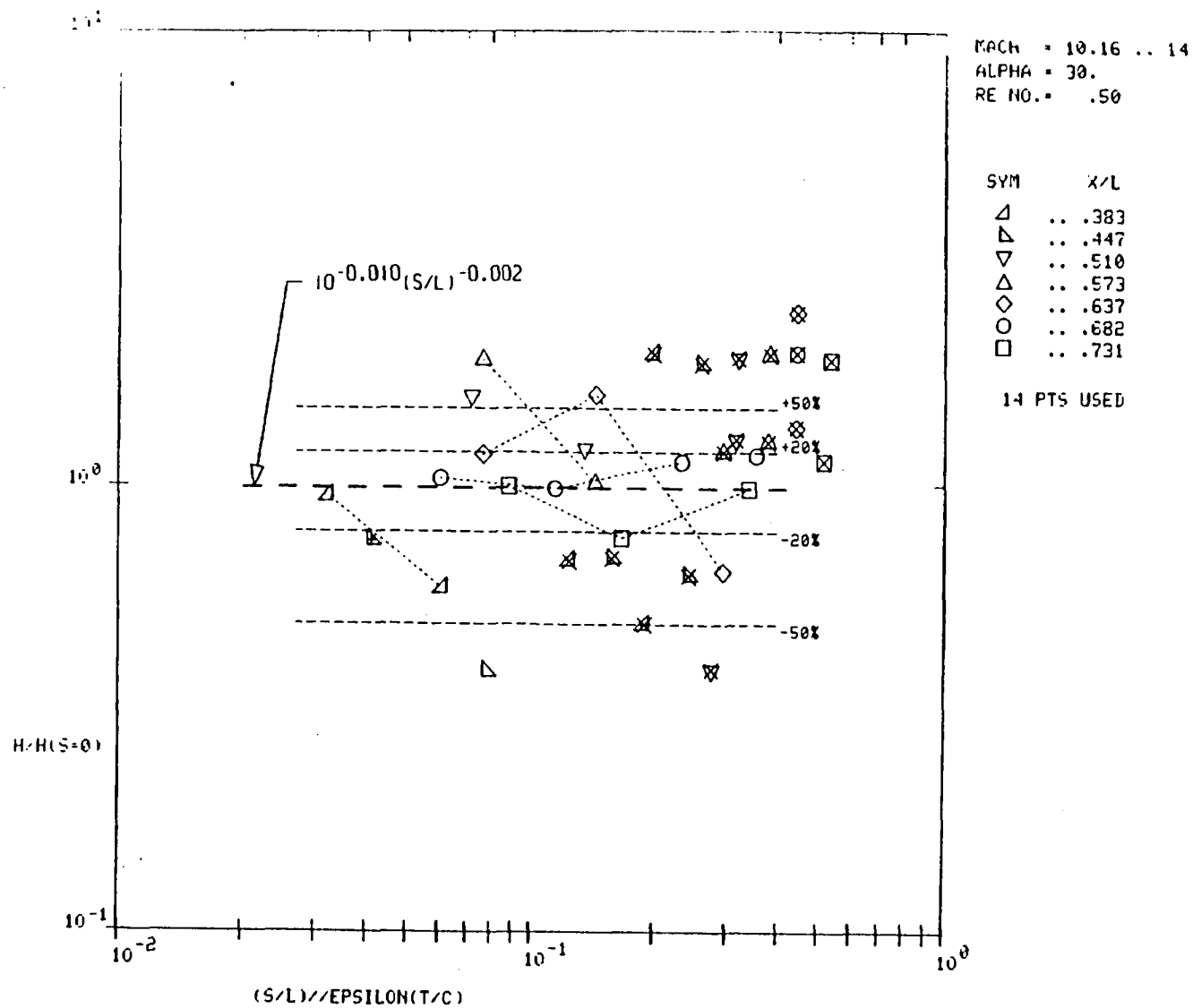


Figure F3c Upper Fuselage Heat Transfer Along Streamlines - Continued

F13

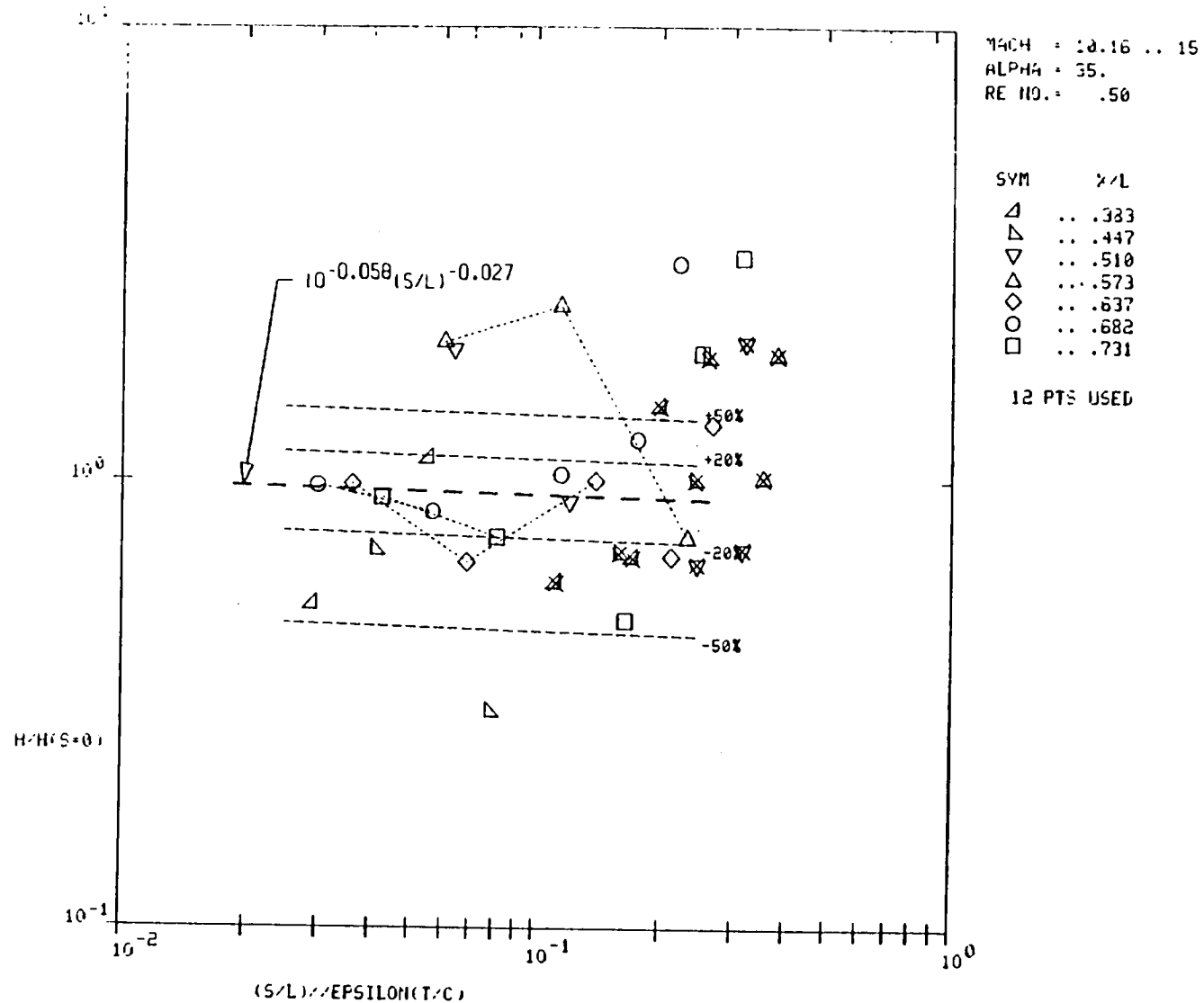


Figure F3d Upper Fuselage Heat Transfer Along Streamlines - Continued

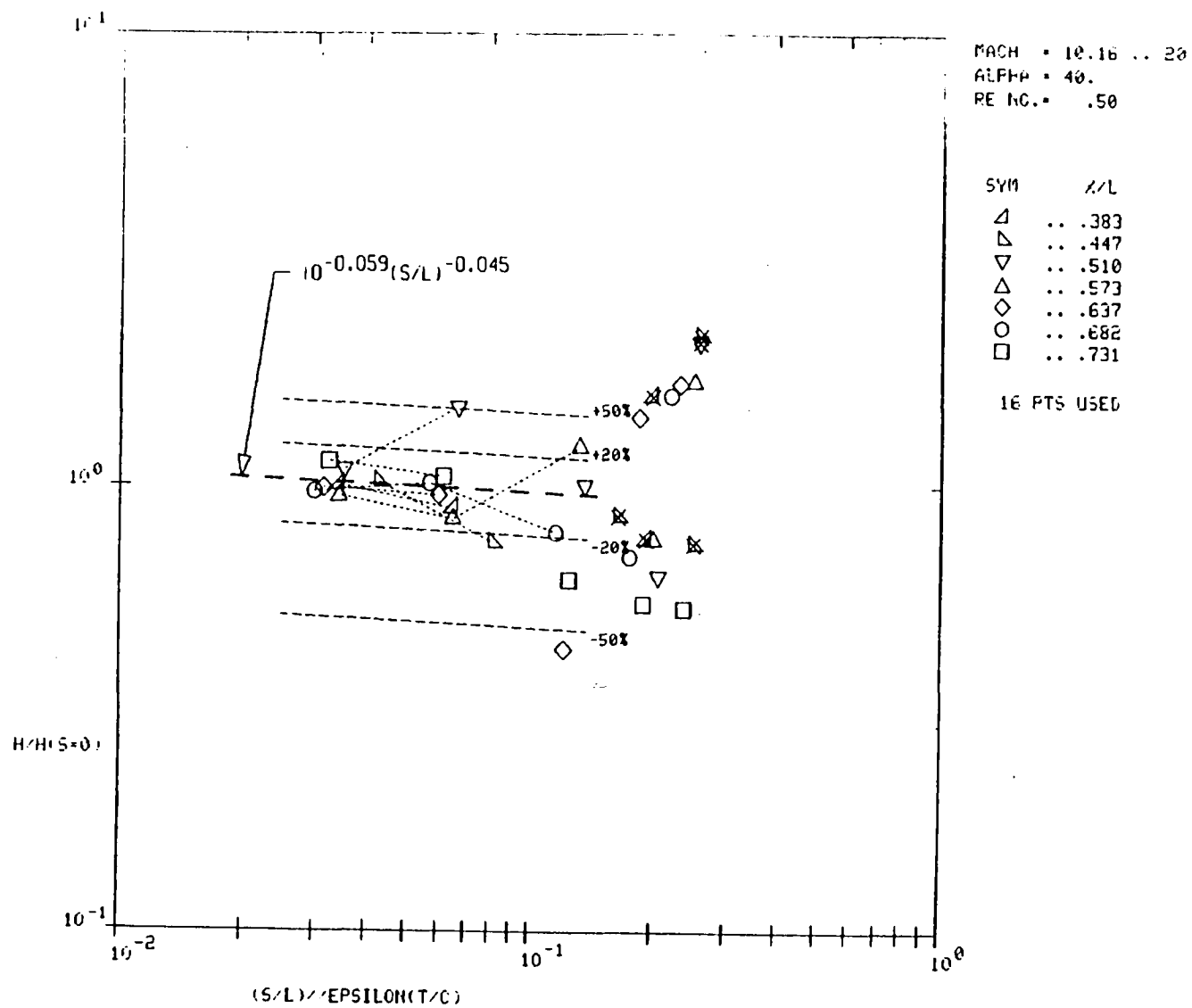


Figure F3e Upper Fuselage Heat Transfer Along Streamlines - Concluded

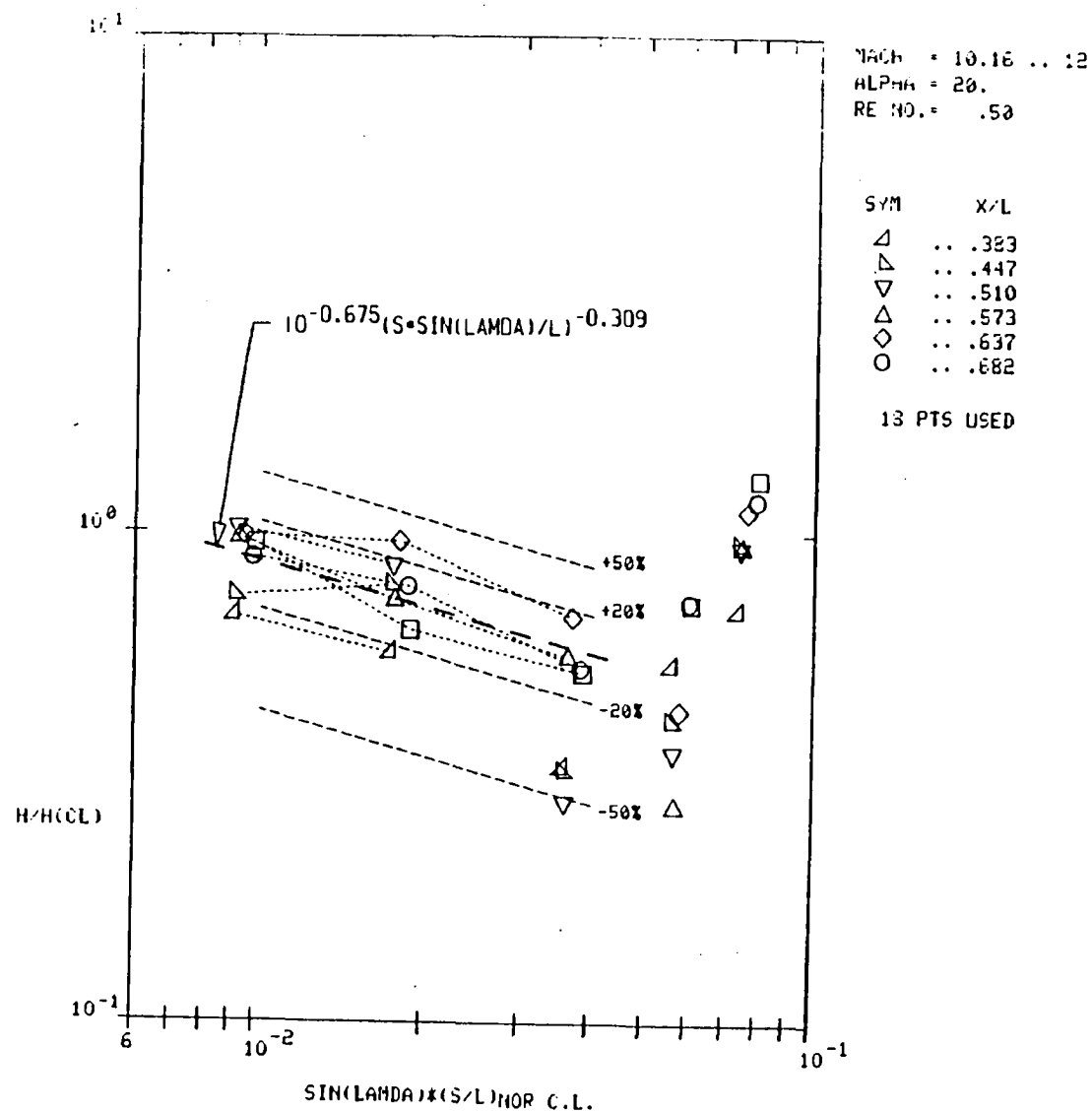


Figure F4a Upper Fuselage Equivalent Swept Cylinder Heating

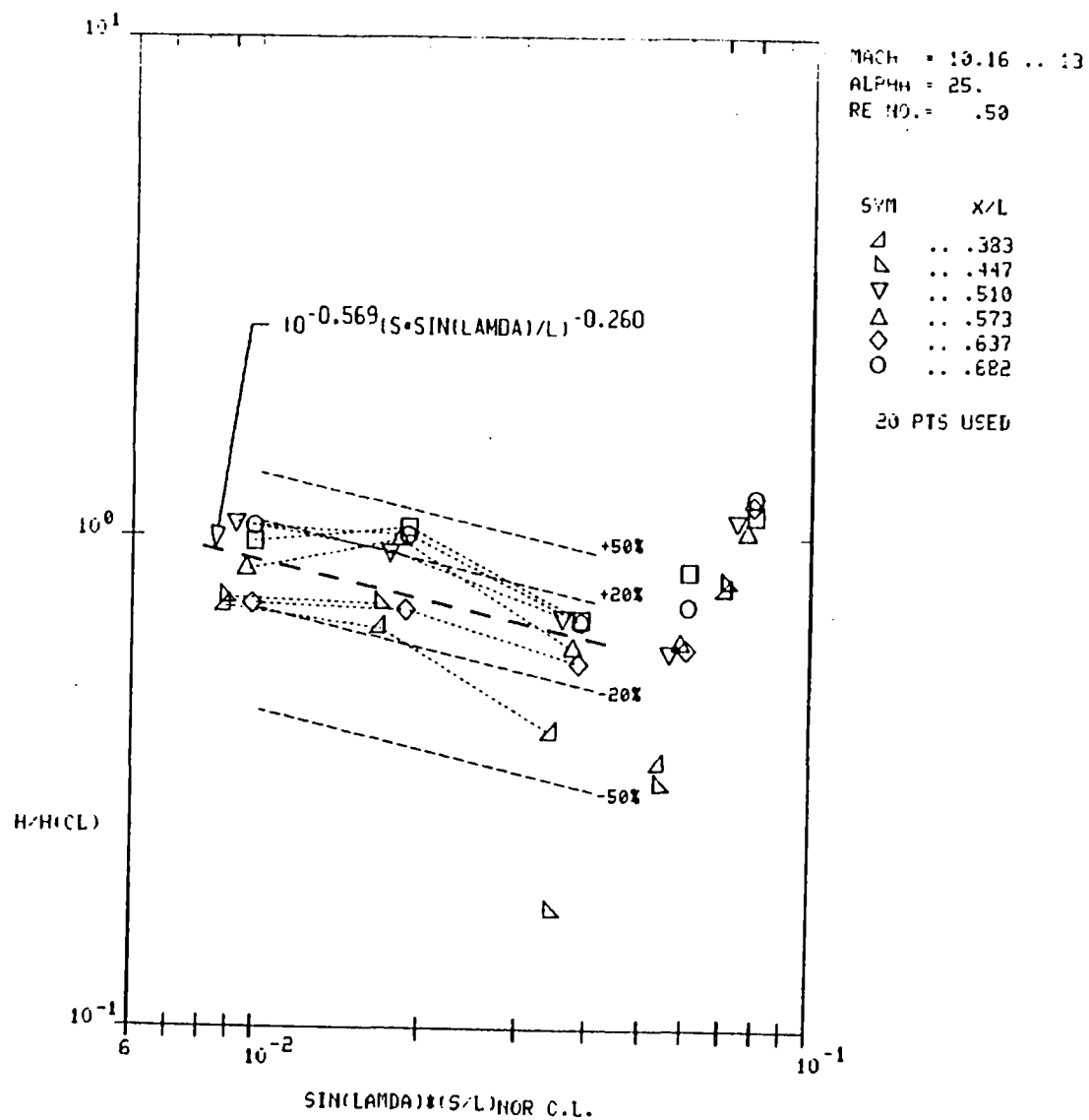


Figure F4b Upper Fuselage Equivalent Swept Cylinder Heating - Continued

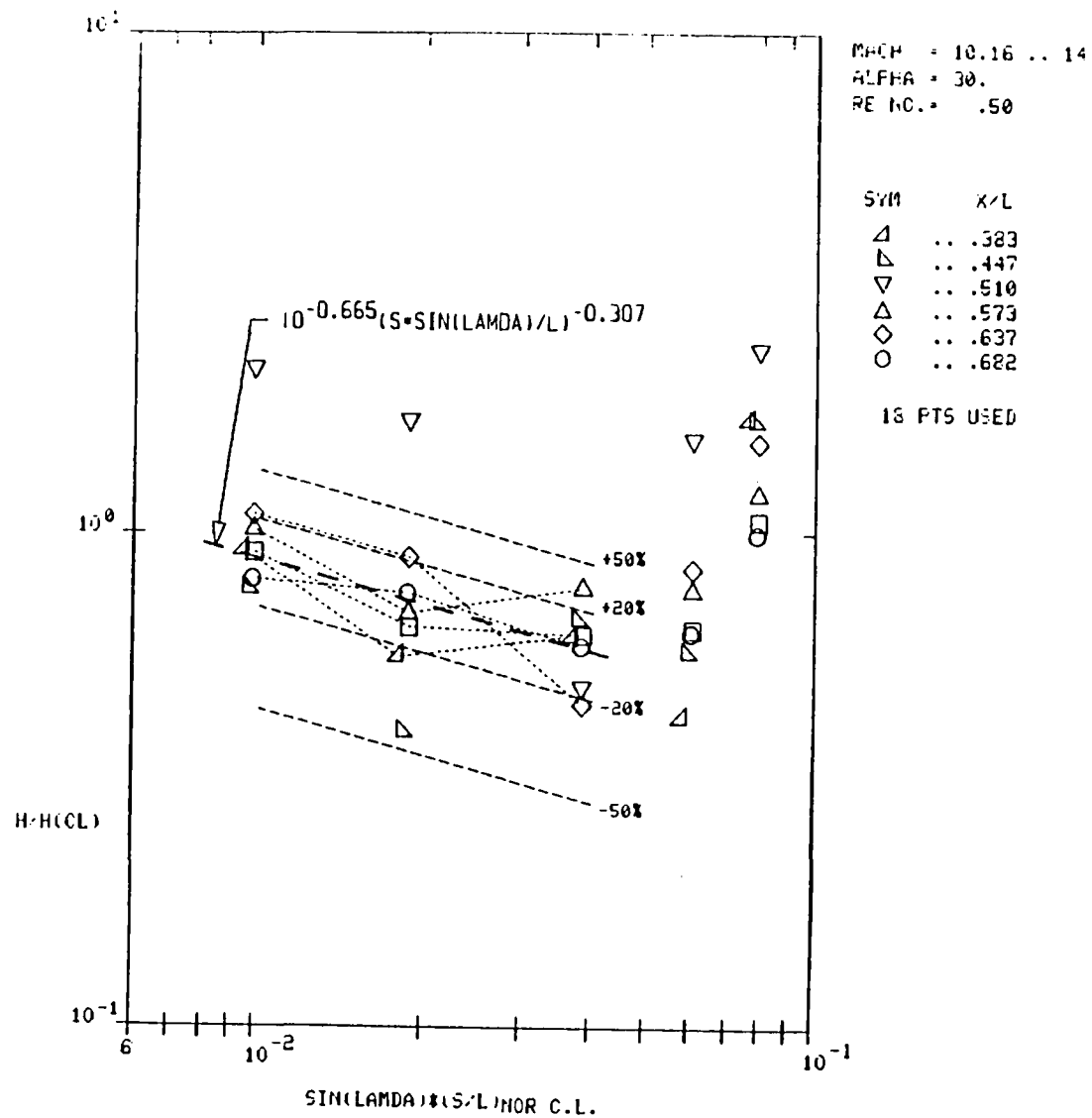


Figure F4c Upper Fuselage Equivalent Swept Cylinder Heating - Continued

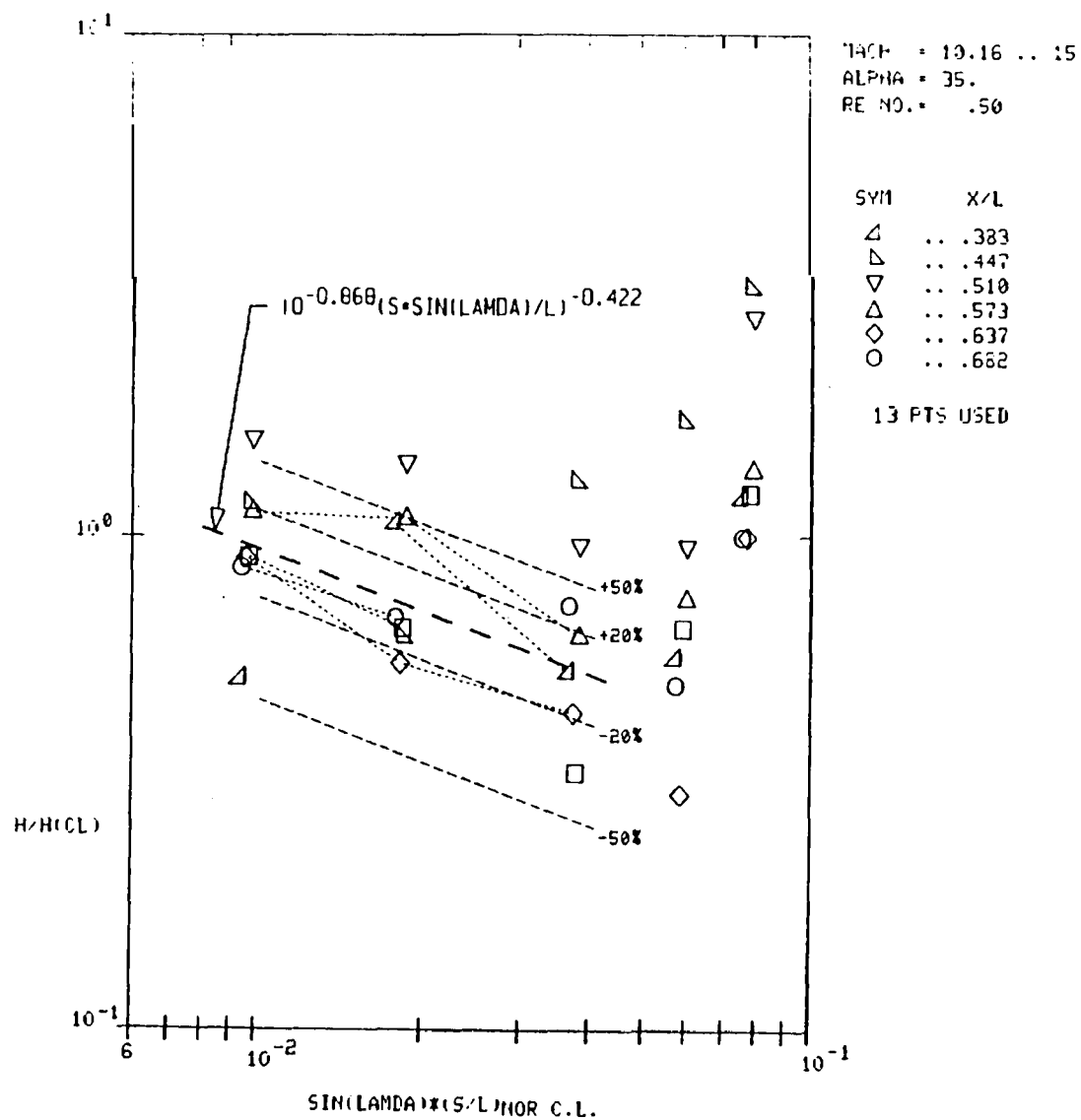


Figure F4d Upper Fuselage Equivalent Swept Cylinder Heating - Continued

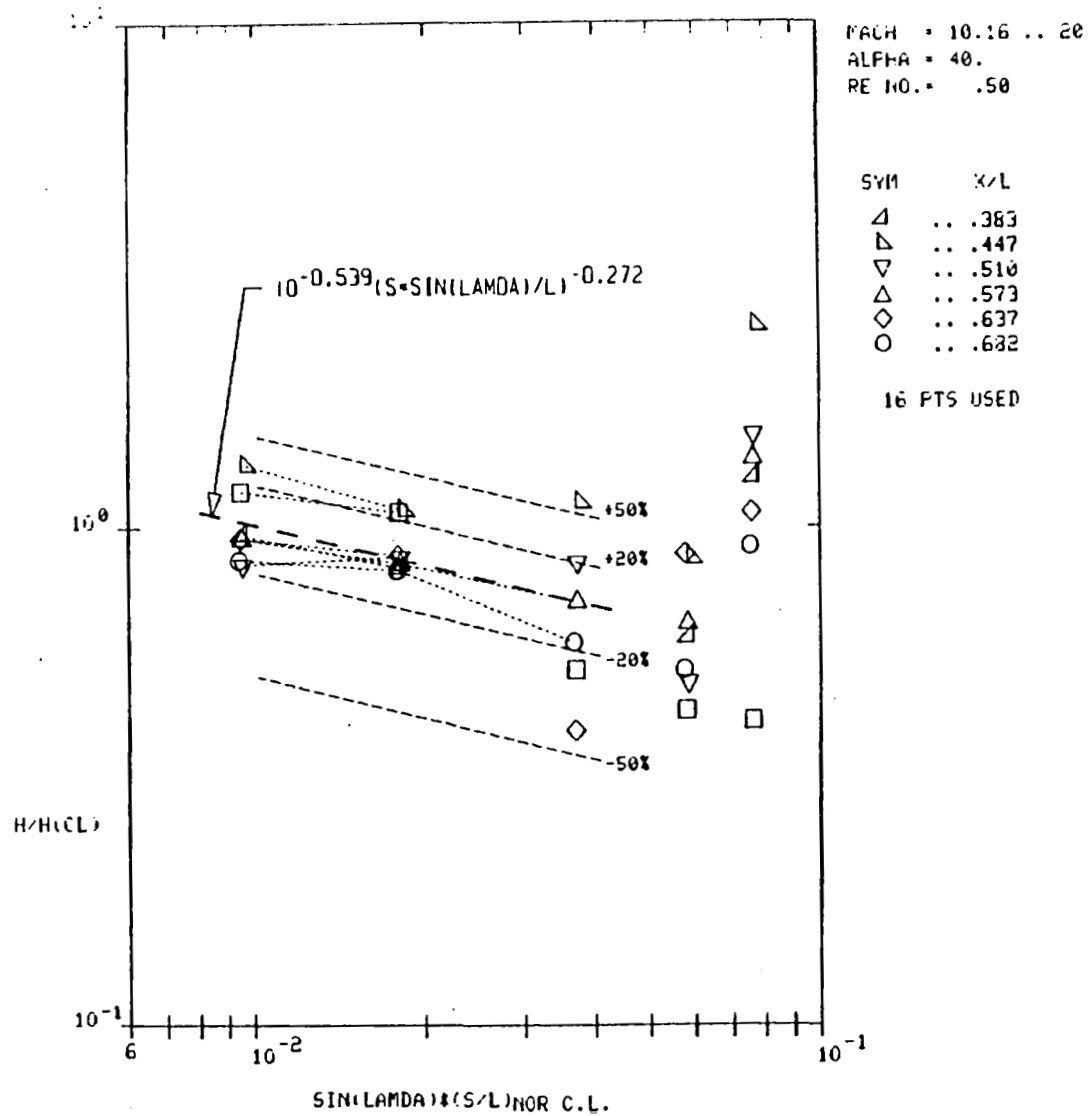


Figure F4e Upper Fuselage Equivalent Swept Cylinder Heating - Concluded

APPENDIX G

Effects of Flow Processing on Heat Transfer

Prepared by H. W. Kipp

The flow field of the Space Shuttle is relatively complex when compared with those of axisymmetric ballistic reentry vehicles. The Shuttle flow is asymmetric and contains embedded shocks, as well as large regions of boundary layer separation and smaller regions of boundary layer reattachment. For these reasons, a very simple analytical investigation was performed to determine the effects of shock strength, flow expansion and embedded shocks on heat transfer to a reference sphere. The calculations were performed for ideal air having $\gamma = 1.4$. The conclusions derived from these results are applicable to leading edges affected by the bow shock. The results illustrate the importance of local flow conditions to the calculation of heat transfer.

Figure G1 illustrates the simple flow geometry employed in the calculations. Essential features are:

- 1) Freestream flow of specified M_∞ , P_∞ and T_∞ (the effects of P_∞ and T_∞ cancel during the calculations). Calculations were performed for values of M_∞ of 4, 6 and 10.
- 2) A bow shock which varies in strength from a normal shock at the nose to a Mach wave. The shock angle, θ_{S1} , was used as an independent variable.
- 3) A shock, $S2$, was considered embedded within the bow shock. The wave angle, θ_{S2} , was also used as an independent variable.
- 4) Flow conditions immediately behind the bow shock were calculated for a range of θ_{S1} values.
- 5) Flow behind the bow shock was permitted to expand to P_∞ . This condition was arbitrarily selected as representative of flow downstream of the bow shock.
- 6) The expanded flow (from Step 5) was recompressed through the embedded shock and conditions immediately downstream of the embedded shock were calculated.
- 7) Flow behind the embedded shock was reexpanded to P_∞ .
- 8) Heat transfer rates to a unit sphere were calculated for the free stream (Step 1) as well as for Steps 4, 5, 6 and 7.
- 9) Heat transfer rates computed in Steps 4, 5, 6 and 7 were normalized to the free stream rate and the normalized results plotted.

Normalized heating rates behind the bow shock and for the re-expanded flow are shown in Figure G2 as functions of bow shock angle θ_{S1} for free stream Mach numbers of 4, 6 and 10. The following observations are drawn from Figure G2.

- For θ_{S1} approaching 90° , normalized reference sphere heating behind the shock is less than for free stream conditions.
- For moderate bow shock angles, reference sphere heating behind the shock is "amplified" above the free stream value and increases with Mach number.
- Heating in the expanded flow is always less than free stream heating and decreases with increasing M_∞ and θ_{S1} .
- The range between the maximum and minimum likely heating rates at any given flight condition is the area between the solid curve and the corresponding dashed curve. Notice that this range increases significantly with Mach number.
- The results in Figure G2 can be used to estimate leading edge heating if the flow direction at the leading edge is known. The local flow direction must be known to determine local wing sweep and local angle of attack. The sweep angle determines the sweep correction and the angle of attack determines the leading edge effective radius.
- If the bow shock intersects the leading edge, the intersection is likely to occur where the shock angle is small (20° - 40°) resulting in high heating. On the other hand, the wing root is likely to intercept flow which has expanded from a large shockwave angle (60° - 90°) resulting in low heating.

Figure G3 illustrates the effects of an embedded leading edge shock on reference sphere normalized heating. The results in this figure were computed for $M_\infty \approx 10$. The flow was assumed to have passed through the bow shock at angles of 30° , 40° , and 50° before passing through the embedded shock. Embedded shock angles of 30° and 40° were considered (this is the appropriate range for Shuttle). The following observations can be made regarding Figure G3.

- Heating rates immediately behind the embedded shock ($S2$) and for the expanded flow ($P = P_\infty$) are both lower than corresponding values downstream of the bow shock. This reduction is attributed to the total pressure loss suffered in traversing the embedded shock.
- Heating rate sensitivity to embedded shockwave angle appears small when compared with $M_\infty = 10$ curves in Figure G2, however the sensitivity compares favorably with the $M_\infty = 4$ curves. A check of the calculations shows that

the Mach numbers preceding the embedded shock range from 4.9 to 6.6, explaining the observed sensitivity.

To what conclusions do the above results lead? Simply this; that in calculating heat transfer there is a need for accurate definition of the flow field surrounding a vehicle. And, the necessity for defining the flow field increases significantly with flight Mach number.

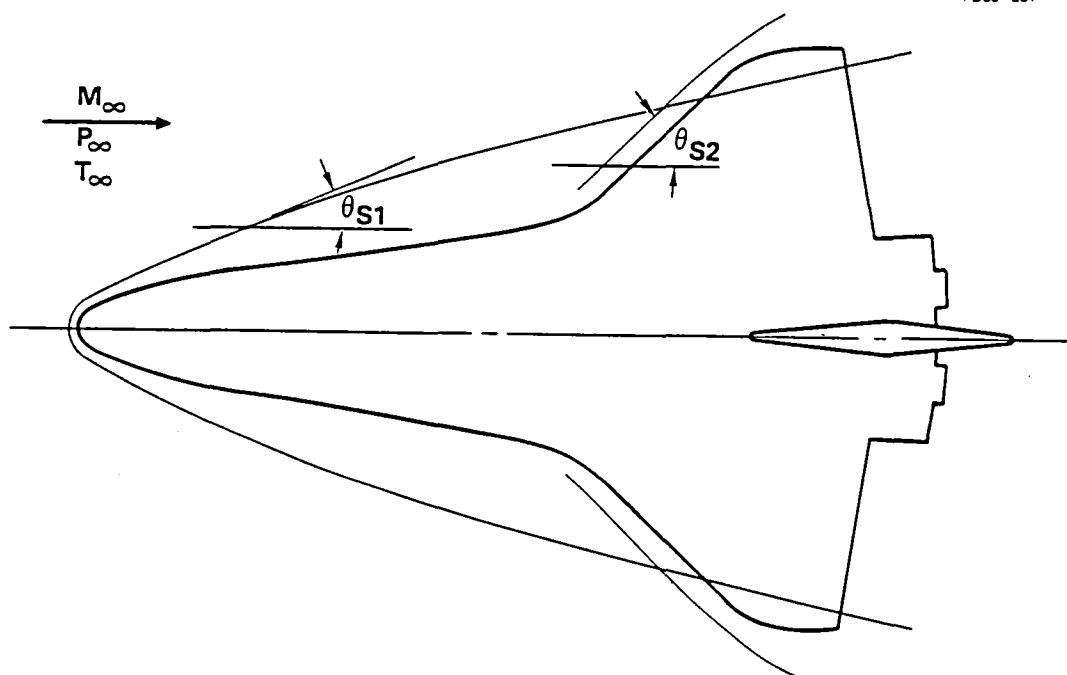


Figure G1 Shock Structure Effect on Wing Heating

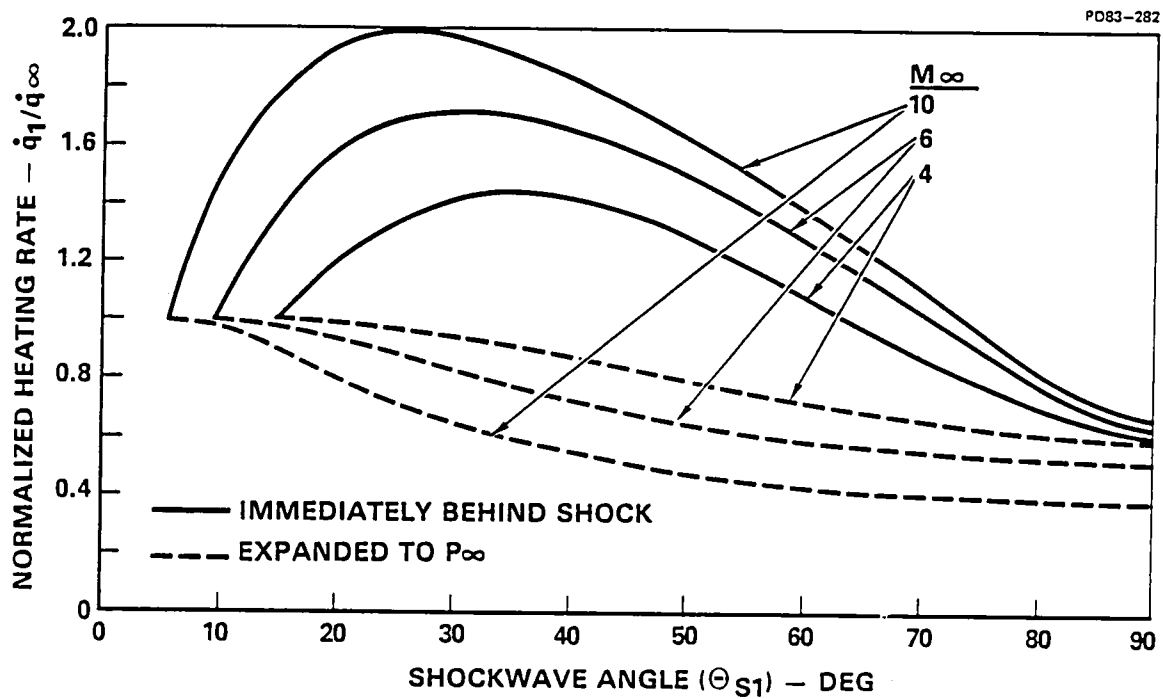


Figure G2 Reference Sphere Heating Downstream of Bow Shock

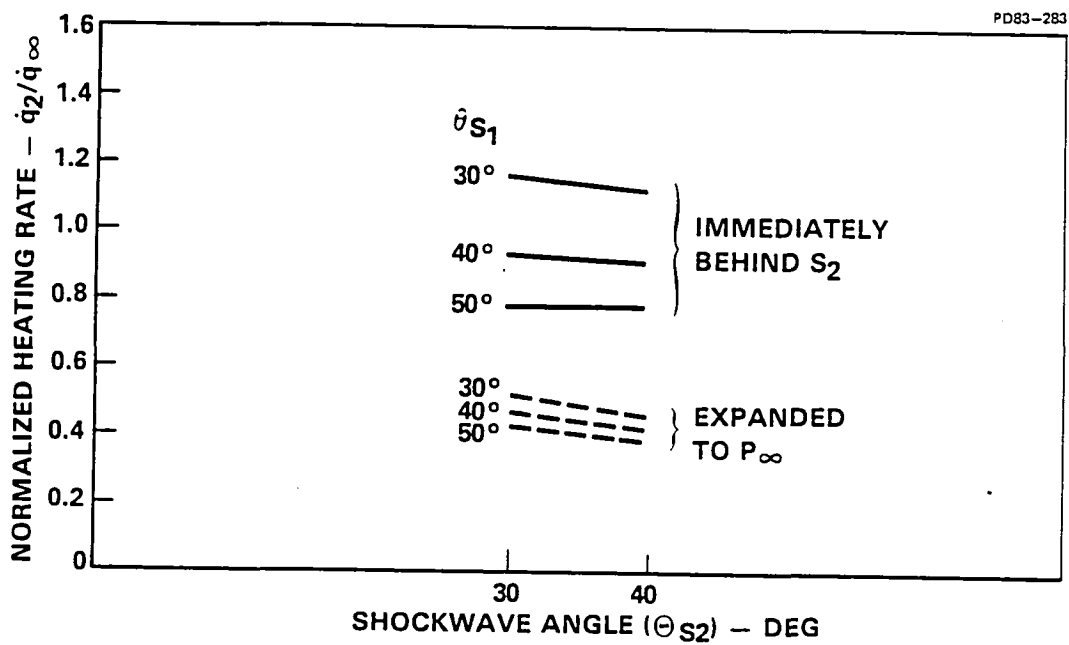


Figure G3 Reference Sphere Heating Downstream of Embedded Shock
 $M_\infty = 10$

APPENDIX H

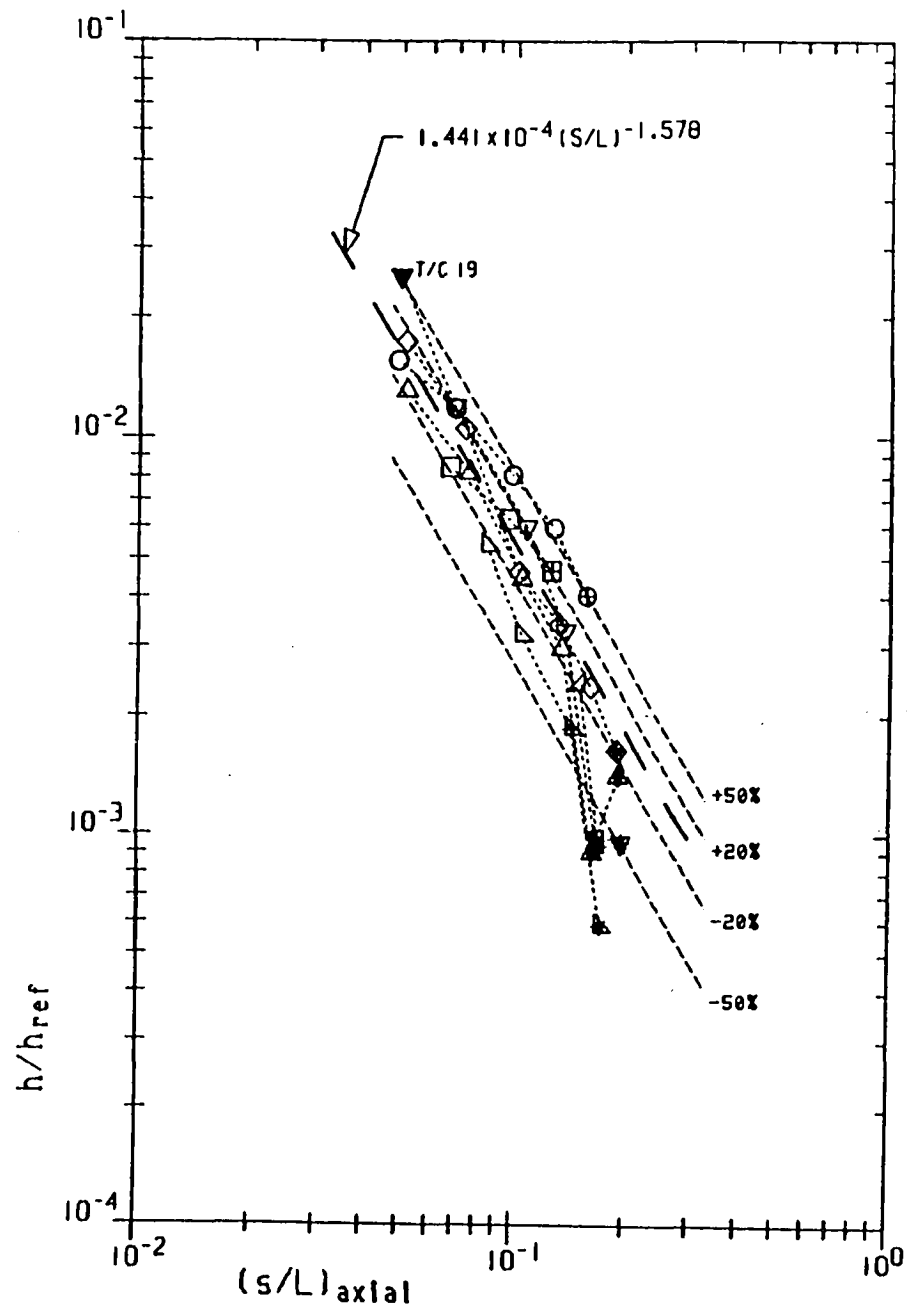
Wing Leaside Surface Heating Correlations

This appendix contains all the correlations of heat transfer distributions for attached flow on the wing leaside surface.

All the attached and pre-separated flow data, even those considered affected by shock interactions, are shown. Most of the separated flow data have been omitted since they were not used in formulating the correlations. These figures also include curves for +20% and +50% deviations from the correlation curve-fits.

A guide for the state of the flow at individual locations is given for each test condition. The guide consists of symbols for the rows (of constant Y/L) of the location and code numbers for the state of local flow, defined by an accompanying legend. The numbers for the associated locations are arranged in a pattern similar to the lay-out of instrumentation shown in Figure 3 of the main text.

This guide also shows the number of data points in each row used to compute the logarithmic least-squares curve fit and the root-mean-square deviation of these data from the correlation.



$M_\infty = 9.02 \dots$
 $\alpha = 20^\circ$
 $Re_L = 0.550 \times 10^6$

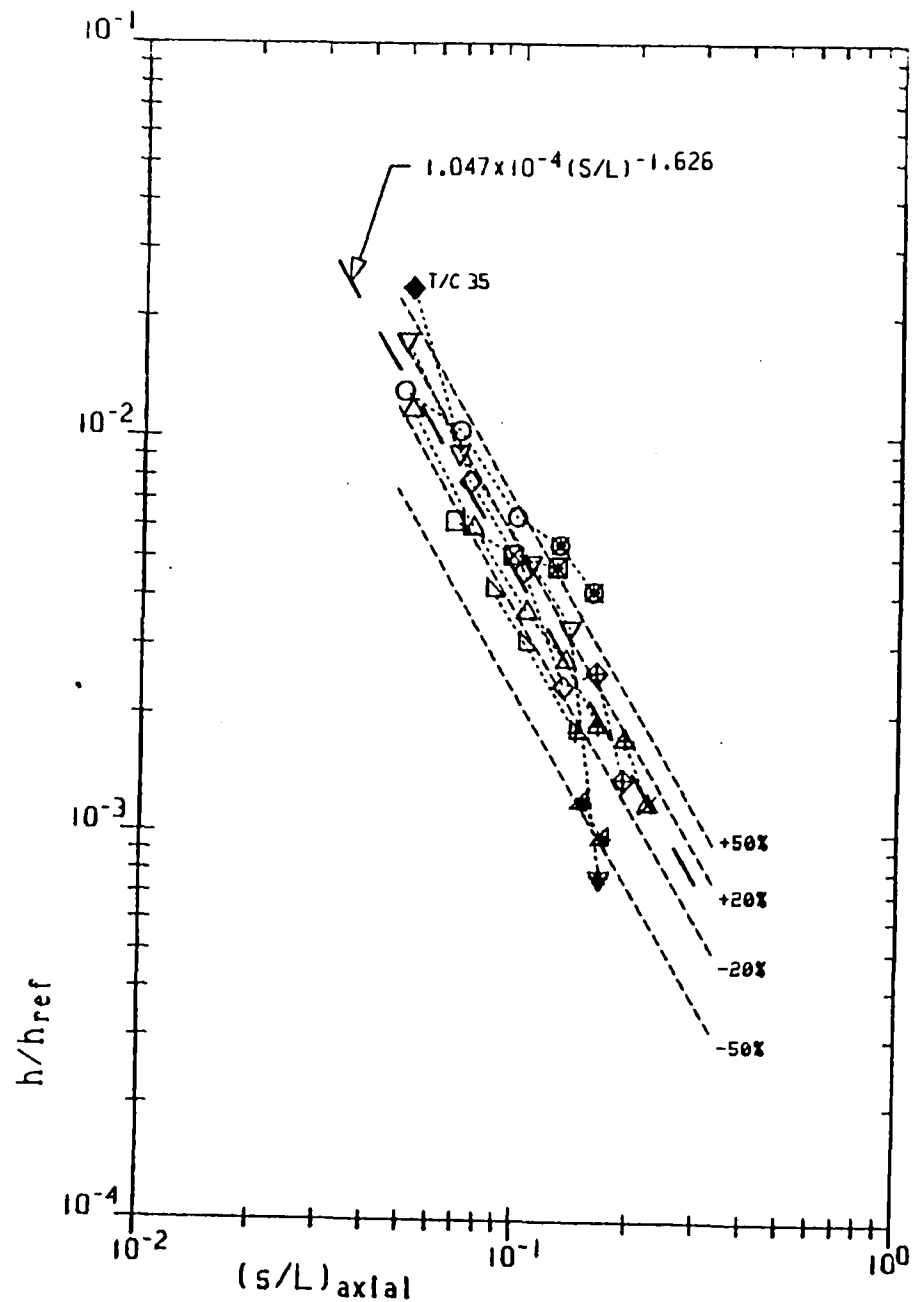
SYM γ/L

\triangle	.1405 .. 1	1-2 0 0 0 0 0 0 0
∇	.1719 .. 3	1 1 2-2 0 0 0 0 0
∇	.2034 .. 3	-4 1 1 1-2-2 0 0 0
\triangle	.2349 .. 4	1 1 1 1-2-2 0
\diamond	.2653 .. 5	1 1 1 1 1-2
\circ	.2978 .. 5	1 1 1 1 2
\square	.3278 .. 3	1 1 2

0 • SEPARATED
 1 • ATTACHED
 2 • PRESEPARATED
 4 • STRAKE SHOCK?
 - - - NOT USED - USUALLY DATA ANOMOLY

24 PTS USED

RMS DEV = 25.85 %



$$M_{\infty} = 9.82 \dots 2$$

$$\alpha = 25.$$

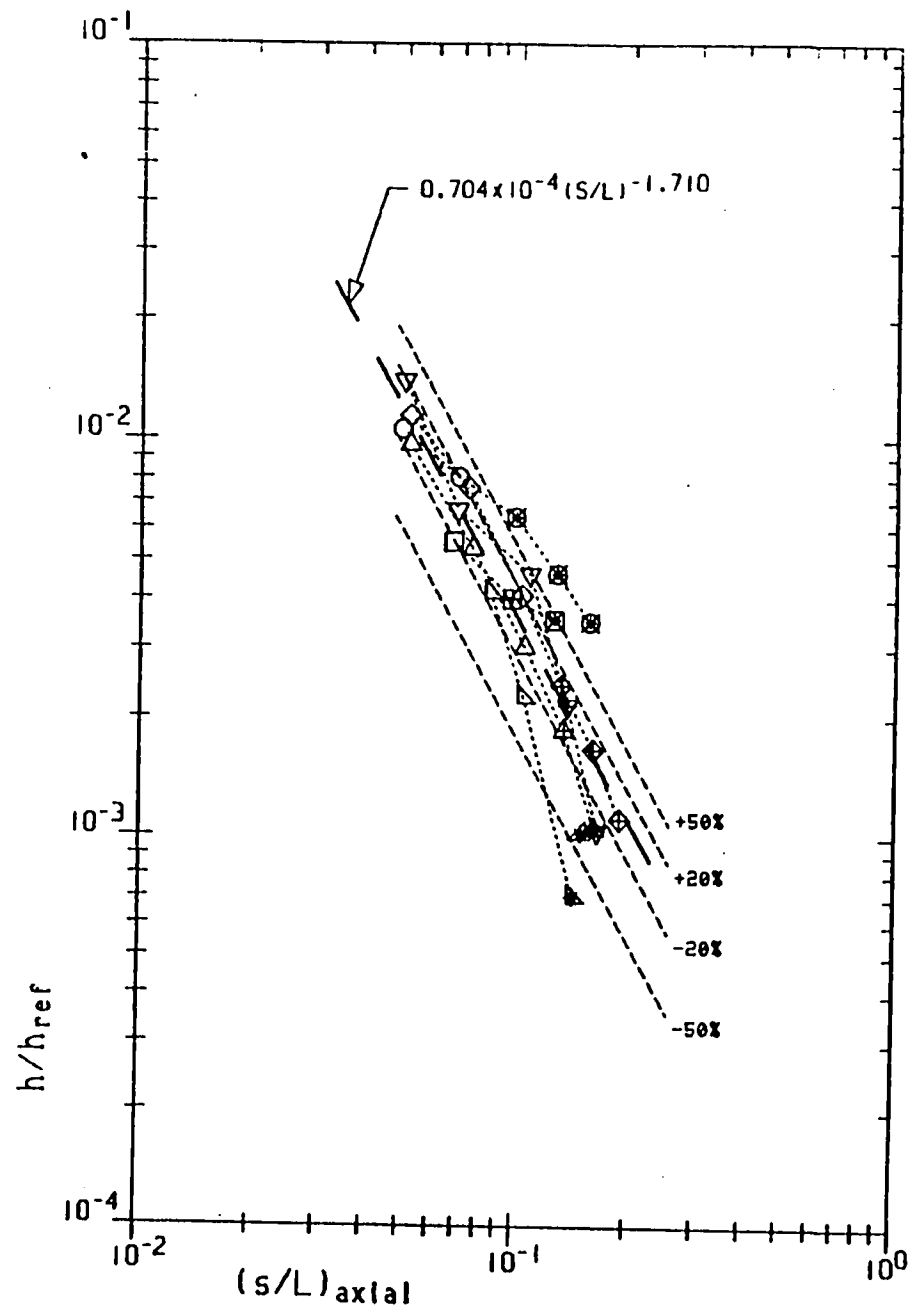
$$Re_L = 0.550 \times 10^6$$

SYM	Y/L	
△	.1405	-2-2 0 0 0 0 0 0 0
△	.1719 .. 3	1 1 2-2 0 0 0 0 0
▽	.2034 .. 4	1 1 1 1-2 0 0 0 0
△	.2349 .. 6	1 1 1 1 2 2-8
◇	.2653 .. 5	-4 1 1 1 2 2
○	.2978 .. 3	1 1 1-3-3
□	.3278 .. 2	1 3-3

- 0 = SEPARATED FLOW
- = 1 = ATTACHED FLOW
- ⊕ = 2 = PRESEPARATED FLOW
- ⊗ = 3 = ANOMOLOUS FLOW
- = 4 = STRAKE SHOCK?
- ⊠ = 8 = SEPARATED, NOT USED BUT SHOWN
- ⊞ = NOT USED - USUALLY DATA ANOMOLY

23 PTS USED

RMS DEV = 20.85 %



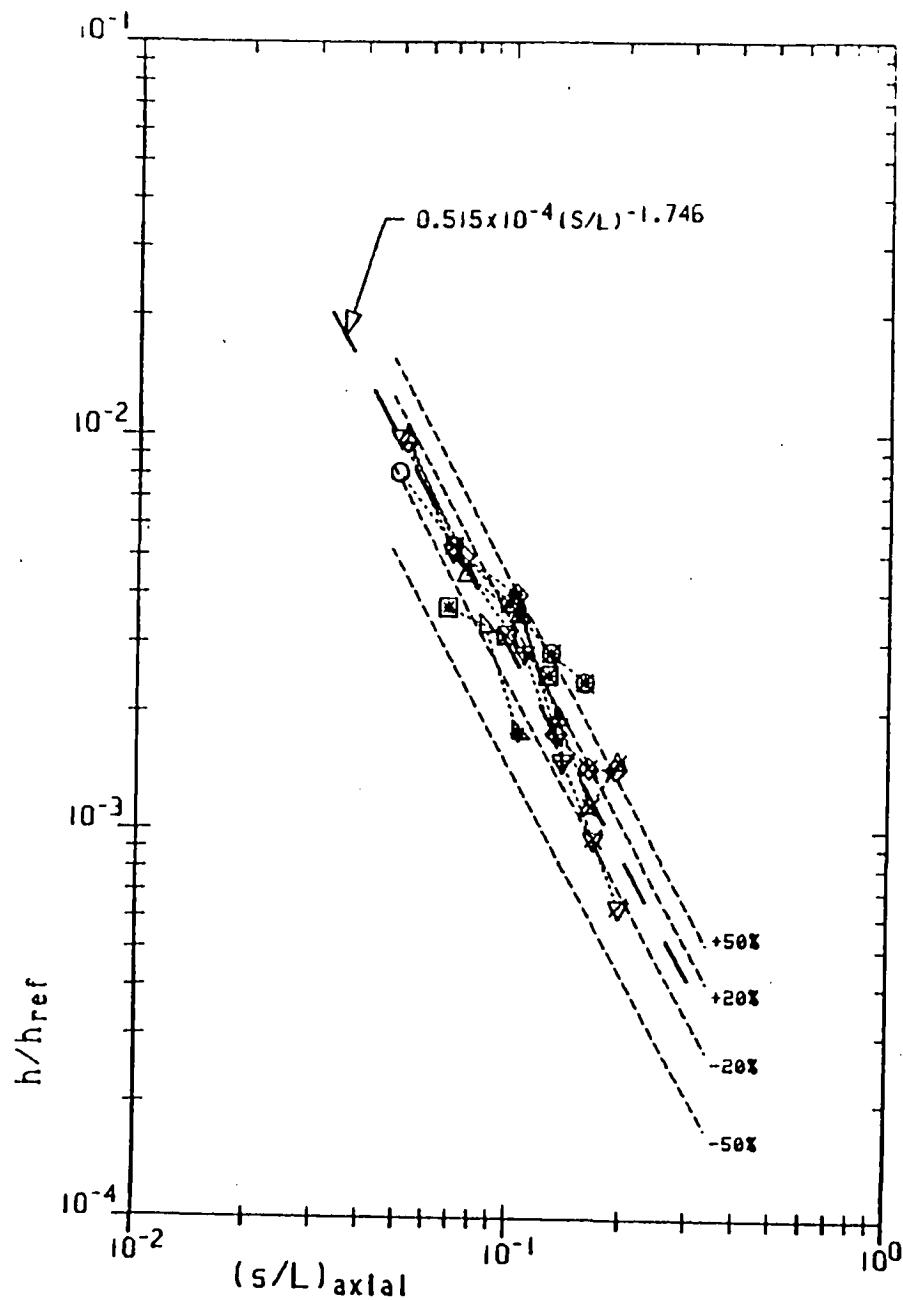
$M_\infty = 9.82 \dots 4$
 $\alpha = 30.$
 $Re_L = 0.550 \times 10^6$

SYM	Y/L	
\triangle	.1405	-2-2 0 0 0 0 0 0 0
∇	.1719 .. 2	1 1-2 0 0 0 0 0 0
\triangle	.2034 .. 4	1 1 1 2-8 0 0 0 0
\triangle	.2349 .. 4	1 1 1 2-2 0 0
\diamond	.2653 .. 6	1 1 1 2 2 2
\circ	.2978 .. 2	1 1-3-3-3
\square	.3278 .. 2	1 2-3

0 = SEPARATED FLOW
 1 = ATTACHED FLOW
 2 = PRESEPARATED FLOW
 3 = ANOMOLOUS FLOW
 8 = SEPARATED, NOT USED BUT SHOWN
 - - - NOT USED - USUALLY DATA ANOMOLY

20 PTS USED

RMS DEV = 17.72 %



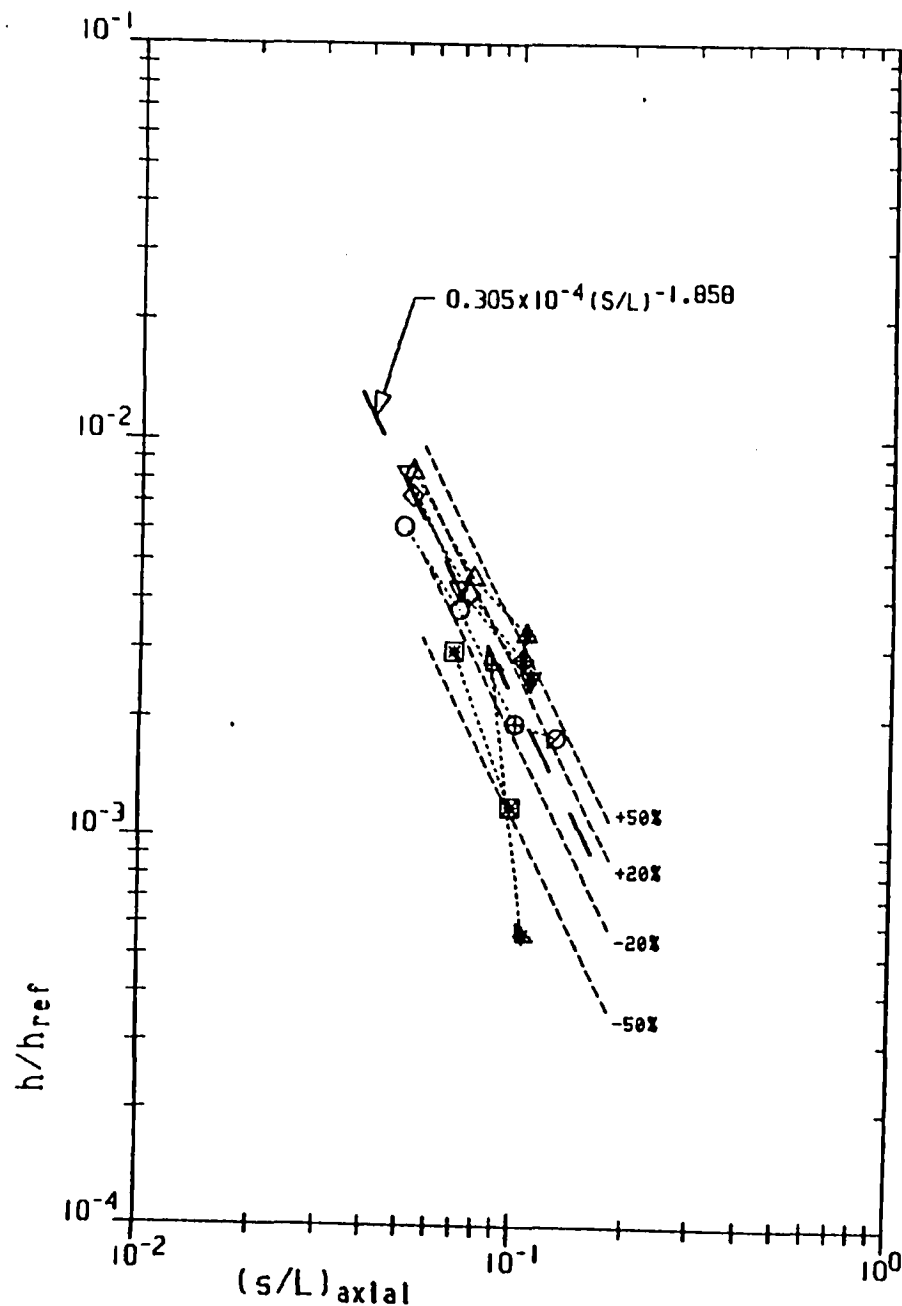
$M_\infty = 9.82 \dots 5$
 $\alpha = 35^\circ$
 $Re_L = 0.550 \times 10^6$

SYM	Y/L	
\triangle	.1405	0 0 0 0 0 0 0 0 0
∇	.1719 .. 1	1-2 0 0 0 0 0 0 0
\triangle	.2034 .. 5	1 1 2 2 3-8 0 0 0
\triangle	.2349 .. 4	1 1-1 2 3-8 0
\diamond	.2653 .. 4	1 1-1 2 3-8
\circ	.2978 .. 2	1 3-3-3-3
\square	.3278 .. 1	-1 3-3

0 = SEPARATED
 1 = ATTACHED
 2 = PRESEPARATED
 3 = ANOMOLOUS
 8 = SEPARATED, NOT USED BUT SHOWN
 - - - NOT USED - USUALLY DATA ANOMOLY

17 PTS USED

RMS DEV = 10.62%



$M_\infty = 9.82 \dots 6$
 $\alpha = 40.$
 $Re_L = 0.550 \times 10^6$

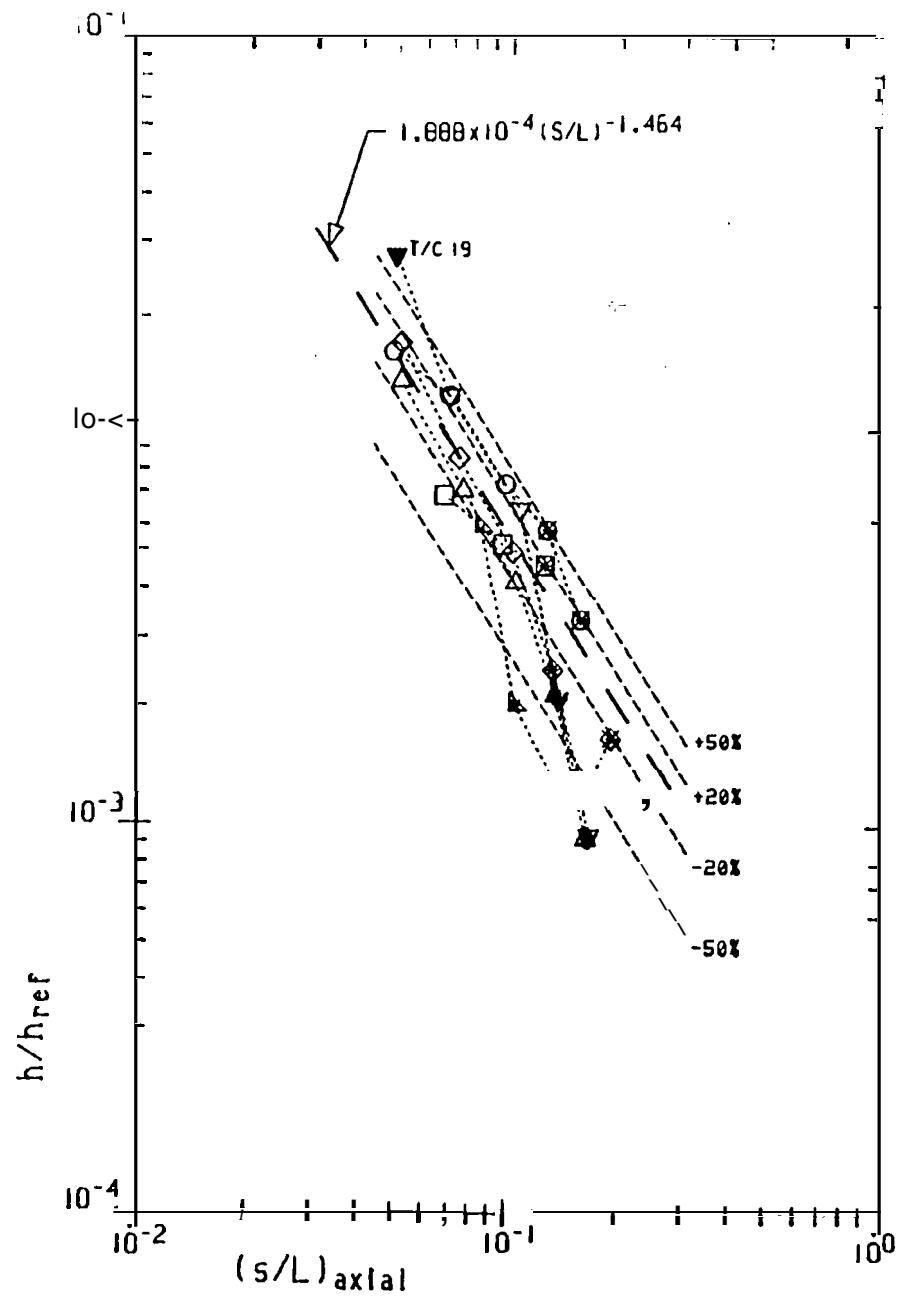
SYM Y/L

\triangle	.1405	0 0 0 0 0 0 0 0 0
∇	.1719 .. 1	2-2 0 0 0 0 0 0 0
\triangle	.2034 .. 2	1 1-2 0 0 0 0 0 0
\triangle	.2349 .. 2	1 1-2 0 0 0 0 0
\diamond	.2653 .. 2	1 1-2 0 0 0 0
\circ	.2978 .. 3	1 1 2-8 0
\square	.3278	-1-3 0

0 • SEPARATED FLOW
 1 • ATTACHED FLOW
 2 • PRESEPARATED FLOW
 3 • ANOMOLOUS FLOW
 8 • SEPARATED, NOT USED BUT SHOWN
 - - - NOT USED - USUALLY DATA ANOMOLY

10 PTS USED

RMS DEV = 14.39 %



$M_\infty = 9.98 \dots 8$
 $\alpha = 20.$
 $Re = 1.070 \times 10^6$

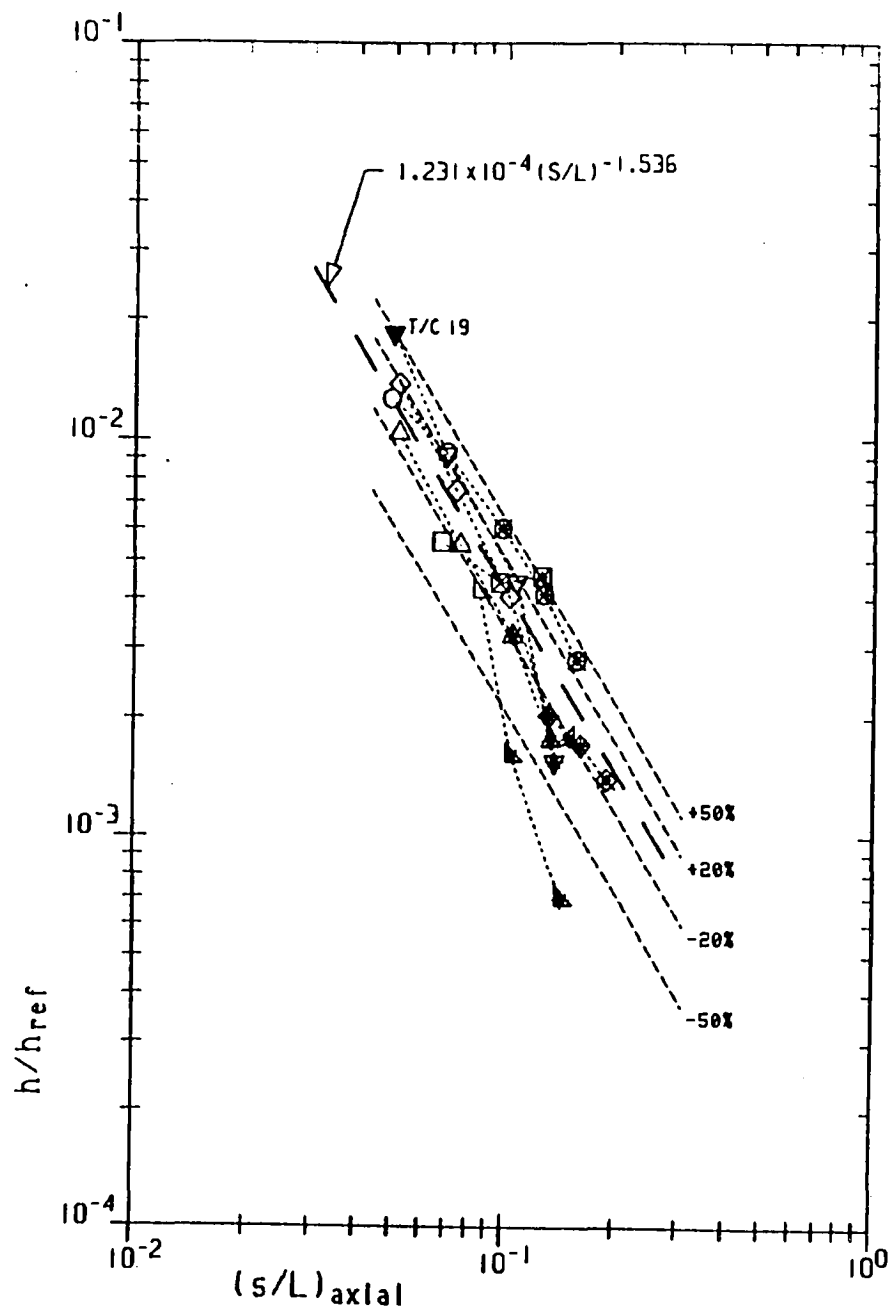
SYM Y/L

△	.1405	-2 0 0 0 0 0 0 0
▽	.1719 .. 1	1-1-2 0 0 0 0 0
▽	.2034 .. 2	-4 1 1-2-2 0 0 0
△	.2349 .. 3	1 1 1-2-2 0 0
◇	.2653 .. 3	1 1 1-1-3-3
○	.2978 .. 3	1 1 1-3-3
□	.3278 .. 2	1 1-3

0 • SEPARATED FLOW
 □ • 1 • ATTACHED FLOW
 ⊞ • 2 • PRESEPARATED FLOW
 ⊠ • 3 • ANOMOLOUS FLOW
 ● • 4 • STRAKE SHOCK?
 ⊞ • - - - NOT USED - USUALLY DATA ANOMOLY

14 PTS USED

RMS DEV = 19.891



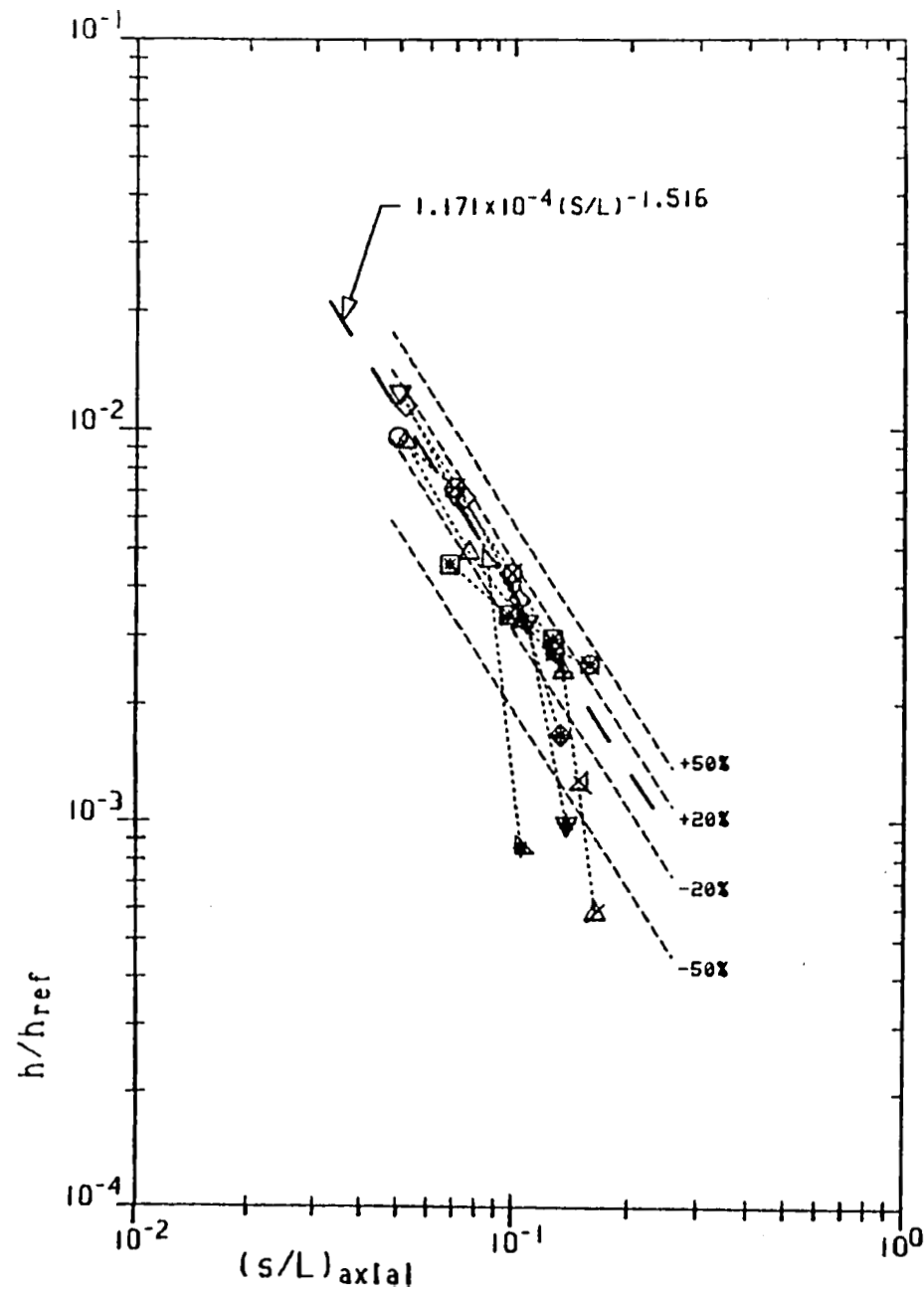
$M_\infty = 9.98 \dots 10$
 $\alpha = 25^\circ$
 $Re_L = 1.070 \times 10^6$

SYM	Y/L	
\triangle	.1405	-2 0 0 0 0 0 0 0 0
∇	.1719 .. 1	1-1-2 0 0 0 0 0 0
\triangle	.2034 .. 2	-4 1 1-2 0 0 0 0 0
\triangle	.2349 .. 2	1 1-2-2 0 0 0
\diamond	.2653 .. 3	1 1 1-2-2-3
\circ	.2978 .. 2	1 1-3-3-3
\square	.3278 .. 2	1 3-3

0 = SEPARATED FLOW
 1 = ATTACHED FLOW
 2 = PRESEPARATED FLOW
 3 = ANOMOLOUS FLOW
 4 = STRAKE SHOCK?
 - - - NOT USED - USUALLY DATA ANOMOLY

12 PTS USED

RMS DEV = 18.72 %



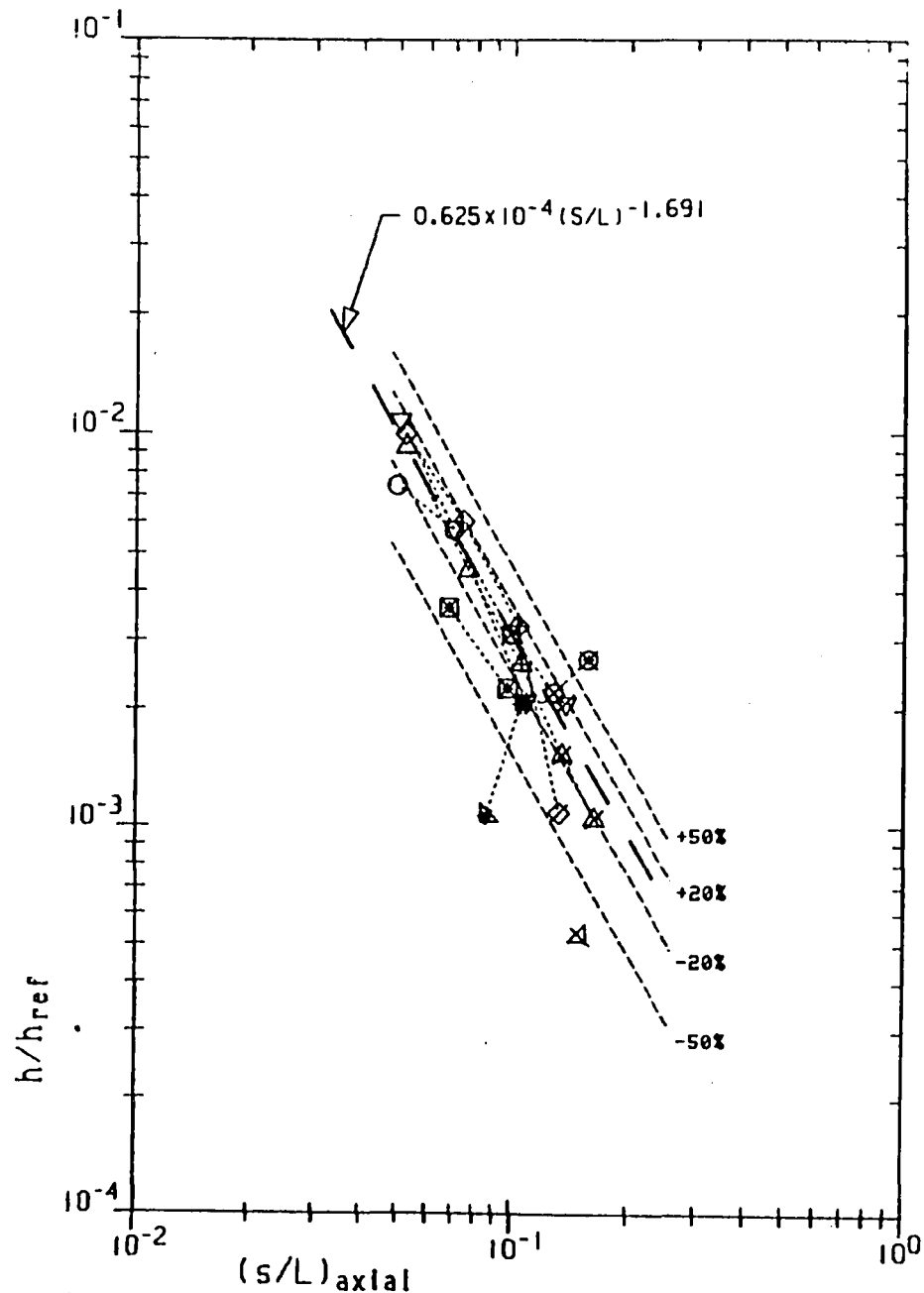
$M_\infty = 9.90 \dots 12$
 $\alpha = 30^\circ$
 $Re_s = 1.030 \times 10^6$

SYM	Y/L	
\triangleleft	.1405	-8 0 0 0 0 0 0 0 0
\triangleleft	.1719 .. 1	1-2 0 0 0 0 0 0 0
∇	.2034 .. 3	1 1 2-2 0 0 0 0 0
\triangle	.2349 .. 4	1 1 2 2-8 0 0 0
\diamond	.2653 .. 3	1 1 1-2 0 0 0
\circ	.2978 .. 4	1 3 3 3-3
\square	.3278	-1-3-3

8 • SEPARATED
 1 • ATTACHED
 ? • PRESEPARATED
 3 • ANOMOLOUS
 8 • SEPARATED. NOT USED BUT SHOWN
 -'- NOT USED - USUALLY DATA ANOMOLY

15 PTS USED

RMS DEV = 9.58 %



$M_{\infty} = 9.98 \dots 14$
 $\alpha = 35.$
 $Re_L = 1.050 \times 10^6$

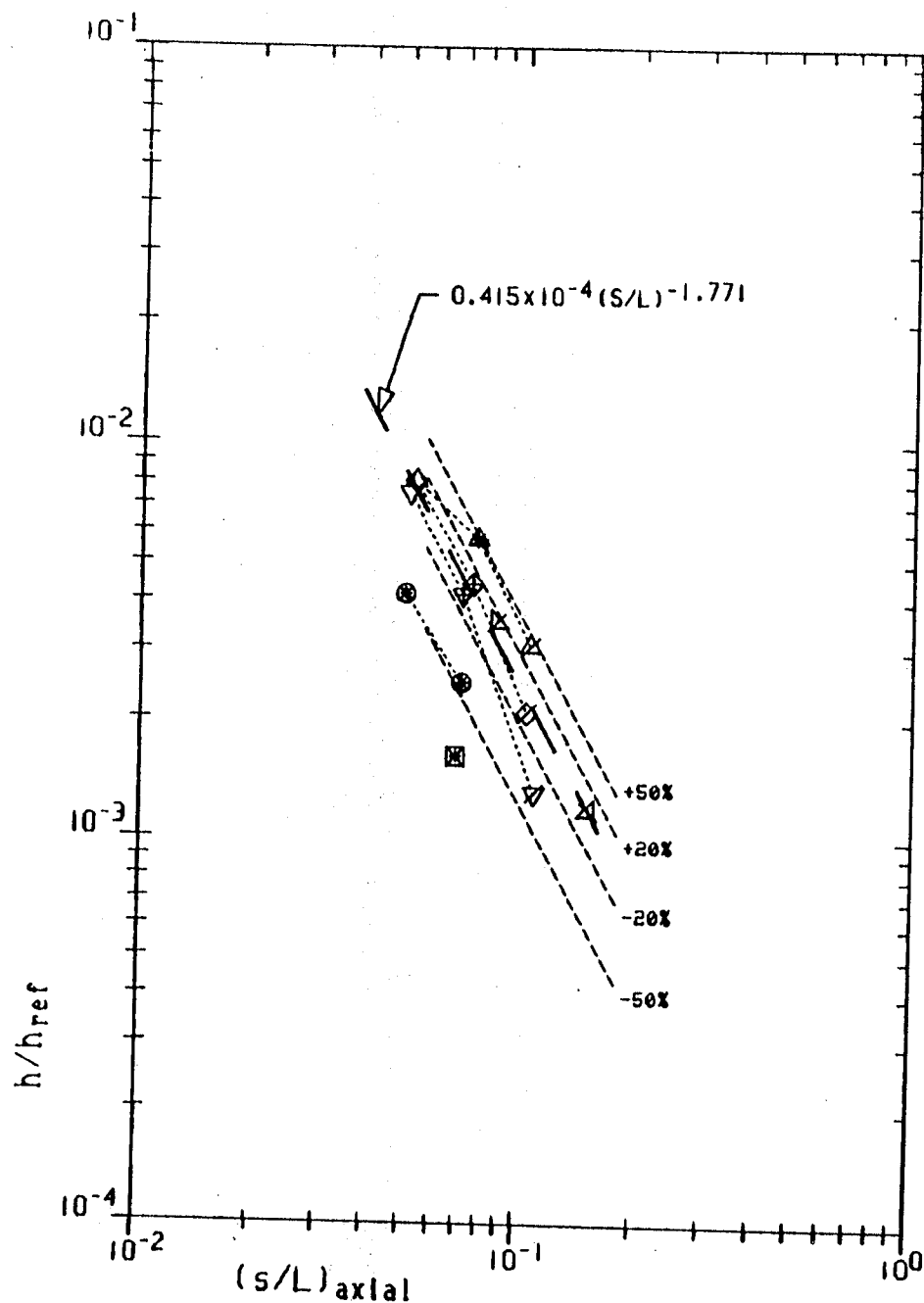
SYM Y/L

△	.1405	-8 0 0 0 0 0 0 0
▽	.1719	-2-2 0 0 0 0 0 0
▽	.2034 .. 2	1 1-2-8 0 0 0 0
△	.2349 .. 4	1 1 2 3-8 0 0
◇	.2653 .. 3	1 1 2-8 0 0
○	.2978 .. 4	1 1 3 3-3
□	.3278	-3-3 0

0 = SEPARATED
 □ = 1 = ATTACHED
 ⊕ = 2 = PRESEPARATED
 ⊗ = 3 = ANOMOLOUS
 ⊠ = 8 = SEPARATED, NOT USED BUT SHOWN
 ⊡ = NOT USED - USUALLY DATA ANOMOLY

13 PTS USED

RMS DEV = 13.55 %

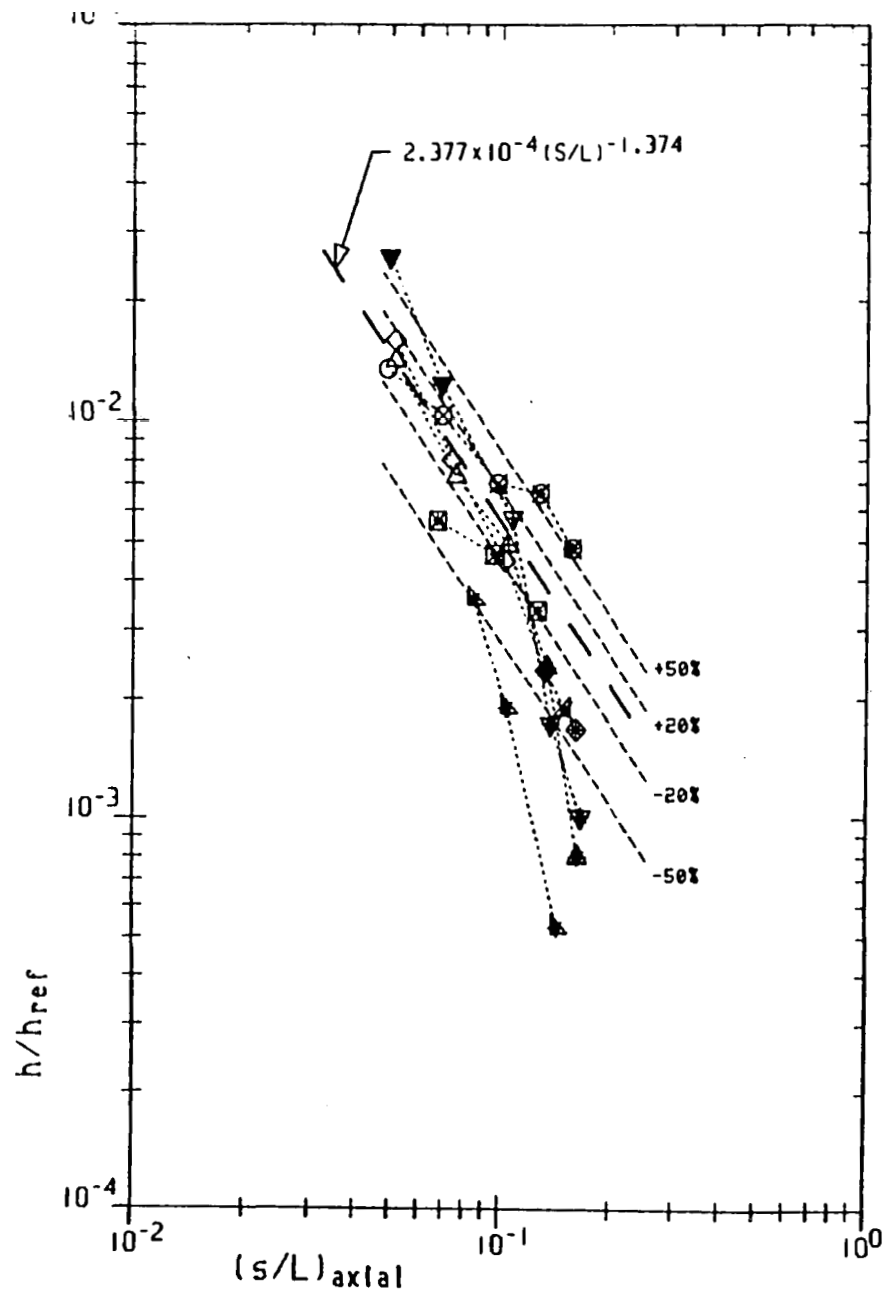

 $M_{\infty} = 9.98 \dots 20$
 $\alpha = 40^\circ$
 $Re_L = 1.090 \times 10^6$

SYM	γ/L	
\triangle	.1405	-8 0 0 0 0 0 0 0 0
∇	.1719	-8 0 0 0 0 0 0 0 0
\triangle	.2034 .. 2	1 2-8 0 0 0 0 0 0
\triangle	.2349 .. 1	1-2-8 0 0 0 0 0
\diamond	.2653 .. 2	1 2-8 0 0 0 0
\circ	.2978	-1-2 0 0 0 0
\square	.3278	-3 0 0

0 = SEPARATED
 1 = ATTACHED
 2 = PRESEPARATED
 3 = ANOMOLOUS
 8 = SEPARATED, NOT USED BUT SHOWN
 - - - NOT USED - USUALLY DATA ANOMOLY

5 PTS USED

RMS DEV = 7.20%



$M_\infty = 0.16 \dots 22$
 $\alpha = 20^\circ$
 $Re_L = 2.500 \times 10^6$

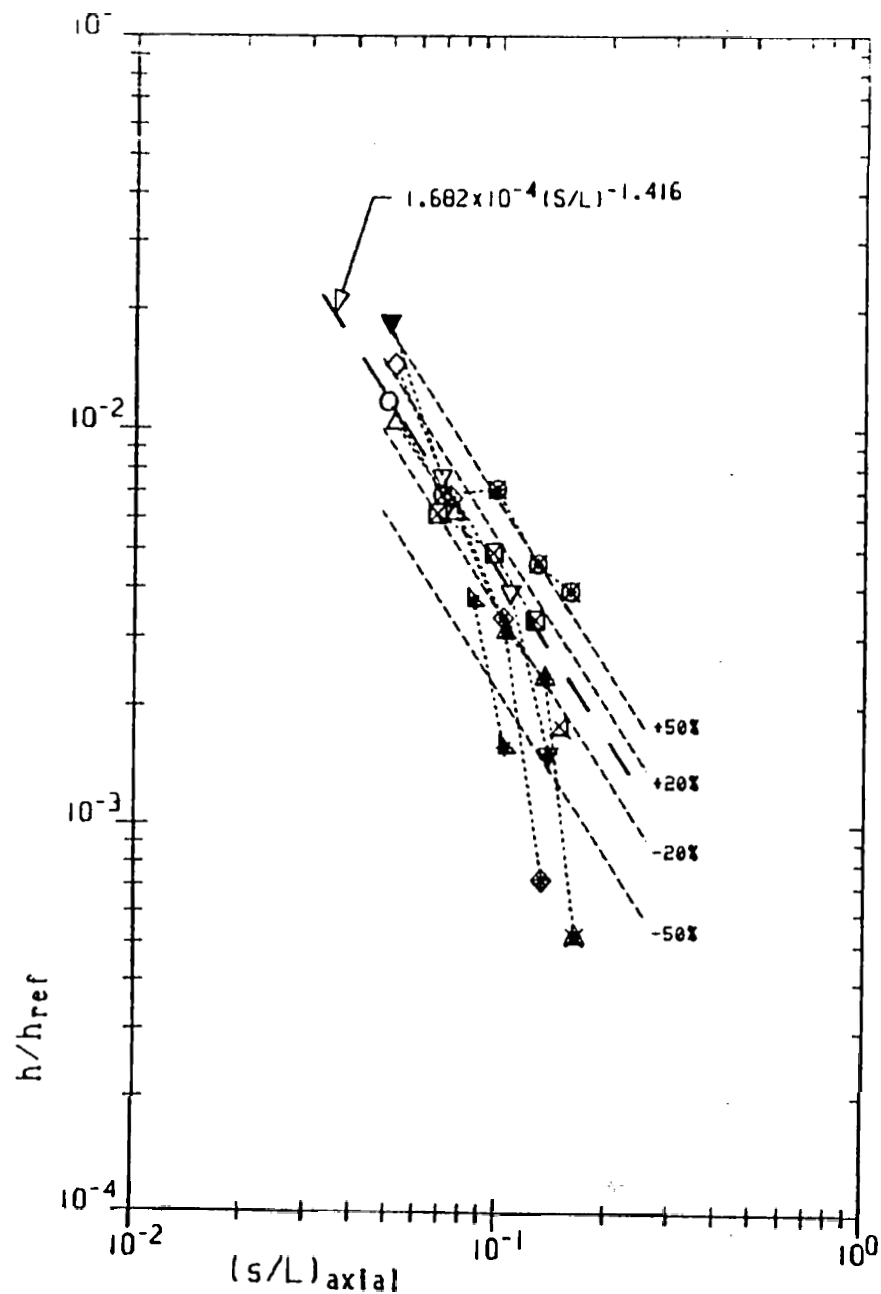
SYM Y/L

\triangle	.1405	-3 0 0 0 0 0 0 0
∇	.1719	-1-2-2 0 0 0 0 0
∇	.2034 .. 1	-4-4 2-2-2 0 0 0 0
\triangle	.2349 .. 3	1 1 2-2-2 0 0
\diamond	.2653 .. 3	1 1 1-2-2 0
\circ	.2978 .. 3	1 3 3-3-3
\square	.3278	-3-3-3

0 • SEPARATED
 1 • ATTACHED
 2 • PRESEPARATED
 3 • ANOMOLOUS
 4 • STRAKE SHOCK?
 ' ' NOT USED - USUALLY DATA ANOMOLY

10 PTS USED

RMS DEU = 12.31 %



$M_\infty = 0.6 \dots 3$
 $\alpha = 25^\circ$
 $Re = 2.500 \times 10^6$

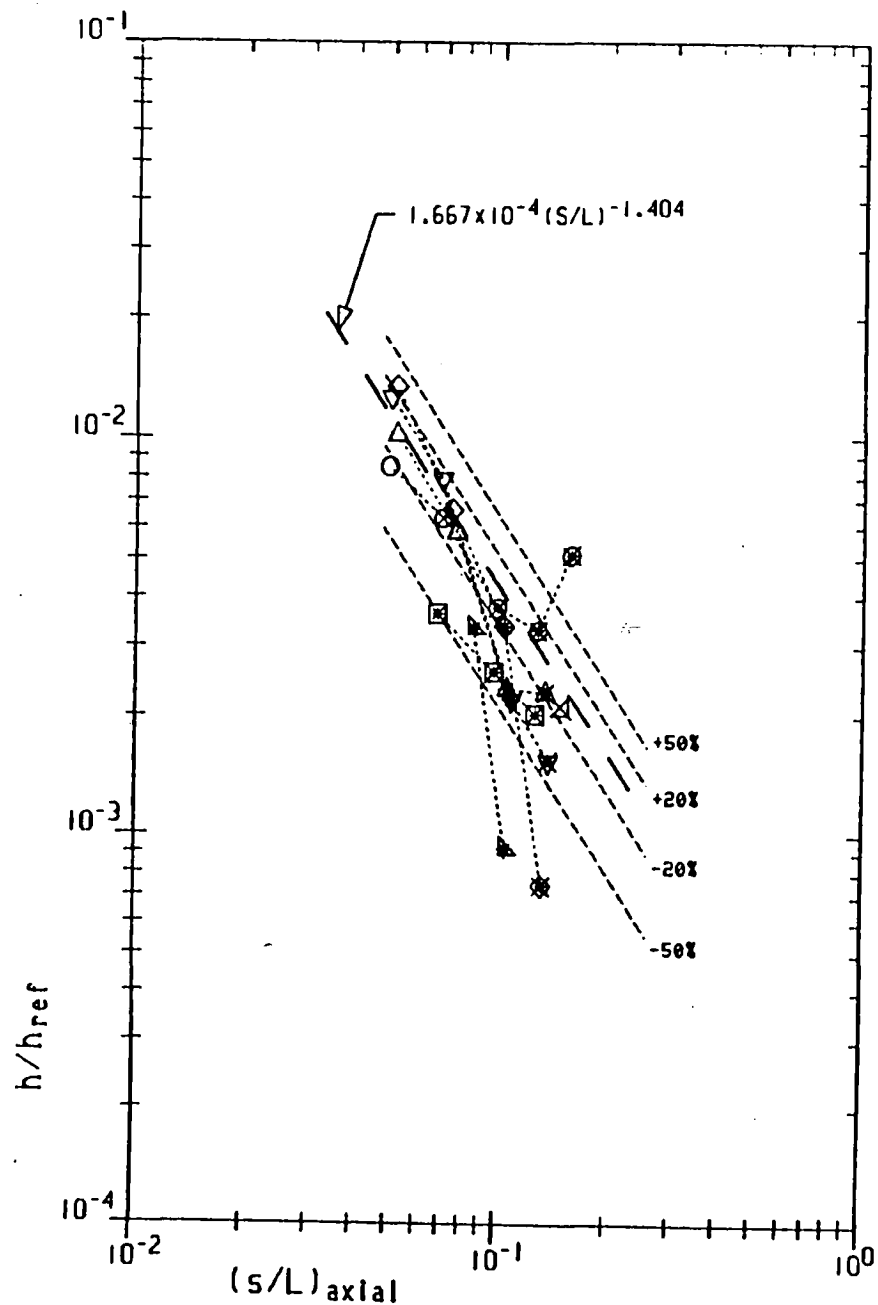
SYM Y/L

∇	.1405	-8 0 0 0 0 0 0 0
\triangle	.1719	-1-2 0 0 0 0 0 0
∇	.2034 .. 2	-4 1 1-2 0 0 0 0
\triangle	.2349 .. 2	1 1-1-2-3 0 0
\diamond	.2653 .. 2	1 1-1-2 0 0
\circ	.2978 .. 2	1 3-3-3-3
\square	.3278 .. 3	3 3 3

- 0 • SEPARATED
- \square • 1 • RTTACHED
- \oplus • 2 • PRESEPARTED
- \boxtimes • 3 • ANOMOLOUS
- \blacksquare • 4 • STRAKE SHOCK?
- \boxdot • 8 • SEPARATED, NOT USED BUT SHOWN
- \circ • NOT USED - USUALLY DATR ANOMOLY

11 PTS USED

RMS DEU • 10.88 %



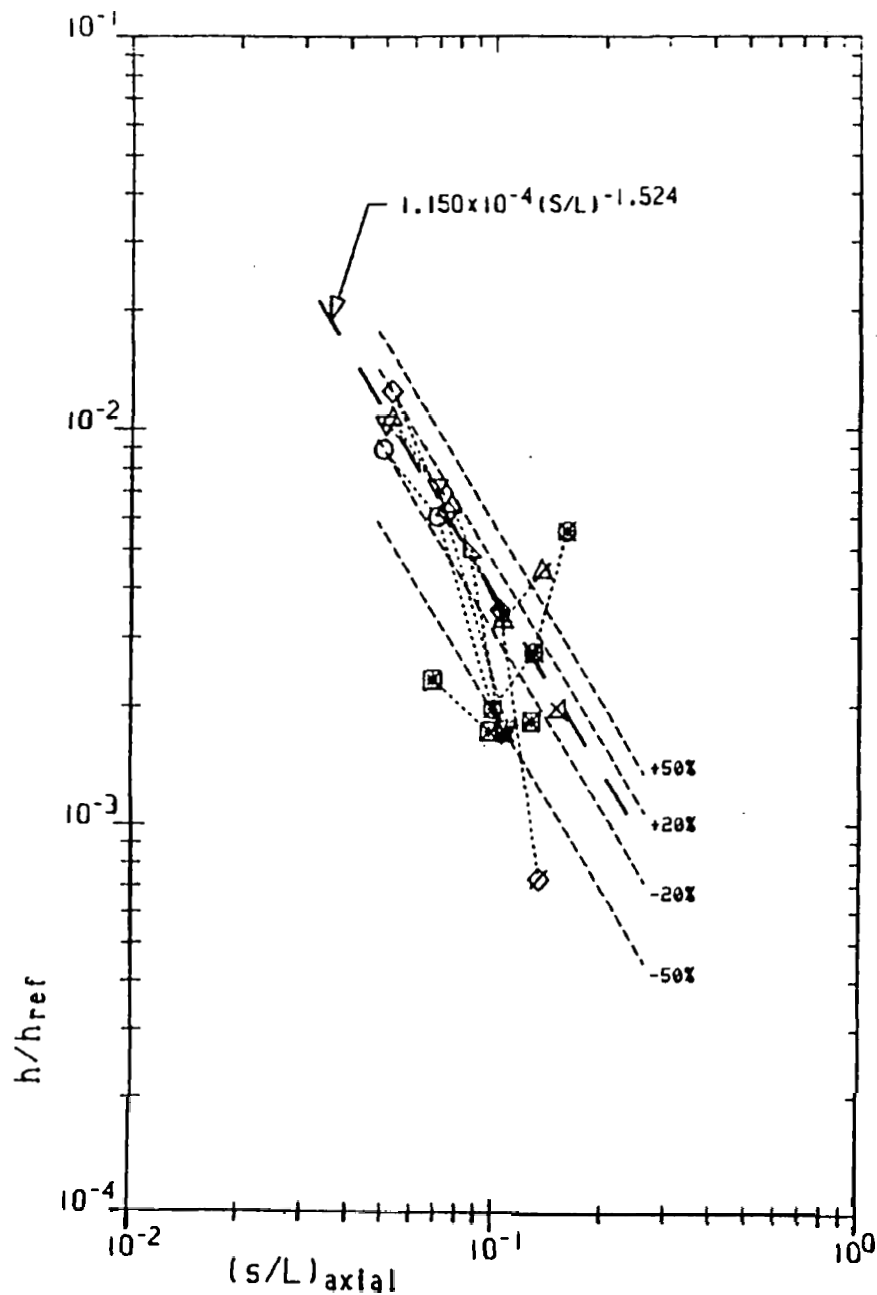
$M_\infty = 10.16 \dots 18$
 $\alpha = 30^\circ$
 $Re_L = 2.430 \times 10^6$

SYM	Y/L	
\triangle	.1405	-8 0 0 0 0 0 0 0 0
\triangle	.1719	-1-2 0 0 0 0 0 0 0
∇	.2034 .. 2	1 1-2-3 0 0 0 0 0
\triangle	.2349 .. 2	1 1-2-3 0 0 0
\diamond	.2653 .. 2	1 1-2-3 0 0
\circ	.2978 .. 2	1 3-3-3-3
\square	.3278	-1-3-3

0 = SEPARATED
 1 = ATTACHED
 2 = PRESEPARATED
 3 = ANOMOLOUS
 8 = SEPARATED, NOT USED BUT SHOWN
 - - - NOT USED - USUALLY DATA ANOMOLY

8 PTS USED

RMS DEV = 15.85 %



$M_{\infty} = 10.16 \dots 6$
 $\alpha = 35.$
 $Re_L = 2.430 \times 10^6$

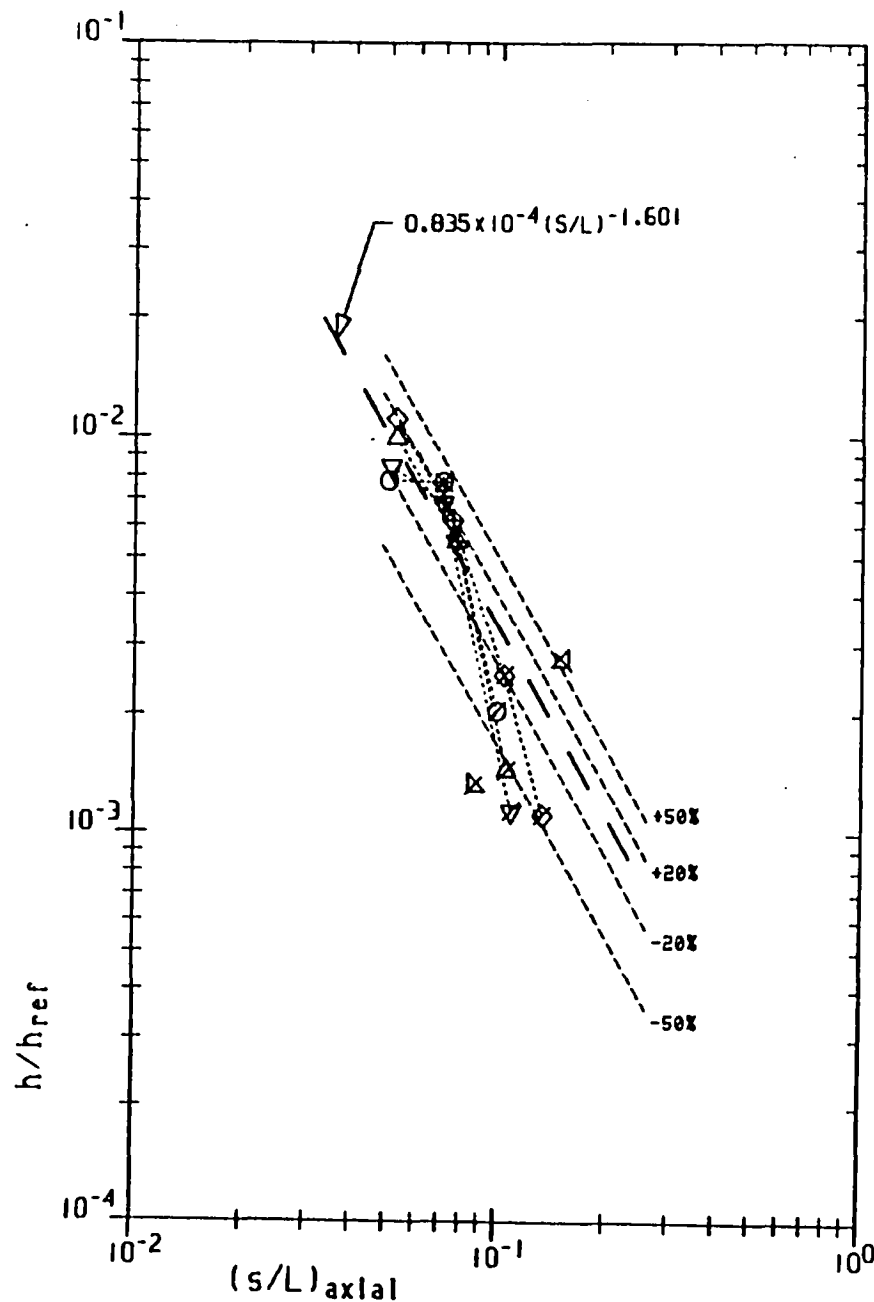
SYM Y/L

\triangle	.1405	-8 0 0 0 0 0 0 0 0
\triangle	.1719 .. 1	1-2 0 0 0 0 0 0 0
∇	.2034 .. 2	1 1-2 0 0 0 0 0 0
\triangle	.2349 .. 3	1 1 2-8 0 0 0
\diamond	.2653 .. 3	1 1 2-8 0 0
\circ	.2978 .. 2	1 1-3-3-3
\square	.3278	-1-3-3

0 • SEPARATED
 1 • ATTACHED
 2 • PRESEPARATED
 3 • ANOMOLOUS
 8 • SEPARATED, NOT USED BUT SHOWN
 NOT USED - USUALLY DATA ANOMOLY

11 PTS USED

RMS DEU • 10.82 %



$M_\infty = 10.16 \dots 7$
 $\alpha = 40.$
 $Re_L = 2.400 \times 10^6$

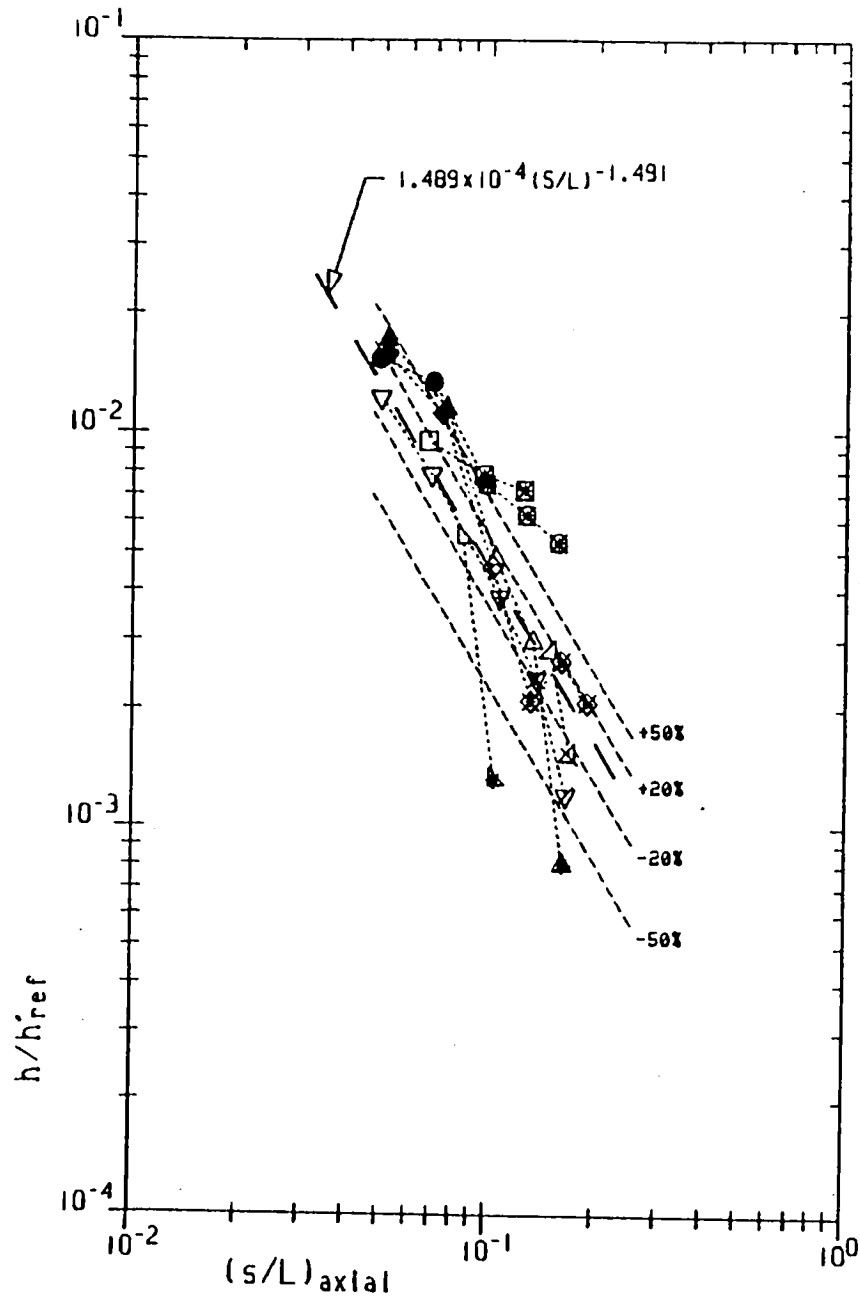
SYM Y/L

△	.1405	-8 0 0 0 0 0 0 0 0
△	.1719	-8 0 0 0 0 0 0 0 0
▽	.2034 .. 2	1 2-8 0 0 0 0 0 0
△	.2349 .. 2	1 2-8 0 0 0 0
◇	.2653 .. 3	1 2 3-8 0 0
○	.2978 .. 1	1-3-8 0 0
□	.3278	0 0 0

0 = SEPARATED
 □ = 1 = ATTACHED
 ⊕ = 2 = PRESEPARATED
 ⊗ = 3 = ANOMOLOUS
 ⊠ = 8 = SEPARATED, NOT USED BUT SHOWN
 ⊞ = NOT USED - USUALLY DATA ANOMOLY

8 PTS USED

RMS DEV = 17.72 %



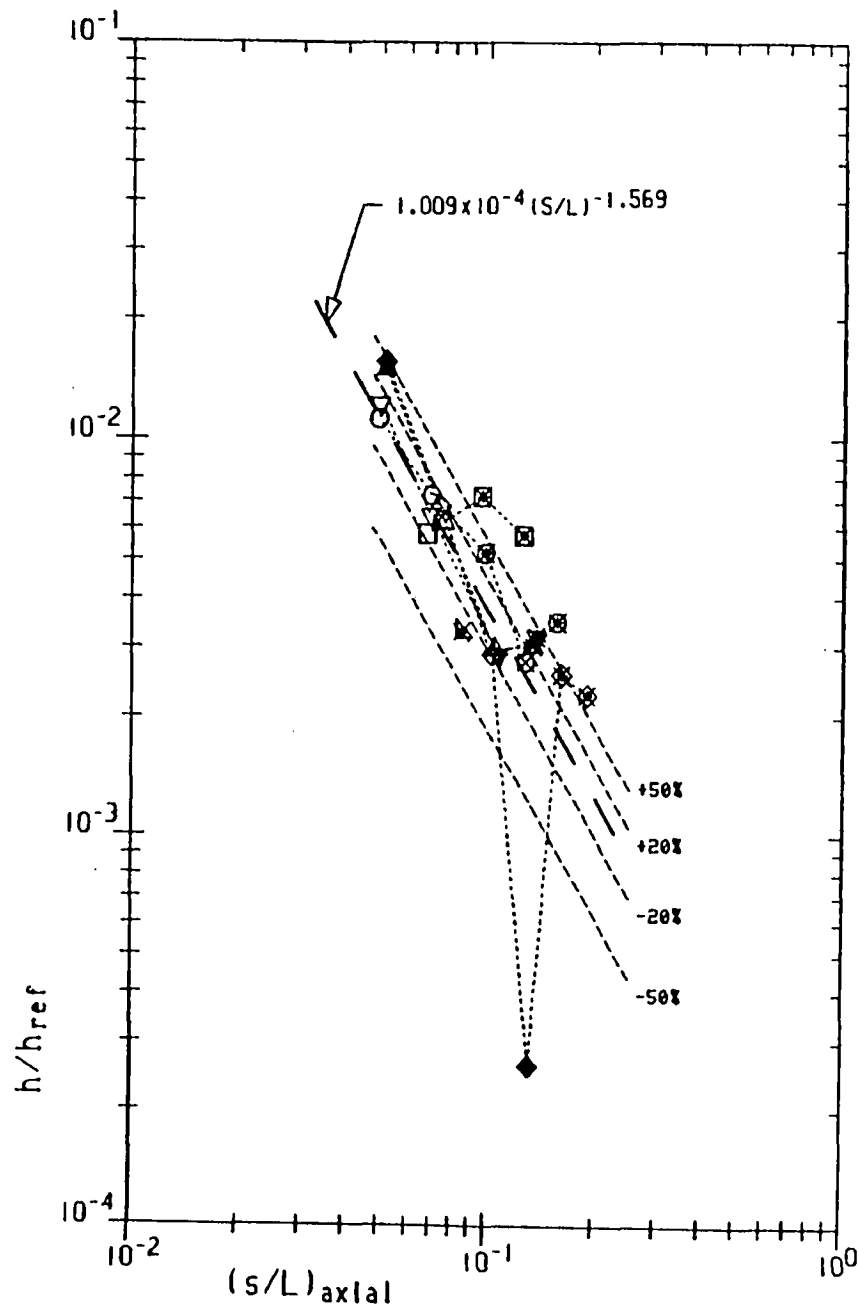
$M_{\infty} = 6. \dots 3$
 $\alpha = 20.$
 $Re_L = 0.840 \times 10^6$

SYM	Y/L	
\triangle	.1405 .. 1	1-8 0 0 0 0 0 0 0
∇	.1719 .. 1	1-2 0 0 0 0 0 0 0
∇	.2034 .. 4	1 1 2 3-8 0 0 0 0
\triangle	.2349 .. 2	-4-4 1 1-2 0 0
\diamond	.2653 .. 1	-4-4 1-3-3-3
\circ	.2978	-4-4-3-3-3
\square	.3278 .. 1	1-3-3

- \emptyset - SEPARATED
- \square - 1 - ATTACHED
- \boxplus - 2 - PRESEPARATED
- \boxtimes - 3 - ANOMOLOUS
- \bullet - 4 - STRAKE/BOX SHOCK?
- \boxminus - 8 - SEPARATED, NOT USED BUT SHOWN
- \boxdot - NOT USED - USUALLY DATA ANOMOLY

10 PTS USED

RMS DEV - 9.87%



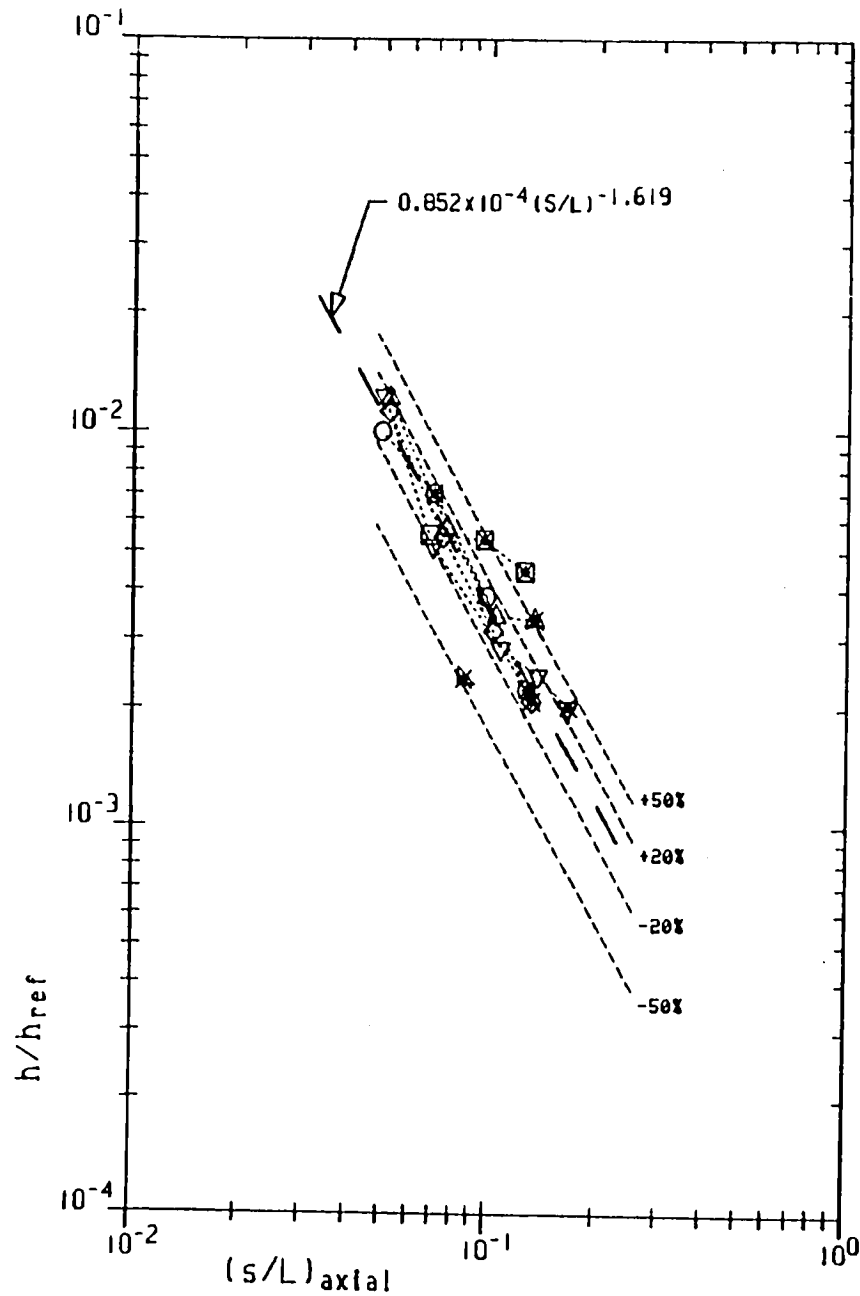
$M_{\infty} = 6. \dots 7$
 $\alpha = 25.$
 $Re_L = 0.800 \times 10^6$

SYM	Y/L	
△	.1405	0 0 0 0 0 0 0 0 0
▽	.1719	-3 0 0 0 0 0 0 0 0
▽	.2034 .. 3	1 1 2-3 0 0 0 0 0
△	.2349 .. 3	-4 1 2 3 0 0 0
◇	.2653 .. 2	-4 1 1-2-3-3
○	.2978 .. 3	1 1-3 3-3
□	.3278 .. 1	1-3-3

0 • SEPARATED
 □ • 1 • ATTACHED
 ⊞ • 2 • PRESEPARATED
 ⊠ • 3 • ANOMOLOUS
 ● • 4 • STRAKE/BOW SHOCK?
 ⊞ • NOT USED - USUALLY DATA ANOMOLY

12 PTS USED

RMS DEV = 13.87%



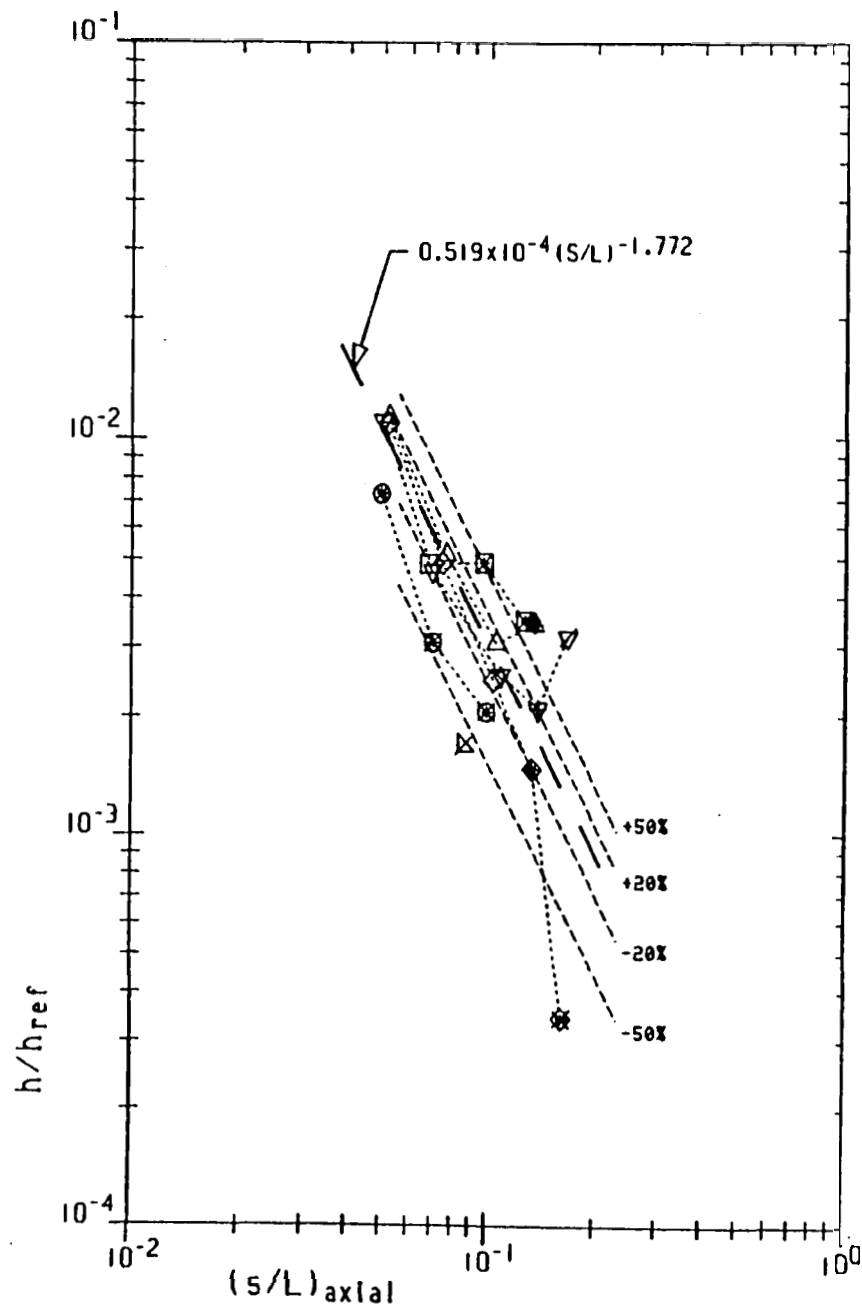
$M_\infty = 6. \dots 8$
 $\alpha = 30.$
 $Re_L = 0.850 \times 10^6$

SYM	Y/L	
\triangle	.1405	0 0 0 0 0 0 0 0
∇	.1719	-3 0 0 0 0 0 0 0
\triangle	.2034 .. 4	1 1 1 1-3 0 0 0
\triangle	.2349 .. 3	1 1 1-3 0 0 0
\diamond	.2653 .. 3	1 1 1-3 0 0
\circ	.2978 .. 2	1-3 1-3 0
\square	.3278 .. 1	1-3-3

0 = SEPARATED
 1 = ATTACHED
 3 = ANOMOLOUS
 - - - NOT USED - USUALLY DATA ANOMOLY

13 PTS USED

RMS DEV = 12.15 %



$M_\infty = 6. \dots 9$
 $\alpha = 35.$
 $Re_L = 0.800 \times 10^6$

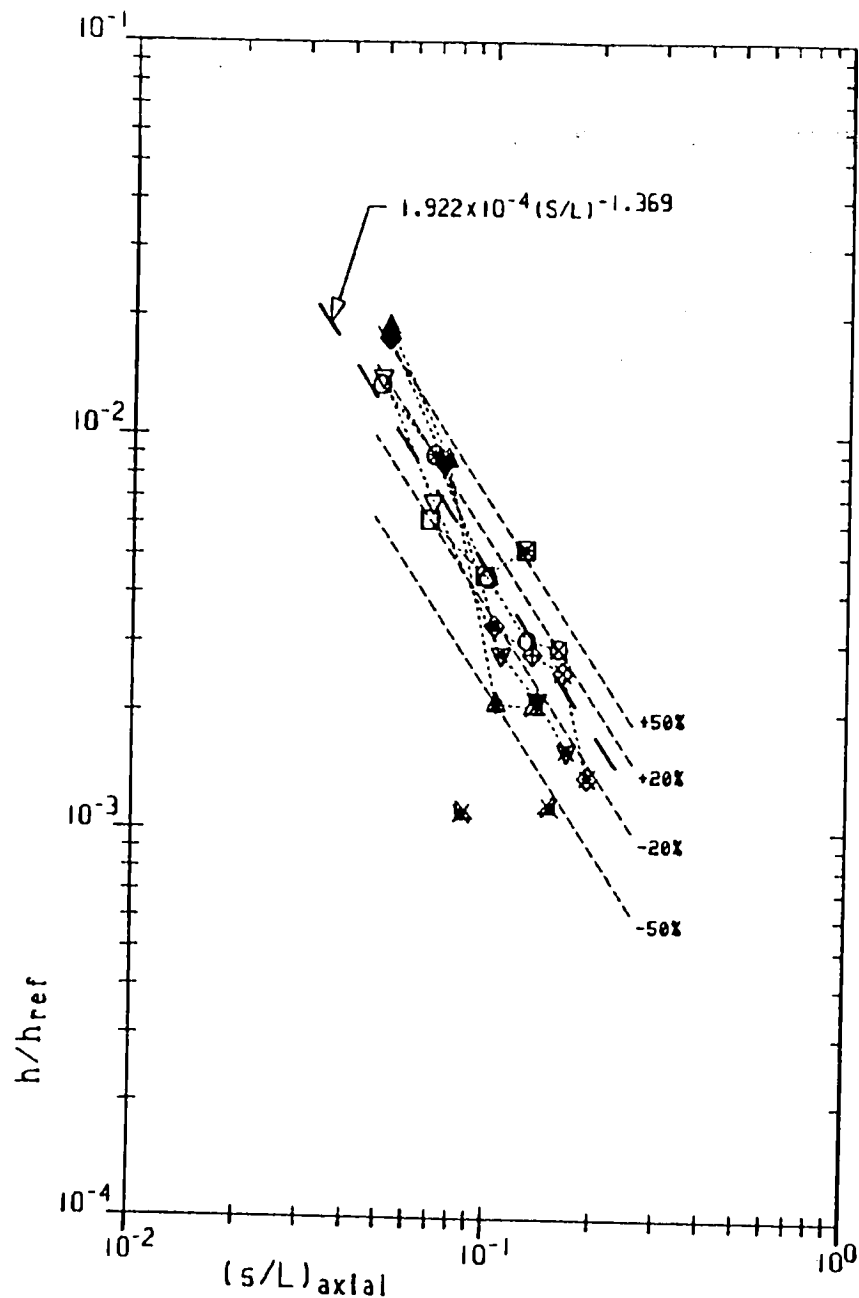
SYM Y/L

\triangle	.1405	0 0 0 0 0 0 0 0 0
∇	.1719	-8 0 0 0 0 0 0 0 0
∇	.2034 .. 4	1 1 1 2-8 0 0 0 0
\triangle	.2349 .. 3	1 1 1-2 0 0 0
\diamond	.2653 .. 3	1 1 1-2-3 0
\circ	.2978	-1-3-3 0 0
\square	.3278 .. 1	1-3-3

0 • SEPARATED
 1 • ATTACHED
 2 • PRESEPARATED
 3 • ANOMOLOUS
 8 • SEPARATED, NOT USED BUT SHOWN
 - - - - - NOT USED - USUALLY DATA ANOMOLY

11 PTS USED

RMS DEV = 14.34%



$M_\infty = 6. \dots 5$
 $\alpha = 20.$
 $Re_L = 2.630 \times 10^6$

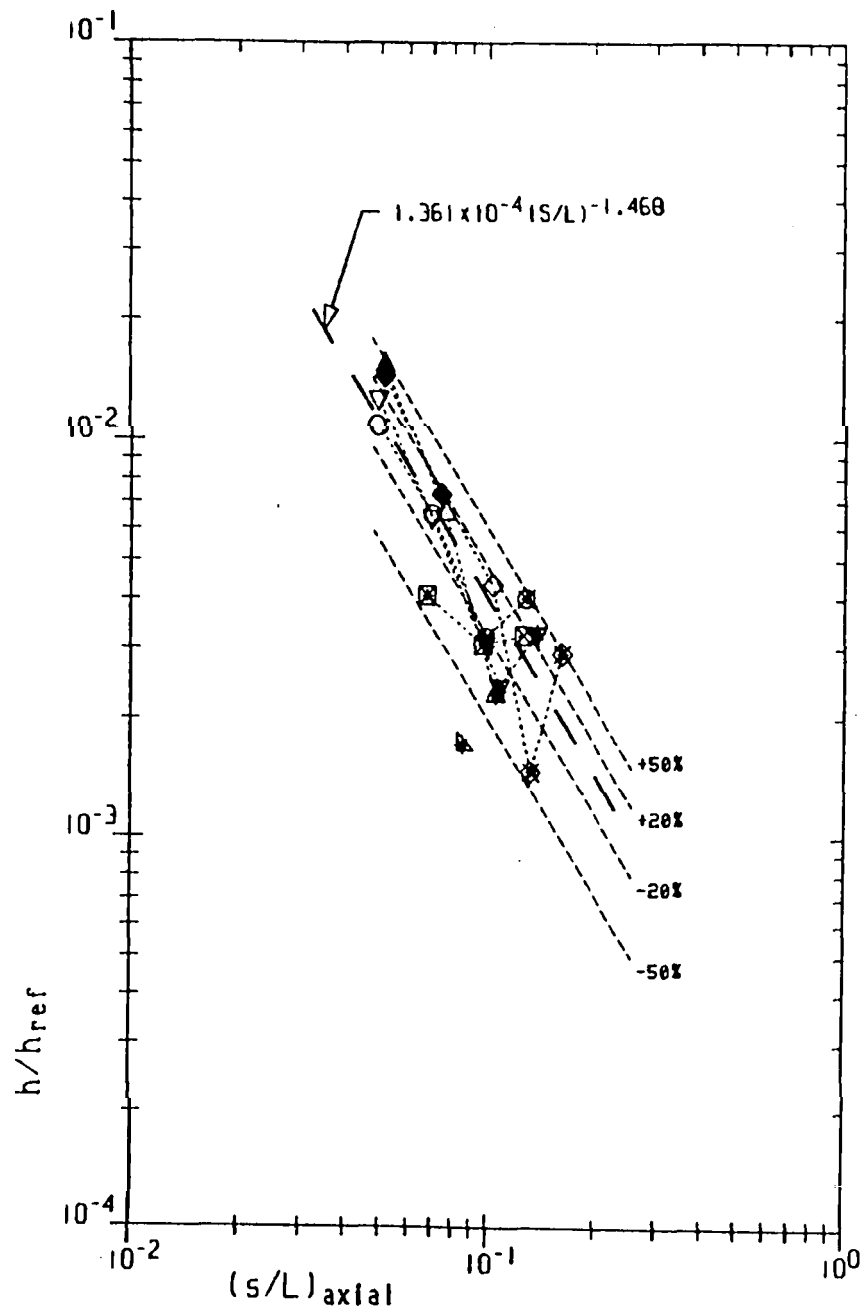
SYM Y/L

\triangle	.1405	-3 0 0 0 0 0 0 0 0
\triangle	.1719	-3 0 0 0 0 0 0 0 0
∇	.2034 .. 2	1 1-1-2-3 0 0 0 0
\triangle	.2349	-4-1-2-8 0 0 0
\diamond	.2653 .. 2	-4-1-1 2 3-3
\circ	.2978 .. 4	1-1 1 1 3
\square	.3278 .. 2	1 1-3

0 • SEPARATED
 1 • ATTACHED
 2 • PRESEPARATED
 3 • ANOMOLOUS
 4 • STRAKE/BOW SHOCK?
 8 • SEPARATED, NOT USED BUT SHOWN
 -'-'- NOT USED - USUALLY DATA ANOMOLY

10 PTS USED

RMS DEV = 12.59 %



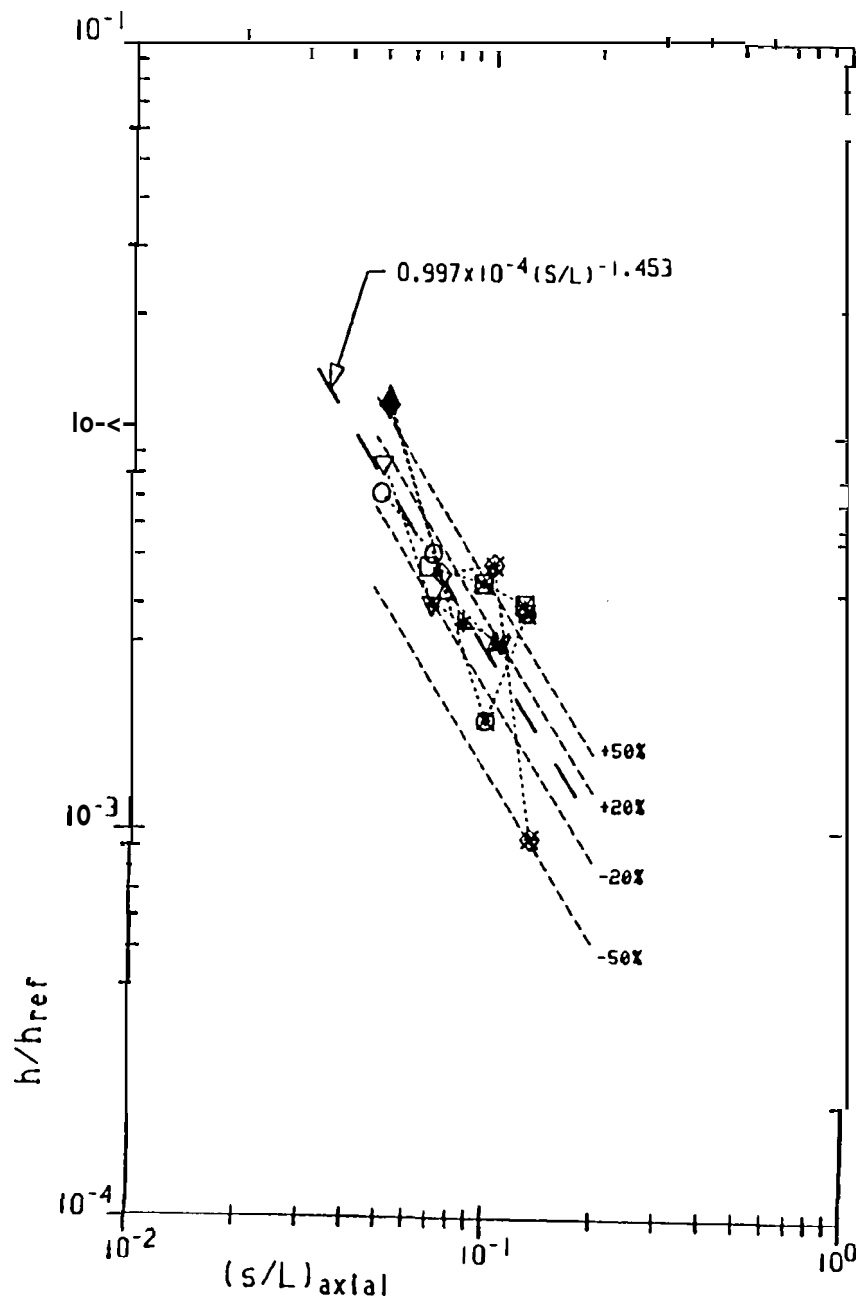
$M_\infty = 6. \dots 10$
 $\alpha = 25.$
 $Re_L = 2.530 \times 10^6$

SYM	Y/L	
\triangle	.1405	0 0 0 0 0 0 0 0 0
∇	.1719	-2 0 0 0 0 0 0 0 0
\triangle	.2034 .. 2	1 1-1-2 0 0 0 0 0
\triangle	.2349 .. 1	-4 1-2 0 0 0 0
\diamond	.2653 .. 1	-4-4 1-3-3 0
\circ	.2978 .. 2	1 1-3-3 0
\square	.3278 .. 2	-3 3 3

0 • SEPARATED
 1 • ATTACHED
 2 • PRESEPARATED
 3 • ANOMOLOUS
 4 • STRAKE/BOW SHOCK?
 - - - NOT USED - USUALLY DATA ANOMOLY

8 PTS USED

RMS DEU = 15.48 %



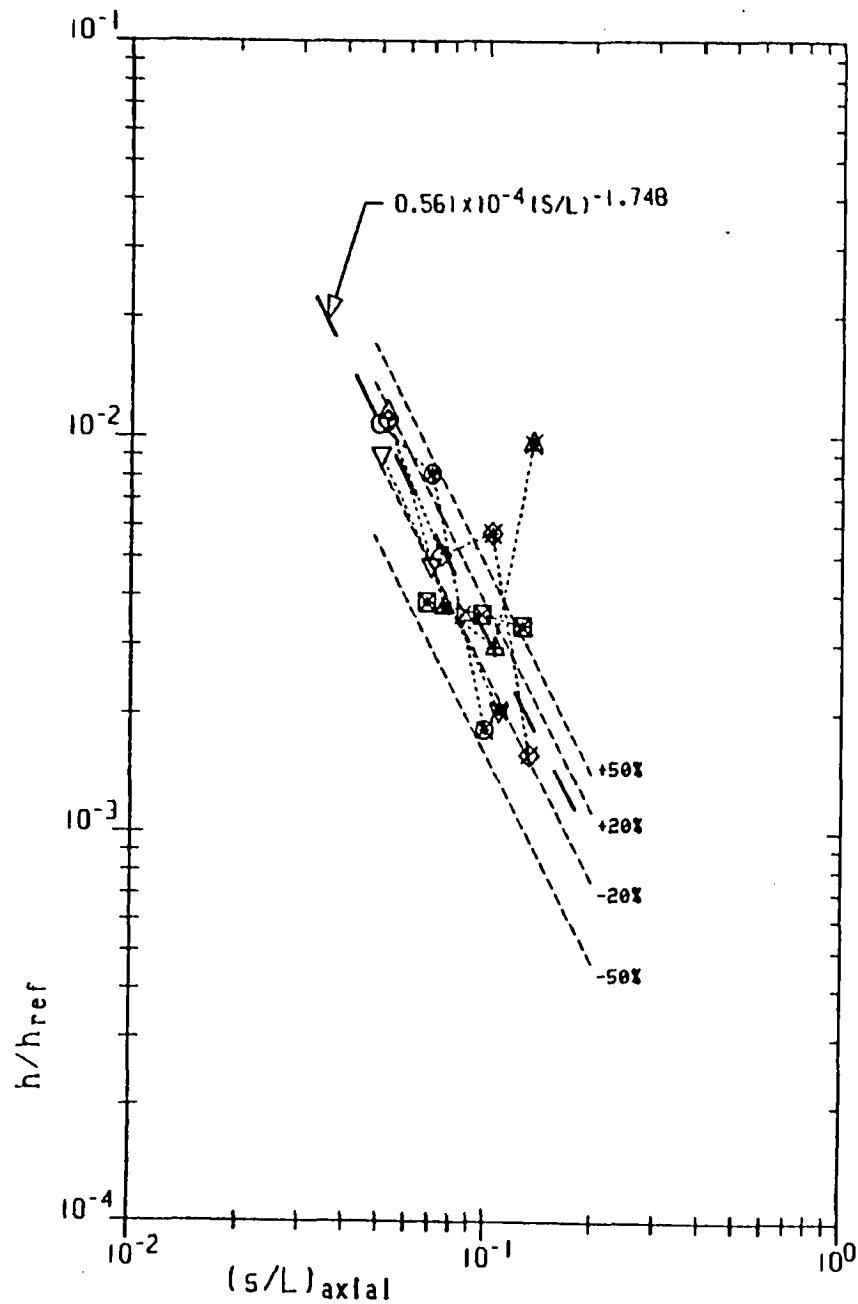
$M_\infty = 6. \dots 13$
 $\alpha = 30.$
 $Re_L = 2.690 \times 10^6$

SYM	Y/L	
\triangle	.1405	0 0 0 0 0 0 0 0 0 0
∇	.1719	-2 0 0 0 0 0 0 0 0 0
	.2034 .. 1	1 - 1 - 3 8 8 8 8 8 0
\triangle	.2349 .. 1	-4 1-3 0 0 0 0
\diamond	.2653 .. 1	-4 1-3-3 8 0
\circ	.2978 .. 2	1 1-3-3 0
\square	.3278 .. 1	1-3-3

8 • SEPARATED
 1 • ATTACHED
 2 • PRESEPARATED
 3 • ANOMOLOUS
 4 • STRAKE/BOX SHOCK?
 - - - NOT USED - USUALLY DATA ANOMOLY

6 PTS USED

RMS DEU = 6.83 %



$M_\infty = 6. \dots 17$
 $\alpha = 35.$
 $Re_L = 2.770 \times 10^6$

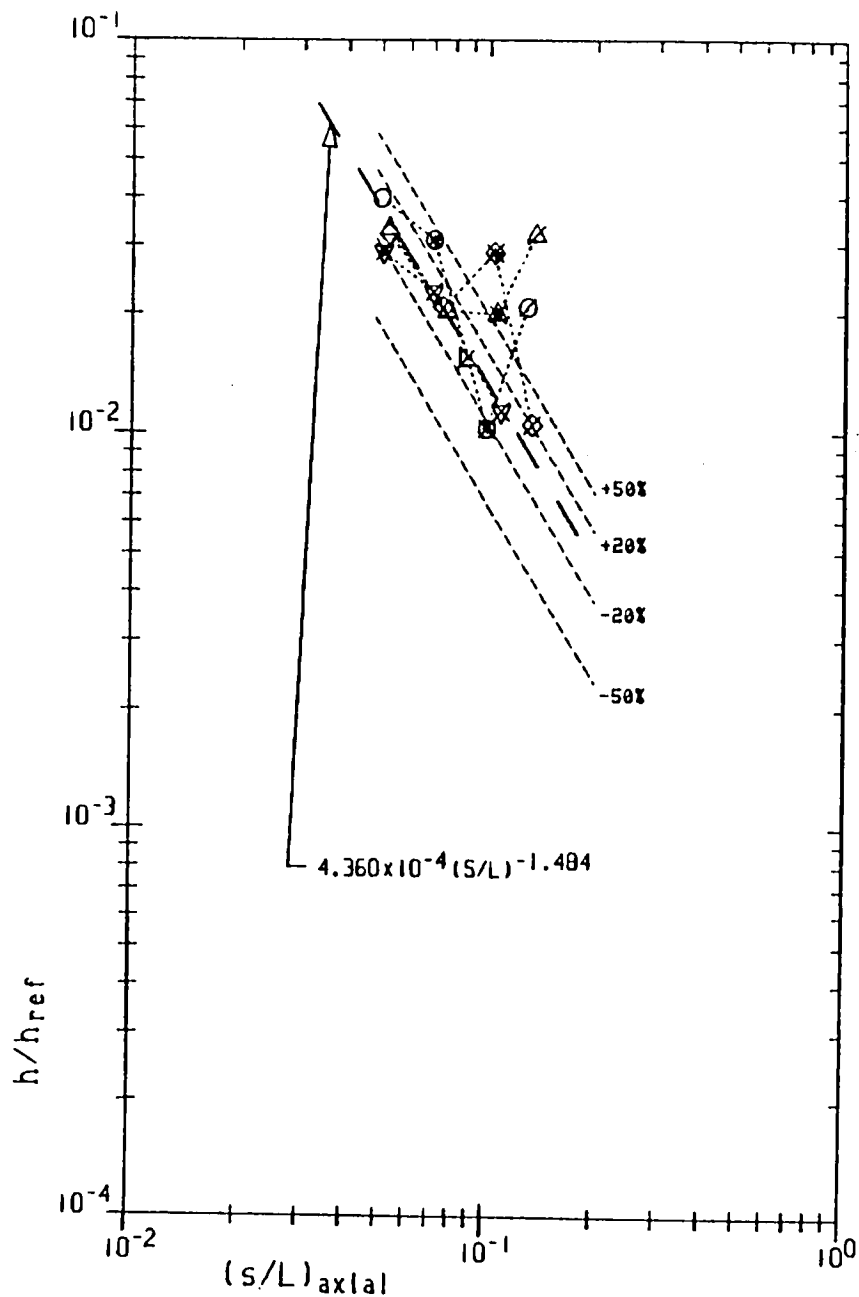
SYM Y/L

\triangle	.1405	0 0 0 0 0 0 0 0 0
∇	.1719	-8 0 0 0 0 0 0 0 0
∇	.2034 .. 2	1 1-3 0 0 0 0 0 0
\triangle	.2349 .. 2	1-1 2-3 0 0 0
\diamond	.2653 .. 2	1 1-3-8 0 0
\circ	.2978 .. 1	1-1-3 0 0
\square	.3278 .. 1	-3 3-3

0 = SEPARATED
 \square = 1 = ATTACHED
 \boxplus = 2 = PRESEPARATED
 \boxtimes = 3 = ANOMOLOUS
 \boxminus = 8 = SEPARATED, NOT USED BUT SHOWN
 \boxdot = NOT USED - USUALLY DATA ANOMOLY

8 PTS USED

RMS DEV = 11.98 %



$M_\infty = 6. \dots 22$
 $\alpha = 40.$
 $Re_L = 3.380 \times 10^6$

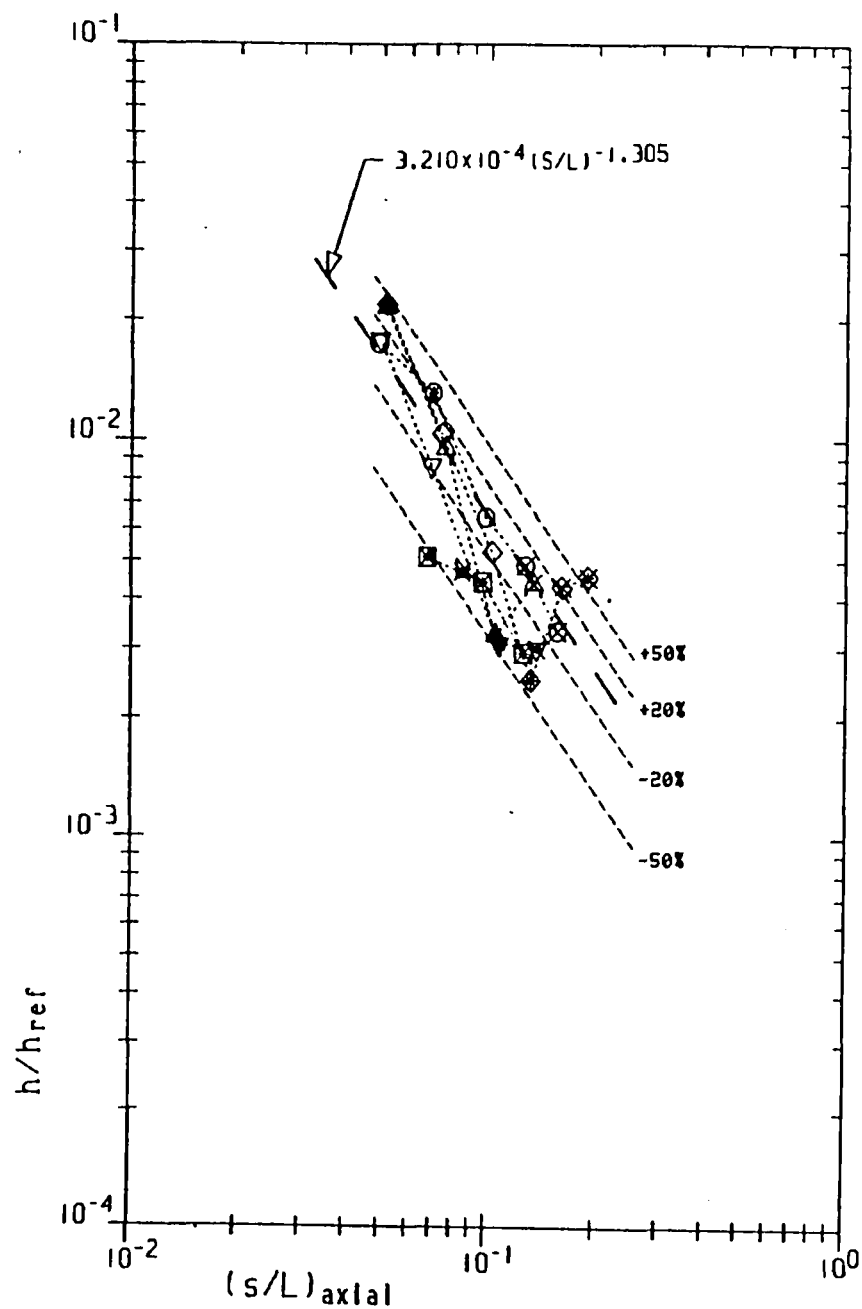
SYM Y/L

\triangle	.1405	0 0 0 0 0 0 0 0 0
\triangle	.1719	-8 0 0 0 0 0 0 0 0
∇	.2034 .. 2	-3 3 3 0 0 0 0 0 0
\triangle	.2349 .. 2	1 1-3-8 0 0 0
\diamond	.2653 .. 2	1 1-3-8 0 0
\circ	.2978 .. 1	1-1-3-8 0
\square	.3278	0 0 0

0 = SEPARATED
 □ = 1 = ATTACHED
 ⊗ = 3 = ANOMOLOUS
 ⊠ = 8 = SEPARATED, NOT USED BUT SHOWN
 ⊞ = NOT USED - USUALLY DATA ANOMOLY

7 PTS USED

RMS DEV = 4.45 %



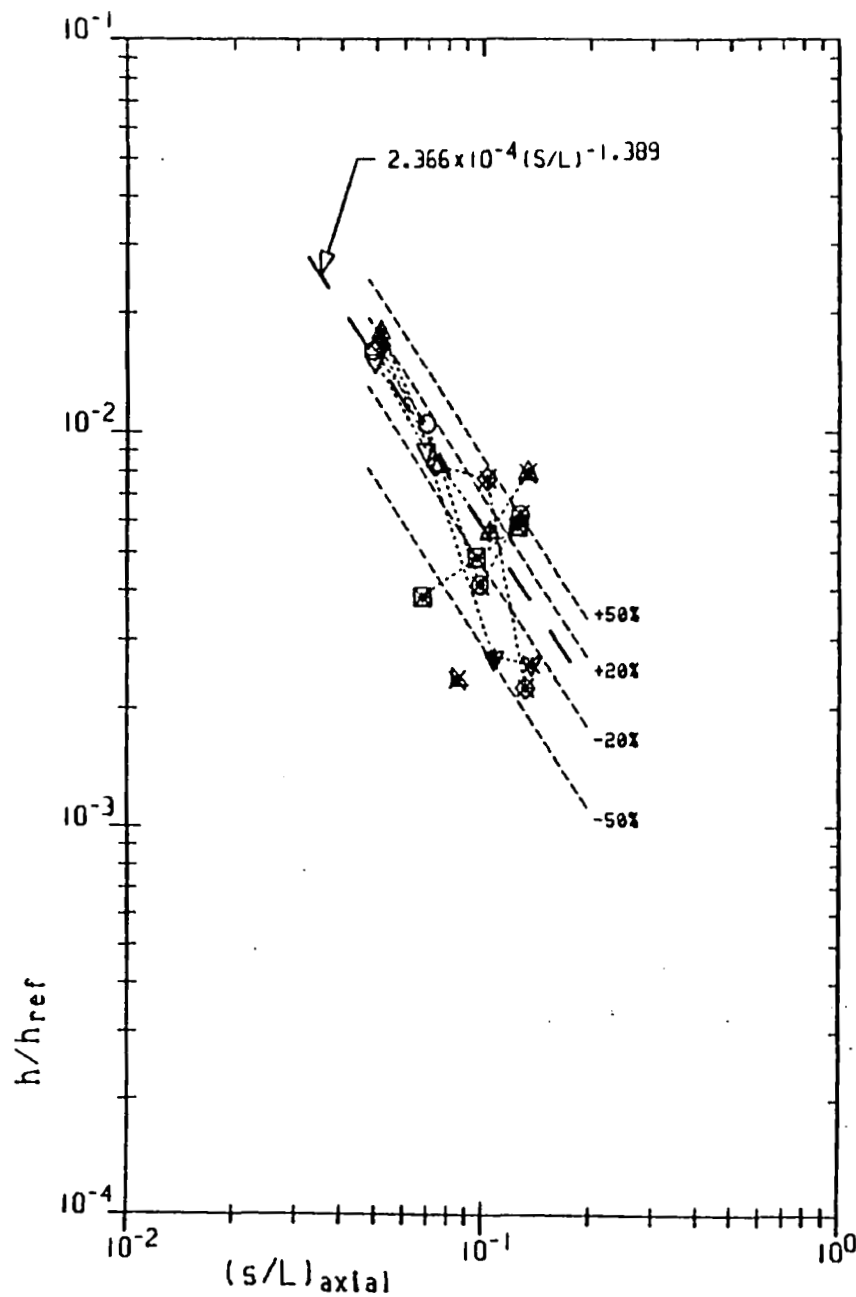
$M_\infty = 6. \dots 6$
 $\alpha = 20.$
 $Re_L = 5.400 \times 10^6$

SYM	Y/L	
△	.1405	0 0 0 0 0 0 0 0
▽	.1719	-3 0 0 0 0 0 0 0
▽	.2034 .. 2	1 1-2-3 0 0 0 0
△	.2349 .. 2	-4 1-2 3 0 0 0
◇	.2653 .. 3	-4 1 1-2 3-3
○	.2978 .. 4	1-1 1 3 3
□	.3278	-3-3-3

0 • SEPARATED
 □ • 1 • ATTACHED
 ⊕ • 2 • PRESEPARATED
 ⊗ • 3 • ANOMOLOUS
 ● • 4 • STRAKE/BOU SHOCK?
 ⊙ • NOT USED - USUALLY DATA ANOMOLY

11 PTS USED

RMS DEV = 11.44 %



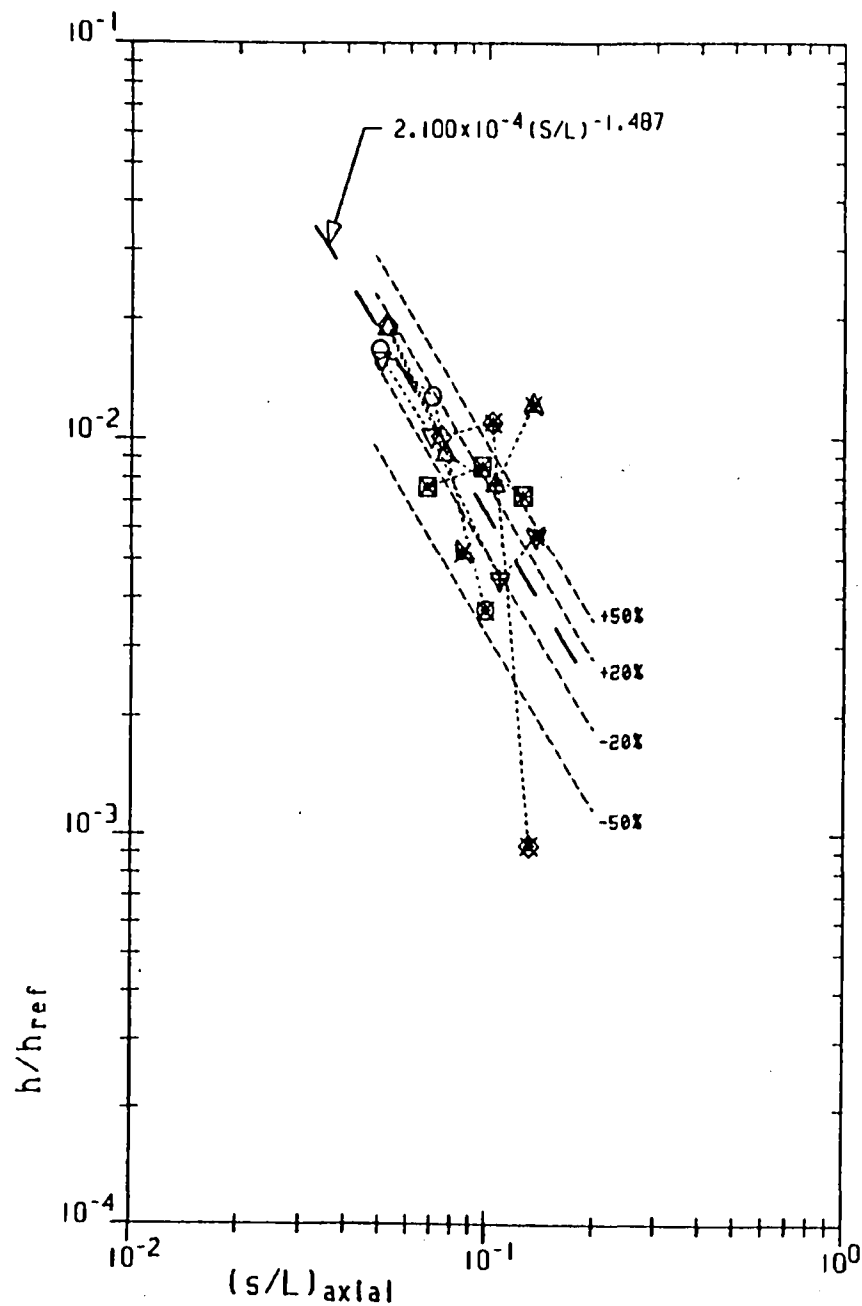
$M_{\infty} = 6. \dots 11$
 $\alpha = 25.$
 $Re_L = 5.120 \times 10^6$

SYM	Y/L	
\triangle	.1405	0 0 0 0 0 0 0 0
∇	.1719	-3 0 0 0 0 0 0 0
∇	.2034 .. 2	1 1-2-3 0 0 0 0
\triangle	.2349 .. 2	-1 1 2-3 0 0 0
\diamond	.2653 .. 1	-1 1-3-3 0 0
\circ	.2978 .. 2	1 1-3-3 0
\square	.3278	-3-3-3

0 - SEPARATED
 1 - ATTACHED
 2 - PRESEPARATED
 3 - ANOMOLOUS
 - - - NOT USED - USUALLY DATA ANOMOLY

7 PTS USED

RMS DEV = 5.19%



$M_\infty = 6. \dots 15$
 $\alpha = 30.$
 $Re_L = 4.690 \times 10^6$

SYM Y/L

\triangle	.1405	0 0 0 0 0 0 0 0 0
∇	.1719	-3 0 0 0 0 0 0 0 0
∇	.2034 .. 3	1 1 2-3 0 0 0 0 0
\triangle	.2349 .. 3	1 1 2-3 0 0 0
\diamond	.2653 .. 2	1 1-3-3 0 0
\circ	.2978 .. 2	1 1-3 0 0
\square	.3278	-3-3-3

0 = SEPARATED

\square = 1 = ATTACHED

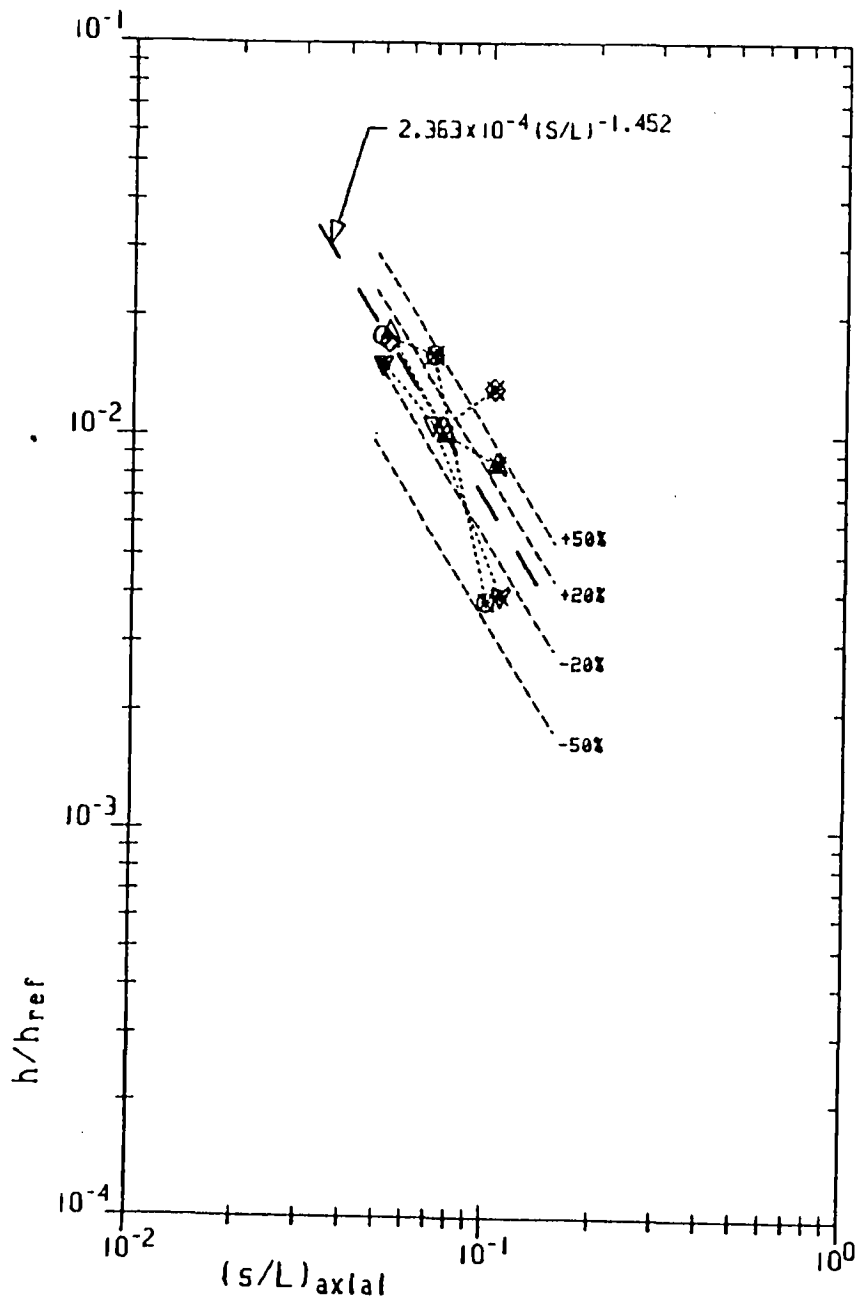
\boxplus = 2 = PRESEPARATED

\boxtimes = 3 = ANOMOLOUS

\star = NOT USED - USUALLY DATA ANOMOLY

10 PTS USED

RMS DEV = 14.46%



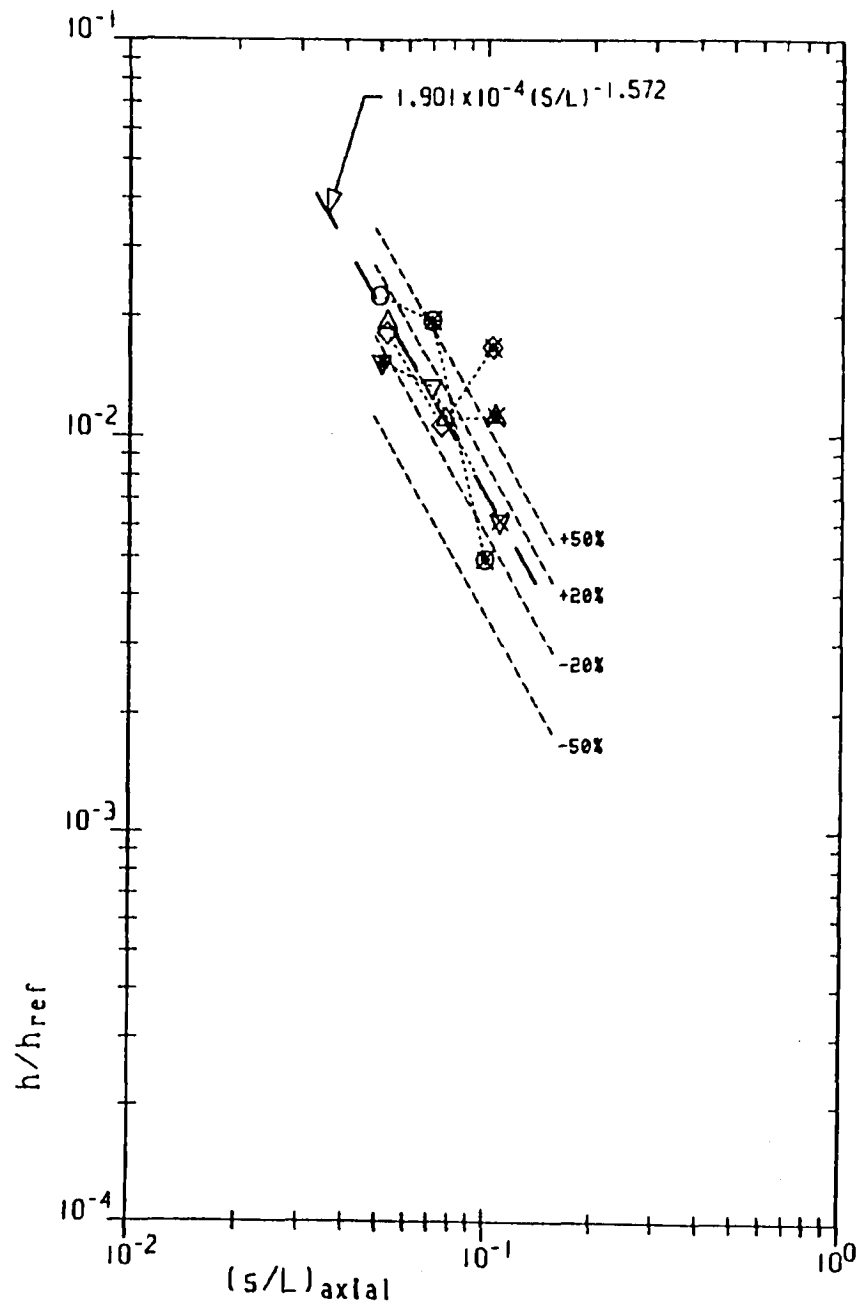
$M_{\infty} = 6. \dots 10$
 $\alpha = 35.$
 $Re_L = 5.150 \times 10^6$

SYM	Y/L	
△	.1405	0 0 0 0 0 0 0 0 0
△	.1719	0 0 0 0 0 0 0 0 0
▽	.2034 .. 1	-1 1-3 0 0 0 0 0 0 0
△	.2349 .. 2	1 1-3 0 0 0 0 0 0 0
◇	.2653 .. 2	1 1-3 0 0 0 0 0 0 0
○	.2978 .. 1	1-3-3 0 0 0 0 0 0
□	.3278	0 0 0

0 = SEPARATED
 □ = 1 = ATTACHED
 ⊗ = 3 = ANOMOLOUS
 ⊛ = NOT USED - USUALLY DATA ANOMOLY

6 PTS USED

RMS DEV = 3.52%



$M_\infty = 6. \dots 21$
 $\alpha = 40.$
 $Re_L = 5.200 \times 10^6$

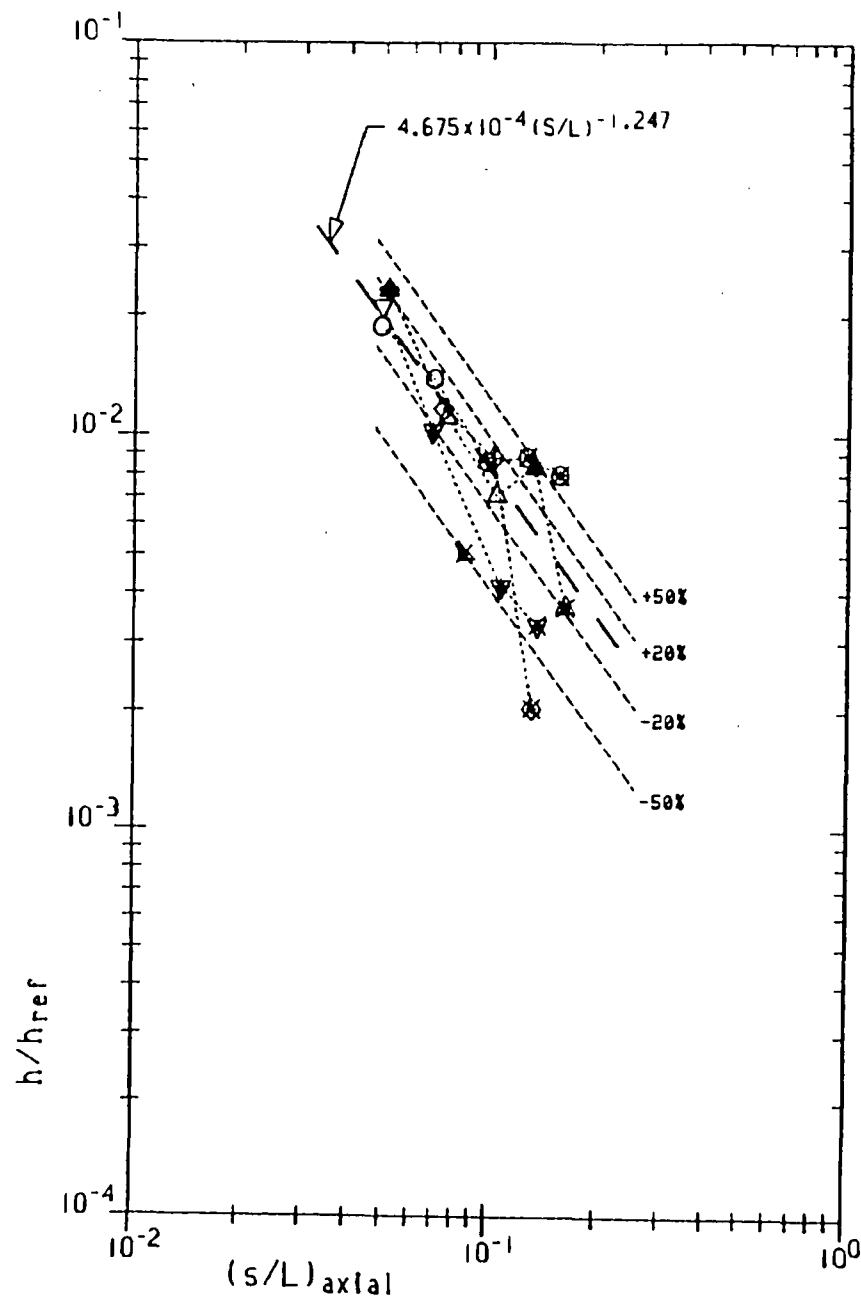
SYM V/L

△	.1405	0 0 0 0 0 0 0 0
△	.1719	0 0 0 0 0 0 0 0
▽	.2034 .. 2	-1 1 3 0 0 0 0 0
△	.2349 .. 2	1 1-3 0 0 0 0
◇	.2653 .. 2	1 1-3 0 0 0
○	.2978 .. 1	1-3-3 0 0
□	.3278	0 0 0

0 = SEPARATED
 □ = 1 = ATTACHED
 ⊗ = 3 = ANOMOLOUS
 ⊠ = - - - NOT USED - USUALLY DATA ANOMOLY

7 PTS USED

RMS DEV = 5.17%



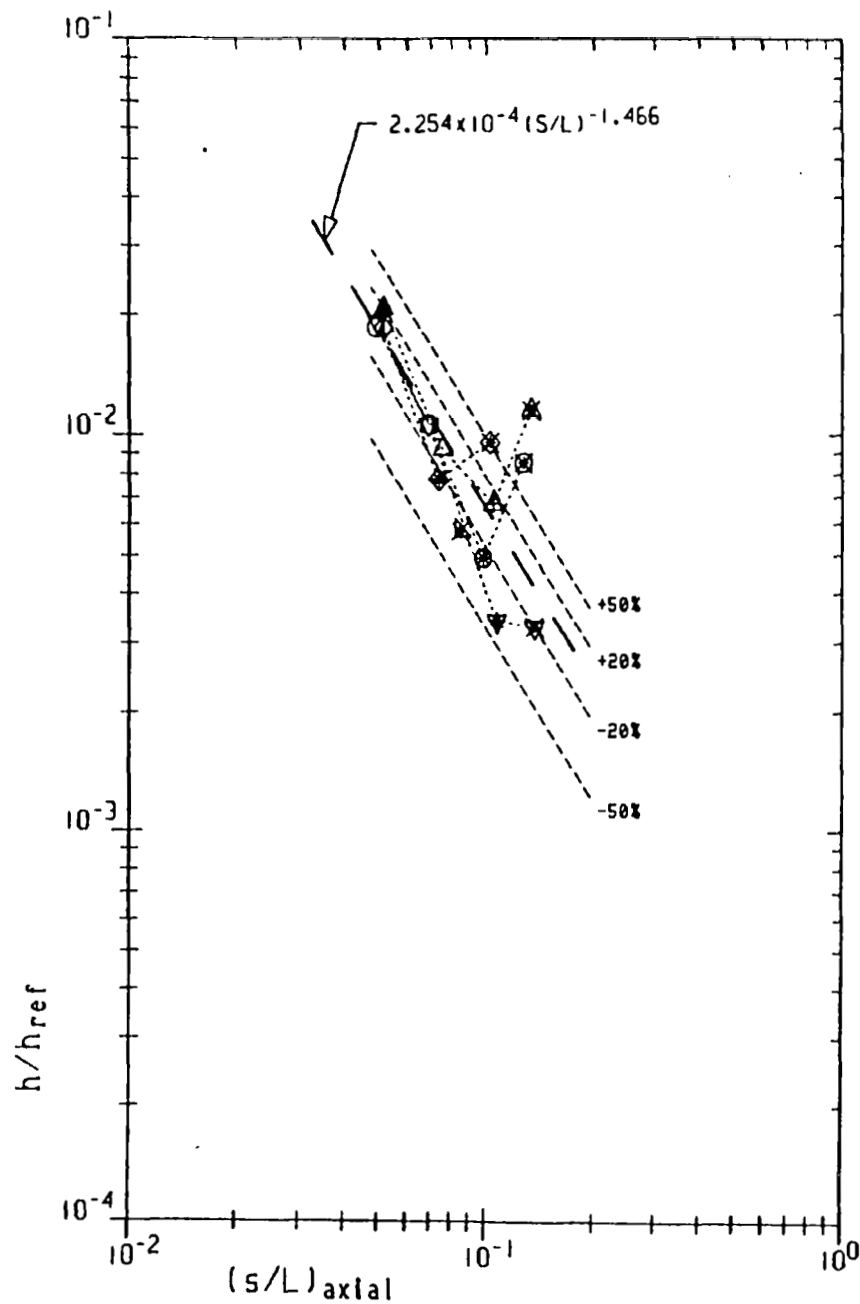
$M_\infty = 6. \dots 2$
 $\alpha = 20.$
 $Re_L = 6.585 \times 10^6$

SYM	Y/L	
\triangle	.1405	0 0 0 0 0 0 0 0 0
\triangle	.1719	-3 0 0 0 0 0 0 0 0
∇	.2034 .. 1	1-2-2-3 0 0 0 0 0
\triangle	.2349 .. 2	-4 1 1-2-3 0 0
\diamond	.2653 .. 2	-4 1 2-3 0 0
\circ	.2978 .. 3	1 1 2-3-3
\square	.3278	0 0 0

0 = SEPARATED
 1 = ATTACHED
 2 = PRESEPARATED
 3 = ANOMOLOUS
 4 = STRAKE/BOW SHOCK?
 -/- NOT USED - USUALLY DATA ANOMOLY

8 PTS USED

RMS DEV = 6.65 %



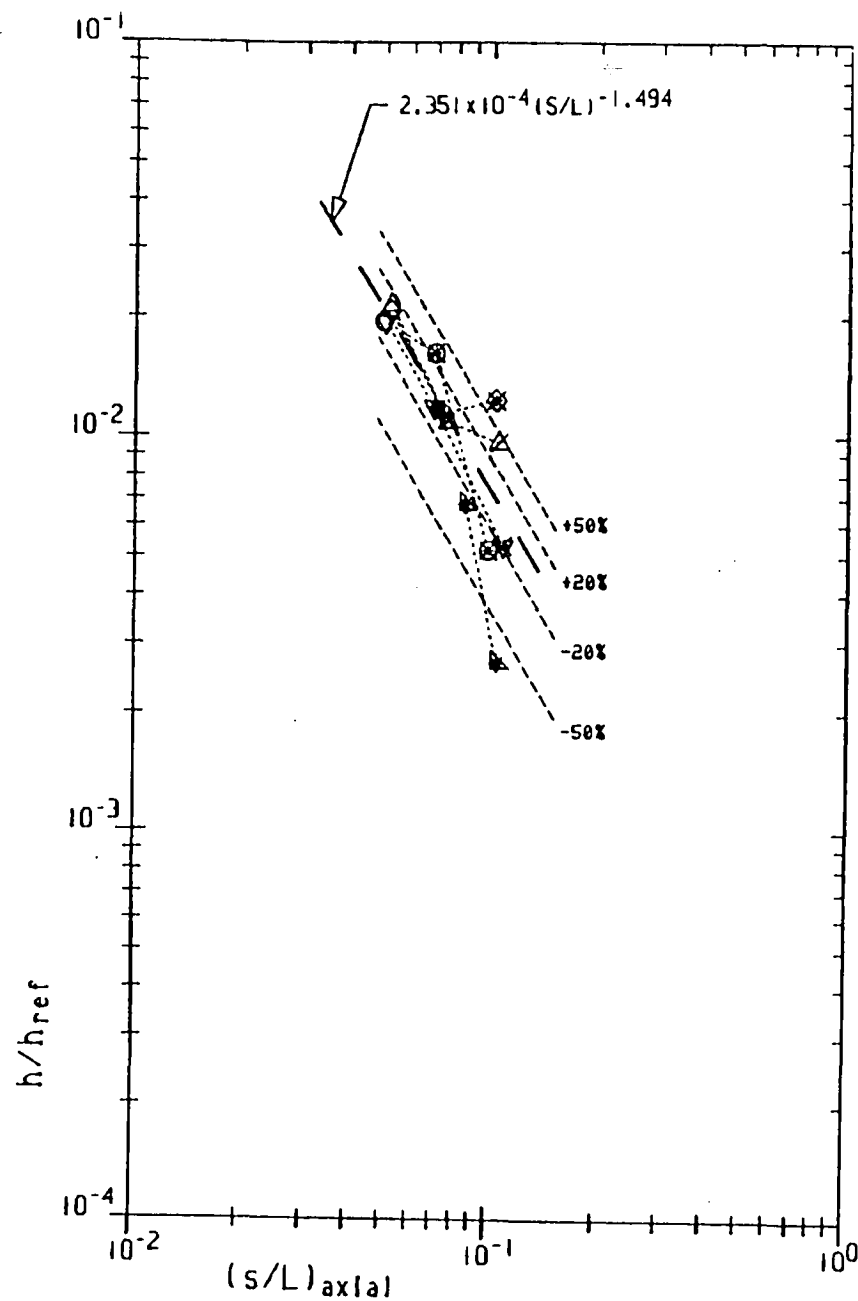
$M_{\infty} = 6. \dots 12$
 $a = 25.$
 $Re_s = 7.100 \times 10^6$

SYM	Y/L	
\triangle	.1405	0 0 0 0 0 0 0 0 0
∇	.1719	-3 0 0 0 0 0 0 0 0
∇	.2034 .. 2	1 1-2-3 0 0 0 0 0
\triangle	.2349 .. 2	-4 1 2-3 0 0 0
\diamond	.2653 .. 1	1-2-3 0 0 0
\circ	.2978 .. 2	1 1-2-3 0
\square	.3278	0 0 0

0 = SEPARATED
 1 = ATTACHED
 2 = PRESEPARATED
 3 = FLNONOIOUS
 4 = STRAKE/BOW SHOCK?
 - - - NOT USED - USUALLY DATA ANOMOLY

7 PTS USED

RMS DEU = 6.19%



$M_\infty = 6. \dots 16$
 $\alpha = 30.$
 $Re_L = 7.070 \times 10^6$

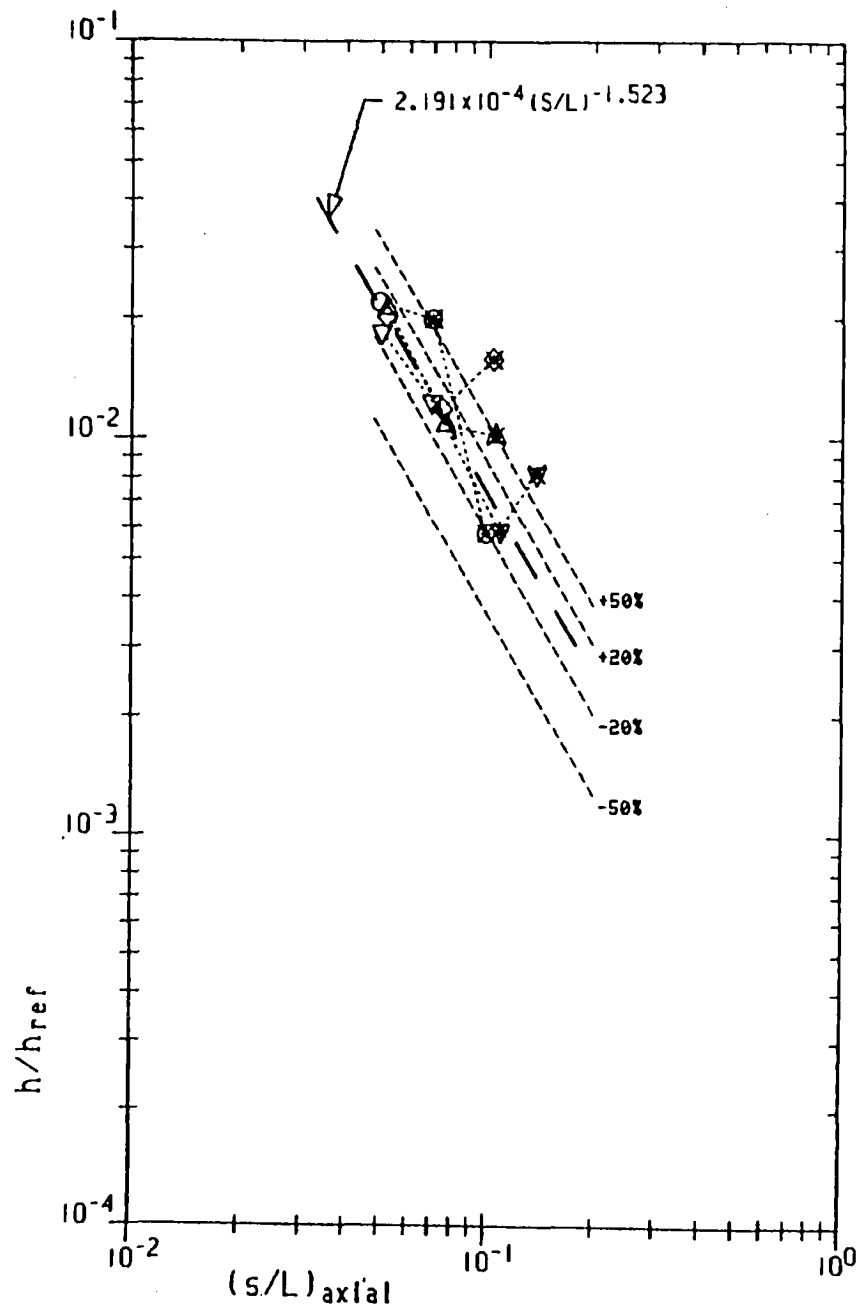
SYM Y/L

\triangle	.1405	0 0 0 0 0 0 0 0 0
∇	.1719	-2-2 0 0 0 0 0 0 0
\triangle	.2034 .. 1	1-2-3 0 0 0 0 0 0
\triangle	.2349 .. 2	1 1-8 0 0 0 0
\diamond	.2653 .. 1	1-2-3 0 0 0
\circ	.2978 .. 1	1-3-3 0 0
\square	.3278	0 0 0

0 = SEPARATED
 1 = ATTACHED
 2 = PRESEPARATED
 3 = ANOMOLOUS
 8 = SEPARATED, NOT USED BUT SHOWN
 -'- NOT USED - USUALLY DATA ANOMOLY

5 PTS USED

RMS DEV = 6.53 %



$M_{\infty} = 6. \dots 19$
 $\alpha = 35.$
 $Re_L = 7.096 \times 10^6$

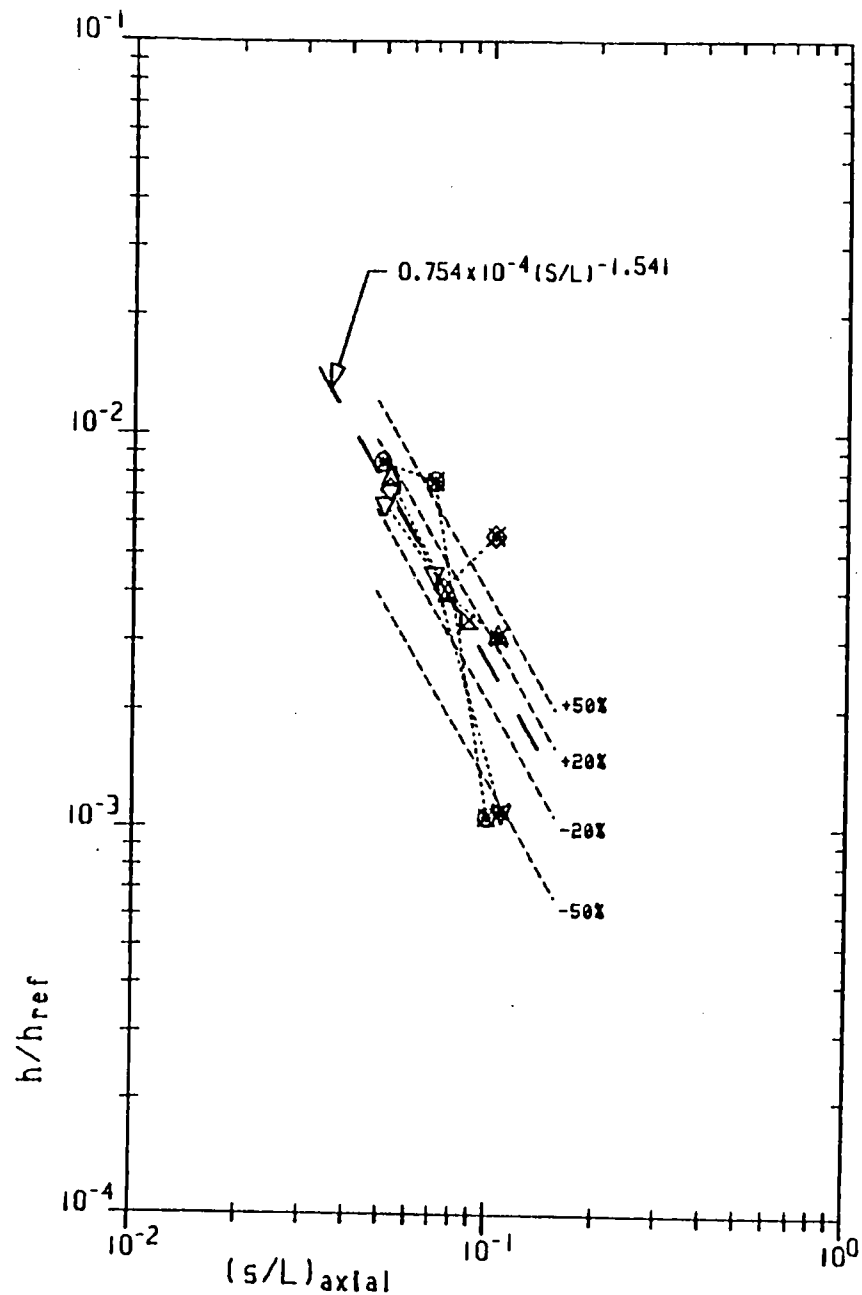
SYM Y/L

\triangle	.1405	0 0 0 0 0 0 0 0 0
\triangle	.1719	0 0 0 0 0 0 0 0 0
∇	.2034 .. 2	1 1-2-3 0 0 0 0 0
\triangle	.2349 .. 2	1 1-3 0 0 0 0 0
\diamond	.2653 .. 2	1 1-3 0 0 0
\circ	.2978 .. 1	1-3-3 0 0
\square	.3278	0 0 0

0 • SEPARATED
 \square • 1 • ATTACHED
 \oplus • 2 • PRESEPARATED
 \boxtimes • 3 • ANOMOLOUS
 \ominus • NOT USED - USUALLY DATA ANOMOLY

7 PTS USED

RMS DEV • 5.93%



$M_\infty = 6. \dots 20$
 $\alpha = 40.$
 $Re_L = 6.730 \times 10^6$

SYM Y/L

\triangle	.1405	0 0 0 0 0 0 0 0 0
∇	.1719	-8 0 0 0 0 0 0 0 0
∇	.2034 .. 2	1 1-3 0 0 0 0 0 0
\triangle	.2349 .. 2	1 1-3 0 0 0 0 0
\diamond	.2653 .. 2	1 1-3 0 0 0
\circ	.2978	-1-3-3 0 0
\square	.3278	0 0 0

0 = SEPARATED
 \square = 1 = ATTACHED
 \boxtimes = 3 = ANOMOLOUS
 \boxdot = 8 = SEPARATED, NOT USED BUT SHOWN
 \boxminus = NOT USED - USUALLY DATA ANOMOLY

6 PTS USED

RMS DEV = 5.96 %

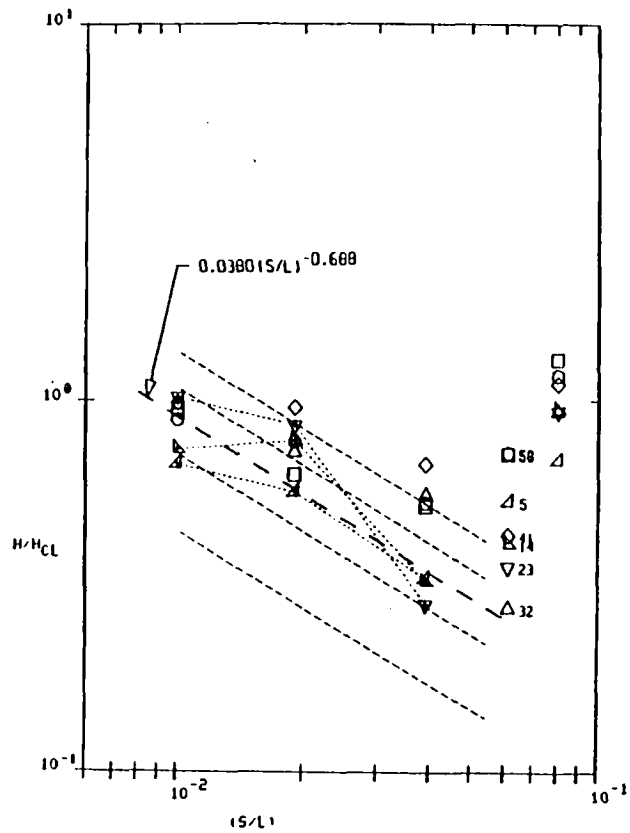
APPENDIX I

Upper Fuselage Heating Correlations

This appendix contains all the correlations of heat transfer ratios for attached flow in the forward and aft regions of the fuselage upper surface.

9 PTS USED

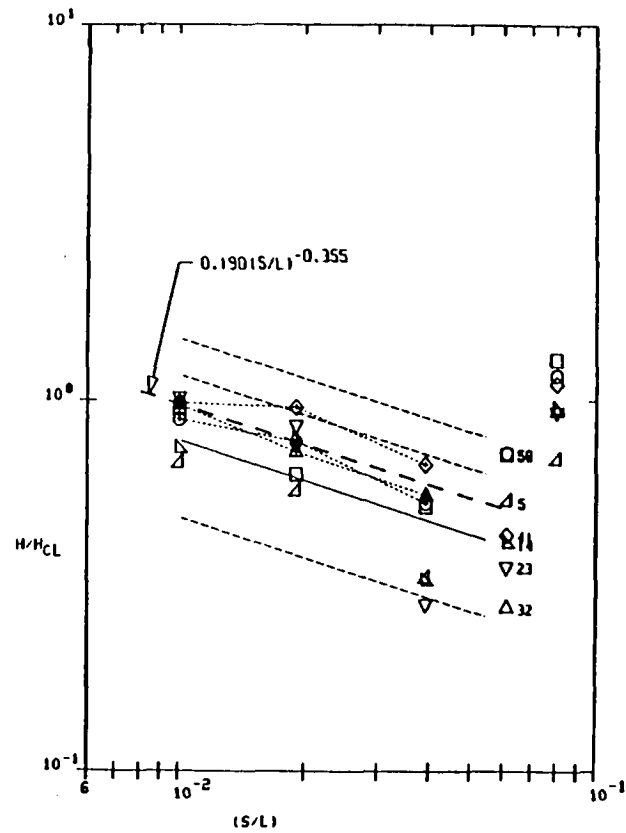
PCT E EST = .21129



Forward

9 PTS USED

PCT E EST = .09636

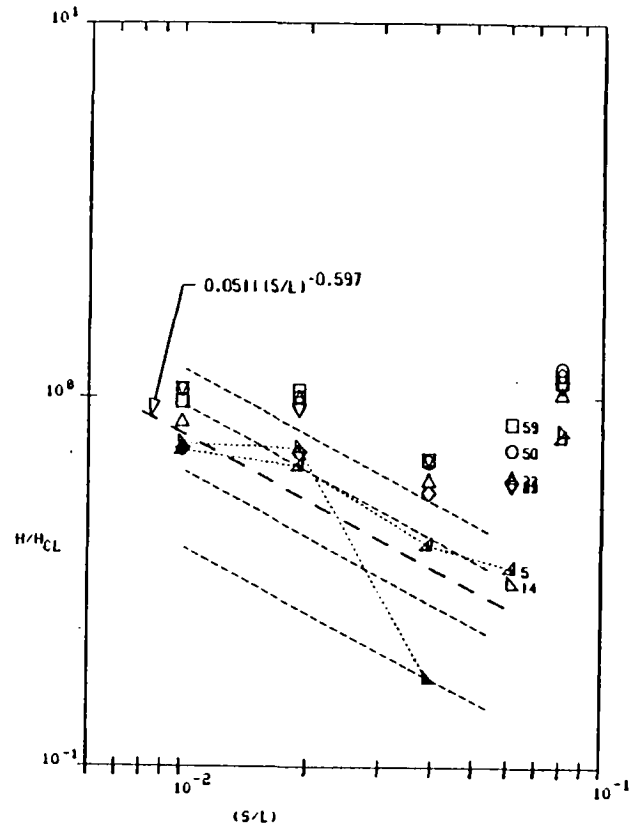


Aft

MACH = 10.16 .. 12
 ALPHA = 20.
 RE NO. = .50

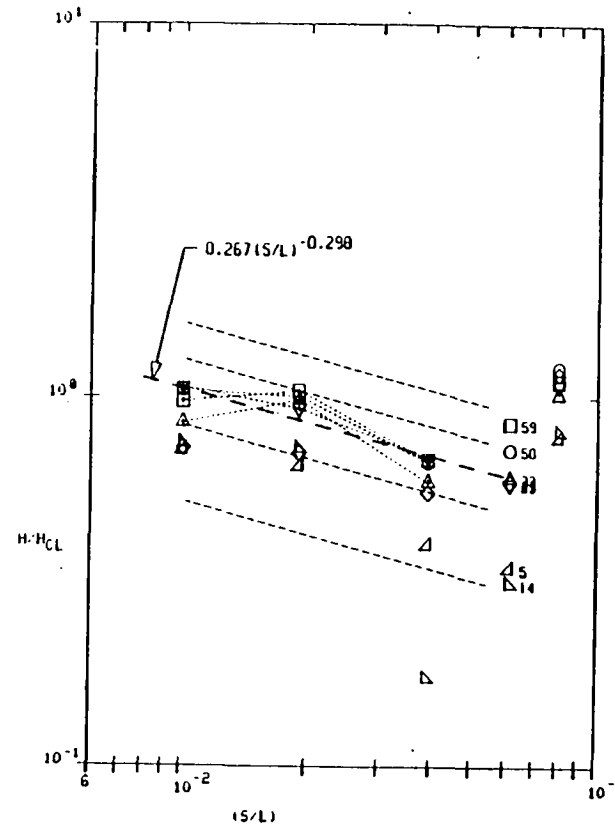
SYM	X/L
△	.. .383
▽	.. .447
◇	.. .510
△	.. .573
○	.. .637
○	.. .682
□	.. .731

7 PTS USED
PCT E EST = .41288



Forward

12 PTS USED
PCT E EST = .11562



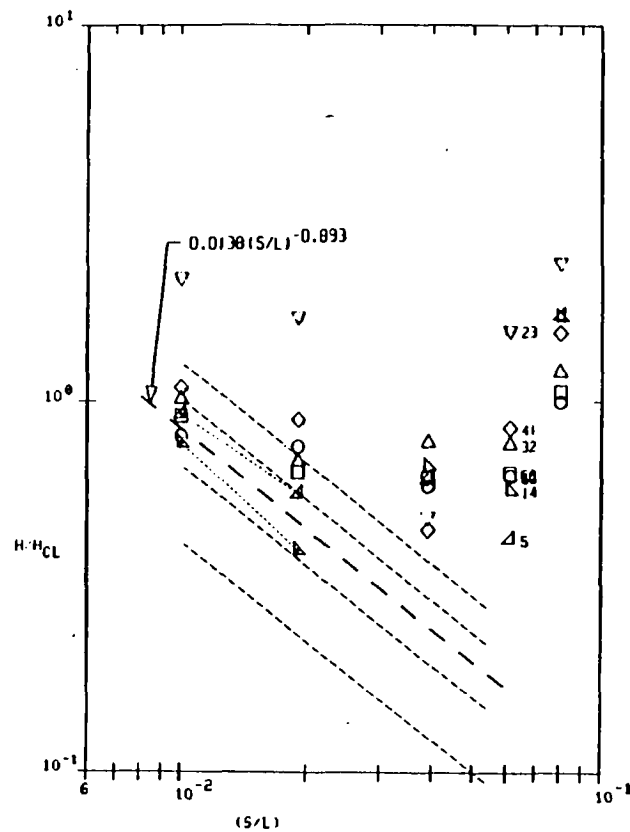
Aft

MACH = 10.16 .. 13
ALPHA = 25.
RE NO. = .50

SYM	X/L
△	.. .383
▽	.. .447
△	.. .510
△	.. .573
○	.. .637
○	.. .682
□	.. .731

4 PTS USED

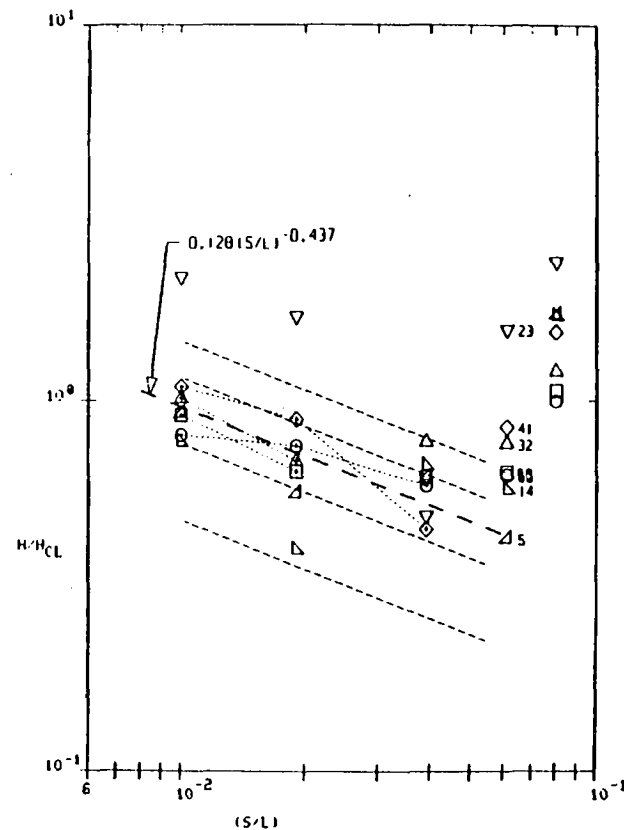
PCT E EST = .13829



Forward

10 PTS USED

PCT E EST = .12166



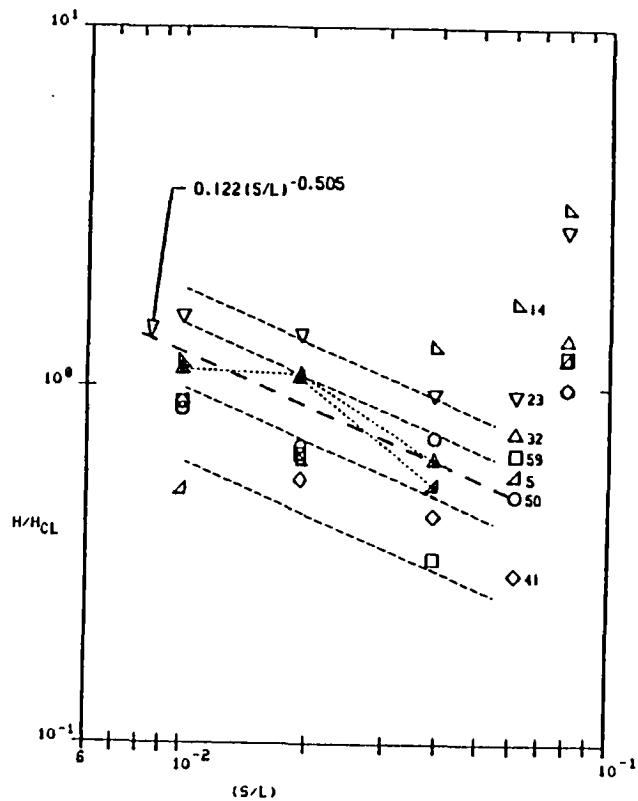
Aft

MACH = 10.16 .. 14
ALPHA = 30.
RE NO. = .50

SYM	X/L
△	.. .383
▽	.. .447
▽	.. .510
△	.. .573
○	.. .637
○	.. .682
□	.. .731

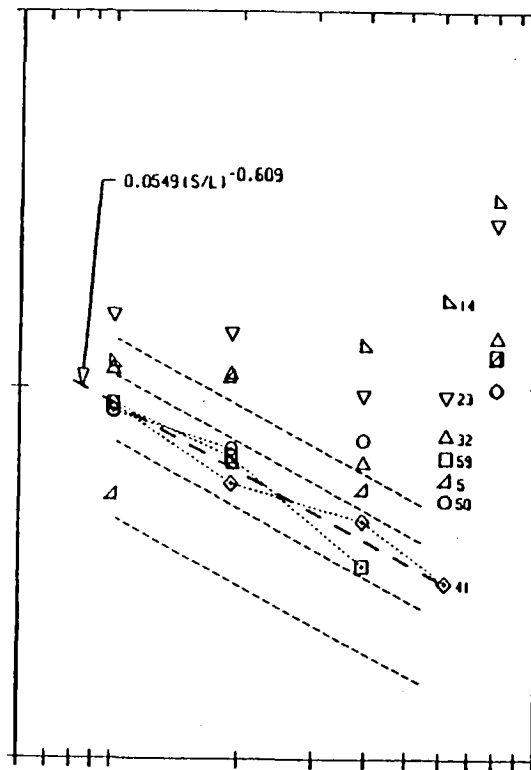
6 PTS USED

PCT E EST = .13949



9 PTS USED

PCT E EST = .08825

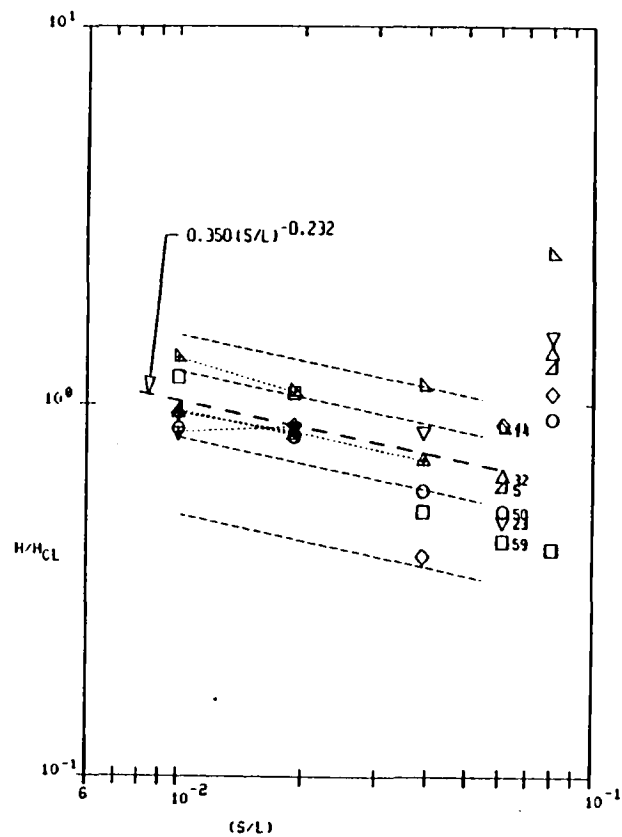


MACH = 10.16 .. 15
 ALPHA = 35.
 RE NO. = .50

SYM - X/L
 Δ383
 ▽447
 ▽510
 Δ573
 ○637
 ○682
 □731

9 PTS USED

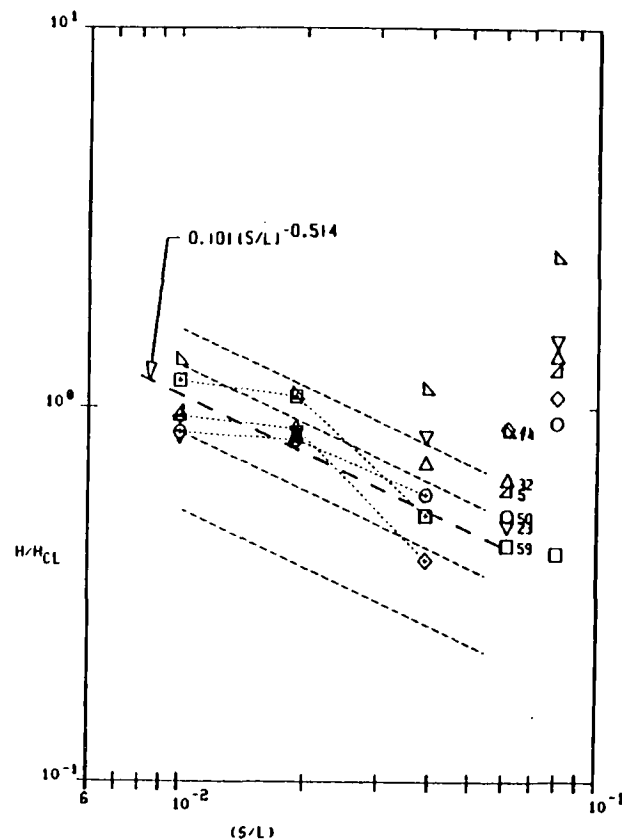
PCT E EST = .12840



Forward

9 PTS USED

PCT E EST = .18751



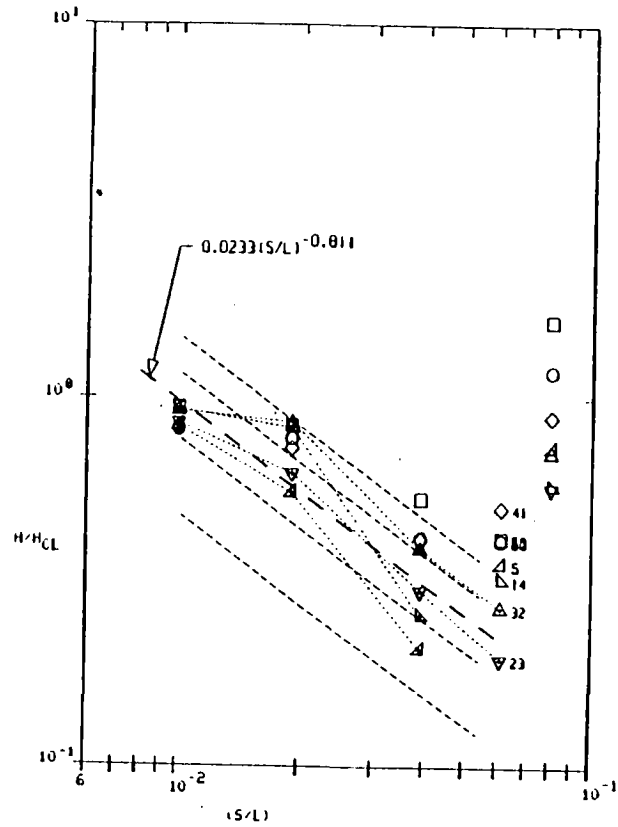
Aft

MACH = 10.16 .. 20
ALPHA = 40.
RE NO. = .50

SYM	X/L
△	.. .383
△	.. .447
▽	.. .510
△	.. .573
○	.. .637
○	.. .682
□	.. .731

14 PTS USED

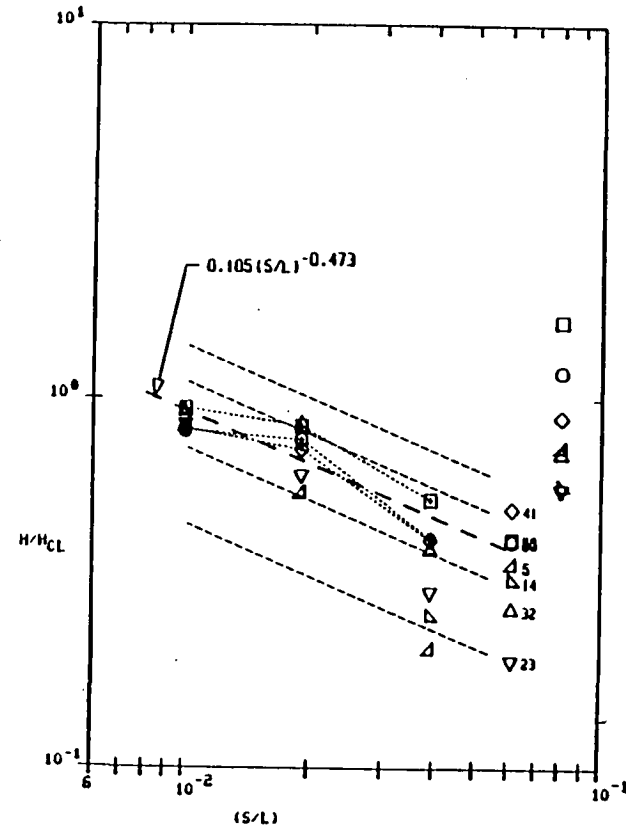
PCT E EST = .21809



Forward

9 PTS USED

PCT E EST = .12477



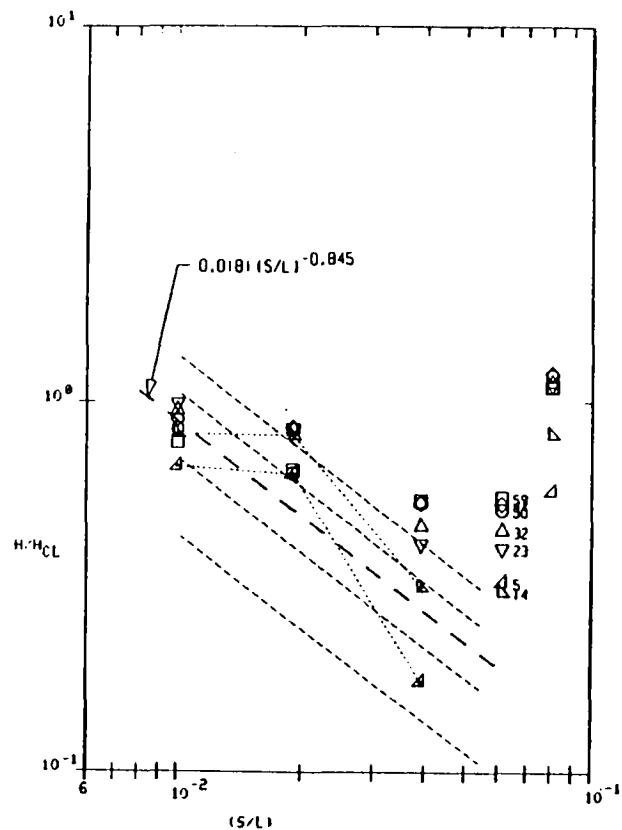
Aft

MACH = 10.34 .. 3
ALPHA = 20.
RE NO. = 1.00

SYM	X/L
△	.. .383
▽	.. .447
△	.. .510
△	.. .573
○	.. .637
○	.. .682
□	.. .731

6 PTS USED

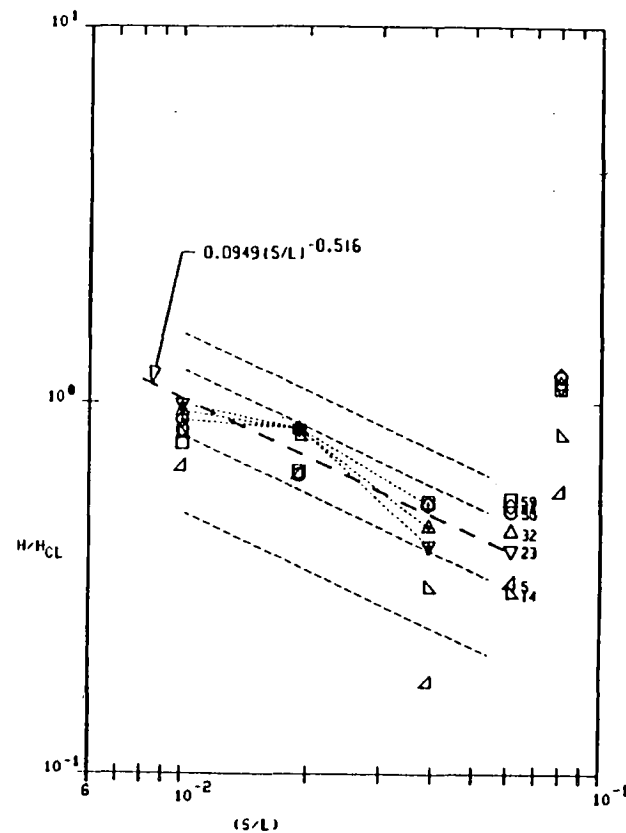
PCT E EST = .32245



Forward

9 PTS USED

PCT E EST = .12384

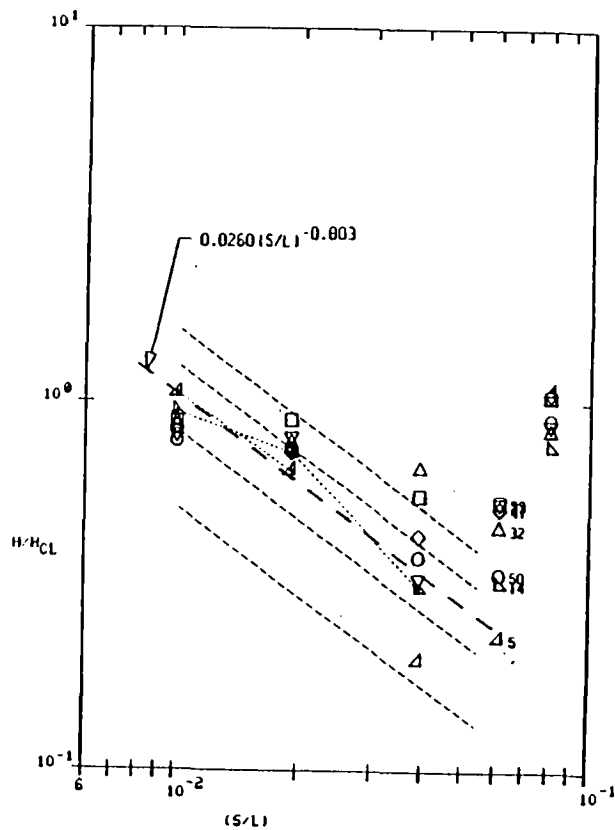


Aft

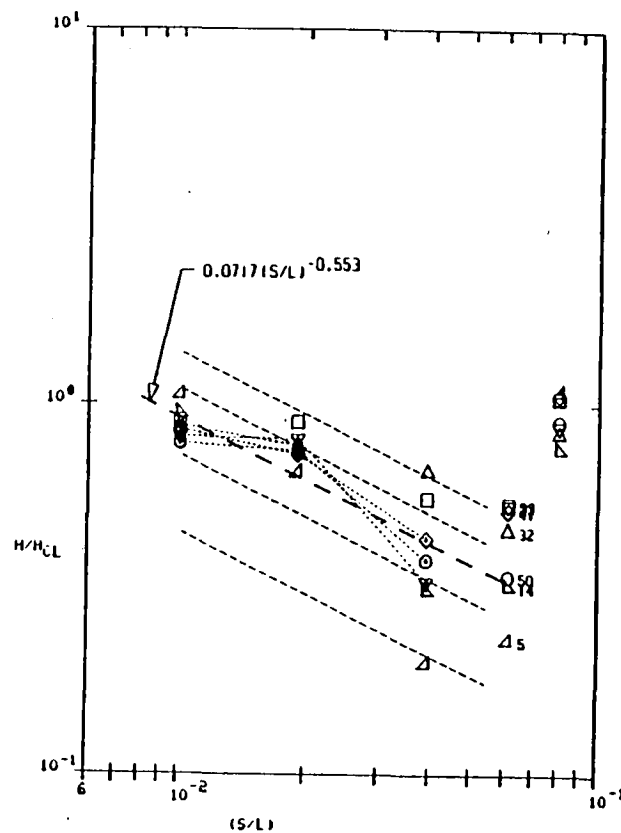
MACH = 10.34 .. 4
ALPHA = 25.
RE NO. = 1.00

SYM	X/L
△	.. .383
△	.. .447
▽	.. .510
△	.. .573
○	.. .637
○	.. .682
□	.. .731

5 PTS USED
PCT E EST = .09610



11 PTS USED
PCT E EST = .14985

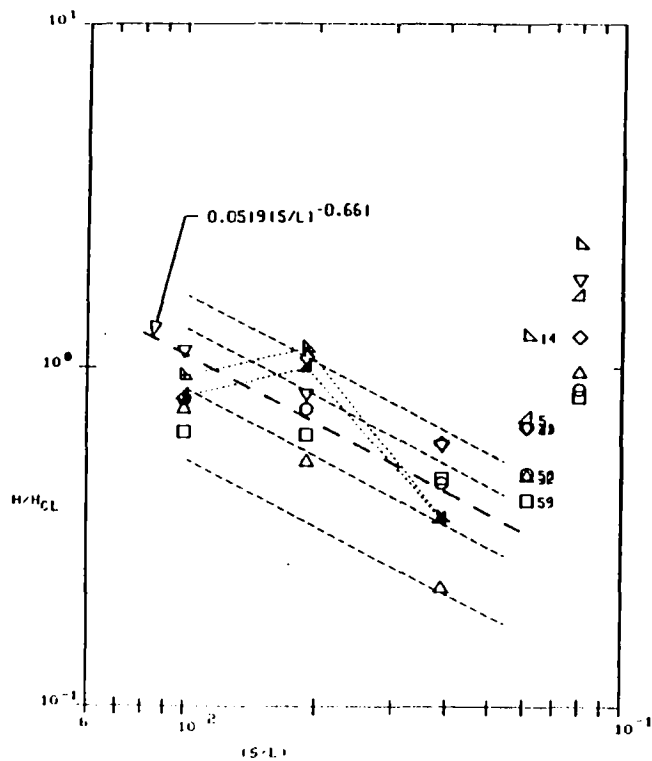


MACH = 10.34 .. 5
ALPHA = 30.
RE NO. = 1.00

SYM	X/L
Δ	.. .383
▽	.. .447
△	.. .510
△	.. .573
○	.. .637
○	.. .682
□	.. .731

6 PTS USED

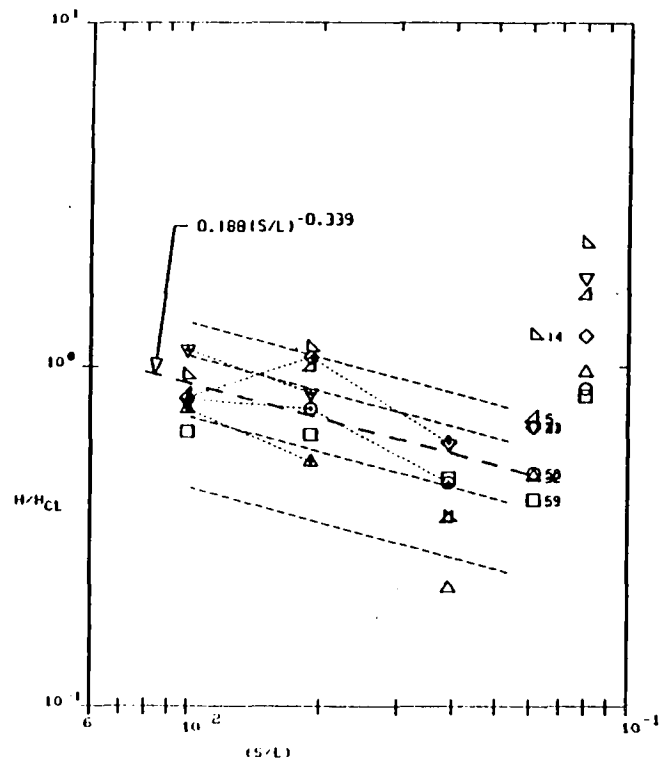
PCT E EST = .26857



Forward

10 PTS USED

PCT E EST = .20079



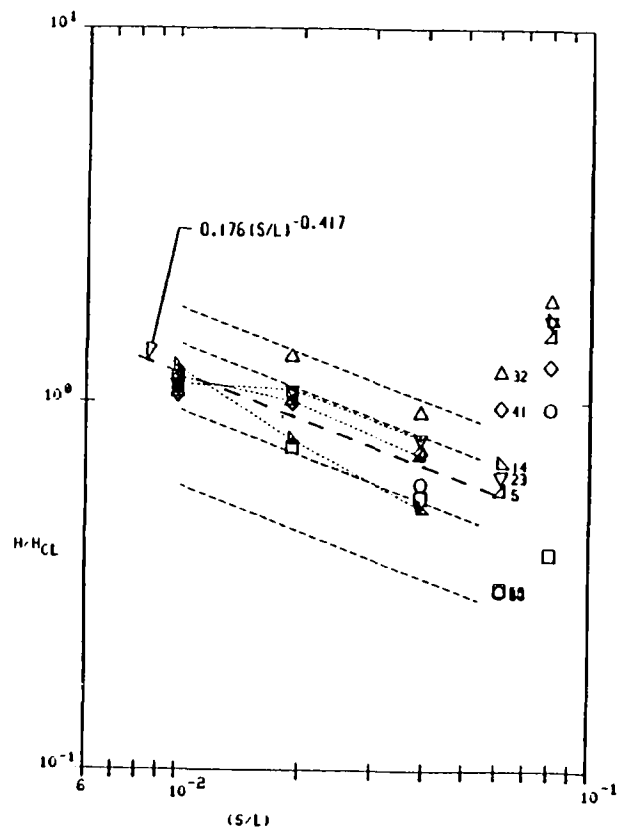
MACH = 10.34 .. 6
ALPHA = 35.
RE NO. = 1.00

SYM	X/L
△	.. .383
▽	.. .447
△	.. .510
◇	.. .573
◇	.. .637
○	.. .682
□	.. .731

Aft

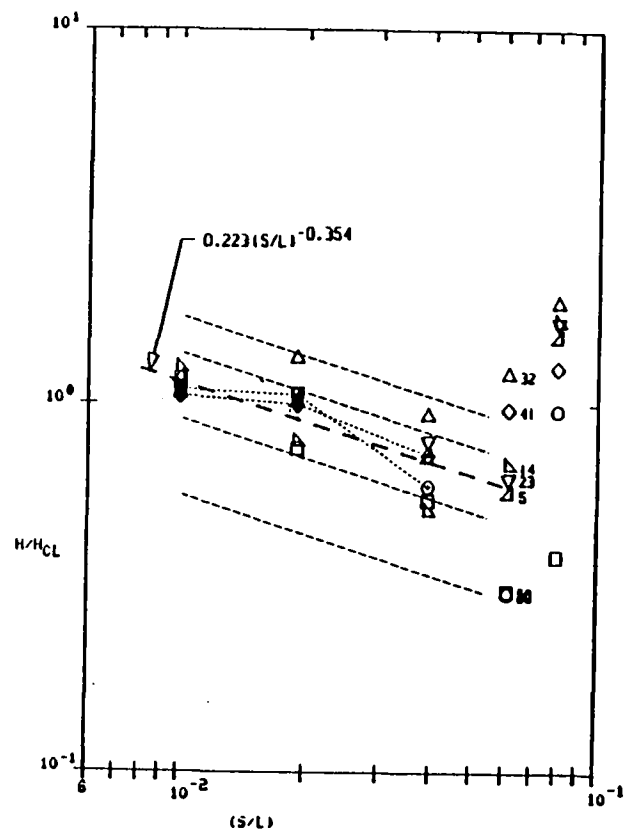
9 PTS USED

PCT E EST = .14355



6 PTS USED

PCT E EST = .10517

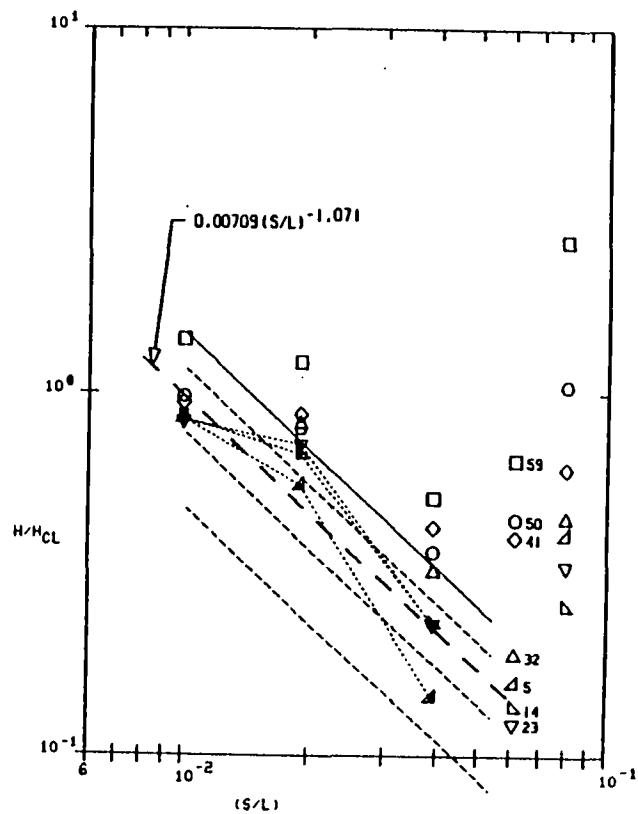


MACH = 10.34 .. 16
ALPHA = 40.
RE NO. = 1.00

SYM	X/L
△	.. .383
▽	.. .447
△	.. .510
△	.. .573
◇	.. .637
○	.. .682
□	.. .731

9 PTS USED

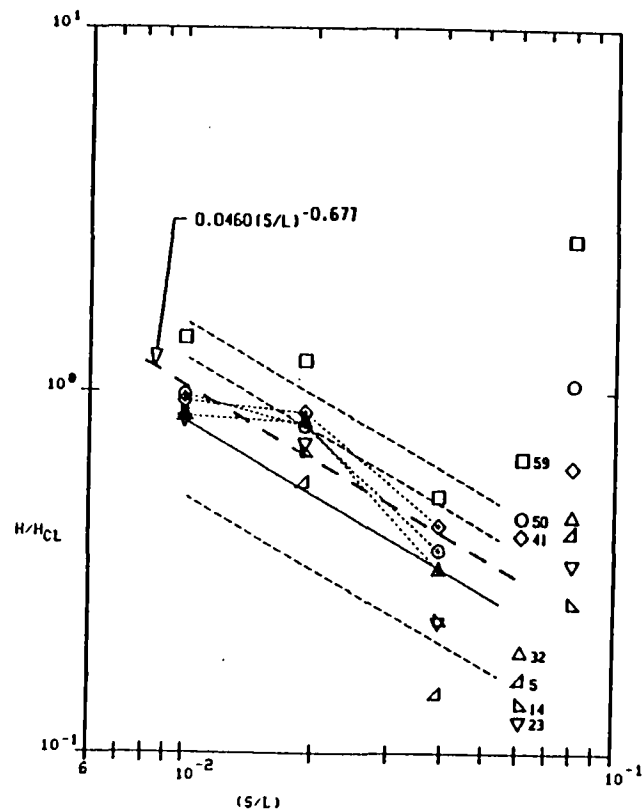
PCT E EST = .25521



Forward

9 PTS USED

PCT E EST = .17848



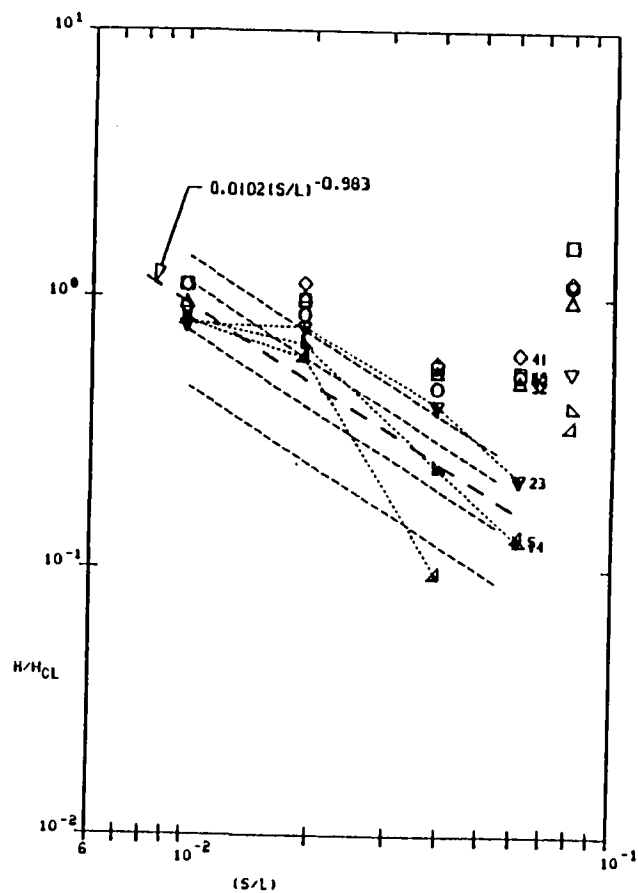
Aft

MACH = 10.36 .. 8
 ALPHA = 20.
 RE NO. = 2.40

SYM	X/L
△	.. .383
△	.. .447
▽	.. .510
△	.. .573
○	.. .637
○	.. .682
□	.. .731

11 PTS USED

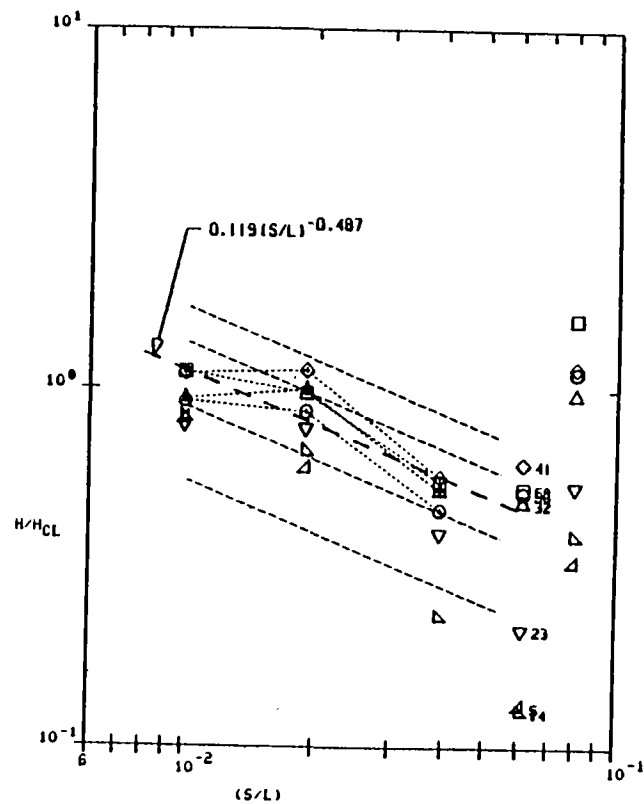
PCT E EST = .53602



Forward

12 PTS USED

PCT E EST = .15355



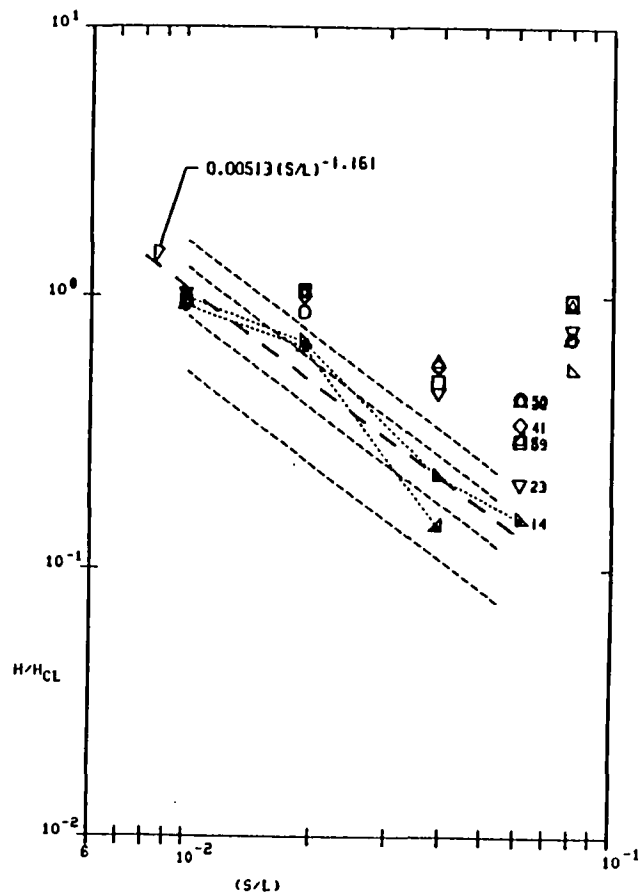
MACH = 10.36 .. 9
 ALPHA = 25.
 RE NO. = 2.40

SYM	X/L
△	.. .383
△	.. .447
▽	.. .510
△	.. .573
○	.. .637
○	.. .682
□	.. .731

Aft

7 PTS USED

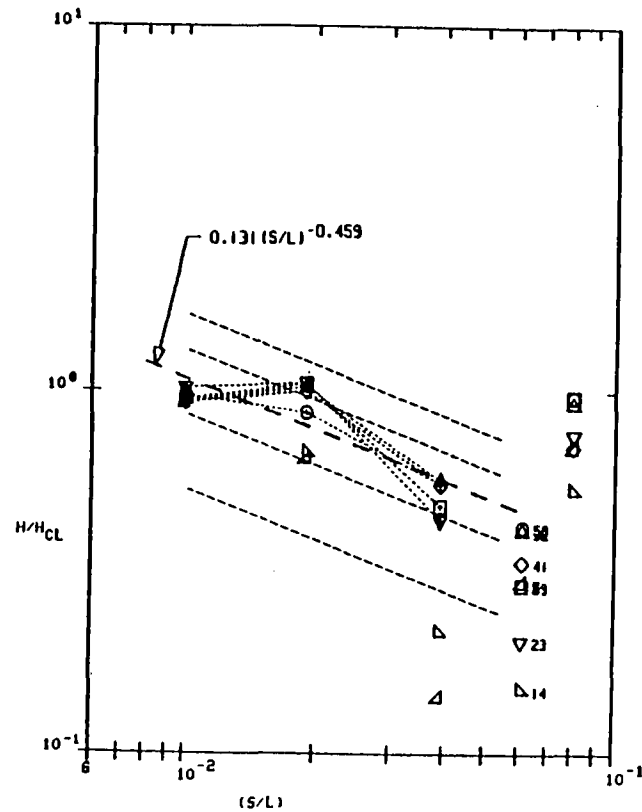
PCT E EST = .25416



Forward

15 PTS USED

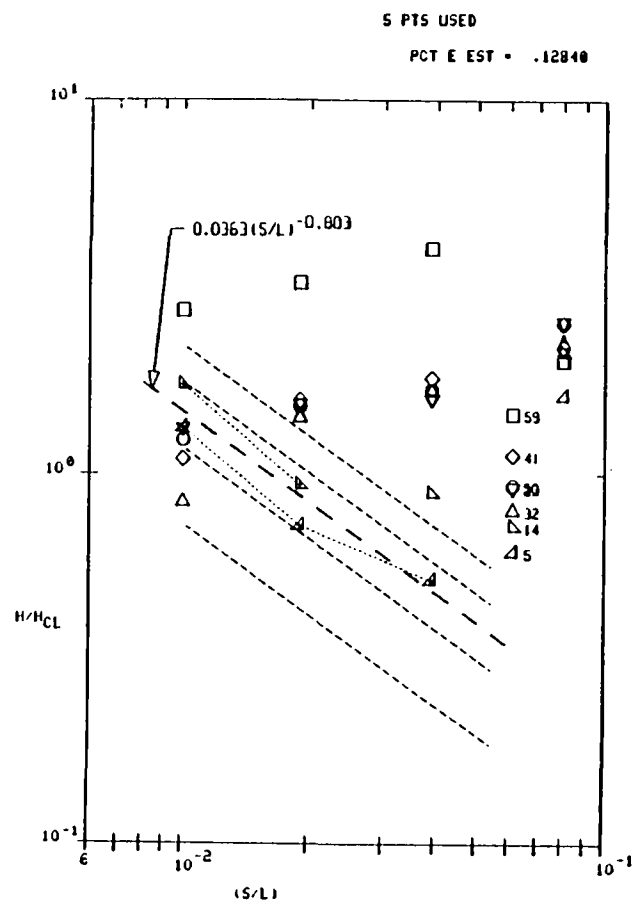
PCT E EST = .16434



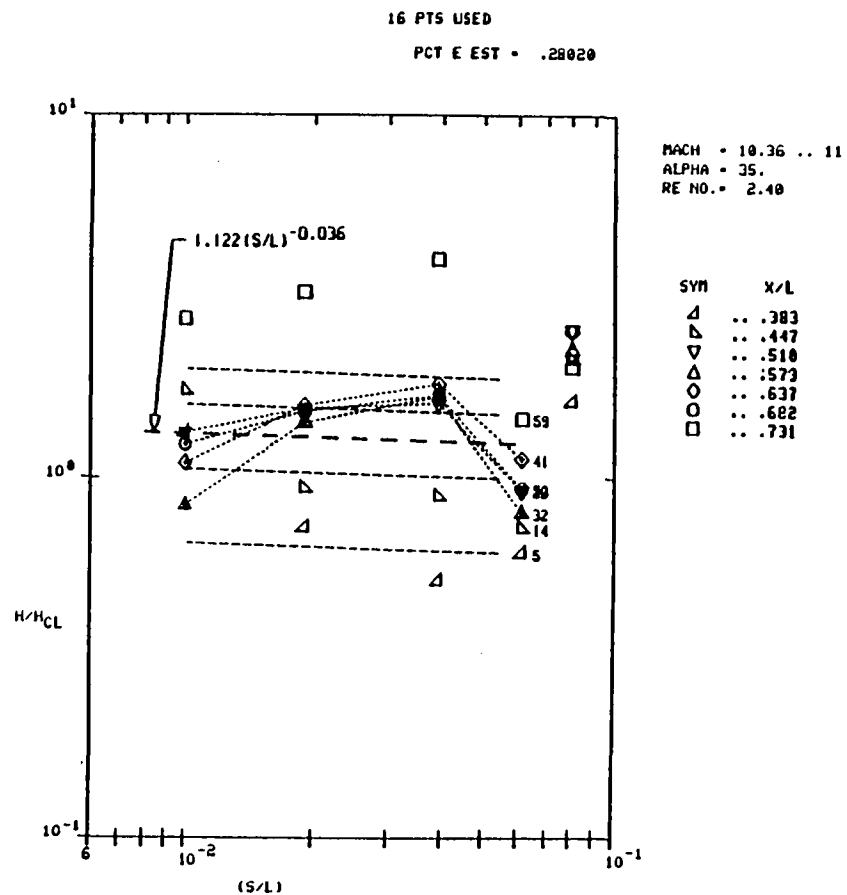
Aft

MACH = 10.36 .. 10
ALPHA = 30.
RE NO. = 2.40

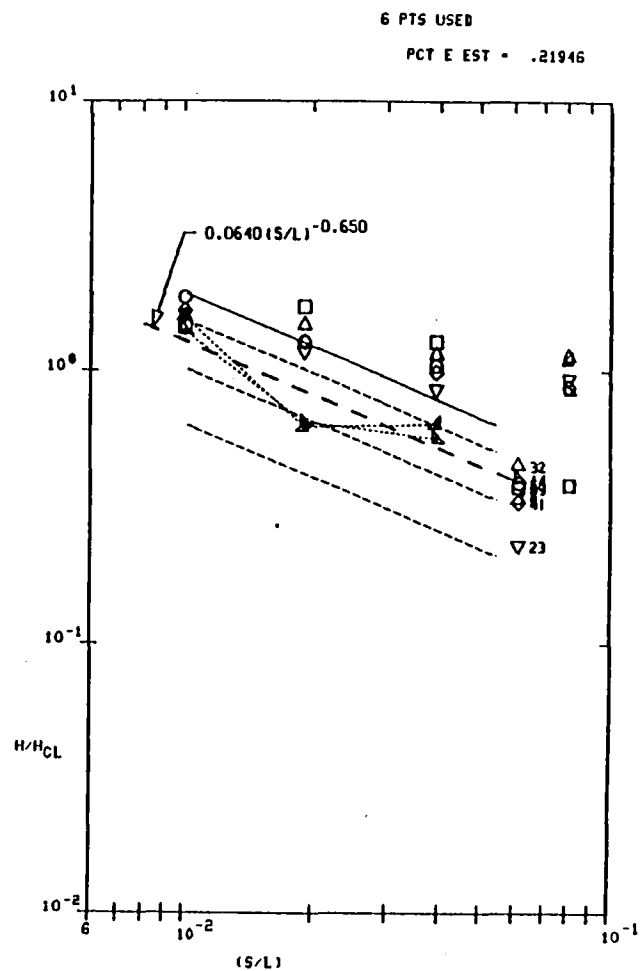
SYM	X/L
△	.. .383
▽	.. .447
△	.. .510
△	.. .573
◇	.. .637
○	.. .682
□	.. .731



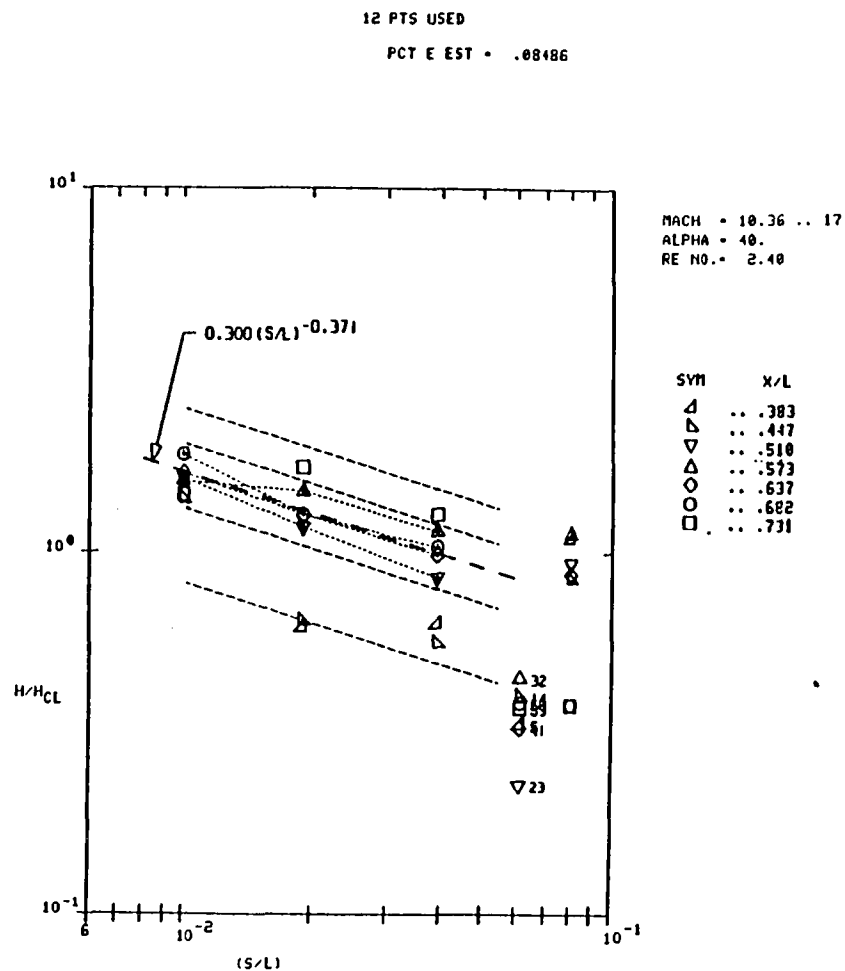
Forward



Aft



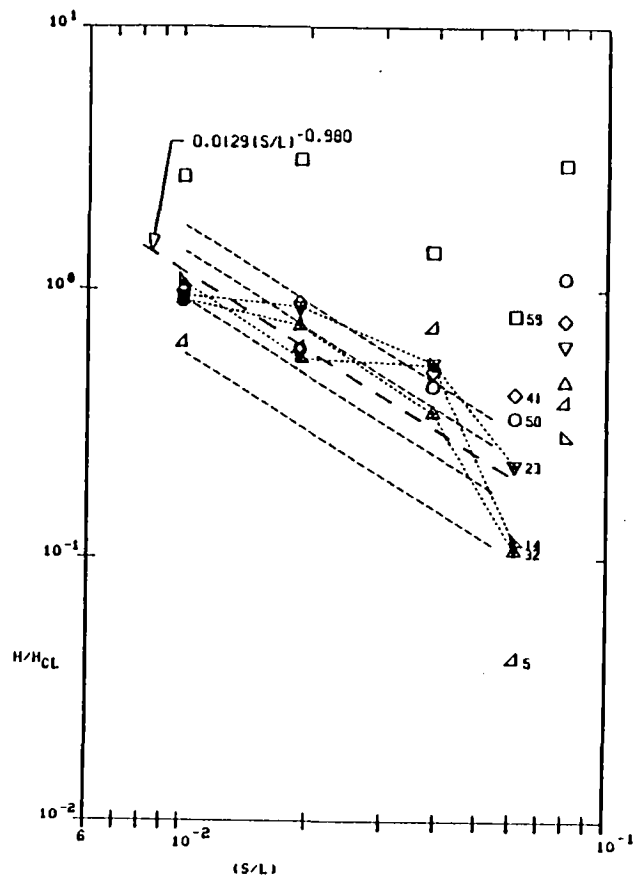
Forward



Aft

12 PTS USED

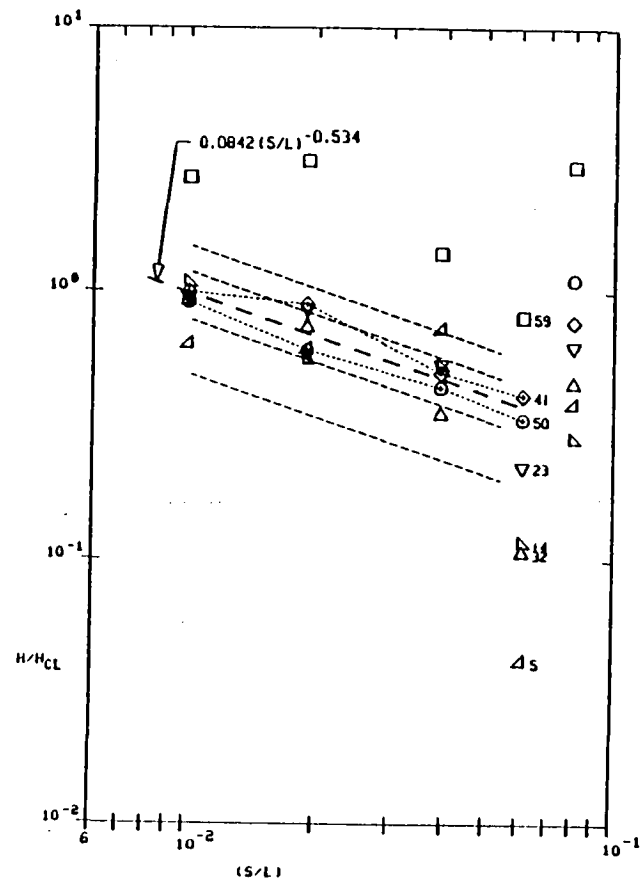
PCT E EST = .39873



Forward

8 PTS USED

PCT E EST = .11626



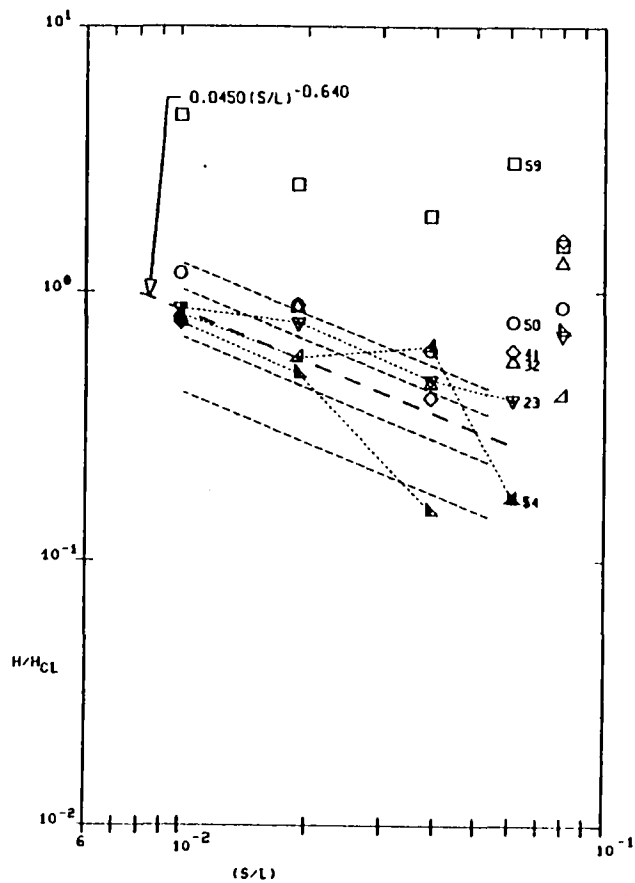
Aft

MACH = 6.00 .. 20
ALPHA = 20.
RE NO. = 1.10

SYM	X/L
△	.. .383
▽	.. .447
◇	.. .510
△	.. .573
○	.. .637
○	.. .682
□	.. .731

11 PTS USED

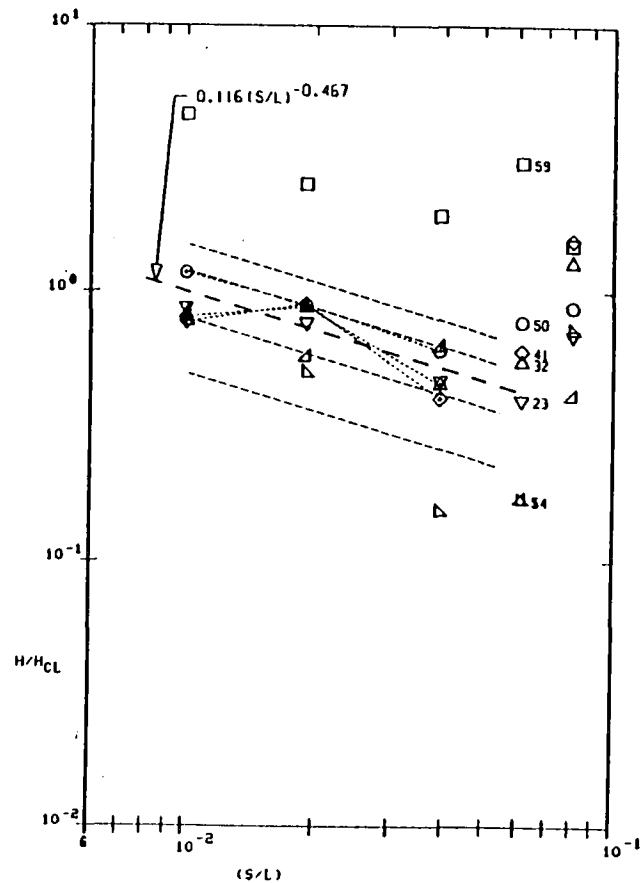
PCT E EST = .48171



Forward

9 PTS USED

PCT E EST = .20580



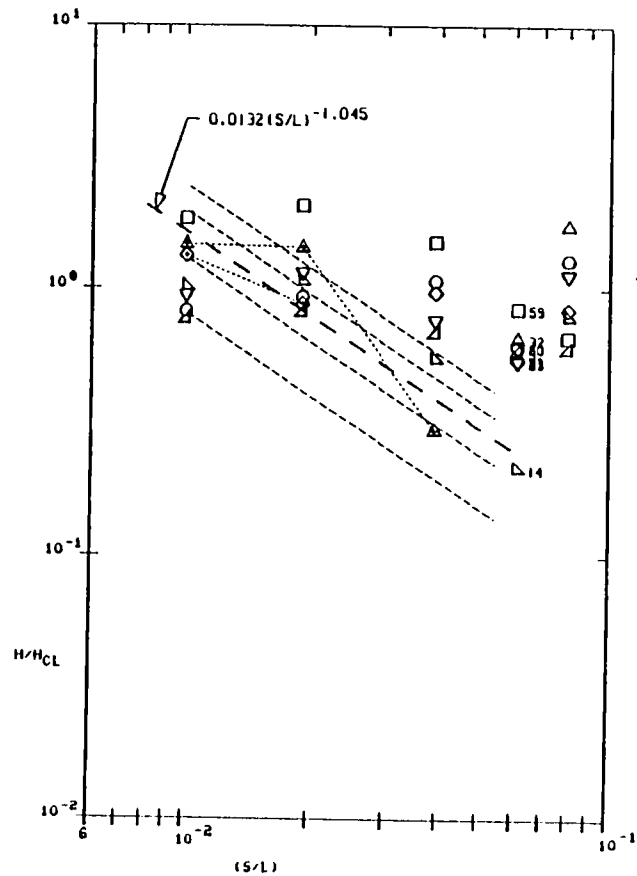
MACH = 6.00 ± .21
ALPHA = 25.
RE NO. = 1.10

SYM	X/L
△	.. .383
△	.. .447
▽	.. .510
△	.. .573
○	.. .637
○	.. .682
□	.. .731

Aft

5 PTS USED

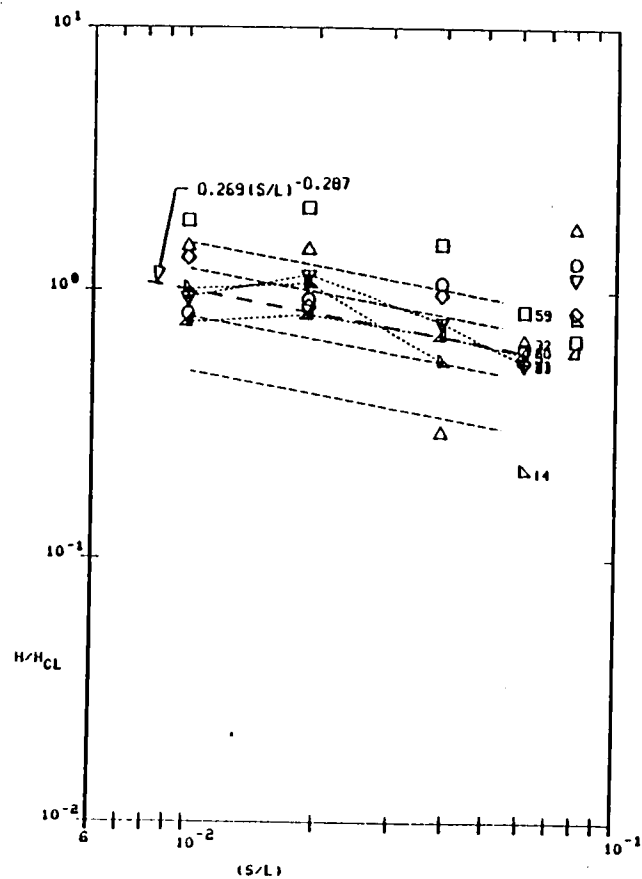
PCT E EST = .26266



Forward

11 PTS USED

PCT E EST = .16713



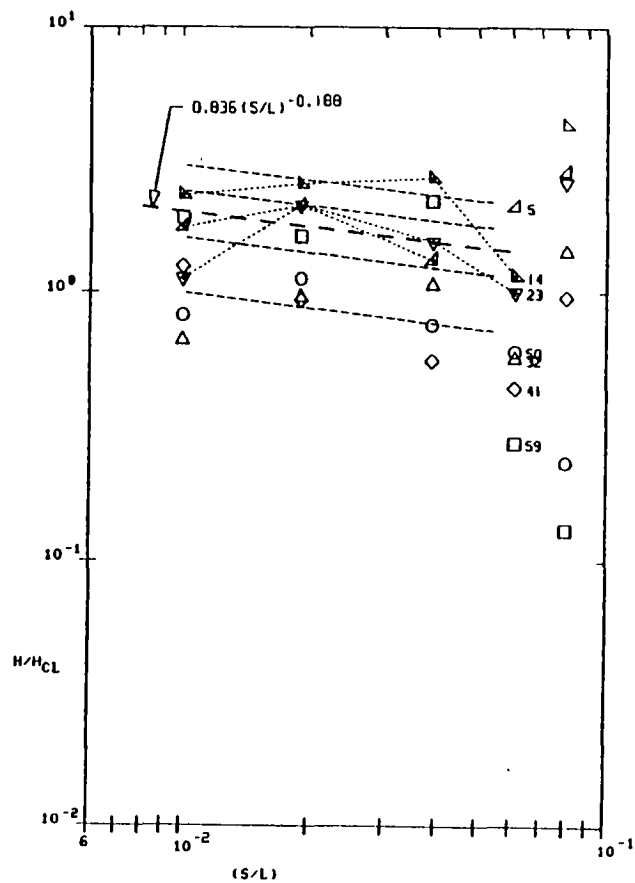
MACH = 6.00 .. 22
ALPHA = 30.
RE NO. = 1.10

SYM	X/L
△	.. .383
▽	.. .447
△	.. .510
▽	.. .573
△	.. .637
▽	.. .682
△	.. .731

Aft

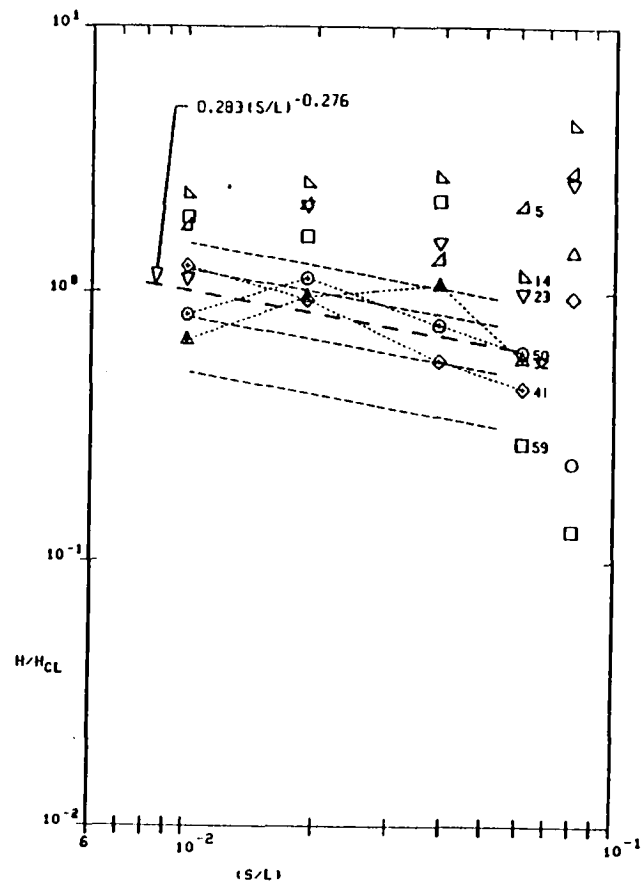
11 PTS USED

PCT E EST = .33205



12 PTS USED

PCT E EST = .25602

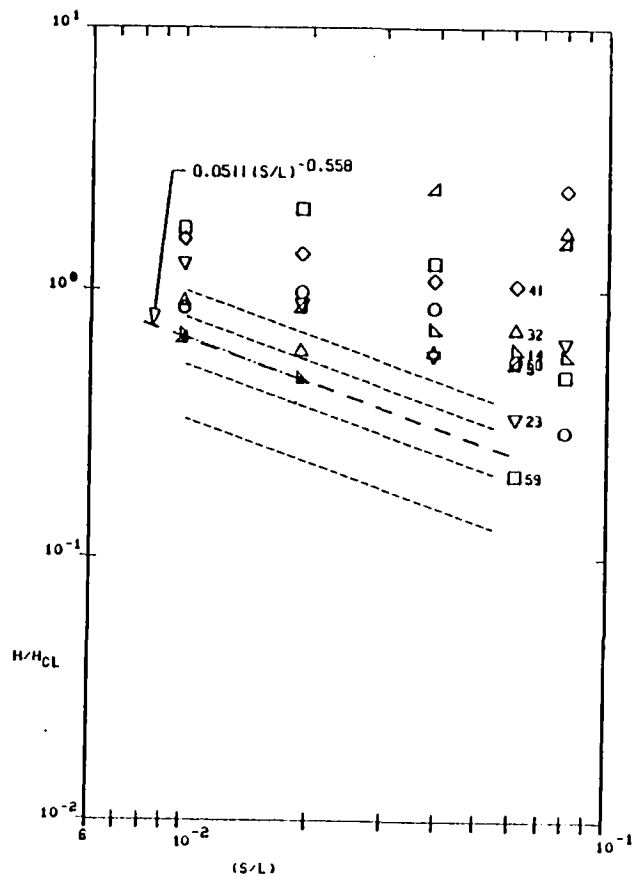


MACH = 6.00 .. 23
 ALPHA = 35.
 RE NO. = 1.10

SYM	X/L
△	.. .383
▽	.. .447
△	.. .510
△	.. .573
◇	.. .637
○	.. .682
□	.. .731

3 PTS USED

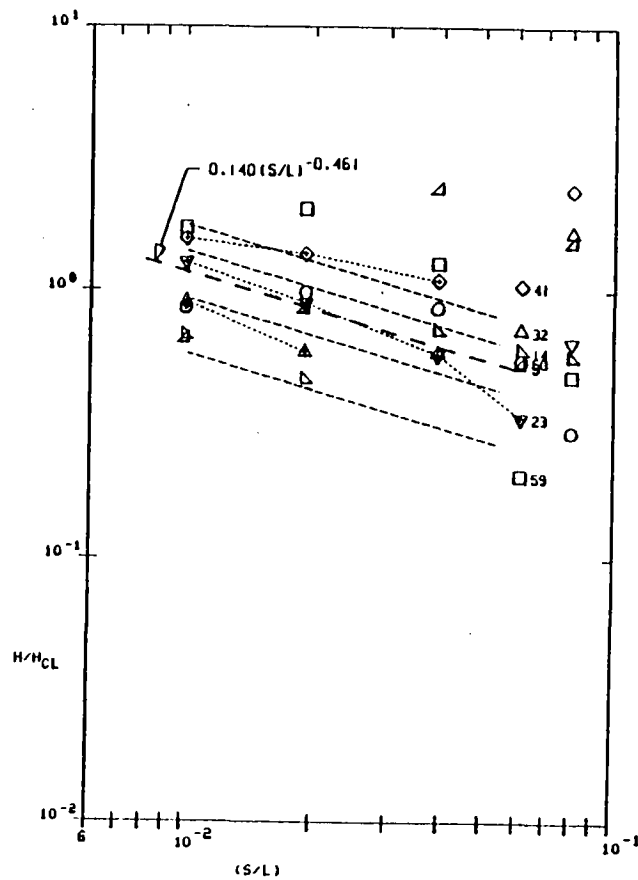
PCT E EST = .01191



Forward

10 PTS USED

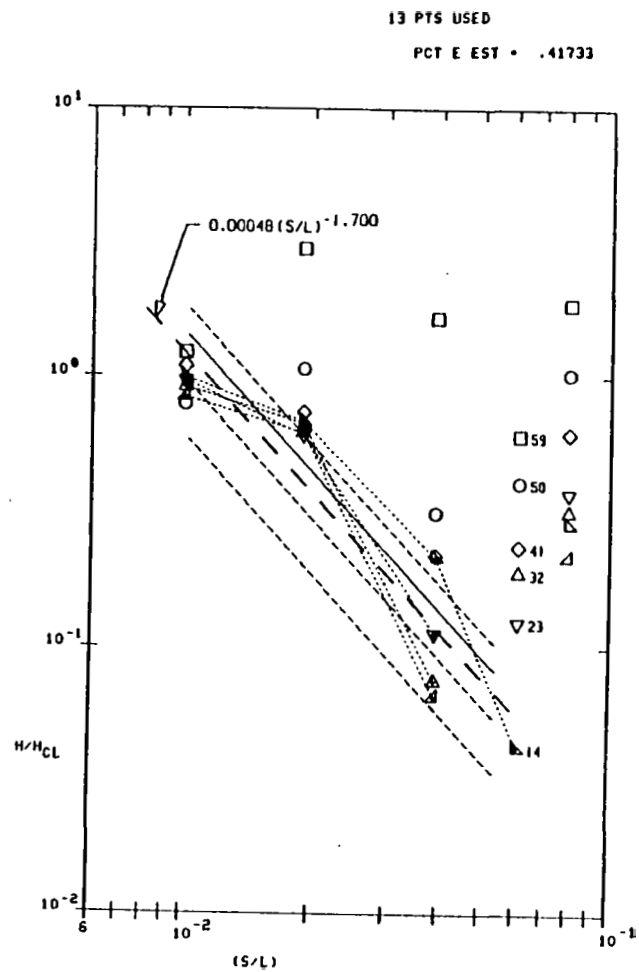
PCT E EST = .32752



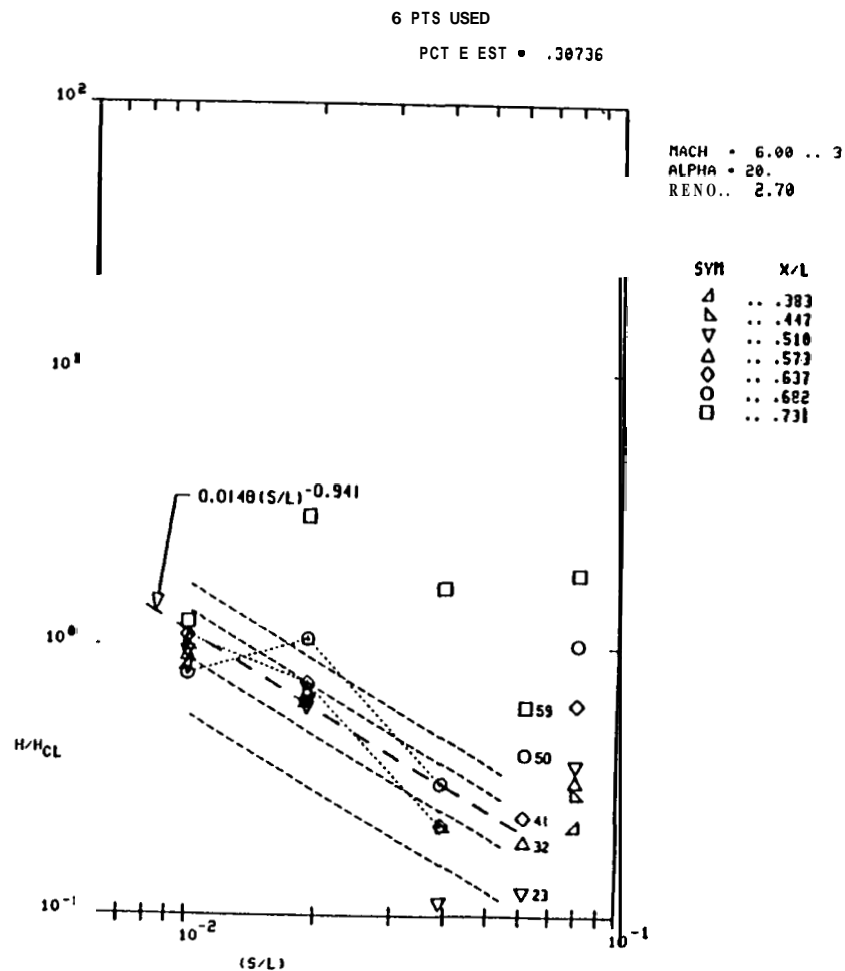
MACH = 6.00 .. 24
 ALPHA = 40.
 RE NO. = 1.10

SYM	X/L
△	.. .383
▽	.. .447
△	.. .510
△	.. .573
○	.. .637
○	.. .682
□	.. .731

Aft

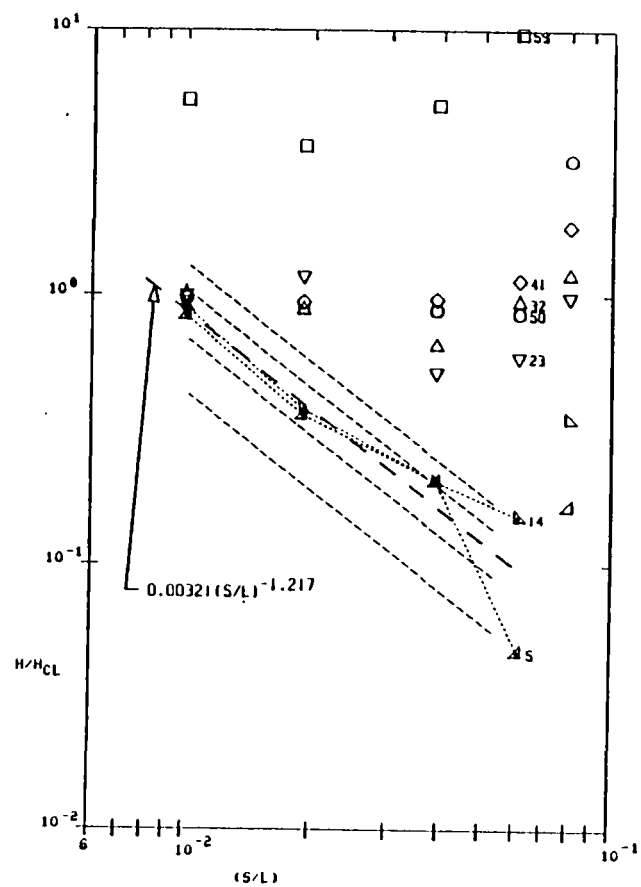


Forward



8 PTS USED

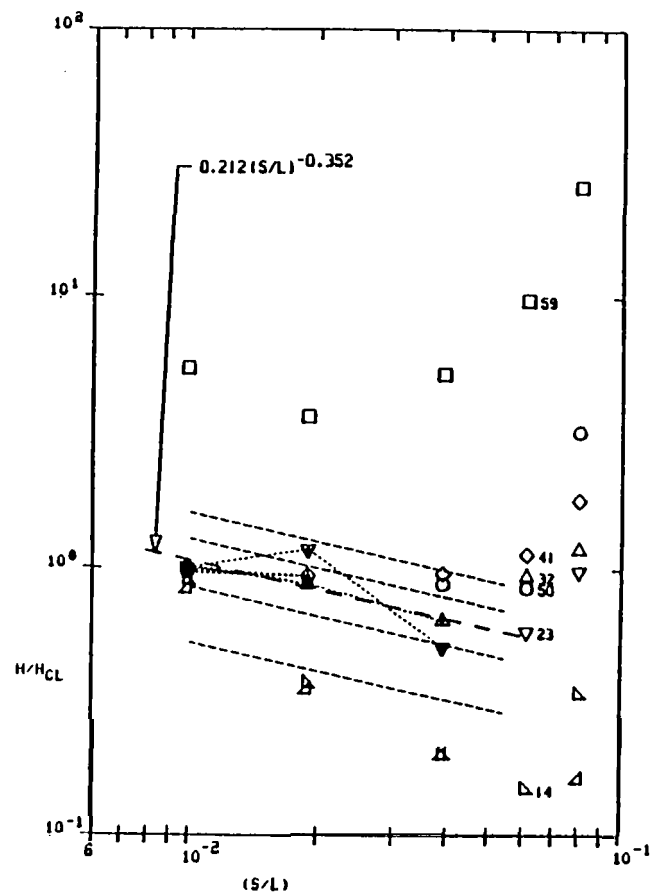
PCT E EST = .39639



Forward

18 PTS USED

PCT E EST = .13945



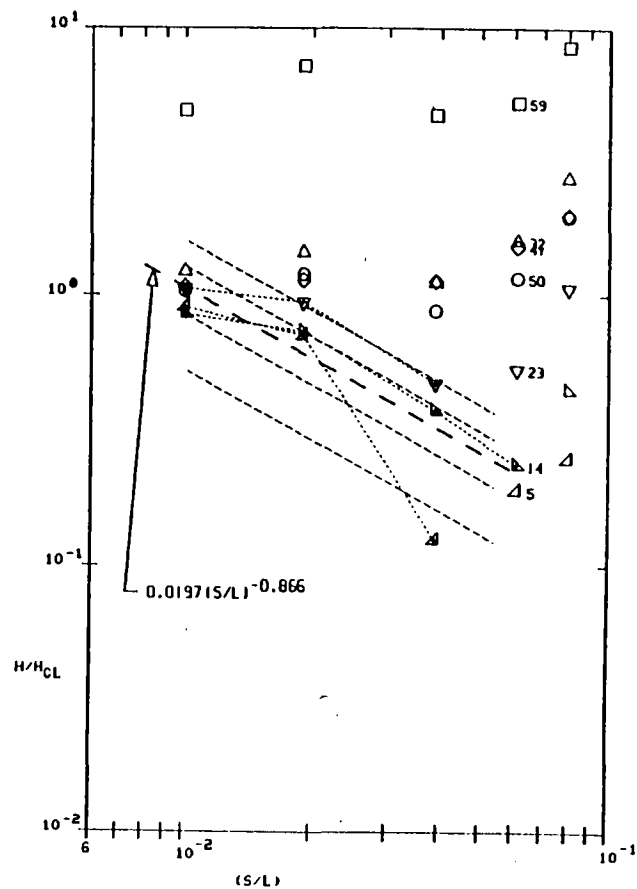
Aft

MACH = 6.88 .. 4
 ALPHA = 25.
 RE NO. = 2.70

SYM	X/L
△	.. .383
△	.. .447
▽	.. .510
△	.. .573
○	.. .637
○	.. .682
□	.. .731

10 PTS USED

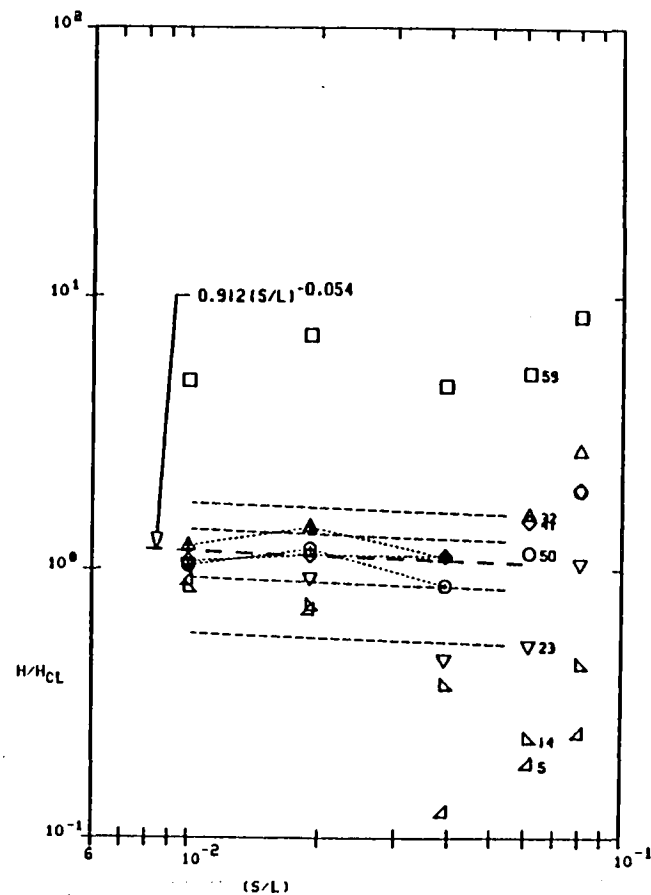
PCT E EST = .54835



Forward

9 PTS USED

PCT E EST = .12165



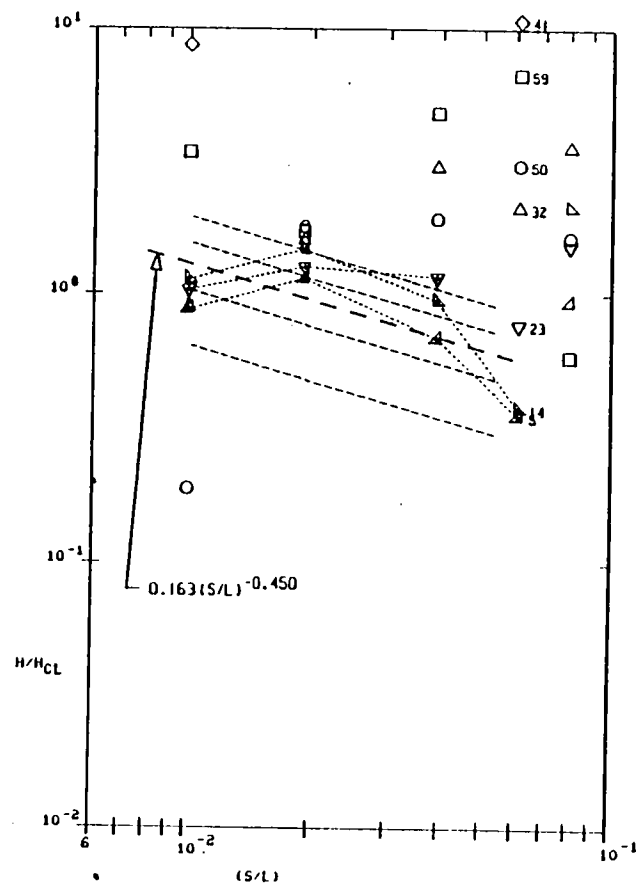
Aft

MACH = 6.00 .. 6
 ALPHA = 30.
 RE NO. = 2.70

SYM	X/L
△	.. .383
▽	.. .447
△	.. .510
△	.. .573
○	.. .637
○	.. .682
□	.. .731

11 PTS USED

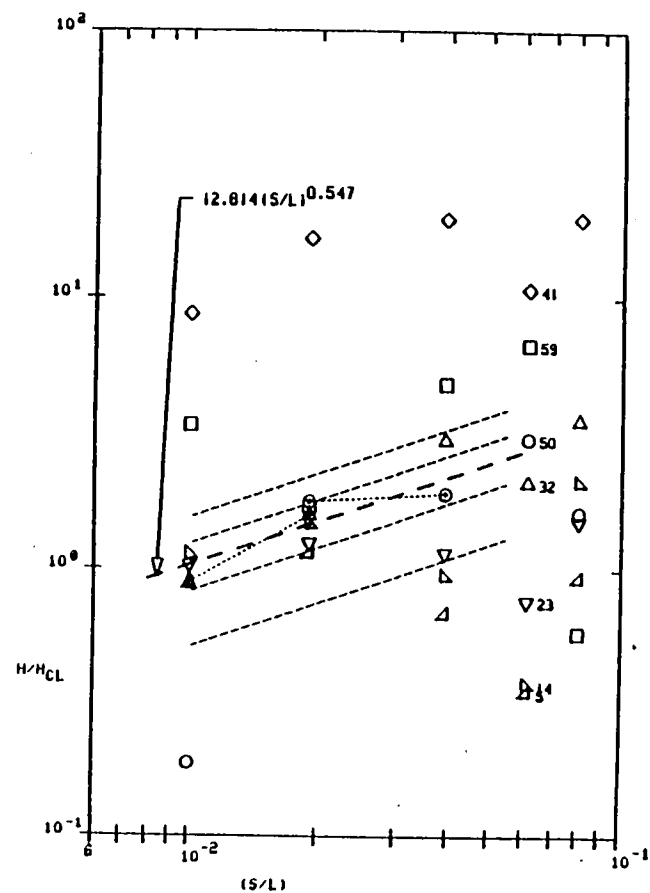
PCT E EST = .35301



Forward

4 PTS USED

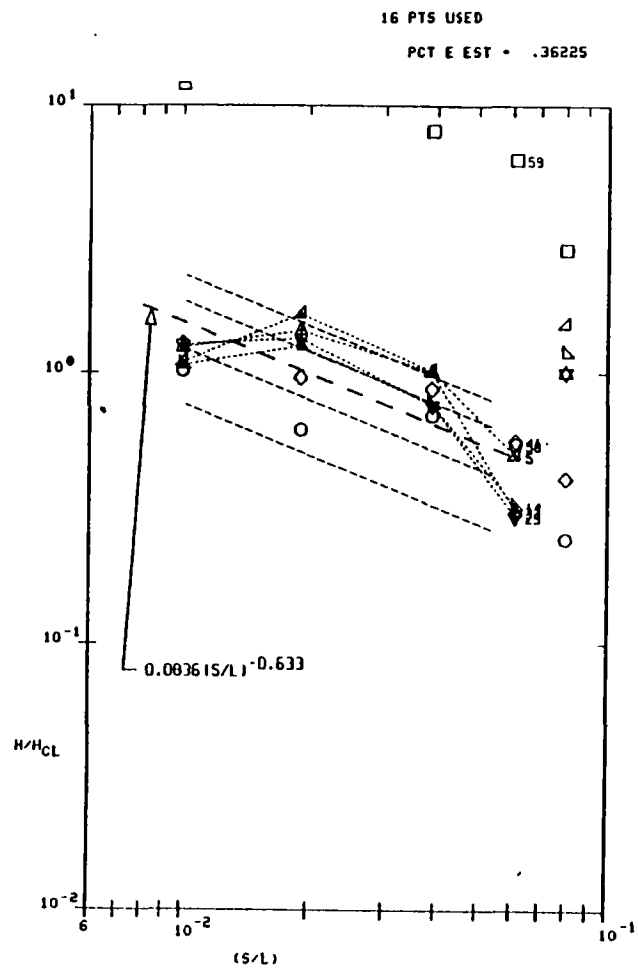
PCT E EST = .14195



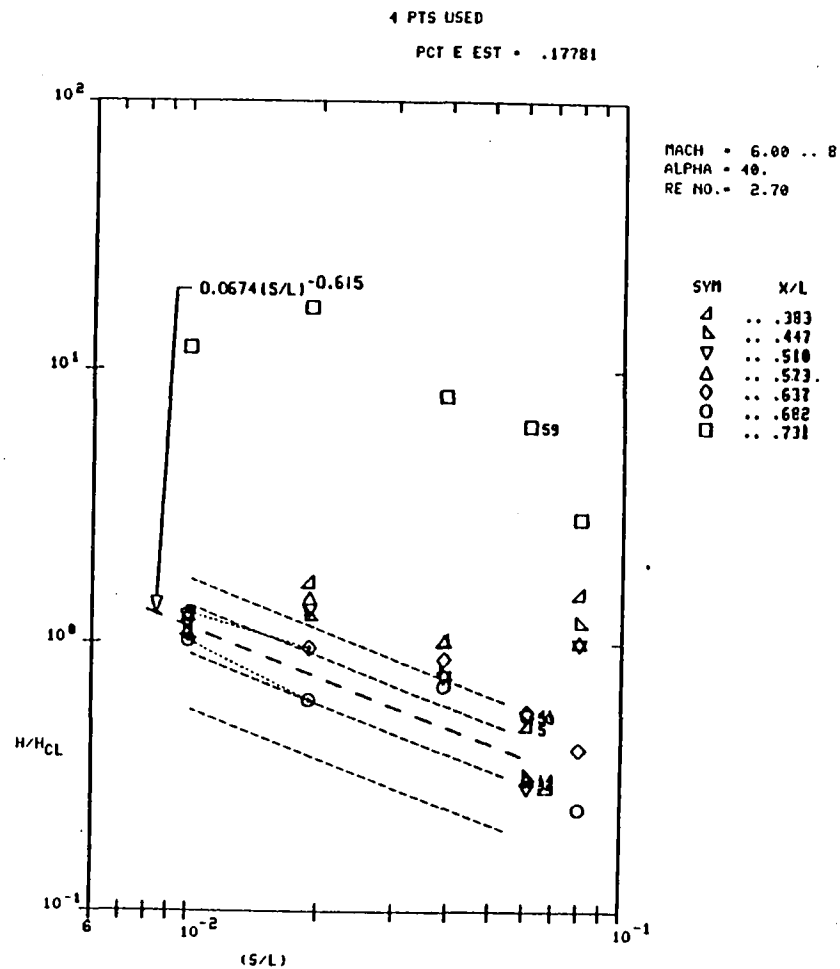
Aft

MACH = 6.00 .. 7
 ALPHA = 35.
 RE NO. = 2.70

SYM	X/L
△	.. .383
▽	.. .447
△	.. .510
▽	.. .573
○	.. .637
○	.. .682
□	.. .731



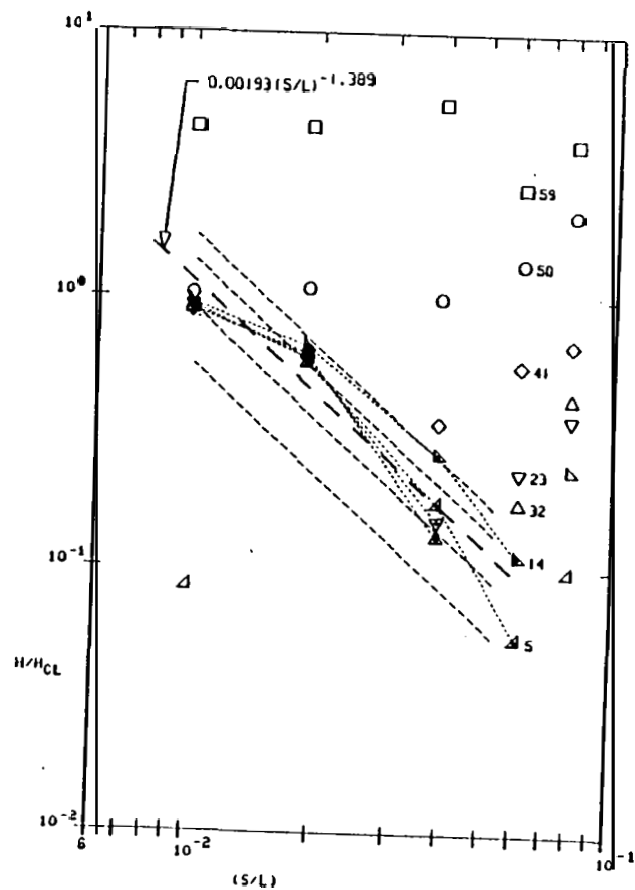
Forward



Aft

13 PTS USED

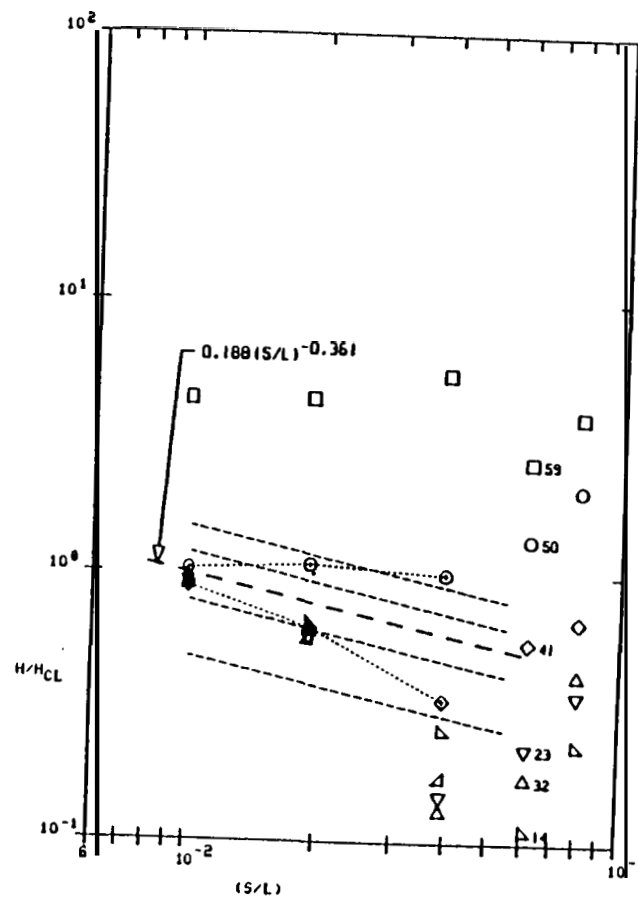
PCT E EST = .29726



Forward

6 PTS USED

PCT E EST = .37758



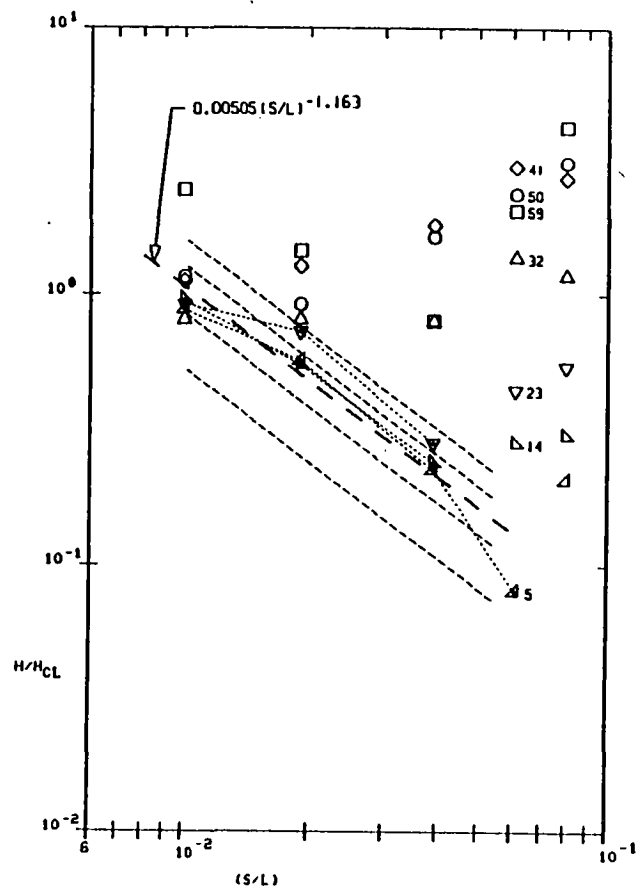
MACH = 6.00 .. 13
 ALPHA = 20.
 RE NO. = 5.40

SYM	x/L
△	.. .383
△	.. .447
▽	.. .518
△	.. .573
○	.. .637
○	.. .682
□	.. .731

Aft

10 PTS USED

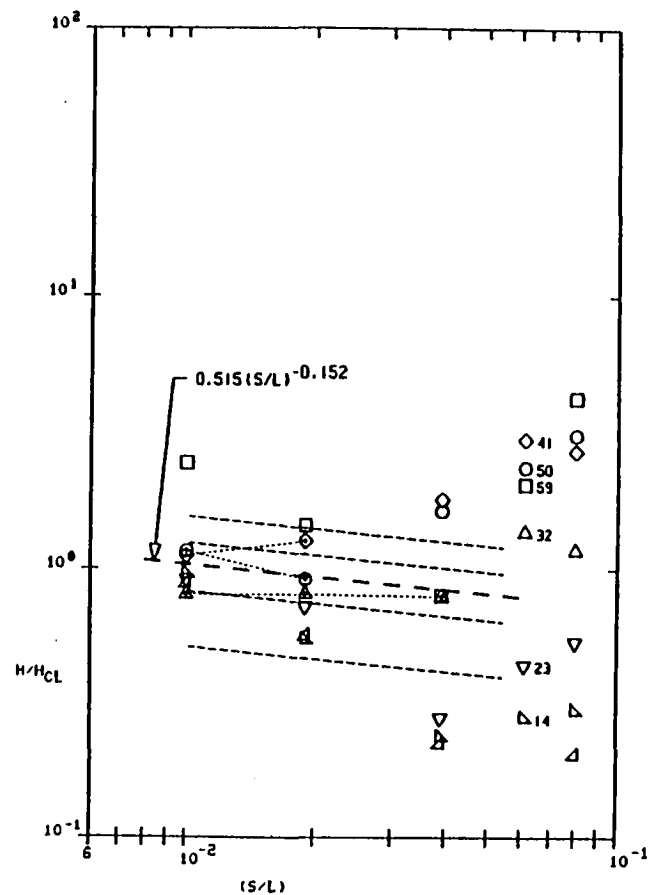
PCT E EST = .25335



Forward

7 PTS USED

PCT E EST = .16773



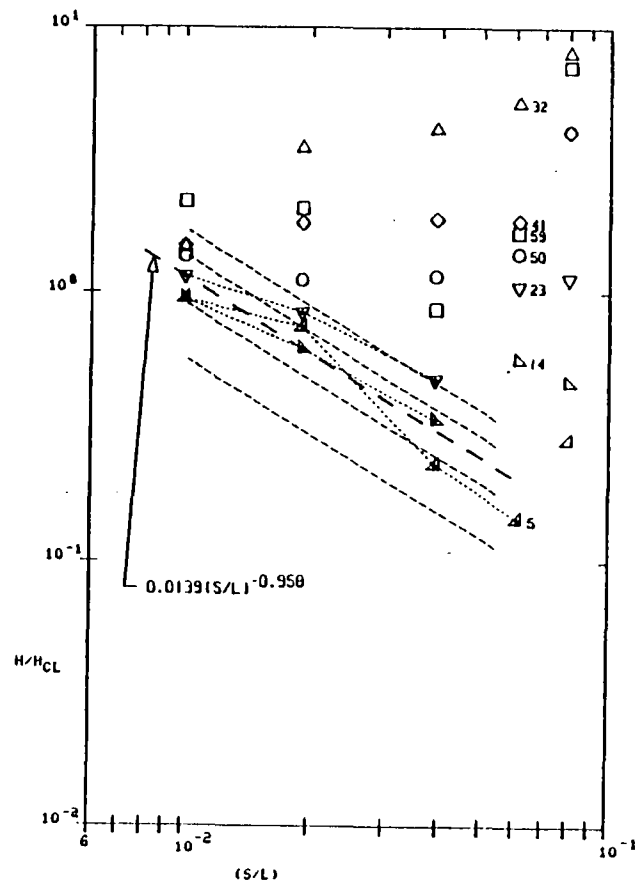
MACH = 6.00 .. 12
 ALPHA = 25.
 RE NO. = 5.40

SYM	X/L
△	.. .383
▷	.. .447
▽	.. .510
△	.. .573
○	.. .637
○	.. .682
□	.. .731

Aft

10 PTS USED

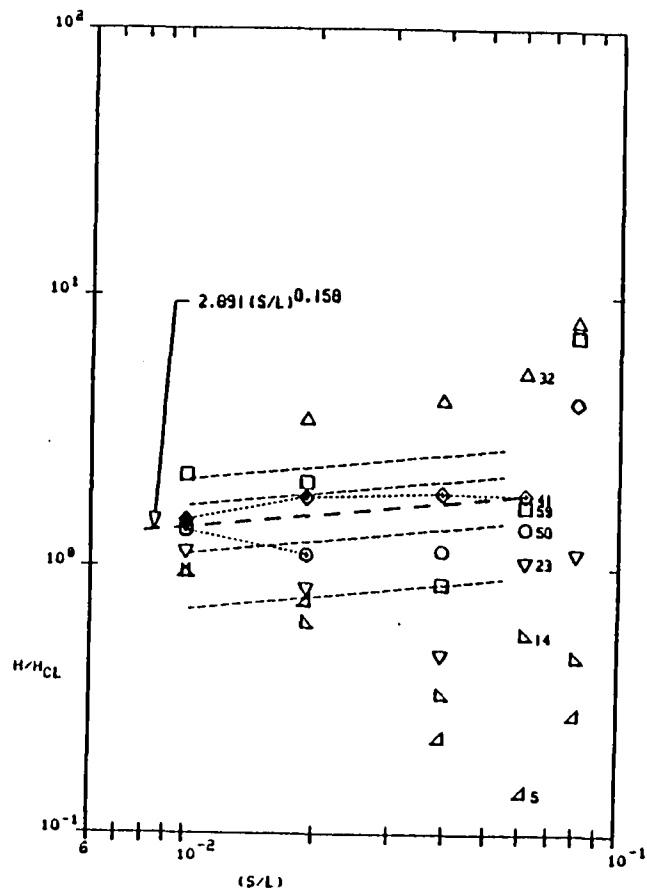
PCT E EST = .24556



Forward

7 PTS USED

PCT E EST = .16221



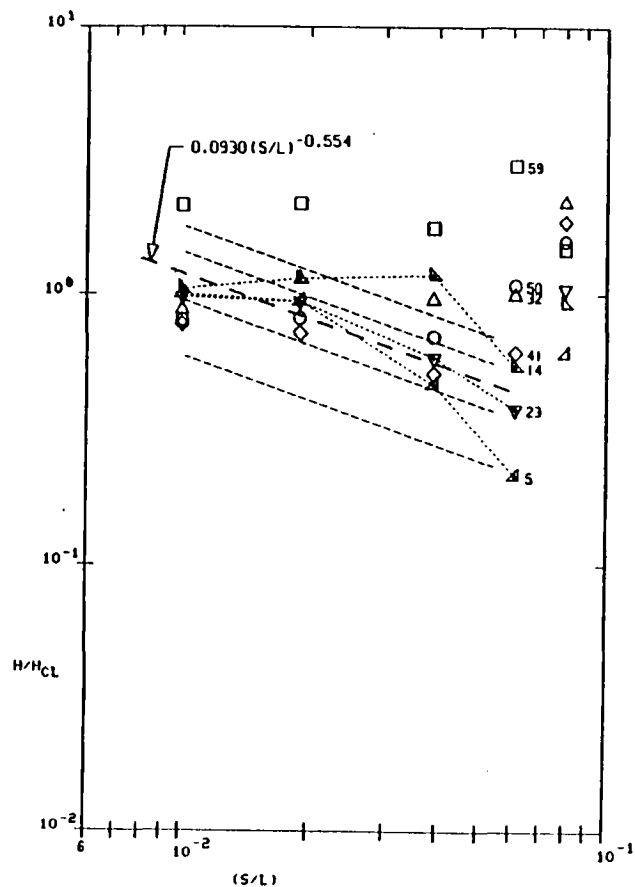
MACH = 6.00 .. 11
 ALPHA = 30.
 RE NO. = 5.40

SYN	X/L
Δ	.. .383
△	.. .447
▽	.. .510
◇	.. .573
○	.. .637
○	.. .682
□	.. .731

Aft

12 PTS USED

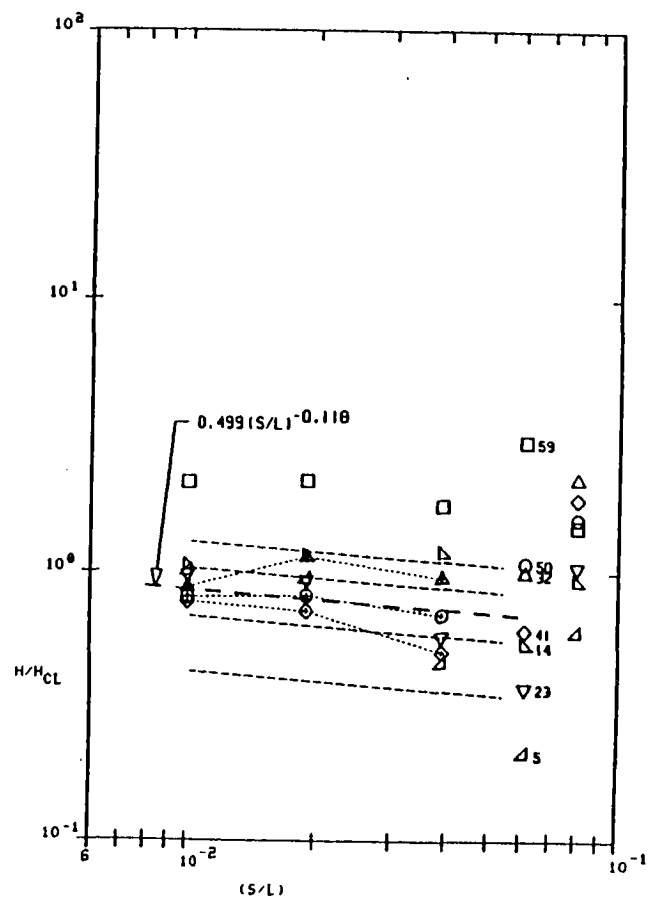
PCT E EST = .37305



Forward

9 PTS USED

PCT E EST = .20054



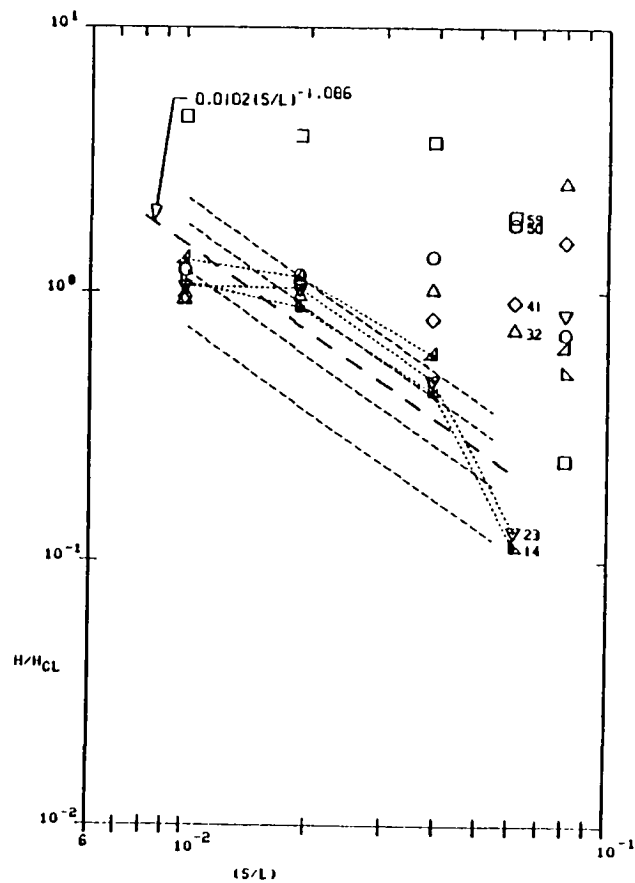
Aft

MACH = 6.00 .. 10
 ALPHA = 35.
 RE NO. = 5.40

SYM	X/L
△	.. .383
▽	.. .447
△	.. .510
△	.. .573
◇	.. .637
○	.. .682
□	.. .731

11 PTS USED

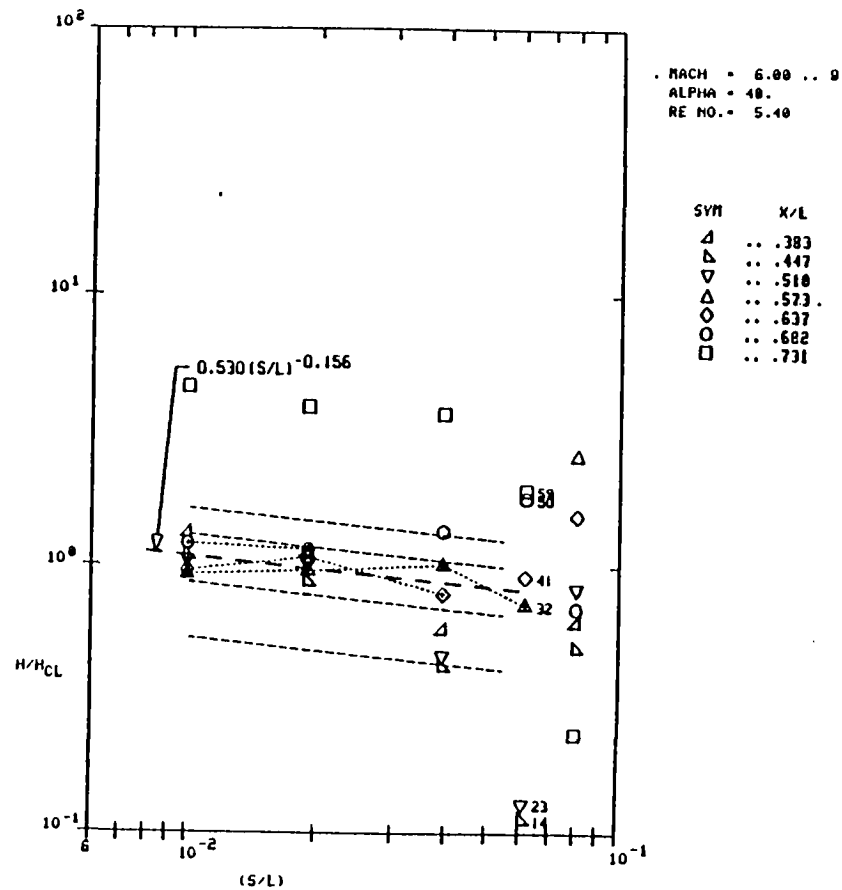
PCT E EST = .42794



Forward

9 PTS USED

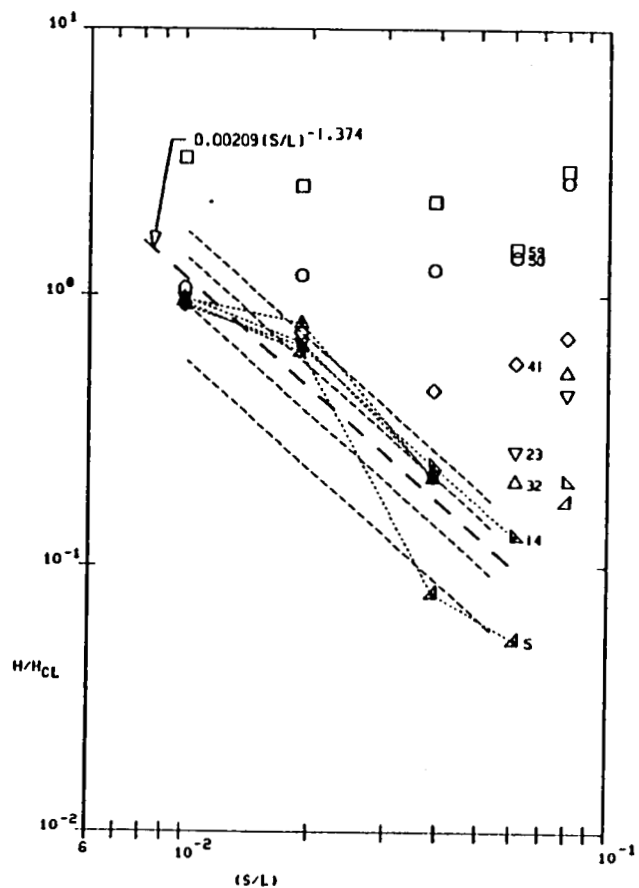
PCT E EST = .12070



Aft

14 PTS USED

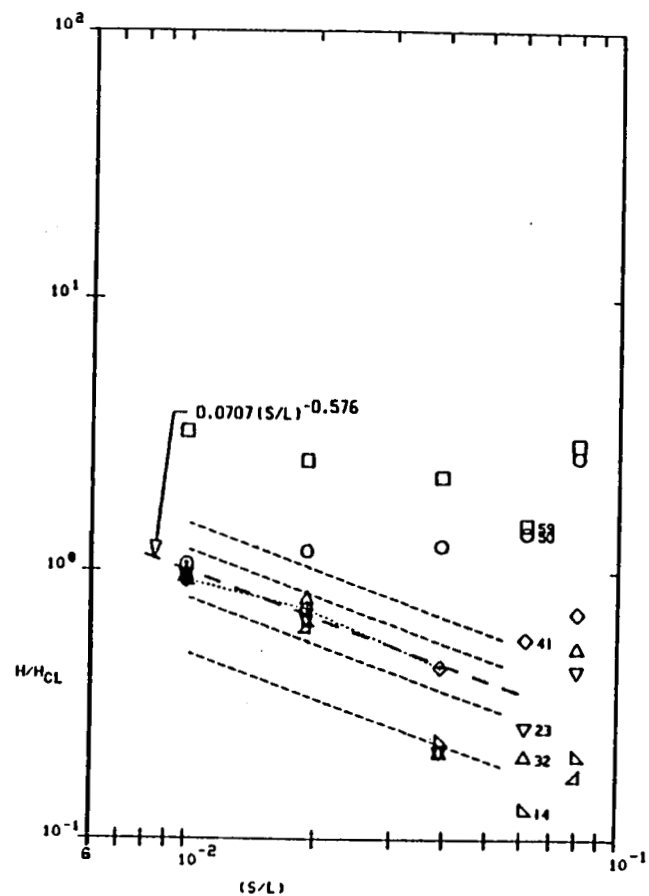
PCT E EST = .46546



Forward

4 PTS USED

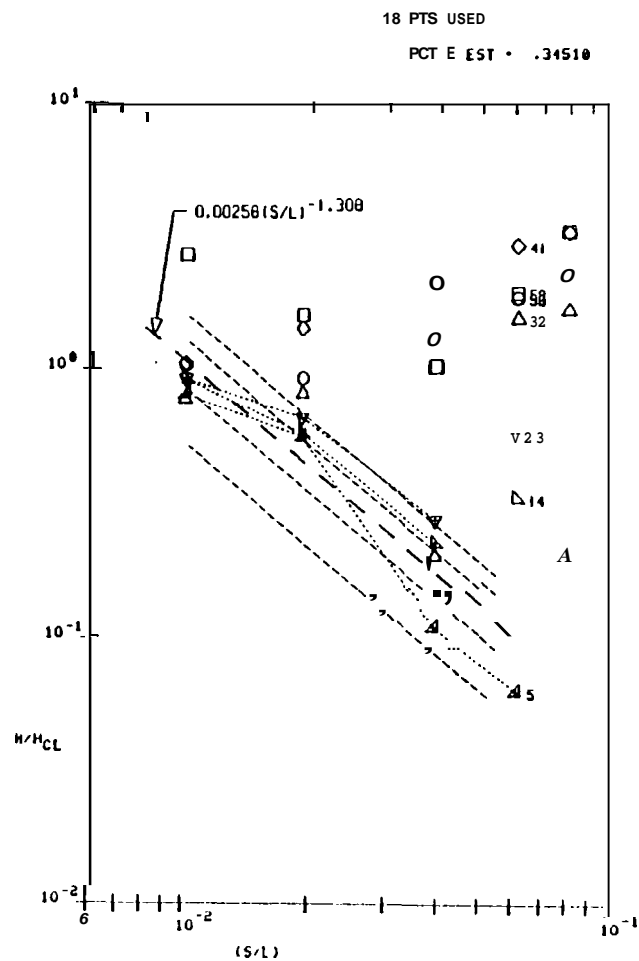
PCT E EST = .05651



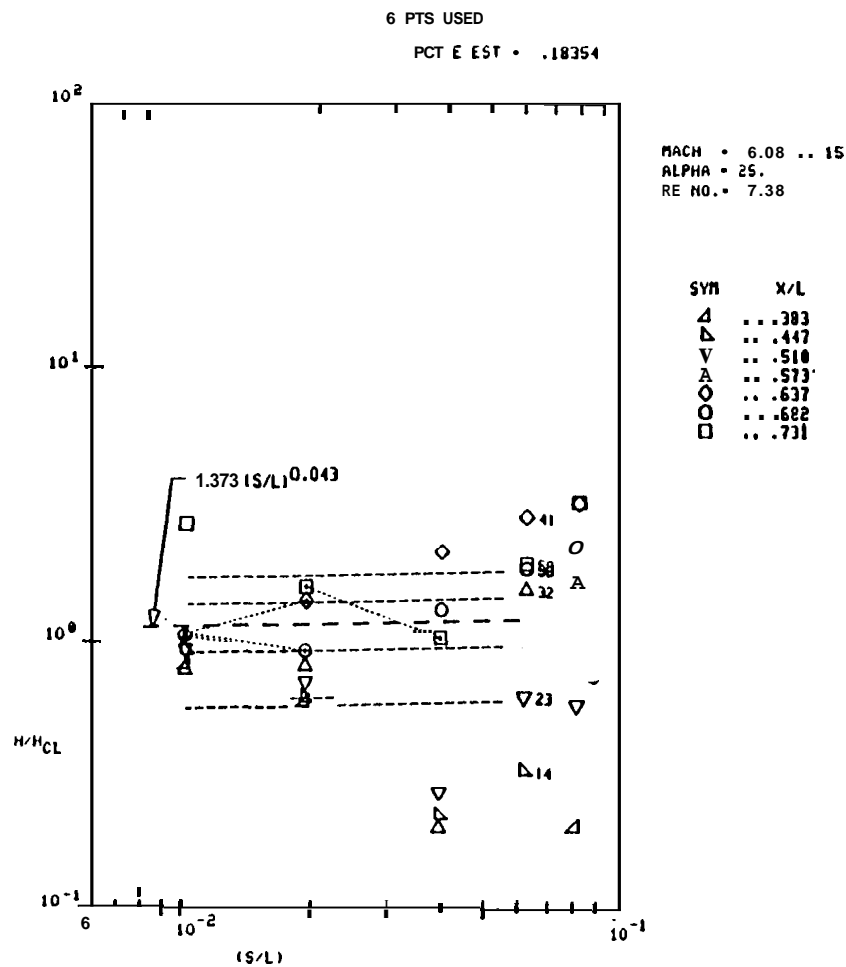
Aft

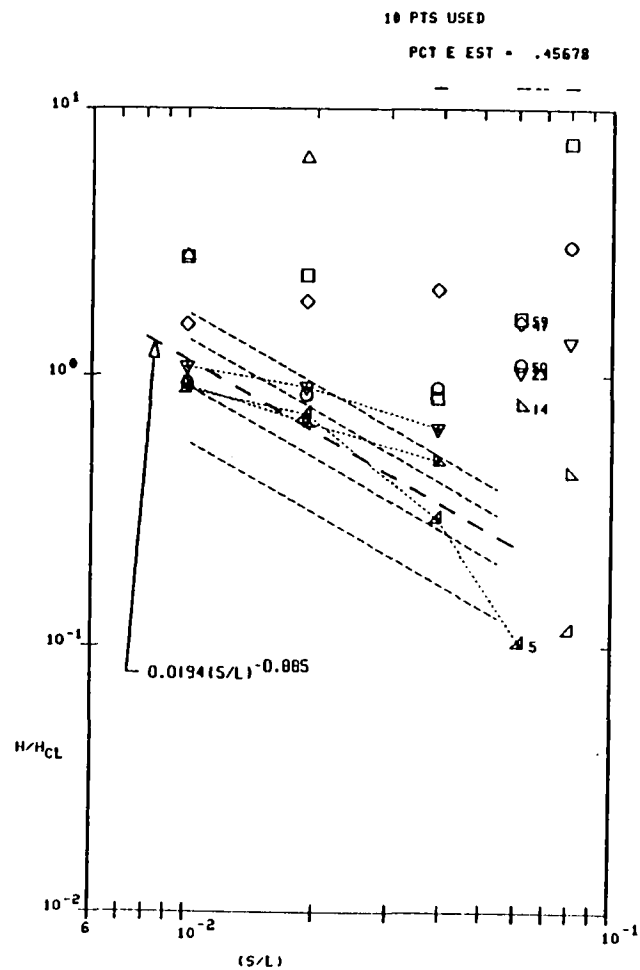
MACH = 6.00 .. 14
 ALPHA = 20.
 RE NO. = 7.30

SYM	X/L
△	.. .383
▽	.. .447
△	.. .510
△	.. .573
○	.. .637
○	.. .682
□	.. .731

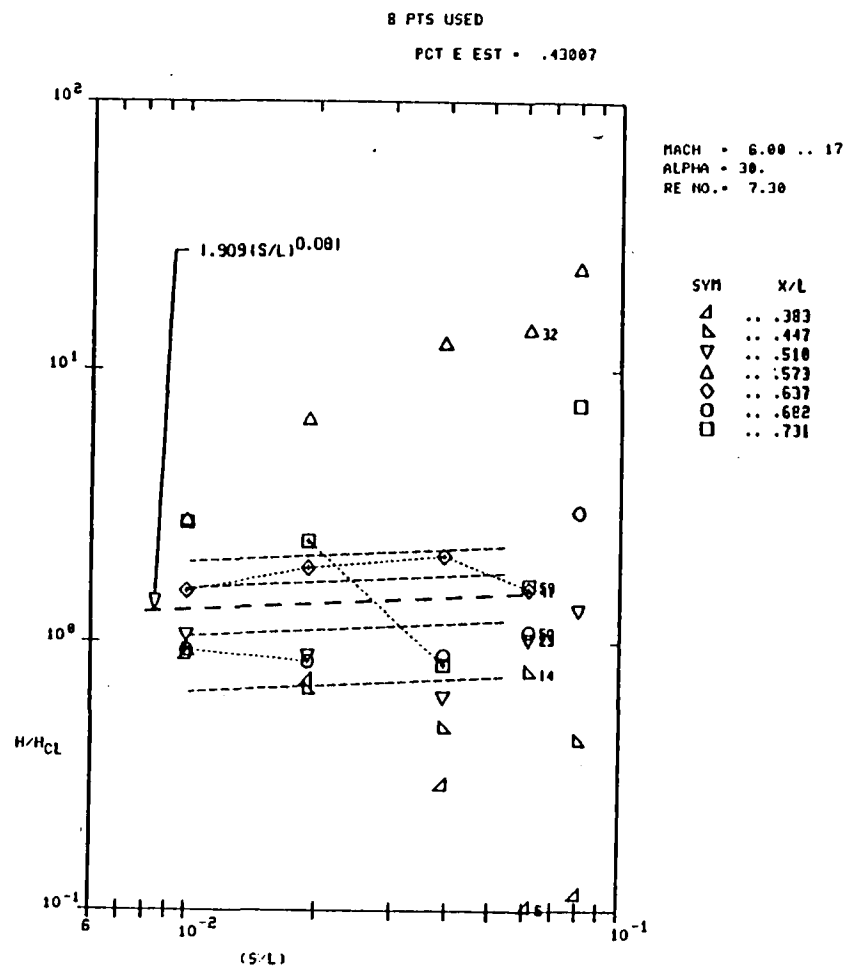


Forward





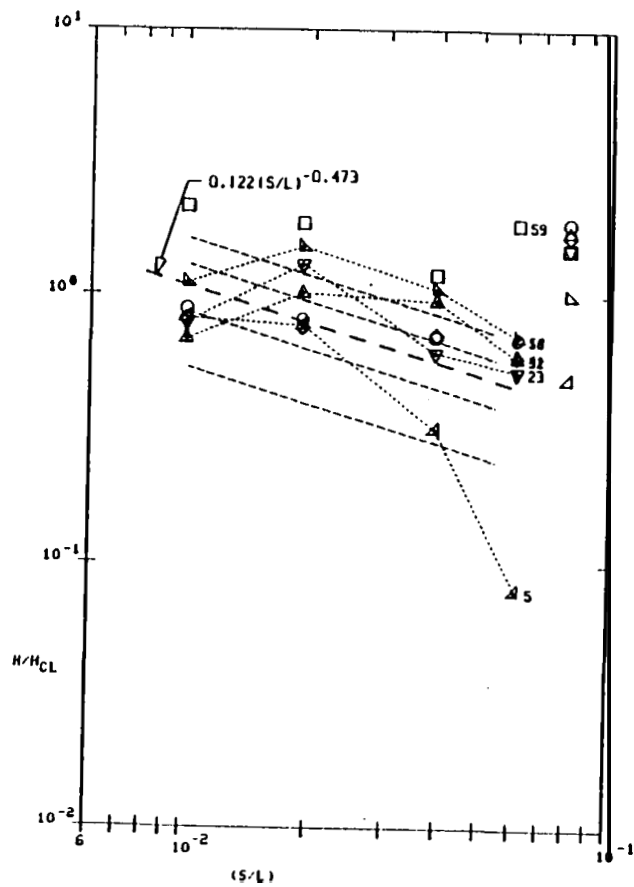
Forward



Aft

16 PTS USED

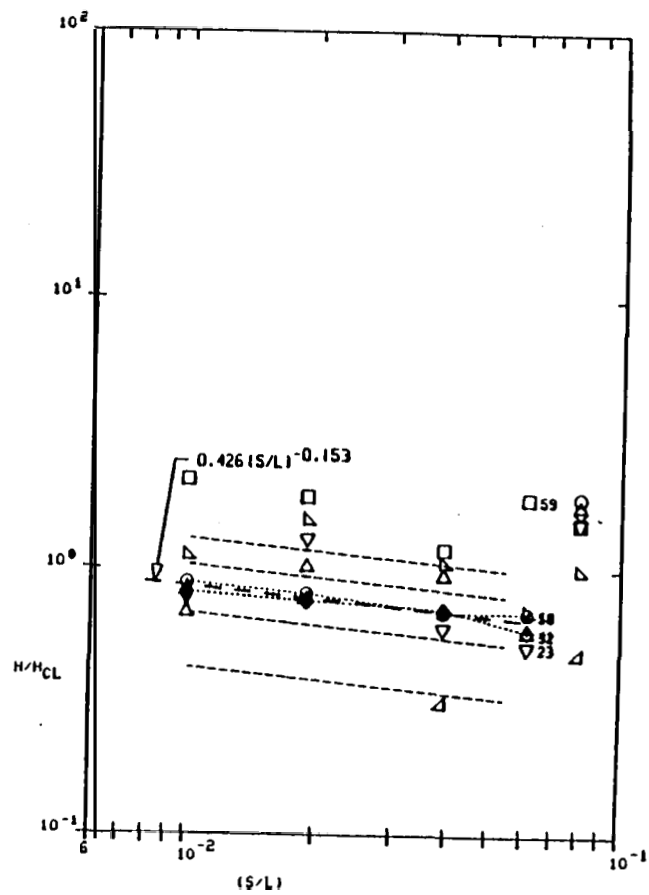
PCT E EST = 1.24113



Forward

8 PTS USED

PCT E EST = .04846



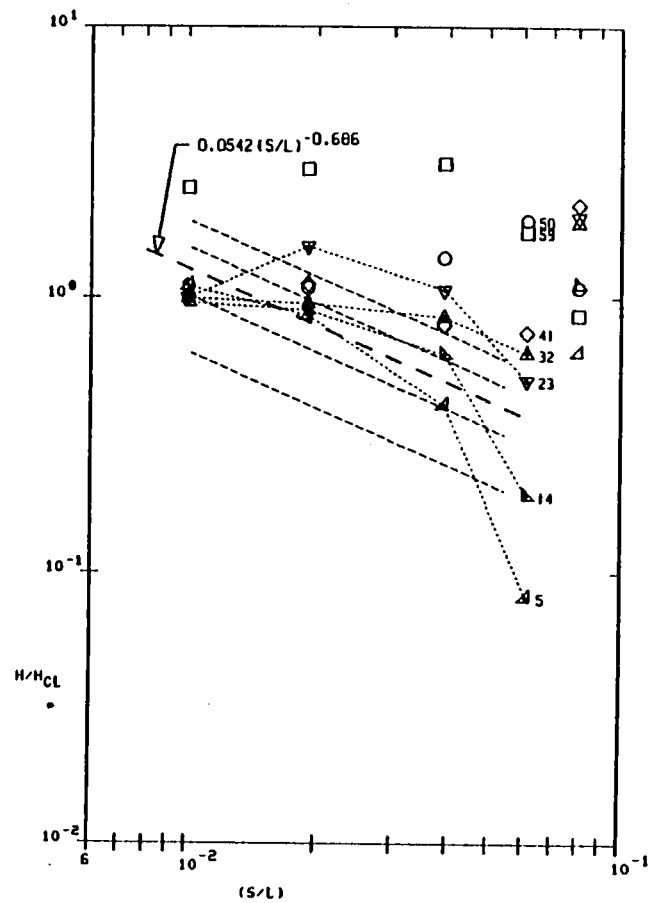
MACH = 6.00 .. 18
 ALPHA = 35.
 RE NO. = 7.30

SYM	X/L
Δ	.. .383
△	.. .447
▽	.. .510
△	.. .573
○	.. .637
○	.. .682
□	.. .731

Aft

16 PTS USED

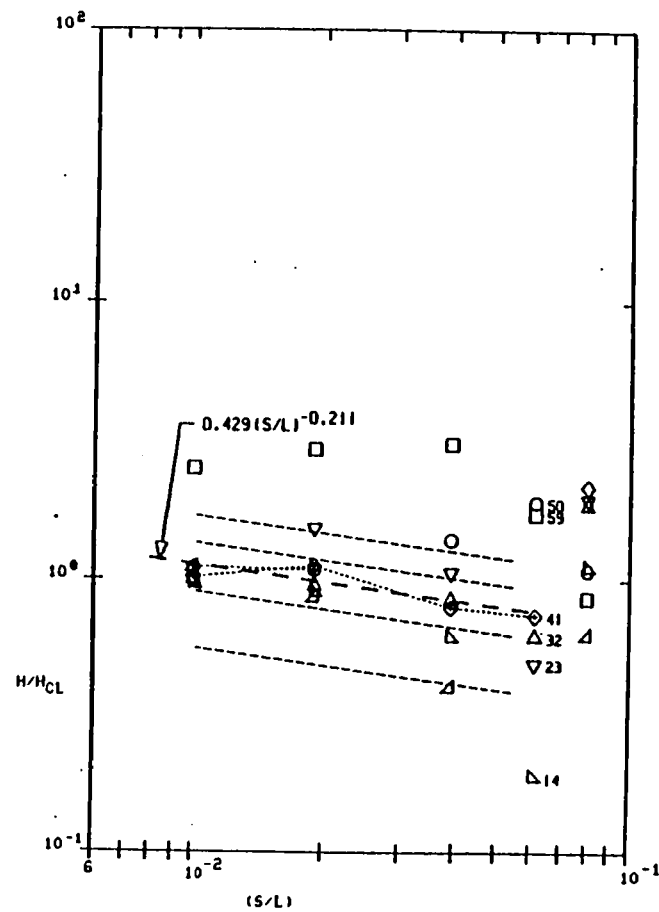
PCT E EST = .94950



Forward

6 PTS USED

PCT E EST = .08217



Aft

MACH = 6.00 .. 19
 ALPHA = 40.
 RE NO. = 7.30

SYM	X/L
△	.. .383
▽	.. .447
△	.. .510
△	.. .573
○	.. .637
○	.. .682
□	.. .731

APPENDIX J
Sample Calculations

This appendix presents sample calculations of the wing leeside heating using the correlations developed in the main text. The calculations are made for DFI location V07T9623A at three flight conditions. The flight conditions correspond to two early entry times at $\alpha = 40^\circ$, and a later entry time at $\alpha = 25^\circ$ when agreement between predictions and flight data was both good and bad. These calculations are repeated utilizing the correlation parameter variations recommended to account for local boundary layer state. This is done primarily in an attempt to reconcile the disagreement between predictions and flight data during the later portion of the entry trajectory.

The calculated heating rates correspond to entry times (t_E) of 866, 1076 and 1346 seconds. Flight conditions and data correlation parameters for these times are listed in Table J1. The location is that of DFI Surface Thermo-couple V07T9623A which has a normalized wetted length (s/L) of about 0.065 (see Figures 39 and 41 of the main text).

To determine the normalized heating ratio from the relation

$$q/q_{\text{ref}} = C_w (s/L)^{-n_w} \quad (\text{J1})$$

values of the coefficient, C_w , and exponent, n_w , are obtained from Figure 37 of the main text. Values of the parameters C_w and $-n_w \log(C_w)$ obtained for the specific flight Reynolds number from the Mach 10 and Mach 6 correlations are shown in Table J1. Values for $\alpha = 40^\circ$ are not available from the Mach 6 correlation because of reasons cited in the main text. The exponent n_w also shown in Table J1 is determined from these parameters using the relation

$$n_w = -n_w \log(C_w) / -\log(C_w) \quad (\text{J2a})$$

for example, at $t_E = 866$ s,

$$n_w = 7.1 / -\log(6.2 \times 10^{-5}) = 1.69 \quad (\text{J2b})$$

The normalized heating ratios at the location of V07T9623A are obtained by substituting the values for C_w and n_w (shown in Table J1) and the value of $s/L = 0.065$ in equation (J1). At $t_E = 866$ s, for example,

$$q/q_{ref} = 6.2 \times 10^{-5} (0.065)^{-1.69} = 0.0063 \quad (J3)$$

The normalized heating rates obtained using the individual Mach number correlations are shown in Table J2. For comparison, this table also includes the heating ratios reduced from the flight data at this location. As discussed in the main text, agreement with flight data during the early portion of the entry trajectory is good for predictions obtained from the Mach 10 data correlations. However, the agreement diminishes as entry time increases and the associated angle of attack decreases.

For the flight condition at the lower angle of attack ($\alpha = 25^\circ$), this calculation is repeated using the variations of the exponent, n_w , and the parameter $(\log(C_w) + n_w)$ shown in Figures 12 and 46 of the main text. In Figure 12, the variation of n_w is shown as relatively independent of Reynolds and Mach numbers. For $\alpha = 25^\circ$, the exponent has a value of about 1.5 ± 0.1 from correlations of both the Mach 10 and Mach 6 data. In Figure 46, the parameter $(\log(C_w) + n_w)$ from both Mach number data has a value of $-2.4 \pm 2\%$ for $Re_{\infty,L} \leq 2.5 \times 10^6$. No Mach 10 data is available for larger Reynolds numbers. However, based on the agreement of this parameter from both the Mach 6 and Mach 10 data for the lower Reynolds numbers, this agreement is assumed to extend to the higher Reynolds numbers. Hence, extrapolating the parameter for $\alpha = 25^\circ$ in Figure 46b to the value of $Re_{\infty,L} = 1.75 \times 10^7$ using the available Mach 6 data, yields a value of $(\log(C_w) + n_w) = -2.02$, and the coefficient is determined from the relation

$$\begin{aligned} C_w &= 10^{(\log(C_w) + n_w) - n_w} \\ &= 10^{-2.02 - 1.5} \\ &= 10^{-3.52} = 3.02 \times 10^{-4} \end{aligned} \quad (J4)$$

Thus, the normalized heating rate is obtained by substituting these new values of C_w and n_w in equation (J1), yielding

$$q/q_{\text{ref}} = 3.02 \times 10^{-4} (0.065)^{-1.5} = 0.018 \quad (\text{J5})$$

which agrees much better with the flight data at this time than does the prediction obtained from the Mach 10 data correlation.

TABLE J1
CORRELATION PARAMETER

FLIGHT CONDITION				DATA CORRELATION					
t_E (SEC)	α (DEG)	$Re_{\infty,L}$ (10^6)	M_{∞}	$M_{\infty} = 10$			$M_{\infty} = 6$		
				C_w	$-n_w \log C_w$	n_w	C_w	$-n_w \log C_w$	n_w
866	40.4	1.66	19.2	6.2×10^{-5}	7.1	1.69	N/A	N/A	-
1076	39.8	4.06	13.3	1.15×10^{-4}	6.1	1.55	N/A	N/A	-
1346	25.0	17.5	6.1	3.1×10^{-4}	4.2	1.20	4.0×10^{-4}	4.8	1.41

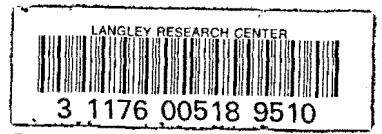
TABLE J2
DFI V07T9623A HEATING ENVIRONMENT DURING STS-2 ENTRY

FLIGHT CONDITION			FLIGHT DATA		PREDICTED	
t_E (SEC)	α (DEG)	$\dot{q}_{ref}^{(a)}$ (BTU/FT ² -S)	T_{SURF} (°F)	$\dot{q}_c / \dot{q}_{ref}^{(b)}$	$\dot{q}_c / \dot{q}_{ref}$	
					$M_{\infty} = 10$	$M_{\infty} = 6$
866	40.4	68.0	462	0.0052	0.0063	N/A
1076	39.8	49.5	480	0.0065	0.0080	N/A
1346	25.0	11.1	450	0.027	0.0082	0.019

(a) \dot{q}_{ref} for $T_w = T_{surf}$

(b) \dot{q}_c from one-dimensional reduction of T_{surf} data with corrections for solar- and cross-radiation.

1. Report No. NASA CR-172362		2. Government Accession No.		3. Recipient's Catalog No.	
4. Title and Subtitle A Study of Leeside Flow Field Heat Transfer on Shuttle Orbiter Configuration				5. Report Date August 1984	
				6. Performing Organization Code	
7. Author(s) Leroy C. Baranowski and H. W. Kipp				8. Performing Organization Report No.	
9. Performing Organization Name and Address McDonnell Douglas Astronautics Company P.O. Box 516 St. Louis, MO 63166				10. Work Unit No.	
				11. Contract or Grant No. NAS1-16839	
12. Sponsoring Agency Name and Address National Aeronautics and Space Administration Washington, DC 20546				13. Type of Report and Period Covered Contractor Report	
				14. Sponsoring Agency Code 506-51-33-01	
15. Supplementary Notes Final Report. Project Monitor, Vernon Helms III, Aerothermodynamics Branch, Space Systems Division, NASA Langley Research Center, Hampton, Virginia					
16. Abstract The purpose of this study was to develop simplified methods for predicting entry heating on leeside surfaces of the Shuttle orbiter. Wind tunnel heat transfer and oil flow data at Mach 6 and 10 and Reynolds numbers ranging from 0.5×10^6 to 7.3×10^6 were used to develop correlations for the wing upper surface and the top surface of the fuselage. These correlations were extrapolated to flight Reynolds number and compared with heating data obtained during the Shuttle STS-2 reentry. Efforts directed toward the wing leeside surface resulted in an approach which agreed adequately with the flight data.					
17. Key Words (Suggested by Author(s)) Shuttle heat transfer data leeward surface separated flow				18. Distribution Statement Unclassified-Unlimited Subject Category 15	
19. Security Classif. (of this report) Unclassified		20. Security Classif. (of this page) Unclassified		21. No. of Pages 318	
				22. Price	



LANGLEY RESEARCH CENTER



3 1176 00518 9510